Methods in Molecular Biology 965

Springer Protocols

Lorenzo Galluzzi
Ilio Vitale
Oliver Kepp
Guido Kroemer *Editors*

Cell Senescence

Methods and Protocols

Humana Press

METHODS IN MOLECULAR BIOLOGY™

Series Editor
John M. Walker
School of Life Sciences
University of Hertfordshire
Hatfield, Hertfordshire, AL10 9AB, UK

For further volumes:
http://www.springer.com/series/7651

Cell Senescence

Methods and Protocols

Edited by

Lorenzo Galluzzi, Ilio Vitale, Oliver Kepp, and Guido Kroemer

Institut Gustave Roussy (IGR), INSERM U848, Villejuif, France

Humana Press

Editors
Lorenzo Galluzzi
Institut Gustave Roussy
Université Paris Descartes
Sorbonne Paris Cité
Villejuif, France

Oliver Kepp
Institut Gustave Roussy
INSERM U848
Villejuif, France

Ilio Vitale
Institut Gustave Roussy
INSERM U848
Villejuif, France

Guido Kroemer
Institut Gustave Roussy
INSERM U848
Villejuif, France

ISSN 1064-3745 ISSN 1940-6029 (electronic)
ISBN 978-1-62703-238-4 ISBN 978-1-62703-239-1 (eBook)
DOI 10.1007/978-1-62703-239-1
Springer New York Heidelberg Dordrecht London

Library of Congress Control Number: 2012950333

Printed on acid-free paper

Humana Press is a brand of Springer
Springer is part of Springer Science+Business Media (www.springer.com)

Preface

In Vitro and In Vivo Cell Senescence

Cell senescence, i.e., the process whereby cells permanently lose the possibility to proliferate without undergoing cell death, can be observed in vitro as well as in vivo, and occurs in a plethora of distinct model organisms. In both cases, cell senescence can be physiological, constituting a safeguard mechanism against cells that have accumulated potentially dangerous genetic alterations, or can be triggered by exogenous perturbations, such as the administration of DNA-damaging agents at low doses. This book provides a detailed description of the most common techniques for the investigation of cell senescence, in model organisms encompassing bacteria (*Escherichia coli*), fungi (*Saccharomyces cerevisiae* and *Podospora anserina*), worms (*Caenorhabditis elegans*), flies (*Drosophila melanogaster*), zebrafish (*Danio rerio*), and mammalian cells. The techniques presented in this book not only cover the study of all the biochemical and functional manifestations of senescence at the cellular level but also include protocols for population analysis and high-throughput approaches in suitable model organisms, as described by worldwide renowned experts of the field.

Chapter Organization

The book is composed of three types of chapters. Four review chapters open the book to provide a solid theoretical background on cell senescence, its morphological and biochemical manifestations and its pathophysiological relevance. Twenty-three protocol chapters follow, detailing the methods to investigate the morphological and biochemical features of senescence at the cellular level, in cultured mammalian cells. Finally, seven protocol chapters provide techniques for the study of cell senescence in lower model organisms, including methods for population studies. Each of these 30 protocols starts with an Abstract and includes four major sections: Introduction, Materials, Methods, and Notes. The "Abstract" presents an overview of the technique(s) detailed in the chapter. The "Introduction" provides a short theoretical view of the procedure and of its applications. "Materials" recapitulate the buffers, reagents, solutions, disposables, and equipments necessary to carry out the protocol(s). "Methods" describe step-by-step how the technique(s) must be carried out. Finally, the "Notes" section, which is the hallmark of *Methods in Molecular Biology* series, indicates not only the sources of problems and how to identify and overcome them, but also safety information, alternative procedures, and hints for the correct interpretation of experimental results.

Brief Content of the Chapters

Chapter 1 provides an overview on cell senescence and its dynamic links with autophagy, an important cytoprotective mechanism. Chapters 2 and 3 discuss the regulation of cell senescence by critical signaling molecules such as the mammalian target of rapamycin (mTOR) and p53. Chapter 4 summarizes the morphological and biochemical markers that have been associated with cell senescence. In Chapters 5–23, protocols for the investigation of senescence-associated alterations in cultured cells are provided, including the following: morphological features (Chapter 5), cell cycle blockage (Chapter 6), cell cycle-arresting proteins (Chapter 7), senescence-associated β-galactosidase (Chapters 8 and 9), senescence-associated secretory phenotype and chemokyne signaling (Chapters 10 and 11), senescence-associated heterochromatin foci (Chapter 12), DNA damage (Chapter 13), telomerase activity and telomere length (Chapters 14 and 15), alterations of the nuclear envelope (Chapter 16), multiple markers of oxidative stress (Chapters 17–20), BRAF, sirtuin, and $p66^{SHC}$ signaling during senescence (Chapters 21–23). In Chapters 24–27, protocols for the study of cell senescence in global terms are detailed, including a method for the study of metabolomic alterations (Chapter 24), a technique to apply genome-wide RNAi approaches to cell senescence research (Chapter 25), and multiparametric strategies (Chapters 26 and 27). Finally, in Chapters 28–34, protocols applicable to lower model organisms are described, encompassing techniques to assess senescence in *Escherichia coli* (Chapter 28), *Podospora anserina* (Chapter 29), *Saccharomyces cerevisiae* (Chapter 30), *Caenorhabditis elegans* (Chapters 31 and 32), *Drosophila melanogaster* (Chapter 33), and *Danio rerio* (Chapter 34).

Potential Audience of This Book

In the first instance, this book will be of interest not only for undergraduate and graduate students but also for more experienced scientists who are approaching the study of cell senescence. In addition, the audience of this book encompasses:

- Libraries of universities and public biological/biomedical research institutions.
- Scientists interested in molecular and cell biology, biochemistry, pharmacology, genetics, systems biology, medicine, public health, and in life sciences in general.
- Specialists and experts in model organisms including bacteria, fungi, worms, flies, and mammals.
- Medical oncologists and scientists working in oncology.
- Pharmaceutical companies and developers of new drugs.

Villejuif, France

Lorenzo Galluzzi
Ilio Vitale
Oliver Kepp
Guido Kroemer

Contents

Contributors

Juan Carlos Acosta • *Cell Proliferation Group, MRC Clinical Sciences Centre, Imperial College, London, UK*

Sandy Adjemian • *INSERM, U848, Villejuif, France; Institut Gustave Roussy, Villejuif, France*

Katherine M. Aird • *Women's Cancer Program, Epigenetics and Progenitor Cells Keystone Program, Fox Chase Cancer Center, Philadelphia, PA, USA*

Reza Ardekani • *Molecular and Computational Biology Program, Department of Biological Sciences, University of Southern California, Los Angeles, CA, USA*

Bo Bai • *Department of Pharmacology and Pharmacy, Li Ka Shing Faculty of Medicine, University of Hong Kong, Hong Kong, China*

Clea Bárcena • *Departamento de Bioquímica y Biología Molecular, Instituto Universitario de Oncología, Universidad de Oviedo, Oviedo, Spain*

Vinicius Bassaneze • *Laboratory of Genetics and Molecular Cardiology/LIM 13, Heart Institute (InCor), University of Sao Paulo Medical School, Sao Paulo, Brazil*

J. Renwick Beattie • *Centre for Vision and Vascular Science, School of Medicine and Dentistry, Queen's University, Belfast, UK*

Jacob G. Bundy • *Biomolecular Medicine, Department of Surgery and Cancer, Imperial College, London, UK*

Amancio Carnero • *Instituto de Biomedicina, Hospital Universitario Virgen del Rocio, Sevilla, Spain*

Maria Castedo • *INSERM, U848, Villejuif, France; Institut Gustave Roussy, Villejuif, France*

Xinbin Chen • *Comparative Oncology Laboratory, University of California, Davis, CA, USA*

Zhanna V. Chitikova • *Institute of Cytology, Russian Academy of Sciences, St. Petersburg, Russia; St. Petersburg State University, St. Petersburg, Russia*

Clara Correia-Melo • *Ageing Research Laboratories, Centre for Integrated Systems Biology of Ageing and Nutrition, Institute for Ageing and Health, Newcastle University, Newcastle upon Tyne, UK*

Zbigniew Darzynkiewicz • *Department of Pathology, Brander Cancer Research Institute, New York Medical College, Valhalla, NY, USA*

Sara K. Deibler • *Howard Hughes Medical Institute, Chevy Chase, MD, USA; Programs in Gene Function and Expression and Molecular Medicine, University of Massachusetts Medical School, Worcester, MA, USA*

Goberdhan P. Dimri • *Department of Biochemistry and Molecular Biology, The George Washington University Medical Center, Washington, DC, USA*

Sandra Donnini • *Department of Biotechnology, University of Siena, Siena, Italy*

Vjekoslav Dulic • *Institut de Génétique Moléculaire, Montpellier, France; CNRS, UMR5535, Montpellier, France; Université Montpellier 1, Montpellier, France*

José Maria Pérez Freije • *Departamento de Bioquímica y Biología Molecular, Instituto Universitario de Oncología, Universidad de Oviedo, Oviedo, Spain*

Silke Fuchs • *Cell and Molecular Biology, Department of Life Sciences, Imperial College, London, UK*

Lorenzo Galluzzi • *Institut Gustave Roussy, Villejuif, France; Université Paris Descartes, Sorbonne Paris Cité, Paris, France*
Ana Cipak Gasparovic • *Rudjer Boskovic Institute, Zagreb, Croatia*
Florian M. Geier • *Biomolecular Medicine, Department of Surgery and Cancer, Imperial College, London, UK*
Antonio Giachetti • *Department of Biotechnology, University of Siena, Siena, Italy*
Jesús Gil • *Cell Proliferation Group, MRC Clinical Sciences Centre, Imperial College, London, UK*
Stavros Gonidakis • *Department of Biological Sciences, Ethel Percy Andrus Gerontology Center, University of Southern California, Los Angeles, CA, USA*
Michael R. Green • *Howard Hughes Medical Institute, Chevy Chase, MD, USA; Programs in Gene Function and Expression and Molecular Medicine, University of Massachusetts Medical School, Worcester, MA, USA*
Andrea Hamann • *Faculty of Biosciences, Institute of Molecular Biosciences, Johann Wolfgang Goethe University Frankfurt, Frankfurt, Germany; Frankfurt Cluster of Excellence "Macromolecular Complexes", Frankfurt, Germany*
Jia Hu • *Ethel Percy Andrus Gerontology Center, Davis School of Gerontology, University of Southern California, Los Angeles, CA, USA*
Koji Itahana • *Duke-NUS Graduate Medical School Singapore, Singapore, Singapore*
Yoko Itahana • *Duke-NUS Graduate Medical School Singapore, Singapore, Singapore*
Morana Jaganjac • *Rudjer Boskovic Institute, Zagreb, Croatia*
Mohamed Jemàa • *INSERM, U848, Villejuif, France; Institut Gustave Roussy, Villejuif, France*
Diana Jurk • *Ageing Research Laboratories, Centre for Integrated Systems Biology of Ageing and Nutrition, Institute for Ageing and Health, Newcastle University, Newcastle upon Tyne, UK*
Oliver Kepp • *INSERM, U848, Villejuif, France; Institut Gustave Roussy, Villejuif, France*
José Eduardo Krieger • *Laboratory of Genetics and Molecular Cardiology/LIM 13, Heart Institute (InCor), University of Sao Paulo Medical School, Sao Paulo, Brazil*
Guido Kroemer • *Centre de Recherche des Cordeliers, Paris, France; INSERM, U848, Villejuif, France; Metabolomics Platform, Institut Gustave Roussy, Villejuif, France; Pôle de Biologie, Hôpital Européen Georges Pompidou, AP-HP, Paris, France; Université Paris Descartes, Sorbonne Paris Cité, Paris, France*
Armand M. Leroi • *Ecology and Evolution, Department of Life Sciences, Imperial College, London, UK*
Rodney L. Levine • *Laboratory of Biochemistry, National Heart, Lung, and Blood Institute, NIH, Bethesda, MD, USA*
Eirini Lionaki • *Institute of Molecular Biology and Biotechnology, Foundation for Research and Technology, Heraklion, Greece*
Valter D. Longo • *Davis School of Gerontology, Ethel Percy Andrus Gerontology Center, University of Southern California, Los Angeles, CA, USA*
Carlos López-Otín • *Departamento de Bioquímica y Biología Molecular, Instituto Universitario de Oncología, Universidad de Oviedo, Oviedo, Spain*
Isabelle Martins • *INSERM, U848, Villejuif, France; Institut Gustave Roussy, Villejuif, France*
Karen L. MacKenzie • *Cancer Cell Development Group, Children's Cancer Institute Australia, Randwick, Australia; Lowy Cancer Research Centre, University of New South Wales, Randwick, Australia*

Michelle F. Maritz • *Cancer Cell Development Group, Children's Cancer Institute Australia, Randwick, Australia; Lowy Cancer Research Centre, University of New South Wales, Randwick, Australia*
John J. McGarvey • *School of Chemistry and Chemical Engineering, Queen's University, Belfast, UK*
Laurie Menger • *INSERM, U848, Villejuif, France; Institut Gustave Roussy, Villejuif, France*
Didier Metivier • *INSERM, U848, Villejuif, France; Institut Gustave Roussy, Villejuif, France*
Mickaël Michaud • *INSERM, U848, Villejuif, France; Institut Gustave Roussy, Villejuif, France*
Branka Mihaljevic • *Rudjer Boskovic Institute, Zagreb, Croatia*
Mario G. Mirisola • *Department of Medical and Forensic Biopathology e Biotechnology, University of Palermo, Palermo, Italy*
Satomi Miwa • *Ageing Research Laboratories, Centre for Integrated Systems Biology of Ageing and Nutrition, Institute for Ageing and Health, Newcastle University, Newcastle upon Tyne, UK*
Ayumi Aurea Miyakawa • *Laboratory of Genetics and Molecular Cardiology/LIM 13, Heart Institute (InCor), University of Sao Paulo Medical School, Sao Paulo, Brazil*
Asako J. Nakamura • *Department of Anatomy and Cell Biology, Osaka Medical College, Takatsuki, Japan*
Masako Narita • *Cancer Research UK, Cambridge Research Institute, Cambridge, UK*
Masashi Narita • *Cancer Research UK, Cambridge Research Institute, Cambridge, UK*
Glyn Nelson • *Ageing Research Laboratories, Centre for Integrated Systems Biology of Ageing and Nutrition, Institute for Ageing and Health, Newcastle University, Newcastle upon Tyne, UK*
Heinz D. Osiewacz • *Faculty of Biosciences, Institute of Molecular Biosciences, Johann Wolfgang Goethe University Frankfurt, Frankfurt, Germany; Frankfurt Cluster of Excellence "Macromolecular Complexes", Frankfurt, Germany*
Fernando G. Osorio • *Departamento de Bioquímica y Biología Molecular, Instituto Universitario de Oncología, Universidad de Oviedo, Oviedo, Spain*
Giovambattista Pani • *Institute of General Pathology, Catholic University Medical School, Rome, Italy*
João F. Passos • *Ageing Research Laboratories, Centre for Integrated Systems Biology of Ageing and Nutrition, Institute for Ageing and Health, Newcastle University, Newcastle upon Tyne, UK*
Valery A. Pospelov • *Institute of Cytology, Russian Academy of Sciences, St. Petersburg, Russia; St. Petersburg State University, St. Petersburg, Russia*
Tatiana V. Pospelova • *Institute of Cytology, Russian Academy of Sciences, St. Petersburg, Russia; St. Petersburg State University, St. Petersburg, Russia*
Yingjuan Qian • *Comparative Oncology Laboratory, University of California, Davis, CA, USA*
Sofia Chiatamone Ranieri • *Clinical Chemistry, Laboratory and Endocrinology Unit, Departement of Laboratory Medicine, Azienda Ospedaliera ASMN, Istituto di Ricovero e Cura a Carattere Scientifico, Reggio Emilia, Italy*
Laura A. Richards • *Cancer Cell Development Group, Children's Cancer Institute Australia, Randwick, Australia; Lowy Cancer Research Centre, University of New South Wales, Randwick, Australia*

Helen Rizos • *Melanoma Institute Australia, North Sydney, Australia University of Sydney, Sydney, Australia; Westmead Institute for Cancer Research, Westmead Millennium Institute for Medical Research, Westmead, Australia*
Francis Rodier • *Institut du cancer de Montréal, Centre de recherche du CHUM, Montréal, Canada*
Ambrosius P. Snijders • *Biomolecular Mass Spectrometry and Proteomics Laboratory, MRC Clinical Sciences Centre, Imperial College, London, UK*
Alan W. Stitt • *Centre for Vision and Vascular Science, School of Medicine and Dentistry, Queen's University, Belfast, UK*
Abdul Qader Sukkurwala • *INSERM, U848, Villejuif, France; Institut Gustave Roussy, Villejuif, France*
Suzana Borovic Sunjic • *Rudjer Boskovic Institute, Zagreb, Croatia*
Simon Tavaré • *Molecular and Computational Biology Program, Department of Biological Sciences, University of Southern California, Los Angeles, CA, USA; Department of Oncology, University of Cambridge, Cambridge, UK; Cancer Research UK, Cambridge Research Institute, Cambridge, UK*
Nektarios Tavernarakis • *Institute of Molecular Biology and Biotechnology, Foundation for Research and Technology, Heraklion, Greece*
John Tower • *Molecular and Computational Biology Program, Department of Biological Sciences, University of Southern California, Los Angeles, CA, USA*
Sieu L. Tran • *Melanoma Institute Australia, North Sydney, Australia; University of Sydney, Sydney, Australia; Westmead Institute for Cancer Research, Westmead Millennium Institute for Medical Research, Westmead, Australia*
Gabriel Valbuena • *Biomolecular Medicine, Department of Surgery and Cancer, Imperial College, London, UK*
Ilio Vitale • *INSERM, U848, Villejuif, France; Institut Gustave Roussy, Villejuif, France*
Thomas von Zglinicki • *Ageing Research Laboratories, Centre for Integrated Systems Biology of Ageing and Nutrition, Institute for Ageing and Health, Newcastle University, Newcastle upon Tyne, UK*
Narendra Wajapeyee • *Department of Pathology, Yale University School of Medicine, New Haven, CT, USA*
Yu Wang • *Department of Pharmacology and Pharmacy, Li Ka Shing Faculty of Medicine, University of Hong Kong, Hong Kong, China*
Nancy B. Wehr • *Laboratory of Biochemistry, National Heart, Lung, and Blood Institute, NIH, Bethesda, MD, USA*
Min Wei • *Davis School of Gerontology, Ethel Percy Andrus Gerontology Center, University of Southern California, Los Angeles, CA, USA*
Andrew R.J. Young • *Cancer Research UK, Cambridge Research Institute, Cambridge, UK*
Neven Zarkovic • *Rudjer Boskovic Institute, Zagreb, Croatia*
Rugang Zhang • *Women's Cancer Program, Epigenetics and Progenitor Cells Keystone Program, Fox Chase Cancer Center, Philadelphia, PA, USA*
Hong Zhao • *Department of Pathology, Brander Cancer Research Institute, New York Medical College, Valhalla, NY, USA*
Marina Ziche • *Department of Biotechnology, University of Siena, Siena, Italy*
Sandra Zintel • *Faculty of Biosciences, Institute of Molecular Biosciences, Johann Wolfgang Goethe University Frankfurt, Frankfurt, Germany; Frankfurt Cluster of Excellence "Macromolecular Complexes", Frankfurt, Germany*

Chapter 1

Cell Senescence as Both a Dynamic and a Static Phenotype

Andrew R.J. Young, Masako Narita, and Masashi Narita

Abstract

It has been 50 years since cellular senescence was first described in human diploid fibroblasts (HDFs), yet its mechanism as well as its physiological and clinical implications are still not fully appreciated. Recent progress suggests that cellular senescence is a collective phenotype, composed of complex networks of effector programs. The balance and quality within the effector network varies depending on the cell type, the nature of the stress as well as the context. Therefore, understanding each of these effectors in the context of the whole network will be necessary in order to fully understand senescence as a whole. Furthermore, searching for new effector programs of senescence will help to define this heterogeneous and complex phenotype according to cellular contexts.

Key words: Autophagy, mTOR, Oncogene, SAHFs, SASP, Senescence, SMS, TASCC

1. Introduction

Cellular senescence is, fundamentally, a stress responsive cell cycle arrest. The senescence phenotype is extremely stable, and thus, senescence is often described as a state of "irreversible" or "permanent" cell cycle arrest, as opposed to the readily reversible quiescent state. The senescence phenotype was originally identified in genetically normal, primary, human diploid fibroblasts (HDFs), which "refused" to proliferate indefinitely in culture (1). At that time this behavior was attributed to the culture medium lacking some essential nutrients (2), but it has since been formally attributed to the limits imposed by telomeres (3). When HDFs become senescent, in addition to their stable cell cycle exit, their morphology drastically changes. Typically the cells have enlarged cell and nuclear bodies, prominent nucleoli, and numerous cytoplasmic vacuoles.

Lorenzo Galluzzi et al. (eds.), *Cell Senescence: Methods and Protocols*, Methods in Molecular Biology, vol. 965,
DOI 10.1007/978-1-62703-239-1_1,

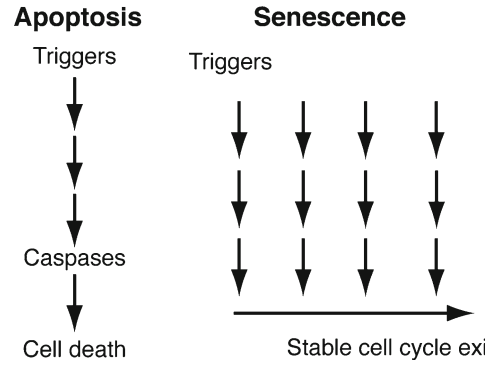

Fig. 1. The juxtaposition of senescence and apoptosis. The contrast between these two stress responsive phenotypes may be due to the way the signals are conveyed. In apoptosis, a variety of triggers can converge to the executioner caspases through a common mechanism. In contrast, in senescence, a number of effector mechanisms, which can each contribute to the process, have been proposed and it is likely that these effectors collectively define the phenotype, and also that the eventual phenotype maybe different depending on the signals and effectors that induced it. In addition, senescence is typically a delayed and progressive process. Thus, as schematically illustrated here, the senescence process can be viewed as a "matrix" composed of a series of signal transductions, rather than the signal "vectors" of apoptosis.

While it is widely accepted that both the p53 and p16/Rb tumor suppressor pathways are involved in senescence, the precise mechanisms underlying the phenotype are still elusive. Cells respond to cytotoxic stimuli differently depending upon the cell type and the strength of the stress. HDFs are relatively resistant to apoptosis, and are highly prone to senescence. Compared to apoptosis, senescence is a delayed and much longer process. The contrast in these two stress responsive phenotypes may be due to the way the signals are conveyed. In apoptosis, a variety of triggers can converge to the executioner caspases through a common mechanism (4). In contrast, in senescence a number of effector mechanisms, each contributing to the process, have been proposed and it is likely that these effectors collectively define the phenotype. Thus, the senescence process can be viewed as a "matrix" composed of a series of signaling transductions, rather than the single "vector" of signals in apoptosis (Fig. 1). Such effector programs of senescence include senescence associated heterochromatic foci (SAHFs) and epigenetic gene regulation, the DNA damage response, senescence associated secretory phenotype (SASP)/Senescence-messaging secretome (SMS), and macroautophagy (5–16). Due to the highly heterogeneous nature of the senescence phenotype, it has not been possible to identify a universal marker for senescence that applies in all cases. However, the use of a combination of various markers often associated with effector programs of senescence has successfully contributed to extending the concept of senescence outside the HDF system: a similar phenotype can be induced by various

cellular stresses in different types of somatic cells, as well as different tissues in animals (17–20). Importantly, the effector mechanisms and markers used in these studies were mostly identified in experiments using HDFs, and thus, HDFs are still the best-characterized model system for this topic. Therefore, in this review, most descriptions are derived from this system unless specifically mentioned otherwise. We also use the term "senescence" to specifically describe the cellular phenotype, distinct from "aging" at the organism level.

The complexity of senescence also implies a "time axis," by which senescence can be understood as a delayed and progressive process. Therefore, it would be sensible to view senescence not only as a static endpoint, but also as a dynamic process of phenotypic establishment (Fig. 1). This distinction becomes more relevant in acute types of senescence, such as oncogene-induced senescence (OIS). Here, we overview the static and dynamic aspects of senescence and discuss our current understanding of the complex interactions between the effector programs during senescence, with a particular focus on the regulation of gene expression.

2. Oncogenic, Ras-Induced Senescence

It was shown in 1997 that oncogenic Ras could induce premature senescence, in both HDFs and mouse embryonic fibroblasts (MEFs) (21). As the paradoxical name suggests, the Ras-induced senescence (RIS) phenotype is nonlinear. Due to the direct impact of the abnormal mitogenic stimuli, the cells initially proliferate more rapidly (22). This mitotic phenotype is then gradually replaced by the senescence phenotype. Interestingly, the in vivo counterpart of OIS is well represented by some pre-neoplastic or benign tumors, such as melanocytic nevi, lung adenomas, and pancreatic intraductal neoplasias, and chemically induced skin papillomas (23–28) (see ref. 20). These tumors are likely to be a consequence of cell proliferation during this mitotic phase. Thus, OIS/RIS may be a model for the initial steps of tumorigenesis, which include the series of events from the first reaction of the cells to the mitotic stress, following activation of various effector programs, and the maintenance of the phenotype. Importantly, each effector program is typically involved not only in senescence but also in its original, physiological, role outside of senescence. Thus, studying the OIS/RIS system should extend our understanding of each of these effector programs and provide insight into the more general concepts in dynamic alterations of phenotype, such as differentiation and transformation.

3. Transcriptional Regulation During Senescence

The strong stability of the phenotype, compared to the readily reversible G0 arrest of quiescence, is a critical aspect of senescence, implying its biological relevance in, for instance, tumor suppression and therapy (29, 30), aging (31), and the efficiency of reprogramming to pluripotent stem cells (32–37). Not surprisingly, one focus of the earlier studies on senescence was on the irreversibility of the cell cycle exit. For example, the Campisi group showed that the refractoriness of cells to mitogens is a hallmark of senescence, and that some growth-related genes are not responsive to growth factors (38, 39). The same group later examined the reversibility of senescence caused by telomere dysfunction using different types of HDFs, with varying levels of the CDK inhibitor p16. They found that the replicative senescence arrest could be reversed by p53 depletion in p16-low cells (such as BJ cells), whereas in p16-high cells (such as WI38 cells) senescence could not be so easily reversed (40). Thus, while p53 contributes to continuous cell cycle arrest signaling, the p16/Rb pathway provides a dominant barrier to the immortalization of human cells. A primary role for the p53 pathway has also been shown in OIS, where it is activated by a persistent DNA damage response (41). These data also reinforce the classical view that, in human cells, it is required to abrogate both the p53 and p16/Rb pathways in order to bypass senescence, and that most cancers do indeed have defects in both pathways.

We and others have previously shown that HDFs exhibit dramatic alterations in heterochromatin during senescence (SAHF) in a p16/Rb dependent manner, and have proposed that SAHF formation is involved in the stable silencing of at least some cell cycle genes (42, 43). Interestingly, senescent HDFs with high p16 (nonreversible by p53 depletion) show more prominent SAHFs compared to p16-low HDFs (reversible by p53 depletion), indicating a correlation between SAHF formation and the stability of senescence arrest (5). Furthermore, we have identified chromatin architectural proteins, HMGA1 and HMGA2, as SAHF components. SAHF disruption by HMGA1 depletion made cellular senescence bypass easier, reinforcing the correlation between phenotype stability and high-order chromatin architecture (44). However, both heterochromatin structure and the related epigenetic marks can also be dynamic. Thus, it is conceivable that cells need to have additional mechanisms to achieve the ultimate irreversibility of senescence.

The precise relationship between high-order SAHF structure and individual gene regulation is still unclear. To investigate this connection it would be necessary to effectively combine both imaging and biochemical data for SAHF markers, which to date has not been managed. It is tempting, however, to speculate that such a clear segregation between euchromatin and heterochromatin in

the static condition might allow a rather fixed gene expression profile, giving up dynamic and complex gene expression regulation. In this sense, SAHFs may be important not only for gene repression as originally proposed, but may also play a role in the stable maintenance of gene activation in the euchromatic regions. This interpretation would extend our understanding of SAHFs beyond senescence, and rather put the concept of SAHFs in the context of gene plasticity that is associated with distinct cellular phenotypes.

Conceivably, senescent cells may exhibit a distinct mRNA expression profile compared to their growing or quiescent counterparts (45). A flurry of papers in the late 2000s defined the functionality of the plethora of factors secreted by senescent cells. This heterogenous collection of cytokines, chemokines and other factors, termed the SASP or SMS has been shown to have autocrine and paracrine functions (10–13, 45, 46)—the autocrine function being to reinforce the senescence phenotype in the cell of origin and one potential paracrine function being to induce senescence in other cells sharing the same DNA damaging/tumorigenic microenvironment. Another paracrine function may be the non-serendipitous promotion of the transformation of premalignant—but not of normal—cells within the microenvironment (47, 48).

Among the series of papers describing the functional significance of SASP/SMS, the Peeper group notably identified SASP/SMS as a "secretome" specifically associated with OIS (10). Microarray experiments showed a set of transcripts highly upregulated in OIS cells, which were upregulated neither in cells that had bypassed OIS nor in quiescent cells (10). Thus, it is tempting to speculate that the "open" areas of chromatin generated by SAHF formation may permit and promote the expression of the secretome as a unit. Interestingly, SASP/SMS can also influence SAHF, in that depletion of IL-6 (a central component of SASP/SMS) in OIS correlated with reduced formation of SAHF as well as p15, a senescence-related CDK inhibitor (CDKI) (10). It has been shown that over-expression of p16, another CDKI, which is sufficient to induce senescence and SAHFs in HDFs, fails to trigger SASP/SMS, indicating that SAHF formation per se cannot activate the secretome (49). However, in our time series microarray experiments in RIS HDFs, upregulation of SASP/SMS components starts during the transition phase of RIS, when SAHF formation is not yet fully established (15). Thus, the two processes may mutually reinforce each other during the course of OIS establishment: SASP/SMS facilitating SAHF formation (possibly in part through p15 upregulation), while high-order chromatin reorganization might reinforce the stable expression of SASP/SMS components in the late stages of RIS.

Thus, it is useful to think of OIS as a whole process, not just a static phenotype, and, along those lines, we recently identified another effector mechanism that affects SASP/SMS during the

RIS-transition, namely macroautophagy (referred to hereafter as autophagy). As well as transcriptional effects, SASP/SMS is also facilitated at the posttranscription level.

4. Autophagy and SASP/SMS in Senescence

To study the process and the dynamic features of the senescence phenotype, 4OHT-inducible RIS is very useful. In the 4OHT RIS system in HDFs, it typically takes around 7 days to establish the senescence phenotype (Fig. 2) (15). In this system, much of the dynamic transcriptional alteration occurs during the RIS transition (15). However, if rapid protein turnover were to happen at the same time it would make achieving gene expression changes far more efficient, and perhaps allow emergent cell remodeling. Consistent with this idea, autophagy is highly active during the RIS transition (15).

Autophagy is, essentially, the "trash collector" of the cell, or rather the "recycling collection truck." Eukaryotic cells have two main known mechanisms for protein degradation: the proteasome and autophagy. The proteasome takes only one protein at a time and targets are signaled for selection, whereas autophagy can collect cellular components *en masse* (although, degrees of specificity are emerging for autophagy too (50)). In autophagy, vesicles form within the cytoplasm and can be seen to have enclosed cytoplasmic content. That cytoplasmic content is then trafficked along microtubules to the lysosome. Lysosomes contain the degradative enzymes of the cell: lipases, proteases, DNase, etc. (51). Autophagosomes then fuse with lysosomes, the product of which is termed an autolysosome, and pass their content inside for degradation and recycling. That content is then actively released from the lysosome (52), and thus, presumably a gradient of metabolites emanates from the lysosome.

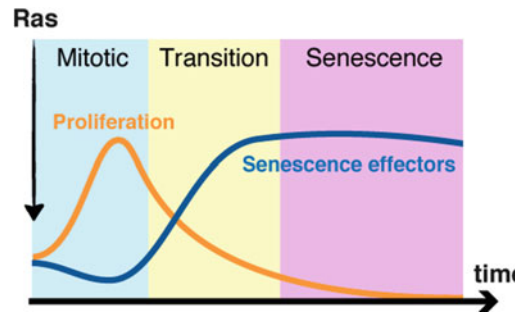

Fig. 2. A schematic view of oncogenic Ras-induced senescence (RIS) in human diploid fibroblasts (HDFs). RIS can be acutely induced by adding 4OHT to HDFs stably expressing ER:Ras, mediated by retrovirus-mediated gene transfer. The whole process is typically completed in ~7 days.

The emerging dogma is thus that autophagy represents the "guardian" of the proteome (53), which could be broadened out to the macromolecule-ome. As macromolecules become damaged, for instance through oxidation, they become misfunctional. Hence constant degradation and resynthesis of macromolecules is required, and is especially required in dire times of cellular stress, such as oxidative or metabolic stress. In addition to that role, however, we have shown that autophagy can have quite unforeseen consequences for the cell, impacting on cell fate, in that it can facilitate the establishment of senescence both cell autonomously and non-cell-autonomously through its role in the production of SASP/SMS in RIS, and beyond.

4.1. Autophagy in RIS

As mentioned in the introduction, the characteristics of senescent cells are that they typically have enlarged cell and nuclear bodies, prominent nucleoli, as well as numerous cytoplasmic vacuoles. Part of this vacuolation may come from enlargement of the ER (54) but a good part comes from the accumulation of autolysosomes (15). Upon the induction of Ras, the HDFs at first proliferate more often, or in other words they go through a "proliferative burst," and then gradually proliferation declines as they approach the "permanent" proliferative arrested state of senescence. It is during the transition phase (from this proliferative phase to the senescent, proliferative arrest) that autophagy becomes active. Inhibition of autophagy causes the downregulation of SASP/SMS, such as IL6 and IL8, at the posttranscriptional level. Presumably autophagy plays a role in delivering the "raw material," the proteins for degradation, for their reuse in the synthesis of these SASP/SMS factors, thus supporting the translation of the upregulated SASP/SMS transcripts.

A similar positive role for autophagy in senescence associated secretory protein synthesis has recently been observed in senescent HDFs induced by oxidative stress (55). The authors showed that H_2O_2 induced senescence with activated autophagy, and that the inhibition of autophagy not only delayed senescence but also reduced the secretory phenotype. Furthermore, autophagy seems to affect SASP/SMS outside fibroblasts. Sasaki et al. (56) showed that autophagy can mediate cellular senescence in primary biliary cirrhosis (PBC). PBC is a liver-specific autoimmune disease that eventually leads to the extensive loss of small bile ducts. The authors had previously demonstrated cellular senescence in the damaged small bile ducts and suggested that it may be involved in the pathogenesis of progressive bile duct loss in PBC (57). They went on to look for autophagy in their bank of biopsied or surgically resected human liver specimens. Immunohistochemistry staining for autophagy and lysosomal markers showed large vesicles in PBC, chronic viral hepatitis, nonalcoholic steatohepatitis and extrahepatic biliary obstruction. By far the highest level of these vesicles

was seen in PBC. The autophagy positive small bile ducts also stained for markers of senescence. Moving into cultured biliary epithelial cells (BECs), Sasaki et al. showed that if autophagy was pharmacologically inhibited then the extent of senescence was significantly decreased, as was the BEC SASP/SMS.

These studies support the idea that active protein turnover can promote the *en masse* production of secretory proteins during senescence. However, it is also possible that autophagy modulates the senescence phenotype through its ability to maintain the quality of macromolecules. Gamerdinger et al. identified activated autophagy during replicative senescence in HDFs as well as in the neurons of aged rodent brains (14, 58). The authors showed that BAG3, a co-chaperone, together with other chaperons, Hsp70 and HspB8, promoted the targeting of misfolded and aggregation prone proteins to autophagosomes. Thus, damaged proteins accumulated during senescence or aging can be eliminated by autophagy. Of note, replicative senescence is also associated with activation of a secretome (49), although how autophagy affects SASP/SMS in the context of replicative senescence remains to be tested. Therefore, autophagy would seem to have, at least, two distinct levels of influence on senescence; through its specific role in SASP/SMS and also through its general activity in the quality control of macromolecules. How can we reconcile these roles, or does this suggest another controversy, as in the association between autophagy and cell death: do cells become senescent due to autophagy or despite autophagy? The potentially mixed roles for autophagy in senescence might reflect the complex effector networks of senescence mentioned above (Fig. 1). The collective outcome of the combinatorial consequences of those effector programs would shift within the range of the senescence phenotype depending on the situation. Therefore, the dominant effect of autophagy might be different between RIS (a highly dynamic process) and replicative senescence (a slow and adaptive process). Consistent with this idea, we have recently identified an additional mechanism occurring during RIS by which autophagy can support SASP/SMS, which involves a TOR-autophagy spatial coupling compartment (TASCC) (15).

TASCC—more defined mechanistic insight into the relationship between autophagy and senescence. Autophagy and protein synthesis are typically regulated in opposite directions. For example, when cells are starved, autophagy is activated while protein synthesis is suppressed, allowing the degradation products (such as amino acids) to be used as an alternative energy source. This reciprocal regulation of anabolic and catabolic processes is achieved through target of rapamycin (TOR), the master regulator of protein synthesis (59). TOR coordinately senses cellular nutrient and energy status as well as growth factor signals. TOR then integrates those signals and "decides" whether sufficient metabolites and energy are available to synthesize protein (60). TOR is a protein kinase

and, if conditions are right, it in turn phosphorylates its substrates, such as eIF4E binding protein (4EBP) and S6 kinase (S6K), and facilitates protein synthesis (59).

However, it is possible that the simultaneous activation of protein degradation and synthesis may allow cells to "regenerate" themselves very efficiently, and this seems to be occurring during RIS, where both autophagy and protein synthesis are active (15). In addition, it has also been shown that Rapamycin, which inhibits TOR, can divert senescence into quiescence; thus, mTOR is required for senescence maintenance (61). One potential explanation for the apparently paradoxical simultaneous activation of protein degradation and protein synthesis may be the spatial separation of these processes within the cell. By immunostaining, we identified a unique cellular compartment, the TASCC, in which both mammalian TOR (mTOR) and autolysosomes (the end stage of autophagy) are enriched in the vicinity of the rER-Golgi apparatus (GA). Aside from growth factor signaling, mTOR can also be activated by amino acids (the ultimate end product of autophagic protein degradation). The inhibitory point where mTOR acts on autophagy is the initial step of autophagosome formation; thus, it is possible that the physical coupling of these two opposing processes causes them to reinforce each other. Indeed, we have shown that amino acids derived from autolysosomes are required for mTOR localization to the TASCC, and that early stage autophagosomes are only detected outside of the TASCC. Our data is highly consistent with emerging evidence from the Sabatini group, indicating that mTOR is recruited to, and activated at, the lysosomal surface, where Rheb resides, and that this process is dependent on Rag GTPases, which also localize to lysosomes (62, 63).

Furthermore, the TASCC is consistently surrounded by the trans-side of the GA. The rER-GA is the place where both secretory proteins as well as lysosomal and other membrane components are synthesized and processed. Thus, the encompassing of the TASCC by the rER-GA raises an interesting possibility: that the TASCC, together with the associated rER-GA, may form a protein "factory" for both the SASP/SMS to be secreted, and lysosomal and other membrane proteins (which would, in turn, reinforce TASCC formation itself). This could be tested using the technique of fluorescent noncanonical amino acid tagging (FUNCAT) to specifically visualize newly synthesized proteins in situ (FUNCAT was developed by the Schuman laboratory (64–66), and is now licensed to Invitrogen). This system is essentially a more modern alternative to radioactive, e.g., ^{35}S, methionine metabolic labeling. Pulse–chase experiments with the "tagged" amino acid revealed that as early as 3 min the nascent proteins are enriched around the GA, and subsequently move to the GA, and about 2 h later are detected in the TASCC. In addition, by immunolabelling, IL6 and IL8 were specifically detected in the TASCC as well as the

surrounding GA, suggesting that the same compartment facilitates the synthesis of proteins for both the degradation machinery and for SASP/SMS. Consistently, inhibition of Rag GTPase activity during RIS blocked mTOR enrichment to the TASCC and reduced the synthesis of SASP/SMS components (15). Although direct evidence for the regulation of protein synthesis within the TASCC by mTOR remains to be shown, the TASCC demonstrates additional complexity in terms of its functional associations between SASP/SMS, senescence and autophagy.

Importantly, we also found that the TASCC was in close association with the GA in other cellular conditions, such as macrophage-like differentiation in culture, during which cells acutely produce abundant IL8 (15). In addition, TASCC-like compartments were detected specifically in the glomerular podocytes of mouse kidneys (15). Podocytes are highly enriched for constitutive autophagy as well as prominent GA, and produce abundant secretory proteins to support the constant turnover of the glomerular basement membrane (67, 68). The TASCC may thus be associated more generally with the acute, abundant production of secretory proteins, rather than senescence per se. Consistent with this interpretation, replicative senescent HDFs do not show a prominent TASCC (Masako Narita & Masashi Narita, unpublished data), suggesting that the rate or amount of synthesis of SASP/SMS components in this adaptive condition may not require such self-reinforcing machinery. Although the exact molecular basis for the necessity of the TASCC in facilitating the production of secretory proteins in some cases but not in others remains to be elucidated, the TASCC might provide a mechanism to modulate the downstream effects of activated autophagy.

5. Conclusions

Taken together, the studies outlined in this review reinforce the higher-order network of the different effector programs of senescence and its complexity, in which the same effector might even produce different outcomes through the different aspects—dynamic or static—of senescence. Furthermore when it is considered, as mentioned in Subheading 3, that SASP can affect SAHF, then the new role for autophagy in the regulation of SASP/SMS and its spatial association with mTOR implies a functional cooperation between nuclear (transcription) and cytoplasmic phenotypes (protein turnover) toward the expression of a subset of genes. While we only focus on the limited aspects of gene regulation in RIS in this review, there are other mechanisms that are also involved in the phenotype and we expect, in this model system, additional unexpected interactions between them, as well as new effector mechanisms to be identified in the future.

Acknowledgments

Our work is supported by Cancer Research UK.

References

1. Hayflick L (1961) The serial cultivation of human diploid cell strains. Exp Cell Res 25: 585–621
2. Shay JW, Wright WE (2000) Hayflick, his limit, and cellular ageing. Nat Rev Mol Cell Biol 1:72–76
3. Harley CB, Futcher AB, Greider CW (1990) Telomeres shorten during ageing of human fibroblasts. Nature 345:458–460
4. Strasser A, Cory S, Adams JM (2011) Deciphering the rules of programmed cell death to improve therapy of cancer and other diseases. EMBO J 30:3667–3683
5. Narita M, Nũnez S, Heard E, Narita M, Lin AW, Hearn SA, Spector DL, Hannon GJ, Lowe SW (2003) Rb-mediated heterochromatin formation and silencing of E2F target genes during cellular senescence. Cell 113:703–716
6. Zhang R, Poustovoitov MV, Ye X, Santos HA, Chen W, Daganzo SM, Erzberger JP, Serebriiskii IG, Canutescu AA, Dunbrack RL, Pehrson JR, Berger JM, Kaufman PD, Adams PD (2005) Formation of MacroH2A-containing senescence-associated heterochromatin foci and senescence driven by ASF1a and HIRA. Dev Cell 8:19–30
7. Di Micco R, Fumagalli M, Cicalese A, Piccinin S, Gasparini P, Luise C, Schurra C, Garre M, Giovanni Nuciforo P, Bensimon A, Maestro R, Giuseppe Pelicci P, D'adda Di Fagagna F (2006) Oncogene-induced senescence is a DNA damage response triggered by DNA hyper-replication. Nature 444:638–642
8. Bartkova J, Rezaei N, Liontos M, Karakaidos P, Kletsas D, Issaeva N, Vassiliou L-VF, Kolettas E, Niforou K, Zoumpourlis VC, Takaoka M, Nakagawa H, Tort F, Fugger K, Johansson F, Sehested M, Andersen CL, Dyrskjot L, Ørntoft T, Lukas J, Kittas C, Helleday T, Halazonetis TD, Bartek J, Gorgoulis VG (2006) Oncogene-induced senescence is part of the tumorigenesis barrier imposed by DNA damage checkpoints. Nature 444:633–637
9. Mallette FA, Gaumont-Leclerc M-F, Ferbeyre G (2007) The DNA damage signaling pathway is a critical mediator of oncogene-induced senescence. Genes Dev 21:43–48
10. Kuilman T, Michaloglou C, Vredeveld LCW, Douma S, van Doorn R, Desmet CJ, Aarden LA, Mooi WJ, Peeper DS (2008) Oncogene-induced senescence relayed by an interleukin-dependent inflammatory network. Cell 133:1019–1031
11. Acosta JC, O'Loghlen A, Banito A, Guijarro MV, Augert A, Raguz S, Fumagalli M, Da Costa M, Brown C, Popov N, Takatsu Y, Melamed J, D'adda Di Fagagna F, Bernard D, Hernando E, Gil J (2008) Chemokine signaling via the CXCR2 receptor reinforces senescence. Cell 133:1006–1018
12. Wajapeyee N, Serra RW, Zhu X, Mahalingam M, Green MR (2008) Oncogenic BRAF induces senescence and apoptosis through pathways mediated by the secreted protein IGFBP7. Cell 132:363–374
13. Coppé J-P, Patil CK, Rodier F, Sun Y, Muñoz DP, Goldstein J, Nelson PS, Desprez P-Y, Campisi J (2008) Senescence-associated secretory phenotypes reveal cell-nonautonomous functions of oncogenic RAS and the p53 tumor suppressor. PLoS Biol 6:2853–2868
14. Gamerdinger M, Hajieva P, Kaya AM, Wolfrum U, Hartl FU, Behl C (2009) Protein quality control during aging involves recruitment of the macroautophagy pathway by BAG3. EMBO J 28:889–901
15. Young ARJ, Narita M, Ferreira M, Kirschner K, Sadaie M, Darot JFJ, Tavaré S, Arakawa S, Shimizu S, Watt FM, Narita M (2009) Autophagy mediates the mitotic senescence transition. Genes Dev 23:798–803
16. Narita M, Young ARJ, Arakawa S, Samarajiwa SA, Nakashima T, Yoshida S, Hong S, Berry LS, Reichelt S, Ferreira M, Tavaré S, Inoki K, Shimizu S, Narita M (2011) Spatial coupling of mTOR and autophagy augments secretory phenotypes. Science 332(6032):966–970
17. Romanov SR, Kozakiewicz BK, Holst CR, Stampfer MR, Haupt LM, Tlsty TD (2001) Normal human mammary epithelial cells spontaneously escape senescence and acquire genomic changes. Nature 409:633–637
18. Lin AW, Lowe SW (2001) Oncogenic ras activates the ARF-p53 pathway to suppress epithelial cell transformation. Proc Natl Acad Sci U S A 98:5025–5030
19. Shay JW, Roninson IB (2004) Hallmarks of senescence in carcinogenesis and cancer therapy. Oncogene 23:2919–2933
20. Narita M, Lowe SW (2005) Senescence comes of age. Nat Med 11:920–922

21. Serrano M, Lin AW, McCurrach ME, Beach D, Lowe SW (1997) Oncogenic ras provokes premature cell senescence associated with accumulation of p53 and p16INK4a. Cell 88:593–602
22. Lin AW, Barradas M, Stone JC, Van Aelst L, Serrano M, Lowe SW (1998) Premature senescence involving p53 and p16 is activated in response to constitutive MEK/MAPK mitogenic signaling. Genes Dev 12:3008–3019
23. Lazzerini Denchi E, Attwooll C, Pasini D, Helin K (2005) Deregulated E2F activity induces hyperplasia and senescence-like features in the mouse pituitary gland. Mol Cell Biol 25:2660–2672
24. Braig M, Lee S, Loddenkemper C, Rudolph C, Peters AH, Schlegelberger B, Stein H, Dörken B, Jenuwein T, Schmitt CA (2005) Oncogene-induced senescence as an initial barrier in lymphoma development. Nature 436:660–665
25. Chen Z, Trotman LC, Shaffer D, Lin H-K, Dotan ZA, Niki M, Koutcher JA, Scher HI, Ludwig T, Gerald W, Cordon-Cardo C, Paolo Pandolfi P (2005) Crucial role of p53-dependent cellular senescence in suppression of Pten-deficient tumorigenesis. Nature 436:725–730
26. Collado M, Gil J, Efeyan A, Guerra C, Schuhmacher AJ, Barradas M, Benguría A, Zaballos A, Flores JM, Barbacid M, Beach D, Serrano M (2005) Tumour biology: senescence in premalignant tumours. Nature 436:642
27. Michaloglou C, Vredeveld LCW, Soengas MS, Denoyelle C, Kuilman T, Van Der Horst CMAM, Majoor DM, Shay JW, Mooi WJ, Peeper DS (2005) BRAFE600-associated senescence-like cell cycle arrest of human naevi. Nature 436:720–724
28. DeNicola GM, Karreth FA, Humpton TJ, Gopinathan A, Wei C, Frese K, Mangal D, Yu KH, Yeo CJ, Calhoun ES, Scrimieri F, Winter JM, Hruban RH, Iacobuzio-Donahue C, Kern SE, Blair IA, Tuveson DA (2011) Oncogene-induced Nrf2 transcription promotes ROS detoxification and tumorigenesis. Nature 475: 106–109
29. Schmitt CA, Fridman JS, Yang M, Lee S, Baranov E, Hoffman RM, Lowe SW (2002) A senescence program controlled by p53 and p16INK4a contributes to the outcome of cancer therapy. Cell 109:335–346
30. te Poele RH, Okorokov AL, Jardine L, Cummings J, Joel SP (2002) DNA damage is able to induce senescence in tumor cells in vitro and in vivo. Cancer Res 62:1876–1883
31. Sharpless NE, Depinho RA (2007) How stem cells age and why this makes us grow old. Nat Rev Mol Cell Biol 8:703–713
32. Hong H, Takahashi K, Ichisaka T, Aoi T, Kanagawa O, Nakagawa M, Okita K, Yamanaka S (2009) Suppression of induced pluripotent stem cell generation by the p53-p21 pathway. Nature 460:1132–1135
33. Kawamura T, Suzuki J, Wang YV, Menendez S, Morera LB, Raya A, Wahl GM, Belmonte JCI (2009) Linking the p53 tumour suppressor pathway to somatic cell reprogramming. Nature 460:1140–1144
34. Marión RM, Strati K, Li H, Murga M, Blanco R, Ortega S, Fernandez-Capetillo O, Serrano M, Blasco MA (2009) A p53-mediated DNA damage response limits reprogramming to ensure iPS cell genomic integrity. Nature 460: 1149–1153
35. Li H, Collado M, Villasante A, Strati K, Ortega S, Cañamero M, Blasco MA, Serrano M (2009) The Ink4/Arf locus is a barrier for iPS cell reprogramming. Nature 460:1136–1139
36. Krizhanovsky V, Lowe SW (2009) Stem cells: the promises and perils of p53. Nature 460:1085–1086
37. Banito A, Rashid ST, Acosta JC, Li S, Pereira CF, Geti I, Pinho S, Silva JC, Azuara V, Walsh M, Vallier L, Gil J (2009) Senescence impairs successful reprogramming to pluripotent stem cells. Genes Dev 23:2134–2139
38. Seshadri T, Campisi J (1989) Growth-factor-inducible gene expression in senescent human fibroblasts. Exp Gerontol 24:515–522
39. Seshadri T, Campisi J (1990) Repression of c-fos transcription and an altered genetic program in senescent human fibroblasts. Science 247:205–209
40. Beauséjour CM, Krtolica A, Galimi F, Narita M, Lowe SW, Yaswen P, Campisi J (2003) Reversal of human cellular senescence: roles of the p53 and p16 pathways. EMBO J 22: 4212–4222
41. D'adda Di Fagagna F (2008) Living on a break: cellular senescence as a DNA-damage response. Nat Rev Cancer 8:512–522
42. Narita M (2007) Cellular senescence and chromatin organisation. Br J Cancer 96:686–691
43. Adams PD (2007) Remodeling of chromatin structure in senescent cells and its potential impact on tumor suppression and aging. Gene 397:84–93
44. Narita M, Narita M, Krizhanovsky V, Nuñez S, Chicas A, Hearn SA, Myers MP, Lowe SW (2006) A novel role for high-mobility group a proteins in cellular senescence and heterochromatin formation. Cell 126:503–514
45. Shelton DN, Chang E, Whittier PS, Choi D, Funk WD (1999) Microarray analysis of replicative senescence. Curr Biol 9:939–945
46. Young ARJ, Narita M (2009) SASP reflects senescence. EMBO Rep 10:228–230

47. Krtolica A, Parrinello S, Lockett S, Desprez PY, Campisi J (2001) Senescent fibroblasts promote epithelial cell growth and tumorigenesis: a link between cancer and aging. Proc Natl Acad Sci U S A 98:12072–12077
48. Campisi J, D'adda Di Fagagna F (2007) Cellular senescence: when bad things happen to good cells. Nat Rev Mol Cell Biol 8:729–740
49. Rodier F, Coppé J-P, Patil CK, Hoeijmakers WAM, Muñoz DP, Raza SR, Freund A, Campeau E, Davalos AR, Campisi J (2009) Persistent DNA damage signalling triggers senescence-associated inflammatory cytokine secretion. Nature 11:973–979
50. Kraft C, Peter M, Hofmann K (2010) Selective autophagy: ubiquitin-mediated recognition and beyond. Nature 12:836–841
51. Holtzman E (1989) Lysosomes. Springer, New York, p 439
52. Mancini GM, Havelaar AC, Verheijen FW (2000) Lysosomal transport disorders. J Inherit Metab Dis 23:278–292
53. Ryan KM (2011) p53 and autophagy in cancer: guardian of the genome meets guardian of the proteome. Eur J Cancer 47:44–50
54. Denoyelle C, Abou-Rjaily G, Bezrookove V, Verhaegen M, Johnson TM, Fullen DR, Pointer JN, Gruber SB, Su LD, Nikiforov MA, Kaufman RJ, Bastian BC, Soengas MS (2006) Anti-oncogenic role of the endoplasmic reticulum differentially activated by mutations in the MAPK pathway. Nat Cell Biol 8:1053–1063
55. Luo Y, Zou P, Zou J, Wang J, Zhou D, Liu L (2011) Autophagy regulates ROS-induced cellular senescence via p21 in a p38 MAPKα dependent manner. Exp Gerontol 46:860–867
56. Sasaki M, Miyakoshi M, Sato Y, Nakanuma Y (2010) Autophagy mediates the process of cellular senescence characterizing bile duct damages in primary biliary cirrhosis. Lab Invest 90:835–843
57. Sasaki M, Ikeda H, Haga H, Manabe T, Nakanuma Y (2005) Frequent cellular senescence in small bile ducts in primary biliary cirrhosis: a possible role in bile duct loss. J Pathol 205:451–459
58. Gamerdinger M, Kaya AM, Wolfrum U, Clement AM, Behl C (2011) BAG3 mediates chaperone-based aggresome-targeting and selective autophagy of misfolded proteins. EMBO Rep 12:149–156
59. Wullschleger S, Loewith R, Hall MN (2006) TOR signaling in growth and metabolism. Cell 124:471–484
60. Sengupta S, Peterson TR, Sabatini DM (2010) Regulation of the mTOR complex 1 pathway by nutrients, growth factors, and stress. Mol Cell 40:310–322
61. Korotchkina LG, Leontieva OV, Bukreeva EI, Demidenko ZN, Gudkov AV, Blagosklonny MV (2010) The choice between p53-induced senescence and quiescence is determined in part by the mTOR pathway. Aging (Albany NY) 2:344–352
62. Sancak Y, Peterson TR, Shaul YD, Lindquist RA, Thoreen CC, Bar-Peled L, Sabatini DM (2008) The Rag GTPases bind raptor and mediate amino acid signaling to mTORC1. Science 320:1496–1501
63. Sancak Y, Bar-Peled L, Zoncu R, Markhard AL, Nada S, Sabatini DM (2010) Ragulator-Rag complex targets mTORC1 to the lysosomal surface and is necessary for its activation by amino acids. Cell 141:290–303
64. Dieterich DC, Link AJ, Graumann J, Tirrell DA, Schuman EM (2006) Selective identification of newly synthesized proteins in mammalian cells using bioorthogonal noncanonical amino acid tagging (BONCAT). Proc Natl Acad Sci U S A 103:9482–9487
65. Dieterich DC, Lee JJ, Link AJ, Graumann J, Tirrell DA, Schuman EM (2007) Labeling, detection and identification of newly synthesized proteomes with bioorthogonal non-canonical amino-acid tagging. Nat Protoc 2: 532–540
66. Dieterich DC, Hodas JJL, Gouzer G, Shadrin IY, Ngo JT, Triller A, Tirrell DA, Schuman EM (2010) In situ visualization and dynamics of newly synthesized proteins in rat hippocampal neurons. Nat Neurosci 13:897–905
67. Hartleben B, Gödel M, Meyer-Schwesinger C, Liu S, Ulrich T, Köbler S, Wiech T, Grahammer F, Arnold SJ, Lindenmeyer MT, Cohen CD, Pavenstädt H, Kerjaschki D, Mizushima N, Shaw AS, Walz G, Huber TB (2010) Autophagy influences glomerular disease susceptibility and maintains podocyte homeostasis in aging mice. J Clin Invest 120:1084–1096
68. Pavenstädt H, Kriz W, Kretzler M (2003) Cell biology of the glomerular podocyte. Physiol Rev 83:253–307

Chapter 2

Senescence Regulation by mTOR

Vjekoslav Dulic

Abstract

The senescence program is activated in response to diverse stress stimuli potentially compromising genetic stability and leads to an irreversible cell cycle arrest. The mTOR pathway plays a crucial role in the regulation of cell metabolism and cellular growth. The goal of this chapter is to present evidence linking these two processes, which have one common regulator—the tumor suppressor p53. While the role of mTOR in senescence is still controversial, recent papers have shed new light onto this issue. This review, far from being exhaustive given the complexity of the field, will hopefully stimulate further research in this domain, whose relevance for ageing is becoming increasingly documented.

Key words: AKT, CDK, CKI, Cell cycle exit, D-type cyclins, mTOR, pRB, Quiescence, Senescence

Abbreviations

ARF	Alternative reading frame
ATM	Ataxia telangiectasia mutated
ATR	ATM and Rad3-related kinase
Bmi1	B lymphoma Mo-MLV insertion region 1
Cdc25	Cell division cycle 25 (CDK-activating phosphatase)
CDK	Cyclin-dependent kinase
Chk1/2	Checkpoint kinase 1/2
CKI	CDK inhibitor
ERK1/2	Extracellular regulated kinase (also called MAPK)
FOXO	Forkhead box protein O
FKBP12	Peptidyl-prolyl *cis/trans* isomerase that forms a complex with rapamycin
HES1	Hairy enhancer of Split1
IGF	Insulin-like growth factors
IRS	Insulin receptor substrate
INK4A	Inhibitor of Cdk4 A
MAPK	Mitogen-activated protein kinase
mTOR	Mechanistic (mammalian) target of rapamycin
TORC1/2	TOR complex 1 and 2
PcG	Polycomb group

Lorenzo Galluzzi et al. (eds.), *Cell Senescence: Methods and Protocols*, Methods in Molecular Biology, vol. 965,
DOI 10.1007/978-1-62703-239-1_2,

PDK1	3-Phosphoinositide-dependent kinase 1
PI3K	Phosphoinositide 3-kinase
PIKK	Phosphoinositide 3-kinase (PI3K)-related protein serine/threonine kinase family
PML	Promyelocytic leukemia protein
PTEN	Phosphatase and tensin homologue
pRb	Retinoblastoma protein
RHEB	Ras homologue enriched in brain
SAHF	Senescence-associated heterochromatin foci
SASP	Senescence-associated secretory phenotype
SGK	Serum- and glucocorticoid-regulated kinase
TSC1/2	Tuberous sclerosis 1,2 GTPase
TGFβ	Transforming growth factor β

1. Introduction

Cellular senescence was originally described by Leonard Hayflick, who showed that, after a finite number of population doublings (mitotic clock), primary human cells irreversibly cease to proliferate in vitro (1). This so-called Hayflick limit was later shown to be provoked, at least in part, by telomere erosion (2), the gradual loss of DNA at the ends of chromosomes, a consequence of the "replication problem" predicted by Olovnikov in the early 1970—hence "replicative senescence" (3). It has been therefore proposed that telomere erosion could activate a DNA damage response (DDR) and cause G1 cell cycle arrest similar to the one elicited by ionizing radiation (4). Moreover, following an excellent intuition, Hayflick associated cellular senescence with both cancer and ageing—with cancer, because cells must acquire certain characteristics of tumor cells to escape senescence, and with ageing, because accumulation of senescent cells could contribute to the global deterioration of an organism. We now know that these original hypotheses were fundamentally right, and since then, senescence, from a "tissue culture artifact," became an ever-expanding field of intense research largely due to its tumor suppression potential and contribution to age-related pathologies. In addition to telomere dysfunction, senescence can be induced by a large variety of stress stimuli, including strong mitogenic signals generated by hyperactivation of certain oncogenes (Ras, Raf, Myc), irreparable DNA damage, or oxidative stress. This invariably inhibits cyclin-dependent kinases (CDK), key cell division regulators, leading to the cell cycle arrest that requires activities of two major tumor suppressors, p53 and pRb (Fig. 1).

As a number of excellent recent reviews extensively covered this topic (5–7), we shall here briefly outline the aspects of cellular senescence and the pathways implicated in its implementation that are relevant for this chapter.

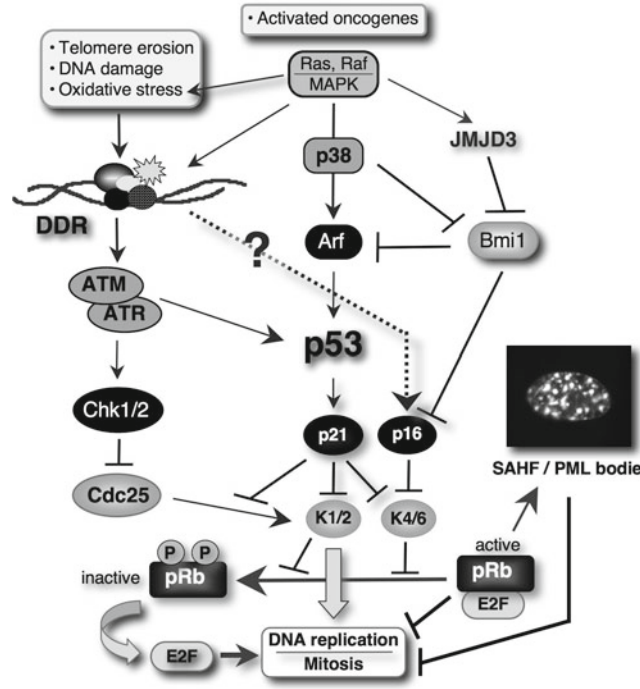

Fig. 1. Molecular pathways leading to senescence-associated irreversible cell cycle arrest. Pro-senescence stimuli activate DNA damage response pathway (DDR) leading to permanent inactivation of cyclin-dependent kinases (CDK) that control DNA replication and mitosis (K1/2). In addition, together with Cdk4/6 (K4/6), they keep inactive tumor suppressor pRb (and related pocket proteins p107 and p130). Genotoxic stress and activated oncogenes induce expression of CDK inhibitors $p21^{Waf1/Cip1}$ (p21) and $p16^{Ink4A}$ (p16) that block cell cycle progression and pRb inactivation. Active pRb blocks expression of genes controlling cell cycle (in part by sequestering E2F family of transcription factors) and contributes to chromatin reorganization in the form of SAHF or PML nuclear bodies. The pathways leading to induction of p16 are not entirely elucidated but, in the case of OIS (oncogene-induced senescence), it has been shown that demethylase JMJD3 blocks repression of Ink4A locus by PcG protein Bmi1. Arf ($p19^{ARF}$), another product of this locus, plays a major role in senescence in mice, while p16 is more important in humans. Figure adapted from ref. 119.

2. How is Permanent Cell Cycle Arrest Achieved?

Senescence is a viable and metabolically active state, which is characterized by a virtually permanent (irreversible) cessation of cell division. It is associated with dramatic changes in cell morphology (large flat cells), metabolism, gene expression and secretion patterns (senescence-associated secretory phenotype or SASP), originally described by Campisi and colleagues (8). Senescence has recently been shown to play a crucial role in age-related pathologies associated with accumulation of senescent cells (9, 10). Both in vitro and in vivo, senescent cells can be detected by virtue of β-galactosidase activity (β-gal) (11), a lysosomal enzyme, which probably does not play a direct role in senescence (12), but serves as a reliable biomarker

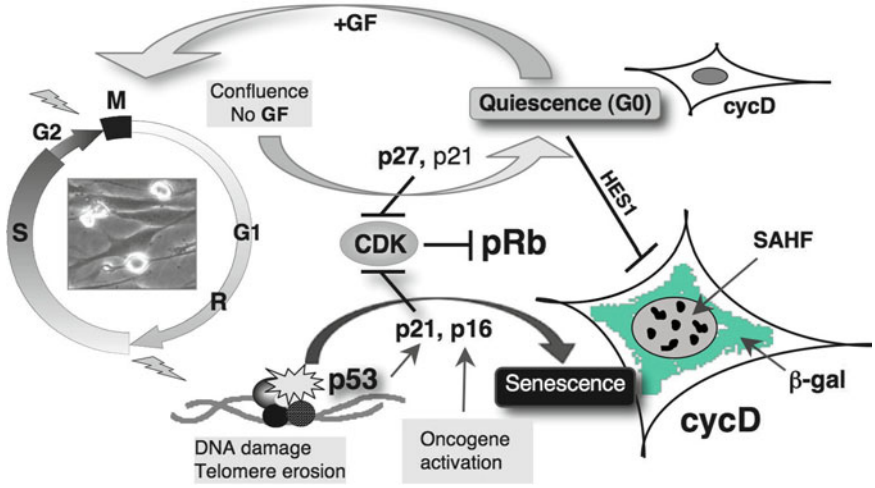

Fig. 2. Senescence versus quiescence. Quiescence (or G0) is reversible and hypotrophic cell cycle exit that occurs in G1 prior to restriction (R) point. It is mediated preferentially by p27-dependent CDK inactivation and cyclin D1 downregulation. Some results suggest that genes expressed in quiescent cells can block senescence (HES1). By contrast, senescence is irreversible and hypertrophic cell cycle exit that takes place either in G1 or G2, depending on the activated checkpoint. Cell cycle arrest is mediated by p16/p21-dependent CDK inactivation (Fig. 1) and senescent cells contain high levels of G1 cyclins (cyclin D and cyclin E) associated with inactive CDK. While the cytoplasm could be frequently stained for β-galactosidase (see Chapters 4, 8 and 9), senescent nuclei are often large and sometimes binuclear (due to endoreplication or defective cytokinesis) and could contain heterochromatin in the forms of SAHF (see Chapter 12) or PML bodies. Both events require active pRb family pocket proteins but in senescence only pRb is essential (ref. 19). *GF* growth factors.

(see Chapter 4 and Fig. 2). In addition, senescent cells often exhibit dramatic rearrangement of chromatin structure, in the forms of PML (promyelocytic leukemia protein) nuclear bodies (13, 14) and senescence-associated heterochromatin foci (SAHF) (15). These heterochromatin structures, whose formation requires active pRb, are thought to play an important role in conferring irreversibility of the cell cycle arrest by repressing the genes controlling cell proliferation (Figs. 1 and 2). However, SAHFs are not observed in all cell types and in all forms of senescence (15), and recent work associates SAHF formation with oncogene induced senescence and repression of DNA damage signaling (16).

The pro-senescence stimuli all converge on one major pathway to permanently arrest the cell cycle (Fig. 1). The senescence program is initiated by inactivation of CDK (17), the key cell cycle regulators. CDKs play two distinct roles. First, they control the onset and progression of DNA replication and mitosis, thus enabling and orchestrating the cell cycle. Second, CDKs, particularly Cdk4/6 associated with D-type cyclins, phosphorylate, thus keeping inactive, the retinoblastoma (pRb) tumor suppressor and related "pocket-proteins" (p107, p130). This is essential for cell cycle progression, since active (hypo-phosphorylated) pocket proteins drive cell cycle exit by sequestering E2F family transcription factors and by repressing the genes required for cell division (18).

Despite often-overlapping functions between different members of the pocket protein family, pRb was shown to play a unique and nonredundant role in senescence by repressing E2F target genes involved in DNA replication (19) (Fig. 1). Recent data suggest that this process requires a recruitment of promoter-bound pRb and E2Fs to PML nuclear bodies (14). More recently, p130/E2F4 complex was also implicated in senescence by repressing, via PML, T-box protein 2 (TBX2) frequently overexpressed in cancer (20).

The presence of diverse genotoxic stresses that induce senescence activates a DDR network, controlled by ATM/ATR kinases, which blocks CDK activation via CDC25 family phosphatases, thereby temporarily halting cell cycle progression (Fig. 1). While not required for this transient arrest, p53 and its transcriptional target $p21^{Waf1/Cip1/Sdi1}$ (p21), a CDK inhibitor (CKI), are essential parts of irreversible cell cycle arrest by the senescence program (21, 22). Permanent CDK inactivation by p21 stably blocks DNA synthesis and mitotic entry and, via activation of pRb, drives exit from the cell cycle (19, 23) (Fig. 1). Another CKI, $p16^{Ink4A}$ (p16), which targets specifically pRb kinases Cdk4/6, also plays an important role in senescence and, along with β-gal, it is often used as a biomarker both in vitro and in vivo (9, 24). However, unlike p21, p16 does not seem to be involved in the cell cycle arrest associated with replicative senescence (21) and its late induction, which occurs after p21-mediated cell cycle arrest, might promote a stabilization of senescent state (25, 26). Nevertheless, p16 is a key regulator of oncogene-induced senescence (OIS) (27) and recent work in a mouse model strongly implicated this inhibitor in acquisition of age-related pathologies (9). Although p16 is widely considered as an essential part of the senescence program, the pathways regulating its induction in response to senescence-promoting stimuli are still not entirely elucidated. It has been suggested that, in the case of OIS, activation of histone demethylase JMJD3 suppresses the repression of the INK4A-ARF locus by Polycomb group proteins (PcG), Bmi1; (5). Another protein encoded by this locus is tumor suppressor $p19^{ARF}$ (ARF) that plays a prominent role in senescence in mice but not in humans (27). ARF stabilizes p53 by inhibiting MDM2 and, via its effector p21 blocks cell cycle. Thus, ultimate targets of both products of the INK4A-ARF locus are CDKs that inactivate pRb, and their dysregulation invariably compromises genome integrity (Fig. 1).

3. Quiescence Versus Senescence

What distinguishes senescence from another non-proliferating state, quiescence, also referred to as G0 or G0/G1 phase (28)? In contrast to senescence, quiescence is a *reversible* cell cycle arrest,

which is induced by the absence of mitogens or growth factors, nutrient starvation, or increasing cell density (confluence) (Fig. 2). Typical examples of quiescent cells are lymphocytes, whose activation is part of the immune response, adult stem cells, or dermal fibroblasts, which actively participate in wound healing (29). In general, quiescence is characterized by low metabolism and protein synthesis, lack of cellular growth, and, the absence of global heterochromatin structures such as PML bodies (30) or SAHF (15). The latter feature is probably responsible for the reversible nature of quiescence. However, much against the prevailing view, recent results showed that fibroblasts rendered quiescent by contact inhibition exhibit comparable metabolic activity to actively proliferating cells. In addition to promote recycling of damaged macromolecules via autophagy, high metabolic activity might serve for biosynthesis and secretion of extracellular matrix proteins (31). Importantly, while downregulating expression of genes involved in cell division, quiescent cells upregulate genes, such as HES1, that inhibit senescence, differentiation and apoptosis (32, 33). Unlike senescence, which can occur either in the G1 or G2 phase of the cell cycle (34), depending on when the damage is detected and the efficiency of the checkpoints (23, 35), quiescence essentially takes place in G1, prior to the restriction (R) checkpoint (36). A teleological explanation for this observation could be given by the unidirectionality of the cell cycle—G0 state always precedes DNA replication (S phase). Therefore, if cells became quiescent in the G2 phase, cell cycle entry upon stimulation would result in genome reduplication giving rise to undesirable tetraploidy.

Like senescence, quiescence is characterized by CDK inactivation, the absence of S-phase- and Mitosis-promoting cyclins and the presence of hypo-phosphorylated pocket proteins. However, unlike senescence, where CDKs are inhibited by p21 or/and p16, the major CKI involved in quiescent arrest is $p27^{Kip1}$ (p27) (37–39). Unlike p21, p27 induction is independent of the p53 pathway (39) and its levels/activity is primarily regulated by translation, phosphorylation, and Skp2-mediated degradation (40). Although p53 and p21 were also implicated in the cell cycle arrest following growth factor removal (41, 42), p53 integrity does not seem to be essential for quiescence (43) (Fig. 2). However, a redundancy of p27 with p21 might explain why contact inhibition is not impaired in $p27^{-/-}$ cells (44). Interestingly, the expression of D-type cyclins, regulatory subunits of Cdk4/6 kinases and key signal integrators, strikingly differs between quiescence and senescence (Fig. 2). Downregulation of cyclin Ds is a hallmark of quiescence and their rapid mitogen-dependent induction is invariably associated with cell cycle entry (42, 45, 46). In sharp contrast, D cyclins are stabilized (cyclin D1) and even overexpressed (cyclin D2) in senescent cells (17, 35, 43, 47). In conjunction with the large-cell phenotype that is observed in senescent cells, these results suggest that the

mitogenic pathways involved in cell growth are active in senescent cells (see below) and might even have a positive role in senescence regulation. Indeed, several recent publications have connected the "hypertrophic" phenotype of senescent cells with activity of mTOR, a master cell growth regulator (48), although this topic is still controversial (49).

4. The mTOR Pathway Essentials

Originally identified in budding yeast mutants conferring resistance to a potent antifungal metabolite (50), the *t*arget *o*f *r*apamycin (TOR) is at the core of a vast signaling pathway regulating cell growth and metabolism in virtually all eukaryotes. The complexity of this pathway, which couples energy and nutrient abundance to the execution of cellular growth and division, relies on the fact that TOR simultaneously senses energy (ATP state), nutrients, stress, as well as growth factors (51, 52). In addition to its growth-related functions, the TOR pathway is also wired to the regulators of cell cycle machinery such as G1 cyclins (D-type and E-type) controlling G1/S-phase progression (see below and Fig. 3). It is therefore not surprising that TOR is essential for many developmental and physiological processes (53) while deregulation in its signaling has been implicated in a wide variety of diseases (52). mTOR ("m" stands for mammalian or, more recently, mechanistic), which belongs to the phosphoinositide 3-kinase (PI3K)-related protein serine/threonine kinase family (PIKK), forms two distinct multiprotein complexes, having distinctive physical structures and functions: mTOR complex 1 (mTORC1), which is sensitive to rapamycin owing to association with the peptidyl-prolyl *cis/trans* isomerase FKBP12 (50), and mTORC2, which is not sensitive to rapamycin in most cases. Their assembly, substrate specificity, and regulation are defined by specific accessory proteins: Raptor (regulatory associated protein of mTOR) being the most prominent for mTORC1, and Rictor (rapamycin-insensitive companion of mTOR), which is specific for mTORC2. Since the regulatory inputs and the cellular actions of mTOR are far too complex for the scope of this chapter (and are reviewed in ref. 53, 54), I outline only some "essentials" focusing mainly on mTORC1, the better characterized of the two.

mTORC1, which is activated by nutrients, growth factors, and cellular energy status, regulates temporal aspects of cellular growth including protein synthesis, ribosome biogenesis, lipid synthesis, nutrient import, and autophagy. Best-known substrates of mTORC1 are p70 ribosomal protein S6 kinases (S6K1 and S6K2) and the eIF4E binding proteins (4E-BP1 and 4E-BP2) by which it controls protein synthesis. The positive and negative control of

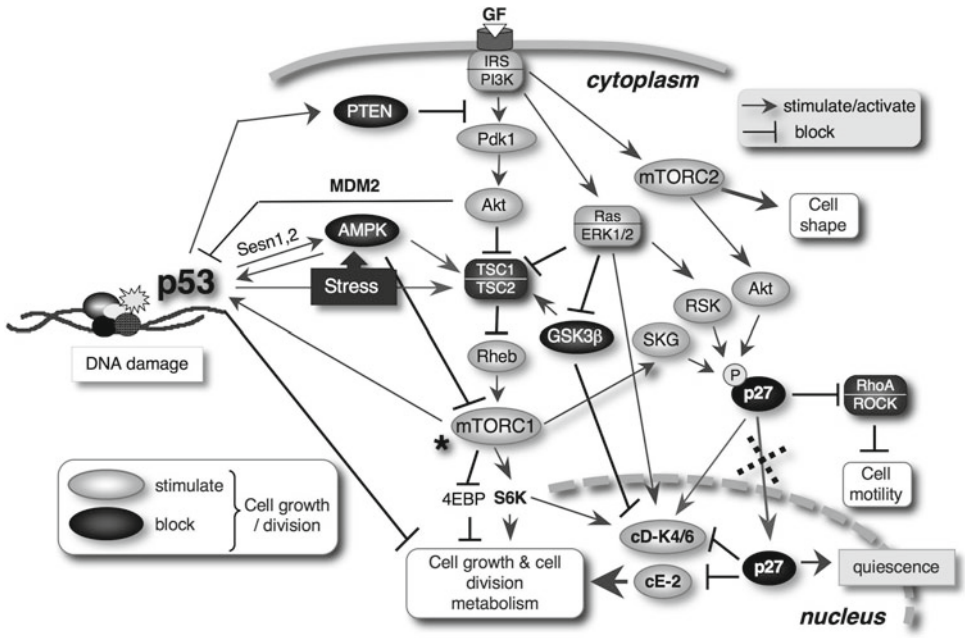

Fig. 3. Interactions between mTOR signaling, p53 and cell cycle regulators. While mTORC1 controls cell growth/division and metabolism, TORC2 mainly controls cell shape and activates Akt. TSC1/TSC2 complex plays a pivotal role as a hub for both positive and negative cues that control mTORC1 activity via signaling kinases (see ref. 53). mTOR controls cell division by regulating synthesis of cyclin D and activity/localization of CDK inhibitor p27. While in the nucleus, p27 inhibits CDKs (cD-K4/K6 and cE-K2) thereby blocking cell cycle progression (like in quiescence). Growth factors stimulate mTOR and ERK1/2 that, via Akt, RSK and SGK, mediate p27 phosphorylation leading to its cytoplasmic sequestration. Cytoplasmic p27 promotes proliferation by stabilizing cyclin D-Cdk4/6 assembly and cell motility by inhibiting RhoA/ROCK (see ref. 71). In response to DNA damage or other stresses, p53 negatively regulates mTORC1 by activating AMPK and PTEN and inducing TSC2. Constitutive activation of mTOR (*asterisk*) could induce p53 translation (see ref. 86). Figure adapted from ref. 119. *GF* growth factors (insulin, IGF1); Sesn, sestrin.

mTORC1 in response to intracellular and extracellular stimuli is mediated by the phosphorylation and subsequent inhibition of Tuberous sclerosis 1 (TSC1, hamartin)/TSC2 (tuberin) complex (Fig. 3). TSC2 subunit, a hub for a variety of cues impinging on mTORC1, serves as GTPase activating protein (GAP), which itself inhibits the small GTPase Rheb, a direct mTORC1 activator (51, 53, 55). TSC2 activity is regulated by several kinases: negatively, by Akt and ERK1/2 (activate mTORC1) and positively, by AMPK and GSK3β (inhibit mTORC1). Importantly, the Wnt pathway also regulates TSC1/TSC2, via inhibition of GSK3β (53) (see Fig. 4). mTORC2 is thought to regulate mainly cytoskeleton organization and cell survival by phosphorylating of AGC kinase family members, including Akt, SGK1, and PKC (52, 53) (Fig. 3). Although little is known about upstream regulators of mTORC2 (56), recent reports showing that its activation requires association with ribosomes suggest that it is active only in growing cells (57).

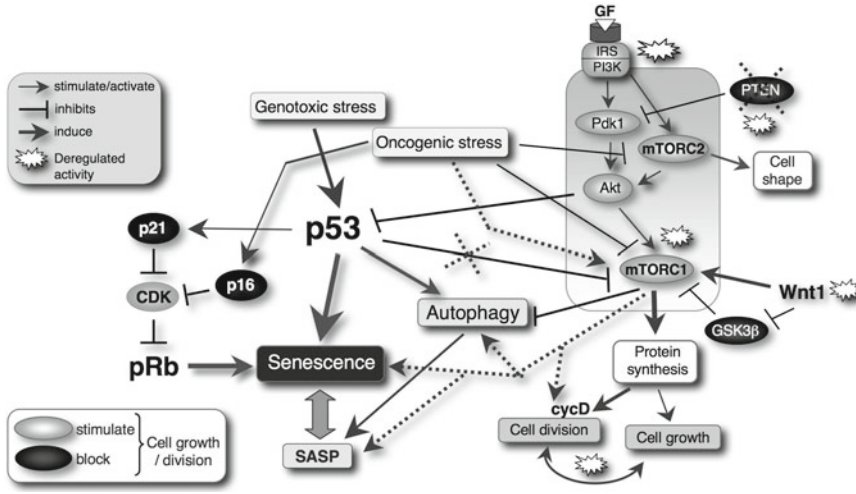

Fig. 4. Possible roles of p53 and mTOR in senescence. Genotoxic stress (via p53–p21) and activated oncogenes (via p16) induce senescence by inactivating CDK and activating pRb (see Fig. 1). Classically, p53 and activated oncogenes induce autophagy by inhibiting mTOR pathway (*grey box*). Autophagy is implicated in senescence by stimulating specific secretory phenotype (SASP) that also promotes senescence. However, recent data suggest that mTOR might positively regulate senescence (*grey dotted lines*) as in the case of persistent Wnt1 signaling or PTEN knockdown. Pro-senescence mTOR activity could be also activated via oncogenic stress—by inducing autophagy, or via low p53 levels (*grey dotted cross*)—by promoting cell growth and D-type cyclin synthesis. Hypertrophy of senescent cells could be explained by deregulated cell signaling (not responding to extracellular cues) resulting in permanent mTOR activation. This is in agreement with results showing that in senescent cells cell growth and cell division are uncoupled events. For more details regarding mTOR regulation, see Fig. 3 and ref. 53. Figure adapted from ref. 119. *GF* growth factors.

5. mTOR and Cell Cycle

As eluded above, mTOR pathway is also implicated in cell division, in part by controlling the synthesis of D-type cyclins (58, 59), major regulators of G1-S phase progression, whose induction in response to growth factors is regulated by the Ras-ERK1/2 pathway (60, 61) (Fig. 3). Recent data show that mTORC1 controls cell proliferation, but not growth, via its targets 4E-BPs, by stimulating the translation of proteins involved in cell cycle progression, including cyclin D3 (62). In addition, in the fission yeast model, TOR was also shown to control mitotic entry in response to nutrients. In this system, both rapamycin (by inhibiting TOR) and poor nitrogen sources stimulate the stress MAPK pathway (Spc1/Sty1), which, by activating Polo kinase and Cdc2 (Cdk1 ortholog, the main mitotic regulator) accelerated mitosis with reduced cell size as consequence (63). While no equivalent pathway was yet reported in other models, these observations are consistent with earlier results that linked mTOR signaling with cell-size control (64). Nevertheless, despite general downregulation of

protein translation in mitosis (65), several recent papers suggest that mTORC1 might also control protein synthesis in mitosis by regulating expression of human Cdk1, which phosphorylates eukaryotic elongation factor 2 (eEF2); (66). Moreover, it seems that, at G2/M transition, Cdk1 might also regulate mTORC1 activity by phosphorylating Raptor (67, 68).

The mTOR pathway also positively controls cell cycle by regulating the activity and subcellular localization of the CKI p27, negative regulator of G1/S progression (Fig. 3). In the presence of growth factors, Akt (activated by mTORC2), RSK (activated by ERK1/2), and SKG (activated by mTORC1, mTORC2 and Pdk1) phosphorylate p27, resulting in its cytoplasmic retention (69–71). This not only prevents p27 to exert its nuclear role as CDK inhibitor, by inactivating CDKs controlling DNA replication (as cyclin E-Cdk2), but also promote cell proliferation by stabilizing assembly of cyclin D-CDK4/6 complexes and increasing cell motility, via inhibition of RhoA signaling (71) (Fig. 3). In addition, mTORC2 regulates cell proliferation via AKT-mediated inhibition of forkhead box protein O (FOXO) transcription factors playing a key role in promoting apoptosis (72). Importantly, the FOXO family members were also shown to block cell cycle by inducing p27 (73) or repressing D-type cyclins (74).

6. TOR, p53, and Genotoxic Stress

In the light of increasing evidence that altered metabolism is not only a common feature of many cancer cells but that it can also greatly contribute to malignant transformation (75), the discovery that p53 also regulates metabolic pathways and interacts with mTOR/AKT pathways is not that surprising (reviewed in refs. 76, 77) (Fig. 3 and 4). Indeed, it has been shown that, in response to diverse stress signals, activation of p53 directly or indirectly inhibits mTOR activity, thus regulating its downstream targets, including those involved in the activation of autophagy, a recently described tumor suppression mechanism that is involved in senescence (54, 78) (see also Chapter 3). The role of autophagy in senescence is discussed in more detail in the chapter by M. Narita (see Chapter 1). In addition to its housekeeping role in the maintenance of energy homeostasis, autophagy, which is negatively regulated by mTOR, is also induced by a variety of stress stimuli, such as nutrient depletion (when mTOR is inhibited), playing a vital role in preserving cellular viability through the degradation of cellular proteins and organelles (53, 79).

The mechanism by which p53 negatively regulates mTOR involves, in part, the activation of AMPK and requires its target TSC1/TSC2 complex (Fig. 3), both of which respond to energy deprivation in cells (53, 80). In response to genotoxic stress caused by DNA damage, p53 inhibits mTORC1 pathway, by phosphorylating Sestrin 1 and 2 that activate AMPK (81), as well as the IGF-1/Akt pathway, by inducing transcription of PTEN (82) (Fig. 3). In addition, p53 can repress mTORC1 by inducing directly TSC2 (83) or AMPK, which suppresses translation by activating TSC2 (80) or by directly inhibiting mTORC1 (54, 84). However, it has been reported that AMPK might also control the p53 activity, like in the case of glucose starvation, which induces the transient AMPK–mediated phosphorylation and activation of p53 leading to reversible cell cycle arrest (85, 86). There are several examples showing that conversely, mTOR can also control p53. Upon glucose removal, mTOR negatively regulates p53 by activating PP2A (87). However, some results suggest that deregulated (constitutive) mTOR activity might, in response to nutrient or genomic stress, induce p53 translation, which in conjunction with activation by AMPK, induces apoptosis (88). This implies that, at least in certain biological contexts, mTOR downregulation/inactivation is required to prevent cell death caused by stress stimuli. Thus, p53 and mTOR signaling networks can cross-talk and coordinately regulate cell growth, proliferation and death.

7. mTOR' s Role in Senescence: Repressor or Inducer?

The mTOR pathway has been shown to have opposing roles on cellular senescence. On the one hand, by inhibiting autophagy (78, 86, 89), mTOR is considered as a negative regulator of senescence (Fig. 4), which is in agreement with its widely accepted negative role in organismal ageing (90). Moreover, as mentioned above, mTOR is inhibited by p53, a *bona fide* pro-senescence positive regulator (Figs. 3 and 4). On the other hand, the hypertrophic phenotype of senescent cells (Fig. 2) and increased production of secretory proteins (SASP; Fig. 4), which requires high metabolic activity, are in apparent contradiction with cellular shrinkage that is usually associated with autophagy and mTOR inhibition (as in quiescence). Indeed, in the case of oncogene or DNA damage-induced senescence, the onset of both senescence and autophagy correlates with inhibition of mTORC1 and mTORC2 activity (91). This might suggest a negative feedback between mTOR and senescence. These findings are also in agreement with earlier observations that activation of p53 by genotoxic stress inhibits mTOR pathway by activating both AMPK and PTEN (Fig. 3) (81, 86). Likewise, persistent

AMPK activation leads to senescence in mouse embryo fibroblasts (MEF) in the presence of functional p53 (85), which is consistent with earlier observation that AMP levels strongly increase in senescent cells (92).

However, it is also possible that mTOR activation via different stimuli could be involved in the induction of senescence. This pro-senescence role of mTOR was first uncovered by manipulation of its upstream regulators or downstream targets. Pandolfi and colleagues found that overexpression of an mTOR target eIF-4E induced senescence both in vitro and in vivo (93). More recently, activation of the PI3K/Akt and mTOR pathways by PTEN knockdown has been shown to induce senescence by promoting accumulation of p53 and p21 (94). Similarly, in an elegant in vivo skin model, Gutkind and colleagues showed that continuous mTOR activation induced by persistent Wnt1 signaling (via inhibiting GSK3; (95)) promoted epithelial stem cell exhaustion by provoking senescence (96). Importantly, senescence and hair loss were abolished by the presence of the mTOR inhibitor rapamycin suggesting that mTOR stimulation is a direct consequence of Wnt1 expression (96) (Fig. 4). These results connect persistent mitogen stimulation and mTOR activation with senescence. Moreover, they are in agreement with accumulated evidence connecting accumulation of senescent cells with ageing (7, 9). Indeed, increased mTOR activity was also observed in hematopoietic stem cells from old mice (97), whereas mTOR inhibition by rapamycin could extend lifespan both in invertebrates (98, 99) and in mice (97, 100, 101).

In the context of OIS, mTOR promotes lysosome biogenesis, which is required for autophagy and senescence-specific secretory phenotype, in a newly identified cytoplasmic compartment (termed TOR-autophagy spatial coupling compartment or TASCC) (102). While these results clearly indicate that mTOR has pro-senescence functions (Fig. 4), they are surprising in light of earlier report, connecting the induction of senescence by oncogenic ras with mTOR downregulation (91). However, in this previous report it was clearly shown that increased phosphorylation of both mTORC1 and mTORC2 substrates (S6K and FoxO3a, respectively) coincided more with the onset of cycle arrest (and senescence) than with ras-induced cell cycle entry, as proposed by the authors. Indeed, transient activation of mTOR was also observed in cells in which senescence was triggered by the genotoxic agent etoposide. Therefore, while the results showing that appearance of late senescence and autophagy markers coincided with downregulation of mTOR activity, overall this work supports a positive role of mTOR pathway in the induction of autophagy at the onset of senescence.

Although mainly focused on autophagy-related roles of mTOR, the above results are consistent with the model proposed by Blagosklonny and coworkers, whose recent experiments suggest

that cellular growth and persistent mTOR activity might be implicated in the onset of the senescence program. Consistent with their finding that serum stimulation is required for both the senescent phenotype (large flat cells) and irreversibility of the cell cycle arrest induced by overexpression of the CDK inhibitor p21 or DNA damage, they observed that a key mTOR target, S6K, is strongly phosphorylated in senescent cells (103). Moreover, in agreement with our earlier observation (17), senescent cells also accumulated another mTOR target, cyclin D1, but the biological significance of its presence is not clear (see below). Interestingly, while rapamycin, like serum starvation, prevented S6K phosphorylation and diminished the senescent marker β-gal staining, it failed to completely abolish large flat cell morphology and to inhibit cyclin D1 induction. While these results imply that mTORC1 is not essential for these events, it would be interesting to test whether they are controlled by mTORC2, which is less sensitive to rapamycin and which is implicated in both cell shape and, via its target Akt, in cyclin D1 stability (Figs. 3 and 4). In addition, rapamycin prevents the onset of senescence if added simultaneously with senescence inducers (p21 induction, genotoxic agents), but fails to revert the already established senescence (104).

Taken together, the above results suggest that (transient?) mTOR activity might positively control senescence but it is still unclear how DDR network controls activity of this pathway.

8. Connections Between mTOR and p53 in Senescence—Lessons from Nutlin-3A

How one can reconcile the data suggesting a positive role of mTOR in senescence with those showing that p53 inhibits the mTOR pathway (76, 77)? In the work of Narita's team the possible interactions between p53 and the mTOR pathway were not examined, because in OIS cell cycle arrest is mainly mediated by the CDK inhibitor p16, which is not regulated by p53 (91) (Fig. 1). In the quest to decipher the respective roles of mTOR and p53 in the senescence program, Blagosklonny and coworkers took advantage of nutlin-3A, a specific small-molecule MDM2 antagonist, which strongly induces p53 expression thereby triggering its transcriptional activity in a non-genotoxic manner (105). Surprisingly, while previous work has shown that nutlin-3A induces senescence in mouse fibroblasts (106), in human fibrosarcoma cells HT1080 and WI-38 human fibroblasts, nutlin-3A induces reversible cell cycle exit resembling quiescence (107). By exploiting a HT1080-derived cell line in which p21 is expressed from an inducible promoter, Demidenko et al. showed that nutlin-3A or p53 overexpression could "convert" p21-induced senescence into a quiescence-like state (108). Nutlin-3A was, however, much less efficient

in preventing senescence in the presence of DNA damage by H_2O_2, which also stimulates the phosphorylation of mTOR (108). In addition, both nutlin-3A and rapamycin suppress senescence without interfering with cell cycle arrest, which led the authors to suggest that high p53 levels preclude the onset of senescence by inhibiting mTOR and inducing quiescence (108, 109). Accordingly, knockdown of TSC2, a negative mTORC1 regulator (Fig. 3), partially compromises nutlin-3-induced quiescence, resulting in accumulation of senescent cells (110). In agreement with the positive role of mTOR in senescence, in cell lines in which nutlin-3A did induce senescence (termed "senescence-prone"), mTOR was not inhibited, whereas the quiescence was "restored" in the presence of rapamycin (110). Unfortunately, these studies did not provide insight into molecular mechanisms explaining differences between "senescence-prone" and "quiescence-prone" cells. In agreement with the above experiments, when exposed to etoposide, serum-deprived or rapamycin-treated fibroblasts (or epithelial cells) failed to become senescent despite p21 induction, as drug removal, concomitant with serum addition, enabled proliferation (111). In contrast, serum addition in the presence of etoposide induced senescence, presumably by activating mTOR. These results support the hypothesis that quiescence (or mTOR inhibition) compromises senescence. However, it is not clear why the checkpoints were not activated once cells exposed to etoposide reentered the cell cycle (assuming that the DNA damage had not been repaired) and how the cells got rid of high p21 levels.

This work, however, did not address the role of the CKI p27 in p53-induced quiescence. This point is relevant for understanding the mechanism that induces quiescence, since mTOR inhibition by rapamycin or p53 overexpression might also block SGK/Akt-mediated p27 phosphorylation and cytoplasmic localization leading to its nuclear accumulation and activation (70, 71) (Fig. 3). One could imagine that, in the presence of rapamycin or absence of serum, p27-dependent CDK inactivation together with cyclin D1 down-regulation could also contribute to quiescence. Reactivation of mTOR (by serum addition) would revert this process, enabling cell cycle entry and progression, probably by degrading p27 and p21 and inducing G1 cyclins (D- and E-type).

Overall, the results of Blagosklonny's team are consistent with the idea that mTOR positively regulates senescence, which might be because p53 levels are not sufficient to inhibit mTOR-dependent cell growth. According to their hypothesis, the "true role" of p53 (when highly expressed) would be to induce quiescence by inhibiting mTOR, which in turn would block the onset of senescence. Consequently, senescence occurs in situations where "the conditions for quiescence are not met" (low p53 levels) and where p53 "fails" to suppress the mTOR pathway (108, 112). This hypothesis is consistent with the data showing that quiescence prevents

p21-induced senescence or inappropriate differentiation due to expression of the transcriptional repressor HES1, playing a key role in the reversibility of this non-proliferative state (33) (Fig. 2).

There are, however, several caveats regarding the use of nutlin-3A as a tool to study the role of p53 and mTOR in senescence. For example, strong p53 induction by nutlin-3A is not usually observed in either quiescence or senescence and it is not clear which biological event produces equivalent amounts of p53. As a matter of fact, primary fibroblasts expressing the HPV16-E6 (hereafter E6) oncogene that degrades p53 (113) can become quiescent in the absence of serum or confluence, whereas strong p21 induction in senescent cells occurs in the absence of significant increases in p53 protein levels (43). Therefore, the hypothesis that high p53 levels induce quiescence while low p53 levels lead to senescence (108, 109) should be verified in other experimental models. For example, our recent results showed that irreversible cell cycle arrest by genotoxic drugs in non-transformed human cells is independent on the degree of p53 activation (or levels) or even p21 levels but rather on the efficiency of p21 to inhibit different CDKs (Lossaint, 2011). Finally, as mentioned above, this model is in apparent contradiction with the results showing that in other cell lines nutlin-3A does not induce quiescence but instead elicits endoreduplication, giving rise to tetraploid cells (114), senescence—due to persistent p21 expression (106, 115), or even apoptosis (116). One explanation could be that nutlin-3A might have other targets than p53 (pRb?) or that its effects might be dependent on the experimental protocol and cell type.

9. mTOR and Senescence: Constitutive Activation or Deregulation?

The above-mentioned work mostly addressed the role of mTOR in premature (induced) senescence but less is known regarding its implication in replicative senescence. Several earlier observations, however, are consistent with the notion that the mTOR pathway might be active in senescent cells and that it is not controlled by p53 or affected by its status. In fact, in human fibroblasts aged in vitro a suppression of the p53/p21 pathway compromises cell cycle arrest, senescence-specific cyclin D2 induction (see below), as well as formation of SAHF, but it does not prevent large flat cell morphology or cyclin D1 accumulation (43). This implies that these two sets of key events associated with senescence, i.e. irreversible cell cycle arrest and cell growth, might be uncoupled, which can also explain the senescent phenotype (Fig. 4). In addition, some data suggest that mitogenic pathways in senescent cells might be also deregulated. Firstly, in sharp contrast to early passage fibroblasts, serum withdrawal in senescent fibroblasts does not

affect cyclin D1 mRNA or cyclin E1 expression or protein synthesis. The CDKs associated with these cyclins are, however, inhibited by p21, explaining the absence of DNA replication (17, 26) (Fig. 1). Interestingly, in agreement with other publications (35, 117), late senescence is associated with strong accumulation of cyclin D2, whose levels are not affected by serum withdrawal. The presence of G1 cyclins, and especially of cyclin D2, in senescent cells is intriguing and it is not clear whether they might play a role in senescence or they merely reflect deregulated mTOR activity. One possibility is that cyclin D1 is part of the DNA repair machinery, as suggested recently (118). Secondly, late-passage p53-deficient fibroblasts (E6) failed to become quiescent upon serum withdrawal, which is documented by both the absence of cyclin D1 or cyclin A down-regulation and p27 induction (or activation). Consequently, CDKs controlling DNA replication were highly active even in the absence of serum. However, these cells failed to proliferate due to deleterious effects of DNA damage resulting in aberrant mitoses, endoreplication, or cell death (43). It is therefore possible that, concomitant with increased population doubling, gradual deregulation of the mTOR pathway contributes to the senescent phenotype. In the absence of the p53/pRb safeguard system, this deregulation provides a fertile ground for tumorigenesis.

In conclusion, the role of the mTOR pathway in senescence is still controversial, partly due to the various models and experimental designs employed in different studies. Apart from the studies manipulating upstream mTOR regulators (PTEN, Wnt1) that reveal pro-senescence mTOR-functions, most of the work has focused on the autophagy-related aspects of senescence, which appeared to exclude mTOR as an important regulator of senescence. Few researchers, however, considered a hypertrophic phenotype of senescent cells and elevated levels of D-type cyclins as an evidence of mTOR activity. Future work will show whether or not this activity is actually required for the onset of senescence, as some investigators proposed, or it is merely the result of senescence-associated deregulation of the mTOR pathway. If the former is the case, it will be interesting to learn whether, and if so, how p53 and/or pRb networks contribute to its induction.

Acknowledgments

I am grateful to Drs Anne Brunet (Stanford University, Palo Alto, USA) and Jacques Piette (CRBM, Montpellier, France) for their insightful comments.

References

1. Hayflick L (1965) The limited in vitro lifetime of human diploid cell strains. Exp Cell Res 37:614–636
2. Harley CB, Futcher AB, Greider CW (1990) Telomeres shorten during ageing of human fibroblasts. Nature 345:458–460
3. Olovnikov AM (1973) A theory of marginotomy. The incomplete copying of template margin in enzymic synthesis of polynucleotides and biological significance of the phenomenon. J Theor Biol 41:181–190
4. Stein GH, Dulic V (1995) Origins of G1 arrest in senescent human fibroblasts. Bioessays 17:537–543
5. Kuilman T, Michaloglou C, Mooi WJ, Peeper DS (2010) The essence of senescence. Genes Dev 24:2463–2479
6. Adams PD (2009) Healing and hurting: molecular mechanisms, functions, and pathologies of cellular senescence. Mol Cell 36: 2–14
7. Rodier F, Campisi J (2011) Four faces of cellular senescence. J Cell Biol 192:547–556
8. Rodier F, Coppe JP, Patil CK, Hoeijmakers WA, Munoz DP, Raza SR, Freund A, Campeau E, Davalos AR, Campisi J (2009) Persistent DNA damage signalling triggers senescence-associated inflammatory cytokine secretion. Nat Cell Biol 11:973–979
9. Baker DJ, Wijshake T, Tchkonia T, LeBrasseur NK, Childs BG, van de Sluis B, Kirkland JL, van Deursen JM (2011) Clearance of p16Ink4a-positive senescent cells delays ageing-associated disorders. Nature 479:232–236
10. Kang TW, Yevsa T, Woller N, Hoenicke L, Wuestefeld T, Dauch D, Hohmeyer A, Gereke M, Rudalska R, Potapova A, Iken M, Vucur M, Weiss S, Heikenwalder M, Khan S, Gil J, Bruder D, Manns M, Schirmacher P, Tacke F, Ott M, Luedde T, Longerich T, Kubicka S, Zender L (2011) Senescence surveillance of pre-malignant hepatocytes limits liver cancer development. Nature 479:547–551
11. Dimri GP, Lee X, Basile G, Acosta M, Scott G, Roskelley C, Medrano EE, Linskens M, Rubelj I, Pereira-Smith O et al (1995) A biomarker that identifies senescent human cells in culture and in aging skin in vivo. Proc Natl Acad Sci U S A 92:9363–9367
12. Lee BY, Han JA, Im JS, Morrone A, Johung K, Goodwin EC, Kleijer WJ, DiMaio D, Hwang ES (2006) Senescence-associated beta-galactosidase is lysosomal beta-galactosidase. Aging Cell 5:187–195
13. Bernardi R, Pandolfi PP (2007) Structure, dynamics and functions of promyelocytic leukaemia nuclear bodies. Nat Rev Mol Cell Biol 8:1006–1016
14. Vernier M, Bourdeau V, Gaumont-Leclerc MF, Moiseeva O, Begin V, Saad F, Mes-Masson AM, Ferbeyre G (2011) Regulation of E2Fs and senescence by PML nuclear bodies. Genes Dev 25:41–50
15. Narita M, Nunez S, Heard E, Narita M, Lin AW, Hearn SA, Spector DL, Hannon GJ, Lowe SW (2003) Rb-mediated heterochromatin formation and silencing of E2F target genes during cellular senescence. Cell 113:703–716
16. Di Micco R, Sulli G, Dobreva M, Liontos M, Botrugno OA, Gargiulo G, Dal Zuffo R, Matti V, d'Ario G, Montani E, Mercurio C, Hahn WC, Gorgoulis V, Minucci S, d'Adda di Fagagna F (2011) Interplay between oncogene-induced DNA damage response and heterochromatin in senescence and cancer. Nat Cell Biol 13:292–302
17. Dulic V, Drullinger LF, Lees E, Reed SI, Stein GH (1993) Altered regulation of G1 cyclins in senescent human diploid fibroblasts: accumulation of inactive cyclin E-Cdk2 and cyclin D1-Cdk2 complexes. Proc Natl Acad Sci U S A 90:11034–11038
18. Burkhart DL, Sage J (2008) Cellular mechanisms of tumour suppression by the retinoblastoma gene. Nat Rev Cancer 8:671–682
19. Chicas A, Wang X, Zhang C, McCurrach M, Zhao Z, Mert O, Dickins RA, Narita M, Zhang M, Lowe SW (2010) Dissecting the unique role of the retinoblastoma tumor suppressor during cellular senescence. Cancer Cell 17:376–387
20. Martin N, Benhamed M, Nacerddine K, Demarque MD, van Lohuizen M, Dejean A, Bischof O (2012) Physical and functional interaction between PML and TBX2 in the establishment of cellular senescence. EMBO J 31:95–109
21. Herbig U, Jobling WA, Chen BP, Chen DJ, Sedivy JM (2004) Telomere shortening triggers senescence of human cells through a pathway involving ATM, p53, and p21(CIP1), but not p16(INK4a). Mol Cell 14:501–513
22. Vousden KH, Prives C (2009) Blinded by the light: the growing complexity of p53. Cell 137:413–431
23. Baus F, Gire V, Fisher D, Piette J, Dulic V (2003) Permanent cell cycle exit in G2 phase after DNA damage in normal human fibroblasts. EMBO J 22:3992–4002

24. Krishnamurthy J, Torrice C, Ramsey MR, Kovalev GI, Al-Regaiey K, Su L, Sharpless NE (2004) Ink4a/Arf expression is a biomarker of aging. J Clin Invest 114:1299–1307
25. Alcorta DA, Xiong Y, Phelps D, Hannon G, Beach D, Barrett JC (1996) Involvement of the cyclin-dependent kinase inhibitor p16 (INK4a) in replicative senescence of normal human fibroblasts. Proc Natl Acad Sci U S A 93:13742–13747
26. Stein GH, Drullinger LF, Soulard A, Dulic V (1999) Differential roles for cyclin-dependent kinase inhibitors p21 and p16 in the mechanisms of senescence and differentiation in human fibroblasts. Mol Cell Biol 19: 2109–2117
27. Gil J, Peters G (2006) Regulation of the INK4b-ARF-INK4a tumour suppressor locus: all for one or one for all. Nat Rev Mol Cell Biol 7:667–677
28. Coller HA (2011) Cell biology. The essence of quiescence. Science 334:1074–1075
29. Coller HA (2007) What's taking so long? S-phase entry from quiescence versus proliferation. Nat Rev Mol Cell Biol 8:667–670
30. Ferbeyre G, de Stanchina E, Querido E, Baptiste N, Prives C, Lowe SW (2000) PML is induced by oncogenic ras and promotes premature senescence. Genes Dev 14: 2015–2027
31. Lemons JM, Feng XJ, Bennett BD, Legesse-Miller A, Johnson EL, Raitman I, Pollina EA, Rabitz HA, Rabinowitz JD, Coller HA (2010) Quiescent fibroblasts exhibit high metabolic activity. PLoS Biol 8:e1000514
32. Coller HA, Sang L, Roberts JM (2006) A new description of cellular quiescence. PLoS Biol 4:e83
33. Sang L, Coller HA, Roberts JM (2008) Control of the reversibility of cellular quiescence by the transcriptional repressor HES1. Science 321:1095–1100
34. Blagosklonny MV (2006) Cell senescence: hypertrophic arrest beyond the restriction point. J Cell Physiol 209:592–597
35. Shelton DN, Chang E, Whittier PS, Choi D, Funk WD (1999) Microarray analysis of replicative senescence. Curr Biol 9:939–945
36. Pardee AB (1989) G1 events and regulation of cell proliferation. Science 246:603–608
37. Polyak K, Kato JY, Solomon MJ, Sherr CJ, Massague J, Roberts JM, Koff A (1994) p27Kip1, a cyclin-Cdk inhibitor, links transforming growth factor-beta and contact inhibition to cell cycle arrest. Genes Dev 8:9–22
38. Fero ML, Rivkin M, Tasch M, Porter P, Carow CE, Firpo E, Polyak K, Tsai LH, Broudy V, Perlmutter RM, Kaushansky K, Roberts JM (1996) A syndrome of multiorgan hyperplasia with features of gigantism, tumorigenesis, and female sterility in p27(Kip1)-deficient mice. Cell 85:733–744
39. Sherr CJ, Roberts JM (1999) CDK inhibitors: positive and negative regulators of G1-phase progression. Genes Dev 13:1501–1512
40. Chu IM, Hengst L, Slingerland JM (2008) The Cdk inhibitor p27 in human cancer: prognostic potential and relevance to anticancer therapy. Nat Rev Cancer 8:253–267
41. Itahana K, Dimri GP, Hara E, Itahana Y, Zou Y, Desprez PY, Campisi J (2002) A role for p53 in maintaining and establishing the quiescence growth arrest in human cells. J Biol Chem 277:18206–18214
42. Pajalunga D, Mazzola A, Salzano AM, Biferi MG, De Luca G, Crescenzi M (2007) Critical requirement for cell cycle inhibitors in sustaining nonproliferative states. J Cell Biol 176:807–818
43. Dulic V, Beney GE, Frebourg G, Drullinger LF, Stein GH (2000) Uncoupling between phenotypic senescence and cell cycle arrest in aging p21-deficient fibroblasts. Mol Cell Biol 20:6741–6754
44. Nakayama K, Ishida N, Shirane M, Inomata A, Inoue T, Shishido N, Horii I, Loh DY (1996) Mice lacking p27(Kip1) display increased body size, multiple organ hyperplasia, retinal dysplasia, and pituitary tumors. Cell 85:707–720
45. Matsushime H, Roussel MF, Ashmun RA, Sherr CJ (1991) Colony-stimulating factor 1 regulates novel cyclins during the G1 phase of the cell cycle. Cell 65:701–713
46. Baldin V, Lukas J, Marcote MJ, Pagano M, Draetta G (1993) Cyclin D1 is a nuclear protein required for cell cycle progression in G1. Genes Dev 7:812–821
47. Atadja P, Wong H, Veillette C, Riabowol K (1995) Overexpression of cyclin D1 blocks proliferation of normal diploid fibroblasts. Exp Cell Res 217:205–216
48. Pani G (2011) From growing to secreting: new roles for mTOR in aging cells. Cell Cycle 10:2450–2453
49. Blagosklonny MV (2011) Cell cycle arrest is not senescence. Aging (Albany NY) 3:94–101
50. Heitman J, Movva NR, Hall MN (1991) Targets for cell cycle arrest by the immunosuppressant rapamycin in yeast. Science 253:905–909
51. Wullschleger S, Loewith R, Hall MN (2006) TOR signaling in growth and metabolism. Cell 124:471–484

52. Dazert E, Hall MN (2011) mTOR signaling in disease. Curr Opin Cell Biol 23:744–755
53. Zoncu R, Efeyan A, Sabatini DM (2011) mTOR: from growth signal integration to cancer, diabetes and ageing. Nat Rev Mol Cell Biol 12:21–35
54. Sengupta S, Peterson TR, Sabatini DM (2010) Regulation of the mTOR complex 1 pathway by nutrients, growth factors, and stress. Mol Cell 40:310–322
55. Conn CS, Qian SB (2011) mTOR signaling in protein homeostasis: less is more? Cell Cycle 10:1940–1947
56. Oh WJ, Jacinto E (2011) mTOR complex 2 signaling and functions. Cell Cycle 10: 2305–2316
57. Zinzalla V, Stracka D, Oppliger W, Hall MN (2011) Activation of mTORC2 by association with the ribosome. Cell 144:757–768
58. Averous J, Fonseca BD, Proud CG (2008) Regulation of cyclin D1 expression by mTORC1 signaling requires eukaryotic initiation factor 4E-binding protein 1. Oncogene 27:1106–1113
59. Balcazar N, Sathyamurthy A, Elghazi L, Gould A, Weiss A, Shiojima I, Walsh K, Bernal-Mizrachi E (2009) mTORC1 activation regulates beta-cell mass and proliferation by modulation of cyclin D2 synthesis and stability. J Biol Chem 284:7832–7842
60. Lavoie JN, L'Allemain G, Brunet A, Muller R, Pouyssegur J (1996) Cyclin D1 expression is regulated positively by the p42/p44MAPK and negatively by the p38/HOGMAPK pathway. J Biol Chem 271:20608–20616
61. Hitomi M, Stacey DW (1999) Cyclin D1 production in cycling cells depends on ras in a cell-cycle- specific manner. Curr Biol 9:1075–1084
62. Dowling RJ, Topisirovic I, Alain T, Bidinosti M, Fonseca BD, Petroulakis E, Wang X, Larsson O, Selvaraj A, Liu Y, Kozma SC, Thomas G, Sonenberg N (2010) mTORC1-mediated cell proliferation, but not cell growth, controlled by the 4E-BPs. Science 328:1172–1176
63. Petersen J, Nurse P (2007) TOR signalling regulates mitotic commitment through the stress MAP kinase pathway and the Polo and Cdc2 kinases. Nat Cell Biol 9:1263–1272
64. Fingar DC, Salama S, Tsou C, Harlow E, Blenis J (2002) Mammalian cell size is controlled by mTOR and its downstream targets S6K1 and 4EBP1/eIF4E. Genes Dev 16: 1472–1487
65. Pyronnet S, Dostie J, Sonenberg N (2001) Suppression of cap-dependent translation in mitosis. Genes Dev 15:2083–2093
66. Smith EM, Proud CG (2008) cdc2-cyclin B regulates eEF2 kinase activity in a cell cycle- and amino acid-dependent manner. EMBO J 27:1005–1016
67. Ramirez-Valle F, Badura ML, Braunstein S, Narasimhan M, Schneider RJ (2010) Mitotic raptor promotes mTORC1 activity, G(2)/M cell cycle progression, and internal ribosome entry site-mediated mRNA translation. Mol Cell Biol 30:3151–3164
68. Gwinn DM, Asara JM, Shaw RJ (2010) Raptor is phosphorylated by cdc2 during mitosis. PLoS One 5:e9197
69. Hong F, Larrea MD, Doughty C, Kwiatkowski DJ, Squillace R, Slingerland JM (2008) mTOR-raptor binds and activates SGK1 to regulate p27 phosphorylation. Mol Cell 30: 701–711
70. Toker A (2008) mTOR and Akt signaling in cancer: SGK cycles in. Mol Cell 31:6–8
71. Wander SA, Zhao D, Slingerland JM (2011) p27: a barometer of signaling deregulation and potential predictor of response to targeted therapies. Clin Cancer Res 17:12–18
72. Guertin DA, Stevens DM, Thoreen CC, Burds AA, Kalaany NY, Moffat J, Brown M, Fitzgerald KJ, Sabatini DM (2006) Ablation in mice of the mTORC components raptor, rictor, or mLST8 reveals that mTORC2 is required for signaling to Akt-FOXO and PKCalpha, but not S6K1. Dev Cell 11: 859–871
73. Medema RH, Kops GJ, Bos JL, Burgering BM (2000) AFX-like Forkhead transcription factors mediate cell-cycle regulation by Ras and PKB through p27kip1. Nature 404:782–787
74. Schmidt M, Fernandez de Mattos S, van der Horst A, Klompmaker R, Kops GJ, Lam EW, Burgering BM, Medema RH (2002) Cell cycle inhibition by FoxO forkhead transcription factors involves downregulation of cyclin D. Mol Cell Biol 22:7842–7852
75. Kroemer G, Pouyssegur J (2008) Tumor cell metabolism: cancer's Achilles' heel. Cancer Cell 13:472–482
76. Vousden KH, Ryan KM (2009) p53 and metabolism. Nat Rev Cancer 9:691–700
77. Feng Z (2010) p53 regulation of the IGF-1/AKT/mTOR pathways and the endosomal compartment. Cold Spring Harb Perspect Biol 2:a001057
78. Young AR, Narita M (2010) Connecting autophagy to senescence in pathophysiology. Curr Opin Cell Biol 22:234–240
79. Kroemer G, Marino G, Levine B (2010) Autophagy and the integrated stress response. Mol Cell 40:280–293

80. Inoki K, Zhu T, Guan KL (2003) TSC2 mediates cellular energy response to control cell growth and survival. Cell 115:577–590
81. Budanov AV, Karin M (2008) p53 target genes sestrin1 and sestrin2 connect genotoxic stress and mTOR signaling. Cell 134: 451–460
82. Feng Z, Hu W, de Stanchina E, Teresky AK, Jin S, Lowe S, Levine AJ (2007) The regulation of AMPK beta1, TSC2, and PTEN expression by p53: stress, cell and tissue specificity, and the role of these gene products in modulating the IGF-1-AKT-mTOR pathways. Cancer Res 67:3043–3053
83. Feng Z, Zhang H, Levine AJ, Jin S (2005) The coordinate regulation of the p53 and mTOR pathways in cells. Proc Natl Acad Sci U S A 102:8204–8209
84. Gwinn DM, Shackelford DB, Egan DF, Mihaylova MM, Mery A, Vasquez DS, Turk BE, Shaw RJ (2008) AMPK phosphorylation of raptor mediates a metabolic checkpoint. Mol Cell 30:214–226
85. Jones RG, Plas DR, Kubek S, Buzzai M, Mu J, Xu Y, Birnbaum MJ, Thompson CB (2005) AMP-activated protein kinase induces a p53-dependent metabolic checkpoint. Mol Cell 18:283–293
86. Feng Z, Levine AJ (2010) The regulation of energy metabolism and the IGF-1/mTOR pathways by the p53 protein. Trends Cell Biol 20:427–434
87. Kong M, Fox CJ, Mu J, Solt L, Xu A, Cinalli RM, Birnbaum MJ, Lindsten T, Thompson CB (2004) The PP2A-associated protein alpha4 is an essential inhibitor of apoptosis. Science 306:695–698
88. Lee CH, Inoki K, Karbowniczek M, Petroulakis E, Sonenberg N, Henske EP, Guan KL (2007) Constitutive mTOR activation in TSC mutants sensitizes cells to energy starvation and genomic damage via p53. EMBO J 26:4812–4823
89. Kim J, Kundu M, Viollet B, Guan KL (2011) AMPK and mTOR regulate autophagy through direct phosphorylation of Ulk1. Nat Cell Biol 13:132–141
90. Selman C, Tullet JM, Wieser D, Irvine E, Lingard SJ, Choudhury AI, Claret M, Al-Qassab H, Carmignac D, Ramadani F, Woods A, Robinson IC, Schuster E, Batterham RL, Kozma SC, Thomas G, Carling D, Okkenhaug K, Thornton JM, Partridge L, Gems D, Withers DJ (2009) Ribosomal protein S6 kinase 1 signaling regulates mammalian life span. Science 326:140–144
91. Young AR, Narita M, Ferreira M, Kirschner K, Sadaie M, Darot JF, Tavare S, Arakawa S, Shimizu S, Watt FM, Narita M (2009) Autophagy mediates the mitotic senescence transition. Genes Dev 23:798–803
92. Zwerschke W, Mazurek S, Stockl P, Hutter E, Eigenbrodt E, Jansen-Durr P (2003) Metabolic analysis of senescent human fibroblasts reveals a role for AMP in cellular senescence. Biochem J 376:403–411
93. Ruggero D, Montanaro L, Ma L, Xu W, Londei P, Cordon-Cardo C, Pandolfi PP (2004) The translation factor eIF-4E promotes tumor formation and cooperates with c-Myc in lymphomagenesis. Nat Med 10: 484–486
94. Astle MV, Hannan KM, Ng PY, Lee RS, George AJ, Hsu AK, Haupt Y, Hannan RD, Pearson RB (2011) AKT induces senescence in human cells via mTORC1 and p53 in the absence of DNA damage: implications for targeting mTOR during malignancy. Oncogene 31:1949–1962
95. Inoki K, Ouyang H, Zhu T, Lindvall C, Wang Y, Zhang X, Yang Q, Bennett C, Harada Y, Stankunas K, Wang CY, He X, MacDougald OA, You M, Williams BO, Guan KL (2006) TSC2 integrates Wnt and energy signals via a coordinated phosphorylation by AMPK and GSK3 to regulate cell growth. Cell 126: 955–968
96. Castilho RM, Squarize CH, Chodosh LA, Williams BO, Gutkind JS (2009) mTOR mediates Wnt-induced epidermal stem cell exhaustion and aging. Cell Stem Cell 5:279–289
97. Chen C, Liu Y, Liu Y, Zheng P (2009) mTOR regulation and therapeutic rejuvenation of aging hematopoietic stem cells. Sci Signal 2:ra75
98. Vellai T, Takacs-Vellai K, Zhang Y, Kovacs AL, Orosz L, Muller F (2003) Genetics: influence of TOR kinase on lifespan in C. elegans. Nature 426:620
99. Kaeberlein M, Powers RW 3rd, Steffen KK, Westman EA, Hu D, Dang N, Kerr EO, Kirkland KT, Fields S, Kennedy BK (2005) Regulation of yeast replicative life span by TOR and Sch9 in response to nutrients. Science 310:1193–1196
100. Harrison DE, Strong R, Sharp ZD, Nelson JF, Astle CM, Flurkey K, Nadon NL, Wilkinson JE, Frenkel K, Carter CS, Pahor M, Javors MA, Fernandez E, Miller RA (2009) Rapamycin fed late in life extends lifespan in genetically heterogeneous mice. Nature 460:392–395
101. Kapahi P, Chen D, Rogers AN, Katewa SD, Li PW, Thomas EL, Kockel L (2010) With TOR, less is more: a key role for the conserved

nutrient-sensing TOR pathway in aging. Cell Metab 11:453–465

102. Narita M, Young AR, Arakawa S, Samarajiwa SA, Nakashima T, Yoshida S, Hong S, Berry LS, Reichelt S, Ferreira M, Tavare S, Inoki K, Shimizu S, Narita M (2011) Spatial coupling of mTOR and autophagy augments secretory phenotypes. Science 332:966–970
103. Demidenko ZN, Blagosklonny MV (2008) Growth stimulation leads to cellular senescence when the cell cycle is blocked. Cell Cycle 7:3355–3361
104. Demidenko ZN, Zubova SG, Bukreeva EI, Pospelov VA, Pospelova TV, Blagosklonny MV (2009) Rapamycin decelerates cellular senescence. Cell Cycle 8:1888–1895
105. Vassilev LT, Vu BT, Graves B, Carvajal D, Podlaski F, Filipovic Z, Kong N, Kammlott U, Lukacs C, Klein C, Fotouhi N, Liu EA (2004) In vivo activation of the p53 pathway by small-molecule antagonists of MDM2. Science 303:844–848
106. Efeyan A, Ortega-Molina A, Velasco-Miguel S, Herranz D, Vassilev LT, Serrano M (2007) Induction of p53-dependent senescence by the MDM2 antagonist nutlin-3a in mouse cells of fibroblast origin. Cancer Res 67: 7350–7357
107. Korotchkina LG, Demidenko ZN, Gudkov AV, Blagosklonny MV (2009) Cellular quiescence caused by the Mdm2 inhibitor nutlin-3A. Cell Cycle 8:3777–3781
108. Demidenko ZN, Korotchkina LG, Gudkov AV, Blagosklonny MV (2010) Paradoxical suppression of cellular senescence by p53. Proc Natl Acad Sci U S A 107:9660–9664
109. Leontieva OV, Gudkov AV, Blagosklonny MV (2010) Weak p53 permits senescence during cell cycle arrest. Cell Cycle 9:4323–4327
110. Korotchkina LG, Leontieva OV, Bukreeva EI, Demidenko ZN, Gudkov AV, Blagosklonny MV (2010) The choice between p53-induced senescence and quiescence is determined in part by the mTOR pathway. Aging (Albany NY) 2:344–352
111. Leontieva OV, Blagosklonny MV (2010) DNA damaging agents and p53 do not cause senescence in quiescent cells, while consecutive re-activation of mTOR is associated with conversion to senescence. Aging (Albany NY) 2:924–935
112. Maki CG (2010) Decision-making by p53 and mTOR. Aging (Albany NY) 2:324–326
113. Scheffner M, Huibregtse JM, Vierstra RD, Howley PM (1993) The HPV-16 E6 and E6-AP complex functions as a ubiquitin-protein ligase in the ubiquitination of p53. Cell 75:495–505
114. Shen H, Moran DM, Maki CG (2008) Transient nutlin-3a treatment promotes endoreduplication and the generation of therapy-resistant tetraploid cells. Cancer Res 68: 8260–8268
115. Shen H, Maki CG (2010) Persistent p21 expression after Nutlin-3a removal is associated with senescence-like arrest in 4 N cells. J Biol Chem 285:23105–23114
116. Villalonga-Planells R, Coll-Mulet L, Martinez-Soler F, Castano E, Acebes JJ, Gimenez-Bonafe P, Gil J, Tortosa A (2011) Activation of p53 by nutlin-3a induces apoptosis and cellular senescence in human glioblastoma multiforme. PLoS One 6:e18588
117. Meyyappan M, Wong H, Hull C, Riabowol KT (1998) Increased expression of cyclin D2 during multiple states of growth arrest in primary and established cells. Mol Cell Biol 18:3163–3172
118. Jirawatnotai S, Hu Y, Michowski W, Elias JE, Becks L, Bienvenu F, Zagozdzon A, Goswami T, Wang YE, Clark AB, Kunkel TA, van Harn T, Xia B, Correll M, Quackenbush J, Livingston DM, Gygi SP, Sicinski P (2011) A function for cyclin D1 in DNA repair uncovered by protein interactome analyses in human cancers. Nature 474:230–234
119. Brondello JM, Prieur A, Philipot D, Lemaitre JM, Lenaers G, Piette J, Dulic V (2012) La sénescence cellulaire: un nouveau mythe de Janus? Med Sci (Paris) 28:288–296

Chapter 3

Senescence Regulation by the p53 Protein Family

Yingjuan Qian and Xinbin Chen

Abstract

p53, a guardian of the genome, exerts its tumor suppression activity by regulating a large number of downstream targets involved in cell cycle arrest, DNA repair, apoptosis, and cellular senescence. Although p53-mediated apoptosis is able to kill cancer cells, a role for cellular senescence in p53-dependent tumor suppression is becoming clear. Mouse studies showed that activation of p53-induced premature senescence promotes tumor regression in vivo. However, p53-mediated cellular senescence also leads to aging-related phenotypes, such as tissue atrophy, stem cell depletion, and impaired wound healing. In addition, several p53 isoforms and two p53 homologs, p63 and p73, have been shown to play a role in cellular senescence and/or aging. Importantly, p53, p63, and p73 are necessary for the maintenance of adult stem cells. Therefore, understanding the dual role the p53 protein family in cancer and aging is critical to solve cancer and longevity in the future. In this chapter, we provide an overview on how p53, p63, p73, and their isoforms regulate cellular senescence and aging.

Key words: Aging, p53, p63, p73, Senescence

1. Introduction

p53, originally identified as a protein associated with the simian virus 40 large T antigen in 1979 (1–4), guards genomic integrity via regulating numerous cellular processes, including cell cycle arrest, DNA repair, apoptosis, and cellular senescence, in response to various stress signals (5, 6). The p53 pathway is commonly lost in human cancers due to either inactivation of p53 protein or mutations in the *TP53* gene, leading to accumulation of damaged cells and cancer progression, (7). Consistent with this, mice deficient in the *Tp53* gene are highly prone to spontaneous malignancy at a young age (8, 9). In addition, Li–Fraumeni syndrome patients carrying a *TP53* mutation display increased risk of early onset of several types of cancer (10, 11).

Lorenzo Galluzzi et al. (eds.), *Cell Senescence: Methods and Protocols*, Methods in Molecular Biology, vol. 965,
DOI 10.1007/978-1-62703-239-1_3,

Clearance of tumor cells by induction of programmed cell death is well documented as a tumor suppression activity of p53. Recent studies demonstrated that induction of p53-dependent senescence plays a pivotal role in limiting tumor progression in vivo (12–14). Thus, further understanding the mechanism by which p53 is implicated in regulating cellular senescence is of great interest for developing new cancer therapies. Cellular senescence was originally described by Hayflick and Moorhead in the 1960s (15, 16). They found that normal human diploid fibroblasts have a limited lifespan in culture and eventually enter a state of permanent cell cycle arrest called replicative senescence. Senescent cells exhibit enlarged cell size, flattened morphology, inability to synthesize DNA, metabolic active, and expression of the senescence-associated β-galactosidase (SA-β-gal), the latter of which can be detected at pH 6.0 (17, 18). Further studies showed that this life timing is controlled by repeats of telomere, a nucleoprotein structure at chromosome tips, which is undergoing progressive loss during cell divisions (19–21). Due to insufficient telomere after a number of cell doublings exposed or fused chromosome ends trigger DNA damage signals (telomeric stress signals), leading to senescence. As a major mediator of the DNA damage pathway, p53 has been shown to be critical for telomeric stress-induced cellular senescence (22, 23). In addition, multiple stress signals, including aberrant oncogene activation (24–26) and cancer chemotherapeutic drugs (22, 23, 27), are able to induce senescence-like phenotypes (premature senescence) in both primary and tumor cells via activating the p53 and/or p16 pathways (28). In this chapter, we provide an overview of the role of p53, its isoforms, and its family members, p63 and p73, in regulating cellular senescence and aging.

2. The Role of p53 in Cellular Senescence in Response to Different Stress Signals

2.1. The p53 Protein

The wild-type p53 protein is composed of 393 amino acids and contains several functional domains (Fig. 1). These are the N-terminal activation domain 1 (AD1) and 2 (AD2), the proline-rich domain (PRD), the central core DNA-binding domain (DBD), the nuclear localization signal region (NLS), the tetramerization domain (TD), and the C-terminal regulatory basic domain (BD) (29). As a sequence-specific transcription factor, p53 regulates gene expression by directly binding to a p53-responsive element (p53-RE) in the target gene as a tetramer. The consensus p53-RE is composed of two half sites (RRRC$^{A}/_{T}{}^{A}/_{T}$GYYY, where R represents purine and Y pyrimidine) separated by up to 13 nucleotides (30). Hundreds of p53 targets have been identified and shown to be involved in a variety of cellular responses, such as cell cycle arrest, DNA repair, apoptosis, and cellular senescence, attributing to the tumor suppressor activity of p53.

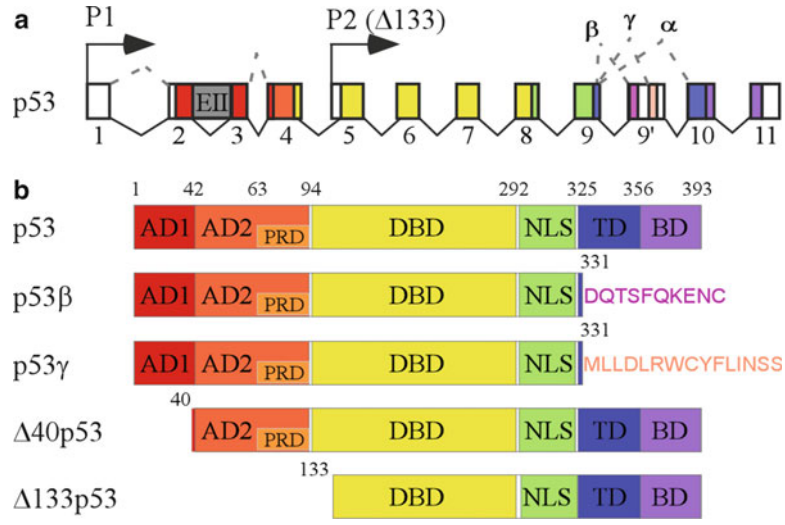

Fig. 1. The p53 gene and protein structure. (**a**) *TP53* locus, location of the P1 and P2 promoters, and patterns of alternative splicing. p53, also called α isoform, is a full-length p53 generated from the P1 promoter. Transcripts initiated from an internal promoter (P2) in intron 4 leads to production of an N-terminal truncated p53 starting from residue 133, named as Δ133p53. Alternative translation initiation at an AUG codon at position 40 leads to production of a p53 protein with a deletion of the first 39 amino acids (Δ40p53). Although alternative splicing of intron 2 gives rise to a transcript containing intron 2 sequence, the presence of a stop codon in intron 2 also leads to production of Δ40p53. Compared to the α isoforms, the β and γ isoforms have 10 and 15 unique amino acids at C-termini, respectively. (**b**) p53 isoforms and functional domains. *AD* activation domain, *PRD* proline-rich domain, *DBD* DNA binding domain, *NLS* nuclear localization domain, *TD* teramerization domain, *BD* basic domain.

The level and activity of p53 protein are primarily regulated through posttranslational modifications (Fig. 2). In normal cells, p53 is a short-lived protein which is continuously undergoing ubiquitination and subject to proteasomal degradation. Mouse double minute 2 (MDM2, HDM2 in human), one of the first characterized p53 targets, serves as a major E3 ubiquitin ligase for p53 degradation and thus forms a negative autoregulatory loop to maintain the low level of p53 expression in unstressed conditions (31–34). Upon genotoxic stresses, rapid phosphorylation of p53 at Ser-15 by the Ataxia telangiectasia mutated (ATM), a serine/threonine protein kinase, and at Ser-20 by the checkpoint kinase 2 (Chk2) results in dissociation of p53 from MDM2, leading to p53 stabilization and activation of its downstream processes (35–37). Likewise, phosphorylation of MDM2 at Ser-395 by ATM attenuates the capability of MDM2 in exporting nuclear p53 to cytoplasm for subsequent p53 degradation, thereby enabling p53 accumulation (38, 39). In addition to ubiquitination and phosphorylation, p53 activity is modulated by acetylation (35, 40). Acetylation by histone acetyltransferases (HATs) and deacetylation by histone deacetylases (HDACs) were initially discovered to regulate

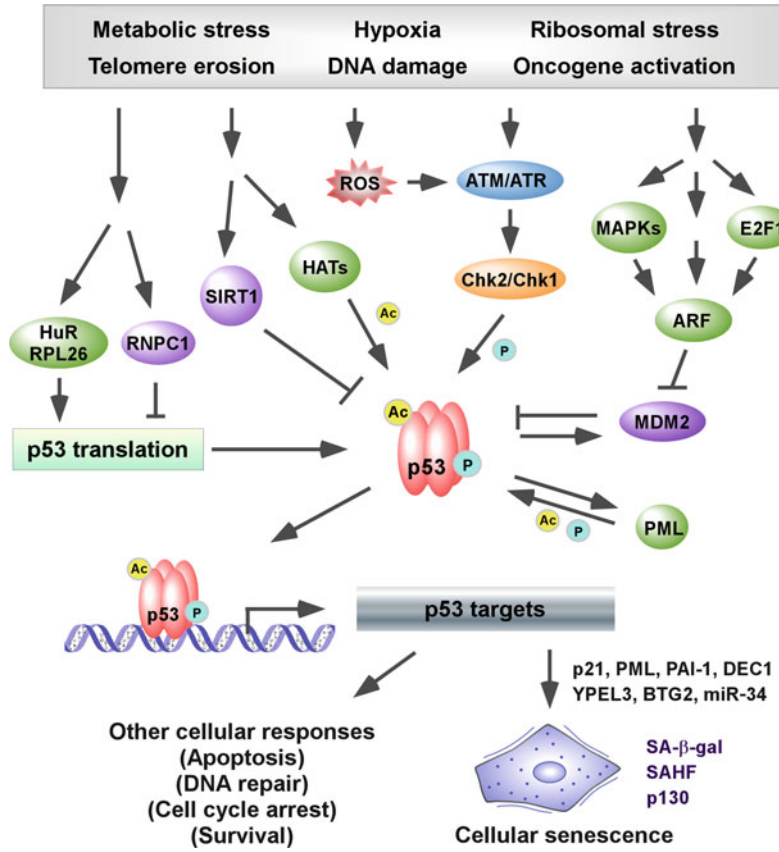

Fig. 2. The role of p53 in cellular senescence. Upon exposure to numerous stress signals, p53 is regulated by phosphorylation (ATM/ATR-Chk2/Chk1), by acetylation (p300/CBP, PCAF, Tip60/hMOF, and SIRT1), by increased protein stability (ARF-MDM2), and by increased translation rates (RNPC1, HuR, and RPL26). Once activated, p53 regulates a set of downstream targets leading to cellular senescence and other cellular responses. Several senescence markers, including p21, PML, PAI-1, and DEC1, are identified as p53 target genes and promote cellular senescence. In addition, PML positively feeds back to promote p53 phosphorylation and acetylation. As a result, senescent cells induced by p53 activation exhibit flattened morphology, enlarged cell size, expression of SA-β-gal, formation of SAHF, and deregulated expression of p53 targets. In some cases, increased hypophosphorylated p130 is detected in cellular senescence induced by p53 and/or DNA damage.

the extent of histone acetylation and play a critical role in gene transcription (41). p53 was identified as the first non-histone substrate of HATs and HDACs (42, 43). In response to DNA damage, CBP/p300 acetylates p53 on six C-terminal lysine (K) residues (K370, K372, K373, K381, K382, and K386), the same target sites of MDM2-mediated ubiquitination, and hence leads to enhanced stability and DNA binding activity of p53 (44). In addition, acetylation of p53 on K320 by PCAF preferentially directs

p53 to activate target genes involved in cell cycle arrest (45), whereas acetylation of p53 on K120 by Tip60/hMOF promotes p53-mediated cell death (46–48). Moreover, acetylation of p53 on K164 by CBP/p300 is required for p53-induced cell cycle arrest and apoptosis (49). Interestingly, emerging evidence showed that *TP53* mRNA stability and translation are regulated by multiple RNA binding proteins including HuR (50), ribosomal protein L26 (RPL26) (51, 52), nucleolin (51), and RNPC1 (53), and microRNAs including miR-125b (54), miR-125a (55), and miR-504 (56).

2.2. The Role of p53 in Replicative Senescence

Detection of γ-H2AX foci, a sensitive marker for DNA double-strand break (DSB), on dysfunctional telomeres (shortened telomeres or altered telomere state) in senescent cells indicates that telomere-dependent replicative senescence is stress-dependent (57–59) (Fig. 2). These foci contain multiple DNA damage responsive proteins, such as 53BP1 and MRN complex (MRE11, RAD51, and NBS1), and are indistinguishable from the γ-H2AX foci originated from ionizing radiation-induced DNA DSB (60, 61). Activation of ATM at sites of DNA DSBs elicits phosphorylation of Chk2 and upregulation of p53 (62, 63). ATM is a primary mediator for telomere dysfunction-induced damage signaling. However, in the absence of ATM, ATR (ATM and Rad3-related) substitutes the role of ATM to activate p53 through Chk1-induced p53 phosphorylation at Ser-15 (63). Consistently, enhanced expression of p53 in mice deficient in Terc, the RNA component of telomerase, leads to activation of senescence and reduced tumor formation (64). In contrast, mice deficient in both Terc and p53 bypass senescence and develop tumors (65). These indicate that p53 plays a pivotal role in maintaining telomere dysfunction-initiated senescence.

2.3. The Role of p53 in Oncogene-Induced Senescence

In addition to spontaneous senescence, OIS was discovered as a cancer prevention mechanism in cells exposed to oncogenic Ras. It has been shown that expression of oncogenic Ras promotes acute senescence-like G1 arrest in primary human or rodent cells containing wild-type p53 (24), but initiates cellular transformation in those lacking p53 (66). This indicates that p53 plays a critical role in OIS. There are two underlying mechanisms by which Ras activates the p53-dependent senescence pathway in OIS (67–69) (Fig. 2). First, Ras regulates p53 through the MAPK pathways. It has been shown that Ras utilizes the MAPK signal-transduction pathway, including Raf-1, MEKs (MEK1/2), and MAPKs (ERK1/2), to promote cell cycle arrest in primary cells but malignant transformation in immortal cells (70–72). However, the cell cycle arrest induced by expression of Ras or MEK is abolished in cells lacking p53 (70). In addition, activation of the p38/MAPK pathway, especially its downstream kinase PRAK, leads to p53-dependent senescence by phosphorylating and activating p53 (73, 74). Indeed, ARF can be activated by the Ras/Raf signaling

cascade via E2F1 or Dmp1 (75, 76). E2F1 and Dmp1 are capable of directly binding to, and activating, the promoter of the ARF gene (77, 78). $p19^{ARF}$ ($p14^{ARF}$ in human) is encoded from an alternative reading frame within the INK4a/ARF locus which also encodes p16 (79, 80). ARF blocks MDM2-mediated degradation of p53 by repressing MDM2 E3 ligase activity and nuclear export as well as promoting MDM2 degradation (81–84). Interestingly, ARF mediates Ras signaling to p53 in mouse cells but is not required for OIS in human cells (85). Second, Ras regulates p53 by activation of DNA damage response (DDR). It has been shown that ectopic expression of HRasV12 in human diploid fibroblasts induces DNA hyper-replication resulting in prematurely terminated DNA replication and collapse of DNA replication forks, which in turn lead to accumulation of DSBs and subsequent activation of the ATM/ATR-p53 pathway to induce senescence (86–89). In addition, oncogene activation leads to accumulation of reactive oxygen species (ROS), which induces DNA damage (89, 90). Consistent with this, human diploid fibroblasts grown in a restrictive culture condition with low or no ROS production bypass oncogene-induced senescence (91).

2.4. The Role of p53 in Genotoxic Stress-Induced Senescence

Given the importance of the DDR-p53 pathway in both replicative senescence and OIS, it is not surprising that numerous stress signals, such as DNA damage, oxidative stress, insufficient nutrients/growth factors, and improper cell contacts, induce premature senescence in normal human and murine cells (27, 92). Since induction of permanent cell cycle arrest is a potential cancer prevention mechanism by eliminating damaged pre-cancer cells at the initial stage of transformation, it was postulated that evasion of senescence might be a prerequisite for pre-cancer cells to complete transformation into cancer cells (93–95). Surprisingly, senescence-like growth arrest is induced by ectopic expression of a tumor suppressor gene or treatment with chemotherapeutic drugs in a broad range of human cancer cells, including those derived from colon, ovarian, lung, prostate, and cervical carcinomas (25). Importantly, reports showed that restoration of p53-mediated premature senescence is able to promote cancer regression in mice with hepatocarcinoma and sarcomas (12, 96). Indeed, ectopic expression of wild-type p53 triggers premature senescence in tumor cells lacking endogenous p53 (97, 98). In addition, p53-dependent premature senescence is induced by a variety of chemotherapeutic drugs, including camptothecin, doxorubicin, etoposide, cisplatin, and resveratrol (99). However, treatment with therapeutic agents also induces p53-independent premature senescence. For instance, doxorubicin induces senescence in a number of cancer cell lines deficient in p53 (25, 100, 101).

3. Characteristics of p53-Mediated Cellular Senescence

3.1. Cell Cycle Arrest

Since senescent cells must initially undergo cell cycle arrest, DNA histogram analysis is expected to show decreased number of cells in S phase (cell uptake of BrdU) and increased number of cells in G1 or sometimes also G2/M phase, but no change in the number of cells in sub-G1 phase (dead cells) (101, 102). However, the cell cycle profile for senescent cells is indistinguishable from that for quiescent cells and terminally differentiated cells.

3.2. SA-β-Gal

SA-β-gal is a commonly used senescence biomarker, which can be detected at pH 6.0 (18). This phenomenon is due to the fact that senescent cells express a high level of lysosomal β-gal (103–105). It is important to note that overexpression of lysosomal β-gal itself is not able to initiate senescence (103). Nevertheless, SA-β-gal staining is a convenient and accepted method to detect cellular senescence in vitro and even in vivo (18, 26). However, β-gal positive alone is not sufficient to judge whether a cell is in the senescent state. For example, TGF-β stimulation induces SA-β-gal independent of senescence in both cultured human prostate basal cells and epithelial cells in benign prostatic hyperplasia (106). In addition, expression of lysosomal galactosidase beta-1 (GLB1), which accounts for the SA-β-gal activity in some cancer cells, is not correlated with senescence (103). Moreover, in order to measure cellular senescence in vivo, fresh or frozen tissues are required for this staining assay.

3.3. Senescence-Associated Heterochromatic Foci

Cellular senescence is accompanied by formation of facultative heterochromatin, also called senescence-associated heterochromatic foci (SAHF), wherein DAPI staining would show spot-staining patterns (107). In contrast, DAPI staining would show homogenous staining patterns in non-senescent cells (107). SAHF contains histone H3K9 methylation whereas euchromatin contains histone H3K9 acetylation and K4 methylation (107). Meanwhile, the increased incorporation of heterochromatin protein 1γ (HP1γ) into SAHF is distinct from the pericentric heterochromatin (107). Furthermore, γ-H2AX colocalizes with SAHF (108). Importantly, a combination of positive SAHF and γ-H2AX with negative Ki67 (a proliferation index) is a reliable indicator of senescence for cells in culture and in tissues (109, 110). However, SAHF formation is often detected but not a prerequisite for p53-dependent senescence (107, 111).

3.4. p53 Targets Genes

As mentioned above, activation of the p53 pathway is a common cellular response leading to cellular senescence upon exposure to

stress signals (Fig. 2). As a result, senescent cells are characterized by enhanced expression of some p53 targets, such as p21 (30), PML (112), plasminogen activator inhibitor (PAI-1) (113), and DEC1 (101), all of which are recognized as senescence markers, and in turn are able to induce senescence themselves (69, 95, 114–117). p21, a cyclin-dependent kinase inhibitor, plays a critical role in inducing G1 cell cycle arrest by inhibiting the activity of cyclin-CDK2/4 complexes, E2F, and PCNA (118–121). Promyelocytic leukemia protein PML, an essential component of PML nuclear bodies (PML-NBs) that accumulates in senescent cells, is induced by several factors, including oncogenic stress and p53 (112, 116). In turn, PML recruits p16, p53, and pRb/E2F complex to the PML-NBs and hence modulates the expression of downstream target genes of these factors, leading to senescence (116, 122). Importantly, PML forms a positive feedback loop with p53 to trigger cellular senescence by promoting p53 acetylation and phosphorylation or inhibiting p53 degradation by MDM2 (115, 116, 123–125). By contrast, inhibition of p53 acetylation by SIRT1 (a NAD+-dependent class III histone deacetylase) blocks PML-mediated premature senescence (126). PAI-1 induces cellular senescence by inhibiting the activity of uPA, a secreted protein which is capable of activating the MAPK pathway, and subsequently promoting G1/S transition (127). DEC1, a basic helix-loop-helix transcription factor, is capable of inducing DNA damage-induced premature senescence via inhibiting ID1, an oncogene which is found to be downregulated in arrested or senescent cells (128, 129). A recent report showed that Yippee-like-3 (YPEL3), a member of the putative zinc finger motif coding gene family, is regulated by p53 and triggers premature senescence in normal and tumor cells (130). In addition, BTG2, a member of the antiproliferative BTG gene family, is a p53-responsive gene and plays an essential role in replicative senescence (131). Moreover, the miR-34 family is a p53 target and elicits cellular senescence in both primary and tumor cells in response to DNA damage and oncogenic stress (132, 133). It is important to note that p130 is the major pocket protein associated with induction of premature senescence via the DNA damage-p53 signaling cascade in both normal and tumor cells (134–136). However, the mechanism by which p53 increases p130 activity during senescence is still not clear.

Detection of p53 and its downstream effectors can be used to measure the state of senescence for cells both in vitro and in vivo. However, these genes are not always induced in senescent cells by p53 in response to a specific stress signal. Therefore, a combination of multiple senescence markers discussed above together with one or more p53 targets is required to implicate the state of p53-mediated cellular senescence.

4. The Role of p53 Isoforms in Cellular Senescence

The *TP53* gene encodes at least nine different isoforms due to the use of two promoters, two translation initiation sites, and alternative splicing (137) (Fig. 1). The *TP53* gene contains 11 exons. p53, also called α isoform, is a full-length p53 generated from the P1 promoter. An internal promoter in intron 4 leads to production of an N-terminal truncated p53 starting from residue 133, named as Δ133p53 (138). In addition, internal initiation of translation at an AUG codon at position 40 or alternative splice of intron 2 leads to expression of a p53 protein with deletion of the first 39 amino acids, named as Δ40p53 (also called ΔNp53, p47, p53/47, and p44) (138–142). Moreover, alternative splicing of intron 9 produces β and γ isoforms (138), which lack C-terminal oligomerization domain but contain 10 and 15 unique amino acids at C-termini, respectively (Fig. 1). As a result, nine p53 isoforms, p53α (full-length p53, referred to as p53 in this chapter), p53β (also called p53I9 (143)), p53γ, Δ40p53α, Δ40p53β, Δ40p53γ, Δ133p53α, Δ133p53β, and Δ133p53γ, are expressed. These p53 isoforms are found to be expressed in normal human tissues in a tissue-dependent manner as well as in some tumor tissues (137). This suggests that the expression pattern of p53 isoforms may play a role in tumor formation and affect the outcomes of cancer therapy.

Under an unstressed condition, p53β itself preferentially binds to the p21 and Bax (a pro-apoptotic gene) promoters rather than to the MDM2 promoter, but has no effect on p53 activity (138). However, in response to a stress signal, p53β specifically enhances the Bax gene transcription through physical interaction with p53 and slightly increases p53-mediated apoptosis (138). In contrast, Δ133p53, which lacks the entire N-terminal AD, is dominant-negative over p53 and diminishes p53-mediated apoptosis (138). Interestingly, it has been shown that induction of p53β and suppression of Δ133p53 lead to induction of p21 and miR-34, resulting in senescence in cultured cells and colon adenomas (144). This indicates that the biological activity of full-length p53 is likely modulated by its isoforms in normal and tumor tissues. However, other groups have reported that p53β, which lacks the C-terminal BD and most of the TD, is deficient in DNA binding activity and unable to modulate p53-dependent stress responses (143, 145). Furthermore, ΔNp53 is implicated in G2 cell cycle arrest (146). Therefore, further studies are needed to clarify the mechanism by which p53 isoforms affect each other's functions.

5. The Role of p53 Protein Isoforms in Aging

It has been proposed that aging is characterized by decreased capability to maintain and repair somatic cells (147). One of the causes for aging is associated with senescence-mediated decline in the number and/or proliferative capacity of adult stem cells (148, 149). Indeed, elevated expression of senescence-associated markers, SA-β-gal and p16, is detected in aging tissues (18, 150). As a major mediator of cellular senescence, activation of p53 not only inhibits neoplasia but also promotes organismal aging. Because *Tp53* homozygous knockout mice die from tumors at a young age (8), several mouse models with altered p53 activity have been generated to analyze the role of p53 in aging. These are $Tp53^{+/m}$, Δ40p53-knockin, pL53, and super p53 mouse models (9, 151).

$Tp53^{+/m}$ mice contain a mutant p53 *m* allele with a deletion mutation in the first six exons of the *Tp53* gene and express an N-terminal truncated p53 protein, called M protein (152). $Tp53^{+/m}$ mice display reduced tumor formation and shortened longevity compared with wild-type littermates (152). However, $Tp53^{m/m}$ mice die before birth and $Tp53^{-/m}$ mice develop tumors similarly to $Tp53^{-/-}$ mice. This suggests that M protein-induced aging phenotypes in $Tp53^{+/m}$ are p53-dependent. Indeed, it has been shown that M protein interacts with and stabilizes p53 by facilitating p53 nuclear localization in the absence of a stress (153). Therefore, it is possible that the resulting phenotypes observed in $Tp53^{+/m}$ mice are due to increased p53 activity. However, this mutant allele also contains a deletion of 24 genes, including *Aloxe3*, *Alox12b*, *Alox15b*, *Chd3*, *Aurkb*, and *Per1*, adjacent to the *Tp53* gene (154). Thus, it is necessary to further analyze whether haploinsufficiency of these 24 genes contributes to altered p53 activity and decreased tumor formation but accelerated aging phenotypes.

Similar to $Tp53^{+/m}$ mice, Δ40p53-knockin mice, that express a naturally occurring N-terminal truncated p53 isoform, exhibit decreased lifespan and several premature aging phenotypes, including shortened reproductive span, lordokyphosis, and a reduced tumor incidence (155). These phenotypes are likely due to enhanced wild-type p53 activity and hyperactivation of insulin-like growth factor 1 (IGF-1) signaling cascade (155), the latter of which is associated with lifespan in many species (156, 157). The elevated IGF-1 signaling in Δ40p53 mice leads to sustained induction of p21 through the MAPK pathway and consequently causes cellular senescence and premature aging phenotypes (155). Similar premature aging phenomena were observed in another line of transgenic mice containing multiple copies of a temperature-sensitive mutant allele p53V135A derived from BALB/c liver DNA, named as

pL53 (158). Together, these results indicate that enhanced p53 activity contributes to aging. This hypothesis is supported by several other accelerated aging mouse models, such as mice deficient in Terc (64), Ku80 (also called Ku86, a regulatory unit of DNA-PK) (159), BRCA1 (a tumor suppressor) (160), and Zmpste24 (also called FACE-1, a metalloproteinase involved in the maturation of Lamin A) (161). Conversely, mice deficient in p66shc, a cytoplasmic signal transducer from activated receptors to Ras, live longer along with decreased p53 activity than wild-type controls (162). However, this hypothesis is challenged by another mouse model, called the "super p53" mice.

The super p53 mice carry extra copies of a complete p53 gene, including the p53 promoter and upstream regulatory region (163). As expected, these mice display augmented p53 activity in response to DNA damage and are tumor-resistant. Interestingly, the super p53 mice have normal lifespan without showing any sign of accelerated aging. Similarly, a "super Ink4a/ARF" mouse strain, which carries a transgenic copy of the entire Ink4a/ARF locus (164), and a mouse strain, which carries a hypomorphic allele of MDM2 (165), were generated, both of which have decreased MDM2 activity and hence enhanced p53 activity. Like the super p53 mice, MDM2 hypomorphic and super Ink4a/ARF mice are resistant to spontaneous and carcinogene-induced tumor formation without premature aging. Moreover, the super p53/p19^{ARF} mice, carrying additional copies of both *Tp53* and ARF alleles, were generated by cross-breeding the super p53 mice with the super Ink4a/ARF mice and hence p53 can be further activated (166). Surprisingly, the super p53/p19^{ARF} mice are not only cancer free but also have a significantly extended lifespan. These findings suggest that there is no causal relationship between increased p53-mediated tumor suppression and decreased longevity. Instead, p53 activation in certain circumstances exerts benefits on longevity. There are several potential explanations. First, aging is a consequence of accumulation of DNA damage in tissues, and therefore, by modulating the DDR, p53 is able to reduce age-associated DNA damage and accumulation of damaged cells. Second, p53 activation plays a role in maintaining the stem-cell pool in adult tissues. Third, p53 regulates aging process by modulating other signaling pathways affecting longevity, such as the insulin/IGF-1 and mTOR signaling (167–169). Fourth, p53 may have pro-longevity effects by restraining secretion of the senescence-associated pro-inflammatory cytokines (170, 171), which are known to contribute to chronic age-related inflammation. However, the precise mechanism by which p53 controls the balance between anti-aging and pro-aging needs to be further explored.

6. The Role of p63 and p73 in Cellular Senescence and Aging

p63 and p73, two p53-ancestral genes (172, 173), share highly amino-acid identity with p53 within the AD, DBD, and TD (174, 175) (Fig. 3). The highest degree of homology among the three members is observed within the DBD (>60% amino-acid identity between p53 and p63/p73, and ~85% amino-acid identity between p63 and p73). Unlike p53, the alpha isoforms of p63 and p73 contain a C-terminal sterile alpha motif (SAM), a protein interaction domain involved in developmental regulation. In addition, multiple protein products are generated from both p63 and p73 genes due to the usage of two promoters and alternative RNA splicing (Fig. 3). Therefore, p63 and p73 isoforms possess one of two N termini, transcriptional active (TA) and N-terminally deleted (ΔN), each with five different C termini for p63 (α–ε) (173, 176) and at least ten different C termini for p73 (α–η, η1, η′, and θ)

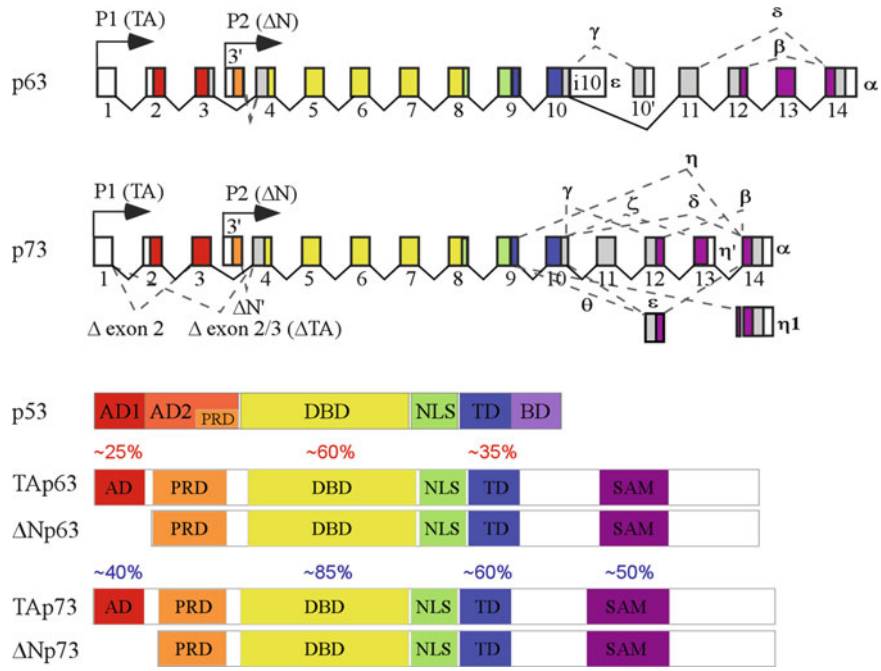

Fig. 3. The p63 and p73 genes and protein structures. (**a**) *TP63* and *TP73* genes. Transcripts initiated from P1 and P2 promoters give rise to TA and ΔN protein isoforms, respectively. Alternative splicing at C-termini of *TP63* transcripts leads to production of p63α, β (Δ exon 13), γ (Δ exons 11–14 and incorporated with additional sequence from exon 10′), δ (Δ exons 12 and 13), and ε (generated by alternative termination in exon 10). Alternative splicing at C-termini of *TP73* transcripts leads to production of p73α, β (Δ exon 13), g (Δ exon 11), δ (Δ exons 11–13), ζ (Δ exons 11 and 12), ε (Δ exons 11 and 13), θ (Δ exons 10, 11, and 13), η (Δ exons 10–13), η1 (Δ 2 nucleotides at 3′-end of exon 9 and contains 18 nucleotides from exon 13, compared with h), and η′ (generated by alternative termination in exon 13). Alternative splicing at N-termini of *TP73* transcripts leads to production of ΔN′p73 and ΔTAp73 (ΔEx2 and ΔEx2/3). Δ, deleted. (**b**) Homology among the p53 family members. Compared to p53, the α isoforms of p63 and p73 have a unique C-terminal SAM (sterile alpha motif) domain. A high degree of sequence identity is seen between p53 and p63/p73 (on *top*) and between p63 and p73 (at *bottom*).

(172, 177–180). Furthermore, alternative splicing of p73 exon 2 and 3 gives rise to two additional p73 isoforms, ΔN′p73 and ΔTAp73 (ΔEx2 and ΔEx2/3) (172, 179, 181).

Unlike *Tp53* knockout mice that are prone to tumor formation, *Tp63* knockout mice show severe defect in limb formation and epidermal development (182, 183) and p73-null mice exhibit developmental defects in central nervous system and inflammatory response (184). These suggest that p63 and p73 play a key role in development. However, due to the high sequence similarity among the p53 family, p63 and p73 act synergistically or antagonistically with p53 in regulating p53-mediated biological activities. Indeed, p63 and p73, especially their TA isoforms, are able to bind to p53-responsive elements and transactivate a set of p53 targets, such as p21, MDM2, Bax, and PUMA, and regulate cell cycle arrest and cell death (174, 185, 186). Recent reports showed that p63 and p73 are also involved in regulating cellular senescence (Fig. 4).

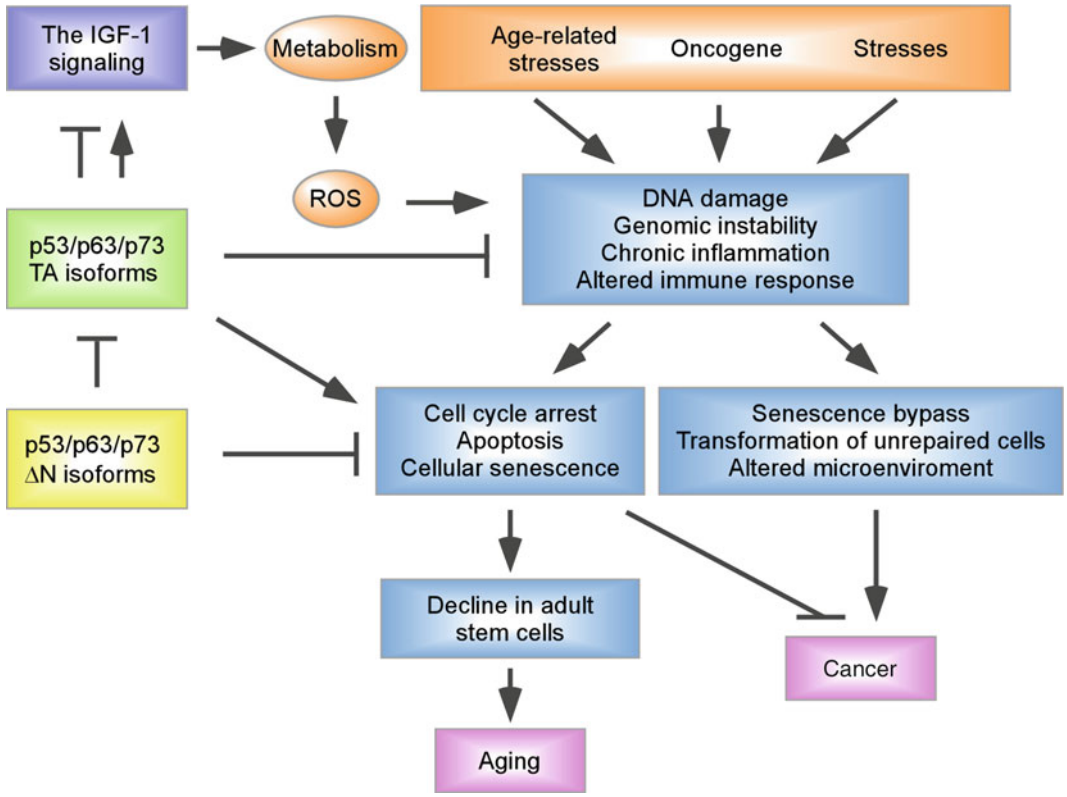

Fig. 4. The role of p53 family proteins in cancer and aging. Accumulation of abnormal cells caused by aging-associated damage, aberrant oncogenic activity, and other stress signals, contributes to both aging and cancer. Activation of the p53 pathway in response to these stress signals is able to protect adult stem cells to promote longevity and prevent malignant transformation by repairing or eliminating damaged cells. However, accumulation of senescent cells in tissues due to activation of TA isoforms of p53 family members, leads to decline in adult stem cells and accelerated aging. In addition, p53 family members are capable of targeting the IGF-1 signaling cascade, a pathway known to be involved in organismal aging, to regulate longevity. In contrast, ΔN isoforms of p53 family are found to be required for maintenance of stem cell proliferation and act as dominate negative inhibitors of TA counterparts.

Results obtained from *Tp63* knockout mice suggest that p63 is an essential regulator for epidermal homeostasis (182, 183). Indeed, ΔNp63 plays a predominant role in epidermal commitment during embryogenesis (187, 188). In addition, ΔNp63 is highly expressed in the basal layer of stratified epithelia to maintain proliferative potential and direct proper differentiation of progenitor cells (189, 190). Moreover, *TAp63*-specific knockout mice do not display the same impaired skin development as p63-null mice (191), whereas ΔNp63-null mice develop lesions that resemble those seen in AEC (ankyloblepharon ectodermal dysplasia and clefting) patients, an ectodermal dysplasia characterized by skin fragility (192). This further confirms the critical role of ΔNp63 in epidermal morphogenesis. However, as a p53 homolog, mice deficient in TAp63 develop metastatic tumors (193). In addition, loss of p63 or TAp63 increases the number of metastatic tumors in $Tp53^{+/-}$ and $Tp53^{-/-}$ mice (193, 194). Surprisingly, although *Tp53* heterozygous mice develop tumors, *Tp63* heterozygous mice are tumor-resistant or develop a few tumors along with a decreased lifespan and accelerated aging phenotypes, similar to $Tp53^{+/m}$ mice (195). Consistently, ablation of p63 induces cellular senescence in primary kerotinocytes (195). In addition, germline- or tissue-specific p63 deficiency also leads to enhanced expression of senescence markers, including SA-β-gal and PML, concomitant with premature aging features (195). Importantly, a report showed that four females from a family with Rapp–Hodgkin syndrome (RHS), a disease associated with *TP63* mutations, present not only typical RHS (anhidrotic ectodermal dysplasia with cleft lip and palate) but also ophthalmic anomalies such as corneal dystrophy and premature menopause (around 30 years) (196). These data suggest that p63 is implicated in aging progression. It has been shown that overexpression of ΔNp63α inhibits OIS and promotes tumorigenesis in vivo (197), whereas ectopic expression of TAp63 induces senescence and inhibits progression of established tumors in vivo (198). However, the $TAp63^{-/-}$ mice exhibit signs of premature aging, including hair loss, impaired wound healing, kyphosis, and a shortened lifespan (191). It is postulated that TAp63 is necessary for the survival of adult skin stem cells and thus prevents premature aging (191). In addition, TAp63 was shown to regulate senescence and aging via modulating the p53, p16, and IGF pathways (199, 200). These together indicate that TA and ΔN isoforms of p63 play a dual role in cellular senescence and tissue aging in cell-type and stress-specific manners.

Like p53, p73 is activated in response to various stress signals, including DNA damage and oncogenic activation, and regulates a set of p53-dependent and -independent genes involved in cell cycle arrest and apoptosis (185, 201, 202). In the absence of p53, p73 can compensate for p53 function to induce apoptosis in cancer cells and the status of the *TP73* gene is correlated with the survival

rate for cancer patients (201, 203–207). Likewise, mice heterozygous of both *Tp53* and *Tp73* exhibit increased tumor burden and metastasis compared to mice heterozygous of *Tp53* alone (194). Mice specifically deficient in TAp73 isoform develop spontaneous and carcinogen-induced tumors and cells from TAp73-null mice display genomic instability associated with enhanced aneuploidy (208). By contrast, cells from ΔNp73-null mice are more sensitive to DNA damage-induced apoptosis in a p53-dependent manner and high levels of ΔNp73 expression associates with poor prognosis in human cancers (209). These results demonstrate that TAp73 is a tumor suppressor whereas ΔNp73 acts as an oncogene. However, to date, knowledge on the role of p73 in senescence is limited. Similar to p53 and p63, p73 plays a function in the maintenance of stem cells (Fig. 4). Specifically, it has been shown that ΔNp73 is a potent prosurvival factor for neurons (210–212) and TAp73 is required for the long-term maintenance of neural stem cells to elicit neurogenesis in adults (213). As a result, mice heterozygous of TA or ΔNp73 isoforms display age-related neurodegeneration (214). Similar to p53 and p63, p73 has been shown to inhibit expression of IGF-1 receptor (200, 215, 216). This indicates that the IGF-1 signaling is a common target of the p53 family to modulate aging (Fig. 4). Importantly, a recent report provided evidence for the role of TAp73 in aging. It has been shown that tumor-free TAp73-null mice develop premature aging phenotypes with impaired ROS scavenging compared to wild-type littermates (217). Indeed, TAp73 is crucial to maintain proper mitochondrial functions by directly regulating the expression of mitochondrial complex IV subunit Cox4i1 (cytochrome C oxidase subunit 4 isoform 1) (217). However, the molecular basis for p73 in aging-associated disorders needs to be further uncovered.

7. Summary and Remarks

Proliferating cells can exit from the cell cycle and enter a state of permanent cell cycle arrest when they encounter stress signals originated from telomere shortening, aberrant oncogenic activities, and other DNA damage signals. Senescent cells are distinct from quiescent cells by expression of senescence-associated markers, including SA-β-gal, SAHF, and activation of the p53 or p16 pathway followed by altered gene expression profile. Emerging evidence showed that cellular senescence associates with multiple pathological disorders, including cancer and aging. Importantly, it has been demonstrated in vivo that induction of cellular senescence is a tumor suppression mechanism by blocking malignant transformation at the initial step of tumorigenesis and by clearance of cancer cells at the late stage of tumor progression. However, the

benefit of the cellular senescence-mediated tumor suppression is countered by the cost of accelerated aging. Therefore, a future challenge to develop senescence-based cancer therapy is to reveal the target and pathways that control the balance between cancer and longevity.

As we discussed in this chapter, the p53 family plays a pivotal role in cellular senescence and thus affect cancer progression and aging (Fig. 4). Although induction of cellular senescence by activation of the p53 family contributes to tumor suppression and accelerated aging, reports also showed that the p53 family promotes longevity and maintains tissue homeostasis through protecting renewable stem cells. In addition, studies with the "super p53" mouse models indicate that cancer resistance could be achieved by modulation of p53 activity without causing undesirable effects. Importantly, a combination of increased p53 and ARF activities not only inhibits tumor formation but also increases longevity. Therefore, the p53 pathway is a promising target for senescence-based cancer treatment. However, there are still unsolved questions. For instance, how are p53 isoforms, p63 and p73, involved in making a balance between cancer and aging? What is the molecular basis for p63/p73-mediated cellular senescence? How does p53 family integrate with other signaling pathways related to aging? Therefore, further exploration of these puzzles in vitro and in vivo will enhance our knowledge about the p53 family in senescence-associated diseases and may provide applicable clues for clinical use.

References

1. DeLeo AB, Jay G, Appella E, Dubois GC, Law LW, Old LJ (1979) Detection of a transformation-related antigen in chemically induced sarcomas and other transformed cells of the mouse. Proc Natl Acad Sci U S A 76:2420–2424
2. Lane DP, Crawford LV (1979) T antigen is bound to a host protein in SV40-transformed cells. Nature 278:261–263
3. Linzer DI, Levine AJ (1979) Characterization of a 54 K dalton cellular SV40 tumor antigen present in SV40-transformed cells and uninfected embryonal carcinoma cells. Cell 17:43–52
4. Melero JA, Stitt DT, Mangel WF, Carroll RB (1979) Identification of new polypeptide species (48–55 K) immunoprecipitable by antiserum to purified large T antigen and present in SV40-infected and -transformed cells. Virology 93:466–480
5. Zilfou JT, Lowe SW (2009) Tumor suppressive functions of p53. Cold Spring Harb Perspect Biol 1:a001883
6. Beckerman R, Prives C (2010) Transcriptional regulation by p53. Cold Spring Harb Perspect Biol 2:a000935
7. Petitjean A, Mathe E, Kato S, Ishioka C, Tavtigian SV, Hainaut P, Olivier M (2007) Impact of mutant p53 functional properties on TP53 mutation patterns and tumor phenotype: lessons from recent developments in the IARC TP53 database. Hum Mutat 28:622–629
8. Donehower LA, Harvey M, Slagle BL, McArthur MJ, Montgomery CA Jr, Butel JS, Bradley A (1992) Mice deficient for p53 are developmentally normal but susceptible to spontaneous tumours. Nature 356:215–221
9. Donehower LA (2009) Using mice to examine p53 functions in cancer, aging, and longevity. Cold Spring Harb Perspect Biol 1:a001081
10. Srivastava S, Zou ZQ, Pirollo K, Blattner W, Chang EH (1990) Germ-line transmission of a mutated p53 gene in a cancer-prone family with Li–Fraumeni syndrome. Nature 348:747–749

11. Malkin D, Li FP, Strong LC, Fraumeni JF Jr, Nelson CE, Kim DH, Kassel J, Gryka MA, Bischoff FZ, Tainsky MA et al (1990) Germ line p53 mutations in a familial syndrome of breast cancer, sarcomas, and other neoplasms. Science 250:1233–1238
12. Xue W, Zender L, Miething C, Dickins RA, Hernando E, Krizhanovsky V, Cordon-Cardo C, Lowe SW (2007) Senescence and tumour clearance is triggered by p53 restoration in murine liver carcinomas. Nature 445:656–660
13. Ventura A, Kirsch DG, McLaughlin ME, Tuveson DA, Grimm J, Lintault L, Newman J, Reczek EE, Weissleder R, Jacks T (2007) Restoration of p53 function leads to tumour regression in vivo. Nature 445:661–665
14. Chen Z, Trotman LC, Shaffer D, Lin HK, Dotan ZA, Niki M, Koutcher JA, Scher HI, Ludwig T, Gerald W, Cordon-Cardo C, Pandolfi PP (2005) Crucial role of p53-dependent cellular senescence in suppression of Pten-deficient tumorigenesis. Nature 436:725–730
15. Hayflick L, Moorhead PS (1961) The serial cultivation of human diploid cell strains. Exp Cell Res 25:585–621
16. Hayflick L (1965) The limited in vitro lifetime of human diploid cell strains. Exp Cell Res 37:614–636
17. Matsumura T, Zerrudo Z, Hayflick L (1979) Senescent human diploid cells in culture: survival, DNA synthesis and morphology. J Gerontol 34:328–334
18. Dimri GP, Lee X, Basile G, Acosta M, Scott G, Roskelley C, Medrano EE, Linskens M, Rubelj I, Pereira-Smith O et al (1995) A biomarker that identifies senescent human cells in culture and in aging skin in vivo. Proc Natl Acad Sci U S A 92:9363–9367
19. d'Adda di Fagagna F, Teo SH, Jackson SP (2004) Functional links between telomeres and proteins of the DNA-damage response. Genes Dev 18:1781–1799
20. Bodnar AG, Ouellette M, Frolkis M, Holt SE, Chiu CP, Morin GB, Harley CB, Shay JW, Lichtsteiner S, Wright WE (1998) Extension of life-span by introduction of telomerase into normal human cells. Science 279:349–352
21. Hayflick L (2000) The illusion of cell immortality. Br J Cancer 83:841–846
22. Dimri GP (2005) What has senescence got to do with cancer? Cancer Cell 7:505–512
23. Artandi SE, Attardi LD (2005) Pathways connecting telomeres and p53 in senescence, apoptosis, and cancer. Biochem Biophys Res Commun 331:881–890
24. Serrano M, Lin AW, McCurrach ME, Beach D, Lowe SW (1997) Oncogenic ras provokes premature cell senescence associated with accumulation of p53 and p16INK4a. Cell 88:593–602
25. Chang BD, Broude EV, Dokmanovic M, Zhu H, Ruth A, Xuan Y, Kandel ES, Lausch E, Christov K, Roninson IB (1999) A senescence-like phenotype distinguishes tumor cells that undergo terminal proliferation arrest after exposure to anticancer agents. Cancer Res 59:3761–3767
26. te Poele RH, Okorokov AL, Jardine L, Cummings J, Joel SP (2002) DNA damage is able to induce senescence in tumor cells in vitro and in vivo. Cancer Res 62:1876–1883
27. Ben-Porath I, Weinberg RA (2005) The signals and pathways activating cellular senescence. Int J Biochem Cell Biol 37:961–976
28. Honma S, Kawamoto T, Takagi Y, Fujimoto K, Sato F, Noshiro M, Kato Y, Honma K (2002) Dec1 and Dec2 are regulators of the mammalian molecular clock. Nature 419:841–844
29. Harms KL, Chen X (2006) The functional domains in p53 family proteins exhibit both common and distinct properties. Cell Death Differ 13(6):890–897
30. el-Deiry WS, Kern SE, Pietenpol JA, Kinzler KW, Vogelstein B (1992) Definition of a consensus binding site for p53. Nat Genet 1:45–49
31. Barak Y, Juven T, Haffner R, Oren M (1993) mdm2 expression is induced by wild type p53 activity. EMBO J 12:461–468
32. Haupt Y, Maya R, Kazaz A, Oren M (1997) Mdm2 promotes the rapid degradation of p53. Nature 387:296–299
33. Honda R, Tanaka H, Yasuda H (1997) Oncoprotein MDM2 is a ubiquitin ligase E3 for tumor suppressor p53. FEBS Lett 420:25–27
34. Kubbutat MH, Jones SN, Vousden KH (1997) Regulation of p53 stability by Mdm2. Nature 387:299–303
35. Lavin MF, Gueven N (2006) The complexity of p53 stabilization and activation. Cell Death Differ 13:941–950
36. Olsson A, Manzl C, Strasser A, Villunger A (2007) How important are post-translational modifications in p53 for selectivity in target-gene transcription and tumour suppression? Cell Death Differ 14:1561–1575
37. Toledo F, Wahl GM (2006) Regulating the p53 pathway: in vitro hypotheses, in vivo veritas. Nat Rev Cancer 6:909–923
38. Khosravi R, Maya R, Gottlieb T, Oren M, Shiloh Y, Shkedy D (1999) Rapid ATM-dependent phosphorylation of MDM2

precedes p53 accumulation in response to DNA damage. Proc Natl Acad Sci U S A 96:14973–14977

39. Maya R, Balass M, Kim ST, Shkedy D, Leal JF, Shifman O, Moas M, Buschmann T, Ronai Z, Shiloh Y, Kastan MB, Katzir E, Oren M (2001) ATM-dependent phosphorylation of Mdm2 on serine 395: role in p53 activation by DNA damage. Genes Dev 15:1067–1077
40. Vousden KH, Lane DP (2007) p53 in health and disease. Nat Rev Mol Cell Biol 8:275–283
41. Jenuwein T, Allis CD (2001) Translating the histone code. Science 293:1074–1080
42. Gu W, Roeder RG (1997) Activation of p53 sequence-specific DNA binding by acetylation of the p53 C-terminal domain. Cell 90:595–606
43. Luo J, Su F, Chen D, Shiloh A, Gu W (2000) Deacetylation of p53 modulates its effect on cell growth and apoptosis. Nature 408:377–381
44. Dai C, Gu W (2010) p53 post-translational modification: deregulated in tumorigenesis. Trends Mol Med 16:528–536
45. Knights CD, Catania J, Di Giovanni S, Muratoglu S, Perez R, Swartzbeck A, Quong AA, Zhang X, Beerman T, Pestell RG, Avantaggiati ML (2006) Distinct p53 acetylation cassettes differentially influence gene-expression patterns and cell fate. J Cell Biol 173:533–544
46. Sykes SM, Mellert HS, Holbert MA, Li K, Marmorstein R, Lane WS, McMahon SB (2006) Acetylation of the p53 DNA-binding domain regulates apoptosis induction. Mol Cell 24:841–851
47. Tang Y, Luo J, Zhang W, Gu W (2006) Tip60-dependent acetylation of p53 modulates the decision between cell-cycle arrest and apoptosis. Mol Cell 24:827–839
48. Charvet C, Wissler M, Brauns-Schubert P, Wang SJ, Tang Y, Sigloch FC, Mellert H, Brandenburg M, Lindner SE, Breit B, Green DR, McMahon SB, Borner C, Gu W, Maurer U (2011) Phosphorylation of Tip60 by GSK-3 determines the induction of PUMA and apoptosis by p53. Mol Cell 42:584–596
49. Tang Y, Zhao W, Chen Y, Zhao Y, Gu W (2008) Acetylation is indispensable for p53 activation. Cell 133:612–626
50. Mazan-Mamczarz K, Galban S, Lopez de Silanes I, Martindale JL, Atasoy U, Keene JD, Gorospe M (2003) RNA-binding protein HuR enhances p53 translation in response to ultraviolet light irradiation. Proc Natl Acad Sci U S A 100:8354–8359
51. Takagi M, Absalon MJ, McLure KG, Kastan MB (2005) Regulation of p53 translation and induction after DNA damage by ribosomal protein L26 and nucleolin. Cell 123:49–63
52. Ofir-Rosenfeld Y, Boggs K, Michael D, Kastan MB, Oren M (2008) Mdm2 regulates p53 mRNA translation through inhibitory interactions with ribosomal protein L26. Mol Cell 32:180–189
53. Zhang J, Cho SJ, Shu L, Yan W, Guerrero T, Kent M, Skorupski K, Chen H, Chen X (2011) Translational repression of p53 by RNPC1, a p53 target overexpressed in lymphomas. Genes Dev 25:1528–1543
54. Le MT, Teh C, Shyh-Chang N, Xie H, Zhou B, Korzh V, Lodish HF, Lim B (2009) MicroRNA-125b is a novel negative regulator of p53. Genes Dev 23:862–876
55. Zhang Y, Gao JS, Tang X, Tucker LD, Quesenberry P, Rigoutsos I, Ramratnam B (2009) MicroRNA 125a and its regulation of the p53 tumor suppressor gene. FEBS Lett 583:3725–3730
56. Hu W, Chan CS, Wu R, Zhang C, Sun Y, Song JS, Tang LH, Levine AJ, Feng Z (2010) Negative regulation of tumor suppressor p53 by microRNA miR-504. Mol Cell 38:689–699
57. Karlseder J, Smogorzewska A, de Lange T (2002) Senescence induced by altered telomere state, not telomere loss. Science 295:2446–2449
58. von Zglinicki T, Saretzki G, Ladhoff J, d'Adda di Fagagna F, Jackson SP (2005) Human cell senescence as a DNA damage response. Mech Ageing Dev 126:111–117
59. Harley CB, Futcher AB, Greider CW (1990) Telomeres shorten during ageing of human fibroblasts. Nature 345:458–460
60. d'Adda di Fagagna F, Reaper PM, Clay-Farrace L, Fiegler H, Carr P, Von Zglinicki T, Saretzki G, Carter NP, Jackson SP (2003) A DNA damage checkpoint response in telomere-initiated senescence. Nature 426:194–198
61. Takai H, Smogorzewska A, de Lange T (2003) DNA damage foci at dysfunctional telomeres. Curr Biol 13:1549–1556
62. Pandita TK (2002) ATM function and telomere stability. Oncogene 21:611–618
63. Herbig U, Jobling WA, Chen BP, Chen DJ, Sedivy JM (2004) Telomere shortening triggers senescence of human cells through a pathway involving ATM, p53, and p21(CIP1), but not p16(INK4a). Mol Cell 14:501–513
64. Chin L, Artandi SE, Shen Q, Tam A, Lee SL, Gottlieb GJ, Greider CW, DePinho RA (1999) p53 deficiency rescues the adverse effects of telomere loss and cooperates with telomere dysfunction to accelerate carcinogenesis. Cell 97:527–538

65. Artandi SE, Chang S, Lee SL, Alson S, Gottlieb GJ, Chin L, DePinho RA (2000) Telomere dysfunction promotes non-reciprocal translocations and epithelial cancers in mice. Nature 406:641–645
66. Kemp CJ, Donehower LA, Bradley A, Balmain A (1993) Reduction of p53 gene dosage does not increase initiation or promotion but enhances malignant progression of chemically induced skin tumors. Cell 74:813–822
67. McDuff FK, Turner SD (2011) Jailbreak: oncogene-induced senescence and its evasion. Cell Signal 23:6–13
68. Kuilman T, Michaloglou C, Mooi WJ, Peeper DS (2010) The essence of senescence. Genes Dev 24:2463–2479
69. Qian Y, Chen X (2010) Tumor suppression by p53: making cells senescent. Histol Histopathol 25:515–526
70. Lin AW, Barradas M, Stone JC, van Aelst L, Serrano M, Lowe SW (1998) Premature senescence involving p53 and p16 is activated in response to constitutive MEK/MAPK mitogenic signaling. Genes Dev 12:3008–3019
71. Campbell PM, Groehler AL, Lee KM, Ouellette MM, Khazak V, Der CJ (2007) K-Ras promotes growth transformation and invasion of immortalized human pancreatic cells by Raf and phosphatidylinositol 3-kinase signaling. Cancer Res 67:2098–2106
72. Land H, Parada LF, Weinberg RA (1983) Tumorigenic conversion of primary embryo fibroblasts requires at least two cooperating oncogenes. Nature 304:596–602
73. Sun P, Yoshizuka N, New L, Moser BA, Li Y, Liao R, Xie C, Chen J, Deng Q, Yamout M, Dong MQ, Frangou CG, Yates JR 3rd, Wright PE, Han J (2007) PRAK is essential for ras-induced senescence and tumor suppression. Cell 128:295–308
74. Wang W, Chen JX, Liao R, Deng Q, Zhou JJ, Huang S, Sun P (2002) Sequential activation of the MEK-extracellular signal-regulated kinase and MKK3/6-p38 mitogen-activated protein kinase pathways mediates oncogenic ras-induced premature senescence. Mol Cell Biol 22:3389–3403
75. Sreeramaneni R, Chaudhry A, McMahon M, Sherr CJ, Inoue K (2005) Ras-Raf-Arf signaling critically depends on the Dmp1 transcription factor. Mol Cell Biol 25:220–232
76. Palmero I, Pantoja C, Serrano M (1998) p19ARF links the tumour suppressor p53 to Ras. Nature 395:125–126
77. Bates S, Phillips AC, Clark PA, Stott F, Peters G, Ludwig RL, Vousden KH (1998) $p14^{ARF}$ links the tumour suppressors RB and p53. Nature 395:124–125
78. Inoue K, Roussel MF, Sherr CJ (1999) Induction of ARF tumor suppressor gene expression and cell cycle arrest by transcription factor DMP1. Proc Natl Acad Sci U S A 96:3993–3998
79. Kamb A, Gruis NA, Weaver-Feldhaus J, Liu Q, Harshman K, Tavtigian SV, Stockert E, Day RS 3rd, Johnson BE, Skolnick MH (1994) A cell cycle regulator potentially involved in genesis of many tumor types. Science 264:436–440
80. Quelle DE, Zindy F, Ashmun RA, Sherr CJ (1995) Alternative reading frames of the INK4a tumor suppressor gene encode two unrelated proteins capable of inducing cell cycle arrest. Cell 83:993–1000
81. Pomerantz J, Schreiber-Agus N, Liegeois NJ, Silverman A, Alland L, Chin L, Potes J, Chen K, Orlow I, Lee HW, Cordon-Cardo C, DePinho RA (1998) The Ink4a tumor suppressor gene product, p19Arf, interacts with MDM2 and neutralizes MDM2's inhibition of p53. Cell 92:713–723
82. Honda R, Yasuda H (1999) Association of p19(ARF) with Mdm2 inhibits ubiquitin ligase activity of Mdm2 for tumor suppressor p53. EMBO J 18:22–27
83. Zhang Y, Xiong Y, Yarbrough WG (1998) ARF promotes MDM2 degradation and stabilizes p53: ARF-INK4a locus deletion impairs both the Rb and p53 tumor suppression pathways. Cell 92:725–734
84. Tao W, Levine AJ (1999) P19(ARF) stabilizes p53 by blocking nucleo-cytoplasmic shuttling of Mdm2. Proc Natl Acad Sci U S A 96: 6937–6941
85. Wei W, Hemmer RM, Sedivy JM (2001) Role of p14(ARF) in replicative and induced senescence of human fibroblasts. Mol Cell Biol 21:6748–6757
86. Bartkova J, Rezaei N, Liontos M, Karakaidos P, Kletsas D, Issaeva N, Vassiliou LV, Kolettas E, Niforou K, Zoumpourlis VC, Takaoka M, Nakagawa H, Tort F, Fugger K, Johansson F, Sehested M, Andersen CL, Dyrskjot L, Ornтoft T, Lukas J, Kittas C, Helleday T, Halazonetis TD, Bartek J, Gorgoulis VG (2006) Oncogene-induced senescence is part of the tumorigenesis barrier imposed by DNA damage checkpoints. Nature 444:633–637
87. Di Micco R, Fumagalli M, Cicalese A, Piccinin S, Gasparini P, Luise C, Schurra C, Garre M, Nuciforo PG, Bensimon A, Maestro R, Pelicci PG, d'Adda di Fagagna F (2006) Oncogene-induced senescence is a DNA damage response

triggered by DNA hyper-replication. Nature 444:638–642

88. Halazonetis TD, Gorgoulis VG, Bartek J (2008) An oncogene-induced DNA damage model for cancer development. Science 319: 1352–1355
89. Mallette FA, Gaumont-Leclerc MF, Ferbeyre G (2007) The DNA damage signaling pathway is a critical mediator of oncogene-induced senescence. Genes Dev 21:43–48
90. Irani K, Xia Y, Zweier JL, Sollott SJ, Der CJ, Fearon ER, Sundaresan M, Finkel T, Goldschmidt-Clermont PJ (1997) Mitogenic signaling mediated by oxidants in Ras-transformed fibroblasts. Science 275: 1649–1652
91. Lee AC, Fenster BE, Ito H, Takeda K, Bae NS, Hirai T, Yu ZX, Ferrans VJ, Howard BH, Finkel T (1999) Ras proteins induce senescence by altering the intracellular levels of reactive oxygen species. J Biol Chem 274:7936–7940
92. Lloyd AC (2002) Limits to lifespan. Nat Cell Biol 4:E25–E27
93. Wynford-Thomas D (1999) Cellular senescence and cancer. J Pathol 187:100–111
94. Lowe SW, Cepero E, Evan G (2004) Intrinsic tumour suppression. Nature 432:307–315
95. Collado M, Gil J, Efeyan A, Guerra C, Schuhmacher AJ, Barradas M, Benguria A, Zaballos A, Flores JM, Barbacid M, Beach D, Serrano M (2005) Tumour biology: senescence in premalignant tumours. Nature 436:642
96. Martins CP, Brown-Swigart L, Evan GI (2006) Modeling the therapeutic efficacy of p53 restoration in tumors. Cell 127:1323–1334
97. Wang Y, Blandino G, Oren M, Givol D (1998) Induced p53 expression in lung cancer cell line promotes cell senescence and differentially modifies the cytotoxicity of anti-cancer drugs. Oncogene 17:1923–1930
98. Sugrue MM, Shin DY, Lee SW, Aaronson SA (1997) Wild-type p53 triggers a rapid senescence program in human tumor cells lacking functional p53. Proc Natl Acad Sci U S A 94:9648–9653
99. Ewald JA, Desotelle JA, Wilding G, Jarrard DF (2010) Therapy-induced senescence in cancer. J Natl Cancer Inst 102:1536–1546
100. Chang BD, Xuan Y, Broude EV, Zhu H, Schott B, Fang J, Roninson IB (1999) Role of p53 and p21waf1/cip1 in senescence-like terminal proliferation arrest induced in human tumor cells by chemotherapeutic drugs. Oncogene 18:4808–4818
101. Qian Y, Zhang J, Yan B, Chen X (2008) DEC1, a basic helix-loop-helix transcription factor and a novel target gene of the p53 family, mediates p53-dependent premature senescence. J Biol Chem 283:2896–2905
102. Fang L, Igarashi M, Leung J, Sugrue MM, Lee SW, Aaronson SA (1999) p21Waf1/Cip1/Sdi1 induces permanent growth arrest with markers of replicative senescence in human tumor cells lacking functional p53. Oncogene 18:2789–2797
103. Lee BY, Han JA, Im JS, Morrone A, Johung K, Goodwin EC, Kleijer WJ, DiMaio D, Hwang ES (2006) Senescence-associated beta-galactosidase is lysosomal beta-galactosidase. Aging Cell 5:187–195
104. Kurz DJ, Decary S, Hong Y, Erusalimsky JD (2000) Senescence-associated (beta)-galactosidase reflects an increase in lysosomal mass during replicative ageing of human endothelial cells. J Cell Sci 113(Pt 20):3613–3622
105. Le Gall JY, Khoi TD, Glaise D, Le treut A, Brissot P, Guillouzo A (1979) Lysosomal enzyme activities during ageing of adult human liver cell lines. Mech Ageing Dev 11:287–293
106. Untergasser G, Gander R, Rumpold H, Heinrich E, Plas E, Berger P (2003) TGF-beta cytokines increase senescence-associated beta-galactosidase activity in human prostate basal cells by supporting differentiation processes, but not cellular senescence. Exp Gerontol 38:1179–1188
107. Narita M, Nunez S, Heard E, Lin AW, Hearn SA, Spector DL, Hannon GJ, Lowe SW (2003) Rb-mediated heterochromatin formation and silencing of E2F target genes during cellular senescence. Cell 113:703–716
108. Zhang R, Chen W, Adams PD (2007) Molecular dissection of formation of senescence-associated heterochromatin foci. Mol Cell Biol 27:2343–2358
109. Rastogi S, Joshi B, Dasgupta P, Morris M, Wright K, Chellappan S (2006) Prohibitin facilitates cellular senescence by recruiting specific corepressors to inhibit E2F target genes. Mol Cell Biol 26:4161–4171
110. Lawless C, Wang C, Jurk D, Merz A, Zglinicki T, Passos JF (2010) Quantitative assessment of markers for cell senescence. Exp Gerontol 45:772–778
111. Chan HM, Narita M, Lowe SW, Livingston DM (2005) The p400 E1A-associated protein is a novel component of the p53−>p21 senescence pathway. Genes Dev 19:196–201
112. de Stanchina E, Querido E, Narita M, Davuluri RV, Pandolfi PP, Ferbeyre G, Lowe SW (2004) PML is a direct p53 target that modulates p53 effector functions. Mol Cell 13:523–535

113. Kunz C, Pebler S, Otte J, von der Ahe D (1995) Differential regulation of plasminogen activator and inhibitor gene transcription by the tumor suppressor p53. Nucleic Acids Res 23:3710–3717
114. Noda A, Ning Y, Venable SF, Pereira-Smith OM, Smith JR (1994) Cloning of senescent cell-derived inhibitors of DNA synthesis using an expression screen. Exp Cell Res 211:90–98
115. Pearson M, Carbone R, Sebastiani C, Cioce M, Fagioli M, Saito S, Higashimoto Y, Appella E, Minucci S, Pandolfi PP, Pelicci PG (2000) PML regulates p53 acetylation and premature senescence induced by oncogenic Ras. Nature 406:207–210
116. Ferbeyre G, de Stanchina E, Querido E, Baptiste N, Prives C, Lowe SW (2000) PML is induced by oncogenic ras and promotes premature senescence. Genes Dev 14:2015–2027
117. Mu XC, Higgins PJ (1995) Differential growth state-dependent regulation of plasminogen activator inhibitor type-1 expression in senescent IMR-90 human diploid fibroblasts. J Cell Physiol 165:647–657
118. el-Deiry WS, Tokino T, Velculescu VE, Levy DB, Parsons R, Trent JM, Lin D, Mercer WE, Kinzler KW, Vogelstein B (1993) WAF1, a potential mediator of p53 tumor suppression. Cell 75:817–825
119. Afshari CA, Nichols MA, Xiong Y, Mudryj M (1996) A role for a p21-E2F interaction during senescence arrest of normal human fibroblasts. Cell Growth Differ 7:979–988
120. Li R, Waga S, Hannon GJ, Beach D, Stillman B (1994) Differential effects by the p21 CDK inhibitor on PCNA-dependent DNA replication and repair. Nature 371:534–537
121. Waga S, Hannon GJ, Beach D, Stillman B (1994) The p21 inhibitor of cyclin-dependent kinases controls DNA replication by interaction with PCNA. Nature 369:574–578
122. Vernier M, Bourdeau V, Gaumont-Leclerc MF, Moiseeva O, Begin V, Saad F, Mes-Masson AM, Ferbeyre G (2011) Regulation of E2Fs and senescence by PML nuclear bodies. Genes Dev 25:41–50
123. Bischof O, Kirsh O, Pearson M, Itahana K, Pelicci PG, Dejean A (2002) Deconstructing PML-induced premature senescence. EMBO J 21:3358–3369
124. Bernardi R, Scaglioni PP, Bergmann S, Horn HF, Vousden KH, Pandolfi PP (2004) PML regulates p53 stability by sequestering Mdm2 to the nucleolus. Nat Cell Biol 6:665–672
125. Louria-Hayon I, Grossman T, Sionov RV, Alsheich O, Pandolfi PP, Haupt Y (2003) The promyelocytic leukemia protein protects p53 from Mdm2-mediated inhibition and degradation. J Biol Chem 278:33134–33141
126. Langley E, Pearson M, Faretta M, Bauer UM, Frye RA, Minucci S, Pelicci PG, Kouzarides T (2002) Human SIR2 deacetylates p53 and antagonizes PML/p53-induced cellular senescence. EMBO J 21:2383–2396
127. Andreasen PA, Egelund R, Petersen HH (2000) The plasminogen activation system in tumor growth, invasion, and metastasis. Cell Mol Life Sci 57:25–40
128. Qian Y, Chen X (2008) ID1, inhibitor of differentiation/DNA binding, is an effector of the p53-dependent DNA damage response pathway. J Biol Chem 283:22410–22416
129. Hara E, Yamaguchi T, Nojima H, Ide T, Campisi J, Okayama H, Oda K (1994) Id-related genes encoding helix-loop-helix proteins are required for G1 progression and are repressed in senescent human fibroblasts. J Biol Chem 269:2139–2145
130. Kelley KD, Miller KR, Todd A, Kelley AR, Tuttle R, Berberich SJ (2010) YPEL3, a p53-regulated gene that induces cellular senescence. Cancer Res 70:3566–3575
131. Wheaton K, Muir J, Ma W, Benchimol S (2010) BTG2 antagonizes Pin1 in response to mitogens and telomere disruption during replicative senescence. Aging Cell 9:747–760
132. He L, He X, Lim LP, de Stanchina E, Xuan Z, Liang Y, Xue W, Zender L, Magnus J, Ridzon D, Jackson AL, Linsley PS, Chen C, Lowe SW, Cleary MA, Hannon GJ (2007) A microRNA component of the p53 tumour suppressor network. Nature 447:1130–1134
133. Tazawa H, Tsuchiya N, Izumiya M, Nakagama H (2007) Tumor-suppressive miR-34a induces senescence-like growth arrest through modulation of the E2F pathway in human colon cancer cells. Proc Natl Acad Sci U S A 104:15472–15477
134. Kapic A, Helmbold H, Reimer R, Klotzsche O, Deppert W, Bohn W (2006) Cooperation between p53 and p130(Rb2) in induction of cellular senescence. Cell Death Differ 13:324–334
135. Jackson JG, Pereira-Smith OM (2006) Primary and compensatory roles for RB family members at cell cycle gene promoters that are deacetylated and downregulated in doxorubicin-induced senescence of breast cancer cells. Mol Cell Biol 26:2501–2510
136. Helmbold H, Komm N, Deppert W, Bohn W (2009) Rb2/p130 is the dominating pocket protein in the p53-p21 DNA damage response pathway leading to senescence. Oncogene 28:3456–3467

137. Khoury MP, Bourdon JC (2010) The isoforms of the p53 protein. Cold Spring Harb Perspect Biol 2:a000927
138. Bourdon JC, Fernandes K, Murray-Zmijewski F, Liu G, Diot A, Xirodimas DP, Saville MK, Lane DP (2005) p53 isoforms can regulate p53 transcriptional activity. Genes Dev 19:2122–2137
139. Courtois S, Verhaegh G, North S, Luciani MG, Lassus P, Hibner U, Oren M, Hainaut P (2002) DeltaN-p53, a natural isoform of p53 lacking the first transactivation domain, counteracts growth suppression by wild-type p53. Oncogene 21:6722–6728
140. Ghosh A, Stewart D, Matlashewski G (2004) Regulation of human p53 activity and cell localization by alternative splicing. Mol Cell Biol 24:7987–7997
141. Yin Y, Stephen CW, Luciani MG, Fahraeus R (2002) p53 Stability and activity is regulated by Mdm2-mediated induction of alternative p53 translation products. Nat Cell Biol 4:462–467
142. Rovinski B, Munroe D, Peacock J, Mowat M, Bernstein A, Benchimol S (1987) Deletion of 5′-coding sequences of the cellular p53 gene in mouse erythroleukemia: a novel mechanism of oncogene regulation. Mol Cell Biol 7:847–853
143. Flaman JM, Waridel F, Estreicher A, Vannier A, Limacher JM, Gilbert D, Iggo R, Frebourg T (1996) The human tumour suppressor gene p53 is alternatively spliced in normal cells. Oncogene 12:813–818
144. Fujita K, Mondal AM, Horikawa I, Nguyen GH, Kumamoto K, Sohn JJ, Bowman ED, Mathe EA, Schetter AJ, Pine SR, Ji H, Vojtesek B, Bourdon JC, Lane DP, Harris CC (2009) p53 isoforms Delta133p53 and p53beta are endogenous regulators of replicative cellular senescence. Nat Cell Biol 11:1135–1142
145. Graupner V, Schulze-Osthoff K, Essmann F, Janicke RU (2009) Functional characterization of p53beta and p53gamma, two isoforms of the tumor suppressor p53. Cell Cycle 8:1238–1248
146. Olivares-Illana V, Fahraeus R (2010) p53 isoforms gain functions. Oncogene 29: 5113–5119
147. Kirkwood TB, Austad SN (2000) Why do we age? Nature 408:233–238
148. Sharpless NE, DePinho RA (2007) How stem cells age and why this makes us grow old. Nat Rev Mol Cell Biol 8:703–713
149. Sharpless NE, DePinho RA (2004) Telomeres, stem cells, senescence, and cancer. J Clin Invest 113:160–168
150. Kim WY, Sharpless NE (2006) The regulation of INK4/ARF in cancer and aging. Cell 127:265–275
151. Papazoglu C, Mills AA (2007) p53: at the crossroad between cancer and ageing. J Pathol 211:124–133
152. Tyner SD, Venkatachalam S, Choi J, Jones S, Ghebranious N, Igelmann H, Lu X, Soron G, Cooper B, Brayton C, Hee Park S, Thompson T, Karsenty G, Bradley A, Donehower LA (2002) p53 mutant mice that display early ageing-associated phenotypes. Nature 415:45–53
153. Moore L, Lu X, Ghebranious N, Tyner S, Donehower LA (2007) Aging-associated truncated form of p53 interacts with wild-type p53 and alters p53 stability, localization, and activity. Mech Ageing Dev 128:717–730
154. Gentry A, Venkatachalam S (2005) Complicating the role of p53 in aging. Aging Cell 4:157–160
155. Maier B, Gluba W, Bernier B, Turner T, Mohammad K, Guise T, Sutherland A, Thorner M, Scrable H (2004) Modulation of mammalian life span by the short isoform of p53. Genes Dev 18:306–319
156. Tatar M, Bartke A, Antebi A (2003) The endocrine regulation of aging by insulin-like signals. Science 299:1346–1351
157. Kurosu H, Yamamoto M, Clark JD, Pastor JV, Nandi A, Gurnani P, McGuinness OP, Chikuda H, Yamaguchi M, Kawaguchi H, Shimomura I, Takayama Y, Herz J, Kahn CR, Rosenblatt KP, Kuro-o M (2005) Suppression of aging in mice by the hormone Klotho. Science 309:1829–1833
158. Lavigueur A, Maltby V, Mock D, Rossant J, Pawson T, Bernstein A (1989) High incidence of lung, bone, and lymphoid tumors in transgenic mice overexpressing mutant alleles of the p53 oncogene. Mol Cell Biol 9:3982–3991
159. Lim DS, Vogel H, Willerford DM, Sands AT, Platt KA, Hasty P (2000) Analysis of ku80-mutant mice and cells with deficient levels of p53. Mol Cell Biol 20:3772–3780
160. Cao L, Li W, Kim S, Brodie SG, Deng CX (2003) Senescence, aging, and malignant transformation mediated by p53 in mice lacking the Brca1 full-length isoform. Genes Dev 17:201–213
161. Varela I, Cadinanos J, Pendas AM, Gutierrez-Fernandez A, Folgueras AR, Sanchez LM, Zhou Z, Rodriguez FJ, Stewart CL, Vega JA, Tryggvason K, Freije JM, Lopez-Otin C (2005) Accelerated ageing in mice deficient in Zmpste24 protease is linked to p53 signalling activation. Nature 437:564–568

162. Migliaccio E, Giorgio M, Mele S, Pelicci G, Reboldi P, Pandolfi PP, Lanfrancone L, Pelicci PG (1999) The p66shc adaptor protein controls oxidative stress response and life span in mammals. Nature 402:309–313
163. Garcia-Cao I, Garcia-Cao M, Martin-Caballero J, Criado LM, Klatt P, Flores JM, Weill JC, Blasco MA, Serrano M (2002) "Super p53" mice exhibit enhanced DNA damage response, are tumor resistant and age normally. EMBO J 21:6225–6235
164. Matheu A, Pantoja C, Efeyan A, Criado LM, Martin-Caballero J, Flores JM, Klatt P, Serrano M (2004) Increased gene dosage of Ink4a/Arf results in cancer resistance and normal aging. Genes Dev 18:2736–2746
165. Mendrysa SM, O'Leary KA, McElwee MK, Michalowski J, Eisenman RN, Powell DA, Perry ME (2006) Tumor suppression and normal aging in mice with constitutively high p53 activity. Genes Dev 20:16–21
166. Matheu A, Maraver A, Klatt P, Flores I, Garcia-Cao I, Borras C, Flores JM, Vina J, Blasco MA, Serrano M (2007) Delayed ageing through damage protection by the Arf/p53 pathway. Nature 448:375–379
167. Feng Z, Lin M, Wu R (2011) The regulation of aging and longevity: a new and complex role of p53. Genes Cancer 2:443–452
168. Feng Z, Levine AJ (2010) The regulation of energy metabolism and the IGF-1/mTOR pathways by the p53 protein. Trends Cell Biol 20:427–434
169. Korotchkina LG, Leontieva OV, Bukreeva EI, Demidenko ZN, Gudkov AV, Blagosklonny MV (2010) The choice between p53-induced senescence and quiescence is determined in part by the mTOR pathway. Aging (Albany NY) 2:344–352
170. Coppe JP, Patil CK, Rodier F, Sun Y, Munoz DP, Goldstein J, Nelson PS, Desprez PY, Campisi J (2008) Senescence-associated secretory phenotypes reveal cell-nonautonomous functions of oncogenic RAS and the p53 tumor suppressor. PLoS Biol 6:2853–2868
171. de Keizer PL, Laberge RM, Campisi J (2010) p53: pro-aging or pro-longevity? Aging (Albany NY) 2:377–379
172. Kaghad M, Bonnet H, Yang A, Creancier L, Biscan JC, Valent A, Minty A, Chalon P, Lelias JM, Dumont X, Ferrara P, McKeon F, Caput D (1997) Monoallelically expressed gene related to p53 at 1p36, a region frequently deleted in neuroblastoma and other human cancers. Cell 90:809–819
173. Yang A, Kaghad M, Wang Y, Gillett E, Fleming MD, Dotsch V, Andrews NC, Caput D, McKeon F (1998) p63, a p53 homolog at 3q27-29, encodes multiple products with transactivating, death-inducing, and dominant-negative activities. Mol Cell 2:305–316
174. Harms K, Nozell S, Chen X (2004) The common and distinct target genes of the p53 family transcription factors. Cell Mol Life Sci 61:822–842
175. Moll UM, Slade N (2004) p63 and p73: roles in development and tumor formation. Mol Cancer Res 2:371–386
176. Mangiulli M, Valletti A, Caratozzolo MF, Tullo A, Sbisa E, Pesole G, D'Erchia AM (2009) Identification and functional characterization of two new transcriptional variants of the human p63 gene. Nucleic Acids Res 37:6092–6104
177. De Laurenzi V, Costanzo A, Barcaroli D, Terrinoni A, Falco M, Annicchiarico-Petruzzelli M, Levrero M, Melino G (1998) Two new p73 splice variants, gamma and delta, with different transcriptional activity. J Exp Med 188:1763–1768
178. De Laurenzi VD, Catani MV, Terrinoni A, Corazzari M, Melino G, Costanzo A, Levrero M, Knight RA (1999) Additional complexity in p73: induction by mitogens in lymphoid cells and identification of two new splicing variants epsilon and zeta. Cell Death Differ 6:389–390
179. Ishimoto O, Kawahara C, Enjo K, Obinata M, Nukiwa T, Ikawa S (2002) Possible oncogenic potential of DeltaNp73: a newly identified isoform of human p73. Cancer Res 62:636–641
180. Scaruffi P, Casciano I, Masiero L, Basso G, Romani M, Tonini GP (2000) Lack of p73 expression in mature B-ALL and identification of three new splicing variants restricted to pre B and C-ALL indicate a role of p73 in B cell ALL differentiation. Leukemia 14:518–519
181. Stiewe T, Theseling CC, Putzer BM (2002) Transactivation-deficient Delta TA-p73 inhibits p53 by direct competition for DNA binding: implications for tumorigenesis. J Biol Chem 277:14177–14185
182. Mills AA, Zheng B, Wang XJ, Vogel H, Roop DR, Bradley A (1999) p63 is a p53 homologue required for limb and epidermal morphogenesis. Nature 398:708–713
183. Yang A, Schweitzer R, Sun D, Kaghad M, Walker N, Bronson RT, Tabin C, Sharpe A, Caput D, Crum C, McKeon F (1999) p63 is essential for regenerative proliferation in limb, craniofacial and epithelial development. Nature 398:714–718
184. Yang A, Walker N, Bronson R, Kaghad M, Oosterwegel M, Bonnin J, Vagner C,

Bonnet H, Dikkes P, Sharpe A, McKeon F, Caput D (2000) p73-deficient mice have neurological, pheromonal and inflammatory defects but lack spontaneous tumours. Nature 404:99–103

185. Zhu J, Jiang J, Zhou W, Chen X (1998) The potential tumor suppressor p73 differentially regulates cellular p53 target genes. Cancer Res 58:5061–5065
186. Dohn M, Zhang S, Chen X (2001) p63alpha and DeltaNp63alpha can induce cell cycle arrest and apoptosis and differentially regulate p53 target genes. Oncogene 20:3193–3205
187. Shalom-Feuerstein R, Lena AM, Zhou H, De La Forest Divonne S, Van Bokhoven H, Candi E, Melino G, Aberdam D (2011) DeltaNp63 is an ectodermal gatekeeper of epidermal morphogenesis. Cell Death Differ 18:887–896
188. Medawar A, Virolle T, Rostagno P, de la Forest-Divonne S, Gambaro K, Rouleau M, Aberdam D (2008) DeltaNp63 is essential for epidermal commitment of embryonic stem cells. PLoS One 3:e3441
189. Lee H, Kimelman D (2002) A dominant-negative form of p63 is required for epidermal proliferation in zebrafish. Dev Cell 2:607–616
190. Koster MI, Kim S, Mills AA, DeMayo FJ, Roop DR (2004) p63 is the molecular switch for initiation of an epithelial stratification program. Genes Dev 18:126–131
191. Su X, Paris M, Gi YJ, Tsai KY, Cho MS, Lin YL, Biernaskie JA, Sinha S, Prives C, Pevny LH, Miller FD, Flores ER (2009) TAp63 prevents premature aging by promoting adult stem cell maintenance. Cell Stem Cell 5:64–75
192. Koster MI, Marinari B, Payne AS, Kantaputra PN, Costanzo A, Roop DR (2009) DeltaNp63 knockdown mice: a mouse model for AEC syndrome. Am J Med Genet A 149A:1942–1947
193. Su X, Chakravarti D, Cho MS, Liu L, Gi YJ, Lin YL, Leung ML, El-Naggar A, Creighton CJ, Suraokar MB, Wistuba I, Flores ER (2010) TAp63 suppresses metastasis through coordinate regulation of Dicer and miRNAs. Nature 467:986–990
194. Flores ER, Sengupta S, Miller JB, Newman JJ, Bronson R, Crowley D, Yang A, McKeon F, Jacks T (2005) Tumor predisposition in mice mutant for p63 and p73: evidence for broader tumor suppressor functions for the p53 family. Cancer Cell 7:363–373
195. Keyes WM, Wu Y, Vogel H, Guo X, Lowe SW, Mills AA (2005) p63 deficiency activates a program of cellular senescence and leads to accelerated aging. Genes Dev 19:1986–1999
196. Holder-Espinasse M, Martin-Coignard D, Escande F, Manouvrier-Hanu S (2007) A new mutation in TP63 is associated with age-related pathology. Eur J Hum Genet 15:1115–1120
197. Keyes WM, Pecoraro M, Aranda V, Vernersson-Lindahl E, Li W, Vogel H, Guo X, Garcia EL, Michurina TV, Enikolopov G, Muthuswamy SK, Mills AA (2011) DeltaNp63alpha is an oncogene that targets chromatin remodeler Lsh to drive skin stem cell proliferation and tumorigenesis. Cell Stem Cell 8:164–176
198. Guo X, Keyes WM, Papazoglu C, Zuber J, Li W, Lowe SW, Vogel H, Mills AA (2009) TAp63 induces senescence and suppresses tumorigenesis in vivo. Nat Cell Biol 11:1451–1457
199. Keyes WM, Mills AA (2006) p63: a new link between senescence and aging. Cell Cycle 5:260–265
200. Nahor I, Abramovitch S, Engeland K, Werner H (2005) The p53-family members p63 and p73 inhibit insulin-like growth factor-I receptor gene expression in colon cancer cells. Growth Horm IGF Res 15:388–396
201. Stiewe T, Putzer BM (2000) Role of the p53-homologue p73 in E2F1-induced apoptosis. Nat Genet 26:464–469
202. Jost CA, Marin MC, Kaelin WG Jr (1997) p73 is a simian [correction of human] p53-related protein that can induce apoptosis. Nature 389:191–194
203. Irwin M, Marin MC, Phillips AC, Seelan RS, Smith DI, Liu W, Flores ER, Tsai KY, Jacks T, Vousden KH, Kaelin WG Jr (2000) Role for the p53 homologue p73 in E2F-1-induced apoptosis. Nature 407:645–648
204. Lissy NA, Davis PK, Irwin M, Kaelin WG, Dowdy SF (2000) A common E2F-1 and p73 pathway mediates cell death induced by TCR activation. Nature 407:642–645
205. Irwin MS, Kondo K, Marin MC, Cheng LS, Hahn WC, Kaelin WG Jr (2003) Chemosensitivity linked to p73 function. Cancer Cell 3:403–410
206. Zhu J, Nozell S, Wang J, Jiang J, Zhou W, Chen X (2001) p73 cooperates with DNA damage agents to induce apoptosis in MCF7 cells in a p53-dependent manner. Oncogene 20:4050–4057
207. Gong JG, Costanzo A, Yang HQ, Melino G, Kaelin WG Jr, Levrero M, Wang JY (1999) The tyrosine kinase c-Abl regulates p73 in apoptotic response to cisplatin-induced DNA damage. Nature 399:806–809

208. Tomasini R, Tsuchihara K, Wilhelm M, Fujitani M, Rufini A, Cheung CC, Khan F, Itie-Youten A, Wakeham A, Tsao MS, Iovanna JL, Squire J, Jurisica I, Kaplan D, Melino G, Jurisicova A, Mak TW (2008) TAp73 knockout shows genomic instability with infertility and tumor suppressor functions. Genes Dev 22:2677–2691

209. Wilhelm MT, Rufini A, Wetzel MK, Tsuchihara K, Inoue S, Tomasini R, Itie-Youten A, Wakeham A, Arsenian-Henriksson M, Melino G, Kaplan DR, Miller FD, Mak TW (2010) Isoform-specific p73 knockout mice reveal a novel role for delta Np73 in the DNA damage response pathway. Genes Dev 24:549–560

210. Pozniak CD, Radinovic S, Yang A, McKeon F, Kaplan DR, Miller FD (2000) An anti-apoptotic role for the p53 family member, p73, during developmental neuron death. Science 289:304–306

211. Pozniak CD, Barnabe-Heider F, Rymar VV, Lee AF, Sadikot AF, Miller FD (2002) p73 is required for survival and maintenance of CNS neurons. J Neurosci 22:9800–9809

212. Tissir F, Ravni A, Achouri Y, Riethmacher D, Meyer G, Goffinet AM (2009) DeltaNp73 regulates neuronal survival in vivo. Proc Natl Acad Sci U S A 106:16871–16876

213. Fujitani M, Cancino GI, Dugani CB, Weaver IC, Gauthier-Fisher A, Paquin A, Mak TW, Wojtowicz MJ, Miller FD, Kaplan DR (2010) TAp73 acts via the bHLH Hey2 to promote long-term maintenance of neural precursors. Curr Biol 20:2058–2065

214. Wetzel MK, Naska S, Laliberte CL, Rymar VV, Fujitani M, Biernaskie JA, Cole CJ, Lerch JP, Spring S, Wang SH, Frankland PW, Henkelman RM, Josselyn SA, Sadikot AF, Miller FD, Kaplan DR (2008) p73 regulates neurodegeneration and phospho-tau accumulation during aging and Alzheimer's disease. Neuron 59:708–721

215. Werner H, Karnieli E, Rauscher FJ, LeRoith D (1996) Wild-type and mutant p53 differentially regulate transcription of the insulin-like growth factor I receptor gene. Proc Natl Acad Sci U S A 93:8318–8323

216. Feng Z, Hu W, de Stanchina E, Teresky AK, Jin S, Lowe S, Levine AJ (2007) The regulation of AMPK beta1, TSC2, and PTEN expression by p53: stress, cell and tissue specificity, and the role of these gene products in modulating the IGF-1-AKT-mTOR pathways. Cancer Res 67:3043–3053

217. Rufini A, Niklison-Chirou MV, Inoue S, Tomasini R, Harris IS, Marino A, Federici M, Dinsdale D, Knight RA, Melino G, and Mak TW (2012) TAp73 depletion accelerates aging through metabolic dysregulation. Genes Dev 26:2009–2014

Chapter 4

Markers of Cellular Senescence

Amancio Carnero

Abstract

Cellular senescence is a tumor suppression mechanism that evolved to limit duplication in somatic cells. Senescence is imposed by natural replicative boundaries or stress-induced signals, such as oncogenic transformation. Neoplastic cells can be forced to undergo senescence through genetic manipulations and epigenetic factors, including anticancer drugs, radiation, and differentiating agents. Senescent cells show distinct phenotypic and molecular characteristics, both in vitro or in vivo. These biomarkers might either cause or result from senescence induction, but could also be the byproducts of physiological changes in these non-replicating cells.

Key words: Cellular senescence, Immortality, Senescence pathways, Senescence markers, Telomere shortening

1. Introduction

Somatic cells demonstrate a spontaneous decline in growth rate in continuous culture that is not related to time elapsed but to a decreasing number of population doublings. Somatic cell aging eventually terminates in a quiescent but viable state known as replicative senescence (1). These cells show a flat, enlarged morphology with low pH β-gal activity, and they are commonly multinucleated and unresponsive to mitogens or apoptotic stimuli. This behavior is observed in a wide variety of normal cells, and it is widely accepted (2) that normal human somatic cells have an intrinsically limited proliferative lifespan, even under ideal growth conditions. Moreover, the senescent phenotype is associated with dramatic changes in gene-expression (3–6). However, cells displaying characteristics of senescence are observed in response to other stimuli, such as oncogenic stress, DNA damage, or cytotoxic drugs (7).

Senescent features involve most of the physiological aspects of the cell (Fig. 1).

Lorenzo Galluzzi et al. (eds.), *Cell Senescence: Methods and Protocols*, Methods in Molecular Biology, vol. 965,
DOI 10.1007/978-1-62703-239-1_4,

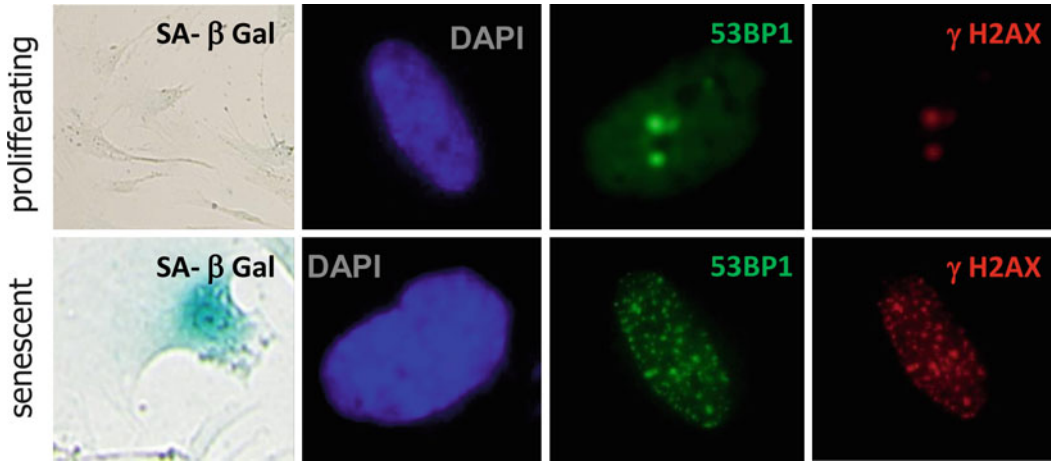

Fig. 1. Examples of molecular markers used to identify cellular senescence. Examples of senescence-associated β-galactosidase (SA-β-gal) activity; senescence-associated heterochromatin foci (SAHF), as identified by immunofluorescence microscopy upon chromatin staining with DAPI; and senescence-associated DNA damage, as visualized by immunofluorescence microscopy upon staining with antibodies that recognize 53BP1 and phosphorylated histone 2AX (γH2AX).

- *Morphological features of senescence*. Senescent cells show flat, enlarged morphology and are commonly multinucleated (see Chapter 5).
- *G1 arrest*. Senescent cells are terminally arrested at G1, showing increased levels of many cell cycle inhibitors (see Chapters 6 and 7).
- *Altered lysosome/vacuoles*. The recycling centers inside of cells are lysosomes. Abnormal chemical structures, which resist degradation, accumulate in the lysosomes during the lifespan of the cells or during stress-induced senescence. The result is the eradication of lysosomal recycling capacity for proteins, lipids, and mitochondria. Consequently, damaged mitochondria accumulate in these cells, which lower ATP production and elevate reactive oxygen species (ROS) production. Furthermore, oxidative damaged enzymes accumulate in the cytosol, which reduces the rate of essential cellular functions.
- *Senescence-associated β-galactosidase* (SA-β-gal), which is detected by histochemical staining of cells with the artificial substrate X-gal. The presence of the SA-β-gal biomarker is independent of DNA synthesis and generally distinguishes senescent cells from quiescent cells. The detection method for SA-β-gal is a convenient, single cell-based assay, which can identify senescent cells even in heterogeneous cell populations and aging tissues, such as skin biopsies from older individuals. Because it is easy to detect, SA-β-gal is a popular biomarker of senescence (see Chapters 8 and 9).

- *Altered methylation*. Genomic methylation status, which influences many cellular processes, such as gene expression and chromatin organization, generally declines during cellular senescence. Hypomethylation has been observed in both replicative senescence and premature senescence, which suggests that genome hypomethylation is necessary to confer an unstable internal environment and conceivably promote cellular senescence (8, 9).
- *Senescence-associated heterochromatin foci (SAHF)*. The initiation of senescence triggers the generation and accumulation of distinct heterochromatic structures, known as senescence-associated heterochromatic foci. The formation of SAHF coincides with the recruitment of heterochromatic proteins and the pRB tumor suppressor to E2F-responsive promoters. SAHF accumulation is associated with stable repression of E2F target genes and does not occur in reversibly arrested cells. SAHF formation and promoter repression depend on the integrity of the pRB pathway (10). These results provide an explanation for the stability of the senescent state. Accordingly, with these results, genome-wide expression analysis indicates that genes whose expression is upregulated during replicative senescence in human cells are physically clustered (11). This phenomenon suggests that senescence is accompanied by alterations in chromatin structure and the opening of certain chromatin domains is responsible for the concurrent upregulation of gene expression during senescence (see Chapter 12).
- *Oxidative stress*. The redox potential poise of some cells changes in response to chemical modifications. This modification results in altered gene expression, enzyme activity, and signaling pathways (see Chapter 17). Finally, oxidative stress results in DNA damage and well in the damage of other molecular species, including proteins and lipids.
- *DNA damage*. Markers of a DNA damage response localize at telomeres in senescent cells after serial passage (12–14), which indicates that the DNA damage response can be triggered by telomere shortening. These markers include nuclear foci of phosphorylated histone H2AX, the localization at double-strand break sites of DNA-repair and DNA-damage checkpoint factors, such as 53BP1, MDC1, and NBS1 (6, 12). Senescent cells also contain activated forms of the DNA-damage checkpoint kinases Chk1 and Chk2. These markers and others suggest that telomere shortening initiates senescence through a DNA damage response. These characteristics also explain why other DNA damage stressors, such as culture shock, potentially initiate senescence without telomere involvement (see Chapter 13).

- *Protein and lipid modification*. Oxidation, glycation, cross-linking, and other chemical modifications impair the molecular functions of multiple vital components, including DNA, membranes, the extracellular matrix (ECM), enzymes, and structural proteins. Modifications that accumulate faster than they are repaired or recycled will cause progressive deterioration over time (see Chapters 18–20).
- *Telomere length*. The telomerase gene is deactivated in many adult human cells. As a result, these cells lose small portions of the ends (telomeres) of their chromosomes each time they divide. This process appears linked to their finite replicative lifespan in cell culture (The Hayflick Limit). However, oncogene- or culture stress-induced senescence does not rely on telomere shortening (see Chapters 14 and 15).
- *Nuclear modifications*. Nuclear structures, such as the nuclear lamina, nucleoli, the nuclear matrix, nuclear bodies (such as promyelocytic leukemia bodies), as well as the overall nuclear morphology are altered within growth-arrested or senescent cells. It is especially interesting that multinucleation is probably the consequence of the failure of nuclear envelope breakdown (see Chapter 16).
- *Senescence-associated secretory phenotype (SASP)*. Senescent cells undergo widespread changes in protein expression and secretion, which ultimately develops into the SASP (15, 16). Senescent cells upregulate the expression and secretion of several matrix metalloproteinases that comprise a conserved genomic cluster and interleukins that promote the growth of premalignant epithelial cells. A limited number of cell culture and mouse xenograft studies support the idea that senescent cells secrete factors that can disrupt tissue structure, alter tissue function and promote cancer progression (17–19). Recent studies on the SASP of human and mouse fibroblasts show it is conserved across cell types and species; moreover, specific secreted factors are strong candidates for stimulating malignant phenotypes in neighboring cells (20–22). The idea that a biological process, such as cellular senescence, can be beneficial (tumor suppressive) and deleterious (pro-tumorigenic) is consistent with a major evolutionary theory of aging termed antagonistic pleiotropy (22). The SASP is possibly the major reason for the deleterious side of the senescence response (23) (see Chapter 11).

Cells displaying senescent characteristics have been observed in cell culture and in their natural tissue environment. Several reports note reduced cellular lifespan with metabolic disease, stress sensitivity, progeria syndromes, and impaired healing, which indicates that entry into cellular senescence possibly contributes to human disease.

It has been suggested that cellular senescence is partially responsible for pathogenesis is numerous human diseases, such as atherosclerosis, osteoarthritis, muscular degeneration, ulcer formation, Alzheimer's dementia, diabetes, and immune exhaustion. Consistent with a role in aging, senescent cells accumulate with age in many rodent and human tissues (24). Moreover, they are found at sites of age-related pathology in degenerative disorders, such as osteoarthritis and atherosclerosis (24), and hyperproliferative lesions, such as benign prostatic hyperplasia (25) and melanocytic nevi (26). Most cancers contain cell populations that have escaped the normal constraints on proliferative potential. Cancer immortality contrasts with the limited lifespan of normal somatic cells. Therefore, it has been proposed that cellular senescence is a major tumor suppressor mechanism that must be overcome during tumorigenesis (2).

The kinetics of replicative senescence do not display abrupt arrest in the whole population, but a gradual decline in a proportion of dividing cells (27). The exact timing of this event varies between cell types and sister clones (28). This behavior is best explained by: (1) an intrinsic control mechanism linked to elapsed cell divisions—the senescence clock—which progressively desensitizes the cell-cycle machinery to growth factor stimulation, and (2) a stochastic component possibly with same basis as that observed in immortal cells under conditions of growth factor restriction. Stem cells can give rise to differentiated progeny and are capable of auto-renewal. In some renewing tissues, stem cells undergo more than 1,000 divisions in a lifetime with no morphological signs of senescence (28). This observation indicates that differentiated cells activate the senescence clock that ultimately induces cell senescence through a series of effectors at a certain point in the lineage.

Due to the broad changes observed in senescent cells, many theories were proposed to explain senescent drift in culture and in vivo. Several hypotheses for cellular clocks driving senescence have been proposed. Most of them focus on error-catastrophe theories, which suggest senescence is a byproduct of life, and deterministic theories, which suggest a genetic program for cellular senescence. A portion of the most representative theories are summarized in Table 1. The finite number of divisions during replicative senescence—referred to as the "Hayflick limit"—is attributed to the progressive shortening of chromosomal ends. Telomere shortening is considered the most probable molecular mechanism for the existence of a senescence clock (29, 30). Eukaryotic cells cannot replicate the distal ends of their chromosomes, the telomeres, which shortens their lengths with every cell division until they reach a critical threshold where cells stop replicating (31). However, enforced replication despite short telomeres generates high chromosomal instability and apoptosis, which is called crisis.

In addition to telomere dysfunction, cellular senescence can be elicited by other types of stress, including oncogene activation (32).

Table 1
Theories explaining cellular senescence (cellular clocks)

Cellular clock	Cause	Molecular outcome
Error-catastrophe theories		
Somatic mutation accumulation	Metabolism/oxygen free radicals	Altered protein function, DNA damage
Mitochondrial DNA mutation	Oxygen free radicals	Altered mitochondrial function
Posttranslational modification of proteins	Oxidation, glycosylation, acetylation, methylation, etc.	Altered protein function
Altered proteolysis	Errors in proteolysis machinery	Accumulation of nonfunctional proteins
Altered lysosomal function	Accumulation of nonrecyclable elements	Accumulation of nonfunctional proteins, mitochondria, or lipids
Deterministic theories		
Telomere shortening	No replication of the telomere ends	DNA damage, exposure of telomere ends, liberation of regulatory proteins, etc.
Changes in hetero-chromatin domains		Altered transcription
Changes in DNA methylation		Altered transcription
Codon restriction	Switching codon preferences in early development restricts availability later in life	Altered protein synthesis
Terminal differentiation	Senescence is a form of genetically controlled terminal differentiation	Changes in physiology

These theories are based on experimental observations of altered features in senescent cells. Although they are implicated in senescence, many of these features are consequences and/or by-products of the induction of senescence

This phenomenon is not observed for oncogenic RAS exclusively; many, but not all, of its effectors, including activated mutants of RAF, MEK, and BRAF, were shown to cause senescence as well as PI3K or AKT (33–36). Also, loss of tumor suppressor such as PTEN or NF1, and other oncogenes such as CDC6, cyclin E, and STAT5 induce senescence and trigger a DNA damage response. This response is associated with DNA hyper-replication and appears causally involved in oncogene-induced senescence (OIS) in vitro (37–40). In contrast to replicative senescence, the occurrence of stress-induced senescence is independent of telomere status (41, 42). Stress-induced premature senescence shares some of the morphological and biochemical features with replicative senescence activated by telomere shortening (43–47), which provides credence to the suggestion that senescence is a common response to cellular damage (48). For the majority of the last decade, OIS has been studied predominantly in cell culture systems, which has triggered a long debate as to whether or not OIS corresponds to a physiologically

relevant phenomenon in vivo. In favor of OIS representing an in vitro-specific phenomenon, artificial conditions (e.g., the use of bovine serum, plastic dishes and the presence of supraphysiologic O2) generate a stress signal that contributes to triggering a cellular senescence response at the very least (49, 50). Conversely, senescence bypass screens have identified several genuine human oncogenes or tumor suppressor genes, including TBX2, BCL6, KLF4, hDRIL, BRF1, PPP1CA, and others (51). Furthermore, virtually all human cancers lack functional p53/pRB pathways, two key senescence signaling routes (52), and often carry mutations in sets of genes that are known to collaborate in vitro in bypassing the senescence response. As of today, many groups have documented the presence of senescent cells induced by oncogenic signaling in several precancerous tissues from human and mouse (26, 32, 53–55). These studies indicate that OIS is an authentic process that does occur in vivo. More importantly, these studies suggest that OIS is an active process in response to oncogenic stimuli and offers a protective mechanism against tumor development.

2. Effector Pathways

Cellular senescence pathways are believed to have multiple layers of regulation, with additional redundancy built into these layers (56–58). Many of the functional studies in which a putative senescence gene is overexpressed in cells indicate that a single gene/pathway is required for repair and subsequent reversion to senescence, suggesting that senescence is essentially a recessive phenomenon.

The effector pathways known to regulate cellular senescence/immortalization, including the $p16^{INK4a}$/pRB pathway and the $p19^{ARF}$/p53/$p21^{CIP1/WAF1}$ pathway are reviewed in (9, 46, 51, 59, 60). Other genes that have been implicated in senescence include PPP1A (61), SAHH (62, 63), Csn2, Arase and BRF1 (64), PGM (65), IGFBP3 and IGFBPrP1 (66), PAI-1 (67, 68), MKK3 (69), MKK6 (69, 70), Smurf2 (71), and HIC-5 (72). Most of these genes can be ascribed to one of the two major senescence pathways. All of these genes have been linked to human tumorigenesis, and these genes and their pathways can act sequentially in a well-regulated process (73).

Replicative senescence, cellular stress or oncogenic Ras can activate p53 to promote cellular senescence, which limits the transforming potential of excessive signaling (74–76). Inhibiting p53 function with dominant negative mutants, specific p53 antisense mRNA, oligonucleotides or viral oncoproteins (such as SV40 T antigen or HPV16 E6) is sufficient to substantially extend the lifespan of several cell types in culture (77). Consistent with these findings, senescence is associated with the transactivation of p53 in

culture (78). Coincident with telomere shortening, DNA-damage checkpoint activation and its associated genomic instability, p53 is also activated in vivo (79). Deletion of p53 attenuated the cellular and organismal effects of telomere dysfunction, which establishes a key role for p53 in telomere shortening (79).

Other p53 regulatory proteins are involved in senescence. MDM2 protein has p53 ubiquitin ligase activity and forms an autoregulatory loop with p53 (80). Overexpression of MDM2 targets p53 for degradation and induces functional p53 depletion (81). Expression of another factor that is upregulated in senescence—$p14^{ARF}$—can release p53 from MDM2 inhibition and cause growth arrest in young fibroblasts (81). Seeding mouse embryonic fibroblasts (MEFs) into culture induces the synthesis of ARF protein, which continues to accumulate until the cells enter senescence (82). MEFs derived from ARF-disrupted mice (82) or wild-type fibroblasts expressing an efficient ARF antisense construct (83) are efficiently immortalized. Concomitant with this observation, overexpression of MDM2 in naïve MEFs produces efficient immortalization (83).

Activation of p53 induces the upregulation of the cyclin-dependent kinase (CDK) inhibitor $p21^{WAF1}$, which directly inhibits cell-cycle machinery (52) and correlates well with declining growth rate in senescing cultures. However, in mouse embryo fibroblasts, the absence of $p21^{WAF1}$ does not overcome senescence (84, 85). This finding suggests that at least one additional downstream effector is needed for p53-induced growth arrest in senescence. In contrast, a different behavior is observed in human cells, where elimination of p21 by a double round of homologous recombination is sufficient to bypass senescence (86). Other p53 effectors are also potentially involved, such as 14-3-3 and GADD45, which inhibit G2/M transition, or downregulation of myc (87) (Leal and Carnero, unpublished results).

The p53 transcriptional program includes the activation of a number of cell cycle inhibitors and proapoptotic proteins, which results in apoptosis, reversible proliferative arrest or cellular senescence (88). The various outcomes of p53 activation might be influenced by quantitative or qualitative mechanisms (89). Two different, though not mutually exclusive, models have been proposed to explain the various biological outcomes associated with p53 activation. The quantitative model implies that differences in p53 levels are sufficient to determine the outcome (90, 91), which is perhaps based on differential p53 affinity for p53 response elements. A qualitative model of p53 action implies that nonquantitative factors controlled by a stimulus, either the tissue origin or the cell genotype, influence the outcome of p53 activation. This model raises the possibility that the activating signal potentially modulates p53 activity in a qualitative manner by directing p53 to different promoters (92). Similarly, the ability of oncogenes to promote either apoptosis or senescence is correlated with different p53 modifications.

Recently, it was demonstrated that Ras modifies p53-dependent transcriptional activation in a quantitative rather than qualitative manner, and the senescence response depends on factors other than p53 activation (6). P53 activation appears necessary, but not sufficient, to induce senescence, as other signals are possibly required for the full onset of senescence. For example, Ras-induced activation of PPP1CA, the catalytic subunit of PP1α, is necessary to induce Ras-dependent senescence (61). It is therefore possible to split the senescence response into two physiological processes. The first category involves induction of growth arrest that is dependent on p53 activation or other physiological signals that activate a proliferative brake similar to p53. The second process occurs later and operates on pRB to stabilize its active unphosphorylated form, independent of p53. Unphosphorylated pRB will bind and inactivate E2F factors. This action blocks cell cycle progression and alters local chromatin (10). PPP1CA activation participates in this second process and contributes to irreversible proliferative arrest by enforcing pRB dephosphorylation.

This finding might explain why genome-wide gene expression analysis has revealed that there is very limited overlap among the gene expression profiles in cells induced to senescence by telomere shortening, oncogene overexpression, oxidative stress, or inadequate culture conditions (93–98). The data indicate that fundamental differences exist in gene regulation during senescence activated by various signals, while cell cycle arrest possibly has a similar concurrent program in all types of senescence.

The retinoblastoma tumor suppressor pathway, pRB, has also been connected to senescence (99). Its tumor suppressor activity is mainly attributed to its ability to bind and inactivate the E2F family of transcription factors, which transactivates genes encoding cell cycle proteins and DNA replication factors required for cell growth (100). pRB is a member of the pocket protein family along with its related proteins p107 and p130 (101). The pocket proteins are substrates for cyclin/CDK complexes, which phosphorylate them, release the E2F transcription factors, and allow progression through the cell cycle (102). The CDKs are inhibited by the CDK inhibitors $p16^{INK4a}$ and $p15^{INK4b}$, both are upregulated during cellular senescence (32), which reduces phosphorylation of pRB and E2F inactivation. These transitions result in the accumulation of heterochromatin around E2F-responsive promoters in senescent cells, which stably silences E2F-regulated genes and forms SAHFs (10).

Overexpression of pRB as well as some of the regulators of the pRB pathway, such as CDK inhibitors, trigger growth arrest, which mimics the senescent phenotype (33). Moreover, inactivation of pRB by viral oncoproteins, such as E7, SV40 large T antigen and E1A, extends lifespan (103–105). Other members of the pocket protein family, comprised of pRB, p130, and p107, might also be involved. In MEFs, p130 levels decrease with population doublings, and MEFs from triple pRB, p130, and p107 knockout mice are

immortal (106). Nevertheless, a certain degree of complementation has been observed among the pocket protein family (106); thus, it is difficult to assess the role of each protein in replicative senescence.

It is likely that pRB possesses more tumor suppressive activity than the other pocket proteins, as mutations that alter p107 and p130 are very rarely observed in human cancers (107). Indeed, pRB seems to have a nonredundant role in tumor suppression by permanently repressing E2F target genes during cellular senescence, but not quiescence. These observations mean that loss of pRB, but not p107 or p130, results in a defective senescence response (108).

Given that $p16^{INK4a}$ inhibits the inactivation of pRB by CDKs (109), a loss-of-function of $p16^{INK4a}$ conceivably has similar consequences as a loss-of-function of pRB. Several types of human cells accumulate $p16^{INK4a}$ protein as they approach senescence (110). Senescent fibroblasts potentially contain $p16^{INK4a}$ levels 40 times greater than early passage cells. The deletion of $p16^{INK4a}$ is common in immortalized tumor cell lines (111), and several non-tumorigenic in vitro immortalized cell lines also lack functional $p16^{INK4a}$ protein. Expression of $p16^{INK4a}$-specific antisense in naïve MEFs increases the probability of immortalization of these cells (83). In accordance with this observation, mice cells that are made nullizygous for $p16^{INK4a}$ by targeted deletion undergo immortalization more readily than normal control cells (112, 113). However, these cells show normal senescence kinetics. $P16^{INK4a}$ knockout mice develop normally to adulthood and are fertile, which indicates that the individual INK4 proteins are not essential for development. However, $p16^{INK4a}$ deficiency results in a low susceptibility to spontaneous tumor development and increased tumor susceptibility under specific carcinogenic protocols (112, 113).

The polycomb group of proteins is critical for the transcriptional repression of the *INK4A-ARF* locus. MEFs deficient for the polycomb group protein BMI1 underwent premature cellular senescence, due to the de-repression of *INK4A* and *ARF* genes (114). The polycomb group proteins are chromatin remodelers that repress gene expression by shaping chromatin structure (115, 116).

The Id family of helix–loop–helix (HLH) transcriptional regulatory proteins coordinates cell growth along with differentiation pathways and regulates G1-S cell-cycle transitions. Loss of Id1 increases the expression of the tumor suppressor p16yInk4a but not p19yARF. Id1 depletion also reduces cyclin-dependent kinase (CDK) 2 and CDK4 kinase activity, which leads to premature senescence (117, 118). Id1 directly inhibits p16yInk4a, but not p19yARF, promoter activity via its HLH domain. Therefore, Id1 is an inhibitor of cellular senescence via the repression of $p16^{INK4a}$.

Crosstalk among the different pathways involved in senescence has been found (83). This crosstalk might ensure the accurate execution of the senescence program. Moreover, genes, such as *myc*,

that are involved in these pathways bypass senescence in human primary cells. Myc can bypass CDK4/6 inhibition by activating CDK2-cyclinA/E complexes and inducing the CDK-activating phosphatase CDC25A (119). Moreover, *myc* induces degradation of p27, which influences the inhibitory effects of PTEN. Finally, expression of myc induces telomerase activity by activating the transcription of the catalytic subunit (120). The overall result is a single step immortalization of human cells induced by *myc* gene amplification (121).

3. MicroRNAs in Senescence

MicroRNAs (miRNAs) are small noncoding endogenous RNA molecules that regulate gene expression and protein coding by base pairing with the 3′ untranslated region (UTR) of target mRNAs. MiRNA expression is associated with cancer pathogenesis because miRNAs are intimately linked to cancer development. Senescence blocks cell proliferation and represents an important barrier that cells must bypass to reach malignancy. Importantly, certain miRNAs have an important role during cellular senescence, which is also involved in human tumorigenesis (122).

Several miRNAs are differentially expressed in senescent cells when compared to primary cells, which implies a role for miRNAs in senescence. Recently, miR-34a overexpression has been reported during senescence and can cause senescence in a p53-independent manner through repression of c-myc (123). MiR-34a is downregulated in pancreatic cancer cells, neuroblastomas, colon cancer cells, and lung cancer cells (124, 125), which suggests a mechanism for immortalization. The expression levels of miR-29 and miR-30 increase during cellular senescence, and these microRNAs directly repress B-Myb in conjunction with Rb-E2F complexes, which results in senescence (126). MiR-29 is downregulated in cell lymphomas (127), and the overexpression of miR-29 is suppressed during tumorigenicity in lung cancer cells (128). MiR-449a suppresses pRB phosphorylation, which induces senescence (129–131). A recent study has shown that miR-449a is downregulated in prostate cancer, which indicates that this miRNA regulates cell growth and viability, in part by repressing the expression of HDAC-1 (131). MiR-128a directly targets the Bmi-1 oncogene (polycomb ring finger oncogene; BMI1), which increases $p16^{INK4A}$ expression and ROS. Collectively, these effects promote cellular senescence in medulloblastoma cell lines. MiR-217, which is expressed in endothelial cells during aging, promotes premature senescence by inhibiting SIRT1 expression. This occurrence increases forkhead box O1 (FoxO1) expression (132). In addition,

miR-217 has been reported to be a novel tumor suppressive miRNA that targets K-Ras in pancreatic ductal adenocarcinoma due to decreases in tumor cell growth both in vitro and in vivo (133). MiR-20a induces senescence in MEFs by directly downregulating the transcriptional regulator leukemia/lymphoma-related factor (LRF), which induces $p19^{ARF}$ (134). In addition, miR-519 induces senescence in cancer cell lines by repressing HuR expression (135). In contrast, there are miRNAs that are downregulated during senescence, such as miR-15b, miR-24, miR-25, and miR-141, which directly target mitogen-activated protein kinase kinase (MKK4) (136).

Recently, it was shown that 28 miRNAs prevented senescence induced by oncogenic RasG12V (134). These miRNAs bypass RasG12V-induced senescence by directly targeting the 3′UTR of $p21^{Cip1}$. Moreover, miR-372, miR-373, miR-302, and miR-520 also bypass RasG12V-induced senescence through the downregulation of LATS2 in addition to $p21^{Cip1}$ (134). These identified proliferative miRNAs are associated with cancer development (122, 137).

4. DNA Methylation in Senescence

DNA methylation regulates the expression of senescence genes and is capable of controlling the process (9). In human cancers, the silencing of tumor suppressor genes through aberrant DNA methylation of the CpG island(s) in gene promoters is a common epigenetic change (138). Genes from an assortment of pathways are hypermethylated in cancer cells, including ones involved with DNA repair, cell-cycle control, invasion and metastasis. The tumor suppressor genes BRCA1, $p16^{INK4a}$, $p15^{INK4b}$, $p14^{ARF}$, p73, and APC are among those silenced by hypermethylation, although the frequency of aberrant methylation is somewhat tumor-type specific. Recently, we found that inactivation of S-adenosylhomocysteine hydrolase (SAHH) confers resistance to p53- and p16(INK4)-induced proliferation arrest and senescence (62). SAHH was previously identified in an independent short hairpin RNA (shRNA) screen (139). SAHH catalyzes the hydrolysis of S-adenosylhomocysteine to adenosine and homocysteine. In eukaryotes, this function is the major route for disposal of S-adenosylhomocysteine, which is formed as a common product of each of the many S-adenosylmethionine-dependent methyltransferases. Thus, SAHH regulates the methylation processes. Interestingly, SAHH inactivation inhibits p53 transcriptional activity and impairs DNA-damage-induced transcription of $p21^{Cip1}$. SAHH messenger RNA (mRNA) was lost in 50 % of tumor tissues from 206 patients with different kinds of tumors in comparison with normal tissue counterparts. Moreover, SAHH protein was also affected in some colon cancers (62, 63).

5. Conclusions

Heterogeneity exists in the senescent responses among different types of senescence induction and tissues, and this diversity originates at the molecular level. However, some markers are common among the senescence types. P53 transcriptional activation increases along with the expression its targets and the INK4a proteins, while pRB phosphorylation is reduced. These characteristics are commonly viewed as biomarkers of senescence either in vitro or in vivo. Furthermore, drastic changes in the physiology of cells are observed in most known types of senescence. Clear biological signs follow senescent biology including: an increase in DNA-damage signals, the secretory phenotype proteins, and SA-β-gal activity; changes in the cellular and nuclear morphology, heterochromatin compaction and DNA methylation; changes in posttranslational modifications in proteins (oxidation, glycosylation, acetylation, ubiquitination, etc.), which alter protein degradation, etc. Despite heterogeneity, the assessment of several of these markers should be sufficient to identify the senescence response.

Acknowledgments

This work was supported by grants from the Spanish Ministry of Science and Innovation and FEDER Funds (SAF2009-08605), Consejeria de Ciencia e Innovacion and Consejeria de Salud of the Junta de Andalucia (CTS-6844 and PI-0142). AC's laboratory is also funded by a fellowship from Fundacion Oncologica FERO, supported by Fundació Josep Botet.

References

1. Hayflick L (1965) The limited in vitro lifetime of human diploid cell strains. Exp Cell Res 37:614–636
2. Hanahan D, Weinberg RA (2000) The hallmarks of cancer. Cell 100:57–70
3. Untergasser G, Koch HB, Menssen A, Hermeking H (2002) Characterization of epithelial senescence by serial analysis of gene expression: identification of genes potentially involved in prostate cancer. Cancer Res 62: 6255–6262
4. Mason DX, Jackson TJ, Lin AW (2004) Molecular signature of oncogenic ras-induced senescence. Oncogene 23:9238–9246
5. Schwarze SR, Fu VX, Desotelle JA, Kenowski ML, Jarrard DF (2005) The identification of senescence-specific genes during the induction of senescence in prostate cancer cells. Neoplasia 7:816–823
6. Ruiz L, Traskine M, Ferrer I, Castro E, Leal JF, Kaufman M, Carnero A (2008) Characterization of the p53 response to oncogene-induced senescence. PLoS One 3:e3230
7. Shay JW, Roninson IB (2004) Hallmarks of senescence in carcinogenesis and cancer therapy. Oncogene 23:2919–2933
8. Zhang W, Ji W, Yang J, Yang L, Chen W, Zhuang Z (2008) Comparison of global DNA methylation profiles in replicative versus premature senescence. Life Sci 83:475–480
9. Carnero A, Lleonart ME (2011) Epigenetic mechanisms in senescence, immortalisation

and cancer. Biol Rev Camb Philos Soc 86: 443–455

10. Narita M, Nunez S, Heard E, Lin AW, Hearn SA, Spector DL, Hannon GJ, Lowe SW (2003) Rb-mediated heterochromatin formation and silencing of E2F target genes during cellular senescence. Cell 113:703–716
11. Zhang H, Pan KH, Cohen SN (2003) Senescence-specific gene expression fingerprints reveal cell-type-dependent physical clustering of up-regulated chromosomal loci. Proc Natl Acad Sci U S A 100:3251–3256
12. d'Adda di Fagagna F (2008) Living on a break: cellular senescence as a DNA-damage response. Nat Rev Cancer 8:512–522
13. d'Adda di Fagagna F, Reaper PM, Clay-Farrace L, Fiegler H, Carr P, Von Zglinicki T, Saretzki G, Carter NP, Jackson SP (2003) A DNA damage checkpoint response in telomere-initiated senescence. Nature 426:194–198
14. Herbig U, Jobling WA, Chen BP, Chen DJ, Sedivy JM (2004) Telomere shortening triggers senescence of human cells through a pathway involving ATM, p53, and p21(CIP1), but not p16(INK4a). Mol Cell 14:501–513
15. Campisi J, Andersen JK, Kapahi P, Melov S (2011) Cellular senescence: a link between cancer and age-related degenerative disease? Semin Cancer Biol 21:354–359
16. Campisi J (2011) Cellular senescence: putting the paradoxes in perspective. Curr Opin Genet Dev 21:107–112
17. Krtolica A, Parrinello S, Lockett S, Desprez PY, Campisi J (2001) Senescent fibroblasts promote epithelial cell growth and tumorigenesis: a link between cancer and aging. Proc Natl Acad Sci U S A 98:12072–12077
18. Bavik C, Coleman I, Dean JP, Knudsen B, Plymate S, Nelson PS (2006) The gene expression program of prostate fibroblast senescence modulates neoplastic epithelial cell proliferation through paracrine mechanisms. Cancer Res 66:794–802
19. Parrinello S, Coppe JP, Krtolica A, Campisi J (2005) Stromal-epithelial interactions in aging and cancer: senescent fibroblasts alter epithelial cell differentiation. J Cell Sci 118:485–496
20. Coppe JP, Patil CK, Rodier F, Krtolica A, Beausejour CM, Parrinello S, Hodgson JG, Chin K, Desprez PY, Campisi J (2010) A human-like senescence-associated secretory phenotype is conserved in mouse cells dependent on physiological oxygen. PLoS One 5:e9188
21. Coppe JP, Patil CK, Rodier F, Sun Y, Munoz DP, Goldstein J, Nelson PS, Desprez PY, Campisi J (2008) Senescence-associated secretory phenotypes reveal cell-nonautonomous functions of oncogenic RAS and the p53 tumor suppressor. PLoS Biol 6:2853–2868
22. Coppe JP, Desprez PY, Krtolica A, Campisi J (2010) The senescence-associated secretory phenotype: the dark side of tumor suppression. Annu Rev Pathol 5:99–118
23. Davalos AR, Coppe JP, Campisi J, Desprez PY (2010) Senescent cells as a source of inflammatory factors for tumor progression. Cancer Metastasis Rev 29:273–283
24. Campisi J (2005) Senescent cells, tumor suppression, and organismal aging: good citizens, bad neighbors. Cell 120:513–522
25. Castro P, Giri D, Lamb D, Ittmann M (2003) Cellular senescence in the pathogenesis of benign prostatic hyperplasia. Prostate 55:30–38
26. Michaloglou C, Vredeveld LC, Mooi WJ, Peeper DS (2008) BRAF(E600) in benign and malignant human tumours. Oncogene 27:877–895
27. Thomas E, al-Baker E, Dropcova S, Denyer S, Ostad N, Lloyd A, Kill IR, Faragher RG (1997) Different kinetics of senescence in human fibroblasts and peritoneal mesothelial cells. Exp Cell Res 236:355–358
28. Rubin H (2002) The disparity between human cell senescence in vitro and lifelong replication in vivo. Nat Biotechnol 20:675–681
29. Wright WE, Shay JW (1995) Time, telomeres and tumours: is cellular senescence more than an anticancer mechanism? Trends Cell Biol 5:293–297
30. Kipling D, Wynford-Thomas D, Jones CJ, Akbar A, Aspinall R, Bacchetti S, Blasco MA, Broccoli D, DePinho RA, Edwards DR, Effros RB, Harley CB, Lansdorp PM, Linskens MH, Prowse KR, Newbold RF, Olovnikov AM, Parkinson EK, Pawelec G, Ponten J, Shall S, Zijlmans M, Faragher RG (1999) Telomere-dependent senescence. Nat Biotechnol 17:313–314
31. Olovnikov AM (1973) A theory of marginotomy. The incomplete copying of template margin in enzymic synthesis of polynucleotides and biological significance of the phenomenon. J Theor Biol 41:181–190
32. Collado M, Serrano M (2006) The power and the promise of oncogene-induced senescence markers. Nat Rev Cancer 6:472–476
33. Carnero A, Link W, Martinez JF, Renner O, Castro ME, Blanco F et al (2003) Cellular senescence and cancer. Adv Cancer Res 3: 183–198
34. Chandeck C, Mooi WJ (2010) Oncogene-induced cellular senescence. Adv Anat Pathol 17:42–48

35. Braig M, Schmitt CA (2006) Oncogene-induced senescence: putting the brakes on tumor development. Cancer Res 66:2881–2884
36. Courtois-Cox S, Jones SL, Cichowski K (2008) Many roads lead to oncogene-induced senescence. Oncogene 27:2801–2809
37. Bartek J, Bartkova J, Lukas J (2007) DNA damage signalling guards against activated oncogenes and tumour progression. Oncogene 26:7773–7779
38. Ruzankina Y, Asare A, Brown EJ (2008) Replicative stress, stem cells and aging. Mech Ageing Dev 129:460–466
39. Kenyon J, Gerson SL (2007) The role of DNA damage repair in aging of adult stem cells. Nucleic Acids Res 35:7557–7565
40. Di Micco R, Fumagalli M, Cicalese A, Piccinin S, Gasparini P, Luise C, Schurra C, Garre M, Nuciforo PG, Bensimon A, Maestro R, Pelicci PG, d'Adda di Fagagna F (2006) Oncogene-induced senescence is a DNA damage response triggered by DNA hyper-replication. Nature 444:638–642
41. Wei S, Sedivy JM (1999) Expression of catalytically active telomerase does not prevent premature senescence caused by overexpression of oncogenic Ha-Ras in normal human fibroblasts. Cancer Res 59:1539–1543
42. Shay JW, Wright WE (2002) Telomerase: a target for cancer therapeutics. Cancer Cell 2:257–265
43. Di Leonardo A, Linke SP, Clarkin K, Wahl GM (1994) DNA damage triggers a prolonged p53-dependent G1 arrest and long-term induction of Cip1 in normal human fibroblasts. Genes Dev 8:2540–2551
44. Serrano M, Lin AW, McCurrach ME, Beach D, Lowe SW (1997) Oncogenic ras provokes premature cell senescence associated with accumulation of p53 and p16INK4a. Cell 88:593–602
45. Robles SJ, Adami GR (1998) Agents that cause DNA double strand breaks lead to p16INK4a enrichment and the premature senescence of normal fibroblasts. Oncogene 16:1113–1123
46. Serrano M, Blasco MA (2001) Putting the stress on senescence. Curr Opin Cell Biol 13:748–753
47. Sharpless NE, DePinho RA (2004) Telomeres, stem cells, senescence, and cancer. J Clin Invest 113:160–168
48. Ben-Porath I, Weinberg RA (2005) The signals and pathways activating cellular senescence. Int J Biochem Cell Biol 37:961–976
49. Passos JF, Von Zglinicki T (2006) Oxygen free radicals in cell senescence: are they signal transducers? Free Radic Res 40: 1277–1283
50. Parrinello S, Samper E, Krtolica A, Goldstein J, Melov S, Campisi J (2003) Oxygen sensitivity severely limits the replicative lifespan of murine fibroblasts. Nat Cell Biol 5:741–747
51. Vergel M, Carnero A (2010) Bypassing cellular senescence by genetic screening tools. Clin Transl Oncol 12:410–417
52. Malumbres M, Carnero A (2003) Cell cycle deregulation: a common motif in cancer. Prog Cell Cycle Res 5:5–18
53. Braig M, Lee S, Loddenkemper C, Rudolph C, Peters AH, Schlegelberger B, Stein H, Dorken B, Jenuwein T, Schmitt CA (2005) Oncogene-induced senescence as an initial barrier in lymphoma development. Nature 436:660–665
54. Chen Z, Trotman LC, Shaffer D, Lin HK, Dotan ZA, Niki M, Koutcher JA, Scher HI, Ludwig T, Gerald W, Cordon-Cardo C, Pandolfi PP (2005) Crucial role of p53-dependent cellular senescence in suppression of Pten-deficient tumorigenesis. Nature 436:725–730
55. Blanco-Aparicio C, Canamero M, Cecilia Y, Pequeno B, Renner O, Ferrer I, Carnero A (2010) Exploring the gain of function contribution of AKT to mammary tumorigenesis in mouse models. PLoS One 5:e9305
56. Smith JR, Pereira-Smith OM (1996) Replicative senescence: implications for in vivo aging and tumor suppression. Science 273: 63–67
57. Duncan EL, Whitaker NJ, Moy EL, Reddel RR (1993) Assignment of SV40-immortalized cells to more than one complementation group for immortalization. Exp Cell Res 205:337–344
58. Barrett JC, Annab LA, Alcorta D, Preston G, Vojta P, Yin Y (1994) Cellular senescence and cancer. Cold Spring Harb Symp Quant Biol 59:411–418
59. Schmitt CA (2007) Cellular senescence and cancer treatment. Biochim Biophys Acta 1775:5–20
60. Mooi WJ, Peeper DS (2006) Oncogene-induced cell senescence–halting on the road to cancer. N Engl J Med 355:1037–1046
61. Castro ME, Ferrer I, Cascon A, Guijarro MV, Lleonart M, Ramón y Cajal S, Leal JF, Robledo M, Carnero A (2008) PPP1CA contributes to the senescence program induced by oncogenic Ras. Carcinogenesis 29:491–499
62. Leal JF, Ferrer I, Blanco-Aparicio C, Hernandez-Losa J, Ramon YCS, Carnero A, Lleonart ME (2008) S-adenosylhomocysteine

hydrolase downregulation contributes to tumorigenesis. Carcinogenesis 29:2089–2095

63. LLeonart ME, Vidal F, Gallardo D, Diaz-Fuertes M, Rojo F, Cuatrecasas M, Lopez-Vicente L, Kondoh H, Blanco C, Carnero A, Ramón y Cajal S (2006) New p53 related genes in human tumors: significant downregulation in colon and lung carcinomas. Oncol Rep 16:603–608
64. Leal JF, Fominaya J, Cascon A, Guijarro MV, Blanco-Aparicio C, Lleonart M, Castro ME, Ramon YCS, Robledo M, Beach DH, Carnero A (2008) Cellular senescence bypass screen identifies new putative tumor suppressor genes. Oncogene 27:1961–1970
65. Kondoh H, Lleonart ME, Gil J, Wang J, Degan P, Peters G, Martinez D, Carnero A, Beach D (2005) Glycolytic enzymes can modulate cellular life span. Cancer Res 65: 177–185
66. Fridman AL, Rosati R, Li Q, Tainsky MA (2007) Epigenetic and functional analysis of IGFBP3 and IGFBPrP1 in cellular immortalization. Biochem Biophys Res Commun 357: 785–791
67. Kortlever RM, Bernards R (2006) Senescence, wound healing and cancer: the PAI-1 connection. Cell Cycle 5:2697–2703
68. Kortlever RM, Higgins PJ, Bernards R (2006) Plasminogen activator inhibitor-1 is a critical downstream target of p53 in the induction of replicative senescence. Nat Cell Biol 8: 877–884
69. Wang W, Chen JX, Liao R, Deng Q, Zhou JJ, Huang S, Sun P (2002) Sequential activation of the MEK-extracellular signal-regulated kinase and MKK3/6-p38 mitogen-activated protein kinase pathways mediates oncogenic ras-induced premature senescence. Mol Cell Biol 22:3389–3403
70. Haq R, Brenton JD, Takahashi M, Finan D, Finkielsztein A, Damaraju S, Rottapel R, Zanke B (2002) Constitutive p38HOG mitogen-activated protein kinase activation induces permanent cell cycle arrest and senescence. Cancer Res 62:5076–5082
71. Zhang H, Cohen SN (2004) Smurf2 up-regulation activates telomere-dependent senescence. Genes Dev 18:3028–3040
72. Shibanuma M, Mochizuki E, Maniwa R, Mashimo J, Nishiya N, Imai S, Takano T, Oshimura M, Nose K (1997) Induction of senescence-like phenotypes by forced expression of hic-5, which encodes a novel LIM motif protein, in immortalized human fibroblasts. Mol Cell Biol 17:1224–1235
73. Campisi J, d'Adda di Fagagna F (2007) Cellular senescence: when bad things happen to good cells. Nat Rev Mol Cell Biol 8:729–740
74. Lin AW, Barradas M, Stone JC, van Aelst L, Serrano M, Lowe SW (1998) Premature senescence involving p53 and p16 is activated in response to constitutive MEK/MAPK mitogenic signaling. Genes Dev 12: 3008–3019
75. Lin AW, Lowe SW (2001) Oncogenic ras activates the ARF-p53 pathway to suppress epithelial cell transformation. Proc Natl Acad Sci U S A 98:5025–5030
76. Pearson M, Carbone R, Sebastiani C, Cioce M, Fagioli M, Saito S, Higashimoto Y, Appella E, Minucci S, Pandolfi PP, Pelicci PG (2000) PML regulates p53 acetylation and premature senescence induced by oncogenic Ras. Nature 406:207–210
77. Wynford-Thomas D (1996) p53: guardian of cellular senescence. J Pathol 180:118–121
78. Bond J, Haughton M, Blaydes J, Gire V, Wynford-Thomas D, Wyllie F (1996) Evidence that transcriptional activation by p53 plays a direct role in the induction of cellular senescence. Oncogene 13:2097–2104
79. Chin L, Artandi SE, Shen Q, Tam A, Lee SL, Gottlieb GJ, Greider CW, DePinho RA (1999) p53 deficiency rescues the adverse effects of telomere loss and cooperates with telomere dysfunction to accelerate carcinogenesis. Cell 97:527–538
80. Ashcroft M, Taya Y, Vousden KH (2000) Stress signals utilize multiple pathways to stabilize p53. Mol Cell Biol 20:3224–3233
81. Blaydes JP, Wynford-Thomas D (1998) The proliferation of normal human fibroblasts is dependent upon negative regulation of p53 function by mdm2. Oncogene 16:3317–3322
82. Kamijo T, Zindy F, Roussel MF, Quelle DE, Downing JR, Ashmun RA, Grosveld G, Sherr CJ (1997) Tumor suppression at the mouse INK4a locus mediated by the alternative reading frame product p19ARF. Cell 91:649–659
83. Carnero A, Hudson JD, Price CM, Beach DH (2000) p16INK4A and p19ARF act in overlapping pathways in cellular immortalization. Nat Cell Biol 2:148–155
84. Carnero A, Beach DH (2004) Absence of p21WAF1 cooperates with c-myc in bypassing Ras-induced senescence and enhances oncogenic cooperation. Oncogene 23:6006–6011
85. Pantoja C, Serrano M (1999) Murine fibroblasts lacking p21 undergo senescence and are resistant to transformation by oncogenic Ras. Oncogene 18:4974–4982
86. Brown JP, Wei W, Sedivy JM (1997) Bypass of senescence after disruption of p21CIP1/

WAF1 gene in normal diploid human fibroblasts. Science 277:831–834

87. Ho JS, Ma W, Mao DY, Benchimol S (2005) p53-Dependent transcriptional repression of c-myc is required for G1 cell cycle arrest. Mol Cell Biol 25:7423–7431
88. Vergel M, Marin JJ, Estevez P, Carnero A (2010) Cellular senescence as a target in cancer control. J Aging Res 2011:725365
89. Sionov RV, Haupt Y (1999) The cellular response to p53: the decision between life and death. Oncogene 18:6145–6157
90. Zhao R, Gish K, Murphy M, Yin Y, Notterman D, Hoffman WH, Tom E, Mack DH, Levine AJ (2000) The transcriptional program following p53 activation. Cold Spring Harb Symp Quant Biol 65:475–482
91. Chen X, Ko LJ, Jayaraman L, Prives C (1996) p53 levels, functional domains, and DNA damage determine the extent of the apoptotic response of tumor cells. Genes Dev 10: 2438–2451
92. Oda K, Arakawa H, Tanaka T, Matsuda K, Tanikawa C, Mori T, Nishimori H, Tamai K, Tokino T, Nakamura Y, Taya Y (2000) p53AIP1, a potential mediator of p53-dependent apoptosis, and its regulation by Ser-46-phosphorylated p53. Cell 102:849–862
93. Shelton DN, Chang E, Whittier PS, Choi D, Funk WD (1999) Microarray analysis of replicative senescence. Curr Biol 9:939–945
94. Schwarze SR, DePrimo SE, Grabert LM, Fu VX, Brooks JD, Jarrard DF (2002) Novel pathways associated with bypassing cellular senescence in human prostate epithelial cells. J Biol Chem 277:14877–14883
95. de Magalhaes JP, Chainiaux F, de Longueville F, Mainfroid V, Migeot V, Marcq L, Remacle J, Salmon M, Toussaint O (2004) Gene expression and regulation in H2O2-induced premature senescence of human foreskin fibroblasts expressing or not telomerase. Exp Gerontol 39:1379–1389
96. Collado M, Serrano M (2005) The senescent side of tumor suppression. Cell Cycle 4: 1722–1724
97. Darbro BW, Schneider GB, Klingelhutz AJ (2005) Co-regulation of p16INK4A and migratory genes in culture conditions that lead to premature senescence in human keratinocytes. J Invest Dermatol 125:499–509
98. Franco N, Lamartine J, Frouin V, Le Minter P, Petat C, Leplat JJ, Libert F, Gidrol X, Martin MT (2005) Low-dose exposure to gamma rays induces specific gene regulations in normal human keratinocytes. Radiat Res 163:623–635
99. Sherr CJ, McCormick F (2002) The RB and p53 pathways in cancer. Cancer Cell 2: 103–112
100. Serrano M (2003) Proliferation: the cell cycle. Adv Exp Med Biol 532:13–17
101. Classon M, Harlow E (2002) The retinoblastoma tumour suppressor in development and cancer. Nat Rev Cancer 2:910–917
102. Classon M, Salama S, Gorka C, Mulloy R, Braun P, Harlow E (2000) Combinatorial roles for pRB, p107, and p130 in E2F-mediated cell cycle control. Proc Natl Acad Sci U S A 97:10820–10825
103. Jarrard DF, Sarkar S, Shi Y, Yeager TR, Magrane G, Kinoshita H, Nassif N, Meisner L, Newton MA, Waldman FM, Reznikoff CA (1999) p16/pRb pathway alterations are required for bypassing senescence in human prostate epithelial cells. Cancer Res 59: 2957–2964
104. Haferkamp S, Tran SL, Becker TM, Scurr LL, Kefford RF, Rizos H (2009) The relative contributions of the p53 and pRb pathways in oncogene-induced melanocyte senescence. Aging (Albany NY) 1:542–556
105. Ye X, Zerlanko B, Zhang R, Somaiah N, Lipinski M, Salomoni P, Adams PD (2007) Definition of pRB- and p53-dependent and -independent steps in HIRA/ASF1a-mediated formation of senescence-associated heterochromatin foci. Mol Cell Biol 27:2452–2465
106. Mulligan G, Jacks T (1998) The retinoblastoma gene family: cousins with overlapping interests. Trends Genet 14:223–229
107. Burkhart DL, Sage J (2008) Cellular mechanisms of tumour suppression by the retinoblastoma gene. Nat Rev Cancer 8:671–682
108. Sage J, Miller AL, Perez-Mancera PA, Wysocki JM, Jacks T (2003) Acute mutation of retinoblastoma gene function is sufficient for cell cycle re-entry. Nature 424:223–228
109. Carnero A, Hannon GJ (1998) The INK4 family of CDK inhibitors. Curr Top Microbiol Immunol 227:43–55
110. Palmero I, McConnell B, Parry D, Brookes S, Hara E, Bates S, Jat P, Peters G (1997) Accumulation of p16INK4a in mouse fibroblasts as a function of replicative senescence and not of retinoblastoma gene status. Oncogene 15:495–503
111. Okamoto A, Demetrick DJ, Spillare EA, Hagiwara K, Hussain SP, Bennett WP, Forrester K, Gerwin B, Greenblatt MS, Serrano M et al (1994) p16INK4 mutations and altered expression in human tumors and cell lines. Cold Spring Harb Symp Quant Biol 59:49–57

112. Krimpenfort P, Quon KC, Mooi WJ, Loonstra A, Berns A (2001) Loss of p16Ink4a confers susceptibility to metastatic melanoma in mice. Nature 413:83–86
113. Sharpless NE, Bardeesy N, Lee KH, Carrasco D, Castrillon DH, Aguirre AJ, Wu EA, Horner JW, DePinho RA (2001) Loss of p16Ink4a with retention of p19Arf predisposes mice to tumorigenesis. Nature 413: 86–91
114. Jacobs JJ, Kieboom K, Marino S, DePinho RA, van Lohuizen M (1999) The oncogene and Polycomb-group gene bmi-1 regulates cell proliferation and senescence through the ink4a locus. Nature 397:164–168
115. Sparmann A, van Lohuizen M (2006) Polycomb silencers control cell fate, development and cancer. Nat Rev Cancer 6:846–856
116. Bernard D, Martinez-Leal JF, Rizzo S, Martinez D, Hudson D, Visakorpi T, Peters G, Carnero A, Beach D, Gil J (2005) CBX7 controls the growth of normal and tumor-derived prostate cells by repressing the Ink4a/Arf locus. Oncogene 24:5543–5551
117. Alani RM, Young AZ, Shifflett CB (2001) Id1 regulation of cellular senescence through transcriptional repression of p16/Ink4a. Proc Natl Acad Sci U S A 98:7812–7816
118. Cummings SD, Ryu B, Samuels MA, Yu X, Meeker AK, Healey MA, Alani RM (2008) Id1 delays senescence of primary human melanocytes. Mol Carcinog 47:653–659
119. Amati B, Alevizopoulos K, Vlach J (1998) Myc and the cell cycle. Front Biosci 3: d250–d268
120. Wang J, Xie LY, Allan S, Beach D, Hannon GJ (1998) Myc activates telomerase. Genes Dev 12:1769–1774
121. Gil J, Kerai P, Lleonart M, Bernard D, Cigudosa JC, Peters G, Carnero A, Beach D (2005) Immortalization of primary human prostate epithelial cells by c-Myc. Cancer Res 65:2179–2185
122. Feliciano A, Sanchez-Sendra B, Kondoh H, Lleonart ME (2011) MicroRNAs regulate key effector pathways of senescence. J Aging Res 2011:205378
123. Christoffersen NR, Shalgi R, Frankel LB, Leucci E, Lees M, Klausen M, Pilpel Y, Nielsen FC, Oren M, Lund AH (2010) p53-independent upregulation of miR-34a during oncogene-induced senescence represses MYC. Cell Death Differ 17:236–245
124. Bommer GT, Gerin I, Feng Y, Kaczorowski AJ, Kuick R, Love RE, Zhai Y, Giordano TJ, Qin ZS, Moore BB, MacDougald OA, Cho KR, Fearon ER (2007) p53-mediated activation of miRNA34 candidate tumor-suppressor genes. Curr Biol 17:1298–1307
125. Tazawa H, Tsuchiya N, Izumiya M, Nakagama H (2007) Tumor-suppressive miR-34a induces senescence-like growth arrest through modulation of the E2F pathway in human colon cancer cells. Proc Natl Acad Sci U S A 104:15472–15477
126. Martinez I, Cazalla D, Almstead LL, Steitz JA, DiMaio D (2011) miR-29 and miR-30 regulate B-Myb expression during cellular senescence. Proc Natl Acad Sci U S A 108:522–527
127. Zhao JJ, Lin J, Lwin T, Yang H, Guo J, Kong W, Dessureault S, Moscinski LC, Rezania D, Dalton WS, Sotomayor E, Tao J, Cheng JQ (2010) microRNA expression profile and identification of miR-29 as a prognostic marker and pathogenetic factor by targeting CDK6 in mantle cell lymphoma. Blood 115:2630–2639
128. Fabbri M, Garzon R, Cimmino A, Liu Z, Zanesi N, Callegari E, Liu S, Alder H, Costinean S, Fernandez-Cymering C, Volinia S, Guler G, Morrison CD, Chan KK, Marcucci G, Calin GA, Huebner K, Croce CM (2007) MicroRNA-29 family reverts aberrant methylation in lung cancer by targeting DNA methyltransferases 3A and 3B. Proc Natl Acad Sci U S A 104:15805–15810
129. Marasa BS, Srikantan S, Martindale JL, Kim MM, Lee EK, Gorospe M, Abdelmohsen K (2010) MicroRNA profiling in human diploid fibroblasts uncovers miR-519 role in replicative senescence. Aging (Albany NY) 2:333–343
130. Noonan EJ, Place RF, Basak S, Pookot D, Li LC (2010) miR-449a causes Rb-dependent cell cycle arrest and senescence in prostate cancer cells. Oncotarget 1:349–358
131. Noonan EJ, Place RF, Pookot D, Basak S, Whitson JM, Hirata H, Giardina C, Dahiya R (2009) miR-449a targets HDAC-1 and induces growth arrest in prostate cancer. Oncogene 28:1714–1724
132. Garzon R, Garofalo M, Martelli MP, Briesewitz R, Wang L, Fernandez-Cymering C, Volinia S, Liu CG, Schnittger S, Haferlach T, Liso A, Diverio D, Mancini M, Meloni G, Foa R, Martelli MF, Mecucci C, Croce CM, Falini B (2008) Distinctive microRNA signature of acute myeloid leukemia bearing cytoplasmic mutated nucleophosmin. Proc Natl Acad Sci U S A 105:3945–3950
133. Menghini R, Casagrande V, Cardellini M, Martelli E, Terrinoni A, Amati F, Vasa-Nicotera M, Ippoliti A, Novelli G, Melino G, Lauro R, Federici M (2009) MicroRNA 217 modulates

endothelial cell senescence via silent information regulator 1. Circulation 120:1524–1532

134. Borgdorff V, Lleonart ME, Bishop CL, Fessart D, Bergin AH, Overhoff MG, Beach DH (2010) Multiple microRNAs rescue from Ras-induced senescence by inhibiting p21(Waf1/Cip1). Oncogene 29:2262–2271
135. Voorhoeve PM, le Sage C, Schrier M, Gillis AJ, Stoop H, Nagel R, Liu YP, van Duijse J, Drost J, Griekspoor A, Zlotorynski E, Yabuta N, De Vita G, Nojima H, Looijenga LH, Agami R (2006) A genetic screen implicates miRNA-372 and miRNA-373 as oncogenes in testicular germ cell tumors. Cell 124:1169–1181
136. Cho WJ, Shin JM, Kim JS, Lee MR, Hong KS, Lee JH, Koo KH, Park JW, Kim KS (2009) miR-372 regulates cell cycle and apoptosis of ags human gastric cancer cell line through direct regulation of LATS2. Mol Cells 28:521–527
137. Leal JA, Feliciano A, Lleonart ME (2011) Stem cell MicroRNAs in senescence and immortalization: novel players in cancer therapy. Med Res Rev
138. Baylin SB, Belinsky SA, Herman JG (2000) Aberrant methylation of gene promoters in cancer–concepts, misconcepts, and promise. J Natl Cancer Inst 92:1460–1461
139. Brummelkamp TR, Berns K, Hijmans EM, Mullenders J, Fabius A, Heimerikx M, Velds A, Kerkhoven RM, Madiredjo M, Bernards R, Beijersbergen RL (2004) Functional identification of cancer-relevant genes through large-scale RNA interference screens in mammalian cells. Cold Spring Harb Symp Quant Biol 69:439–445

Chapter 5

Biomarkers of Cell Senescence Assessed by Imaging Cytometry

Hong Zhao and Zbigniew Darzynkiewicz

Abstract

The characteristic features of senescent cells such as their "flattened" appearance, enlarged nuclei and low saturation density at the plateau phase of cell growth, can be conveniently measured by image-assisted cytometry such as provided by a laser scanning cytometer (LSC). The "flattening" of senescent cells is reflected by a decline in local density of DNA-associated staining with 4,6-diamidino-2-phenylindole (DAPI) and is paralleled by an increase in nuclear area. Thus, the ratio of the maximal intensity of DAPI fluorescence per nucleus to the nuclear area provides a very sensitive morphometric biomarker of "depth" of senescence, which progressively declines during senescence induction. Also recorded is cellular DNA content revealing cell cycle phase, as well as the saturation cell density at plateau phase of growth, which is dramatically decreased in cultures of senescent cells. Concurrent immunocytochemical analysis of expression of $p21^{WAF1}$, $p16^{INK4a}$, or $p27^{KIP1}$ cyclin kinase inhibitors provides additional markers of senescence. These biomarker indices can be expressed in quantitative terms ("senescence indices") as a fraction of the same markers of the exponentially growing cells in control cultures.

Key words: Cell aging, Chromatin structure, Cell cycle, Apoptosis, Nuclear size, Laser scanning cytometry, $p21^{WAF1}$, $p16^{INK4a}$, $p27^{KIP1}$, Premature cell senescence

1. Introduction

Cellular senescence can be subdivided into two distinct categories. The first is replicative senescence, observed after certain rounds of division as a loss of replicative capacity of normal proliferating diploid cells in culture ("Hayflick's limit") (1). This type of senescence is a consequence of a progressive shortening of telomeres with each division until a cell reaches the state of telomere dysfunction (2). The second category is independent of telomere shortening or dysfunction and is referred to as premature cell senescence (3). Persistent cellular stress including oxidative DNA damage leading

Lorenzo Galluzzi et al. (eds.), *Cell Senescence: Methods and Protocols*, Methods in Molecular Biology, vol. 965,
DOI 10.1007/978-1-62703-239-1_5,

to constitutive replication stress (4, 5), activation of oncogenes (6) and loss of tumor suppressor genes (7) are among the factors and mechanisms inducing premature cells senescence. Although during chemo- or radiotherapy apoptosis is the preferred mode of cell death in certain malignancies such as acute leukemia, in solid tumors the mechanism of growth suppression often relies on irreversible impairment of cell reproductive capacity defined as a drug- or radiation-induced senescence, which also belongs to the category of premature senescence (8, 9). There is growing body of evidence that induction of premature senescence in vivo plays also a critical role as barrier in tumor development, including prevention of tumorigenesis of the induced pluripotent stem cells (iPSCs) (10).

Regardless of the category and the mechanism of induction of senescence there are common markers to identify senescent cells. The most characteristic are morphological features (11). Senescent cells are characterized by "flattened" appearance, enlarged and often irregular-shaped nuclei, cytoplasmic granules and low saturation density at the plateau phase of growth. An increase in cellular size is accompanied by an increase in nuclear and nucleolar size. There are numerous vacuoles in the cytoplasm, an increased number of cytoplasmic microfilaments, enlarged lysosomal bodies, and a prominent Golgi apparatus (11–13). Also apparent in some types of cells are abnormalities of nuclear chromatin presented as senescence-associated heterochromatic foci (SAHF). SAHF are abundant in histone H3 modified at lysine 9 (K9M H3) and its binding partner heterochromatin protein 1 (HP1) (13–16).

Several molecular biomarkers also characterize senescent cells. Suppression of proliferation of these cells is to a large degree mediated by an over-expression of inhibitors of cyclin-dependent kinases (CKIs) $p21^{WAF1}$, $p16^{INK4A}$ and/or $p27^{KIP1}$ associated with the activation of tumor suppressor p53 pathways (17–20). Persistent expression of markers of DNA damage response, particularly of Ser139-phosphorylated histone H2AX (γH2AX), is an additional feature of senescent cells (21, 22). These molecular markers, however, are neither unique nor highly specific to senescent cells. Among all biomarkers the most specific are: (1) the characteristic changes in cell morphology, and (2) the induction of senescence-associated β-galactosidase activity, the latter considered being the hallmark of cell senescence (23, 24).

We have recently reported that one of the most specific morphological features of senescent cells, namely their "flattening" and nuclear enlargement, can be quantitatively assessed using imaging cytometry, such as provided by the laser scanning cytometer (LSC) (25, 26). LSC is the microscope-based quantitative-image analyzer that offers the combined advantages of flow cytometry and image analysis (27–29) (Fig. 1). It can analyze over100 cells per second, record a large number of the measured parameters including cell morphometric data, and preserve images of the analyzed cells.

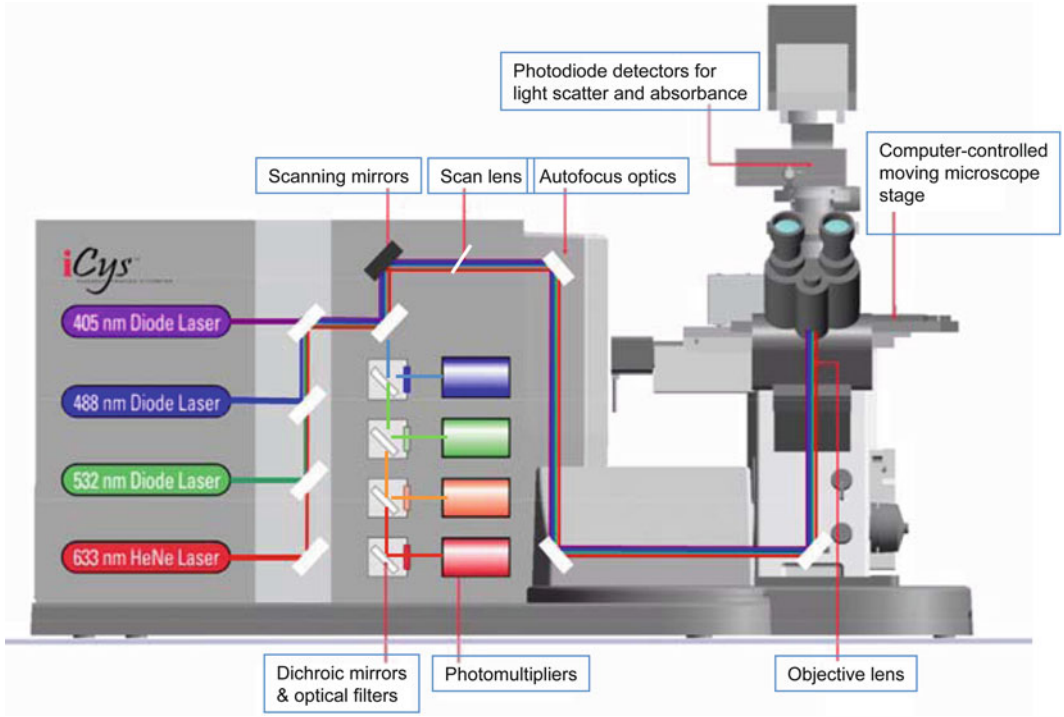

Fig. 1. Schematic illustration of iCys® Research Imaging Cytometer outfitted with 405, 488, 532, and 633 nm lasers.

We have recently shown that a simple assay based on measurement of nuclear size (area) combined with the intensity of maximal pixel of DNA-associated fluorescence per nucleus, after DNA staining with fluorescent dyes like DAPI, provides a convenient marker of the degree ("depth") of cell senescence (26). The protocol for identification of senescent cells and for quantitative assessment of a "depth" of cell senescence is given below. This protocol includes also immunocytochemical detection of CKIs $p21^{WAF1}$, $p27^{KIP1}$ or, $p16^{INK4a}$, which are additional, although as mentioned, not highly specific markers of senescent cells (17–20).

2. Materials

2.1. Common Materials

1. Chambered slides, available from Nunc Lab-Tek II (Fisher Scientific, Pittsburgh, PA): see Subheading 3.1.
2. Phosphate-buffered saline (PBS), pH 7.4.
3. Formaldehyde (methanol-free, "ultrapure") (Polysciences, Warrington, PA), 1% (v/v) in PBS (see Note 1).
4. Ethanol (70%).
5. Coplin jars.

6. Parafilm "M" (American National Can, Greenwich, CT).
7. Solution of 0.1%Triton X-100 (v/v) (Sigma/Aldrich, St. Louis, MO) in PBS.
8. Antifade coverslips mounting medium (Invitrogen/Molecular Probes).

2.2. Immunocytochemical and DNA Staining Reagents

1. Bovine serum albumin (BSA; Sigma/Aldrich) dissolved (1%; w/v) in PBS (BSA solution).
2. $p21^{WAF1}$ and/or $p16^{INK4a}$ and/or $p27^{KIP1}$Ab (Santa Cruz Biotechnology, Santa Cruz, CA) (see Subheading 3).
3. The secondary fluorochrome-tagged Abs: AlexaFluor 488 or AlexaFluor 633 Ab (Invitrogen/Molecular Probes, Eugene, OR).
4. Stock solution of 4′,6-diamidino-2-phenylindole (DAPI; Invitrogen/Molecular Probes). Dissolve 1 mg DAPI dihydrochloride in 1 mL of deionized water (2.66 mM concentration) (see Note 2).
5. Staining solution of DAPI prepared freshly before the use: Add 5 μL of the stock DAPI solution to 2 mL of PBS (final DAPI concentration 2.5 μg/mL).

2.3. Equipment to Measure Cell Fluorescence

1. LSC, preferentially a new model of LSC (iGeneration; Research Imaging Cytometer; iCys®) manufactured by CompuCyte, Westwood, MA (Fig. 1) (see Note 3).

3. Methods

3.1. Induction of Cell Senescence

1. The methodology is applicable to cells growing attached to surface of culture vessel and not to cells growing in suspension. Because morphology of cells undergoing replicative senescence (e.g., due to telomere dysfunction) is similar to that of premature senescence such as that of stress- or drug-induced, this protocol can be used to assess depth of senescence in either case.
2. Prepare cell cultures by seeding cells on single- or multichambered incubation slides (see Notes 4–6) for approaches to induce premature cell senescence in these chambered cultures.

3.2. Cell Fixation and Staining

1. Remove the culture medium from each chamber on the slide and replace it with PBS, to fill up the chamber.
2. Remove PBS and replace it with ice-cold 1% formaldehyde solution in PBS, to fill up the chamber, close chambers caps. Keep cells in formaldehyde on ice for 15 min.

3. Remove formaldehyde and replace it with ice-cold PBS, close chamber caps and transfer slides to refrigerator at 4°C. The slides can be stored in PBS at 4°C for up to 12 h.
4. After storage in PBS, carefully remove the chamber's walls from the slides and incubate the slides in PBS in Coplin jars for 5 min.
5. Remove the slides from Coplin jar and place them horizontally in a moisturized chamber.
6. Carefully layer a small volume (approximately100 μL) of 0.1% Triton X-100 in PBS for 15 min, then 1% BSA solution for 30 min.
7. After 30 min replace the BSA solution with the solution of BSA containing primary p21 or p16 Ab at 1:100 dilution (see Notes 7 and 8), incubate at room temperature for 1.5 h or overnight at 4°C.
8. Rinse the cells with 1% BSA solution in PBS and layer approximately 100 μL of BSA solution containing AlexaFluor 488 or AlexaFluor 633-tagged secondary Ab at 1:100 dilution (see Note 7), incubate for 45 min at room temperature.
9. Rinse the slides with PBS and layer approximately 100 μL of DAPI staining solution.
10. After 15 min, rinse away the DAPI staining solution with PBS, then add a drop of anti-fade mounting medium and mount under the coverslip (see Note 9).

3.3. Fluorescence Measurement and Data Analysis

1. Measure cell fluorescence on LSC. Excite DAPI fluorescence with a 405 nm diode laser, AlexaFluor 488 with a 488 nm diode laser and AlexaFluor 633 with a 633 nm Helium–Neon laser. Collect blue (DAPI), green (AlexaFluor 488) and far red (AlexaFluor 633) fluorescence emission with the respective photomultipliers (see Notes 10–13).

4. Notes

1. Formaldehyde is a *strong carcinogenic agent.* Care should be exercised in handling this reagent. It should be noted that the use of methanol-free formaldehyde, as specified in this protocol, substitutes the use of paraformaldehyde (solid state substance), which is even more hazardous since it requires heating to hydrolyze it to obtain formaldehyde.
2. The stock solution of DAPI is stable for several months when stored at 4°C in the dark.

3. Other type of fluorescence microscope or imaging system may by used provided that its capability for fluorescence analysis (hardware and software) makes possible to assess the cell *nuclear area and intensity of maximal pixel of DNA-associated nuclear fluorescence* (after staining with DAPI or with another DNA-fluorochrome).
4. Premature senescence can be induced by cell treatment with low concentrations of a DNA damaging drug, which leads to persistent replication stress revealed as inhibited progression through S phase. Alternatively one can induce premature senescence by upregulation of expression of CKIs, which often arrests cells in G_1 or G_2. Activation of certain oncogenes that leads to enhancement of transcription and/or translation can also induce senescence. The premature cell senescence is optimally induced by promoting *growth imbalance* which takes place when cell growth (overall transcription and translation) continues concurrently with inhibition of cell cycle progression (26, 30). When the rates of transcription and translation are high (e.g., activated by certain oncogenes) and cell cycle progression is abruptly halted the induction of senescence is rapid, generally seen within the time period equivalent of two to three cell generation times. Slowing the growth rate slows the induction and reduces the depth of cell senescence (26). (see Notes 5 and 6).
5. We induced premature senescence by exposure of cells to low concentration of DNA topoisomerase II inhibitor mitoxantrone (Mxt) (25). Specifically human pulmonary carcinoma A549 cells cultured in Ham's F12K medium (GIBCO/Invitrogen) or WI-38 fibroblasts grown in MEM Eagle–Earle (GIBCO/Invitrogen) were treated with 1 or 2 nM Mxt (Sigma/Aldrich) for 2–4 days. In another set of experiments senescence of A549 or WI-38 cells was induced by treatment with 0.5 or 1.0 μM histone deacetylase inhibitor Trichostatin A (TSA) (Sigma/Aldrich) for 2 or 3 days (26).
6. Other drugs than Mxt or TSA can be used to induce premature cell senescence. As mentioned, their concentration should be high enough to arrest cell cycle progression but not too high to significantly suppress transcription and translation. The "depth" of cell senescence correlates with time interval of treatment with the drug. This protocol can also be used to assess replicative senescence of normal cells resulting from telomeres dysfunction (1, 2).
7. For optimal immunocytochemical detection it is advised to test various dilutions (titer) of the primary and secondary Abs in the

pilot experiments. Specifically, in addition to the concentration advised by the supplier, two and fourfold lower and higher concentrations have to be tested. The *optimal concentration* is the one at which the *signal to noise ratio* (ratio of the highest fluorescence intensity of cells positively stained with Ab to fluorescence intensity of Ab-negative cells) is *maximal*.

8. Primary and/or secondary Abs from suppliers other than listed in this protocol can be used to immunocytochemically to detect $p21^{WAF1}$, $p16^{INK4a}$, or $p27^{KIP1}$ protein. While ordering, check the supplier whether the primary Abs can be used for immunocytochemistry and not only for Western blotting.
9. To preserve the specimen for longer period of time or transport it, seal the cells mounted in anti-fade under coverslip with nail polish or melted paraffin.
10. In addition to measurement of fluorescence of DAPI concurrently with expression of $p21^{WAF1}$, $p16^{INK4a}$, or $p27^{KIP1}$ other markers relevant to cell senescence can be analyzed. Among the latter are markers of DNA damage response such as expression of γH2AX and/or activation of *Ataxia Telangiectasia* mutated (ATM) protein kinase, which can be detected by phospho-specific Abs and measured by LSC (31–33).
11. The integral of DAPI fluorescence intensity per nucleus provides information on cellular DNA content and thereby on cell cycle-phase distribution of the population of senescent cells (Fig. 2; DNA content frequency histograms).
12. Fluorochromes other than DAPI like Hoechst 33342, DyeCycle Violet, DRAQ5 or propidium iodide (PI) can be used to stain DNA (33). The use of PI requires pretreatment of cells with RNase A.
13. Among the measured by LSC parameters useful to characterize "depth" of cell senescence are: (1) intensity of maximal pixel of DNA-associated fluorescence (DAPI); (2) area of nucleus based on the image of DAPI-fluorescence, which equals to the number of DAPI pixels; (3) fluorescence intensity of Ab used as a marker of the respective CKI ($p21^{WAF1}$, $p16^{INK4a}$, or $p27^{KIP1}$) integrated over the nucleus, and (4) intensity of DAPI fluorescence over the nucleus (integral), providing information about position of cell in the cell cycle (G_1 vs. S vs. G_2M). Recorded is also cell density on the slide, which provides information about the saturation density of cells at confluence. Compare changes in these parameters recorded on senescent cells with the control exponentially growing cells to obtain the "Senescence Index" (SI). Examples of analysis of these parameters are provided in Figs. 2 and 3.

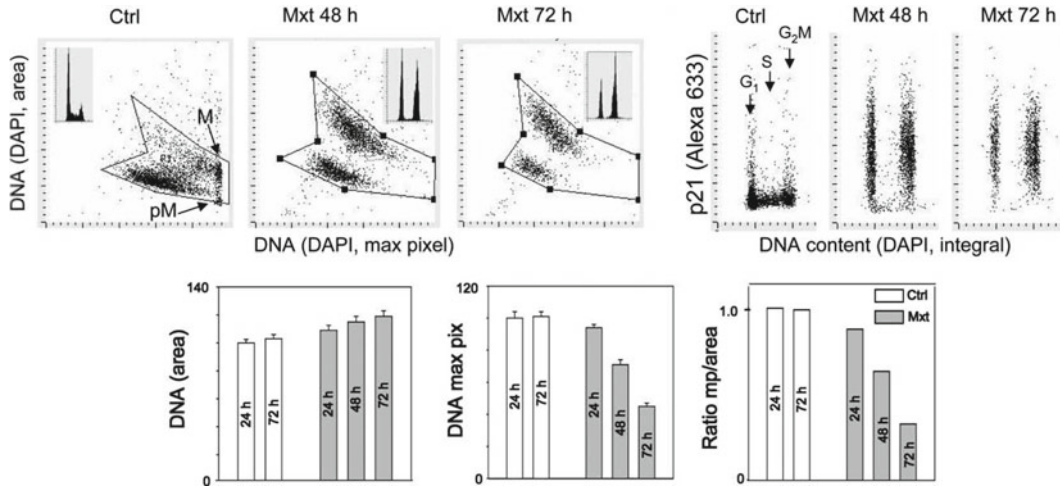

Fig. 2. Analysis of nuclear changes and expression of $p21^{WAF1}$ of A549 cells in cultures treated with mitoxantrone (Mxt) to induce cell senescence. The cells were untreated (Ctrl) or treated with 2 nM Mxt for 24, 48, or 72 h, their DNA was stained with DAPI and expression of $p21^{WAF1}$ was detected immunocytochemically (AlexaFluor 633 nm indirect Ab). The intensity of maximal (max) pixel of DNA-bound DAPI fluorescence reveals highest local level of chromatin condensation per nucleus. In the untreated cultures mitotic (M) and immediately postmitotic (pM) cells have the highest value of maximal pixel, reflecting their highly condensed chromatin. In senescing cells due to "flattening" of the cell and nucleus, the nuclear area is *increased* and intensity of maximal pixel of DAPI fluorescence is *decreased* (25, 26). The insets in the top left panels show DNA frequency histograms of cells from the respective cultures. The bar plots at the bottom panels show *mean values* (±standard deviation) of nuclear DNA (DAPI) area, mean value of DNA (DAPI) fluorescence intensity of maximal pixel per nucleus, and the ratio of maximal pixel to nuclear area. The ratio of maximal pixel to nuclear area of the Mxt-treated cells ("cell senescence index"; SI) is expressed as a fraction of such ratio of the respective control (untreated cells, cells growing exponentially) (SI = 1.0). The lowest is the SI value the greater is "depth" of senescence.

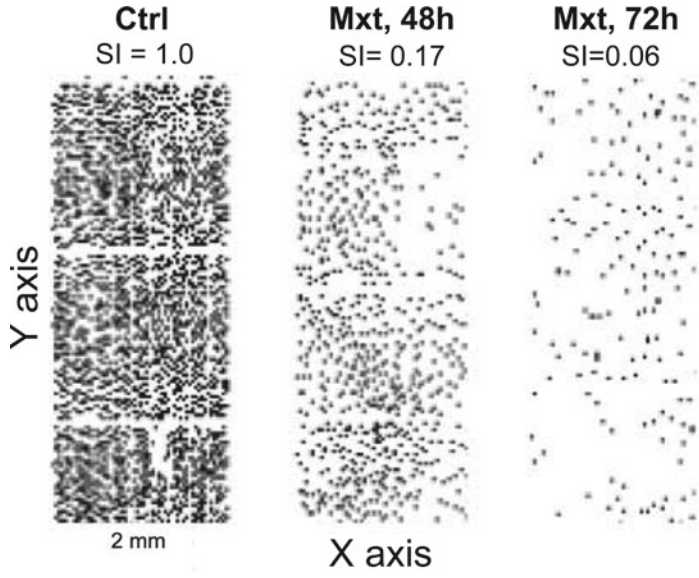

Fig. 3. Decreased cell saturation density at confluence as another marker (senescence index, SI) reflecting "depth" of cell senescence. The A6549 cells were untreated (Ctrl) or grown in the presence of 2 nM mitoxantrone (Mxt) for 48 or 72 h in chamber slide-cultures. The cells were fixed and stained with DAPI as described in the protocol. Their presence and location on the slides concurrently with other parameters (measured as shown in Fig. 2) was recorded by LSC (25, 27–29). The observed decrease in cell density in the Mxt-treated cultures is presented as a fraction (senescence index, SI) of cell density in the untreated exponentially growing culture (SI = 1.00).

Acknowledgment

Supported by NCI grant RO1 28 704 and Robert A. Welke Cancer Research Foundation.

References

1. Hayflick L (1965) The limited in vitro lifetime of human diploid cell strains. Exp Cell Res 37:614–636
2. Harley CB, Futcher AB, Greider CW (1990) Telomeres shorten during ageing of human fibroblasts. Nature 345:458–460
3. Kuilman T, Michaloglou C, Mooi WJ, Peeper DS (2010) The essence of senescence. Genes Dev 24:2463–2479
4. Parrinello S, Samper E, Krtolica A, Goldstein J, Melov S, Campisi J (2003) Oxygen sensitivity severely limits the replicative lifespan of murine fibroblasts. Nat Cell Biol 5:741–747
5. Sherr CJ, DePinho RA (2000) Cellular senescence: mitotic clock or culture shock? Cell 102:407–410
6. Serrano M, Lin AW, McCurrach ME, Beach D, Lowe SW (1997) Oncogenic ras provokes premature cell senescence associated with accumulation of p53 and p16INK4a. Cell 88:593–602
7. Chen Z, Trotman LC, Shaffer D, Lin HK, Dotan ZA, Niki M, Koutcher JA, Scher HI, Ludwig T, Gerald W, Cordon-Cardo C, Pandolfi PP (2005) Crucial role of p53-dependent cellular senescence in suppression of Pten-deficient tumorigenesis. Nature 436:725–730
8. Gewirtz DA, Holt SE, Elmore LW (2008) Accelerated senescence: an emerging role in tumor cell response to chemotherapy and radiation. Biochem Pharmacol 76:947–957
9. Litwiniec A, Grzanka A, Helmin-Basa A, Gackowska L, Grzanka D (2010) Features of senescence and cell death induced by doxorubicin in A549 cells: organization and level of selected cytoskeletal proteins. J Cancer Res Clin Oncol 136:717–736
10. Banito A, Gil J (2010) Induced pluripotent stem cells and senescence: learning the biology to improve the technology. EMBO Rep 11:353–359
11. Cristofalo VJ, Pignolo RJ (1993) Replicative senescence of human fibroblast-like cells in culture. Physiol Rev 73:617–638
12. Cho S, Hwang ES (2011) Fluorescence-based detection and quantification of features of cellular senescence. Methods Cell Biol 103:149–188
13. Funayama R, Ishikawa F (2007) Cellular senescence and chromatin structure. Chromosoma 116:431–440
14. Narita M, Lowe SW (2004) Executing cell senescence. Cell Cycle 3:244–246
15. Zhang R, Adams PD (2007) Heterochromatin and its relationship to cell senescence and cancer therapy. Cell Cycle 6:784–789
16. Li Q, Ma L, Zhang Z, Tong T (2007) SAHF: a new biomarker of cellular senescence. Prog Biochem Biophys 11:1123–1128
17. Qian Y, Chen X (2010) Tumor suppression by p53: making cells senescent. Histol Histopathol 25:515–526
18. Shen H, Maki CG (2010) Persistent p21 expression after Nutlin-3a removal is associated with senescence-like arrest in 4 N cells. J Biol Chem 285:23105–23114
19. Korotchkina LG, Demidenko ZN, Gudkov AV, Blagosklonny MV (2009) Cellular quiescence caused by the Mdm2 inhibitor nutlin-3A. Cell Cycle 8:3777–3781
20. Demidenko ZN, Korotchkina LG, Gudkov AV, Blagosklonny MV (2010) Paradoxical suppression of cellular senescence by p53. Proc Natl Acad Sci U S A 107:9660–9664
21. Mah LJ, El-Osta A, Karagiannis TC (2010) GammaH2AX as a molecular marker of aging and disease. Epigenetics 5:129–136
22. Mallette FA, Ferbeyre G (2007) The DNA damage signaling pathway connects oncogenic stress to cellular senescence. Cell Cycle 6:1831–1836
23. Dimri GP, Lee X, Basile G, Acosta M, Scott G, Roskelley C, Medrano EE, Linskens M, Rubelj I, Pereira-Smith O et al (1995) A biomarker that identifies senescent human cells in culture and in aging skin in vivo. Proc Natl Acad Sci U S A 92:9363–9367
24. Itahana K, Campisi J, Dimri GP (2007) Methods to detect biomarkers of cellular senescence: the senescence-associated beta-galactosidase assay. Methods Mol Biol 371:21–31
25. Nowicki TS, Zhao H, Darzynkiewicz Z, Moscatello A, Shin E, Schantz S, Tiwari RK, Geliebter J (2011) Downregulation of uPAR inhibits migration, invasion, proliferation, FAK/PI3K/Akt signaling and induces

senescence in papillary thyroid carcinoma cells. Cell Cycle 10:100–107

26. Zhao H, Halicka HD, Traganos F, Jorgensen E, Darzynkiewicz Z (2010) New biomarkers probing depth of cell senescence assessed by laser scanning cytometry. Cytometry A 77:999–1007
27. Kamentsky LA, Kamentsky LD (1991) Microscope-based multiparameter laser scanning cytometer yielding data comparable to flow cytometry data. Cytometry 12:381–387
28. Darzynkiewicz Z, Bedner E, Li X, Gorczyca W, Melamed MR (1999) Laser-scanning cytometry: a new instrumentation with many applications. Exp Cell Res 249:1–12
29. Henriksen M, Miller B, Newmark J, Al-Kofahi Y, Holden E (2011) Laser scanning cytometry and its applications: a pioneering technology in the field of quantitative imaging cytometry. Methods Cell Biol 102:161–205
30. Gong J, Traganos F, Darzynkiewicz Z (1995) Growth imbalance and altered expression of cyclins B1, A, E, and D3 in MOLT-4 cells synchronized in the cell cycle by inhibitors of DNA replication. Cell Growth Differ 6:1485–1493
31. Tanaka T, Halicka HD, Huang X, Traganos F, Darzynkiewicz Z (2006) Constitutive histone H2AX phosphorylation and ATM activation, the reporters of DNA damage by endogenous oxidants. Cell Cycle 5:1940–1945
32. Zhao H, Tanaka T, Halicka HD, Traganos F, Zarebski M, Dobrucki J, Darzynkiewicz Z (2007) Cytometric assessment of DNA damage by exogenous and endogenous oxidants reports aging-related processes. Cytometry A 71:905–914
33. Zhao H, Traganos F, Dobrucki J, Wlodkowic D, Darzynkiewicz Z (2009) Induction of DNA damage response by the supravital probes of nucleic acids. Cytometry A 75:510–519

Chapter 6

Cytofluorometric Assessment of Cell Cycle Progression

Ilio Vitale*, Mohamed Jemaà*, Lorenzo Galluzzi, Didier Metivier, Maria Castedo, and Guido Kroemer

Abstract

One of the most prominent features of cellular senescence, a stress response that prevents the propagation of cells that have accumulated potentially oncogenic alterations, is a permanent loss of proliferative potential. Thus, at odds with quiescent cells, which resume proliferation when stimulated to do so, senescent cells cannot proceed through the cell cycle even in the presence of mitogenic factors. Here, we describe a set of cytofluorometric techniques for studying how chemical and/or physical stimuli alter the cell cycle in vitro, in both qualitative and quantitative terms. Taken together, these methods allow for the identification of bona fide cytostatic effects as well as for a refined characterization of cell cycle distributions, providing information on proliferation, DNA content as well as on the presence of cell cycle phase-specific markers. At the end of the chapter, a set of guidelines is offered to assist researchers that approach the study of the cell cycle with the interpretation of results.

Key words: Cancer, Cyclin B1, HCT 116, Histone H3, Mitosis

1. Introduction

The cell cycle is an evolutionarily conserved and tightly regulated series of events by which cells become capable of generating a progeny. To this aim, cells must (1) grow in size (at least to some extent), (2) replicate critical and numerically limited organelles including centrioles, and (3) duplicate their genetic material. These requirements ensure that each of the daughter cells will be provided with one copy of the cellular genome as well as with a set of organelles that will sustain its survival (1). Such newly generated cells will either promptly resume the cell cycle to undertake additional rounds

*I.V. and M.J. equally contributed to this paper.

Lorenzo Galluzzi et al. (eds.), *Cell Senescence: Methods and Protocols*, Methods in Molecular Biology, vol. 965,
DOI 10.1007/978-1-62703-239-1_6, © Springer Science+Business Media, LLC 2013

of cell replication (as in the case of actively proliferating cells), or undergo three distinct non-proliferative fates: differentiation, quiescence, and senescence (2, 3). The first scenario is that of highly specialized cells that acquire their terminal functions, such as cardiomyocytes and neurons. These cells, as well as many others in the body, activate precise genetic programs that allow them to become highly specialized, de facto losing the possibility to proliferate (4, 5). Quiescence is the state of cells that temporarily exit the cell cycle in response to specific stimuli, but do not loose the possibility to enter it again and resume proliferation. An example of this behavior is provided by hematopoietic stem cells, which massively proliferate when the need for mature hematopoietic cells is elevated (such as in response to infections, or upon a consistent blood loss), but "rest" (at least part of them) if the requirements are lower (6). Senescence, on the contrary, constitutes a permanent loss of proliferative potential that occurs in cells that have accumulated potentially mutagenic alterations, including DNA damage and oxidative modifications of lipid and proteins (7, 8).

In somatic cells, the cell cycle includes four sequential steps, or phases: the gap 1 phase (best known as G_1, which was named as such because it appeared as a poorly characterized interval between mitosis and DNA replication, the first processes of the cell cycle to be clearly recognized); the DNA synthesis (S) phase, the gap 2 (G_2) phase, and mitosis (M phase) (9). In G_1, newly generated cells increase in size and prepare for the subsequent S phase, in which DNA replication takes place. In G_2, cell growth continues and multiple control mechanisms ensure that cells are ready to undertake mitosis. The correct progression throughout the cell cycle is driven by the timely activation/inactivation of specific serine/threonine kinases including cyclin-dependent kinases (CDKs) (10). In turn, the catalytic activity of CDKs is regulated by multiple mechanisms: (1) upon their heterodimerization with cyclins, small proteins that are expressed and degraded in a cell cycle-specific fashion; (2) upon the binding of so-called CDK inhibitors, such as $p21^{WAF1}$ and $p27^{KIP1}$; and (3) by posttranslational modifications such as phosphorylation/dephosphorylation events (11–13). Additional serine/threonine kinases participate in the regulation of the cell cycle in a mitosis-restricted fashion. These factors include Aurora kinases (AURKs), Polo-like kinases (PLKs), and MPS1 (14, 15).

The transitions between G_1 and S as well as between G_2 and M are known as G_1 (or restriction) and G_2 checkpoint, respectively. The G_1 checkpoint constitutes a point at which cells arrest if they do not receive appropriate stimuli for proliferation (which is de facto engaged when cells enter the S phase) or if their genetic material is damaged beyond a certain threshold (16, 17). On the contrary, the G_2 checkpoint ensures that cells that bear defects such as partially unreplicated or highly damaged DNA as well as

unreplicated centrioles do not enter a potentially abortive or oncogenic mitosis (16, 18, 19). Additional checkpoint mechanisms that operate throughout the cell cycle include the intra-S checkpoint, blocking cell cycle progression in the presence of stalled replication forks or damaged DNA (20, 21); the spindle-assembly checkpoint (SAC, also known as mitotic checkpoint), which ensures the metaphase-to-anaphase transition only when all chromosomes are properly aligned at the metaphase plate (22, 23); and the so-called tetraploidy (or post-mitotic) checkpoint, a hitherto debated process that would restrict the proliferation/survival of illicitly generated non-diploid cells (24–26). Of note, multiple tumor suppressor proteins, including ATM, BRCA1, p53, and RB, have been shown to contribute to these control mechanisms (27–30). In line with this notion, cell cycle checkpoints appear to be frequently deregulated in cancer, and this has been causally linked to increased aggressiveness, resistance to therapy and worsened prognosis (31, 32).

Nevertheless, the tumor cell-specific deregulation of cell cycle checkpoints might constitute a target for the design of new chemotherapeutic/chemopreventive strategies against cancer. Proof-of-principle for this notion has already been provided in multiple preclinical tumor models. For instance, highly aggressive tetraploid tumor cells rely much more than their diploid counterparts on the SAC, and can be selectively eliminated by the depletion/inactivation of specific SAC components/regulators (33, 34). Along similar lines, inhibitors of mitotic kinases including PLK1, AURKs, and/or MPS1 preferentially kill cells harboring defects in the p53 system, in spite of the fact that these cells are highly resistant to the induction of apoptosis by conventional chemotherapeutics (35–37). Intriguingly, such a preferential toxicity appears to be linked to the incapacity of p53-deficient (but not p53-proficeint) cells to undergo cell cycle arrest in response to tetraploidization, as induced by PLK1 and MPS1 inhibitors.

In this chapter, we outline a few protocols that can be routinely employed to assess proliferation and cell cycle distribution by cytofluorometry. We applied these techniques to compare the effects on cell cycle progression of commercially available drugs that perturb key phases of the cell cycle (such as DNA replication and mitotic entry/execution/completion) and/or activate cell cycle checkpoints. To this aim, we undertook a two-step approach. First, we demonstrated the cytostatic effects of these agents on an easily manageable human cancer cell line (human colon carcinoma HCT 116 cells). Second, we characterized in a refined fashion how these agents affect cell cycle progression in the same cellular model. This procedure is amenable for precisely evaluating cell cycle perturbations as induced by known or novel pharmacological agents.

2. Materials

2.1. Common Materials

2.1.1. Disposables

- 0.22 μm filters.
- 0.5, 1.5, and 2 μL microcentrifuge tubes.
- 15 and 50 mL conical centrifuge tubes.
- 25, 75, or 175 cm^2 flasks for cell culture.
- 5 mL, 12×75 mm FACS tubes.
- 6-, 12-, 24-, 96-well plates for cell culture.
- Counting chamber: Improved Neubauer or Bürker hemocytometer.

2.1.2. Equipment

- Cytofluorometer (see Note 1):
  - FACSVantage (BD, San José, USA), equipped with a UV laser (argon ion laser emitting at 488 nm) and a 70 μm nozzle, and controlled by the operational/analytical software CellQuest™ Pro (BD).
  - Gallios (Beckman Coulter, Miami, USA), equipped with three solid-state lasers emitting at 488, 638, and 405 nm (ten colors), and controlled by the operational Gallios software.
- Bright-field inverted microscope: XDS-1R (Optika, Ponteranica, Italy), equipped with 10×, 25×, and 40× long working distance plan achromatic objectives.

2.1.3. Software

- CellQuest™ Pro (BD).
- Kaluza software (Beckman Coulter).
- Win-MDI 2.9 (©1993–2000, Joe Trotter).

2.1.4. Reagents

- Alignment beads: AlignFlow™ Plus flow cytometry alignment beads, 6 μm, for 350–370 nm (UV) and 488 nm excitation, stock solution at ~1.2×10^8 beads/mL, stored at 4°C under protection from light (see Notes 2 and 3).
- Complete growth medium for HCT 116 human colon carcinoma cells: McCoy's 5A medium containing 4.5 g/L glucose and 4 mM L-glutamine, supplemented with 1 mM sodium pyruvate, 100 mM HEPES buffer, 100 U/mL penicillin G sodium, 100 μg/mL streptomycin sulfate, and 10% fetal bovine serum (FBS); stored at 4°C (see Notes 4 and 5).
- Dimethylsulfoxide (DMSO) (Sigma-Aldrich, St Louis, MO, USA) (see Note 6).
- Phosphate buffered saline (PBS) 1×: 137 mM NaCl, 2.7 mM KCl, 4.3 mM Na_2HPO_4, 1.4 mM KH_2PO_4 in deionized water (dH_2O), adjust pH to 7.4 with 2 N NaOH; stored at room temperature (RT).

- Sheath fluid: FACSFlow™ (BD) and IsoFlow™ Sheath Fluid (Beckman Coulter), stored at RT (see Note 7).
- Trypan blue (TB), stock solution in PBS, 0.4% (w/v), stored at RT (see Notes 8 and 9).
- Trypsin/EDTA: 0.25% trypsin, 0.38 g/L (1 mM) EDTA×4 Na^+ in HBSS, stored at –20°C (see Notes 10–12).
- Chemicals (see Note 13).
  - AZD 1152-HQPA (Selleck Chemicals, Munich, Germany), MW = 507.56 g/mol, stock solution in DMSO at 10 mM, stored at –20°C under protection from light (see Notes 14–16).
  - Nocodazole (Sigma-Aldrich): MW = 301.3 g/mol, stock solution in DMSO at 10 mM, stored at –20°C under protection from light (see Notes 17–19).
  - Roscovitine (Sigma-Aldrich): MW = 354.5 g/mol, stock solution in DMSO at 10 mM, stored at –20°C under protection from light (see Notes 20–22).
  - SP600125 (Sigma-Aldrich): MW = 220 g/mol, stock solution in DMSO at 30 mM, stored at –20°C under protection from light (see Notes 23–25).
  - Thymidine (Sigma-Aldrich): MW = 242.23 g/mol, stock solution in complete medium at 50 mM (see Notes 26–28), stored at +4°C.

2.2. Assessment of Cell Proliferation

- 5(6)-Carboxyfluorescein diacetate N-succinimidyl ester (CFSE) (Molecular Probes-Invitrogen), stock solution in DMSO at 5 mM, stored at –20°C under protection from light (see Notes 29–32).

2.3. Quantification of Cell Cycle Distribution

- Bovine serum albumin (BSA) (Sigma-Aldrich), stock solution 10 mg/mL in dH_2O, stored at 4°C (see Note 33).
- DNA dyes (Molecular Probes-Invitrogen) (see Notes 34 and 35):
  - 4′,6-Diamidino-2-phenylindole, dihydrochloride (DAPI), stock solution in dH_2O at 10 mM, stored at 4°C under protection from light (see Notes 36–38).
  - 7-Aminoactinomycin D (7-AAD), stock solution in DMSO at 1 mg/mL, stored at –20°C under protection from light (see Notes 39–41).
  - FxCycle™ far-red stain (FxCycle), stock solution in DMSO at 200 μM, stored at –20°C under protection from light (see Notes 42–44).
  - Hoechst 33342, stock solution in dH_2O or DMSO at 10 mg/mL, stored at 4°C under protection from light (see Notes 45–48).

– Propidium iodide (PI), stock solution in dH_2O at 1 mg/mL, stored at 4°C under protection from light (see Notes 49–51).

2.3.1. Cell Cycle Profiling

- Fixative solution: Ice-cold 75% ethanol in dH_2O, stored at –20°C (see Note 52).
- Staining solution: 20 μg/mL 7-AAD (see Notes 39–41), 10 μM DAPI (see Notes 36–38), 1 μM FxCycle (see Notes 42–44) or 50 μg/mL PI (see Notes 49–51), in 0.1% (w/v) D-glucose in PBS supplemented with 1 μg/mL (w/v) ribonuclease (RNase) A (Sigma-Aldrich) (see Note 53), prepared extemporarily.

2.3.2. Quantification of Cells in the S Phase: EdU Incorporation Assay

- Click-iT® EdU Flow Cytometry Assay Kit (Molecular Probes-Invitrogen) (see Note 54):
  – 5-Ethynyl-2′-deoxyuridine (EdU), stock solution in DMSO at 10 mM, stored at –20°C in small aliquots (see Notes 55 and 56).
  – Alexa Fluor® 488 Azide, working solution made by adding 260 μL DMSO, stored at –20°C in small aliquots (see Note 57).
  – Click-iT® EdU buffer additive, 10× stock solution in dH_2O, stored at –20°C (see Note 58).
  – Click-iT® EdU reaction buffer, 10× solution containing TBS (see Note 59).
  – Click-iT® fixative: 4% paraformaldehyde in PBS (see Notes 60 and 61).
  – Click-iT® saponin-based permeabilization and wash reagent, 10× solution in 1% (w/v) BSA in PBS, stored at 4°C (see Notes 33 and 62).
  – Click-iT® Triton® X-100-based permeabilization reagent, 1× solution in PBS, stored at 4°C (see Note 63).
  – $CuSO_4$, stock solution in dH_2O at 100 mM stored at 4°C (see Note 64).

2.3.3. Assessment of Histone H3 Phosphorylation and Cyclin B1 Levels

- Primary antibodies (see Note 65).
  – Anti-cyclin B1 (mouse monoclonal IgG_1, #554176, BD Biosciences), provided as a 250 μg/mL solution in aqueous buffer containing ≤0.09% sodium azide (see Note 2).
  – Anti-phosphorylated histone H3 (Ser28) (rabbit antiserum, #07-145, Millipore-Chemicon International, Temecula, CA, USA), provided as a 1 mg/mL solution in buffer containing 0.1 M Tris-Glycine (pH 7.4), 150 mM NaCl, and 0.05% sodium azide (see Note 2).

- Secondary antibodies (see Notes 65 and 66):
  - Alexa Fluor® 488 Goat Anti-mouse IgG (H + L) (Molecular Probes-Invitrogen, #A1101), provided as a 1 mg/mL solution in 0.1 M sodium phosphate, 0.1 M NaCl, 2 mM EDTA, 1% glycerol, ≤0.05% sodium azide (pH 7.5) (see Note 2).
  - Alexa Fluor® 568 Goat Anti-rabbit IgG (H + L) (Molecular Probes-Invitrogen), provided as a 1 mg/mL solution in 0.1 M sodium phosphate, 0.1 M NaCl, 2 mM EDTA, 1% glycerol, ≤0.05% sodium azide (pH 7.5) (see Note 2).
- Tween 20 (see Note 2).

3. Methods

3.1. Cell Culture and Treatment with Chemicals

1. Upon thawing, maintain human colon carcinoma HCT 116 cells in complete growth medium within 75 cm^2 flasks (37°C, 5% CO_2) (see Note 67).
2. When confluence approaches 80–90% (see Note 68), remove and discard culture medium, gently rinse the cell layer with pre-warmed PBS (see Note 69) and detach cells with 0.25% (w/v) Trypsin-EDTA solution or with TrypLE™ Express (see Notes 70–72).
3. Upon detachment, add complete growth medium (see Note 73) and transfer aliquots of the cell suspension to new 75 or 150 cm^2 flasks, to constitute fresh maintenance cultures (see Notes 68 and 74).
4. Alternatively, for experimental determinations, seed cells in 25 cm^2 flasks or 12-well plates, depending on the specific experimental setting (see below) (see Note 75).
5. Twenty-four hour after seeding (to allow cells to adhere, readapt and recover normal growth rates) (see Note 76), chemicals can be administered at the concentration of choice in fresh, complete growth medium (see Note 77).
6. Cells treated with an equivalent volume of the solvent used for the reconstitution of drugs will provide appropriate negative control conditions (see Note 78).

3.2. Assessment of Cell Proliferation

3.2.1. Assessment of Cell Proliferation: Cell Counting with Beads

1. Seed ~0.8×10^5 HCT 116 cells in 12-well plates (1 mL growth medium/well) and let adhere for 24 h.
2. Treat adherent cells by substituting the culture medium with complete medium supplemented with the agent of choice (see Subheading 3.1, steps 5 and 6 and Notes 76–79).
3. At the end of the stimulation period, collect culture supernatants in 5 mL FACS tubes (see Notes 80 and 81).

4. Detach adherent cells with ~0.5 mL trypsin/EDTA per well (see Notes 70–72).
5. Upon detachment, add 1 mL of complete growth medium and transfer cells to the FACS tubes containing the corresponding supernatant (see Note 73).
6. Dilute alignment beads in pre-warmed complete growth medium (1 drop/mL) (see Notes 2 and 3).
7. Centrifuge samples at 300 × g, RT, for 5 min and discard supernatants.
8. Resuspend cell pellets in 0.3 mL of the bead-containing solution (see Notes 82 and 83).
9. Analyze samples by means of a classic cytofluorometer allowing for the acquisition of light scattering data, and fluorescence in (at least) two separate channels (e.g., green and red).
10. Perform acquisition and analysis by first gating on events that are characterized by normal light scattering parameters (forward scatter, FSC; and side scatter, SSC) (see Notes 84 and 85) (Fig. 1a).

3.2.2. Assessment of Cell Proliferation: CellTrace™ CFSE Staining

1. Seed 0.5–1 × 10^6 HCT 116 cells in 5–10 mL complete growth medium in 25 cm^2 flasks and allow them to adhere for 24 h.
2. Discard supernatant (see Notes 76, 80, and 81), wash adherent cells with 5 mL pre-warmed PBS (see Note 69), and detach them with 1–2 mL trypsin-EDTA (see Notes 70–72).
3. Upon detachment, add 5 mL complete growth medium (see Note 73) and collect cells in 15 mL centrifuge tubes.
4. Centrifuge samples at 300 × g, RT, for 5 min, remove supernatants and resuspend cell pellets in 1 mL cold PBS containing 2.5 μM CFSE (see Notes 29 and 86).
5. Incubate cells for 5 min at RT under protection from light.
6. Thereafter, add 1 mL FBS to stop the CFSE labeling, centrifuge as above (see step 4) and wash cells twice with PBS.
7. Check the staining quality by rapidly observing CFSE-labeled cells in fluorescence microscopy (see also Note 32).
8. Seed CFSE-labeled cells in 12-well plates (~0.8 × 10^5 cells/well in 1 mL complete growth medium), let adhere for 24 h, and then treat them with the agents of choice (see Subheading 3.1, steps 5 and 6 and Notes 76–79).
9. After the appropriate time, collect cells as described above (see Subheading 3.2.1, steps 3–5, and 7 and Notes 70–73, 80, 81, and 83), resuspend cell pellets in 0.3 mL cold PBS and perform cytofluorometric acquisition/analysis of the samples upon gating on events characterized by normal light scattering parameters (see Subheading 3.2.1, steps 9 and 10 and Notes 84, 85, and 87) (Fig. 1b).

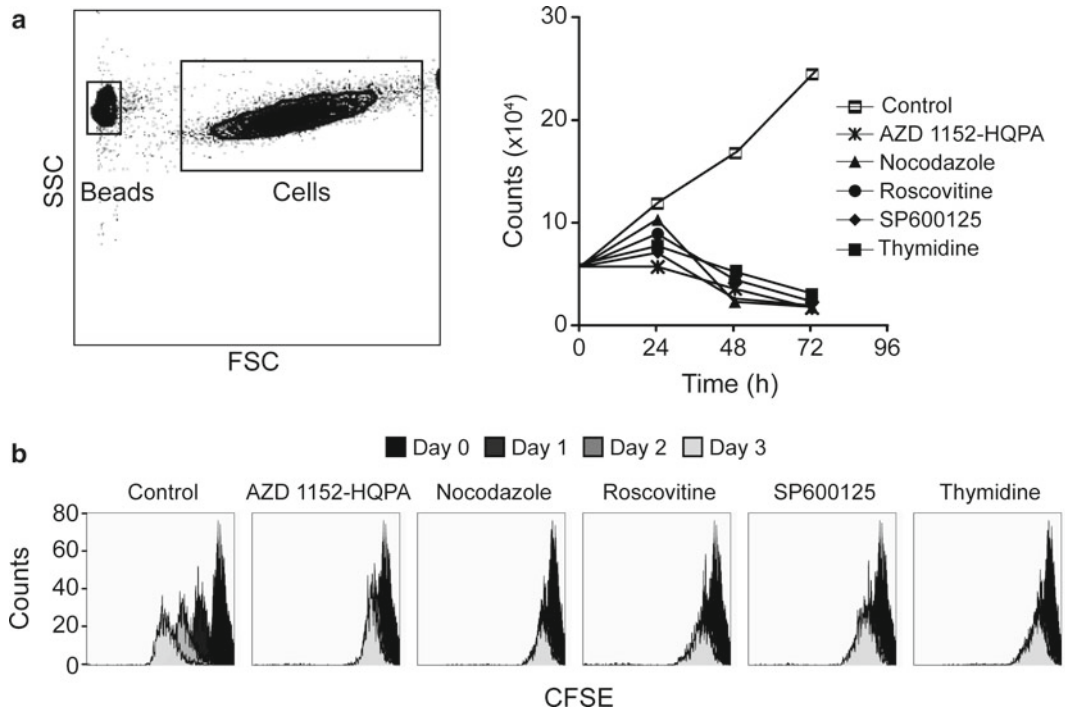

Fig. 1. Proliferation of colon carcinoma cells upon AZD 1152-HQPA, nocodazole, roscovitine, SP600125 or thymidine treatment. (**a**) *Beads-mediated cell counting.* Human colorectal carcinoma HCT 116 cells were left untreated or treated for the depicted time with 1 μM AZD 1152-HQPA, 100 nM nocodazole, 10 μM roscovitine, 30 μM SP600125 or 2 mM thymidine, then collected, resuspended in a bead-containing solution as detailed in Subheading 3.2.1 and analyzed by flow cytometry. Cytofluorometric acquisition was interrupted after 5,000 beads and the corresponding number of events characterized by normal forward scatter (FSC) and side scatter (SSC) was determined. The *left panel* depicts the relative positioning of beads and cells on a FCS versus SSC *dot plot*. On the right, quantitative data are reported. (**b**). *Assessment of cell proliferation by CellTrace™ CFSE staining.* Cells were stained with CFSE as detailed in Subheading 3.2.2, then treated as in (**a**). Thereafter, fluorescence intensity (which diminishes with each cell division) was determined by cytofluorometry at the indicated time points. Histograms depict the overlay of subsequent acquisitions. Please note that control cells proliferate normally—as demonstrated by increased cell numbers (**a**) and decreased CFSE intensity (**b**)—whereas cells exposed to AZD 1152-HQPA, nocodazole, roscovitine, SP600125, or thymidine undergo a proliferative arrest. Data are representative of one out of three independent experiments yielding similar results.

3.3. Cell Cycle Studies

3.3.1. Cell Cycle Profiling

1. Forty-eight hours upon seeding in 12-well plates, collect cells (together with the corresponding supernatants) in FACS tubes, as described Subheading 3.2.1, steps 3–5 and Notes 70–73, 80, 81, and 83.
2. Centrifuge cells as described in Subheading 3.2.1, step 7 and discard supernatants.
3. For live cell staining, resuspend pellets in 0.3 mL pre-warmed growth medium supplemented with 2 μM Hoechst 33342 (see Notes 34, 45, and 83).
4. Keep cells in staining conditions (37°C, 5% CO_2, under protection from light) for 30 min and then proceed to cytofluorometric acquisition (see Subheading 3.2.1, steps 9 and 10 and Notes 84, 85, 88–92) (Fig. 2).

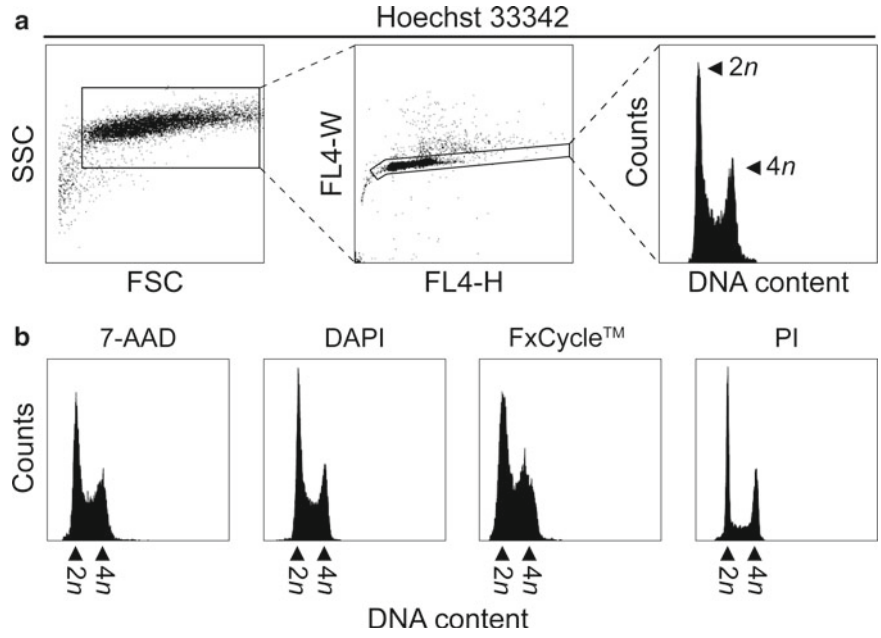

Fig. 2. Comparative analysis of the cell cycle profiling obtained with different DNA dyes. Forty-eight hours after seeding, human colorectal carcinoma HCT 116 cells were collected and stained with Hoechst 33342, or—alternatively—fixed with ethanol and stained with four different dyes: 7-aminoactinomycin D (7-AAD), 4′,6-diamidino-2-phenylindole (DAPI), FxCycle™ far-red, or propidium iodide (PI), as detailed in Subheading 3.3.1. After the appropriate staining time, samples were analyzed by cytofluorometry. In panel (**a**), the gating procedure to sequentially concentrate the analysis on events characterized by normal light scattering parameters (*left panel*) and to exclude doublets (*central panel*) is illustrated. In panel (**b**), representative cell cycle profiles are reported. Please note the high quality and resolution of the cell cycle profile resulting upon PI staining (well defined G_1 and G_2/M peaks) as compared to those obtained with other DNA fluorochromes. Data are representative of one out of three independent experiments yielding similar results.

5. Alternatively, for fixed cell staining, add ice-cold 75% ethanol dropwise (see Note 93) and incubate samples at –20°C for at least 24 h.
6. Centrifuge tubes at 300 × g at 4°C for 5 min, discard ethanol and wash cells 2–3 times with cold PBS.
7. Add 300 μL of the staining solution to cell pellets, incubate for 30 min at 37°C, and then proceed to cytofluorometric acquisition (see Subheading 3.2.1, steps 9 and 10 and Notes 84, 85, 88, 94–97) (Fig. 2).

3.3.2. Quantification of Cells in the S Phase: EdU Incorporation Assay

1. Seed HCT 116 cells in 12-well plates (0.8×10^5/well), allow them to adhere for 24 h and then treat them with the agents of choice (see Subheading 3.1, steps 5 and 6 and Notes 76–79).
2. After the appropriate incubation time, replace the culture medium with 1 mL pre-warmed growth medium supplemented with 10 μM EdU (see Notes 56 and 98). Cells incubated with EdU-free complete growth medium constitute an appropriate negative control.

3. Maintain cells under optimal culture conditions for 30–45 min (see Note 99), then collect them as described in Subheading 3.2.1, steps 3–5, and 7 (see also Notes 70–73, 80, 81, and 83).
4. Wash once with 1% (w:v) BSA in PBS, discard supernatants, and resuspend pellets in 100 μL Click-iT® fixative solution (see Note 60).
5. Incubate cells for 15 min at RT under protection from light (see Notes 60 and 99).
6. After two additional washes with 1% (w:v) BSA in PBS, permeabilize cells with 100 μL Triton® X-100-based permeabilization reagent (see Notes 63 and 100) and incubate for 30 min at RT under protection from light.
7. In the meanwhile, prepare the Click-iT® reaction cocktail (500 μL for tube) by mixing (see Note 101): 438 μL Click-iT® 1× Reaction Buffer (see Note 59), 10 μL $CuSO_4$ (see Note 64), 2.5 μL Alexa Fluor 488 Azide (see Note 57), 50 μL Reaction Buffer Additive (see Note 58).
8. Wash samples once with 1% (w:v) BSA in PBS, remove supernatants and resuspend pellets in 500 μL Click-iT® reaction cocktail (see Notes 83 and 102).
9. Incubate for 30 min at RT under protection from light.
10. Wash again with 1% (w:v) BSA in PBS then add to pellets 500 μL DAPI solution (see Notes 34, 36, 83, and 94).
11. Incubate for 30 min at 37°C in a 5% CO_2 atmosphere and proceed to cytofluorometric acquisitions and analysis (see Subheading 3.2.1, steps 9 and 10 and Subheading 3.3.1, step 7 and Notes 84, 85, 88, 95–96, and 103) (Fig. 3).

3.3.3. Assessment of Histone H3 Phosphorylation and Cyclin B1 Levels

1. Seed HCT 116 cells in 12-well plates (0.8×10^5/well), allow them to adhere for 24 h and then treat them with the agents of choice (see Subheading 3.1, steps 5 and 6 and Notes 76–79).
2. After the appropriate incubation time, collect cells in FACS tubes as described in Subheading 3.2.1, steps 3–5, and 7 (see also Notes 70–73, 80, 81, and 83).
3. Fix cells with ice-cold ethanol as described in Subheading 3.3.1, step 5 (see also Note 93).
4. Upon incubation at −20°C for at least 24 h, centrifuge samples at 300 × g, 4°C, for 5 min, to remove ethanol, then wash cells 2–3 times with cold PBS.
5. Add 1 mL 0.25% (v/v) Tween 20 in PBS to each tube (see Note 2), then incubate samples at 4°C for 15 min.
6. Wash twice with 1% (w/v) BSA in PBS, then block unspecific binding by incubating samples in 3% (w/v) BSA in PBS for at 4°C for 30 min (see Notes 104 and 105).

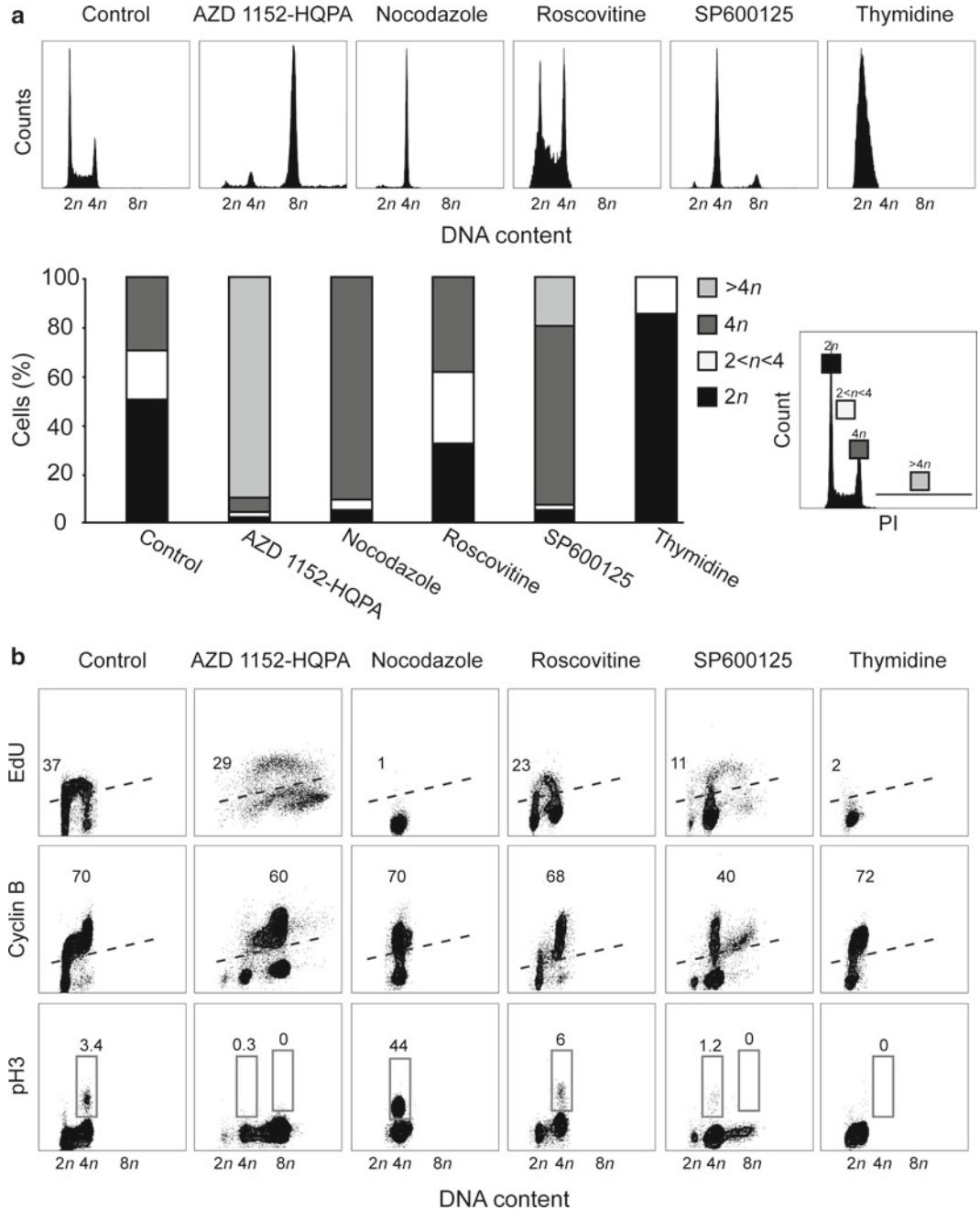

Fig. 3. Impact of AZD 1152-HQPA, nocodazole, roscovitine, SP600125 and thymidine on cell cycle distribution. (**a**) and (**b**). Human colorectal carcinoma HCT 116 cells were left untreated (control) or exposed either for 12 h to 100 nM nocodazole, 10 μM roscovitine and 2 mM thymidine or for 24 h to 1 μM AZD 1152-HQPA and 30 μM SP600125. Thereafter, cells were either labeled with the thymidine analog EdU, as detailed in Subheading 3.3.2, or co-immunostained for the detection of cyclin B1 and phosphorylated histone 3 (pH3), as detailed in Subheading 3.3.3. In both cases, propidium iodide (PI) was employed to monitor DNA content. In panel (**a**), representative cell cycle profiles and quantitative data on DNA content are reported. In representative *dot plots* provided in panel (**b**), the percentage of EdU-incorporating (*upper panels*), cyclin B1$^+$ (*middle panels*) and pH3$^+$ (*lower panels*) cells with the indicated DNA content is reported. Data are representative of one out of three independent experiments yielding similar results.

7. In the meanwhile, dilute primary anti-cyclin B1 and anti-phopho-H3 antibodies 1:100 in 1% (w/v) BSA in PBS (see Notes 65, 106–108).
8. Centrifuge samples at 300 × g, RT, for 5 min, discard supernatants, and resuspend each pellet in 200 μL primary antibody solution (see Note 109).
9. Cells incubated with 200 μL primary antibody-free 1% (w/v) BSA in PBS constitute an appropriate negative control.
10. Incubate samples for 1 h at RT (see Note 110).
11. In the meanwhile, dilute secondary Alexa Fluor® 488 Goat Anti-mouse and Alexa Fluor® 568 Goat Anti-rabbit antibodies 1:300 in 1% (w/v) BSA in PBS (see Notes 65 and 66).
12. Wash cells three times with of 1% (w/v) BSA in PBS (see Note 111), add 200 μL secondary antibody solution to each tube, and incubate at 4°C for 30 min under protection from light (see Note 112).
13. Wash samples twice with 3 mL 1% (w/v) BSA in PBS and resuspend cells in 500 μL 10 μM DAPI in cold PBS (see Notes 34, 36, 83, and 94).
14. Incubate for 30 min at 37°C in a 5% CO_2 atmosphere under protection from light.
15. Store samples at 4°C for 1 h, then analyze them by means of a classic cytofluorometer allowing for UV excitation and acquisition of light scattering data as well as fluorescence in (at least) three separate channels (e.g., green, red, or orange, and blue) (see Subheading 3.2.1, steps 9 and 10—Subheading 3.3.1, step 7 and Notes 84, 85, 88, 95, 96, 113, and 114) (Fig. 3).

3.4. Guidelines for the Correct Interpretation of Cell Cycle Progression Data

Here, we provide a short set of guidelines for researchers approaching the study of drugs that (may) affect cell cycle progression.

1. First, the actual cytostatic potential of the compound(s) under investigation should be determined by cell counting with beads or CellTrace™ CFSE staining. This is important as it allows for the relatively straightforward discrimination between agents that exert bona fide cytostatic effects and agents that do not. As a note, at the concentration and time points tested here, the AURKB inhibitor AZD 1152-HQPA, the microtubular inhibitor nocodazole, the CDKs inhibitor roscovitine, the multikinase inhibitor SP600125, and thymidine all inhibited the proliferation of HCT 116 cells (Fig. 1).
2. Second, drugs that exert bona fide cytostatic effects should be more precisely characterized for their capability to alter cell cycle distribution. To this aim, we recommend to perform preliminary cell cycle profiling experiments on treated versus untreated cells, either upon fixation (PI staining) or not

(Hoechst 33342 staining) (Fig. 2). By this approach, we were able to show that, when administered to HCT 116 cells, (1) thymidine induces a near-to-complete arrest at the G_1/S transition or in early S, (2) nocodazole, SP600125 and roscovitine favor the accumulation of cells with ~4n DNA content, and (3) AZD 1152-HQPA causes an exquisite increase in the fraction of cells bearing an ~8n DNA content. It should be noted that, in this two latter instances, no information can be derived on the cell cycle distribution, as diploid cells in G_2 and M contain as much DNA as tetraploid cells in G_1 and tetraploid cells in G_2 and M contain as much DNA as octaploid cells in G_1 (Fig. 3a).

3. Cell cycle profiling, which is relatively inaccurate, should be followed by a more refined analysis of cell cycle progression. To this aim, we recommend to employ assays that allow for the quantification of cells that actively synthesize DNA such as the EdU incorporation Click-iT® test. In our setting, HCT 116 cells responding to AZD 1152-HQPA, and roscovitine (and at least partially SP600125), but not cells exposed to thymidine and nocodazole, preserved the ability to synthesize DNA (Fig. 3b).
4. Finally, the precise cell cycle distribution of cells responding to the stimuli of choice should be assessed by cytofluorometry upon co-immunostaining with antibodies that recognize cell cycle phase-restricted cyclins (such as cyclin B1, whose intracellular levels begin to raise in S to abruptly fall at the onset of anaphase) and/or cell cycle phase-specific post-translational modifications (such as the phosphorylation of histone H3, which is a mitotic marker). This analysis allows for the precise discrimination between cell cycle phases in mixed cell populations having the same DNA content. As an example, cells with an ~4n DNA content are in a diploid G_2 phase if they display elevated levels of cyclin B1 and low amounts of phosphorylated histone H3 (cyclin $B1^+/pH3^-$), in a diploid metaphase when they stain positively for both cyclin B1 and pH3 (cyclin $B1^+/pH3^+$), or in a tetraploid G_1 phase if they fail to stain for both markers (cyclin $B1^-/pH3^-$). In our setting, (1) roscovitine arrested HCT 116 cells in a diploid G_2 phase (~4n, cyclin $B1^+/pH3^-$); (2) nocodazole induced a mitotic arrest (~4n, cyclin $B1^+/pH3^+$) with a mild generation of tetraploid cells in G_1 (4n, cyclin $B1^-/pH3^-$); while (3) SP600125 and AZD 1152-HQPA efficiently generated polyploids in the absence of an evident mitotic blockage (~4n, cyclin $B1^-/pH3^-$ and ~4n/~8n cyclin $B1^-/pH3^-$ for SP600125 and AZD 1152-HQPA, respectively) (Fig. 3b).
5. The integration of the results obtained with the techniques described above is critical for correctly interpreting the impact of the agents under investigation on cell cycle progression. In addition, this set of techniques—when applied as we described—allows

for the internal validation of (at least part of the observations). To mention a standalone example out of the dataset presented here, the thymidine-induced arrest in G_1/S preliminarily evidenced upon cell cycle profiling (Fig. 3a) is confirmed by the findings that thymidine-treated HCT 116 cells neither incorporate EdU nor stain positively for pH3 (Fig. 3b).

6. Finally, as chemicals that alter the cell cycle often also exert cytotoxic effects (under the same conditions or, more often, at higher concentrations and upon prolonged exposure) (38–40), it is strongly recommendable to have cell cycle determinations performed together with assays to monitor cell death (41). High levels of cell death, indeed, have a dramatic biasing effect on cell cycle distributions and de facto preclude proper cell cycle studies. The detailed description of techniques for the quantification of cell death-associated parameters largely exceeds the scope of this chapter and can be found in refs. 42–44. This said, the sequential approach that we have detailed here allows for a precise characterization of the cytostatic and cell cycle-modulatory effects of chemical and physical stimuli in vitro, which in turn may constitute a basis for subsequent in vivo studies.

4. Notes

1. In order to ensure optimal and long-lasting performances, it is strongly recommended to subject the cytofluorometer to maintenance procedures on a routine basis, following the manufacturer's recommendations. Of note, the flow rate should be controlled—and the system aligned and calibrated with appropriate beads (see also Notes 2 and 3)—on a daily basis, immediately before use.
2. AlignFlow™ Plus flow cytometry alignment beads are provided as suspensions in water containing 2 mM sodium azide (NaN_3) and 0.05% (v/v) Tween 20. NaN_3 is extremely toxic by ingestion and under acidic conditions may release the highly toxic gas hydrazoic acid. Tween 20 is not currently listed as a carcinogen by the National Toxicology Program (NTP), the International Agency for Research on Cancer (IARC) or the Occupational Safety and Health Administration (OSHA), yet may behave as a mild irritant for the eyes, skin, and respiratory system.
3. Under appropriate storage conditions (+4°C, under protection from light), AlignFlow™ Plus flow cytometry alignment beads are stable for at least 1 year.
4. Optimal growth conditions (e.g., medium composition and supplements) vary for different cell lines, and may influence

not only growth rates but also the response to the agent(s) of choice. Unless changes in the composition of the growth medium are part of the experimental protocol, we suggest to use the medium recommended by the American Type Culture Collection (ATCC, Manassas, USA).

5. Penicillin G and streptomycin are included in culture media to prevent bacterial contamination, 4-(2-hydroxyethyl)-1-piperazineethanesulfonic acid (HEPES) is a zwitterionic organic chemical buffering agent, whereas sodium pyruvate represents a readily accessible energy source for propagating cells and a carbon skeleton for their anabolic processes.
6. DMSO may be harmful by inhalation or skin absorption and is inflammable. For these reasons, it should always be handled in a chemical fume hood and by wearing appropriate protective equipment (gloves, clothing, and eyewear). In addition, it should always be kept away from heat, sparks, and open flames.
7. FACSFlow™ and IsoFlow™ Sheath Fluid are a mixture of multiple substances, any of which, at their given concentration, is considered to be hazardous to health.
8. TB is not currently listed as a carcinogen by the NTP, IARC, or OSHA, yet may behave as an irritant for the eyes, skin, gastrointestinal tract, and respiratory system.
9. Undissolved TB appears as a dark purple-brown powder and is stable under ordinary conditions of use and storage (RT, sealed vials). TB is soluble in aqueous solvents (e.g., dH_2O and PBS) but the solution tends to form precipitates with time, which are quickly dissolved by agitation.
10. EDTA is not currently listed as a carcinogen by NTP, IARC, or OSHA, yet may behave as a mild irritant for the eyes, skin, and respiratory system.
11. Under appropriate storage conditions (at –20°C, under protection from light), Trypsin/EDTA is stable for at least 18 months.
12. TrypLE™ Express is a convenient replacement for trypsin, owing to its fully synthetic origin, its storage temperature (+4°C) and its elevated stability at RT.
13. An appropriate exhaust ventilation system is required in rooms where drugs are reconstituted. The manufacturers recommend to avoid the formation of dust and the inhalation of vapors/mists/gases. Containers should be kept tightly closed and stored under protection from light.
14. AZD 1152-HQPA is a potent and specific inhibitor of AURKB.
15. AZD 1152-HQPA is highly toxic if swallowed (may impair fertility and be harmful for fetuses) and may behave as moderate to severe irritant for the skin and the eyes. Therefore, it should always be handled with the maximal care and by wearing suitable protective equipment (gloves, clothing, and eyewear).

16. Undissolved AZD 1152-HQPA has a whitish crystalline appearance. Under appropriate storage conditions (–20°C, under protection from light), AZD 1152-HQPA solutions are stable for at least 1 year.
17. Nocodazole is a microtubule-depolymerizing agent that directly binds to tubulin.
18. Nocodazole is not currently listed as a carcinogen by NTP, IARC, or OSHA, yet it may be harmful or fatal if inhaled, swallowed, or absorbed through skin, and may cause eye irritation. Therefore, this substance should always be handled using suitable protective equipment (gloves, clothing, and eyewear).
19. Undissolved nocodazole appears as a beige powder and has a minimum shelf life of 2–3 years (stored at 4°C, under protection from light). Under appropriate storage conditions (–20°C, under protection from light), nocodazole solutions are stable for several months. However, nocodazole solutions should be aliquoted to avoid repeated freeze-thawing. Nocodazole is stable in biological media for at least 7 days.
20. Roscovitine is a purine analog that acts as CDK1, CDK2, and CDK5 inhibitor.
21. Roscovitine is not currently listed as a carcinogen by NTP, IARC, or OSHA, yet it may be harmful or fatal if inhaled, swallowed, or absorbed through skin, and may cause eye irritation. Therefore, this substance should always be handled using suitable protective equipment (gloves, clothing, and eyewear).
22. Undissolved roscovitine appears as a white powder. It is recommendable to store roscovitine solutions in small aliquots to avoid repeated freeze-thawing.
23. SP600125 is a broad-spectrum inhibitor of serine/threonine kinases including AURKA, AURKB, JNK1, JNK2, and MPS1.
24. SP600125 is not currently listed as a carcinogen by NTP, IARC, or OSHA, yet causes skin and eye irritation and may be harmful by inhalation. Thus, this substance should always be handled by wearing suitable protective equipment (gloves, clothing, and eyewear).
25. Undissolved SP600125, which is insoluble in water, appears as a yellow powder. It is recommendable to store SP600125 stock solutions in small aliquots to avoid repeated freeze-thawing.
26. Thymidine is a pyrimidine deoxynucleoside.
27. Thymidine is not identified as a carcinogen by NTP, IARC, or OSHA. However, as this compound is considered a possible mutagen and may be harmful if inhaled, swallowed or absorbed through skin, it should always be manipulated by wearing suitable protective equipment (gloves, clothing, and eyewear).

28. Undissolved thymidine appears as a white powder. Thymidine solutions are colorless and stable for some days, under appropriate storage conditions (+4°C, under protection from light). However, it is strongly recommended to dissolve thymidine and sterilize the solution by filtration (using a 0.22 μm filter) on the same day of use.
29. CFSE is not currently listed as a carcinogen by NTP, IARC, or OSHA, yet may behave as mild irritants for the eyes, skin and the respiratory system and therefore should be handled by wearing suitable protective equipment (gloves, clothing, and eyewear).
30. Lyophilized CFSE appears as an off-white, nonfluorescent crystalline substance and is stable for at least 6 months, under appropriate storage conditions (−20°C, under protection from light). The manufacturer recommends to avoid repeated freeze-thawing of CSFE solutions.
31. Upon passive diffusion into cells, CFSE is hydrolyzed by intracellular esterases and form fluorescent conjugates with intracellular amines.
32. Upon hydrolysis by intracellular esterases (see also Note 31), CFSE exhibits excitation/emission peaks at approximately 492/517 nm, respectively. CFSE-labeled cells may also be visualized by fluorescence microscopy using the standard fluorescein filter (excitation = 492 nm; emission = 517 nm) .
33. Under appropriate storage conditions (4°C, under protection from light and humidity), undissolved BSA is stable for at least 1 year. BSA stock solutions, on the contrary, should not be stored for more than 2 weeks, owing to problems of bacterial contamination. To circumvent this issue, BSA solutions can be frozen or supplemented with 0.02% (w:v) sodium azide (see also Note 2).
34. Although available information may be inadequate, DNA-binding dyes are potential carcinogens/mutagens and hence should always be manipulated by wearing suitable protective equipment (gloves, clothing, and eyewear).
35. It is strongly recommended to keep DNA-binding dyes in properly labeled and tightly sealed containers, under protection from light. In solution, such compounds almost invariably form precipitates with time. For this reasons, vials should always be properly agitated/vortexed/mixed prior to use.
36. Although the available information is not adequate for making a satisfactory assessment, DAPI should be treated as a potential carcinogen/mutagen. This compound may cause skin, eye and respiratory irritation, and hence should always be manipulated by wearing suitable protective equipment (gloves, clothing, and eyewear).

37. Undissolved DAPI appears as a yellow powder and is soluble in water, but not in PBS. Under appropriate storage conditions (+4°C, under protection from light), DAPI stock solutions are stable for some months.
38. DAPI is a cell-impermeant dye labeling double-stranded nucleic acids (with a binding specificity for AT clusters in the minor groove). DNA-bound DAPI exhibits excitation/emission peaks at ~350/~460 nm, respectively.
39. 7-AAD is considered as a possible carcinogen and as a substance which causes concern for man owing to possible mutagenic effects, but for which the available information is not adequate for making a satisfactory assessment. This product may impair fertility, may harm fetuses and is toxic by inhalation, swallowing and in contact with skin. Thus, 7-AAD should always be manipulated by wearing suitable protective equipment (gloves, clothing, and eyewear).
40. 7-AAD has a moderate water solubility. 7-AAD solutions have a red to dark purple color and are stable for some months under appropriate storage conditions (4°C, under protection from light).
41. 7-AAD is a cell-impermeant fluorochrome that selectively binds GC-rich DNA regions. DNA-bound 7-AAD has an excitation peak at 488 nm and can be detected in the far red range of the spectrum (650 nm long-pass filter).
42. Although the available information is not adequate for making a satisfactory assessment, the FxCycle™ far-red stain may behave as an irritant for the respiratory tract and the eyes, and hence should always be manipulated by wearing suitable protective equipment (gloves, clothing, and eyewear).
43. FxCycle™ far-red stain solutions are stable for at least 1 year, under appropriate storage conditions (–20°C, under protection from light).
44. The FxCycle™ far-red stain is a cell-impermeant dye with excitation/emission peaks at 635/650 nm, respectively.
45. Hoechst 33342 is currently listed among substances that may cause concern to man owing to possible mutagenic effects but for which the available information is inadequate for making satisfactory assessments. This product is harmful by inhalation or if swallowed, causes severe skin and eye burns and may provoke respiratory irritation. Handling Hoechst 33342 with the maximal care by wearing protective equipment (gloves, clothing, and eyewear) is recommended.
46. Undissolved Hoechst 33342 appears as a dark yellow powder. Under appropriate storage conditions (+4°C, under protection from light), Hoechst 33342 solutions are stable for at

least 6 months. Hoechst 33342 is particularly prone to photobleaching.

47. Hoechst 33342 is a cell-permeant fluorochrome that preferentially binds to AT-rich DNA regions. DNA-bound Hoechst 33342 exhibits excitation/emission peaks at ~346/~500 nm, respectively.
48. At appropriate dye dilutions, Hoechst 33342 staining is compatible with cell life. For this reasons, Hoechst 33342 should always be handled in sterile conditions, in particular in laboratories that use it routinely for the sorting/cloning of cells based on DNA content.
49. PI is not currently listed as a carcinogen by NTP, IARC, or OSHA but should be treated as such. PI behaves as an irritant for the eyes, respiratory system and skin, and may be harmful if swallowed. Thus, PI should always be manipulated by wearing suitable protective equipment (gloves, clothing, and eyewear).
50. PI solutions look red-and—under appropriate storage conditions (+4°C, under protection from light)—are stable for at least 18 months.
51. PI is a cell-impermeant fluorochrome that intercalate between DNA bases with little or no sequence specificity. DNA-bound PI exhibits excitation/emission peaks at ~535/~617 nm, respectively.
52. Ethanol is highly inflammable and may be harmful if inhaled, swallowed or absorbed through skin. Therefore, ethanol should always be manipulated by wearing suitable protective equipment (gloves, clothing, and eyewear). In addition, it should always be kept away from heat, sparks, and open flames.
53. RNase A is provided as a 20 mg/mL solution in 50 mM Tris–HCl (pH 8.0) and 10 mM EDTA (see also Note 10). This solution is stable at RT and maintains appropriate enzymatic activity for at least 12 months. RNase A is not considered to be hazardous to health.
54. Under appropriate storage conditions, Click-iT® EdU Flow Cytometry Assay Kit components are stable for up to 1 year. Components that are stored at −20°C should never be subjected to steep temperature changes and should always be kept on ice during use.
55. EdU is a nucleoside analog of thymidine that is incorporated into DNA during DNA replication, as occurring in the S phase of the cell cycle. Detection is based on a click chemistry, implying a copper-catalyzed reaction between an alkyne (contained in EdU itself) and an azide (provided by the detection reagent), generating a stable triazole ring.
56. The toxicity data available for EdU is inadequate for making satisfactory safety assessments. However, due to its potential

hazard to health, EdU should always be manipulated by wearing suitable protective equipment (gloves, clothing, and eyewear).

57. Please note that Alexa Fluor® 488 azide is particularly prone to photobleaching. This product contains sodium azide (see also Note 2).
58. The Click-iT® EdU buffer additive contains no substances that, at their given concentration, are considered to be hazardous to health.
59. The Click-iT® EdU reaction buffer contains no substances that, at their given concentration, are considered to be hazardous to health.
60. PFA is highly toxic by inhalation and should always be handled under an appropriate fume hood.
61. As the stability of PFA in solution is limited, it should be either prepared shortly before use or kept on ice throughout the entire experiment. As an alternative, PFA solutions can be frozen at preparation and thawed shortly before use. In this case, however, refreezing should be avoided.
62. Saponin is not currently listed as a carcinogen by NTP, IARC, or OSHA, yet causes serious irritations of the respiratory system and eyes. According to the manufacturer, this product contains 0.09% sodium azide (see also Note 2). Thus, saponin should always be manipulated by wearing suitable protective equipment (gloves, clothing, and eyewear).
63. Triton X-100 is not currently listed as a carcinogen by NTP, IARC, or OSHA, yet is harmful if swallowed, causes serious damage to eyes and is toxic to aquatic organisms. Thus, Triton X-100 should always be handled by wearing suitable protective equipment (gloves, clothing, and eyewear). In addition, adequate procedures should be established for Triton X-100 disposal.
64. Chronic exposure to copper can be dangerous for the liver and kidney. In addition, copper is harmful to aquatic organisms and may cause long-term effects to aquatic ecosystems. Hence, copper should always be handled by wearing suitable protective equipment (gloves, clothing, and eyewear). In addition, copper-containing solutions should be disposed according to adequate procedures.
65. Primary and secondary antibodies should be handled and stored as instructed by the manufacturer. Antibodies are provided in sodium azide-containing buffers (see also Note 2). These products should never be subjected to steep temperature changes and should always be kept in an ice bath throughout use.
66. Secondary antibodies should be carefully protected from light to prevent photobleaching.

67. Depending on specific requirements (e.g., physical space within incubators, need for very large amounts of cells), 75 cm^2 flasks can be substituted with smaller (25 cm^2 flasks) or larger (175 cm^2 flasks) cell culture supports.
68. The subculture of both under- and over-confluent flasks should be avoided, as it may result in a genetic drift of the cell population or in overcrowding-dependent stress, respectively, both of which may negatively affect experimental assessments.
69. At least one wash in PBS is recommended as it removes serum traces and salts that may inhibit trypsin. However, care should be taken with cell lines that are particularly prone to detachment, as prolonged and/or violent washes may result in a consistent loss of cells.
70. Appropriate amounts of trypsin-EDTA (or TrypLE™ Express) are 0.5, 1.5, 3, and 5/6 mL for 1 well of 12-well plates and for 25, 75, and 175 cm^2 flasks, respectively (see also Notes 10–12).
71. While shaking cell culture supports facilitates detachment, it also promotes cell clumping and hence should be avoided (see also Note 83). Detachment occurs more readily if cell culture supports are maintained at 37°C.
72. The trypsinization time varies as a function of cell type and culture density. For HCT 116 (and most adherent) cells, 3 min at 37°C are amply sufficient to fully detach a totally confluent, healthy population. To avoid a consistent loss of cells, it is recommendable to visualize complete detachment by light microscopy.
73. The serum contained in the complete culture medium definitively inactivates trypsin, rendering trypsinized cells compatible with reseeding. To completely remove trypsin and debris, however, it is recommendable to wash once cells in complete growth medium before seeding.
74. For most human cancer cells, passaging ratios of 1:3–1:8 are appropriate. To avoid genetic drifts of the cell populations, cells should not be subcultured beyond a predetermined number of passages. For this reason, the generation of a large liquid nitrogen stock of cells at the beginning of the experiments, starting from a homogenous and healthy population, is strongly recommended.
75. Upon thawing, allow cells to readapt for at least two passages before using them in experimental determinations.
76. Suboptimal culture conditions (e.g., limited adherence, under-/over-confluence) may dramatically influence the uptake of drugs and fluorochromes, as well as the cellular response to the former. It is therefore good practice to always check density and overall status of the cell cultures by light microscopy before any experimental procedure. As a guideline, cell density

at drug administration and staining should not exceed 40–50 and 80–90%, respectively.

77. To avoid cell detachment, the exhaust culture medium should be removed with the maximal care, and the fresh, drug-containing medium added slowly, while keeping the pipette tip abetted on the plate wall.
78. Organic solvents can be toxic to cells and promote specific cellular responses (e.g., differentiation) even at very low concentrations. It is therefore critical to ensure that, in the amounts employed as a vehicle for the agents under investigation, organic solvents do not influence the biological outcomes studied (e.g., cell cycle distributions).
79. For scarcely available and/or very expensive drugs, the total volume of medium per well can be reduced to 0.8 mL, provided that incubation times do not exceed 48 h. The combination of reduced culture volumes and prolonged incubation times is indeed particularly prone to result in high rates of evaporation, leading to cell stress.
80. The appearance of cells should always be checked by light microscopy before experimental assessments.
81. The supernatants of cultures subjected to chemical/physical stimuli contain the fraction of cells that underwent apoptosis-dependent detachment from the substrate during the stimulation period. Supernatants may be discarded if assays are supposed to include viable cells only.
82. Supernatants must be removed completely, by aspiration, to avoid the unwarranted dilution of the bead-containing solution. Moreover, as beads tend to precipitate very rapidly, the bead-containing solution must be thoroughly mixed before every tube. Importantly, one single bead-containing solution must be employed for all the samples of a single experiment, to ensure internal comparability of the results.
83. To ensure uniform labeling, it is critical to employ single-cell suspensions. If clumps have formed during detachment (see also Note 71), they can normally be resolved by pipetting repeatedly the cell suspension through a 1 mL Gibson pipette tip.
84. FSC depends on cell size while SSC reflects the refractive index, which in turn is influenced by multiple parameters including cellular shape and intracellular complexity (i.e., presence of cytoplasmic organelles and granules).
85. Cytofluorometers are provided with software for instrumental control and analysis. A number of analytical software packages (for both Mac and PC-based systems) are available online free of charge. For PC users, we recommend Win-MDI 2.9 (© 1993–2000, Joe Trotter), (freely available at http://www.cyto.purdue.edu/flowcyt/software.htm).

86. This total amount of CFSE is usually appropriate for labeling 10^5–10^6 cells that are subsequently allowed to proliferate for 72–96 h (3–4 rounds of mitosis). Prolonged follow-ups may require re-staining, as the increasing the initial amount of CFSE may result in (at least some extent of) cytotoxicity (see also Notes 30–32).
87. In our experimental setting, CFSE fluorescence is detected in channel FL1 (see also Note 32).
88. For optimal cytofluorometric assessments of the DNA content, follow these general guidelines: (1) avoid excessive cell confluence, (2) eliminate cell clumps, (3) do not wash cells after staining, (4) keep a sample of diploid cells as a reference, (5) acquire samples at reduced flow rates (≤100 events per second), (6) use linear (rather than logarithmic) signal amplification, and (7) collect an adequate number of events for the intended application (at least 10,000 cells for cell cycle distributions).
89. If the G_1 and G_2/M peaks of the cell cycle distribution are relatively broad, interrupt acquisition and incubate samples for additional 10–15 min at 37°C, 5% CO_2, under protection from light. However, please note that exposure to Hoechst 33342 for more than 45 min may per se affect cell viability.
90. In our experimental settings, Hoechst 33342 fluorescence is detected in channel FL4.
91. Hoechst 33342 can be efficiently excited also with non-UV wavelengths (>360 nm), for instance at ~405 nm. UV excitation, however, is the gold standard for obtaining clear cell cycle distributions and hence reliable results.
92. Unbound Hoechst 33342 has an emission peak at 510–540 nm (green). This fluorescence can be observed when excessive Hoechst 33342 concentrations are employed.
93. The addition of ethanol dropwise is strictly required to conserve the integrity of cells during fixation. Gently vortexing tubes while ethanol is added further increases fixation quality (see also Note 52).
94. Fluorochromes including PI and the FxCycle™ far-red stain bind DNA as well as RNA, making the use of RNase A a strict requirement for proper DNA content studies. This is not the case for dyes that selectively bind chromatin-associated DNA, such as Hoechst 33342 and DAPI.
95. If cell cycle profiles are of insufficient quality, interrupt acquisition and incubate samples at +4°C, under protection from light, overnight. Generally, stained samples can be stored in this conditions for a few days. However, a time-dependent decrease in fluorescence (whose rapidity depends on the fluorochrome in use as well as on storage conditions) will result in the impossibility to analyze the samples. This occurs relatively rapidly for Hoechst 33342 and DAPI.

96. Carefully vortex samples before acquisition.
97. In our experimental setting, the following channels are employed for fluorescence detection: FL3 for PI, FL4 for DAPI and FL6 for 7-AAD and FxCycle.
98. For longer incubations (>24 h), lower concentrations of EdU (e.g., 1–5 μM) are recommended (see also Notes 55 and 56).
99. Fixed samples can be stored at 4°C under protection from light and conveniently sealed for at least 1 week.
100. The Click-iT® saponin-based permeabilization reagent may be used as an alternative its Triton X-100-based counterpart (see also Note 62).
101. The manufacturer recommends to mix thoroughly (to maximize homogeneity) and to protect the solution from prolonged exposure to light (see also Notes 57–59, and 64).
102. The Click-iT™ reaction cocktail should be prepared no earlier than 15 min before use.
103. In our experimental setting, the following channels are employed for fluorescence detection: FL1 for Alexa Fluor® 488 azide, and FL4 for DAPI. The fluorescent signal generated by Alexa Fluor® 488 azide is best detected with logarithmic amplification.
104. An alternative blocking buffer is provided by 10% (v/v) FBS in PBS.
105. Blocking is recommendable (unless specifically indicated in the antibody datasheet), as it generally results in reduced background signal.
106. As an alternative, precise hybridization buffers, as described (or even provided) by antibody manufacturers, can be used. This is often recommendable as hybridization buffers characterized by a strictly defined molecular composition are less prone to interfere with the antibody/antigen interaction.
107. Antibodies should always be agitated before the use in order to eliminate precipitates.
108. To avoid degradation, primary antibody stock solutions should always be kept in near-to-storage conditions, in particular concerning temperature. This can be achieved by preparing hybridization solutions as rapidly as possible, and with the help of ice baths (for antibodies stored at 4°C) or precooled ice packs (for antibodies stored at −20°C). It is a good laboratory practice to split antibodies into aliquots at delivery.
109. Depending on availability and/or price of the antibody, this volume can be reduced to 100/150 μL.

110. Incubation times for optimal immunostaining may slightly vary as a function of the antibody lot. Staining can also be performed at 37°C (30 min) or at 4°C (overnight).
111. To reduce the intensity of the background signal, the number washes can be increased up to five.
112. For secondary antibodies, incubation time should not exceed 1 h.
113. Generally, stained cells can be stored at 4°C under protection from light for several days (see also Note 95).
114. In our experimental setting, the following channels are employed for fluorescence detection: FL1 for Alexa Fluor® 488, FL2 for Alexa Fluor® 568, and FL4 for DAPI.

Acknowledgments

IV, LG and GK are especially grateful to Mr. Sundaramoorthy Balasubramanian, Senior Project Manager at SPi Global for assistance with the production of this book. This work is supported by grants to GK from the Ligue Nationale contre le Cancer (Equipes labellisée), Agence Nationale pour la Recherche (ANR), European Commission (Active p53, Apo-Sys, ChemoRes, ApopTrain), Fondation pour la Recherche Médicale (FRM), Institut National du Cancer (INCa), Cancéropôle Ile-de-France, Fondation Bettencourt-Schueller, and the LabEx Onco-Immunology.

References

1. Alberts B (2008) Molecular biology of the cell, extended version, 5th edn. Garland Science, New York
2. Blomen VA, Boonstra J (2007) Cell fate determination during G1 phase progression. Cell Mol Life Sci 64:3084–3104
3. Pfeuty B, David-Pfeuty T, Kaneko K (2008) Underlying principles of cell fate determination during G1 phase of the mammalian cell cycle. Cell Cycle 7:3246–3257
4. Hobert O (2011) Regulation of terminal differentiation programs in the nervous system. Annu Rev Cell Dev Biol 27:681–696
5. Olson EN, Schneider MD (2003) Sizing up the heart: development redux in disease. Genes Dev 17:1937–1956
6. Oh IH, Humphries RK (2012) Concise review: Multidimensional regulation of the hematopoietic stem cell state. Stem Cells 30:82–88
7. Pazolli E, Stewart SA (2008) Senescence: the good the bad and the dysfunctional. Curr Opin Genet Dev 18:42–47
8. Evan GI, d'Adda di Fagagna F (2009) Cellular senescence: hot or what? Curr Opin Genet Dev 19:25–31
9. Morgan DO (2007) The cell cycle: principles of control. New Science Press, London
10. Hochegger H, Takeda S, Hunt T (2008) Cyclin-dependent kinases and cell-cycle transitions: does one fit all? Nat Rev Mol Cell Biol 9:910–916
11. Morgan DO (1997) Cyclin-dependent kinases: engines, clocks, and microprocessors. Annu Rev Cell Dev Biol 13:261–291
12. Bloom J, Cross FR (2007) Multiple levels of cyclin specificity in cell-cycle control. Nat Rev Mol Cell Biol 8:149–160
13. Satyanarayana A, Kaldis P (2009) Mammalian cell-cycle regulation: several Cdks, numerous cyclins and diverse compensatory mechanisms. Oncogene 28:2925–2939
14. Liu X, Winey M (2012) The MPS1 family of protein kinases. Annu Rev Biochem 81: 561–585

15. Malumbres M (2011) Physiological relevance of cell cycle kinases. Physiol Rev 91:973–1007
16. Sancar A, Lindsey-Boltz LA, Unsal-Kacmaz K, Linn S (2004) Molecular mechanisms of mammalian DNA repair and the DNA damage checkpoints. Annu Rev Biochem 73:39–85
17. Foster DA, Yellen P, Xu L, Saqcena M (2010) Regulation of G1 cell cycle progression: distinguishing the restriction point from a nutrient-sensing cell growth checkpoint(s). Genes Cancer 1:1124–1131
18. Lindqvist A, Rodriguez-Bravo V, Medema RH (2009) The decision to enter mitosis: feedback and redundancy in the mitotic entry network. J Cell Biol 185:193–202
19. Bartek J, Lukas J (2007) DNA damage checkpoints: from initiation to recovery or adaptation. Curr Opin Cell Biol 19:238–245
20. Gottifredi V, Prives C (2005) The S phase checkpoint: when the crowd meets at the fork. Semin Cell Dev Biol 16:355–368
21. Segurado M, Tercero JA (2009) The S-phase checkpoint: targeting the replication fork. Biol Cell 101:617–627
22. Musacchio A (2011) Spindle assembly checkpoint: the third decade. Philos Trans R Soc Lond B Biol Sci 366:3595–3604
23. Musacchio A, Salmon ED (2007) The spindle-assembly checkpoint in space and time. Nat Rev Mol Cell Biol 8:379–393
24. Vitale I, Galluzzi L, Castedo M, Kroemer G (2011) Mitotic catastrophe: a mechanism for avoiding genomic instability. Nat Rev Mol Cell Biol 12:385–392
25. Vitale I, Galluzzi L, Senovilla L, Criollo A, Jemaa M, Castedo M, Kroemer G (2011) Illicit survival of cancer cells during polyploidization and depolyploidization. Cell Death Differ 18:1403–1413
26. Margolis RL, Lohez OD, Andreassen PR (2003) G1 tetraploidy checkpoint and the suppression of tumorigenesis. J Cell Biochem 88:673–683
27. Giacinti C, Giordano A (2006) RB and cell cycle progression. Oncogene 25:5220–5227
28. Giono LE, Manfredi JJ (2006) The p53 tumor suppressor participates in multiple cell cycle checkpoints. J Cell Physiol 209:13–20
29. Deng CX (2006) BRCA1: cell cycle checkpoint, genetic instability, DNA damage response and cancer evolution. Nucleic Acids Res 34: 1416–1426
30. Jiang H, Reinhardt HC, Bartkova J, Tommiska J, Blomqvist C, Nevanlinna H, Bartek J, Yaffe MB, Hemann MT (2009) The combined status of ATM and p53 link tumor development with therapeutic response. Genes Dev 23:1895–1909
31. Stewart ZA, Westfall MD, Pietenpol JA (2003) Cell-cycle dysregulation and anticancer therapy. Trends Pharmacol Sci 24:139–145
32. McDonald ER 3rd, El-Deiry WS (2001) Checkpoint genes in cancer. Ann Med 33: 113–122
33. Vitale I, Senovilla L, Galluzzi L, Criollo A, Vivet S, Castedo M, Kroemer G (2008) Chk1 inhibition activates p53 through p38 MAPK in tetraploid cancer cells. Cell Cycle 7: 1956–1961
34. Vitale I, Galluzzi L, Vivet S, Nanty L, Dessen P, Senovilla L, Olaussen KA, Lazar V, Prudhomme M, Golsteyn RM, Castedo M, Kroemer G (2007) Inhibition of Chk1 kills tetraploid tumor cells through a p53-dependent pathway. PLoS One 2:e1337
35. Jemaà M, Vitale I, Kepp O, Berardinelli F, Galluzzi L, Senovilla L, Marino G, Malik SA, Rello-Varona S, Lissa D, Antoccia A, Tailler M, Schlemmer F, Harper F, Pierron G, Castedo M, Kroemer G (2012) Selective killing of p53-deficient cancer cells by SP600125. EMBO Mol Med 4(6):500–514
36. Degenhardt Y, Greshock J, Laquerre S, Gilmartin AG, Jing J, Richter M, Zhang X, Bleam M, Halsey W, Hughes A, Moy C, Liu-Sullivan N, Powers S, Bachman K, Jackson J, Weber B, Wooster R (2010) Sensitivity of cancer cells to Plk1 inhibitor GSK461364A is associated with loss of p53 function and chromosome instability. Mol Cancer Ther 9:2079–2089
37. Jemaà M, Galluzzi L, Kepp O, Boilève A, Lissa D, Senovilla L, Harper F, Pierron G, Berardinelli F, Antoccia A, Castedo M, Vitale I, Kroemer G (2012) Preferential killing of p53-deficient cancer cells by reversine. Cell Cycle 11(11): 2149–2158
38. Kroemer G, Galluzzi L, Brenner C (2007) Mitochondrial membrane permeabilization in cell death. Physiol Rev 87:99–163
39. Galluzzi L, Vitale I, Abrams JM, Alnemri ES, Baehrecke EH, Blagosklonny MV, Dawson TM, Dawson VL, El-Deiry WS, Fulda S, Gottlieb E, Green DR, Hengartner MO, Kepp O, Knight RA, Kumar S, Lipton SA, Lu X, Madeo F, Malorni W, Mehlen P, Nunez G, Peter ME, Piacentini M, Rubinsztein DC, Shi Y, Simon HU, Vandenabeele P, White E, Yuan J, Zhivotovsky B, Melino G, Kroemer G (2012) Molecular definitions of cell death subroutines: recommendations of the Nomenclature Committee on Cell Death 2012. Cell Death Differ 19:107–120
40. Hoffmann J, Vitale I, Buchmann B, Galluzzi L, Schwede W, Senovilla L, Skuballa W, Vivet S, Lichtner RB, Vicencio JM, Panaretakis T, Siemeister G, Lage H, Nanty L, Hammer S,

Mittelstaedt K, Winsel S, Eschenbrenner J, Castedo M, Demarche C, Klar U, Kroemer G (2008) Improved cellular pharmacokinetics and pharmacodynamics underlie the wide anticancer activity of sagopilone. Cancer Res 68: 5301–5308

41. Vitale I, Senovilla L, Jemaa M, Michaud M, Galluzzi L, Kepp O, Nanty L, Criollo A, Rello-Varona S, Manic G, Metivier D, Vivet S, Tajeddine N, Joza N, Valent A, Castedo M, Kroemer G (2010) Multipolar mitosis of tetraploid cells: inhibition by p53 and dependency on Mos. EMBO J 29:1272–1284
42. Kepp O, Galluzzi L, Lipinski M, Yuan J, Kroemer G (2011) Cell death assays for drug discovery. Nat Rev Drug Discov 10:221–237
43. Tasdemir E, Galluzzi L, Maiuri MC, Criollo A, Vitale I, Hangen E, Modjtahedi N, Kroemer G (2008) Methods for assessing autophagy and autophagic cell death. Methods Mol Biol 445: 29–76
44. Galluzzi L, Aaronson SA, Abrams J, Alnemri ES, Andrews DW, Baehrecke EH, Bazan NG, Blagosklonny MV, Blomgren K, Borner C, Bredesen DE, Brenner C, Castedo M, Cidlowski JA, Ciechanover A, Cohen GM, De Laurenzi V, De Maria R, Deshmukh M, Dynlacht BD, El-Deiry WS, Flavell RA, Fulda S, Garrido C, Golstein P, Gougeon ML, Green DR, Gronemeyer H, Hajnoczky G, Hardwick JM, Hengartner MO, Ichijo H, Jaattela M, Kepp O, Kimchi A, Klionsky DJ, Knight RA, Kornbluth S, Kumar S, Levine B, Lipton SA, Lugli E, Madeo F, Malomi W, Marine JC, Martin SJ, Medema JP, Mehlen P, Melino G, Moll UM, Morselli E, Nagata S, Nicholson DW, Nicotera P, Nunez G, Oren M, Penninger J, Pervaiz S, Peter ME, Piacentini M, Prehn JH, Puthalakath H, Rabinovich GA, Rizzuto R, Rodrigues CM, Rubinsztein DC, Rudel T, Scorrano L, Simon HU, Steller H, Tschopp J, Tsujimoto Y, Vandenabeele P, Vitale I, Vousden KH, Youle RJ, Yuan J, Zhivotovsky B, Kroemer G (2009) Guidelines for the use and interpretation of assays for monitoring cell death in higher eukaryotes. Cell Death Differ 16:1093–1107

Chapter 7

Quantification of Cell Cycle-Arresting Proteins

Oliver Kepp, Isabelle Martins, Laurie Menger, Mickaël Michaud, Sandy Adjemian, Abdul Qader Sukkurwala, Lorenzo Galluzzi, and Guido Kroemer

Abstract

Cellular senescence, which can be defined as a stress response preventing the propagation of cells that have accumulated potentially oncogenic alterations, is invariably associated with a permanent cell cycle arrest. Such an irreversible blockage is mainly mediated by the persistent upregulation of one or more cyclin-dependent kinase inhibitors (CKIs), including (though not limited to) $p16^{INK4A}$ and $p21^{CIP1}$ and $p27^{KIP1}$. CKIs operate by binding to cyclin-dependent kinases (CDKs), de facto inhibiting their enzymatic activity. Here, we provide an immunoblotting-based method for the detection and quantification of CKIs in vitro and ex vivo, together with a set of guidelines for the interpretation of results.

Key words: ARF, Cancer, DNA damage, INK, $p14^{ARF}$, $p57^{KIP2}$

1. Introduction

The cell cycle is a tightly regulated and monodirectional process whereby cells acquire the ability to undergo division and give rise to an offspring. This entails (1) an (at least partial) increase in cell size, (2) the duplication of fundamental, numerically limited organelles (e.g., centrioles), and (3) the replication of the cellular genome. Such requirements ensure that each daughter cell will be viable, provided with a copy of the genetic material and in turn able to replicate (1). Depending on the balance between pro- and anti-mitogenic signals from the extracellular microenvironment as well as from the activation status of intracellular signaling pathways, newly formed cells can either promptly proceed through the cell cycle and undertake subsequent rounds of cell division or undergo one out of three non-proliferative fates: differentiation,

Lorenzo Galluzzi et al. (eds.), *Cell Senescence: Methods and Protocols*, Methods in Molecular Biology, vol. 965,
DOI 10.1007/978-1-62703-239-1_7,

quiescence and senescence. However, while quiescence is reversible (i.e., quiescent cells can resume proliferation in the presence of appropriate growth factors), both differentiation and senescence are permanent (2). Differentiation refers to the process whereby highly specialized cells (e.g., neurons) acquire their terminal functions, which is invariably accompanied by a permanent loss of proliferative potential. On the contrary, senescence operates to prevent the propagation of cells that have accumulated potentially mutagenic alterations, including DNA damage and oxidative modifications of other macromolecules (3).

In both physiological and pathological settings, progression through the cell cycle is tightly regulated by the interplay among three distinct classes of proteins: (1) cyclins, (2) cyclin-dependent kinases (CDKs), and (3) CDK inhibitors (CKIs). In particular, the catalytic activity of CDKs, which de facto controls cell cycle progression, requires their association with cyclins (small proteins that—contrarily to CDKs—are expressed in a cell cycle phase-dependent fashion). Conversely, the binding of CKIs exerts potent cell cycle-inhibitory effects (4). Similar to cyclins, the levels of CKIs normally oscillate, hence maintaining cells in a specific phase of the cell cycle until all the associated process have been properly completed (5). Moreover, cells upregulate CKIs in particular physiological settings, such as during differentiation and development as well as in response to multiple insults, notably upon exposure to DNA-damaging agents. The cell cycle arrest that often accompanies stress responses is crucial as it (1) prevents the proliferation of cells with potentially harmful alterations, and (2) allows repair mechanisms to attempt reestablishing homeostasis. If this can be achieved, CKI-mediated cell cycle inhibition, which is often associated with the induction of an anti-apoptotic state (6, 7), gets relieved and cells resume proliferation. Otherwise, cells die (8–12) or the cell cycle blockage becomes permanent (13).

There are two main classes of CKIs: the inhibitor of kinase 4/alternative reading frame (INK4/ARF) class and the CDK-interacting protein/kinase-inhibitory protein (Cip/Kip) class. The former includes $p15^{INK4B}$, $p16^{INK4A}$, $p18^{INK4C}$, and $p19^{INK4D}$, which specifically bind to CDK4 and CDK6 (Fig. 1), thereby evoking an allosteric change that abrogates the binding of type D cyclins (5). The latter encompasses $p21^{CIP1}$, $p27^{KIP1}$, and $p57^{KIP2}$, which bind to preassembled cyclin E-CDK2, cyclin A-CDK2, and (to a lesser extent) cyclin D-CDK4/6 complexes (at their catalytic cleft) (Fig. 1), hence arresting cell cycle progression at the so-called G_1-to-S transition (5). CKIs have been shown to operate in a context-dependent manner. Thus, whereas $p57^{KIP2}$ exhibits a tissue-restricted expression pattern and seems to function exclusively during embryonic development (14), $p21^{CIP1}$ is ubiquitously expressed and is transactivated by p53 in response to multiple type of

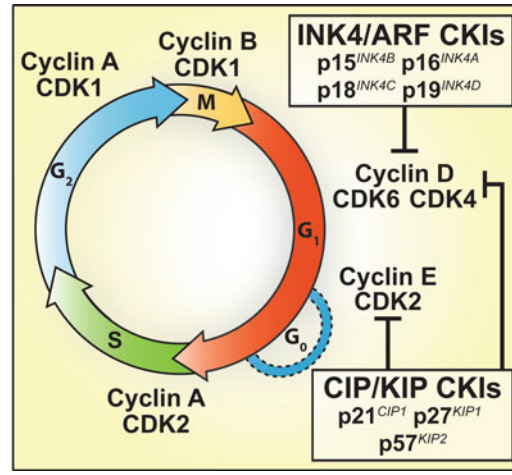

Fig. 1. *Cyclin-dependent kinase inhibitors in cell cycle progression.* Two classes of cyclin-dependent kinase (CDK) inhibitors (CKIs) regulate the cell cycle, either by interfering with the binding of cyclins to CDKs or by forming heteromeric complexes with preformed cyclin-CDK dimers, thereby limiting substrate phosphorylation. The inhibitor of kinase 4/alternative reading frame (INK4/ARF) class includes $p15^{INK4B}$, $p16^{INK4A}$, $p18^{INK4C}$, and $p19^{INK4D}$, which specifically bind to CDK4 and CDK6, thus evoking an allosteric change that abrogates the engagement of type D cyclins. The CDK interacting protein/kinase inhibitory protein (CIP/KIP) class, on the contrary, inhibits the enzymatic functions of pre-assembled cyclin-CDK complexes, by binding to the catalytic cleft of the dimer. The latter class of proteins includes $p21^{CIP1}$, $p27^{KIP1}$, and $p57^{KIP2}$, which bind to cyclin E-CDK, cyclin A-CDK and—to a lesser extent—cyclin D-CDK complexes, hence inducing a cell cycle arrest in the G_1 phase.

DNA damage, including the senescence-associated erosion of telomeres (15). Along similar lines, $p27^{KIP1}$ has a broad expression pattern and predominantly responds to growth factor deprivation (16).

Lost or reduced CKI function (resulting from primary genetic defects as well as from alterations involving upstream/downstream signaling modules) has been detected in multiple types of cancers. In line with these observations, the reintroduction of $p16^{INK4A}$ in human osteosarcoma U2OS cells as well as the ectopic expression of $p21^{CIP1}$ or $p27^{KIP1}$ in human osteosarcoma SAOS-2 cells have been shown to abrogate the tumorigenic phenotype, at least in vitro, by promoting senescence (17). Moreover, multiple distinct chemotherapeutic agents that are currently used in the clinic exert beneficial effects, at least in part, by triggering the senescence of cancer cells (18). Taken together, these observations highlight the key role exerted by CKIs in the regulation of tissue homeostasis.

Here, we provide an immunoblotting-based method for the detection and quantification of CKIs in vitro and ex vivo, together with a set of guidelines for interpreting results.

2. Materials

2.1. Common Materials

Disposables

1. 1.5 mL microcentrifuge tubes.
2. 15 and 50 mL conical centrifuge tubes.
3. 6-well plates for cell culture.
4. 75 or 175 cm^2 flasks for cell culture.

Reagents

1. Cisplatin (CDDP) (Sigma-Aldrich, Saint-Louis, MO, USA), stock solution in *N,N*-dimethylformamide, at 50 mM, stored at room temperature (RT) (see Notes 1 and 2).
2. Complete growth medium for HeLa cells: DMEM containing 4.5 g/L glucose, 4 mM L-glutamine, and 110 mg/L sodium pyruvate supplemented with 100 mM HEPES buffer and 10% fetal bovine serum (FBS) (see Note 3).
3. Trypsin/EDTA: 0.25% trypsin—0.38 g/L (1 mM) EDTA×4 Na^+ in HBSS.

2.2. Quantification of Cell Cycle-Arresting Proteins by Immunoblotting

1. 3 MM® Whatman paper.
2. Antibodies employed are listed in Table 1 (see Note 4).
3. Binding/blocking buffer: 0.1% Tween 20 in TBS (v/v) supplemented with 3% (w/v) bovine serum albumin (BSA), stored at 4°C (see Note 5).
4. BSA, stock solution 10 mg/mL in dH_2O, stored at 4°C (see Note 5).
5. Chemiluminescent substrate: SuperSignal West Pico Chemiluminescent Substrate (Pierce Biotechnology, Rockford, IL, USA), stored at RT (see Note 6).
6. *DC* Protein Assay (Bio-Rad, Hercules, CA, USA), stored at RT (see Notes 7 and 8).
7. De-hybridization buffer: Restore Western Blot Stripping Buffer (Pierce Biotechnology), stored at 4°C (see Note 9).
8. Detection system: ImageQuant LAS 4000 (GE Healthcare life Sciences, Upsala, Sweden).
9. Electrophoresis apparatus: XCell4 SureLock™ Mini-Cell (Life Technologies-Invitrogen, Eugene, CA, USA).
10. Electrophoresis power supply unit: PowerEase® 500 (Life Technologies-Invitrogen).
11. Electrotransfer module: XCell II™ Blot Module (Life Technologies-Invitrogen).
12. Electrotransfer sponges: XCell II™ blotting pads (Life Technologies-Invitrogen).

Table 1
Antibodies for immunoblotting

Primary antibody	Specificity	Source organism	[a]Company	References
Anti-GAPDH (6C5)	Monoclonal IgG_1	Mouse	Chemicon International	mAB374
Anti-p14^{ARF}	Monoclonal IgG_{2A}	Mouse	Cell Signaling Technology	mAB2407
Anti-p16^{INK4A}	Monoclonal IgG_1	Mouse	Santa Cruz Biotechnology	sc-81613
Anti-p21^{CIP1}	Monoclonal IgG	Rabbit	Cell Signaling Technology	mAB2947
Anti-p27^{KIP1}	Monoclonal IgG	Rabbit	Cell Signaling Technology	mAB3688

Secondary antibody	Label	Source organism	[a]Company	References
Anti-mouse	Horseradish peroxidase	Goat	Southern Biotech	1010–05
Anti-rabbit	Horseradish peroxidase	Goat	Southern Biotech	4010–05

Notes: [a]Cell Signaling Technology, Danvers, MA, USA; Chemicon International, Temecula, CA, USA; Santa Cruz Biotechnology, Santa Cruz, CA, USA; Southern Biotech, Birmingham, AL, USA

13. Methanol (see Notes 10 and 11).
14. Nitrocellulose membrane.
15. NP40 lysis buffer: 1% NP40, 20 mM HEPES, 10 mM potassium chloride (KCl), 1 mM ethylenediaminetetraacetic acid (EDTA) (Sigma-Aldrich), 10% glycerol, 1 mM orthovanadate (Sigma-Aldrich), 1 mM phenylmethylsulfonyl fluoride (PMSF) (Sigma-Aldrich), 1 mM dithiothreitol (DTT) (Sigma-Aldrich) + complete EDTA-free protease inhibitor cocktail (Roche Diagnostics GmbH, Mannheim, Germany, 1 tablet/10 mL), stored at –20°C (see Notes 12–15).
16. NuPAGE® antioxidant (1×) (Life Technologies-Invitrogen), stored at 4°C (see Note 16).
17. NuPAGE® LDS sample buffer (4×) (Life Technologies-Invitrogen), stored at 4°C (see Note 17).
18. NuPAGE® MES SDS running buffer (20×) (Life Technologies-Invitrogen), stored at 4°C or RT (see Notes 17 and 18).
19. NuPAGE® Novex 4–12% Bis–Tris precast gels (Life Technologies-Invitrogen), stored at 4°C or RT (see Notes 17 and 19).
20. NuPAGE® Novex gel knife (Life Technologies-Invitrogen).

21. NuPAGE® sample reducing agent (Life Technologies-Invitrogen), stored at 4°C or RT (see Notes 17 and 20).
22. NuPAGE® transfer buffer (20×) (Life Technologies-Invitrogen), stored at 4°C or RT (see Notes 17 and 19).
23. Ponceau S staining solution: 0.1% (w/v) Ponceau S and 5.0% (w/v) acetic acid in dH_2O (or ready-made, commercially available) (see Note 21).
24. Protein molecular weight (MW) markers: Precision Plus Protein™ Standard (Bio-Rad).
25. Rinsing buffer: 0.1% Tween 20 in TBS, stored at 4°C (see Note 22).
26. TBS (1 ×): 150 mM NaCl, 50 mM Tris in dH_2O, adjust pH to 7.4 with 1 N HCl.

3. Methods

3.1. Cell Culture and Treatments

1. Human cervical adenocarcinoma HeLa cells are routinely cultured in complete growth medium at 37°C in a humidified 5% CO_2-enriched atmosphere using 75 cm^2 supports (see Notes 23 and 24).
2. Slightly underconfluent cells are subcultured regularly by trypsin/EDTA detachment (see Notes 25 and 26), dilution and reseeding. This generates maintenance cultures (see Note 27) and provides cells for experimental determinations.
3. The latter are carried out in 6-well plates.
4. Twenty-four hours after seeding (when cells have adhered to the matrix and have resumed proliferation) (see Note 28), culture supernatants are discarded and replaced by complete culture medium in which the compounds of interest have been prediluted at the desired final concentration (see Notes 29–33).

3.2. Quantification of Cell Cycle-Arresting Proteins by Immunoblotting

3.2.1. Preparation of Samples

1. HeLa cells are seeded in 6-well plates (see Note 34), let adhere for 12–24 h and treated with the stimuli of interests (see Subheading 3.1, step 4 and Notes 28–33).
2. After the desired incubation time, supernatants are transferred into 15 mL conical tubes (see Note 35) and adherent cells are washed with PBS (see Note 36). The PBS is pooled with the corresponding supernatant and cells are detached with Trypsin-EDTA (see Notes 37–39).
3. Detached cells and supernatants are pooled and subsequently centrifuged at 300–500 × *g* for 5 min (4°C) (see Note 40).
4. Supernatants are removed and pellets are carefully lysed in 30–50 µL of cold (4°C) NP40 lysis buffer (see Notes 41–43).

5. The protein concentration of each sample is determined by means of the *DC* Protein Assay, following the manufacturer's instructions (see Note 44).
6. 20–80 µg of proteins from each lysate (see Note 45) are mixed with 5–7.5 µL NuPAGE® LDS sample buffer (4×) and the final volume is adjusted to 20–30 µL with lysis buffer (see Notes 46 and 47).
7. Protein denaturation is achieved by the incubation of samples at 100°C for 5 min (see Notes 48 and 49). Normally, samples are allowed to cool down at RT or 4°C prior to loading on polyacrylamide gels (see Note 50).

3.2.2. Electrophoresis

1. These instructions refer to an Invitrogen XCell4 SureLock™ Mini-Cell system for gel electrophoresis and NuPAGE® Novex 4–12% Bis–Tris precast gels.
2. For a single unit, which can accommodate two precast gels, use dH_2O to prepare 500 mL 1× NuPAGE® MES SDS running buffer (see Notes 51 and 52).
3. Unwrap the gel(s), peel off the tape covering the slot on the back of the gel cassette (see Note 53), and gently remove the disposable comb while paying particular attention at preserving the integrity of sample slots (see Note 54).
4. Gently wash wells with 1× running buffer to remove possible polyacrylamide debris, and assemble the electrophoresis unit by following the manufacturer's instructions (see Notes 55 and 56).
5. Fill the inner chamber of the unit with running buffer until sample slots are entirely submerged (see Note 57), add 500 µL 10× NuPAGE® antioxidant (see Note 58), and gently remove bubbles that may have formed.
6. Fill the outer chamber of the unit with running buffer and proceed to load the gel with protein samples prepared as described above (see Subheading 3.2.1, steps 6 and 7 and Notes 45–50). 1–2 wells are loaded with Precision Plus Protein™ Standard MW markers (see Note 59).
7. Following sample loading (see Note 59), connect the unit to the power supply and separate proteins in constant-field mode (see Notes 60 and 61) without further delay. Importantly, the electrophoresis should be stopped before the 15 kDa band of the MW marker reaches the bottom horizontal line that delineates the zone of the gel that will be eliminated before the electrotransfer (see Note 62).

3.2.3. Electrotransfer

1. For a single unit, which can accommodate up to two precast gels, prepare 1 L 1× NuPAGE® transfer buffer by mixing 50 mL 20× NuPAGE® transfer buffer, 200 mL methanol,

1 mL 1× NuPAGE® antioxidant, and 749 mL dH_2O (see Note 52).

2. 5 XCell II™ blotting pads and 4 sheets of 3 MM® Whatman filter paper of approximately the same size than the running gel (9×9 cm) are equilibrated in 1× transfer buffer for 1–2 min at RT.
3. 2 Nitrocellulose membranes of approximately the same size of the running gel (9×9 cm) are activated by incubation in dH_2O for 2–5 min at RT, then equilibrated in transfer buffer (see Note 63).
4. The gel unit is disconnected from the power supply and disassembled. With the help of a NuPAGE® Novex gel knife, precast gels are opened and the upper plastic shield is discarded (see Note 64).
5. The gel "foot" is displaced by means of the gel knife and each gel is deposited on a clean and flat surface previously wetted with transfer buffer. Wells and gel "feet" are cut and discarded (see Notes 65 and 66).
6. The transfer setup is prepared by overlaying the following components (pre wetted in transfer buffer) on top of the cathodic core (−) of the XCell II™ Blot Module (conditions for two gels): two blotting pads, one filter paper, the first gel, the first nitrocellulose membrane, one filter paper, one blotting pad, one filter paper, the second gel, the second nitrocellulose membrane, one filter paper, two blotting pads (as indicated by the manufacturer) (see Notes 67 and 68).
7. The anodic core (+) of the blot module is then used to close the transfer sandwich, which is subsequently inserted into the XCell4 SureLock™ Mini-Cell system.
8. Fill the blot module with 1× transfer buffer until the sandwich is entirely covered (see Note 69).
9. Fill the outer chamber with ~650 mL dH_2O until the water level reaches ~2 cm from the top of the unit (see Note 70).
10. Place the lid on top of the unit, connect it to the power supply and electrotransfer proteins in constant-field mode (30 V) for 1 h, as recommended by the manufacturer (see Notes 71–73).
11. Once the transfer is complete, disconnect the transfer unit from the power supply, disassemble the blot module and withdraw nitrocellulose membranes (see Note 74), on which colored MW markers should be clearly visible (see Notes 75 and 76).
12. At this stage, bound proteins can be visualized (as a preliminary indicator of an adequate electrotransfer as well as of the equal loading of lanes) by incubating membranes in Ponceau S staining solution for 2–5 min (see Notes 77 and 78).

13. After cutting the membrane at the adequate horizontal position estimated by MW markers (in order to detect multiple cell cycle-inhibitory proteins at the same time, if required) the Ponceau S staining solution should be removed by quickly rinsing membranes in rinsing buffer (see Notes 79–82).

3.2.4. Immunoblotting for the Detection of CKI Expression Levels

1. To block unspecific binding sites, nitrocellulose membrane fragments are incubated on an orbital shaker in 10 mL of blocking buffer for 30–60 min at RT.
2. Blocking buffer is discarded, membrane fragments are rapidly washed in rinsing buffer and incubated with the corresponding primary antibodies (see Table 1). The following conditions should be employed: anti-CKI, 1/500–1/1,000 in blocking or binding buffer, as recommended by the manufacturers (overnight at 4°C), anti-GAPDH, 1/10,000 in rinsing, blocking, or binding buffer (1 h at RT) (see Notes 83–86).
3. Primary antibodies are removed (see Note 87) and membrane fragments are washed three times in rinsing buffer (10 min, RT).
4. Upon washing, membranes are incubated for 45–60 min at RT (by means of an orbital shaker) with freshly prepared 1/5,000–1/1,000 dilutions (in blocking buffer) of goat anti-rabbit or goat-anti-mouse horseradish peroxidase (HRP)-coupled secondary antisera.
5. Secondary antibodies are discarded (see Note 88), and membrane fragments are again washed three times in rinsing buffer (10 min, RT).
6. Each membrane fragment is overlaid for 2–5 min with 500–1,000 µL SuperSignal West Pico Maximum Sensitivity chemiluminescent substrate, prepared ex tempore according to the manufacturer's instruction (see Note 89).
7. Finally chemiluminescence is detected by cumulative acquisition in an ImageQuant LAS 4000 equipped with a light-sensitive CCD camera until the signal reaches saturation. Adequately exposed images (see Notes 90–94) are then selected and further analyzed for densitometry with the help of the open-source software ImageJ (NIH, Bethesda, MD, USA; freely available at http://rsb.info.nih.gov/ij/).

3.3. Guidelines for the Correct Evaluation of Cell Cycle Arrest and Cellular Senescence

Depending on both cell-intrinsic and cell-extrinsic variables, the administration of potentially cytotoxic conditions (with CDDP as a model drug for cell cycle arrest) can elicit a number of biochemical cascades whose outcomes are as diverse as adaptation to stress (survival) and cell death. In some cases, various signaling pathways are activated by CDDP in a near-to-simultaneous fashion, which sometimes renders the effects of CDDP on the cell cycle difficult to estimate. As a general rule, CDDP concentrations higher than

50 μM are likely to promote rapid cell death in most cell lines, while in the low micromolar range (1–10 μM) CDDP mainly leads to cell cycle arrest. With these considerations in mind, we propose the following guidelines aimed at providing researchers with a practical tool to approach the study of CDDP-triggered cell cycle arrest.

1. In the experimental settings of choice, the occurrence of bona fide cell death should be assessed by a broad range of concentrations. Sublethal conditions should then be applied for the correct assessment of cell cycle-arresting mechanisms.
2. When an idea has been obtained about these basic parameters, a more precise quantitative and qualitative evaluation of the molecular pathways activated in the experimental setting of choice should be attempted. In particular, the investigator should aim at answering the following questions:
   (a) By which mechanism is the cell cycle arrested and can this be overcome by removing the treatment and restoring normal cell growth conditions?
   (b) In case of an irreversible cell cycle arrest, biochemical markers of cellular senescence (such as senescence associated beta-galactosidase activity) should be evaluated for further insights.
   (c) The long-term stability of the cell cycle arrest should be evaluated by clonogenic assays.

The elucidation of these issues will undoubtedly help researchers to finely characterize cell cycle arrests as induced by a wide array of distinct stimuli.

4. Notes

1. When stored sealed at −20°C, undissolved CDDP (powder) is stable for at least 2 years. It is recommendable to prepare stock solutions of CDDP in small aliquots (10–50 μL), which should be used within 6–8 months from preparation.
2. DMF, which is readily absorbed by inhalation/through the skin, can act as an irritant for the eyes, skin, gastrointestinal tract and respiratory system.
3. Optimal growth conditions (e.g., medium composition, supplements) vary according to the cell line of choice, and may quite dramatically influence not only growth rates but also the response to senescence-inducing stimuli. In particular, suboptimal growth conditions can per se trigger a cell cycle

arrest due to lack of appropriate growth factors or cell-to-cell signaling. Unless changes in the composition of the growth medium are part of the experimental protocol, we suggest to use the medium that is most suitable for the cell line of choice, as recommended by the American Type Culture Collection (ATCC, Manassas, USA).

4. Each antibody should be handled and stored as indicated by the manufacturer. Moreover, antibodies should never be subjected to steep temperature changes and should always be kept on ice when solutions for immunoblotting are prepared.
5. Storage at 4°C of binding and blocking buffers should not exceed 2 weeks, unless 0.02% NaN_3 is added as a preservative to prevent microbial contamination (see also Note 16). The same applies to rehydrated BSA (lyophilized BSA has a shelf life of 1 year at 4°C).
6. This material is considered hazardous by the Occupational Safety and Health Administration (OSHA) Hazard Communication Standard, and may behave as an irritant for the eyes, skin, and respiratory system.
7. The *DC* Protein Assay kit contains sodium hydroxide (NaOH), which is corrosive and might cause severe burns of the skin, eyes and gastrointestinal system upon contact/ingestion.
8. Under appropriate storage conditions, the *DC* Protein Assay kit has a shelf life of at least 6 months.
9. This material is considered hazardous by the OSHA Hazard Communication Standard, is corrosive and may cause severe burns of the skin, eyes and gastrointestinal system upon contact/ingestion.
10. Methanol is volatile and highly toxic due to the formation of formaldehyde and formic acid (an inhibitor of mitochondrial respiration causing hypoxia and lactate accumulation) by hepatic alcohol dehydrogenases.
11. Methanol is highly inflammable and should therefore kept away from heat, fires, sparkling sources, and oxidizers. As a note, methanol flames are almost invisible in normal light conditions, but may be detected by the heat generated or the burning of other materials.
12. EDTA is not currently listed as a carcinogen by the National Toxicology Program (NTP), the International Agency for Research on Cancer (IARC) or OSHA, yet may behave as a mild irritant for the eyes, skin, and respiratory system.
13. PMSF is toxic by inhalation, upon contact with skin and if swallowed, and should therefore always be manipulated with maximal care and preferably under an appropriate fume hood.

14. DTT is considered hazardous by the OSHA Hazard Communication Standard, as it can cause skin irritation and severe ocular damage.
15. Before the addition of the protease inhibitor cocktail, lysis buffer can be stored at 4°C for up to 6 months. Once protease inhibitor tablets have been added, it is recommendable either to use lysis buffer within 24 h (storage at 4°C), or to store small aliquots at –20°C. These are stable for at least 6 months, but should not be refrozen upon first use.
16. This reagent contains sodium bisulfate and DMF (see also Note 2).
17. These products are stable for at least 12 months under ordinary conditions of use and storage (4°C or RT, close bottles or sealed packages).
18. This reagent contains sodium dodecylsulfate (SDS), which can irritate the eyes and the skin, and hence should be handled using protective gloves, clothing, and eyewear.
19. This product contains no substances that, at their given concentration, are considered to be hazardous to health.
20. This reagent contains 500 mM DTT (see also Note 14).
21. Information on the effects on human health deriving from exposure to Ponceau S is limited. It should therefore be handled with the maximal care, by using protective gloves, clothing, and eyewear.
22. Tween 20 is not currently listed as a carcinogen by NTP, IARC, or OSHA, yet may behave as a mild irritant for the eyes, skin, and respiratory system.
23. Depending on specific requirements (e.g., physical room within incubators, need for very large amounts of cells), smaller or larger supports for cell culture can be used in substitution of 75 cm^2 flasks.
24. While HeLa cells conveniently grow on untreated supports, pretreated (e.g., collagen-coated, gelatin-coated) flasks may be required for other cell types.
25. In these conditions, a 75 cm^2 flask contains $5–10 \times 10^6$ HeLa cells. This may considerably vary for other cell lines, mainly depending on cell size.
26. The subculture of both excessively underconfluent and overconfluent flasks should be avoided as it may result in a genetic drift and in the overcrowding-dependent stress of the cell population, respectively, both of which negatively affect experimental determinations.
27. It is recommendable to allow freshly thawed cells to readapt for 2–3 passages before using them in experimental assessments.

Similarly, it is good practice to define a maximal number of passages and to discard maintenance cultures once this limit has been reached, to avoid genetic population drifts. This strategy requires an appropriate liquid nitrogen stock of cells, which should be generated from an homogenous and healthy population prior to the beginning of the experiments.

28. Quickly adhering cells (e.g., HeLa) can be treated after 12 h, whereas at least 24–36 h are necessary for cells with longer adaptation times (e.g., HCT 116). Premature treatment may result in excessive toxicity due to suboptimal culture conditions. Light microscopy-assisted observation of the cell morphology normally suffices to determine the adherence/adaptation status.
29. This is particularly important when stock solutions involve very lipophilic agents (e.g., DMF and dimethylsulfoxide, DMSO), which can results in overt cytotoxicity if directly administered to the cell layer (see also Note 30).
30. Also at very low concentrations, organic solvents like DMF and DMSO may be toxic per se or may promote specific cellular responses (e.g., differentiation). Such effects and the concentration of DMF at which they appear should be carefully determined at a preliminary stage, and should be taken into careful consideration for the definition of the experimental plan.
31. Whenever possible, we recommend to treat cells with (at least) three different concentrations of the compounds of interest (ideally $EC_{50} \times 10^{-1}$, $EC_{50} \times 10^{0}$, $EC_{50} \times 10^{+1}$), in order to avoid insufficient or excessive biological effects.
32. As a positive control for senescence induction, sub-apoptotic doses of a DNA-damaging agent like CDDP can be employed (see also Note 33).
33. Please keep in mind that the final concentration of CDDP and the incubation time required to induce detectable levels of cell cycle arrest and/or cellular senescence may vary significantly with cell type (see also Note 32), and might depend on cell-extrinsic variables (e.g., medium composition and cell density). As a guideline, HeLa cells treated with 1 μM CDDP for 72 h in complete growth medium usually contain 40% cells characterized by morphological traits of cellular senescence.
34. Cell density at seeding depends on cell size, proliferation rate, well surface, and total assay duration. To avoid the appearance of overcrowding-dependent toxicity, control cultures at the end of the assay should exhibit confluence levels that never exceed 85%. For assays lasting no more than 72 h, $100–200 \times 10^3$ ($50–100 \times 10^3$) HeLa cells in 1 (0.5) mL complete growth medium can indicatively be seeded in 12-(24-)well plates.

35. Since they contain the fraction of cells that underwent apoptosis-dependent detachment from the substrate during the stimulation period, supernatants from treated cultures should be discarded if the analysis is planned to focus on viable cells only.
36. This is particularly important for detachment-resistant cells, as serum and salt traces inhibit the enzymatic activity of Trypsin-EDTA (see also Note 38).
37. Trypsinization time is a function of cell type, viability, and culture density. For HeLa cells (and most cell lines), 5 min at 37°C are amply sufficient to fully detach a totally confluent, healthy population. It is however recommendable to check for complete cell detachment by visual inspection or by rapid observation in light microscopy.
38. The detachment of some cell types may require slightly prolonged trypsinization. This may also be necessary if traces of medium remain in the wells after the collection of supernatants (see also Note 36).
39. As a general guideline, excessive trypsinization (>10 min) should be prevented, since it may result per se in some extent of cell sufferance. However, at least initially, this should not affect the expression of cell cycle-inhibitory proteins. Trypsinization can be replaced by mechanical scraping, although this may also promote sufferance in sensible cells.
40. FBS contained in supernatants definitely inactivates trypsin at this stage. Should supernatants be scarce (<500 µL), derive from FBS-free culture conditions, or have been discarded (see also Note 35), complete trypsin inactivation may be guaranteed by adding 3–5 mL pre-warmed complete growth medium to each sample.
41. To minimize proteolytic degradation, from this step onward samples should always be kept on ice (until the addition of loading buffer and denaturation or storage).
42. Lysis should be performed in the minimal volume of lysis buffer that allows for the complete dissolution of cell pellets (30 µL normally suffice for samples derived from 6-well plates). Lysis may be facilitated by thorough pipetting, vortexing, or sonication. If some particulate debris remains undissolved, 5–20 µL supplemental lysis buffer can be added, followed by another round of pipetting, vortexing, or sonication. Keeping the lysate volume to a minimum is important to avoid an excessive dilution of the protein content of samples, which may turn out to be problematic at gel loading.
43. Lysates can be stored at −80°C for prolonged periods (several months) without any significant degradation of their protein content.

44. Protein quantification is performed by interpolating a calibration curve built from a serial dilution of BSA. BSA standards are rarely (if ever) included in protein quantification kits and should be prepared shortly before use. Either dH_2O or (more properly) lysis buffer can be used as solvent.
45. The amount of total proteins that should be loaded onto the polyacrylamide gel for separation depends on multiple variables, including size and expression levels of the protein of interest as well as the performance of the antibodies used at detection. Although CKIs are usually small (most often between 10 and 20 kDa), in our experimental conditions 30–50 μg total proteins normally suffice to visualize the corresponding bands upon immunoblotting.
46. When the amount of total proteins for loading has been determined, lysates that will be separated on the same polyacrylamide gel are diluted in the minimal volume that allows for the loading of the same quantity of proteins and the addition of 4× loading buffer (to a final 1× concentration). Keeping the loading volume to a minimum facilitates the loading procedure.
47. According to the manufacturer, these are the maximal loading volumes for 1 mm-thick NuPAGE® Novex 4–12% Bis–Tris precast gels (Invitrogen): 1-well gel: 700 μL/well; 9-well gel: 28 μL/well; 10-well gel: 25 μL/well; 15-well gel: 18 μL/well; 17-well gel: 15 μL/well. The volume that actually fits into such wells is 10–15% higher if loading is performed very slowly while keeping the pipette tip at the upper limit of wells.
48. Boiling is intended to integrate the denaturing activity of lysis and loading buffers (which contain SDS, reducing agents and calcium chelators), thereby fully resolving inter- and intramolecular bonds that are responsible for tertiary and quaternary protein structures. This step ensures that the subsequent electrophoretic separation is based on the MW of protein subunits with no (or little) influence from protein-to-protein interactions and native structural features.
49. Incomplete denaturation may have either of the following consequences at electrophoresis. (Partially) folded polypeptides often migrate with an apparently lower MW (as compared to the predicted value), as they retain (at least in part) some structural compactness that favors their progression through the molecular sieve provided by the gel. Conversely, proteins that are engaged in unresolved protein-to-protein interactions migrate with an apparently higher MW, which (at least theoretically) reflects the sum of the MW of all interacting polypeptides.
50. Alternatively, samples can be stored at –80°C for prolonged periods (several months) without significant degradation.
51. Running buffer is stable when stored at 4°C.

52. Used 1× NuPAGE® MES SDS running buffer and 1× NuPAGE® transfer buffer can be recycled for at least 2–3 additional electrophoretic runs and electrotransfers, respectively.
53. Failure to do so will result in low or no current during the electrophoretic run, due to failing electric circuitry within the unit.
54. If slots get seriously damaged during gel preparation, adjacent samples may mix at loading. In this case, the use of a new gel is recommended.
55. Polyacrylamide debris may impede correct sample loading, result in the mix up of adjacent samples and/or affect the entry of proteins in gel, and hence should be carefully avoided.
56. If only one polyacrylamide gel is used, replace the second gel cassette with the plastic dummy provided with the XCell4 SureLock™ Mini-Cell unit to confer integrity of the upper and lower chambers of the electrophoresis unit.
57. The running buffer has to completely cover all slots to allow for an homogeneous electrophoresis, yet it should though not create a bypass between the upper and lower chamber, as this would compromise the correct electrical flow within the unit.
58. The reducing agents that are contained in the NuPAGE® LDS sample buffer do not co-migrate with proteins through the gel in a neutral pH environment. Although disulfide bonds are poorly reactive at neutral pH and hence poorly prone to oxidize, some oxidation may occur during electrophoresis in the absence of an antioxidant. The NuPAGE® Antioxidant migrates with the proteins during electrophoresis, thereby fully preventing reoxidization.
59. Pre-stained markers that cover various MW ranges and allow for the visual follow-up of migration are available from distinct commercial provider. For practical reasons, we routinely use the large-range Precision Plus Protein™ Standard MW markers (Bio-Rad), covering from 10 to 250 kDa or low-range Natural Pre-stained SDS-PAGE Standards (Bio-Rad), covering from 14.4 to 97.4 kDa.
60. As a good practice, in order to avoid the diffusion of samples within the gel (in particular of those that were loaded first) and hence maximize resolution, it is recommended to perform loading as quickly as possible (though very carefully) and to start the electrophoresis immediately thereafter.
61. According to the manufacturer, protein samples loaded on NuPAGE® Novex 4–12% Bis–Tris precast gels in NuPAGE® MES SDS running buffer should be separated at 200 V, resulting in a runtime of ~35 min and in expected currents at the start and at the end of the run of 110–125 and 70–80 mA/gel,

respectively. Although it results in increased runtimes, we normally perform separation at 150–180 V, as this relevantly ameliorates resolution.

62. In most cases in which the 15 kDa MW marker trespasses this limit, low molecular weight proteins cannot be detected. This occurs either due to the fact that the corresponding band(s) has (have) run out of the gel at electrophoresis and hence has (have) been lost in the running buffer, or because the band(s) is (are) too close to the gel "foot" and therefore is (are) cut away for the electrotransfer.
63. As an alternative, polyvinylidene fluoride (PVDF) membranes can be employed. In this case, activation should be performed by incubating membranes for 30–60 s in methanol, ethanol or isopropanol, followed by brief rinsing in dH_2O and equilibration in transfer buffer.
64. Use caution while inserting the gel knife between the two plastic shields to avoid excessive pressure toward the gel. While removing the upper plastic shield, to minimize the risk of gel rupture, proceeds slowly and ensure that the gel remains entirely adherent to the lower plastic plate.
65. Alternatively, wells and gel "feet" can be cut away when gels still lay on the lower plastic shield, followed by assembly of the transfer "sandwich."
66. Cutting the gel "feet" is required for the correct assembly of the transfer "sandwich." For this reason, any protein that may have migrated down to this level of the gel is irremediably lost.
67. During assembly, the formation of bubbles between the various layers of the "sandwich" should be carefully avoided, as this will locally interfere with protein transfer and result in the generation of protein-free zones on membranes (which are easily visualized by subsequent Ponceau S staining). To remove bubbles, a common 5 mL pipette can be gently rolled on top of each component before the addition of the next one.
68. During assembly, attention should be made at respecting the reciprocal order among the anodic core (+) of the blot module (attracting proteins that are negatively charged by SDS), membranes, gels and the cathodic core (–) of the blot module. Although this may seem trivial, the loss of proteins due to a "reverse" electrotransfer occurs relatively frequently.
69. Do not fill all the way to the top of the blot module as this will only generate extra conductivity and heat.
70. This serves to dissipate part of the heat produced during the run.
71. Expected currents at the start and at the end of the run are 170 and 110 mA, respectively.

72. These settings are appropriate for both nitrocellulose and PVDF membranes.
73. The efficient electrotransfer of high MW proteins (>100 kDa) may require more than 1 h. In this case, the temperature of the electrotransfer unit might increase excessively, if not controlled, due to the intense current. To avoid this problem, the entire electrotransfer procedure can be performed in a cold room (4°C).
74. Upon careful rinsing in PBS or dH_2O, sponges can be reused. Filter papers are discarded.
75. "Sandwiches" should be removed from the transfer module with the maximal care and the correct transfer of MW markers should be checked prior to their dismantling (by slightly opening the layers of the "sandwich" at one corner). This is very important as it allows for the proper reconstitution of "sandwiches" and for another electrotransfer run if the efficiency of the first one has been suboptimal (see also Note 76).
76. If MW markers are still (partially) visible on the gels (but poorly on membranes), the electrotransfer has occurred with suboptimal efficiency. If an obvious reason for this can be identified, and if "sandwiches" have not been completely dismantled (see also Note 75), the transfer module can be reassembled and another electrotransfer run can be started.
77. Ponceau S staining allows for the identification of gross transfer problems (e.g., bubbles, as well as of highly unequal lane loading). Stained membranes can be wrapped in transparent plastic film and photocopied or scanned, to keep track of the correct transfer.
78. As it contains 5.0% acetic acid, the Ponceau S staining solution favors the fixation of electrotransferred proteins onto nitrocellulose membranes. For this reason, it is advisable to incubate nitrocellulose membranes in Ponceau S staining solution for at least 5 min, whereas 1–2 min normally suffice for PDVF membranes (for which the staining only serves visualization purposes).
79. Cutting should be avoided if—for any reason—the electrophoretic run has not proceeded to completion (as witnessed by the incomplete resolution of MW marker bands along the membrane). In this case, intact membranes should be subjected to one round of immunoblotting for each antibody, separated from each other by multiple washes and de-hybridization (see also Note 93).
80. It is advisable to cut membranes before washing away the Ponceau S staining solution. In this case, colored protein bands provide indeed a valuable guide for cutting membranes along

an approximately straight line that spans a MW range as narrow as possible.

81. Used Ponceau S solutions retain nearly all their staining power, and hence can be reused several times over prolonged periods (several months). Precipitates and polyacrylamide leftovers that may accumulate should be removed every now and then by filtering the solution with a 0.22 μm filter.
82. Alternatively, binding buffer can be used. Binding buffer is recommended for both blocking and hybridization by the majority of antibody suppliers, as it is characterized by a strictly defined molecular composition (and hence is less prone to interfere with the antibody/antigen interaction). Nevertheless, the use of blocking buffer should be preferred (unless specifically indicated in the antibody datasheet) as it generally results in reduced unspecific background signal at revelation.
83. To avoid degradation, primary antibody stocks should always be kept in near-to-storage conditions, in particular concerning temperature. This can be achieved by preparing hybridization solutions as rapidly as possible, and with the help of ice baths (for antibodies stored at 4°C) or pre-cooled ice packs (for antibodies stored at −20°C). It is a good laboratory practice to split antibodies at delivery into aliquots that are sufficient for 1–2 membranes only.
84. Equal lane loading should be performed with an antibody that recognizes a highly expressed protein, whose amount is stable in most experimental settings. As an alternative to GAPDH, α-tubulin (MW = ~52 kDa) or β-actin (MW = ~45 kDa) levels can be monitored to this aim.
85. The primary antibodies that we routinely employ (see also Table 1) are perfectly compatible with blocking buffer. This may not apply to other antibodies. In this case, please refer to the specific manufacturer's recommendations.
86. As an alternative, hybridization with primary antibodies can be achieved by incubating membranes with the antibody solutions for 2 h at RT.
87. Used anti-GAPDH hybridization solutions can be reemployed, if properly stored at −20°C, for at least ten times. Normally, anti-CKI antibodies diluted in hybridization solutions can also be reemployed, if stored at 4°C for no more than 1 week, once or twice more.
88. As secondary antibodies are coupled to an enzymatic activity, it is not recommendable to store them for long periods upon first usage. In exceptional cases, however, they can be stored at 4°C for no more than 24 h and reused once (usually with suboptimal, yet acceptable, results).

89. Attention should be paid to ensure that membranes are entirely covered by the chemiluminescent substrate.
90. Optimal exposure time for the correct visualization of protein bands varies according to the intensity of the HRP-catalyzed chemiluminescent reaction. In turn, this is influenced by several factors including the amount of protein in the band, the affinity of primary and secondary antibodies, the presence of contaminants that inhibit HRP, and the time passed since the addition of the chemiluminescent substrate. Exposure times between 1 and 5 min provide acceptable results for a majority of proteins. When proteins are small or scarcely expressed (or when the antibodies display reduced affinity), however, longer exposures (up to 10–12 h) are required for optimal results. On the contrary, when proteins are large or well represented in the sample (or when the antibodies exhibit high affinity), a few seconds may be sufficient. Of note, the signal from the anti-GAPDH antibody is usually very strong and an exposure in the range of seconds is largely sufficient (see also Note 90).
91. Revelation of the anti-GAPDH antibody is often associated with overexposure (see also Note 90). To circumvent this issue, image acquisition time should be decreased. As an alternative, the anti-GAPDH antibody can be detected 30–120 min after the addition of the chemiluminescent substrate, when the efficiency of the enzymatic reaction has decreased enough to allow for standard exposure times.
92. If the desired bands cannot be detected upon overnight exposure, membranes can be collected and washed three times in rinsing buffer (10 min, RT), followed by re-hybridization with freshly prepared secondary antibodies, washing and revelation with the SuperSignal West Femto Chemiluminescent Substrate (Pierce Biotechnology), as recommended by the manufacturer.
93. If cutting could not be performed (and hence hybridization involved a single primary antibody, see also Note 79), after revelation membranes are washed three times in rinsing buffer (10 min, RT) and antibodies are removed by incubating them in de-hybridization buffer for 30–60 min (RT or 37°C), as recommended by the manufacturer, followed by extensive washing with dH_2O. Membranes processed as such can be re-probed with another primary antibody starting from the saturation of unspecific binding sites onward. In this case, as the anti-GAPDH antibody has a very strong affinity for GAPDH and provides a very high signal (which may be hardly de-hybridized) immunoblotting to monitor the equal loading of lanes should be performed as the final round.
94. Upon revelation, membranes are washed three times in rinsing buffer (10 min, RT) and can be stored at 4°C (in rinsing

buffer) for up to 6 months. If additional immunoblotting rounds become required within this period, stored membranes can be normally processed starting from the saturation of unspecific binding sites onward.

Acknowledgments

OK, LG and GK are especially grateful to Mr. Sundaramoorthy Balasubramanian, Senior Project Manager at SPi Global for assistance with the production of this book. GK is supported by the Ligue Nationale contre le Cancer (Equipe labellisée), Agence Nationale de la Recherche, Cancéropôle Ile-de-France, Fondation pour la Recherche Médicale, Institut National du Cancer, European Commission (Active p53, Apo-Sys, RIGHT, TransDeath, ChemoRes, ApopTrain), Fondation pour la Recherche Médicale, and the LabEx Immuno-Oncology.

References

1. Virchow R (1975) Cellular pathology: Lecture VIII. Blood and lymph. CA Cancer J Clin 25:93–97
2. Cho S, Hwang ES (2012) Status of mTOR activity may phenotypically differentiate senescence and quiescence. Mol Cells 33(6):597–604
3. Hanahan D, Weinberg RA (2000) The hallmarks of cancer. Cell 100:57–70
4. Russo AA, Jeffrey PD, Patten AK, Massague J, Pavletich NP (1996) Crystal structure of the p27Kip1 cyclin-dependent-kinase inhibitor bound to the cyclin A-Cdk2 complex. Nature 382:325–331
5. Sherr CJ, Roberts JM (1999) CDK inhibitors: positive and negative regulators of G1-phase progression. Genes Dev 13:1501–1512
6. Shin HY, Gerritsen ME, Bizios R (2002) Regulation of endothelial cell proliferation and apoptosis by cyclic pressure. Ann Biomed Eng 30:297–304
7. Blagosklonny MV (2002) Are p27 and p21 cytoplasmic oncoproteins? Cell Cycle 1:391–393
8. Kroemer G, Galluzzi L, Brenner C (2007) Mitochondrial membrane permeabilization in cell death. Physiol Rev 87:99–163
9. Kroemer G, Galluzzi L, Vandenabeele P, Abrams J, Alnemri ES, Baehrecke EH, Blagosklonny MV, El-Deiry WS, Golstein P, Green DR, Hengartner M, Knight RA, Kumar S, Lipton SA, Malorni W, Nunez G, Peter ME, Tschopp J, Yuan J, Piacentini M, Zhivotovsky B, Melino G (2009) Classification of cell death: recommendations of the Nomenclature Committee on Cell Death 2009. Cell Death Differ 16:3–11
10. Vandenabeele P, Galluzzi L, Vanden Berghe T, Kroemer G (2010) Molecular mechanisms of necroptosis: an ordered cellular explosion. Nat Rev Mol Cell Biol 11:700–714
11. Vitale I, Galluzzi L, Castedo M, Kroemer G (2011) Mitotic catastrophe: a mechanism for avoiding genomic instability. Nat Rev Mol Cell Biol 12:385–392
12. Galluzzi L, Vitale I, Abrams JM, Alnemri ES, Baehrecke EH, Blagosklonny MV, Dawson TM, Dawson VL, El-Deiry WS, Fulda S, Gottlieb E, Green DR, Hengartner MO, Kepp O, Knight RA, Kumar S, Lipton SA, Lu X, Madeo F, Malorni W, Mehlen P, Nunez G, Peter ME, Piacentini M, Rubinsztein DC, Shi Y, Simon HU, Vandenabeele P, White E, Yuan J, Zhivotovsky B, Melino G, Kroemer G (2012) Molecular definitions of cell death subroutines: recommendations of the Nomenclature Committee on Cell Death 2012. Cell Death Differ 19:107–120
13. Gartel AL, Serfas MS, Gartel M, Goufman E, Wu GS, el-Deiry WS, Tyner AL (1996) p21 (WAF1/CIP1) expression is induced in newly nondividing cells in diverse epithelia and during differentiation of the Caco-2 intestinal cell line. Exp Cell Res 227:171–181
14. Zhang P, Wong C, DePinho RA, Harper JW, Elledge SJ (1998) Cooperation between the

Cdk inhibitors p27(KIP1) and p57(KIP2) in the control of tissue growth and development. Genes Dev 12:3162–3167

15. Herbig U, Jobling WA, Chen BP, Chen DJ, Sedivy JM (2004) Telomere shortening triggers senescence of human cells through a pathway involving ATM, p53, and p21(CIP1), but not p16(INK4a). Mol Cell 14:501–513
16. Levkau B, Koyama H, Raines EW, Clurman BE, Herren B, Orth K, Roberts JM, Ross R (1998) Cleavage of p21Cip1/Waf1 and p27Kip1 mediates apoptosis in endothelial cells through activation of Cdk2: role of a caspase cascade. Mol Cell 1:553–563
17. Dai CY, Enders GH (2000) p16 INK4a can initiate an autonomous senescence program. Oncogene 19:1613–1622
18. Acosta JC, Gil J (2012) Senescence: a new weapon for cancer therapy. Trends Cell Biol 22:211–219

Chapter 8

Colorimetric Detection of Senescence-Associated β Galactosidase

Koji Itahana, Yoko Itahana, and Goberdhan P. Dimri

Abstract

Most normal human cells have a finite replicative capacity and eventually undergo cellular senescence, whereby cells cease to proliferate. Cellular senescence is also induced by various stress signals, such as those generated by oncogenes, DNA damage, hyperproliferation, and an oxidative environment. Cellular senescence is well established as an intrinsic tumor suppressive mechanism. Recent progress concerning senescence research has revealed that cellular senescence occurs in vivo and that, unexpectedly, it has a very complex role in tissue repair, promoting tumor progression and aging via the secretion of various cytokines, growth factors, and enzymes. Therefore, the importance of biomarkers for cellular senescence has greatly increased. In 1995, we described the "senescence-associated β galactosidase" (SA-βgal) biomarker, which conveniently identifies individual senescent cells in vitro and in vivo. Here, we describe an updated protocol for the detection of cell senescence based on this widely used biomarker, which contributed to recent advances in senescence, aging and cancer research. We provide an example of detecting SA-βgal together with other senescence markers and a proliferation marker, EdU, in single cells.

Key words: Aging, Biomarker, Cellular senescence, EdU labeling, SA-βgal, Immunostaining

1. Introduction

In contrast to germ cells, stem cells and cancer cells, most normal human somatic cells do not express a detectable level of telomerase and have a finite replicative capacity, due to the progressive erosion of telomeres that protect the ends of the chromosome (1, 2). This finite replicative lifespan of human cells was originally described by Hayflick and colleagues in cultured human fibroblasts (3). Telomeres become shortened at each round of cell division and, when they reach the critical length for replication, cells are permanently arrested with a G1 DNA content in a state called replicative senescence or cellular senescence (4, 5). Subsequent studies showed that cellular senescence also occurs prematurely in

Lorenzo Galluzzi et al. (eds.), *Cell Senescence: Methods and Protocols*, Methods in Molecular Biology, vol. 965,
DOI 10.1007/978-1-62703-239-1_8, © Springer Science+Business Media, LLC 2013

a telomere-independent manner in response to various kinds of stress such as oncogenic insults mediated by RAS (6) or RAF (7), hyperproliferative signals mediated by E2F1 (8) or ETS2 (9), oxidative stress (10, 11), DNA damage (12, 13), or induction of tumor suppressor proteins such as ARF (8), $p16^{INK4A}$ (14), and PML (15, 16). In addition, we have previously shown that the replicative senescence of human fibroblasts as described by Hayflick is in fact mediated by a mosaic of cells that undergo either telomere-dependent or -independent senescence in culture (17). Cellular senescence has been well established as an intrinsic tumor suppressive mechanism that prevents cells from dividing with faulty short telomeres that may cause genomic instability (1, 18). Cellular senescence is also a protective mechanism against oncogene-induced DNA replication stress, and other cellular stresses such as DNA damage and oxidative stress, to prevent cells with irreparable damage from undergoing further replication. Several studies have suggested that cellular senescence also occurs in vivo. For example, senescent cells were detected in a mouse model of liver fibrosis (19). Additionally, dysfunctional telomeres in mice lacking the RNA component of telomerase have been shown to activate a cellular senescence pathway to suppress tumorigenesis in the absence of apoptosis (20, 21). The existence of senescent cells in vivo was also demonstrated in mouse models of induction of oncogenes such as *Eμ-NRAS* (22), $KRAS^{V12}$ (23) or *BRAF* (24) as well as of loss of tumor suppressor genes such as *PTEN* (25). Importantly, the in vivo connection between aging and cellular senescence in tissues was recently demonstrated using a mouse model in which the removal of senescent cells can prevent or delay tissue dysfunction and extend health span (26). Several laboratories have recently shown that senescent cells also secrete many kinds of growth factors, proteases, and cytokines that can promote cancer progression and aging to cause detrimental effects (27), suggesting very complex roles for senescent cells in vivo (2).

To understand the role of cellular senescence in cancer and aging, developing reliable biomarkers of cellular senescence is very important. Senescent cells show a flat and enlarged morphology with increased cytoplasmic and nuclear volume. Senescent cells do not respond to mitogens. Therefore, senescent cells can be identified by their lack of DNA synthesis, or by genes that are differentially expressed. However, many somatic cells in our body consist of quiescent or terminally differentiated cells, and the DNA synthesis measurement does not distinguish these cells from senescent cells. In addition, downregulation of proliferation-associated genes and upregulation of growth inhibitory genes are common features among senescent, quiescent, and terminally differentiated cells. In 1995, we discovered that senescent cells expressed a β-galactosidase activity, which is histochemically detectable at pH 6.0 (28). We termed this activity “senescence-associated

β galactosidase" (SA-βgal). This biomarker was expressed in senescent, but not in pre-senescent or quiescent fibroblasts, nor in terminally differentiated keratinocytes (28). SA-βgal also showed an age-dependent increase in dermal fibroblasts and epidermal keratinocytes in skin samples from human donors of different ages, suggesting that it could be a good biomarker to identify senescent cells in vivo (28). Although we described that this marker can be detected in a senescent-independent manner, for instance in cells cultured in confluence conditions for long periods of time or in tissue structures such as hair follicles and the lumens of eccrine glands, we showed that SA-βgal activity is tightly associated with the senescent phenotype and increases in frequency in aged tissues, consistent with accumulation of senescent cells with age in vivo (28). Several subsequent studies have reinforced the idea that SA-βgal is a useful biomarker for the detection of senescent cells in culture as well as in vivo, in rodents and primates (5, 29–37). To date, by virtue of the simplicity and its reliability, the SA-βgal assay method is cited in more than 2,400 publications and has been the most extensively utilized biomarker for senescent cells in vitro and in vivo (5, 21–26, 29–37). Interestingly, the SA-βgal assay has also been used with other model organisms such as zebrafish (38) and *Caenorhabditis elegans* (39). The SA-βgal activity has been shown to partly reflect the increase in lysosomal mass (40). Increased expression of the *GLB1* gene, encoding a lysosomal enzyme, contributes to SA-βgal activity (41). Increased levels of lysosomal enzymes and an increased lysosomal activity are known to be one of the hallmarks of cellular senescence (42, 43). Several other senescent biomarkers have also been described such as p16 overexpression, senescence-associated heterochromatic foci (SAHF), which are nuclear DNA domains densely stained by DAPI (44), DNA segments with chromatin alterations reinforcing senescence (DNA-SCARS) (45), and the senescence-associated inflammatory transcriptome (46). However, compared to SA-βgal, these additional markers are not nearly as universal or convenient to use.

As in some exceptional cases the SA-βgal assay can stain non-senescent cells, showing that SA-βgal-positive cells are indeed not cycling is helpful. We have reported the SA-βgal staining protocol with thymidine labeling several years ago (47). BrdU labeling has been widely used to determine the percentage of proliferating cells in culture and tissues. However, BrdU labeling require cells and tissue samples to be subjected to strong denaturing conditions such as concentrated hydrochloric acid or mixtures of methanol and acetic acid. These harsh staining conditions degrade the structure of the specimen and cause poor retention of the cell morphology. Thus, BrdU labeling is not quite suitable for co-staining with SA-βgal. Recently, 5-ethynyl-2′-deoxyuridine (EdU), a thymidine analog, has been developed for labeling DNA (48). EdU labeling

does not require a denaturing step because the fluorescent azide to detect EdU is 1/500 the size of the BrdU antibody. It diffuses and penetrates cells rapidly without denaturation. Therefore, EdU labeling coupled to SA-βgal staining may constitute a convenient method for both in vitro and in vivo assays.

In this chapter, we update the previous SA-βgal assay protocol in detail and describe the protocol for SA-βgal assay together with EdU labeling (marker for cell proliferation), DAPI staining (marker for SAHF), and immunostaining (various protein markers for senescence) to detect cellular senescence in single cells in multiple ways.

2. Materials

2.1. Cell Culture

1. Dulbecco's modified Eagle's medium (DMEM) supplemented with 10% fetal bovine serum.
2. 100× penicillin–streptomycin.
3. 35-mm plates or 6-well plates (see Note 1).
4. WI-38 fetal lung normal human fibroblasts (Coriell Cell Repositories, Camden, NJ, USA) or any other types of cells.

2.2. Fixation and SA-βgal Staining of Cultured Cells

1. Phosphate-buffered saline (PBS) (137 mM NaCl, 2.7 mM KCl, 10 mM Na_2HPO_4, 1.8 mM KH_2PO_4; adjust to pH 7.4 with HCl if necessary).
2. Fixing solution: 4% formaldehyde, neutral buffered (Sigma-Aldrich, Saint-Louis, MO, USA, see Note 2).
3. Staining solution: 1 mg/mL 5-bromo-4-chloro-3-indolyl-beta-d-galactopyranoside (X-gal, Invitrogen, Eugene, CA, USA) (see Note 3), 1× citric acid/sodium phosphate buffer (pH 6.0, *see* below) (see Note 4), 5 mM potassium ferricyanide, 5 *mM* potassium ferrocyanide, (see Note 5), 150 mM NaCl, and 2 mM $MgCl_2$ (Table 1).
4. Mounting medium (Dako, Carpinteria, CA, USA) (see Note 6).
5. 22 × 22 mm cover glasses (see Note 6).

2.3. Fixation and SA-βgal Staining for Tissue Samples

1. Fixing solution: 1% formaldehyde either freshly prepared or diluted from 4% formaldehyde, neutral buffered (Sigma-Aldrich, see Note 2) with PBS.
2. Staining solution: As indicated in Subheading 2.2.
3. Counter staining solution: Eosin (Sigma-Aldrich).

Table 1
SA-βgal staining solution

Component	Stock solution	Amount for 10 mL	Final concentration
Citric acid/sodium phosphate buffer (pH 6.0)	5×	2 mL	1×
Potassium ferricyanide	50 mM	1 mL	5 mM
Potassium ferrocyanide	50 mM	1 mL	5 mM
NaCl	5 M	0.33 mL	150 mM
$MgCl_2$	1 M	20 µL	2 mM
X-gal	20 mg/mL	0.5 mL	1 mg/mL
H_2O	–	5.2 mL	–

2.4. EdU Labeling

1. Fixing solution: 4% formaldehyde, neutral buffered (see Note 2).
2. Permeabilizing solution: 0.5% Triton X-100 in PBS.
3. Click-iT® EdU Alexa Fluor® 594 Imaging Kit (red fluorescence, Invitrogen) or Click-iT® EdU Alexa Fluor® 488 Imaging Kit (green fluorescence, Invitrogen).
4. Hoechst 33342 solution (included in the Click-iT® kit).
5. DAPI (Sigma-Aldrich) 1 mg/mL solution in distilled water is placed at 4°C for short-term or at –20°C for long-term storage. The solution has to be protected from light.
6. Mounting medium (Dako, see Note 6).
7. 22×22 mm cover glasses (see Note 6).

2.5. Immunostaining

1. Fixing solution: 4% formaldehyde, neutral buffered (Sigma-Aldrich, see Note 2).
2. Permeabilizing solution: 0.5% Triton X-100 in PBS.
3. Blocking solution: 0.5% BSA in PBS (see Note 7).
4. Antibody dilution buffer: 0.5% BSA in PBS (see Note 7).
5. Secondary antibody (Jackson ImmunoResearch, West Grove, PA, USA).
6. 1 mg/mL DAPI (Sigma-Aldrich), stored as described above (see Subheading 2.4).
7. Mounting medium (Dako) (see Note 6).
8. 22×22 mm cover glasses (see Note 6).

3. Methods

3.1. SA-βgal Staining for Cultured Cells

1. Seed 2–5 × 10^4 cells in either a 35-mm plate or 6-well plate, and culture for 2–3 days or more (see Note 1).
2. Wash cells twice with PBS.
3. Fix cells with neutral buffered 4% formaldehyde for 3 min at room temperature (see Note 8).
4. Wash cells twice with PBS.
5. Add SA-βgal staining solution (2 mL per 35-mm plate).
6. Incubate cells with staining solution at 37°C (*NOT* in a CO_2 incubator).
7. Blue color is detectable in some cells within 2 h, but staining is generally maximal in 12–16 h (see Note 9).
8. After blue color is fully developed wash cells twice with PBS. Add one drop of mounting medium, and place cover glasses either on a 35-mm plate or 6-well plate.
9. Count the blue SA-βgal-positive cells under a microscope (see Note 10). In general, human normal fibroblast cultures are considered to be senescent if >80% of cells are SA-βgal positive.

3.2. SA-βgal Staining for Tissue Samples

1. Obtain biopsy specimens and rinse briefly in PBS to remove any blood.
2. Place in OCT compound (Miles Scientific, Princeton, MN, USA) in a Tissue-Tek Cryomold and flash freeze in liquid nitrogen containing 2-methylbutane (see Note 11).
3. Unused samples can be stored at −80°C, but the enzyme is not stable after freezing. In general, samples should be processed immediately or within a few hours after freezing.
4. Cut 4-μm sections of the samples.
5. Place sections onto slides that have been treated with silane to make them adhesive.
6. Fix sections in 1% formaldehyde in PBS for 1 min at room temperature.
7. Wash with PBS three times.
8. Immerse sections in SA-βgal staining solution overnight.
9. Counterstain with eosin.
10. View by bright-field microscopy (see Note 12).

3.3. EdU Labeling for Cultured Cells

1. Seed 2–5 × 10^4 cells in either a 35-mm plate or 6-well plate, and culture for 2–3 days or more (see Note 1).

2. Aspirate culture media and add 1 mL of DMEM containing 10% serum and 3 μM EdU provided as Click-iT® EdU Alexa Fluor® (594 or 488) Imaging Kit for 24 h (see Note 13).
3. Wash cells with PBS once.
4. Fix cells with neutral buffered 4% formaldehyde for 5 min at room temperature.
5. Wash cells twice with PBS.
6. Add 1 mL of 0.5% Triton® X-100 in PBS and incubate for 5 min at room temperature for permeabilization.
7. Wash cells twice with PBS.
8. Add 0.5 mL of Click-iT® reaction cocktail prepared according to the manufacturer's instructions (Invitrogen).
9. Incubate the plate for 30 min at room temperature, protected from light.
10. Remove the reaction cocktail and then wash each well once with PBS.
11. Add 1 mL of diluted DAPI solution in PBS (1 μg/mL) to label nuclei for 5 min at room temperature, protected from light.
12. Wash cells twice with PBS, add one drop of mounting medium, and place a cover glass on a plate.
13. Observe cells under an inverted fluorescent microscope (see Note 14).
14. Determine the percent of labeled nuclei (%LN) by counting the number of total (DAPI stained) and labeled (green or red fluorescent) nuclei in several randomly chosen fields (generally 200–500 total nuclei). %LN = (labeled nuclei/total nuclei) × 100. In general, human fibroblast cultures are considered to be senescent if <10% of cells incorporate EdU over a 1-day interval.

3.4. SA-βgal Staining with EdU Labeling for Cultured Cells

1. Incubate cells with 10 μM EdU for 24 h (see Subheading 3.3, steps 1 and 2).
2. Wash, fix, and stain for SA-βgal activity as described above (see Subheading 3.1, steps 2–7 and Note 15).
3. After blue color develops, wash, permeabilize, and add Click-iT® reaction cocktail and DAPI as described above (see Subheading 3.3, steps 5–11).
4. Wash cells twice with PBS, add one drop of mounting medium, and place a cover glass on a plate. Observe cells under an inverted fluorescent microscope (see Note 14).

5. Count cells with blue-colored staining for SA-βgal activity (% of SA-βgal-positive cells) under a bright field and with EdU labeled (%LN) under green or red fluorescence. Count DAPI-stained cells as the total number of cells.

3.5. SA-βgal Staining with Immunostaining for Cultured Cells

1. Culture cells in 35-mm or 6-well plates.
2. Wash, fix, and stain for SA-βgal activity as described above (see Subheading 3.1, steps 2–7 and Note 15).
3. Wash with PBS twice after blue color is developed.
4. Permeabilize cells with 0.5% of Triton X-100 in PBS for 5 min at room temperature.
5. Block plates with 0.5% BSA in PBS for 20 min (see Note 7).
6. Incubate plates with a primary antibody in 0.5% BSA either for 2 h at room temperature or overnight at 4°C (see Note 7).
7. Wash three times with PBS, 10 min each.
8. Incubate slides with secondary antibody in 0.5% BSA for 1 h at room temperature.
9. Wash three times with PBS, 10 min each.
10. Add 1 mL of diluted DAPI solution in PBS (1 μg/mL) to label nuclei for 5 min at room temperature.
11. Wash cells twice with PBS, add one drop of mounting medium, and place a cover glass on a plate. Observe cells under an inverted fluorescent microscope (see Note 14).
12. Count cells with blue-colored staining for SA-βgal activity under a bright field and with immunostaining under green or red fluorescence. Count DAPI-stained cells as the total number of cells.

3.6. SA-βgal Staining with EdU Labeling and Immunostaining for Cultured Cells

1. Culture cells in 35-mm or 6-well plates.
2. Add EdU, stain for SA-βgal activity, and detect EdU labeling as described above except for DAPI staining (see Subheading 3.4, steps 1–3).
3. Wash cells twice with PBS.
4. Follow the immunostaining procedure after the permeabilization step as described above (see Subheading 3.5, steps 5–11 and Note 16).
5. Count cells with blue-colored staining for SA-βgal activity under a bright field microscope and with either EdU or immunostaining under green or red fluorescence. Count DAPI-stained cells as the total number of cells. An example of SA-βgal staining with EdU Labeling and immunostaining is shown in Fig. 1.

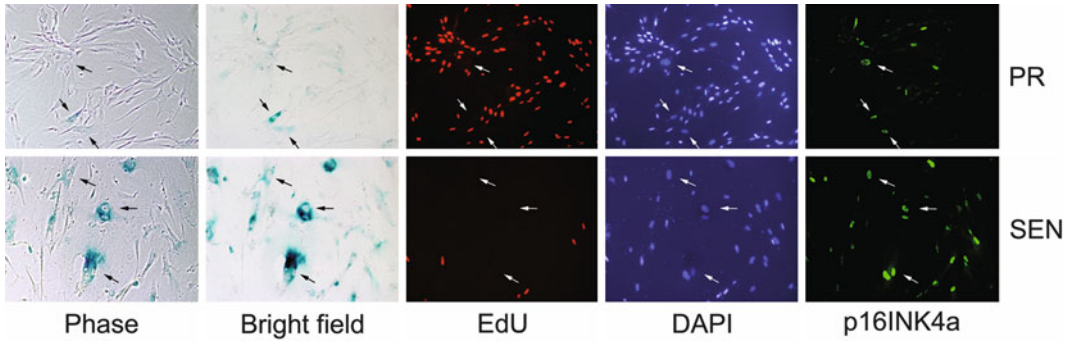

Fig. 1. SA-βgal staining with 5-ethynyl-2′-deoxyuridine (EdU) labeling, DAPI staining, and immunostaining of cultured cells. Early passage WI-38 fibroblasts (passage 25; *upper panel*) were cultured until near-to-senescence (passage 40; *lower panel*). Co-staining was performed as described in Subheading 3.6. SA-βgal staining was visualized and photographed under phase contrast and bright field microscopy as indicated. EdU labeling, DAPI, and immunostaining of $p16^{INK4a}$ were visualized and photographed by fluorescence microscopy. Mouse monoclonal antibody against p16 (Santa Cruz) was used for immunostaining. Note that the strong $p16^{INK4a}$ staining is correlated well with SA-βgal staining and the lack of EdU labeling in both early passage proliferating and senescent cultures (shown with *arrows*). PR and SEN indicate proliferating and senescent culture respectively.

4. Notes

1. For EdU labeling and immunostaining, Lab-Tek II Chamber Slide II (Nunc, Rochester, NY) can be used, although cell morphology and cell attachment are better either on a 35-mm plate or 6-well plate after EdU labeling and immunostaining. Cells should be at or less than 50–80% confluence at the time of assay. SA-βgal staining tends to increase in cells that have been plated for several days. SA-βgal staining of non-adherent cells such as lymphocytes requires a Cytospin centrifuge (Thermo Scientific, Asheville, NY, USA) to deposit cells onto glass slides.
2. For convenience, small aliquots of neutral buffered 4% formaldehyde solution are commercially available. The solution is stored at room temperature and each small container can be used up to a month after opening. For some cells or tissues, freshly prepared 2% formaldehyde plus 0.2% glutaraldehyde in PBS preserves the cell morphology somewhat better. The 25% glutaraldehyde solution can be obtained in small aliquots from Sigma and stored at −20°C. Formaldehyde and glutaraldehyde are toxic and emit toxic vapors. Use a chemical fume hood to avoid inhalation. Wear gloves, safety glasses, and protective clothing to avoid skin contact.
3. 20 mg/mL X-gal solution: X-gal is dissolved at 20 mg/mL in dimethylformamide (DMF) and stored in dark-colored or aluminum foil-wrapped tubes to protect from light. The solution

can be stored at –20°C for a few days. DMF is toxic and emits toxic vapors. Use a chemical fume hood to avoid inhalation. Wear gloves, safety glasses, and protective clothing to avoid skin contact.

4. 0.1 M citric acid solution: citric acid monohydrate ($C_6H_8O_7 \cdot H_2O$) is dissolved at 0.1 M in water. The solution can be kept at room temperature for several months. 0.2 M sodium phosphate solution: sodium dibasic phosphate (Na_2HPO_4) or sodium dibasic phosphate dehydrate ($Na_2HPO_4 \cdot H_2O$) is dissolved in water at 0.2 M. The solution can be stored at room temperature for several months. 5× citric acid/sodium phosphate buffer (pH 6.0): mix 36.85 mL of 0.1 M citric acid solution with 63.15 mL of 0.2 M sodium phosphate (dibasic) solution. Verify that the pH is 6.0. If the pH of the buffer is not 6.0, add either citric acid buffer or sodium phosphate buffer to adjust to pH 6.0. Some cell types, such as mouse fibroblasts or human epithelial cells, stain less intensely for SA-βgal. The staining intensity can sometimes be improved by slightly decreasing the pH. Try several pH ranges from 5.0 to 6.0 to optimize the staining conditions, making sure to include positive and negative controls. Most, if not all, cells stain positive at pH 4.0 because of endogenous lysosomal β galactosidase activity regardless of senescence status; therefore, caution should be exercised when lowering the pH of the staining solution. The buffer can be kept at room temperature for several months.
5. 50 mM potassium ferricyanide solution: potassium ferricyanide is dissolved in water at 50 mM concentration and stored at 4°C in a tube covered with aluminum foil to protect from light. 50 mM potassium ferrocyanide solution: potassium ferrocyanide is dissolved in water at 50 mM concentration and stored at 4°C in a tube covered with aluminum foil to protect from light. Both can be stored for several months. Avoid heating or adding acidic solution to prevent release of highly toxic hydrogen cyanide gas. Mixing the staining solution with other chemical waste by aspirating or dumping is not advisable because waste may contain acidic solutions. Autoclaving waste solution should be avoided.
6. These mounting mediums and cover glasses are suitable for SA-βgal staining, EdU labeling, and immunostaining on either a 35-mm or 6-well plate.
7. The success in co-staining for SA-βgal with immunostaining depends on the antigen and antibody. Senescent cells tend to have high background problems for immunostaining depending on the primary and secondary antibody. If this is the case, blocking with 5% nonfat milk in PBS or diluting the primary and/or secondary antibodies may help.

8. Longer fixation time such as 15 min destroys enzyme activity and significantly decreases the SA-βgal staining. 3–5 min of fixation is enough for SA-βgal staining, EdU labeling, and immunostaining.
9. If cultured fibroblasts are confluent for long period of times, density-induced SA-βgal staining, independent of senescence, may occur (28). Such staining is generally less intense than that observed in senescent cells and disappears within 2 days after the confluent cells are replated.
10. Blue staining is easier to be recognized under a bright field rather than with phase contrast.
11. Direct freezing in liquid nitrogen may fracture the specimen. Thus, placing samples in OCT on top of dry ice is best. Avoid repeated freeze thawing of the samples, which will affect morphology and destroy the SA-βgal enzymatic activity.
12. Some tissues structures, such as hair follicles and the lumens of eccrine glands, show strong age-independent staining (28).
13. EdU labeling is more convenient and less labor intensive compared with traditional thymidine labeling for cultured cells. We described protocols for thymidine labeling and co-staining SA-βgal with thymidine labeling previously (47). The protocol for EdU labeling and detection is slightly modified from manufacturer's instructions (Invitrogen). The best concentration of EdU should be determined according to each cell line and the type of experiment. A high concentration of EdU may lead to excess signals of EdU labeling that may be detected in microscope filters used for monitoring subsequent DAPI staining and immunostaining.
14. If cells are on chamber slides, use a regular (not an inverted) fluorescent microscope.
15. Because enzyme activity for SA-βgal activity is not stable, the SA-βgal assay must be performed before EdU detection. 3–5 min is adequate for fixation and permeabilization for SA-βgal staining with EdU Labeling, respectively. Avoid longer fixation times.
16. The intensity of SA-βgal staining and EdU labeling do not decrease even if plates are kept with primary antibody at 4°C overnight. EdU labeling does not require a denaturation step like BrdU labeling and has been used for tissue samples. Therefore, staining of SA-βgal, EdU-labeled DNA, antigen, and SAHF can be done for tissue samples in a similar order shown for cultured cells. If the intensity of EdU labeling (green fluorescence) is too high, emission from a green fluorophore may be detected through a red emission filter and DAPI filter. Therefore, we recommend to use Click-iT® EdU Alexa Fluor® 594 Imaging Kit (red fluorescence) for EdU labeling together with immunostaining since red fluorophore is difficult to detect through green emission filter and DAPI filter.

Acknowledgments

We thank Drs. Judith Campisi and Peter de Keizer, Buck Institute for Age Research, Novato, CA, for helpful suggestions.

References

1. Campisi J (2005) Senescent cells, tumor suppression, and organismal aging: good citizens, bad neighbors. Cell 120:513–522
2. Rodier F, Campisi J (2011) Four faces of cellular senescence. J Cell Biol 192:547–556
3. Hayflick L, Moorhead PS (1961) The serial cultivation of human diploid cell strains. Exp Cell Res 25:585–621
4. de Lange T (2001) Cell biology. Telomere capping–one strand fits all. Science 292:1075–1076
5. Itahana K, Campisi J, Dimri GP (2004) Mechanisms of cellular senescence in human and mouse cells. Biogerontology 5:1–10
6. Serrano M, Lin AW, McCurrach ME, Beach D, Lowe SW (1997) Oncogenic ras provokes premature cell senescence associated with accumulation of p53 and p16INK4a. Cell 88:593–602
7. Zhu J, Woods D, McMahon M, Bishop JM (1998) Senescence of human fibroblasts induced by oncogenic Raf. Genes Dev 12:2997–3007
8. Dimri GP, Itahana K, Acosta M, Campisi J (2000) Regulation of a senescence checkpoint response by the E2F1 transcription factor and p14(ARF) tumor suppressor. Mol Cell Biol 20:273–285
9. Ohtani N, Zebedee Z, Huot TJ, Stinson JA, Sugimoto M, Ohashi Y, Sharrocks AD, Peters G, Hara E (2001) Opposing effects of Ets and Id proteins on p16INK4a expression during cellular senescence. Nature 409:1067–1070
10. Blander G, de Oliveira RM, Conboy CM, Haigis M, Guarente L (2003) Superoxide dismutase 1 knock-down induces senescence in human fibroblasts. J Biol Chem 278:38966–38969
11. Chen QM, Bartholomew JC, Campisi J, Acosta M, Reagan JD, Ames BN (1998) Molecular analysis of H2O2-induced senescent-like growth arrest in normal human fibroblasts: p53 and Rb control G1 arrest but not cell replication. Biochem J 332(Pt 1):43–50
12. Di Leonardo A, Linke SP, Clarkin K, Wahl GM (1994) DNA damage triggers a prolonged p53-dependent G1 arrest and long-term induction of Cip1 in normal human fibroblasts. Genes Dev 8:2540–2551
13. Robles SJ, Adami GR (1998) Agents that cause DNA double strand breaks lead to p16INK4a enrichment and the premature senescence of normal fibroblasts. Oncogene 16:1113–1123
14. Kato D, Miyazawa K, Ruas M, Starborg M, Wada I, Oka T, Sakai T, Peters G, Hara E (1998) Features of replicative senescence induced by direct addition of antennapedia-p16INK4A fusion protein to human diploid fibroblasts. FEBS Lett 427:203–208
15. Ferbeyre G, de Stanchina E, Querido E, Baptiste N, Prives C, Lowe SW (2000) PML is induced by oncogenic ras and promotes premature senescence. Genes Dev 14:2015–2027
16. Pearson M, Carbone R, Sebastiani C, Cioce M, Fagioli M, Saito S, Higashimoto Y, Appella E, Minucci S, Pandolfi PP, Pelicci PG (2000) PML regulates p53 acetylation and premature senescence induced by oncogenic Ras. Nature 406:207–210
17. Itahana K, Zou Y, Itahana Y, Martinez JL, Beausejour C, Jacobs JJ, Van Lohuizen M, Band V, Campisi J, Dimri GP (2003) Control of the replicative life span of human fibroblasts by p16 and the polycomb protein Bmi-1. Mol Cell Biol 23:389–401
18. Dimri GP (2005) What has senescence got to do with cancer? Cancer Cell 7:505–512
19. Krizhanovsky V, Yon M, Dickins RA, Hearn S, Simon J, Miething C, Yee H, Zender L, Lowe SW (2008) Senescence of activated stellate cells limits liver fibrosis. Cell 134:657–667
20. Cosme-Blanco W, Shen MF, Lazar AJ, Pathak S, Lozano G, Multani AS, Chang S (2007) Telomere dysfunction suppresses spontaneous tumorigenesis in vivo by initiating p53-dependent cellular senescence. EMBO Rep 8:497–503
21. Feldser DM, Greider CW (2007) Short telomeres limit tumor progression in vivo by inducing senescence. Cancer Cell 11:461–469
22. Braig M, Lee S, Loddenkemper C, Rudolph C, Peters AH, Schlegelberger B, Stein H, Dorken B, Jenuwein T, Schmitt CA (2005) Oncogene-induced senescence as an initial barrier in lymphoma development. Nature 436:660–665
23. Collado M, Gil J, Efeyan A, Guerra C, Schuhmacher AJ, Barradas M, Benguria A, Zaballos A, Flores JM, Barbacid M, Beach D,

Serrano M (2005) Tumour biology: senescence in premalignant tumours. Nature 436:642

24. Michaloglou C, Vredeveld LC, Soengas MS, Denoyelle C, Kuilman T, van der Horst CM, Majoor DM, Shay JW, Mooi WJ, Peeper DS (2005) BRAFE600-associated senescence-like cell cycle arrest of human naevi. Nature 436:720–724
25. Chen Z, Trotman LC, Shaffer D, Lin HK, Dotan ZA, Niki M, Koutcher JA, Scher HI, Ludwig T, Gerald W, Cordon-Cardo C, Pandolfi PP (2005) Crucial role of p53-dependent cellular senescence in suppression of Pten-deficient tumorigenesis. Nature 436: 725–730
26. Baker DJ, Wijshake T, Tchkonia T, LeBrasseur NK, Childs BG, van de Sluis B, Kirkland JL, van Deursen JM (2011) Clearance of p16Ink4a-positive senescent cells delays ageing-associated disorders. Nature 479:232–236
27. Campisi J (2011) Cellular senescence: putting the paradoxes in perspective. Curr Opin Genet Dev 21:107–112
28. Dimri GP, Lee X, Basile G, Acosta M, Scott G, Roskelley C, Medrano EE, Linskens M, Rubelj I, Pereira-Smith OM, Peacocke M, Campisi J (1995) A novel biomarker identifies senescent human cells in culture and in aging skin in vivo. Proc Natl Acad Sci U S A 92:9363–9367
29. Cao L, Li W, Kim S, Brodie SG, Deng CX (2003) Senescence, aging, and malignant transformation mediated by p53 in mice lacking the Brca1 full-length isoform. Genes Dev 17:201–213
30. Castro P, Giri D, Lamb D, Ittmann M (2003) Cellular senescence in the pathogenesis of benign prostatic hyperplasia. Prostate 55:30–38
31. Choi J, Shendrik I, Peacocke M, Peehl D, Buttyan R, Ikeguchi EF, Katz AE, Benson MC (2000) Expression of senescence-associated beta-galactosidase in enlarged prostates from men with benign prostatic hyperplasia. Urology 56:160–166
32. Ferlicot S, Durrbach A, Ba N, Desvaux D, Bedossa P, Paradis V (2003) The role of replicative senescence in chronic allograft nephropathy. Hum Pathol 34:924–928
33. Krishnamurthy J, Torrice C, Ramsey MR, Kovalev GI, Al-Regaiey K, Su L, Sharpless NE (2004) Ink4a/Arf expression is a biomarker of aging. J Clin Invest 114: 1299–1307
34. Melk A, Schmidt BM, Takeuchi O, Sawitzki B, Rayner DC, Halloran PF (2004) Expression of p16INK4a and other cell cycle regulator and senescence associated genes in aging human kidney. Kidney Int 65:510–520
35. Mishima K, Handa JT, Aotaki-Keen A, Lutty GA, Morse LS, Hjelmeland LM (1999) Senescence-associated beta-galactosidase histochemistry for the primate eye. Invest Ophthalmol Vis Sci 40:1590–1593
36. Pendergrass WR, Lane MA, Bodkin NL, Hansen BC, Ingram DK, Roth GS, Yi L, Bin H, Wolf NS (1999) Cellular proliferation potential during aging and caloric restriction in rhesus monkeys (Macaca mulatta). J Cell Physiol 180:123–130
37. Sun LQ, Lee DW, Zhang Q, Xiao W, Raabe EH, Meeker A, Miao D, Huso DL, Arceci RJ (2004) Growth retardation and premature aging phenotypes in mice with disruption of the SNF2-like gene, PASG. Genes Dev 18:1035–1046
38. Kishi S, Bayliss PE, Uchiyama J, Koshimizu E, Qi J, Nanjappa P, Imamura S, Islam A, Neuberg D, Amsterdam A, Roberts TM (2008) The identification of zebrafish mutants showing alterations in senescence-associated biomarkers. PLoS Genet 4:e1000152
39. Dmitrieva NI, Burg MB (2007) High NaCl promotes cellular senescence. Cell Cycle 6:3108–3113
40. Kurz DJ, Decary S, Hong Y, Erusalimsky JD (2000) Senescence-associated (beta)-galactosidase reflects an increase in lysosomal mass during replicative ageing of human endothelial cells. J Cell Sci 113(Pt 20):3613–3622
41. Lee BY, Han JA, Im JS, Morrone A, Johung K, Goodwin EC, Kleijer WJ, DiMaio D, Hwang ES (2006) Senescence-associated beta-galactosidase is lysosomal beta-galactosidase. Aging Cell 5:187–195
42. Robbins E, Levine EM, Eagle H (1970) Morphologic changes accompanying senescence of cultured human diploid cells. J Exp Med 131:1211–1222
43. Brunk U, Ericsson JL, Ponten J, Westermark B (1973) Residual bodies and "aging" in cultured human glia cells. Effect of entrance into phase 3 and prolonged periods of confluence. Exp Eye Res 79:1–14
44. Narita M, Nunez S, Heard E, Lin AW, Hearn SA, Spector DL, Hannon GJ, Lowe SW (2003) Rb-mediated heterochromatin formation and silencing of E2F target genes during cellular senescence. Cell 113:703–716
45. Rodier F, Munoz DP, Teachenor R, Chu V, Le O, Bhaumik D, Coppe JP, Campeau E, Beausejour CM, Kim SH, Davalos AR, Campisi J (2011) DNA-SCARS: distinct nuclear structures that sustain damage-induced senescence growth arrest and inflammatory cytokine secretion. J Cell Sci 124:68–81

46. Coppe JP, Desprez PY, Krtolica A, Campisi J (2010) The senescence-associated secretory phenotype: the dark side of tumor suppression. Annu Rev Pathol 5:99–118
47. Itahana K, Campisi J, Dimri GP (2007) Methods to detect biomarkers of cellular senescence: the senescence-associated beta-galactosidase assay. Methods Mol Biol 371:21–31
48. Salic A, Mitchison TJ (2008) A chemical method for fast and sensitive detection of DNA synthesis in vivo. Proc Natl Acad Sci U S A 105:2415–2420

Chapter 9

Chemiluminescent Detection of Senescence-Associated β Galactosidase

Vinicius Bassaneze, Ayumi Aurea Miyakawa, and José Eduardo Krieger

Abstract

Identifying molecules that serve as markers for cell aging is a goal that has been pursued by several groups. Senescence-associated β galactosidase (SA-βgal) staining is broadly used and very easily detected. β-gal is a lysosomal enzyme strongly correlated to the progression of cell senescence. Here, we describe a simple, fast, and quantitative protocol to quantify SA-βgal activity in cell lysate extracts by a chemiluminescent method using galacton as substrate.

Key words: Cell senescence, Chemiluminescence, Quantitative method, SA-βgal

1. Introduction

Despite the fact that senescence-associated β galactosidase (SA-βgal) is not a causative element to cell senescence (1), its accumulation is irreversibly augmented in senescent cells and it is reliable and easy to detect. Moreover, there is no truly specific marker of senescence nor does each senescent cell express all possible senescence markers (2). Generally, SA-βgal activity is quantified by the X-gal staining procedure, a semiquantitative and subjective procedure that demands a laborious counting process of cells stained in variable intensities, even in a homogeneous cell culture. The distinction between faint and negative staining is often difficult to observe, making the methodology inaccurate. To overcome these limitations, new methodologies to detect and quantify β-gal activity using specific substrates and claiming to be more quantitative and less time consuming have been proposed (Table 1).

The methodology described in this chapter uses galacton® (Fig. 1), a 1,2-dioxetane substrate, that is non-isotopic and it is known to provide high signal intensity, low background, and high

Lorenzo Galluzzi et al. (eds.), *Cell Senescence: Methods and Protocols*, Methods in Molecular Biology, vol. 965,
DOI 10.1007/978-1-62703-239-1_9,

Table 1
Different methods for SA-βgal detection

Substrate type		Application	References
Chromogenic	X-gal	Adherent cell cultures and tissue samples	(5, 6)
Fluorescent	C_{12}FDG	Cell culture supernatant or flow cytometry	(7–10)
	MUG	Cell culture extracts	(11)
Chemiluminescent	Galacton®	Cell culture extracts	(12)

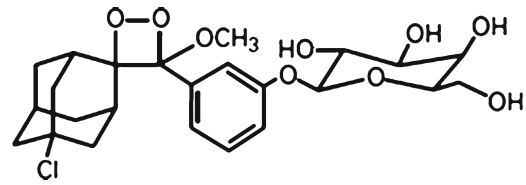

Fig. 1. *Galacton® structure.* (3-(4-methoxyspiro(1,2-dioxetane-3,20-(50-chloro)-tricyclo-(3.3.1.13,7)decan)-4-yl)phenyl-b-D-galactopyranoside)) structural formula.

sensitivity, and it is compatible with multiple assay formats (tubes, microwell plates, or X-ray films) when used to detect prokaryotic β-galactosidase. It was originally designed for the detection of prokaryotic β-gal enzyme (pH 7.8) used as a reporter in transfection studies (3). The methodology was adapted to detect and quantify SA-βgal activity in mammalian cell culture by modifying the pH 7.8 to pH 6.0. In fact, chemiluminescent substrates usually provide a more sensitive result than fluorescent or colorimetric probes, particularly when the amount of samples is limited (4). Therefore, we present methods in detail for the detection and quantification of SA-βgal using the galacton® chemiluminescent substrate.

2. Materials

2.1. Disposables

- Tissue culture dishes and flasks and cell scrappers.
- Specific plastic tubes for Monolight 2010 chemiluminometer (Analytical Luninescence, San Diego, CA, USA).

2.2. Equipment

- Chemiluminometer (Monolight 2010, Analytical Luminescence).
- Spectrophotometer (Victor Wallac 1420, Perking Elmer, Wellesley, MA, USA).

2.3. Reagents

- Human saphenous vein smooth muscle cells (see Note 1).
- Dulbecco's modified Eagle's medium (DMEM) with 4.5 g/L glucose.
- Fetal bovine serum (FBS).
- Penicillin and streptomycin, 100×.
- Phosphate buffer saline (PBS): 0.8% w/v sodium chloride, 0.02% KCl, 1.14% sodium phosphate dibasic heptahydrate, and 0.024% potassium phosphate dibasic (pH 7.4).
- 0.25% trypsin/1 mM EDTA (w/v).
- Magnesium chloride salt.
- Potassium ferricyanide.
- Citric acid.
- Monobasic sodium phosphate salts.
- Dibasic sodium phosphate salts.
- Gelatin from porcine skin (Sigma-Aldrich, St. Louis, MO, USA).
- X-gal (Invitrogen, Eugene, CA, USA).
- 100× Galacton® chemiluminescent substrate (3-(4-methoxyspiro(1,2-dioxetane-3,20-(50-chloro)-tricyclo-(3.3.1.13,7) decan)-4-yl)phenyl-b-D-galactopyranoside) (Applied Biosystems, Carlsbad, CA, USA).
- 10× Emerald Luminescence Enhancer for Solution Assays (Applied Biosystems).
- Cell culture lysis buffer (Promega, Madison, WI, USA).
- Bradford protein determination (Bio-Rad, Hercules, CA, USA).

3. Methods

3.1. Preparation of Smooth Muscle Cell Cultures

- Prepare 6-well plates coated with gelatin. Therefore add a thin layer of 1% gelatin from porcine skin in each well. Incubate the plates (without cover) at room temperature inside a laminar flow and let water completely evaporate.
- Plates can be wrapped with plastic film, stored in the refrigerator, and used on the next day.
- Inside a laminar flow, rinse the veins with PBS in order to remove the remaining blood. Open it longitudinally and cut it in small pieces (1–4 mm^2) using sterile scissors, on a plastic petri dish.
- Place six pieces (explants), with the lumen face down, inside of each well and a small drop (approximately 50 μL) of cell culture

medium supplemented with 1% penicillin/streptomycin and 20% FBS on each explant and maintain the culture in 5% CO_2 atmosphere at 37°C for at least 24 h.

- The following day the explants should have attached to the support; therefore carefully add 1 mL of cell culture medium to (the border of) each well.
- Cell culture medium should be replaced every 2–3 days and the proliferations should be observed under a light microscope. It usually takes at least 2 weeks to observe a considerable cell proliferation, which is the moment when the explant must be removed.
- After 25–30 days cell cultures should have reached confluence. At this moment the cells can be frozen for later usage, or replated and expanded, for experimentation or comparisons with earlier passages.

3.2. Passaging Smooth Muscle Cells

- Discard the cell culture medium and wash the cells twice with PBS, 1 mL per well.
- Aspirate PBS, add 500 μL per well of 0.25% trypsin/1 mM EDTA, and incubate for at most 3 min at the incubator.
- Check under microscope if the cells detached.
- Add 1.5 mL per well of cell culture medium and transfer all content to a 15 mL plastic tube.
- Count the number of cells and note the period between passages for further population doubling accountability.
- Transfer 8×10^4 cells per well and maintain in a 37°C incubator with 5% CO_2.
- For expansion, transfer from 0.8×10^4 to 1.2×10^4 cells/cm^2, depending on cell yield and flask size.

3.3. Stock Preparation

- Discard the cell culture medium and wash the cells twice with PBS, 1 mL per well.
- Aspirate PBS completely, add 500 μL per well of 0.25% trypsin/1 mM EDTA, and incubate for at most 3 min at the incubator, checking under microscope if the cells detached.
- Add 1.5 mL per well of cell culture medium and transfer all content to a 15 mL plastic tube.
- Count the number of cells and spin the cells at $500 \times g$ for 3 min.
- Discard the supernatant and resuspend the cells with cell culture medium to a concentration of 1×10^6 cells/mL.

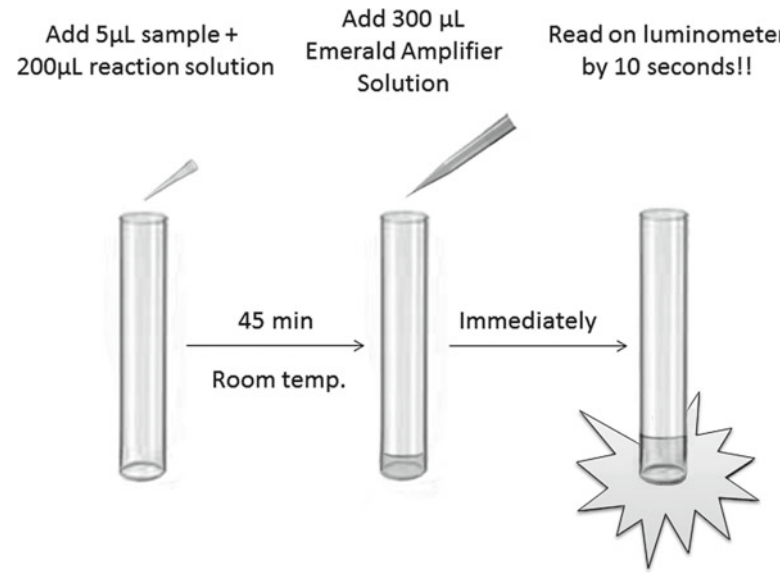

Fig. 2. Reaction steps.

- Transfer 900 µL of cell culture medium to a cryovial and add 100 µL of DMSO. Mix gently.
- Put the vials in –80°C freezer for no more than 1 month. For long-term storage, cells should be transferred to liquid nitrogen containers.

3.4. SA-βgal Activity Determination

- Perform all experiment in duplicate at room temperature.
- Two days after platting the cells, lyse the cells using 300 µL cell culture lysis buffer. Use a cell scraper to facilitate detaching and transfer the content to 1.5 mL tubes (see Note 2).
- Prepare the reaction solution by diluting galacton® substrate 1:100 in 100 mM sodium phosphate buffer (pH 6.0), supplemented with 20 µM magnesium chloride. The reaction solution must be prepared upon use. Prepare enough for immediate use.
- Incubate 5 µL of cell culture lysate in 200 µL reaction solution inside a plastic tube suitable for analysis by means of a luminometer. Incubate at room temperature for 45 min.
- Prepare the Emerald Luminescence Amplifier Solution by adding 600 µL of 5 N NaOH and 300 µL of 10× Emerald Enhancer to a final volume of 2.1 mL milli-Q water. Prepare enough for immediate use.
- After 45 min of reaction, add 300 µL of Emerald Luminescence Amplifier Solution to the tube and immediately perform the reading on luminometer, for 10 s (Fig. 2). The result should be normalized by total protein content (see Note 3).

3.5. Total Protein Content Determination

- Perform a 1:10 dilution of the cell lysate with milli-Q water. Pipet 10 μL of diluted sample in a 96-well plate. It is recommended to do this in triplicate.
- Create a standard curve using bovine serum albumin (BSA) ranging from 0.05 to 0.4 μg/μL. Add 10 μL of each on a 96-well plate, also in triplicate.
- Prepare the diluted Bradford dye reagent (1:5) and add 200 μL of the diluted to each well if possible using a multichannel pipet.
- Incubate at room temperature for at least 5 min.
- Measure absorbance at 595 nm on a spectrophotometer at no more than 1 h.
- Multiply the concentration obtained by 5 μL (volume used to react the samples on SA-βgal activity determination). Use the corresponding values to normalize the luminescence measurement, obtaining final data as a.u./μg protein (see Notes 4 and 5).

4. Notes

1. Experiments involving human materials must be carried out conforming to institutional regulations for biosafety and ethics.
2. Material can be stored at −80°C for future assay. It is strongly recommended to perform the SA-βgal activity of all samples you want to compare in the same assay.
3. This protocol is adjusted for smooth muscle cell. The assay may need to be standardized for each cell type. The basal SA-βgal varies between cell lines.
4. As mentioned before, the basal SA-βgal varies between cell lines. For that reason, the comparison of SA-βgal content between different cell types is not suitable for determining which one is more senescent.
5. To avoid confounding factors, different experiments should be performed with the same confluence (preferably not fully confluent) and without serum deprivation.

References

1. Lee BY, Han JA, Im JS, Morrone A, Johung K, Goodwin EC, Kleijer WJ, DiMaio D, Hwang ES (2006) Senescence-associated beta-galactosidase is lysosomal beta-galactosidase. Aging Cell 5:187–195
2. Campisi J (2011) Cellular senescence: putting the paradoxes in perspective. Curr Opin Genet Dev 21:107–112
3. Bronstein I, Martin CS, Fortin JJ, Olesen CE, Voyta JC (1996) Chemiluminescence: sensitive detection technology for reporter gene assays. Clin Chem 42:1542–1546
4. Jain VK, Magrath IT (1991) A chemiluminescent assay for quantitation of beta-galactosidase in the femtogram range: application to quantitation

of beta-galactosidase in lacZ-transfected cells. Anal Biochem 199:119–124

5. Dimri GP, Lee X, Basile G, Acosta M, Scott G, Roskelley C, Medrano EE, Linskens M, Rubelj I, Pereira-Smith O et al (1995) A biomarker that identifies senescent human cells in culture and in aging skin in vivo. Proc Natl Acad Sci U S A 92:9363–9367
6. Shlush LI, Itzkovitz S, Cohen A, Rutenberg A, Berkovitz R, Yehezkel S, Shahar H, Selig S, Skorecki K (2011) Quantitative digital in situ senescence-associated beta-galactosidase assay. BMC Cell Biol 12:16
7. Kurz DJ, Decary S, Hong Y, Erusalimsky JD (2000) Senescence-associated (beta)-galactosidase reflects an increase in lysosomal mass during replicative ageing of human endothelial cells. J Cell Sci 113(Pt 20):3613–3622
8. Noppe G, Dekker P, de Koning-Treurniet C, Blom J, van Heemst D, Dirks RW, Tanke HJ, Westendorp RG, Maier AB (2009) Rapid flow cytometric method for measuring senescence associated beta-galactosidase activity in human fibroblasts. Cytometry A 75:910–916
9. Yang NC, Hu ML (2004) A fluorimetric method using fluorescein di-beta-D-galactopyranoside for quantifying the senescence-associated beta-galactosidase activity in human foreskin fibroblast Hs68 cells. Anal Biochem 325:337–343
10. Debacq-Chainiaux F, Erusalimsky JD, Campisi J, Toussaint O (2009) Protocols to detect senescence-associated beta-galactosidase (SA-betagal) activity, a biomarker of senescent cells in culture and in vivo. Nat Protoc 4:1798–1806
11. Gary RK, Kindell SM (2005) Quantitative assay of senescence-associated beta-galactosidase activity in mammalian cell extracts. Anal Biochem 343:329–334
12. Bassaneze V, Miyakawa AA, Krieger JE (2008) A quantitative chemiluminescent method for studying replicative and stress-induced premature senescence in cell cultures. Anal Biochem 372:198–203

Chapter 10

Detection of the Senescence-Associated Secretory Phenotype (SASP)

Francis Rodier

Abstract

Cellular senescence suppresses cancer by eliminating potentially oncogenic cells, participates in tissue repair, contributes to cancer therapy, and promotes organismal aging. Numerous activities of senescent cells depend on the aptitude of these cells to secrete myriads of bioactive molecules, a behavior termed the senescence-associated secretory phenotype (SASP). The SASP supports cell-autonomous functions like the senescence-associated growth arrest, and mediates paracrine interactions between senescent cells and their surrounding microenvironment. The biological functions and the regulation of the SASP are beginning to emerge, and current SASP assessment techniques include the analysis of SASP factors at the mRNA level, the direct measurement of factors inside or outside the cell (i.e., secreted), and the detection of SASP-provoked cellular responses. Here, we focus on a simple approach to collect SASP-conditioned media in order to directly measure secreted SASP factors using sandwich enzyme-linked immunosorbent assay. As an example, we discuss the assessment of the major SASP factor interleukin-6 in senescent human fibroblasts. Supplemental notes are provided to easily adapt this procedure to other SASP factors, change cell types, or scale the techniques for different volumes or high-throughput measurements. These techniques should facilitate the discovery of novel functions and regulators of the SASP.

Key words: Aging, Cancer, Cytokines, Growth factors, Inflammation, Interleukin, Proteases, Sandwich enzyme-linked immunosorbent assay, Secretion

1. Introduction

Cellular senescence induces a permanent growth arrest in cells at risk of oncogenic transformation, contributes to normal tissue repair, and plays a role in age-associated pathologies or diseases (1). Many cancer cells retain the ability to undergo cellular senescence in response to damage, suggesting that cell senescence also plays a critical role during cancer therapy (2). Until recently, the cellular senescence response was almost exclusively associated with a state of permanent growth arrest; we now know that cellular senescence comprises an extracellular program that modulates

Lorenzo Galluzzi et al. (eds.), *Cell Senescence: Methods and Protocols*, Methods in Molecular Biology, vol. 965,
DOI 10.1007/978-1-62703-239-1_10,

interactions between senescent cells and their microenvironments (3, 4). The ability of senescent cells to modulate their microenvironment mostly resides in the senescence-associated secretory phenotype (SASP) (5–7). A variety of secreted factors comprise the SASP and their multiplicities of actions influence cell growth, survival, motility, inflammation, and extracellular matrix (ECM) remodeling (8, 9). Importantly, and one more reason to assess it properly, senescent cells do not always develop a SASP (10). Recently, some of the signaling pathways regulating the SASP were identified, including the DNA damage response (DDR), p38MAPK, JAK/STAT signaling pathway, and transcription factors such as NF-κB and C/EBPbeta (5, 6, 8, 11–13). Despite this early push, much remains unknown about the constituents, effects, and regulation of the SASP; thus effective tools to dissect this important phenotype are required.

1.1. Studying the SASP

Originally, the secretion of biologically active SASP factors by senescent cells was identified through the ability of senescent cells to influence the biology of other cells using soluble factors (14). Subsequently, mRNA profiling, proteomics, and genome-wide RNA interference screens were involved in refining a basic list of SASP factors (5–7, 15, 16). Several candidate SASP factors have been directly validated for their ability to modulate the biology of senescent cells, or that of surrounding cells (1, 3, 4). The process of identifying, validating, and characterizing new SASP factors is summarized below:

1. Identification of factors specifically secreted (or upregulated) by senescent cells.
2. Demonstration that these factors influence particular cellular phenotypes (either in senescent cells themselves, such as reinforcement of the growth arrest (5, 6), or in target cells, such as promotion of cancer cell growth or invasion (7, 16)).
3. Characterization of the molecular mechanisms responsible for the biological regulation and the effects of the new SASP factors (in senescent cells themselves, in the extracellular environment, or in target cells).

1.2. Enzyme-Linked Immunosorbent Assay and the SASP

Sandwich enzyme-linked immunosorbent assay (ELISA), a variation of the ELISA assay, is a powerful antibody-based technique highly sensitive and quantitative to detect individual soluble factors. However, Sandwich ELISA also has technical limitations, including a requirement for two separate specific antibodies recognizing the selected target. Because of this, and given the intrinsic limitation of sandwich ELISA to quantify only one soluble factor per experimental reaction, new SASP factors are most effectively discovered using large-scale molecular biology techniques such as mRNA profiling, antibody arrays, proteomics, or multiplex assays (5–7, 15, 16). The discovery strength of these large-scale assays

relies on their ability to simultaneously analyze several potential SASP factors (from tens to thousands). However, under some conditions and particularly with protein samples, the limited linear detection range of these large-scale techniques precludes the discovery of rare factors, and these assays often suffer the drawback of being limited to a smaller number of experimental samples given the relatively high "per sample" cost.

Almost to the opposite, the strength of the sandwich ELISA technique relies on its ability to analyze a lot of experimental samples simultaneously for one selected, potential, or confirmed SASP factor. Sandwich ELISA can do this with high sensitivity over a large linear range of target concentrations and at a much reduced "per sample" cost. Sandwich ELISA is therefore the technique of choice for follow-up confirmation analysis of SASP factors and their regulatory pathways. For example, sandwich ELISA was used to confirm the previously suspected SASP factors interleukin-6 (IL-6), IL-8, and MMP-3 (7, 17), or to study the molecular regulation of the validated SASP factor IL-6, which comprises multiple signaling molecules including ATM, H2AX, p38MAPK, and transcription factors NF-κB and C/EBPbeta (5, 6, 12, 13, 18).

2. Materials

The material described below is used to trigger DNA damage-induced premature cellular senescence in cultures of normal human diploid fibroblasts (HDF), to collect and process the normal (control) and senescent (SASP) conditioned media (CM) from 100 mm cell culture petri dishes, and to perform ELISA analysis of the CM samples for human IL-6.

2.1. Cell Culture

- Low passage or actively growing HDF strains are suitable for these experiments. Cell populations should have a doubling time of 48 h or less and DNA synthesis indices of at least 70 % over a period of 24 h (13). Suggested human fibroblast strains are BJ or HCA2 (foreskin) and WI-38 or IMR-90 (fetal lung) (7). The population doubling (PD) for the suggested cells at the beginning of the experiment should be below PD 25 to avoid the presence of replicatively senescent cells.
- Cells should be cultured at 37°C in 5–10 % CO_2 using DMEM supplemented with 9 % fetal bovine serum and 100 U/mL streptomycin/penicillin. The use of low O_2 levels (less than 5 %) is suggested but optional (19).
- Basic cell culture apparatus and reagents.

2.2. Senescence Induction

- Calibrated Gamma ray or X-ray source in a setup that permits the irradiation of cell culture tubes or flasks/dishes (13).

- Alternatively, bleomycin stock solution of 10 mg/mL in DMSO (radiomimetic drug causing DNA double-strand breaks (20)).

2.3. CM Collection

- Sterile plastic collection tubes (15 mL, suitable for freezing at −80°C).
- Sterile low protein-binding 0.45 μm syringe filters (example: Millex-HV PVDF Millipore SLHV033RS).
- Syringes suitable to filter the expected CM volume (10 mL or bigger).

2.4. ELISA

- Pre-coated quality controlled kits. We suggest using R&D Systems (Minneapolis, MN, USA) but any other human IL-6 ELISA kit should do.
- Extra 96-well plates to use as "loading plates."
- Multichannel (8 or 12) pipettes.

3. Methods

This protocol highlights how to collect a SASP and discusses a direct way to measure predefined SASP factors using ELISA. This protocol can be used as a SASP discovery tool to detect suspected new SASP components, as a SASP assessment tool to test the presence of SASP factors in different cells, or to identify/ascertain pathways regulating the secretion of selected SASP factors.

3.1. Cell Culture

The characteristics of cellular senescence develop over a period of about 10 days following a senescence-inducing dose of DNA damage (1). The following cell culture timelines are given in order to synchronize control and senescent cell population for CM collection on the same day. Senescence should be clearly assessed in experimental cell populations (see Notes 1–5).

1. DNA damage-induced prematurely senescent cell population:

   Day −1: Seed 750,000 cells in one 100 mm cell culture petri dish.

   Day 0: *Induce senescence*; cells roughly at 60 % confluence (change media).

   Day 2: Cells roughly at 75 % confluence (change media).

   Day 5: Cells roughly at 90 % confluence (change media).

   Day 8: Cells roughly at 95 % confluence (change media).

   Day 10: Cells roughly at 100 % confluence (prepare CM).

2. Control cell population:

   Day 7: Seed 750,000 cells in one 100 mm cell culture petri dish.

   Day 8: Cells roughly at 60 % confluence (change media).

   Day 10: Cells roughly at 90 % confluence (prepare CM).

3. Replicatively senescent cell population:

   Day 5: Seed 1,500,000 senescent cells in one 100 mm cell culture petri dish.

   Day 6: Cells roughly 80 % confluent (change media).

   Day 8: *Cells should expand in size*; cells roughly 90 % confluent (change media).

   Day 10: Cells roughly at 90 % confluence (prepare CM).

3.2. Senescence Induction

1. Cells from DNA damage-induced premature senescence populations can be X-irradiated on day 0 at rates equal to or above 0.75 Gy/min for a total dose of 10 Gy or treated with bleomycin at 20 μg/mL for 2 h. Either treatment should be followed by a media change.
2. Alternatively, cells can be grown to replicative senescence until the cell population has a DNA synthesis labeling index of <5 % over 24 h and >75 % of cells express SA-βgal activity.

3.3. CM Collection

1. On day 10, gently wash three times with 12 mL warm PBS making sure to remove as much PBS as possible at every wash.
2. Apply 6 mL serum-free CM (DMEM + Antibiotics, *without serum*, *for fibroblast*).
3. On day 11 (24 h later), collect CM in a tube and reserve for later on ice (4°C).
4. Following CM collection, Trypsinize and count cells in original vessel (*important to adjust CM concentration in cells/mL*).
5. Optional: Pellet cells and freeze at −80°C if intracellular extracts needed (remember that these cells were starved for 24 h).
6. Return to CM and process immediately as follows:
7. Spin down cell debris (5 min at 300 × *g* in cell culture centrifuge).
8. Filter CM supernatant through 0.45 μM syringe filter.
9. Aliquot if necessary and freeze at −80°C.
10. Calculate CM cells/mL concentration (total cell number per dish divided by volume of CM collected).
11. The expected cell concentrations for this protocol is around 200–300 thousand cells per mL of CM.

12. This conditioned media is stable for months at –80°C when planning to measure IL-6 levels. The stability of other SASP factors could vary.

3.4. ELISA

We suggest to use the R&D Systems IL-6 kit and to follow the user's manual. Protocols for other ELISA kits may be slightly different, but the general principle remains the same. However, to successfully detect SASP components, CM concentrations may need to be adjusted to match the linear range and sensitivity of the selected kit. CM-SASP samples have higher concentrations of SASP factors; therefore, they will require a greater dilution compared to CM-control. Alternatively, SASP factors may not be detectable at all in CM-control samples, even without dilutions. Because of the need to think about different dilution ratios for CM-control and CM-SASP samples, we prepare a "loading 96-well plate" prior to starting the true ELISA protocol. This loading plate is an extra 96-well plate, it is *NOT THE ELISA PLATE FROM THE KIT*. For R&D Systems IL-6, proceed as follows:

1. The expected cell concentration for the collection protocol above is around 200–300 thousand cells per mL of CM.
2. Thaw the CM samples that you plan to use and keep them on ice.
3. To effectively detect IL-6, you should use a final concentration of 5,000 cells/mL or less for senescent cells, and 50,000 cells/mL or more for control cells. When trying for the first time, we suggest using multiple dilutions.
4. Once you have selected and made your dilutions, prepare the "loading 96-well plate" as follows:
5. Keep the loading 96-well plate on ice.
6. Pipet 150 µL from your IL-6 standards from the ELISA kit into the wells A1-H1.
7. Pipet 150 µL from the first of your diluted CM samples into wells A2, followed by 150 µL of your second sample into A3, and so forth for up to 88 samples if you wish to run a full ELISA plate.
8. When the loading plate is finally completed, you can use it at the right step in the ELISA protocol to rapidly transfer 100 µL per well from this plate to *the real ELISA plate from the kit (which at that point in the ELISA protocol already contains the assay diluent*). Use a multichannel pipettor.
9. Follow the ELISA protocol from the kit.

Once you get IL-6 concentration data from the ELISA, you need to normalize the concentration of IL-6 detected in every well using the volume and cell concentration of the diluted sample.

You will then obtain a final value of secreted pg of IL-6 per cell per day or IL-6 pg/cell/day (since the CM collection was performed over a 24-h period). For each of the samples, use the following formula:

(Detected IL-6 concentration in pg) divided by (diluted cell concentration per mL) = IL-6 pg/cell/day.

For this formula, *do not use the original cell concentration of the sample*; use the value after dilution that was used to load the ELISA well.

4. Notes

1. It is important to validate the state of cellular senescence. In addition to growth arrest and enlargement (21), cellular senescence is characterized by multiple phenotypes (1). Following growth and visual analysis of cells, we suggest testing your senescent cell cultures for at least two out of the four following phenotypes: (1) Senescent cells express an enzymatic SA-βgal (22); (2) most senescent cells express the gene $p16^{INK4a}$, which is not commonly expressed by quiescent or proliferating cells (23–26); (3) in some senescent cells, $p16^{INK4a}$ causes formation of senescence-associated heterochromatin foci (SAHF), which can be simply tested using a DAPI DNA staining (27); and (4) cells that senesce with persistent DDR signaling harbor persistent DNA damage nuclear foci, termed DNA segments with chromatin alterations reinforcing senescence (DNA-SCARS) (13). These foci can be detected using immunofluorescence and contain activated DDR proteins, including phospho-ATM and phosphorylated ATM/ATR substrates (12, 28–30).
2. In general, avoid cell confluence since this could decrease the accuracy of cell counts following CM collection or induce senescence-independent cellular stresses.
3. The CM does not necessarily need to be centrifuged or filtered, although these steps rule out detection of targets inside floating cells.
4. The techniques described here can be applied to any other cell type or SASP factor. Different SASP factors may need very different dilutions prior to ELISA detection. Different cell types may need the CM to be collected in the presence of serum to avoid cell death or stress.
5. The protocol described here can be scaled up for proteomic studies or down for high-throughput experiments. This scaling can be performed based on the surface area of the target cell culture vessels. For example, to prepare CM from a 96-well

plate (hypothetic well surface area of 0.32 cm^2 versus 56.5 cm^2 for a 100 mm petri dish), you can divide cell numbers from the described protocol by the corresponding ratio of 176 (between the hypothetic 100 mm petri and one well from a 96-well plate). Thus, you can seed (750,000/176), or 4,200 control cells, in one well of a 96-well plate on day 7. You will then collect CM samples from roughly 10,000 cells on days 10–11 (control cells will more than double in 3 days). Since the volume of CM in one well from a 96-well plate will also be reduced accordingly, a similar final concentration of 200–300 thousand cells per mL is expected. This strategy was used successfully to identify small molecules regulating IL-6 secretion by senescent cells (31).

Acknowledgments

This work was supported by grants from the Institut du cancer de Montréal (René Malo initiative for innovative research) and the Canadian Institute of Health Research (CIHR # MOP 114962) to F.R.

References

1. Rodier F, Campisi J (2011) Four faces of cellular senescence. J Cell Biol 192:547–556
2. Collado M, Serrano M (2010) Senescence in tumours: evidence from mice and humans. Nat Rev Cancer 10:51–57
3. Coppé JP, Desprez PY, Krtolica A, Campisi J (2010) The senescence-associated secretory phenotype: the dark side of tumor suppression. Annu Rev Pathol 5:99–118
4. Kuilman T, Peeper DS (2009) Senescence-messaging secretome: SMS-ing cellular stress. Nat Rev Cancer 9:81–94
5. Acosta JC, O'Loghlen A, Banito A, Guijarro MV, Augert A, Raguz S, Fumagalli M, Da Costa M, Brown C, Popov N, Takatsu Y, Melamed J, d'Adda di Fagagna F, Bernard D, Hernando E, Gil J (2008) Chemokine signaling via the CXCR2 receptor reinforces senescence. Cell 133:1006–1018
6. Kuilman T, Michaloglou C, Vredeveld LC, Douma S, van Doorn R, Desmet CJ, Aarden LA, Mooi WJ, Peeper DS (2008) Oncogene-induced senescence relayed by an interleukin-dependent inflammatory network. Cell 133:1019–1031
7. Coppé JP, Patil CK, Rodier F, Sun Y, Munoz DP, Goldstein J, Nelson PS, Desprez PY, Campisi J (2008) Senescence-associated secretory phenotypes reveal cell-nonautonomous functions of oncogenic RAS and the p53 tumor suppressor. PLoS Biol 6:2853–2868
8. Freund A, Orjalo AV, Desprez PY, Campisi J (2010) Inflammatory networks during cellular senescence: causes and consequences. Trends Mol Med 16:238–246
9. Davalos AR, Coppé JP, Campisi J, Desprez PY (2010) Senescent cells as a source of inflammatory factors for tumor progression. Cancer Metastasis Rev 29:273–283
10. Coppe JP, Rodier F, Patil CK, Freund A, Desprez PY, Campisi J (2011) Tumor suppressor and aging biomarker p16(INK4a) induces cellular senescence without the associated inflammatory secretory phenotype. J Biol Chem 286:36396–36403
11. Novakova Z, Hubackova S, Kosar M, Janderova-Rossmeislova L, Dobrovolna J, Vasicova P, Vancurova M, Horejsi Z, Hozak P, Bartek J, Hodny Z (2010) Cytokine expression and signaling in drug-induced cellular senescence. Oncogene 29:273–284
12. Rodier F, Coppé JP, Patil CK, Hoeijmakers WA, Munoz DP, Raza SR, Freund A, Campeau E, Davalos AR, Campisi J (2009) Persistent

DNA damage signalling triggers senescence-associated inflammatory cytokine secretion. Nat Cell Biol 11:973–979

13. Rodier F, Munoz DP, Teachenor R, Chu V, Le O, Bhaumik D, Coppe JP, Campeau E, Beausejour CM, Kim SH, Davalos AR, Campisi J (2011) DNA-SCARS: distinct nuclear structures that sustain damage-induced senescence growth arrest and inflammatory cytokine secretion. J Cell Sci 124:68–81
14. Krtolica A, Parrinello S, Lockett S, Desprez PY, Campisi J (2001) Senescent fibroblasts promote epithelial cell growth and tumorigenesis: a link between cancer and aging. Proc Natl Acad Sci U S A 98:12072–12077
15. Wajapeyee N, Serra RW, Zhu X, Mahalingam M, Green MR (2008) Oncogenic BRAF induces senescence and apoptosis through pathways mediated by the secreted protein IGFBP7. Cell 132:363–374
16. Coppé JP, Patil CK, Rodier F, Krtolica A, Beauséjour CM, Parrinello S, Hodgson JG, Chin K, Desprez PY, Campisi J (2010) A human-like senescence-associated secretory phenotype is conserved in mouse cells dependent on physiological oxygen. PLoS One 5:e9188
17. Parrinello S, Coppé JP, Krtolica A, Campisi J (2005) Stromal-epithelial interactions in aging and cancer: senescent fibroblasts alter epithelial cell differentiation. J Cell Sci 118:485–496
18. Freund A, Patil CK, Campisi J (2011) p38MAPK is a novel DNA damage response-independent regulator of the senescence-associated secretory phenotype. EMBO J 30:1536–1548
19. Parrinello S, Samper E, Krtolica A, Goldstein J, Melov S, Campisi J (2003) Oxygen sensitivity severely limits the replicative lifespan of murine fibroblasts. Nat Cell Biol 5:741–747
20. Regulus P, Duroux B, Bayle PA, Favier A, Cadet J, Ravanat JL (2007) Oxidation of the sugar moiety of DNA by ionizing radiation or bleomycin could induce the formation of a cluster DNA lesion. Proc Natl Acad Sci U S A 104:14032–14037
21. Hayflick L (1965) The limited in vitro lifetime of human diploid cell strains. Exp Cell Res 37:614–636
22. Dimri GP, Lee X, Basile G, Acosta M, Scott G, Roskelley C, Medrano EE, Linskens M, Rubelj I, Pereira-Smith O et al (1995) A biomarker that identifies senescent human cells in culture and in aging skin in vivo. Proc Natl Acad Sci U S A 92:9363–9367
23. Serrano M, Lin AW, McCurrach ME, Beach D, Lowe SW (1997) Oncogenic ras provokes premature cell senescence associated with accumulation of p53 and p16INK4a. Cell 88:593–602
24. Stein GH, Drullinger LF, Soulard A, Dulic V (1999) Differential roles for cyclin-dependent kinase inhibitors p21 and p16 in the mechanisms of senescence and differentiation in human fibroblasts. Mol Cell Biol 19: 2109–2117
25. Beauséjour CM, Krtolica A, Galimi F, Narita M, Lowe SW, Yaswen P, Campisi J (2003) Reversal of human cellular senescence: roles of the p53 and p16 pathways. EMBO J 22:4212–4222
26. Hara E, Smith R, Parry D, Tahara H, Stone S, Peters G (1996) Regulation of p16CDKN2 expression and its implications for cell immortalization and senescence. Mol Cell Biol 16:859–867
27. Narita M, Nunez S, Heard E, Narita M, Lin AW, Hearn SA, Spector DL, Hannon GJ, Lowe SW (2003) Rb-mediated heterochromatin formation and silencing of E2F target genes during cellular senescence. Cell 113:703–716
28. d'Adda di Fagagna F, Reaper PM, Clay-Farrace L, Fiegler H, Carr P, Von Zglinicki T, Saretzki CNP, Jackson SP (2003) A DNA damage checkpoint response in telomere-initiated senescence. Nature 426:194–198
29. Herbig U, Jobling WA, Chen BP, Chen DJ, Sedivy J (2004) Telomere shortening triggers senescence of human cells through a pathway involving ATM, p53, and p21(CIP1), but not p16(INK4a). Mol Cell 14:501–513
30. Takai H, Smogorzewska A, de Lange T (2003) DNA damage foci at dysfunctional telomeres. Curr Biol 13:1549–1556
31. Laberge RM, Zhou L, Sarantos MR, Rodier F, Freund A, de Keizer PL, Liu S, Demaria M, Cong YS, Kapahi P, Desprez PY, Hughes RE, Campisi J (2012) Glucocorticoids suppress selected components of the senescence-associated secretory phenotype. Aging Cell 11: 569–578

Chapter 11

Unbiased Characterization of the Senescence-Associated Secretome Using SILAC-Based Quantitative Proteomics

Juan Carlos Acosta, Ambrosius P. Snijders, and Jesús Gil

Abstract

Approaches based on the combination of mass spectrometry (MS) and quantitative methods have the potential to generate unbiased, thorough proteomic catalogues. In particular, stable isotope labeling with amino acid in cell culture (SILAC) has been used to perform highly accurate quantitative comparisons between the proteomes of different cell lines, treatments, or even animal models. Here, we describe how we have taken advantage of SILAC-based quantitative proteomics and inducible cell systems of oncogene-induced senescence to make an unbiased characterization of the senescence-associated secretome. This approach could be used to analyze the effect of diverse molecules on the senescence secretome or to catalogue unrelated secretomes.

Key words: Mass spectrometry, SILAC, Proteomics, Secreted factors, Conditioned media, Senescence secretome, SASP, SMS

1. Introduction

Senescence is a highly stable form of cell cycle arrest that is engaged in response to replicative exhaustion and a number of other cellular stresses (1). These include DNA damage, treatment with chemotherapeutic agents, or aberrant oncogenic signaling (2). Senescence, and in particular oncogene-induced senescence (OIS), acts as a barrier for tumorigenesis (3). In addition, senescent cells are observed during aging and in multiple pathological stages (1). While most of the effects exerted by senescent cells are cell intrinsic and related to their strict implementation of cell cycle arrest, senescent cells secrete a complex collection of factors. This is often referred to as the senescence-associated secretory phenotype

These authors equally contributed.

Lorenzo Galluzzi et al. (eds.), *Cell Senescence: Methods and Protocols*, Methods in Molecular Biology, vol. 965,
DOI 10.1007/978-1-62703-239-1_11, © Springer Science+Business Media, LLC 2013

(SASP) or the senescence-messaging secretome (SMS) (4, 5). This senescence secretome has been involved in the ability of senescent cells to induce inflammation, cause tissue damage, or promote tumorigenesis, but also can reinforce senescence and exert tumor-suppressive actions (4, 5).

Given all the potential effects that the senescence secretome can mediate, a lot of interest has been focused on identifying its components. Different methods for identifying the composition of the senescence secretome include mRNA expression analysis or the use of antibody arrays (6–8). In recent years, several approaches have been used to perform quantitative analysis of complex mix of proteins. For example, stable isotope labeling with amino acids in culture (SILAC) has been used to catalogue quantitative proteomic changes in cell culture (9) and even in whole mice (10). For SILAC, stable isotope-labeled amino acids are actively incorporated into cells while they are in culture. Cells kept at the two conditions to be compared are grown in different isotope mix (often referred as heavy and light). Samples from the two conditions are then combined and subjected to one-dimensional gel electrophoresis, followed by trypsin digestion. The resulting tryptic peptides can be analyzed by mass spectrometry (MS). The ratio of the heavy versus light-labeled peptide peak intensities in the spectrum mirrors the relative expression levels of the proteins they represent between the compared samples. We explain here a powerful, unbiased method to identify components of the secretome of senescent cells by taking advantage of SILAC-based quantitative proteomics to compare the conditioned media of senescent versus normal cells.

2. Materials

2.1. Cells and Tissue Culture

All the tissue culture is done in standard conditions in humidity at 37°C with 5% CO_2.

1. IMR90 human diploid fibroblast (ATCC).
2. HEK293T cells (ATCC).
3. IMR90 ER:RAS and vector were produced from IMR90 cells by retroviral infection with pLNC-ER:RAS and pLXSN retroviral vectors (11).
4. Tissue culture media for IMR90 and HEK 293T cell growth: Dulbecco's Modified Eagle Medium (DMEM) supplemented with 10% fetal bovine serum (FBS) and Antibiotic–Antimycotic (Invitrogen-Gibco 15240).

2.2. Transfection and Retroviral Infection Reagents

1. pLNC-ER:RAS has been previously described (11).
2. 25 kDa linear polyethylenimine (PEI) reagent (Polysciences) was prepared at a concentration of 1 mg/mL (w/v).

3. Hexadimethrine bromide (Polybrene) (Sigma) is prepared in stocks of 8 mg/mL.
4. 50 mg/mL G418 solution.
5. 4-Hydroxytamoxifen (4OHT, Sigma) was prepared in DMSO at a concentration of 200 mM.

2.3. Stable Isotope Labeling with Amino Acids in Cell Culture

1. DMEM Media for SILAC (Pierce).
2. 10 kDa dialyzed FBS (Biosera).
3. Heavy amino acids $^{13}C_6$, $^{15}N_2$ L-Lysine-2HCl and $^{13}C_6$, $^{15}N_4$ L-Arginine-HCl were from CKGas.
4. Cell culture grade light amino acids.
5. Light SILAC media (L SILAC): DMEM media for SILAC (Pierce) was complemented with 0.1 mg/mL of L-Lysine-2HCl and L-Arginine-HCl, 10% dialyzed FBS and Antibiotic–Antimicotic (Invitrogen-Gibco).
6. Heavy SILAC media (H SILAC): DMEM media for SILAC (Pierce) was complemented with 0.1 mg/mL of $^{13}C_6$, $^{15}N_2$ L-Lysine-2HCl and $^{13}C_6$, $^{15}N_4$ L-Arginine-HCl and 10% dialyzed FBS and Antibiotic–Antimicotic (Invitrogen-Gibco) (see Note 1).
7. Experimental SILAC media (H or L). It refers to the media used to produce CM from normal and senescence cells for the analysis of the secretome. The composition is like the SILAC labeling media heavy and light but without the addition of FBS.

2.4. Reagents for Processing Conditioned Media

1. 20 MWCO 5000 Vivaspin filters (GE Healthcare).
2. Proteomics grade trypsin.
3. LC-MS grade water (ThermoFisher).
4. Acetonitrile (ThermoFisher).
5. Formic acid (FA) (ThermoFisher).
6. Trifluoroacetic acid (TFA) (ThermoFisher).

2.5. Mass Spectrometry

1. Ultimate 3000 Rapid Separations nano LC system (ThermoFisher).
2. LTQ-Orbitrap-Velos Mass Spectrometer (ThermoFisher).
3. 100 × 2 cm Trapcolumn with 5 mm c18 particles (ThermoFisher).
4. Acclaim Pepmap column (75 × 50 cm column, 2 mm c18 particles, ThermoFisher).

2.6. Data-Dependant Acquisition

1. Xcalibur software.
2. DCMS Link software.
3. MaxQuant and embedded Andromeda search engine (12, 13).

3. Methods (Fig. 1)

3.1. Generation of IMR90 ER:RAS Cells

1. The day before transfection, HEK293T cells are seeded so that they reach 50–80% confluence the next day.
2. Mix 20 mg of the pLNC-ER:RAS or LXSN retroviral vectors with 7.5 mg of plasmid encoding the VSV-G envelope protein and 2.5 mg of a vector expressing the gag and pol retroviral proteins in HEK293T cells (see Note 2).
3. Mix 30 μg of DNA with 1 mL of DMEM and 75 μL of PEI at a concentration of 1 mg/mL (w/v).
4. Vortex and incubate for 10 min.
5. Following incubation, add the DNA–PEI mix drop-wise over a 70–80% confluent 10 cm dish of HEK293T cells containing 10 mL of DMEM supplemented with 10% FBS (see Note 3).
6. After 16 h replace the media by DMEM 10% FBS.
7. Thirty-two hours after transfection seed IMR90 cells so that they will be around 50–80% confluency at the moment of infection.
8. Forty-eight hours after transfection, the media enriched in retroviral particles from the transfected HEK-293T cells is collected and filtered using 0.2 mM pore size filters (Anachem). 10 mL of fresh growth media is added to the HEK-293T cells.
9. Complement the filtered media containing retroviral particles with polybrene to a final concentration of 4 mg/mL.

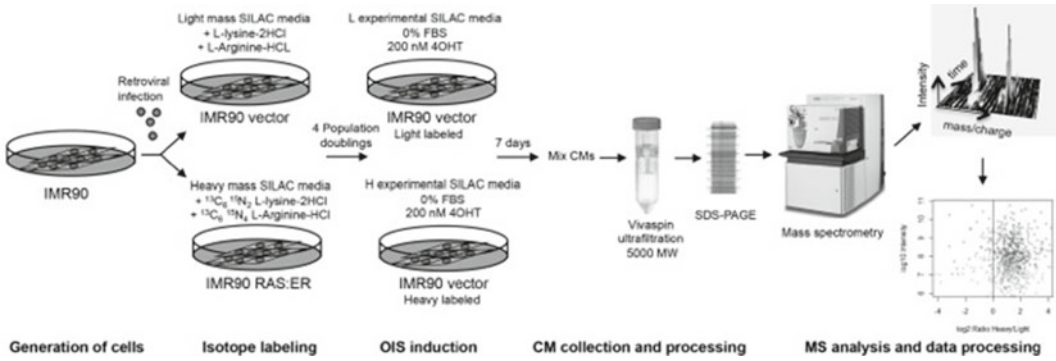

Fig. 1. Flowchart summarizing the protocol for SILAC-based identification of the secretome of senescent cells. Cells are generated by retroviral infection, and grown in SILAC media for at least four population doublings to ensure proper labeling of all proteins. At this stage, they are switched to medium lacking FBS and senescence is induced (by adding 200 nM 4OHT). Conditioned medium is collected at appropriate time, processed, mixed, concentrated, and subjected to Mass spectrometry analysis. Spectra are generated that identifies the peptides by their mass/charge ratio and by comparing the peaks corresponding to the Heavy and Light forms of a given peptide. By plotting the Intensity versus the Heavy/Light ratio a global view of the secreted factors changing during senescence is obtained.

10. Change the media of the IMR90 cells for 6 mL of this supernatant.
11. After 3 h, repeat the infection (from step 8), adding the viral supernatant to IMR-90 cells without aspiration.
12. Repeat the infection process 3 h later.
13. Three hours after the last infection round, change the retroviral enriched media from the IMR90 cells for fresh media to decrease VSVG-induced toxicity.
14. Forty-eight hours after infection, IMR90 cells are split (1:4) and selected with G418 at a final concentration of 400 mg/mL during 1 week (see Note 4).

3.2. Isotope Labeling of the IMR90 ER:RAS and IMR90 LXSN Cells

1. After selection the IMR90-ER:RAS cells or IMR-90-vector cells are incubated with the H or L SILAC labeling media for a minimum of four population doublings (see Note 5).
2. At this stage, a small number of cells (~10^5) are lysed and the heavy label incorporation is assessed by mass spectrometry.

3.3. Induction of Oncogene-Induced Senescence

1. Split a 10 cm dish of confluent IMR90-RAS:ER H- or L-labeled cells in two 10 cm dishes (around two million cells per plate) using the corresponding SILAC labeling H or L media.
2. Split IMR90-vector cells similarly to produce non-senescence conditioned media.
3. The next day, wash the cells thoroughly four times with 10 mL of PBS to remove FBS (see Note 6).
4. Add 10 mL of H or L experimental SILAC media (devoid of FBS), containing 200 nM of 4OHT to induce Ras activity.
5. After 3 days, 1 mL of SILAC experimental media containing 2 mM 4OHT is added to the 10 cm dish.
6. Incubate the cells for an additional 4 days (see Note 7).

3.4. Processing of Conditioned Media for Analysis

1. Collect the conditioned media and centrifuge at 5,000 × *g* to remove cellular debris.
2. Filter the supernatant through a 0.2 mm pore size filter (see Note 8).
3. After filtration, 10 mL each of the H and L "senescence" and "control" conditioned media are mixed in a 1/1 volume proportion. A reciprocal sample and adequate controls are also prepared.
4. The 20 mL H and L mix CM is concentrated by ultrafiltration using vivaspin 20 with 5,000 kDa cutoff by means of centrifugation at 5,000 × *g*. The centrifugation time is variable, and progress should be observed every 10 min (see Note 9). Concentrate the sample about 100–200 times, i.e., until the

sample in the top end of the vivaspin filter is around 200–100 µL. At this stage, the protein concentration can be determined by Pierce 660 nm Protein Assay Reagent (Pierce) and the sample can be stored at –80°C until further analysis (see Note 10).

5. Prior to Liquid Chromatography Mass Spectrometry (LCMS) analysis a protein or peptide pre-fractionation step is highly recommended to reduce the sample complexity. This can be done by liquid chromatography or through gel-based methods. We have successfully applied both approaches to analyze the secretome of OIS cells. When combined with LTQ-Orbitrap mass spectrometry the gel-based method is robust and easy to standardize and therefore discussed here.
6. Load approximately 50–75 mg on a 10–12% SDS-PAGE gel. Stop the gel when the running front has traveled for approximately 4–5 cm (1/3 of the gel) (see Notes 11–13).
7. Stain the gel with Coomasie Blue to confirm that the protein bands are well resolved and vertical streaking is minimized.
8. Cut the gel in 6–10 pieces containing approximately the same amount of protein. Ideally the gel pieces are equally sized. Collect the gel pieces in low-binding 1.5 mL Eppendorf tubes (see Note 14).
9. Reduce and alkylate cysteine residues to make the proteins more accessible to trypsin digestion. Dehydrate and shrink the gel pieces by adding 250–500 mL of acetonitrile (ACN). The gel pieces should shrink in less than 5 min. The process can be speeded up by shaking the tubes at 37°C or by adding additional ACN.
10. Remove the ACN and let air-dry for 5 min.
11. Incubate the gel pieces for 30 min at 55°C in a heating block in 40–80 mL reduction buffer containing 10 mM DTT in 100 mM ammonium bicarbonate.
12. Remove the reduction buffer and shrink gel pieces with ACN as described before.
13. Add alkylation buffer containing 55 mM iodoacetamide in 100 mM ammonium bicarbonate and incubate at room temperature in the dark for 20 min.
14. Carefully remove all liquid and shrink the gel with ACN as described before (see Note 15).
15. Destain the gel pieces with 200–500 mL of 200 mM ammonium bicarbonate in 40% ACN for 30 min at 37°C. Refreshing the solution and vortexing may speed up the process.
16. Add 40–50 mL of trypsin solution (10 nL/mL trypsin in 10 mM ammonium bicarbonate). The gel pieces will swell with

the trypsin solution. This step is best performed on ice for 30 min. Confirm that all pieces are covered in solution and add more trypsin solution when appropriate. Incubate the gel pieces overnight or at least for 6 h at 37°C (see Note 16).

17. Collect the liquid in new low-binding Eppendorf tubes. Perform further peptide extraction by incubating the gel pieces with 50 mL, 5% formic acid in 50% ACN for 20 min. Finally, shrink the gel pieces in 50 mL ACN and pool all extractions per gel piece. Dry down the extracts to completeness using a vacuum centrifuge. Dried extracts may be stored at –20°C for up to several months.
18. Resuspend the peptide mixtures in 10–14 mL of 0.1% TFA using a sonicator water bath. Spin down the samples at 10,000×*g* for 5 min to remove particulates from the solution. When transferring the liquid to HPLC vials take care not to disturb the pellet and check visually whether the sample is clear.

3.5. Mass Spectrometry Analysis and Data Processing

1. Peptide mixtures are separated using a 50 cm analytical column on a 3-h gradient from 3 to 50% ACN (0.1% FA) taking the total LC-MS analysis time to approximately 24 h per lane. Shorter gradients can be used if time is limited but some identifications might be missed.
2. On the LTQ-Orbitrap Mass spectrometry the data was acquired using a top six MSMS collision-induced dissociation (CID) method to ensure that each 3D peak is sampled multiple times, thereby facilitating quantification. The number of MSMS per cycle can be extended up to 20 to increase the number of peptide identifications.
3. All raw data is analyzed through MaxQuant (typically 1.5 GB per sample). Carbamidomethyl of cysteines is used as a fixed modification whereas oxidation of methionine is used as a variable modification. The minimum H/L count is set to 1.
4. The table for protein groups contains the protein heavy/light ratios and can be imported to Perseus or R for further statistical analysis (see Note 17).

4. Notes

1. SILAC labeling is performed with lysine and arginine to ensure that all peptides contain at least one labeled amino acid residue upon proteolytic digestion with trypsin. It is best to use isotopes that introduce a different Δmass for arginine and lysine (e.g., $^{3}C_{6}$, $^{15}N_{2}$ L-Lysine-2HCl and $^{13}C_{6}$, $^{15}N_{4}$ L-Arginine-HCl rather than $^{13}C_{6}$ L-Lysine-2HCl and $^{13}C_{6}$ L-Arginine-HCl).

2. High retroviral titer can be also achieved with classical amphotropic packaging cells like LinxA or PhoenixA. However, we obtained higher retroviral titer cotransfecting the retroviral vector with the VSVG/gag-pol helper plasmid combination. The use of first-generation amphotropic helper for cotransfection should be avoided because of the risk of production of recombinant helper virus production.
3. A key point in retroviral transduction is the state of the packaging cells (HEK293T). The cells have to be frequently passed, avoiding prolonged periods of confluency. HEK293T cells with a tendency to acidify the culture media turning it yellow and to grow in clumps or with a high proportion of big and polynucleated cells should be discarded.
4. It is strongly recommended to use early passage IMR90 to develop the inducible OIS system. We infect IMR90 at passage 8 to produce a stock of frozen IMR90-ER:RAS and IMR90-vector at passage 12.
5. Once the cells are cultured in the SILAC DMEM with the dialyzed FBS, the IMR90 change slightly the morphology to a more spindle shape and they slightly slow down their growth rate. Otherwise, the culture behaves normally. We initiate the SILAC labeling from the stock of IMR90-ER:RAS or vector at passage 12 to produce a stock of frozen H- and L-labeled IMR90-ER:RAS or vector at passage 14 that will be used later to perform the OIS induction.
6. This step is very important to remove FBS as much as possible to avoid contamination during the mass spectrometry. Contaminating proteins such as keratins and components of the FBS can reduce the number of peptides identified from the CM and might interfere with the quantification.
7. It is recommended to prepare cell plates in excess to counteract the loss of CM volume by evaporation and subsequent manipulation (filtering, etc.).
8. The conditioned media from senescent cells is very viscous, so higher pressure should be applied during the filtration and a change of the filter due to saturation could be required.
9. The sample containing the senescence–control mix conditioned media should require more spinning time than the control–control mix again due to its higher viscosity.
10. Note that some protein quantification methods like Lowry cannot be used because of the presence of phenol red from the tissue culture media. Precise protein quantification is not necessary since the SILAC method provides a relative measure.
11. In our setup, the typical yield of secreted proteins is in the order of 4–8 mg/mL, which vastly exceeds the amount required for mass spectrometry analysis.

12. For most standard gel configurations this amount of protein gives an intense signal with most Coomassie blue-based stains and keeps vertical streaking due to in-gel protein precipitation to a minimum. Furthermore, these amounts lead to a desirable TIC signal on the mass spectrometer (10^9 or higher) without compromising the chromatography.
13. Essentially, the function of the gel is twofold. Firstly, it provides a protein pre-fractionation step that reduces the complexity of the sample. Secondly, it provides a robust and reproducible matrix in which the trypsin digestion is performed. It is not necessary to use the whole length of the gel. If more separation is required it is recommended to run a longer gradient during the LC-MS run. A shorter SDS-PAGE run keeps the volume of the gel and thus the processing time down. Furthermore, any contamination and particulates from the gel matrix that can interfere with the LC-MS run are kept to a minimum.
14. To save time, the reduction–alkylation step can be omitted but for secreted proteins it is highly recommended because of the expected large proportion of disulfide bonds in this class of proteins. An optional deglycosylation step (e.g., with PNGase F) could be considered to further facilitate trypsin digestion.
15. Alternatively the reduction–alkylation step can be performed in solution before the SDS-PAGE step.
16. For more detail regarding the in-gel trypsinization protocol refer to (14).
17. Maxquant and Perseus software are freely available from http://maxquant.org/. Further information on the Maxquant algorithm can be found at (12, 13).

Acknowledgments

Core funding from the Medical Research Council funded this work. J. Gil is also supported by the EMBO Young Investigator Programme.

References

1. Kuilman T, Michaloglou C, Mooi WJ, Peeper DS (2010) The essence of senescence. Genes Dev 24:2463–2479
2. Campisi J, d'Adda di Fagagna F (2007) Cellular senescence: when bad things happen to good cells. Nat Rev Mol Cell Biol 8:729–740
3. Collado M, Serrano M (2010) Senescence in tumours: evidence from mice and humans. Nat Rev Cancer 10:51–57
4. Kuilman T, Peeper DS (2009) Senescence-messaging secretome: SMS-ing cellular stress. Nat Rev Cancer 9:81–94

5. Coppe JP, Desprez PY, Krtolica A, Campisi J (2010) The senescence-associated secretory phenotype: the dark side of tumor suppression. Annu Rev Pathol 5:99–118
6. Kuilman T, Michaloglou C, Vredeveld LC, Douma S, van Doorn R, Desmet CJ, Aarden LA, Mooi WJ, Peeper DS (2008) Oncogene-induced senescence relayed by an interleukin-dependent inflammatory network. Cell 133:1019–1031
7. Coppe JP, Patil CK, Rodier F, Sun Y, Munoz DP, Goldstein J, Nelson PS, Desprez PY, Campisi J (2008) Senescence-associated secretory phenotypes reveal cell-nonautonomous functions of oncogenic RAS and the p53 tumor suppressor. PLoS Biol 6:2853–2868
8. Acosta JC, O'Loghlen A, Banito A, Guijarro MV, Augert A, Raguz S, Fumagalli M, Da Costa M, Brown C, Popov N, Takatsu Y, Melamed J, d'Adda di Fagagna F, Bernard D, Hernando E, Gil J (2008) Chemokine signaling via the CXCR2 receptor reinforces senescence. Cell 133:1006–1018
9. Mann M (2006) Functional and quantitative proteomics using SILAC. Nat Rev Mol Cell Biol 7:952–958
10. Zanivan S, Krueger M, Mann M (2012) In vivo quantitative proteomics: the SILAC mouse. Methods Mol Biol 757:435–450
11. Barradas M, Anderton E, Acosta JC, Li S, Banito A, Rodriguez-Niedenfuhr M, Maertens G, Banck M, Zhou MM, Walsh MJ, Peters G, Gil J (2009) Histone demethylase JMJD3 contributes to epigenetic control of INK4a/ARF by oncogenic RAS. Genes Dev 23:1177–1182
12. Cox J, Mann M (2008) MaxQuant enables high peptide identification rates, individualized p.p.b.-range mass accuracies and proteome-wide protein quantification. Nat Biotechnol 26:1367–1372
13. Cox J, Matic I, Hilger M, Nagaraj N, Selbach M, Olsen JV, Mann M (2009) A practical guide to the MaxQuant computational platform for SILAC-based quantitative proteomics. Nat Protoc 4:698–705
14. Shevchenko A, Tomas H, Havlis J, Olsen JV, Mann M (2006) In-gel digestion for mass spectrometric characterization of proteins and proteomes. Nat Protoc 1: 2856–2860

Chapter 12

Detection of Senescence-Associated Heterochromatin Foci (SAHF)

Katherine M. Aird and Rugang Zhang

Abstract

One of the most prominent features of cellular senescence, a stress response that prevents the propagation of cells that have accumulated potentially oncogenic alterations, is a permanent loss of proliferative potential. Thus, at odds with quiescent cells, which resume proliferation when stimulated to do so, senescent cells cannot proceed through the cell cycle even in the presence of mitogenic factors. Here, we describe a set of cytofluorometric techniques for studying how chemical and/or physical stimuli alter the cell cycle in vitro, in both qualitative and quantitative terms. Taken together, these methods allow for the identification of *bona fide* cytostatic effects as well as for a refined characterization of cell cycle distributions, providing information on proliferation, DNA content, as well as the presence of cell cycle phase-specific markers. At the end of the chapter, a set of guidelines is offered to assist researchers that approach the study of the cell cycle with the interpretation of results.

Key words: Cancer, Cyclin B1, HCT 116, Histone H3, Mitosis

1. Introduction

Cellular senescence is a state of irreversible cell growth arrest. Cellular senescence can be triggered by a variety of stimuli such as critically shortened telomeres, which occur after extensive cell division, or activation of certain oncogenes (such as H-RAS^{G12V} or BRAF^{V600E}) (1–3). By definition, senescent cells are irreversibly growth arrested, and one of the necessary steps towards this irreversible cell cycle exit is the suppression of E2F target genes (4), which are mainly involved in promoting cell proliferation and S phase cell cycle progression (5). Promoters of E2F target genes typically acquire heterochromatic features during senescence (4). The heterochromatin associated with this process is specialized domains of facultative heterochromatin that often form in senescent human cells, senescence-associated heterochromatin foci (SAHF) (4, 6–12).

Lorenzo Galluzzi et al. (eds.), *Cell Senescence: Methods and Protocols*, Methods in Molecular Biology, vol. 965,
DOI 10.1007/978-1-62703-239-1_12, © Springer Science+Business Media, LLC 2013

SAHF were first described in 2003 by Narita et al. who observed that the nuclei of senescent cells contain 30–50 bright, punctate DNA-stained dense foci that can be readily distinguished from chromatin in normal cells (4). Importantly, SAHF are not associated with cells undergoing quiescence, indicating that SAHF formation is not associated with reversible cell cycle exit (4). In addition, SAHF have also been shown to be distinct from constitutive heterochromatin because centromeres, telomeres, and other constitutive heterochromatin regions are not included in SAHF (4, 12, 13). Further, SAHF are also different from other facultative heterochromatin such as inactivated X chromosomes (Xi) in female human cells. For example, histone modifications such as lysine 27 trimethylated histone H3 (H3K27Me3) are associated with Xi but not SAHF (4).

SAHF play a role in sequestering proliferation-promoting genes (4), including E2F target genes such as cyclin A (12), which is required for the progression through S phase of the cell cycle (14). Indeed, SAHF do not contain any active transcription sites (4), demonstrating their role in contributing to the senescence-associated cell cycle exit. Significantly, disruption of SAHF formation can cause cell transformation (15), which infers that SAHF contribute to the tumor-suppressive function of senescence. Recently, there is evidence to suggest that SAHF may limit the extent of DNA damage signaling which may prevent senescent cells from undergoing apoptosis induced by high DNA damage signaling, thereby maintaining the viability of senescent cells (11). Finally, there is emerging evidence to suggest that SAHF may play a role in the senescence phenotype in vivo (16–19).

A number of different inducers of senescence cause the formation of SAHF, including activated oncogenes such as H-RAS^{G12V} and BRAF^{V600E} (4, 20, 21), extensive passaging (4), chemotherapeutics such as etoposide (4) and hydroxyurea (9), and bacterial toxins (9). However, SAHF formation and senescence are not always coupled. Indeed, a number of studies have shown that senescence can occur in the absence of SAHF formation. For instance, activation of AKT and knockdown of PTEN do not cause SAHF formation (22, 23). It is also important to note that SAHF formation is cell-line dependent (9). For example, senescence induced by extensive passaging in the primary human embryonic fibroblast cell lines IMR90 and WI38 cells is associated with SAHF, while senescence triggered by extensive passaging in BJ cells (primary human foreskin fibroblasts) is not associated with SAHF formation (4). The difference between these cell lines correlates with a variation in activation of the p16/pRb pathway after extensive passaging (9). Indeed, senescence induced by activated oncogenes (such as H-RAS^{G12V} and BRAF^{V600E}) in BJ cells triggers SAHF formation, which is associated with activation of the p16/

pRb pathway (24, 25). Notably, mouse cells do not form robust SAHF, although they do display a marked increase in staining of certain components of SAHF such as macroH2A (26).

To date, a number of molecular markers of SAHF have been described (reviewed in ref. 6, 10, 27) including macroH2A (8), a histone variant known to contribute to X chromosome inactivation and gene silencing (28); high mobility group A (HMGA) proteins, which coordinate with $p16^{INK4a}$ to induce SAHF formation and are required for maintaining SAHF (15); and di- or tri-methylated lysine 9 histone H3 (H3K9Me2/3) and bound HP1 proteins (4, 12), two common markers of heterochromatin (29). Together with DAPI, co-staining for these markers is a simple and reliable method to determine the presence of SAHF in senescent cells. Here, using oncogenic-RAS ($H\text{-}RAS^{G12V}$) as an inducer of senescence and SAHF, we describe a method for the immunofluorescent detection of SAHF using DAPI and specific antibodies to components of SAHF such as macroH2A, H3K9Me2/3, and HP1 proteins.

2. Materials

2.1. Cell Culture for Expression of Oncogenic RAS

- pBABE-puro and pBABE-puro-$H\text{-}RAS^{G12V}$ constructs (Addgene) (see Note 1).
- 2.5 M $CaCl_2$.
- 2×BBS:50mM *N,N-bis*(2-hydroxyethyl)-2-aminoethanesulfonic acid (BES), 280 mM NaCl, 1.5 mM Na_2HPO_4, pH 6.95 (see Note 2).
- Laemmli sample buffer: 50 mM Tris–HCl, 2% (w/v) sodium dodecyl sulfate (SDS), 100 mM dithiothreitol, 10% (v/v) glycerol, and 0.05% (w/v) bromophenol blue (pH 6.8).
- Equipment and reagents for SDS-polyacrylamide gel electrophoresis (PAGE).
- Bradford reagent (Bio-Rad) and 1 mg/mL bovine serum albumin (BSA) as standard.
- PVDF transfer membrane.
- Towbin transfer buffer: 170 mM glycine, 22 mM Tris–HCl, and 0.01% (w/v) SDS (pH 8.3).
- Anti-RAS antibody (BD Transduction Laboratories).
- 0.45 μm filter.
- Sterile-filtered ddH_2O.
- Phoenix cells (a gift from Gary Nolan) growing in Dulbecco's modified Eagle's medium supplemented with 10% (v/v) fetal bovine serum, 1% (w/v) penicillin–streptomycin, and 1% (w/v)

L-glutamine in a humidified 37°C, 5% (v/v) CO_2 incubator (see Note 3).

- IMR90 cells (ATCC) growing in DMEM supplemented with 20% (v/v) FBS, 1% (w/v) L-glutamine, 1% (v/v) nonessential amino acid solution, 2% (v/v) essential amino acids, 1% (v/v) vitamins, and 1% (w/v) penicillin–streptomycin in a humidified 37°C, 5% (v/v) CO_2 incubator (see Notes 4 and 5).
- 0.25% (w/v) Trypsin + 1 mM EDTA.
- Sterile-filtered Dulbecco's phosphate-buffered saline (PBS), pH 7.3.
- Sterile-filtered, 1 mg/mL puromycin in PBS, pH 7.3.
- Sterile-filtered, 8 mg/mL (w/v) polybrene in ddH_2O (Sigma-Aldrich, St. Louis, MO, USA).
- 10-cm cell culture dishes and 6-well cell culture plates.
- Clean and sterile glass coverslips.

2.2. Fluorescent Staining of SAHF and Microscopic Examination of SAHF

- 4% (w/v) paraformaldehyde (see Note 6).
- PBS, pH 7.3.
- 0.2% (v/v) and 1% (v/v) Triton-X in PBS, pH 7.3.
- 3% (w/v) BSA in PBS, pH 7.3 (see Note 7).
- Primary antibodies to macroH2A, H3K9Me2, H3K9Me3, HP-1α, HP-1β, or HP-1γ (Table 1) (see Note 8).
- Appropriate secondary antibodies (Table 2) (see Note 9).
- 5 mg/mL 4′,6-diamidino-2-phenylindole dihydrochloride (DAPI) in ddH_2O.
- Clean microscope slides.

Table 1
Primary antibodies used to identify SAHF by immunofluorescence

Protein	Source	Dilution	References
MacroH2A	Drs. Rugang Zhang (The Wistar Institute) and Peter D. Adams (University of Glasgow)	1:2,000	(7)
HP-1α	Dr. William Earnshaw (University of Edinburgh)	1:200	(8)
HP-1β	Millipore (MAB3448)	1:20,000	(9)
HP-1γ	Millipore (MAB3450)	1:2,000	(7)
H3K9Me3	Abcam (ab8898)	1:500–1:1,000	(9)
H3K9Me2	Abcam (ab7312)	1:500–1:1,000	(9)

Table 2
Fluorescent secondary antibodies used to visualize SAHF components

Antibody	Catalog numbers	Dilution
Cy3 goat anti-mouse	115-165-003	1:5,000
FITC goat anti-rabbit	111-095-003	1:1,000

- Anti-fade fluorescence mounting media: 0.25 g *p*-phenylenediamine (Sigma-Aldrich) dissolved in 25 mL 1× PBS (pH 9.0) mixed with 225 mL glycerol (see Note 10).
- Fluorescent microscope with the ability to view blue, green, and red channels (e.g., Nikon 80*i*).

3. Methods

3.1. Cell Culture for Expression of Oncogenic RAS

The infectious retrovirus is generated by transfecting the plasmid DNA into a packaging cell line, for example, Phoenix cells (http://www.standford.edu/group/nolan/protocols/pro_helper_dep.html). Transfection-quality DNA of the retrovirus plasmid is made using a Qiafilter Plasmid Maxi kit, according to the manufacturer's instructions. After transfection, the Phoenix cells reverse transcribe the plasmid DNA into an RNA that is packaged into infectious virus and expelled from the cells. Then, the tissue culture supernatant containing the virus is applied to the cells of interest to deliver the activated oncogenes (e.g., H-RAS^{G12V}) to the target cells. The infected cells can be selected in puromycin to enrich for cells that have been infected. To assess the efficiency of puromycin to kill uninfected cells, perform a mock virus infection. To assess the efficiency of infection, infect one plate with a virus known to have a high titer (e.g., pBABE-puro vector, Addgene).

1. Split the Phoenix cells to 5×10^6 cells per 10-cm dish in 10 mL medium 24 h before transfection (see Note 11). Culture in a 37°C, 5% (v/v) CO_2 incubator overnight.
2. Twenty-four hours later, and 4 h prior to transfection, change the medium to 9 mL of pre-warmed, fresh growth media.
3. Dilute the required amount of 2.5 M $CaCl_2$ to 250 mM in sterile ddH_2O and aliquot 0.5 mL per transfection to separate, sterile 15 mL polystyrene tubes.
4. Add 30 μg of the supercoiled plasmid DNA of the intended virus to each tube.

5. Add 0.5 mL of 2× BBS by dripping slowly from a 1 mL pipette vertically down the center of the tube (1–2 drops per second). Do not mix. Incubate the mixture for 15 min. At this time, the precipitate should be barely visible to the naked eye.
6. Use a 1 mL pipette to blow air bubbles through the solution to mix the precipitate. Evenly distribute the mixture drop-wise into the medium of the plate of Phoenix cells.
7. Rock the plates back and forth very gently to mix the calcium phosphate precipitate and then place in a humidified 37°C incubator with 5% (v/v) CO_2 overnight.
8. Change the medium to 6 mL fresh, pre-warmed growth media approximately 24 h later (see Note 12).
9. On the same day as step 8, prepare the target IMR90 primary human embryonic fibroblast cells for infection. A confluent 10 cm dish of cells should be split 1:4 in regular growth media so that cells are 50–60% confluent on the next day (i.e., the first day of infection).
10. Twenty-four hours later, collect the supernatant from the Phoenix cells after step 8 and put through a 0.45 μm filter. Add 6 mL of fresh, pre-warmed growth media to the Phoenix cells (see Note 12).
11. Infect the target cells. Aspirate the IMR90 media from the dish. For a 10 cm dish of target cells, add 3 mL fresh media and 3 mL of virus-containing supernatant harvested from the Phoenix cells drop-wise onto the IMR90 cells.
12. Add 6 μL of 8 mg/mL (w/v) polybrene to make a final concentration of 8 μg/mL, and swirl the dishes to mix. Put the cell dish back into a 5% (v/v) CO_2-containing incubator.
13. Culture the infected cells for 24 h. Repeat the infection (Subheading 3.1, steps 10–12) to increase efficiency.
14. Remove the medium from the IMR90 cells 24 h post infection and replace with 10 mL of fresh, pre-warmed IMR90 growth media that contains puromycin at a final concentration of 1 μg/mL.
15. Typically, 3 days after addition of puromycin, all of the noninfected cells should be dead. At this time, there should be no surviving cells left in the mock virus-infected dish.
16. At the desired time point (see Note 13), split the IMR90 cells into 6-well plates containing clean, sterile glass coverslips.
17. At the same time, harvest an aliquot of the infected cells for Western blot analysis (see Note 14).

3.2. Fluorescent Staining of SAHF

To visualize SAHF, DAPI is used to stain for DNA, while specific antibodies to components of SAHF (e.g., macroH2A, H3K9Me2/3, and HP1 proteins) should be used for indirect immunofluorescence

staining. To assess the specificity of the antibody staining pattern, an isotype-matched control primary antibody and/or omission of the primary antibody should be included as negative controls for immunofluorescence staining. In addition, IMR90 cells infected with vector control-encoding retrovirus should be included as a negative control.

1. Gently wash the coverslips three times with PBS, pH 7.3 to remove all culture media (see Note 15).
2. Fix cells in freshly prepared 4% (w/v) paraformaldehyde for 10 min at room temperature (see Note 16).
3. Wash the coverslips three times with PBS, pH 7.3 to remove fixing solution (see Note 17).
4. Permeabilize the cells by incubating the coverslips in 0.2% (v/v) Triton X-100 in PBS (pH 7.3) for 5 min at room temperature.
5. Block the coverslips with 3% (w/v) BSA in PBS, pH 7.3 for 5 min at room temperature.
6. Incubate the coverslips with the primary antibodies diluted in 3% (w/v) BSA in PBS, pH 7.3 by inverting the coverslip onto 200 μL of diluted antibody spotted on parafilm. Incubate for 1–2 h at room temperature.
7. Put the coverslips back into the 6-well plates with the cell side face up. Wash the coverslips three times with 1% (v/v) Triton X-100 in PBS, pH 7.3.
8. Dilute the appropriate secondary antibodies (Table 2) in 3% (w/v) BSA in PBS, pH 7.3. Incubate the coverslips with 2 mL secondary antibody solution in each well for 1 h at room temperature in the dark.
9. Stain SAHF by incubating the coverslips with 0.15 μg/mL final concentration of DAPI diluted in 3% (w/v) BSA in PBS, pH 7.3 for 3 min at room temperature (see Note 18).
10. Wash the slide three times with PBS, pH 7.3.
11. Mount the inverted coverslips (cells facing the microscope slide) into one drop of mounting media (approximately 20 μL). Aspirate the excess liquid, and seal the coverslips using nail polish (see Note 19).
12. After the slides have dried, observe SAHF using a fluorescent microscope (see Notes 20 and 21).

3.3. Microscopic Examination of SAHF

1. After immunofluorescence staining, the processed slides can be examined under a fluorescent microscope.
2. DAPI staining should reveal punctate staining in oncogenic H-RAS^{G12V}-infected cells, while vector control cells should display diffuse staining across the cell nuclei (Fig. 1).

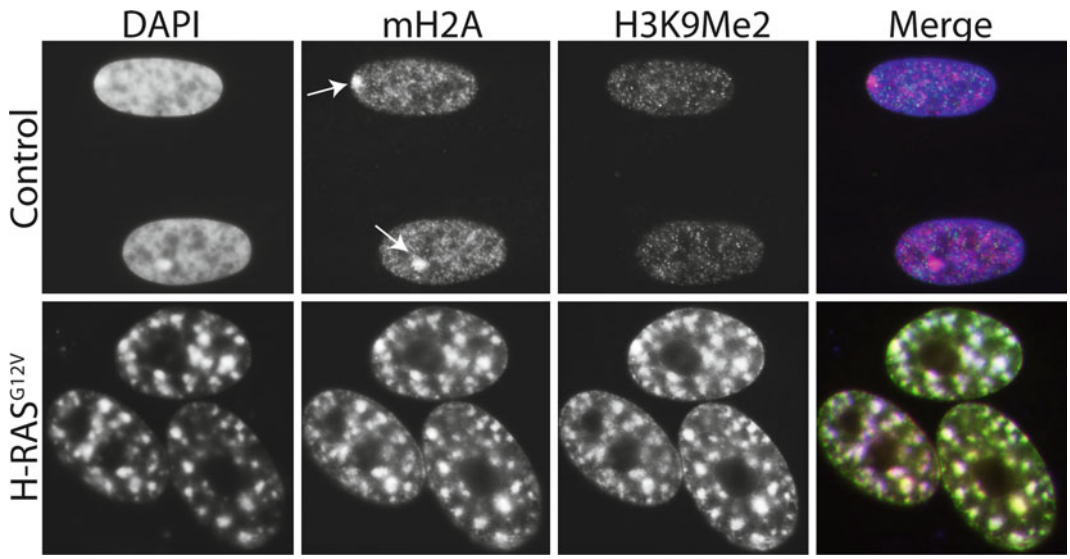

Fig. 1. IMR90 cells were infected with a puromycin-resistant retrovirus encoding oncogenic H-RAS^{G12V} or vector control. Drug-selected cells were stained with antibodies to H3K9Me2 and histone H2A variant macroH2A. DAPI counterstaining was used to visualize SAHF. Note the robust punctate DAPI foci in the H-RAS^{G12V}-infected cells, which co-localize with both macroH2A and H3K9Me2. *Arrows* point to inactivated X chromosome in control IMR90 female fibroblast cells. Chicken anti-macroH2A1.2 primary antibody was obtained from Dr. John R. Pehrson (University of Pennsylvania) (28). Rabbit anti-H3K9Me3 is from AbCam (ab8898) and was used at 1:500. Secondary antibodies were FITC-labeled goat anti-chicken (1:2,500) and Cy3-labeled goat anti-rabbit (1:5,000), which were both obtained from Jackson Immunolabs.

3. The number of cells with SAHF staining depends upon the duration of RAS expression. For example, ~50% of RAS-infected cells display SAHF by DAPI staining 7–9 days post drug selection.
4. Components of SAHF such as macroH2A, HP1 proteins, and H3K9Me2/3 form foci that co-localize with DAPI-stained SAHF in RAS-infected cells. In vector control cells, HP1 protein and H3K9Me2/3 staining is largely diffuse. MacroH2A staining marks the single foci in female mammalian cells (such as IMR90 and WI38 primary human fibroblast cells) that is the inactivated X chromosome (Fig.1).
5. As negative controls, staining using isotype-matched IgG controls as the primary antibody or using the secondary antibody only (without the primary antibody) should not show foci that co-localize with DAPI-stained SAHF. The controls herein will obviously be specific to each component of SAHF.
6. Importantly, regardless of the specific components, not all cells with DAPI-stained SAHF-positive cells will display foci for components of SAHF. This is because relocalization of components of SAHF into DAPI-stained foci is typically a later event compared with formation of DAPI foci (8).

4. Notes

1. As discussed in the introduction, other oncogenes (BRAF/MEK/ERK) and other cellular stressors can cause the formation of SAHF. We recommend using H-RAS^{G12V} as a positive control because activation of RAS induces distinct SAHF formation in a variety of cell types.
2. Correct pH of the 2× BBS solution is necessary for efficient plasmid transfection using this method.
3. Never let cells reach confluence as this may decrease transfection efficiency. Passage Phoenix cells in 300 μg/mL hygromycin (Roche) and 1 μg/mL diptheria toxin (Sigma) for 1 week every month to maintain transfection efficiency. For more information, please visit Gary Nolan's Web site (http://www.stanford.edu/group/nolan/retroviral_systems/retsys.html).
4. For oncogene-induced SAHF formation (or to study other types of stressors), low population doubling (PD) IMR90 cells should be used (PD < 35). However, if you wish to study replicative senescence-induced SAHF, high PD IMR90 cells (e.g., PD65) should be used instead.
5. Other cell lines and cell types form SAHF (9); however, this must be determined on a cell type-by-cell type basis. It is important to note that mouse cells do not form distinct SAHF structures that are visible by DAPI staining alone. Instead, macroH2A may server as a marker for SAHF in senescent mouse cells (26).
6. To make 4% paraformaldehyde, weigh 2 g of paraformaldehyde (Sigma) and add 25 mL of ddH_2O, 25 mL 2× PBS, pH 7.3, and 100 μL 1 N NaOH. Vortex and incubate this mixture at 65°C for 10–15 min to dissolve the paraformaldehyde (vortex the tube every 5 min). Cool the solution to room temperature before use.
7. Adding 0.02% (w/v) sodium azide to the 3% (w/v) BSA in PBS will decrease potential contamination and increase the shelf life.
8. Any of these markers can be used in addition to DAPI staining to identify SAHF. See Table 11 for antibody catalog numbers, dilutions, and references.
9. Secondary antibodies to the appropriate species can be purchased from Jackson Immunolabs. See Table 2 for details.
10. Mounting media should be aliquoted and stored at −80°C. Once the media changes to an orange color, replace with a fresh batch.
11. Although the Phoenix cells are easy to remove from the plate, use 0.25% (w/v) trypsin + 1 mM EDTA to fully separate the cells and avoid cell aggregation.

12. Be very gentle when adding fresh media as Phoenix cells do not adhere very well to the plate. It is typical that Phoenix cells change shape after changing them into fresh medium. They will fully recover after 6–8 h of culture in the newly changed medium.
13. SAHF should start to appear approximately 3–4 days after starting selection and typically reach the highest percentage with ~50% RAS-infected cells positive for DAPI-stained SAHF around 7–9 days after staring drug selection.
14. Protein lysates can be made by directly adding 1× Laemmli sample buffer followed by boiling for 5 min. Samples can be stored at −80°C. Ectopically expressed oncogenic-RAS should be confirmed by Western blotting. Cell extracts should be fractionated by SDS-PAGE, transferred to a PVDF membrane, and then Western blotted with antibody to RAS (BD Biosciences, 610001). An antibody to a housekeeping gene (e.g., β actin) should be used as a loading control.
15. Senescent cells do not adhere very well to coverslips; therefore, rinsing coverslips with PBS before fixation should be done very carefully. In instances where rinsing coverslips with PBS may lead to loss of cells, this step can be skipped, and coverslips can be directly immersed in 4% (w/v) paraformaldehyde for 10 min.
16. At this step, soluble proteins can be removed to only retain tightly bound chromatin proteins. To do so, cells can be pre-extracted with 5 mM $MgCl_2$ in 0.2% (v/v) Triton-X in PBS for 5 min to preserve SAHF while removing the soluble proteins. Extra care should be taken when performing pre-extraction and the following steps of washing and fixation as these pre-extracted cells can be easily washed off the coverslips.
17. After fixation, coverslips can be washed 3× with PBS and stored at 4°C for up to 2 weeks before processing.
18. Higher DAPI concentrations and longer incubation periods will make it harder to distinguish DAPI-stained SAHF.
19. Avoid air bubbles when mounting coverslips.
20. Slides can be stored at −20°C for up to a month. However, it is important to note that the fluorescent signal may fade over time.
21. The same methods can be applied to other cell lines/cell types to determine SAHF formation. As not all cell lines or all causes of cellular senescence induce SAHF formation (see Subheading 1 for details), we recommend the use of IMR90 cells expressing oncogenic H-RAS^{G12V} as a positive control.

Acknowledgments

This work was funded by a NIH/NCI grant (R01CA160331), a Liz Tilberis Scholar Award from the Ovarian Cancer Research Fund and the Department of Defense Ovarian Cancer Academy Award (OC093420). Support of Core Facilities used in this study was provided by Cancer Center Support Grant (CCSG) CA010815 to The Wistar Institute.

References

1. Kuilman T, Michaloglou C, Mooi WJ, Peeper DS (2010) The essence of senescence. Genes Dev 24:2463–2479
2. Campisi J (2005) Senescent cells, tumor suppression, and organismal aging: good citizens, bad neighbors. Cell 120:513–522
3. Campisi J, d'Adda di Fagagna F (2007) Cellular senescence: when bad things happen to good cells. Nat Rev Mol Cell Biol 8:729–740
4. Narita M, Nunez S, Heard E, Narita M, Lin AW, Hearn SA, Spector DL, Hannon GJ, Lowe SW (2003) Rb-mediated heterochromatin formation and silencing of E2F target genes during cellular senescence. Cell 113:703–716
5. Ren B, Cam H, Takahashi Y, Volkert T, Terragni J, Young RA, Dynlacht BD (2002) E2F integrates cell cycle progression with DNA repair, replication, and G(2)/M checkpoints. Genes Dev 16:245–256
6. Zhang R, Adams PD (2007) Heterochromatin and its relationship to cell senescence and cancer therapy. Cell Cycle 6:784–789
7. Zhang R, Liu ST, Chen W, Bonner M, Pehrson J, Yen TJ, Adams PD (2007) HP1 proteins are essential for a dynamic nuclear response that rescues the function of perturbed heterochromatin in primary human cells. Mol Cell Biol 27:949–962
8. Zhang R, Poustovoitov MV, Ye X, Santos HA, Chen W, Daganzo SM, Erzberger JP, Serebriiskii IG, Canutescu AA, Dunbrack RL, Pehrson JR, Berger JM, Kaufman PD, Adams PD (2005) Formation of MacroH2A-containing senescence-associated heterochromatin foci and senescence driven by ASF1a and HIRA. Dev Cell 8:19–30
9. Kosar M, Bartkova J, Hubackova S, Hodny Z, Lukas J, Bartek J (2011) Senescence-associated heterochromatin foci are dispensable for cellular senescence, occur in a cell type- and insult-dependent manner and follow expression of p16(ink4a). Cell Cycle 10:457–468
10. Adams PD (2007) Remodeling of chromatin structure in senescent cells and its potential impact on tumor suppression and aging. Gene 397:84–93
11. Di Micco R, Sulli G, Dobreva M, Liontos M, Botrugno OA, Gargiulo G, dal Zuffo R, Matti V, d'Ario G, Montani E, Mercurio C, Hahn WC, Gorgoulis V, Minucci S, d'Adda di Fagagna F (2011) Interplay between oncogene-induced DNA damage response and heterochromatin in senescence and cancer. Nat Cell Biol 13:292–302
12. Zhang R, Chen W, Adams PD (2007) Molecular dissection of formation of senescence-associated heterochromatin foci. Mol Cell Biol 27:2343–2358
13. Funayama R, Saito M, Tanobe H, Ishikawa F (2006) Loss of linker histone H1 in cellular senescence. J Cell Biol 175:869–880
14. Pagano M, Pepperkok R, Verde F, Ansorge W, Draetta G (1992) Cyclin A is required at two points in the human cell cycle. EMBO J 11:961–971
15. Narita M, Narita M, Krizhanovsky V, Nunez S, Chicas A, Hearn SA, Myers MP, Lowe SW (2006) A novel role for high-mobility group a proteins in cellular senescence and heterochromatin formation. Cell 126:503–514
16. Collado M, Gil J, Efeyan A, Guerra C, Schuhmacher AJ, Barradas M, Benguria A, Zaballos A, Flores JM, Barbacid M, Beach D, Serrano M (2005) Tumour biology: senescence in premalignant tumours. Nature 436:642
17. Herbig U, Ferreira M, Condel L, Carey D, Sedivy JM (2006) Cellular senescence in aging primates. Science 311:1257
18. Kreiling JA, Tamamori-Adachi M, Sexton AN, Jeyapalan JC, Munoz-Najar U, Peterson AL, Manivannan J, Rogers ES, Pchelintsev NA, Adams PD, Sedivy JM (2011) Age-associated increase in heterochromatic marks in murine and primate tissues. Aging Cell 10:292–304

19. Collado M, Serrano M (2010) Senescence in tumours: evidence from mice and humans. Nat Rev Cancer 10:51–57
20. Martin C, Chen S, Heilos D, Sauer G, Hunt J, Shaw AG, Sims PF, Jackson DA, Lovric J (2010) Changed genome heterochromatinization upon prolonged activation of the Raf/ERK signaling pathway. PLoS One 5:e13322
21. Michaloglou C, Vredeveld LC, Soengas MS, Denoyelle C, Kuilman T, van der Horst CM, Majoor DM, Shay JW, Mooi WJ, Peeper DS (2005) BRAFE600-associated senescence-like cell cycle arrest of human naevi. Nature 436:720–724
22. Kennedy AL, Morton JP, Manoharan I, Nelson DM, Jamieson NB, Pawlikowski JS, McBryan T, Doyle B, McKay C, Oien KA, Enders GH, Zhang R, Sansom OJ, Adams PD (2011) Activation of the PIK3CA/AKT pathway suppresses senescence induced by an activated RAS oncogene to promote tumorigenesis. Mol Cell 42:36–49
23. Tu Z, Aird KM, Bitler BG, Nicodemus JP, Beeharry N, Xia B, Yen TJ, Zhang R (2011) Oncogenic RAS regulates BRIP1 expression to induce dissociation of BRCA1 from chromatin, inhibit DNA repair, and promote senescence. Dev Cell 21:1077–1091
24. Deng Q, Liao R, Wu BL, Sun P (2004) High intensity ras signaling induces premature senescence by activating p38 pathway in primary human fibroblasts. J Biol Chem 279:1050–1059
25. Ye X, Zerlanko B, Zhang R, Somaiah N, Lipinski M, Salomoni P, Adams PD (2007) Definition of pRB- and p53-dependent and -independent steps in HIRA/ASF1a-mediated formation of senescence-associated heterochromatin foci. Mol Cell Biol 27: 2452–2465
26. Kennedy AL, McBryan T, Enders GH, Johnson FB, Zhang R, Adams PD (2010) Senescent mouse cells fail to overtly regulate the HIRA histone chaperone and do not form robust senescence associated heterochromatin foci. Cell Div 5:16
27. Funayama R, Ishikawa F (2007) Cellular senescence and chromatin structure. Chromosoma 116:431–440
28. Costanzi C, Pehrson JR (1998) Histone macroH2A1 is concentrated in the inactive X chromosome of female mammals. Nature 393: 599–601
29. Trojer P, Reinberg D (2007) Facultative heterochromatin: is there a distinctive molecular signature? Mol Cell 28:1–13

Chapter 13

Monitoring DNA Damage During Cell Senescence

Glyn Nelson and Thomas von Zglinicki

Abstract

Cellular senescence is a state of irreversible cell cycle arrest, accompanied by and in most cases driven by a persistent DNA damage response (DDR), which may be activated by uncapped telomeres or other forms of DNA damage. DNA damage foci, therefore, are an important part of the signaling pathway that induces cell senescence. However, similar foci can also be observed in proliferating cells, for instance as a result of replicative stress. Identifying the phenotypic differences between the DDR of young, proliferation-competent cells and senescent cells is therefore important for establishing the cellular DDR as a marker of senescence. Here, we describe various methods by which the DDR can be used as a robust marker of cellular senescence, and how to utilize a DDR marker to investigate the induction and stabilization of the senescent phenotype.

Key words: 53BP1, DNA damage, γH2A.X, Microscopy, Senescence

1. Introduction

The senescent phenotype is much more complex than a simple growth arrest, involving a major reprogramming of cellular gene expression and metabolism that can significantly modify the interaction of a senescent cell with its environment (1, 2). For instance, a sustained DNA damage response (DDR) leads to activation of p38MAPK (MAPK14), which in turn triggers mitochondrial dysfunction and enhanced ROS production (1, 3) as well as release of a wide variety of pro-inflammatory cytokines, chemokines, and growth factors (4). The DDR involves the balance of damage induction, recognition, and repair, both at single-strand and double-strand breaks (DSBs). A detailed description of these processes is beyond the scope of this chapter, and has been covered recently by others (5, 6).

There is evidence that frequencies of cells bearing senescence markers increase with age in various tissues (7–10). Furthermore,

Lorenzo Galluzzi et al. (eds.), *Cell Senescence: Methods and Protocols*, Methods in Molecular Biology, vol. 965,
DOI 10.1007/978-1-62703-239-1_13,

dietary restriction, an intervention that slows down aging, decreases frequencies of senescent cells in the hematopoietic system (11) and in multiple solid tissues (12). Development of a simple assay for determination of the frequency of senescence within heterogeneous cultures/organs is therefore of importance for tracking the development of aging in vivo and in vitro.

1.1. Senescence-Associated Changes in the DNA Damage Phenotype

The DDR in senescent cells differs from their young, replication-competent counterparts in various aspects: (1) senescent cells display a larger number of DNA damage foci. In senescent primary human fibroblasts, this amounts to an average of 4–5 DSBs at any one time within the population, compared to a maximum of 1–2 foci in proliferating cells (13); (2) senescent cells contain long-lived, potentially persistent foci. A quantitative kinetic analysis showed that the fraction of foci with lifespans >15 h was about 40–50% in senescent cells versus <20% in proliferation-competent fibroblasts (1); (3) senescent cells contain large DNA damage foci (14); (4) nuclear co-localization of DNA damage foci with PML bodies has been suggested as another marker of cell senescence (14).

Therefore, either observation of *a*; foci number, size, and PML body co-localization or *b*; the DNA damage foci frequency and their longevity would be expected to robustly identify senescent cells. The first method is comparatively simple, requiring only fixation to allow for labeling of DNA damage foci and PML bodies. The second requires monitoring formation and repair of DNA damage in live cells, for which design and expression of a suitable fluorescent fusion protein is needed. Whilst more complex and time consuming, the data are far more rich, plus the cells are kept alive throughout and can therefore be used for other parameter readouts. This is especially useful in replicative senescence, where cellular heterogeneity is a known factor, and one that is not fully understood. However, the method needs careful validation with data from fixed cells to ascertain whether ectopic expression of the fusion protein affects the results obtained. Such problems can be minimized by careful fusion protein choice and design, for which we describe one such possibility.

2. Materials

All chemicals were purchased from Sigma-Aldrich unless stated otherwise.

2.1. Plasmids and cDNA

- Human full-length 53BP1 cDNA (Genbank accession NM_001141980.1), cloned from the plasmid pCMH-6k53BP1, which was a gift from K. Iwabuchi, Kanazawa Medical University (15), but it is also available as an MGC clone (accession BU596747).

- pAcGFP-C2, a vector expressing AcGFP from a CMV promoter (Clontech).
- Clonase recombination vectors pLenti6/UbC/V5-DEST, pENTR2B, Gateway destination cassettes, and lentiviral packaging plasmid mix (all from Invitrogen).

2.2. Immunofluorescence

2.2.1. Antibodies

- Rabbit anti-human PML antibody (Abcam, ab53773); used at a 1:250 dilution.
- Mouse anti-human γH2A.X (Upstate, clone JBW103); used at a 1:1,250 dilution.
- Rabbit anti-53BP1 antibody (Cell Signalling, #4937) recognizing an epitope in the C terminal of 53BP1; used at a 1:200 dilution.
- Secondary antibodies: Goat Alexa fluor conjugated (Alexa 488, Alexa 555, and Alexa 647, Invitrogen); used at a 1:2,000 dilution.

2.2.2. Solutions

- Paraformaldehyde, 4%.
- 1× TBS: 20 mM Tris–HCl, 0.8% (w/v) NaCl; pH adjusted to 7.6 with HCl.
- Blocking buffer:
  - 1× TBS with 5% (v/v) normal goat serum.
  - 1× TBS/Triton: 1× TBS with 0.3% (w/v) Triton X-100.
- Mounting medium: Vectashield with DAPI (Vector labs).

2.3. Cell Culture

2.3.1. Solutions

- Complete medium: DMEM, 10% fetal bovine serum, 1% penicillin/streptomycin, and 1% L-glutamine.
- Trypsin/EDTA.
- 1× PBS, made from 10× PBS diluted with distilled water and autoclaved.
- Blasticidin (Life Technologies-Invitrogen). A killing curve determined a concentration of 2–4 μg/mL for MRC-5 cells.
- G418 (Geneticin). A killing curve determined a concentration of 400 μg/mL.

2.3.2. Cells

- MRC-5 human embryonic lung fibroblasts (ECACC). For stable transformation or transduction the cells were used at as low a population doubling (PD) as possible (usually around PD x+~12, where x is an unknown PD number due to purchasing the cells from ECACC; empirically, we determined it to be ~10 for our cells, since they reach replicative senescence around PD x+45, and should theoretically reach PD ~55). For controls, young cells were considered young when the PD was less than x+~33. Cells were classed as replicatively senescent when the culture grew less than 0.1 PD per month (usually

around PD x+~45). Cells were grown to approximately 95% confluence before trypsinizing, counting, and replating at no less than 25% confluence. Senescent and almost senescent cells not yet requiring passage were fed once per week with complete medium.

- Lentiviral packaging cell line HEK293FT (Life Technologies-Invitrogen), grown following the manufacturer's instructions. Medium with antibiotic selection was replaced every 3 days.

2.3.3. Plates/Dishes

- For immunofluorescence, #1.5 16 mm Ø glass coverslips in 12-well plates.
- For live cell microscopy, glass coverslip-bottomed dishes (Iwaki).

2.4. Live Cell Imaging

We employ two systems for live cell imaging (see Note 1), both of which work well for long-term imaging (tested up to 60 h, but there is no reason not to image longer if your cells are nondividing):

- Zeiss LSM 510 laser scanning microscope (see Note 2).
- Zeiss spinning disk system (see Note 3).

3. Methods

3.1. Production of Fluorescent Reporter Cells

For in vitro analysis of cellular senescence, use of normal diploid cells, with intact DDR machinery and which will reach replicative senescence, is essential. However, we find that such cells are quite difficult to use with transient transfection (<1% transfection after attempting to optimize conditions), possibly owing to their long cell cycle (MRC-5 take approximately 50–55 h per cycle when young). Additionally, transient transfection generates a very heterogeneous population in terms of plasmid copy number transfected and the protein expression level, which can complicate analysis of cellular responses (16). Furthermore, when interested in investigating DNA damage, there is also a high probability of extraneous plasmid DNA within the nucleus degrading over time, and so becoming a target for the DDR machinery, which would skew our results. Therefore it is in our interest to invest the effort to produce stably integrated expression cassettes for analysis of DNA damage formation and repair.

3.1.1. Fusion Protein Design

Choosing a suitable protein to tag to follow any signaling pathway is the critical step. Other considerations include the terminus to attach the tag, as well as the choice of reporter:

1. We found that the adapter protein TP53BP1 (53BP1) fitted the criteria required as a suitable protein to tag and express ectopically (see Note 4).

2. 53BP1 is a large protein (2,231 amino acids), and to create a fusion which is packable into virions required creating a truncated version. Analysis of the literature and Uniprot on structure and function of 53BP1 suggested that the essential part of the protein was the C terminal half. Therefore, we removed the protein's N terminal end, ensuring that we kept the TUDOR and BRCT domains, and replaced it with a fluorescent protein.
3. We opted for a relatively fast-maturing, monomeric fluorescent protein, AcGFP, a human codon optimized green fluorescent protein derived from *Aequorea coerulescens* (Clontech); however there are many other suitable alternatives (see Note 5). It is not the most photostable green monomeric fluorescent protein, but for live cell imaging, this is not a problem, more of a potential benefit (for FRAP studies and determining excitation levels suitable for normal physiology).

3.1.2. Creating a Standard Fusion Protein Expression Plasmid

1. To create an AcGFP-53BP1 C terminal fragment fusion (AcGFP-53BP1c), we internally digested 53BP1 cDNA at a BamHI site and a 3′ XhoI site introduced from the original vector (pCMH6k53BP1) to obtain a truncated 2.77 kb C terminal fragment of 53BP1.
2. This was ligated into the BamHI/XhoI sites of the polylinker of PENTR2A, a Gateway cloning Entry vector with an ampicillin resistance cassette replacing the kanamycin cassette in the original vector, pENTR2B.
3. A mammalian expression vector was then produced using recombination with pG-AcGFP-A, which was created by inserting a Gateway destination cassette "a" into Ecl136II, in the polylinker of pAcGFP-C2, to produce the vector pG-AcGFP-53BP1c. This could also be performed using more standard cloning techniques, ensuring that the C terminal amino acid of the fluorescent protein is in frame with the truncated 53BP1.
4. This vector allowed us to create stable clones expressing AcGFP-53BP1c from a CMV promoter using standard techniques (see Subheading 3.1.4). However, isolating a single clone and generating a stable isogenic cell line would have meant that our cells were practically senescent once we had enough to use. Using a heterogeneous population for analysis worked (17), but we had to discard cells which expressed too much AcGFP-53BP1c, as we were unable to visualize sites of DNA damage against the bright nuclear background fluorescence.
5. Therefore, we also generated stably integrated cells using lentivirus. This method has the benefit of creating a far more homogeneous expression level at low MOI by integrating a more fixed number of copies of the cassette, albeit in random genomic sites.

6. Furthermore, selection is also quicker, as all transduced cells appear to integrate the virus, plus transduction produces a far higher proportion of positive cells than transfection.

3.1.3. Creating a Lentivirus Expression Cassette

1. The 3.9 kb AcGFP-53BP1c fusion construct was excised from pG-AcGFP-53BP1c using NheI and SmaI, blunted, and inserted into the EheI and EcoRV sites of pENTR2B (Invitrogen).
2. The resulting plasmid, pE2B-AcGFP-53BP1c, was then recombined in a Clonase reaction with pLenti6/UbC/V5-DEST (Invitrogen) to create pLenti-AcGFP-53BP1c, which drives expression of AcGFP-53BP1c from a human UbC promoter, and the blasticidin selection gene from an SV40 promoter.

3.1.4. Production of Stably Integrated Cells Using Standard Transfection

1. 1×10^5 MRC-5 cells, at ~50% confluence, were trypsinized and then transfected with 1 μg pG-AcGFP-53BP1c DNA using an Amaxa electroporator (Amaxa) with the manufacturer's V-20 protocol (see Note 6).
2. Cells were replated into one well of a 6-well tissue culture dish.
3. Two days after electroporation, stably integrated cells were selected with 400 μg/mL G418 for 10 days and subsequently maintained in medium supplemented with 50 μg/mL G418.

3.1.5. Fluorescent Reporter Production Using Lentivirus

1. Virions carrying copies of pLenti-AcGFP-53BP1 were created in HEK293FT cells using transfection of pLenti-AcGFP-53BP1c alongside a plasmid packaging kit following the manufacturer's protocol (Invitrogen).
2. Lentiviral transduction of young MRC-5 was carried out using pLenti-AcGFP-53BP1c virions following the manufacturer's protocol with a target MOI of 2.
3. Cells were subsequently maintained in selection medium containing 4 μg/mL blasticidin.

3.2. Sample Preparation

Here we will first describe different sample preparations, for either fixed cells or live cell imaging. In the case of fixed cells, we can either use the fluorescent protein expression and/or use indirect immunofluorescence.

3.2.1. Using Fixed Cells Directly

1. AcGFP-53BP1c-expressing cells were grown on coverslips for at least 1 day prior to fixation (see Subheading 2.3.3).
2. For fixation, cells were washed once in PBS, and then incubated in 4% paraformaldehyde at 37°C for 2 min (see Note 7).
3. The coverslips were then washed three times with PBS before mounting in Vectashield (~10 μL per coverslip).

3.2.2. Using Immunofluorescence

Cells were harvested and fixed as described in Subheading 3.2.1, except that TBS was used instead of PBS for washing after fixation (see Note 8). Antibody staining was then performed:

1. Coverslips were blocked with 220 μL blocking buffer for 1 h at room temperature.
2. Cells were then incubated with the choice of primary antibodies in TBS/Triton (200 μL volume per coverslip/12-well plate well) overnight, gently rocking at 4°C.
3. Wash cells with 3×1 mL washes of TBS for 5 min each with gentle rocking.
4. Apply suitable fluorochrome-conjugated secondary antibodies in TBS/Triton (200 μL per well/coverslip) for 1–2 h at room temperature in the dark, with gentle rocking.
5. Wash cells with 3×1 mL washes of TBS for 5 min each with gentle rocking.
6. Coverslips were then lifted from the multi-well dish, excess TBS wicked away with a piece of tissue, and then mounted with a small volume (~10 μL) of Vectashield.

3.2.3. Using Live Cells to Monitor DNA Damage Foci Kinetics

AcGFP-53BP1c-expressing cells are plated 1–2 days prior to beginning imaging in 35 mm petri dishes with a glass coverslip base (a 12 mm Ø coverslip base is sufficient to image hundreds of fields), and kept growing in complete medium supplemented with the appropriate antibiotic.

3.3. Analysis of Fluorescently Labeled DNA Damage Foci

3.3.1. Fixed Cell Imaging

1. Imaging with any epifluorescence microscope with suitable filter cubes, ideally equipped with a camera, allows one to image fluorescent protein expression and immunofluorescence in fixed cells. To obtain accurate counts of DNA damage foci, a high-power, high-NA objective is essential. We use a Leica upright DM5500B equipped with a 63× 1.4 NA oil immersion objective and the following filter sets:

Fluorophore	Excitation and bandwidth (nm)	Emission and bandwidth (nm)	Dichroic mirror cutoff (nm)
AcGFP, Alexa 488	470/40	525/50	500
Alexa 555	543/22	593/40	562
Alexa 647	620/60	700/75	660
DAPI	360/40	470/40	400

2. For imaging DNA damage foci with immunofluorescence, we always use either red or green secondary antibodies, as they are far brighter than their far red counterparts. Also of note is that the far red fluorophore listed here (Alexa 647) is not visible to

the naked eye, so a camera capable of imaging far red light is essential for its use. Using these single filter sets, we capture sequential images of the cells with a monochrome camera (a Leica DFC360FX) using the software supplied with the camera and microscope, LAS-AF.

3. In general, we find that MRC-5 fibroblasts lie relatively flat on the coverslip, and even the nucleus is no more than ~3–3.5 μm deep. Given that we are interested in the steady-state levels of DNA damage in young and senescent cells, we are never expecting too many foci in a nucleus. We therefore find that taking a single plane image in most cases captures all of the visible foci. In cell lines and/or experiments where this is not the case, we instead use the motorized objective turret to capture *z* stacks encompassing the entire nuclear volume with at least 2× Nyquist sampling, and then deconvolute the resulting *z* stacks using a theoretical point spread function in Huygens (SVI). Whilst this method takes longer, we can be sure that we have counted all possible foci, which are resolvable by standard microscopy. An in-depth explanation of the benefits of deconvolution is beyond the scope of this chapter, but a good accessible review is given by Ref. (18).
4. Using two or more probes, we can use immunofluorescence to verify that the localization of our fusion protein is what we expect. 53BP1 should show a diffuse nuclear fluorescence, and any sites of DNA damage are visible by bright clustering of the fusion protein. We can show that the reporter faithfully shows the same localization as endogenous 53BP1 using an anti-53BP1 antibody and labeling it with an alternative colored fluorophore. In this case, there should be very high colocalization of the fusion protein and immunofluorescence (see Note 9). Alternatively, we can stain with anti-γH2A.X, which only stains the phosphorylated form present at sites of DNA damage, giving sharp colocalization at the DNA damage foci (Fig. 1).
5. Alternatively, one can correlate the number of DNA damage foci per nucleus with other markers, such as PML bodies or specific signaling pathway activation (e.g., phospho p38MAPK or nuclear translocation of transcription factors).
6. For analysis of fixed cells, we either count the number of foci per nucleus manually or use a macro in ImageJ. For this we capture a DAPI nuclear counterstain image, which is used to identify the number of nuclei per field, and then count bright DNA damage foci, the combination of which gives us an average number of foci per nucleus per field. Both counts require transforming the two fluorescent images into binary images, thresholding at the cutoff of nuclear staining for DAPI, and thresholding at the cutoff for bright nuclear foci for the DNA damage marker (Fig. 2), and as an extra precaution, limiting the

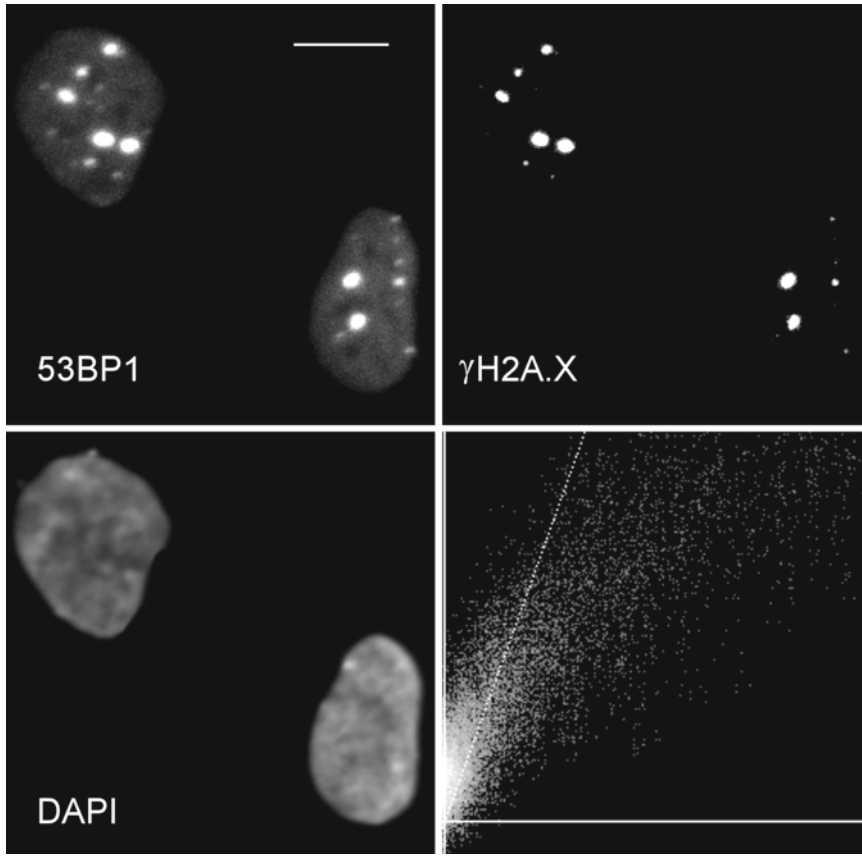

Fig. 1. Immunofluorescence colocalization demonstrates accumulation of AcGFP-53BP1c with sites of DNA damage. AcGFP-53BP1-expressing cells were fixed and then stained for γH2A.X as described in Subheading 3.2.2. Images were captured as epifluorescent *z* stacks (63× 1.4 NA) and deconvoluted as described in Subheading 3.3.1, before representing here as MIPs for each channel. The pixel-by-pixel colocalization between GFP fluorescence and indirectly labeled Alexa555 γH2A.X is shown in the lower right quadrant—a linear regression of best fit is shown (*dashed line*) against the individual pixels with values above background (scatter plot). A regression gradient of 0.5 would describe two colocalizing channels with the same intensity—here it is skewed by the noncolocalizing basal AcGFP-53BP1c fluorescence present in the nucleus. Such methods can generate correlation coefficients (i.e., goodness of fit of the data to the line of regression) on a per nuclear basis, and from *z* stack data without flattening, as was performed for simplification here. Scale bar shown represents 10 μm.

size of identified objects for each channel and removing nuclei on the edge of field when using ImageJ's "Analyse particles" command. Within an experiment we always keep our imaging parameters the same; so this method is possible with only one pre-calculation of background levels per experiment.

3.3.2. Live Cell Imaging

As described in Materials, we use confocal microscopes for live cell imaging. It is feasible to use widefield systems, as long as it is possible to minimize the input of excitation light, which also requires a very sensitive camera. Confocal systems are ideally suited for fine adjustment of light intensities and, coupled with sensitive detectors,

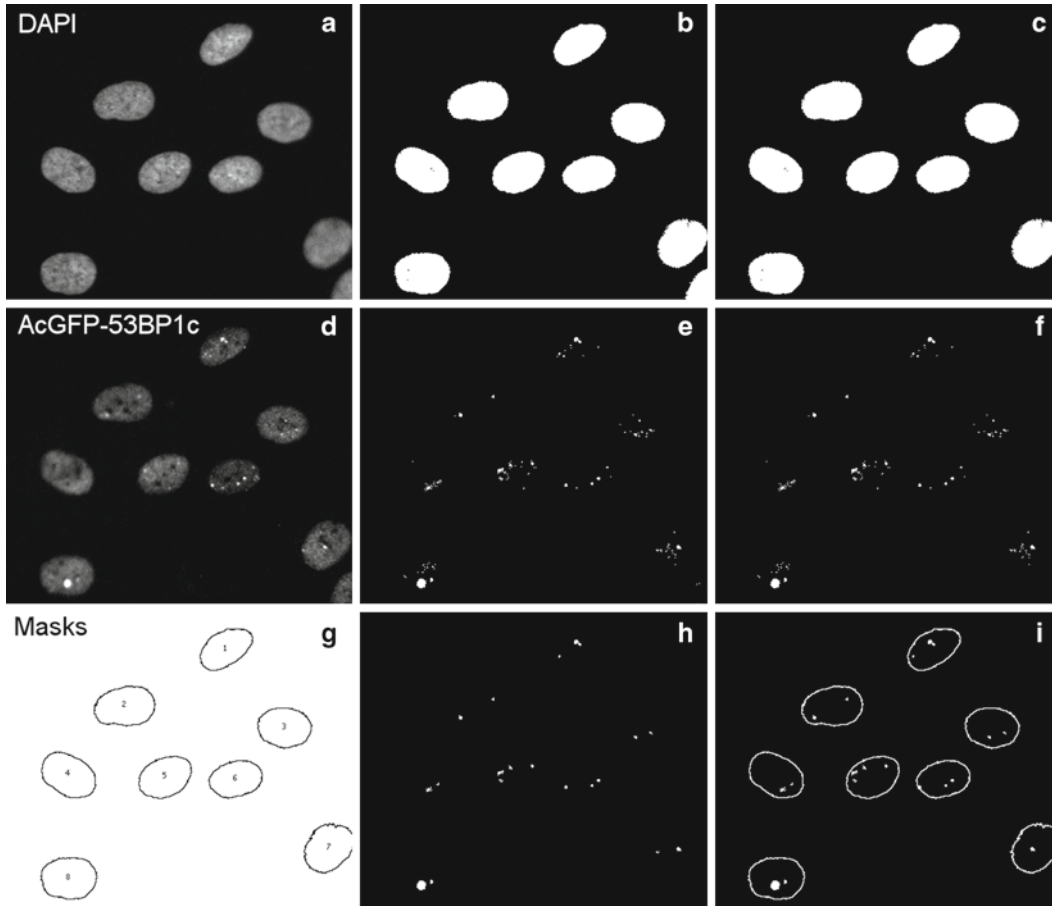

Fig. 2. Automated analysis of DNA damage foci per nucleus using binary images in ImageJ. AcGFP-53BP1-expressing cells were fixed and then mounted in DAPI-containing medium before imaging using single plane widefield epifluorescence (20× 0.7 NA). The steps performed by an ImageJ macro are shown. Firstly the DAPI channel (**a**) is converted to a binary image (**b**), which is used to detect nuclear shapes, specifying the size range of nuclei for the particular cell line (determined a priori), and to ignore any nuclei cut by the edges of the image (**c**). The AcGFP fluorescent channel (**d**) is thresholded to remove any fluorescence that is not in *bright spots* (i.e., DNA damage sites or single bright pixels) (**e**). So that foci of any partial nuclei on the edge of field are not counted, a mask is created by subtraction of (**c**) from (**b**), which is then subtracted from (**e**) to generate (**f**) which contains all the foci of the identified nuclei shown in (**c**). The final row of this Figure displays the output from the "Analyse particles" measurement in ImageJ. Panel (**g**) shows the outlines of the detected nuclei in (**c**). DNA damage foci were detected using image (**f**), stipulating a minimum size of positive signal (~>4 pixels area for this magnification, C mount, and camera pixel size), generating (**h**). An overlay image of the detected nuclei and foci is finally shown in (**i**). Normally, we do not generate these images, as once we are convinced the method works, we are only interested in the counts of foci and nuclei. Per field, we then obtain a measurement of mean foci per nucleus, for which it is very little work to obtain counts from multiple fields, replicates, and treatments.

make ideal systems for live cell imaging, where phototoxicity is the main concern.

1. For imaging, the glass-bottomed cell culture dish is placed in the pre-warmed incubation chamber on the inverted stage. To best maintain normal culture conditions, the cells are kept in normal complete medium for imaging (2.5 mL/35 mm dish);

an advantage of confocal systems is an automatic removal of any autofluorescence from the medium by using a narrow pinhole.

2. We use an automatic stage that enables multiple field imaging throughout the time course in combination with a Zeiss multitime macro (see Note 10). MRC-5 cells grown on glass move around quite a lot when subconfluent, and therefore, to maximize the amount of time we can track an individual cell, we capture multifield images as a tiled area. At each field, we perform an autofocus check prior to capturing a three-slice *z* stack around the optimal focal plane, using a *z* step size 100 nm larger than our pinhole (1.7 μm).
3. To determine a suitable interval for capturing foci formation and removal, we have performed several experiments with different time intervals to ascertain the minimal focus lifespan we could expect to record. The results of this work suggested that foci are hardly ever shorter than 20 min (with the exception of S phase, when many short-lived foci can be observed, presumably as a result of repair between Okazaki fragments).
4. Based on this, we settled on an imaging interval of 10 min—this meant that (a) we should observe almost all foci for at least two consecutive frames and (b) there was a large break between images at each field, minimizing the chances of phototoxicity. Typically, we can easily obtain a 3×3 tiled image *z* stack (GFP and phase transmission image) within 10 min. Using the Zeiss multitime macro, we capture these as individual files for each time point and field, and then concatenate each field. Due to the constraints of using a 32-bit operating system for image concatenation, we ensure that each file is at a max ~2 GB, which equates to approximately 330 time points (~55 h).
5. Subsequent data manipulation is performed using servers and high-specification desktop PCs. We deconvoluted the fluorescence channel using a server and Huygens software in batch mode. This immediately reduces background from photomultiplier tube (PMT) shot noise and increases our capability to ascertain whether two close fluorescent spots are distinct foci or not. As mentioned in Subheading 3.3.1, given the nuclear depth in MRC-5 cells and the foci frequency, the chances of two foci appearing in the same axial plane are very slim. Consequently we create maximum intensity projection (MIP) images of the deconvoluted fluorescent channel; this greatly speeds up our analysis, as we only need to track foci over time, not time and z.
6. For analysis, we have not found a suitable program for tracking both an individual nucleus and then the individual foci within that nucleus. Theoretically, it is not an insurmountable task, but to our knowledge no software exists to perform this task. Therefore, we determine foci lifespans by tracking nuclei and

foci manually. If a cell divides, the brightfield image can be useful to verify it is dividing rather than dying, but otherwise we generally work with the fluorescence image only, as there is enough basal expression within the nucleus to make following an individual cell easy.

7. The task of following foci over time requires patience, but once it has been performed a few times, the user is able to track several at once, noting their time of appearance and disappearance. In cells with several foci, it is usually easy to follow individual foci, as their positions within the nucleus are maintained, even when the nucleus rotates or shifts suddenly, similar to constellations wheeling around the sky (Fig. 3). We disregard anything that appears for only one frame (i.e., less than 20 min), and if a focus appears to be missing for one frame and back again the next, we treat it as one contiguous site of damage (Fig. 3). Based on the lifespan data we obtained from young and senescent cells, we were able to determine a size limit cutoff for large foci (which are long-lived, associated with senescence, very probably critically short telomeres), which corresponded to 0.45 μm^2 (13). Based on such analyses, it is possible to obtain foci frequencies per cell, per time point, foci lifespans per cell, frequencies and lifespans of small and large foci, as well as their correlation to other cellular parameters, such as timing of the cell cycle and their neighborhood to other cells (e.g., senescent or dying neighbors).

4. Notes

1. Successful performance of fluorescent live cell imaging requires maintaining the cells in a viable, healthy state. A good indicator of this is if the cells divide during the time course—this demonstrates that the incubation conditions are optimal and that the light intensity added for fluorescence capture is not damaging the cells. Therefore, the equipment required is based on these criteria. The microscope must be equipped with an incubator, which accurately maintains the desired temperature, gas mixture, and humidity around the cells. Since the incubator and cells are directly attached to the microscope, the performance of the incubator is also dependent on the maintenance of a steady-state room temperature. For high-magnification work (required for imaging DNA damage foci), an inverted microscope is necessary to allow a high-powered objective to work close enough to the cells growing on a glass coverslip (see Subheading 2.3.3). The alternative of using an upright body is not very desirable, even for lower powered work, since

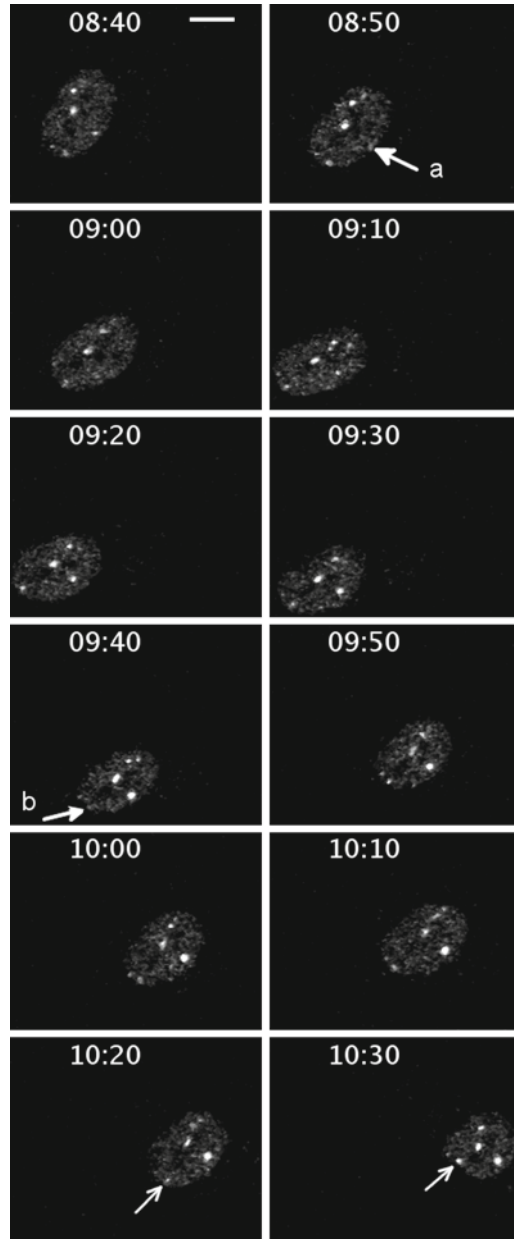

Fig. 3. Manual tracking of foci in live cell time-lapse images. Example MIP images taken from a 55-h time-series captured using line scanning confocal microscopy as described in Subheadings 2.4. and 3.3.2. Scale bar shown represents 10 μm, each frame is time stamped in hh:mm from the start of the experiment. The images show one cell tracked over the time frames shown, and *arrows* indicate examples of foci behavior. Note that the nuclear shape can be traced by eye over time, even with translocation across frames and rotation. Within this shape, the layout/mapping of each focus does not noticeably move any large distance, reflecting the stable nuclear architecture. *Arrow* (**a**) highlights a focus which is just disappearing and no longer visible from that frame, indicating a repaired site. *Arrow* (**b**) points to a focus which appears to almost disappear, but is clearly visible in both the preceding and succeeding frame. In such cases, we assume that the site of DNA damage was not repaired, and the partial disappearance of the focus is more due to imperfections in our imaging (e.g., if the cell has moved slightly so that the site is slightly out of focus in our *z* stacks). Finally, the two open-headed *arrows* describe the same focus—even though the nuclear shape rapidly changes in the final frame shown (10:30), it is clear by its position that this is the same site of DNA damage as highlighted in the preceding frame.

it generally requires using dipping objectives, which makes aseptic technique difficult, and the objective is often mismatched to the refractive index of the cell medium. Finally, suitable excitation and detection systems are required to allow for the minimum amount of light to illuminate the sample—therefore we ideally require brief exposures, which require a sensitive detector.

2. The first is a Zeiss LSM510META on a Zeiss Axiovert 200 M body. Whilst a laser is a very powerful light source, we minimize the light input by dropping the laser output to the lowest possible level, and maximizing our acquisition speed and sensitivity by scanning at a relatively fast rate and keeping the PMT gain high. For our low-expressing AcGFP-53BP1c cells, we use the following parameters: 40× 1.3 NA oil immersion objective on 1× zoom, excitation via 488 nm Argon line, set at 5.9 A power output, and using 0.9% through a 488 nm dichroic mirror. Fluorescence image acquisition is through a BP525/50 nm filter to a standard Zeiss LSM 510 PMT, using no averaging for a $1{,}024 \times 1{,}024 \times 3$ (*xyz*) scan with a pixel dwell time of 0.8 μs whilst also capturing a transmission image via the ChD PMT situated above the condenser. Cells are maintained at normal incubation conditions with the use of a Solent incubator at 37°C, pumping humidified 95% air/5% CO_2 mix into the cell chamber on the stage.
3. This rig is a Zeiss Cellobserver SD, equipped with a Zeiss XL incubator and a Yokagowa CSU-X1 spinning disk head for excitation and emission to an EMCCD camera (Photometrix QuantEM:512C). For long-term live cell imaging of AcGFP-53BP1c-expressing cells, we use a 63× 1.4 NA oil objective, excite with 3% of the 488 nm Argon (set at ~6.5 A), and capture GFP fluorescence through a 520/30 nm filter to the EMCCD set at a gain of 1, EM gain 250, 98-ms exposure, and no binning. The higher laser input does not correspond to a higher laser intensity at the objective due to the spinning disk blocking a high proportion of the light. As with the point scanning confocal, we capture images as *z* stacks to visualize the entire nuclear volume, and maintain cell health using the XL incubation chamber to replicate normal culture conditions. This system will not be referred to in Methods, as it will complicate the descriptions; we mention it here to make the reader aware of the feasibility of using such a system, and give an insight into workable parameters for live cell imaging using spinning disk systems.
4. For following the DDR, we required a protein which is recruited to the site of damage and removed once it is repaired. Since we wished to follow this in live cells, a fluorescent protein fusion was the ideal choice, requiring no other substrates

to be added. However, all fluorescent proteins have a lag after protein translation before the fluorophore has matured (19); so the tagged protein also had to be one which resides within the cell at a basal level of expression, not transcribed/translated after damage induction. Additionally, as best as we could determine, the protein had to be one which, if expressed at higher levels than normally found endogenously, would not alter/break any downstream signaling/processes, since building a targeted insertion would take so long that we would have an almost senescent cell line before we could use it. We found that the adapter protein TP53BP1 (53BP1) fitted these criteria, as its expression appears stable, and is recruited to sites of DNA damage for as long as histone H2A.X is phosphorylated and ubiquitinated (20). Ubiquitinated γH2A.X appears to increase binding affinity for 53BP1, which binds at DSBs based upon exposure of constitutively methylated lysine residues of histones 3 and 4, which are only visible when a break alters chromatin structure, exposing the nucleosome core (20–22).

5. (19) gives a succinct overview of fluorescent protein choices, which, whilst quite an old article, is still relevant. A lot of the more recent fluorescent protein design has been focused towards improved FRET, photoactivation, and conversion, especially regarding super-resolution microscopy techniques (23).
6. Amaxa lipid/electroporation protocol in our hands produced a lot of cell death (~50% cells), but did produce a reasonably high transfection level compared to what we would normally obtain from using lipid only-based systems such as Lipofectamine or Fugene. We removed the unattached/dead cells the day after electroporation. However, we still found that the surviving cells took a long time to reenter the cell cycle afterwards, possibly due to the combination of stress and antibiotic addition. For MRC-5, we optimized the cell number and DNA quantity, but did not try an alternative electroporation protocol than that suggested by Amaxa for this cell line. Ensuring that most cells are growing (i.e., at sub-confluence) is essential for higher transfection efficiency.
7. To preserve the maximum amount of fluorescence from fluorescent proteins, paraformaldehyde is the preferred fixation method. Methanol desiccates the sample too much, which quenches fluorescent protein fluorescence. Glutaraldehyde should work, but is a comparatively slow fixation method. The fixation can be performed for longer (10 min) at room temperature if preferred, with no noticeable effect upon AcGFP localization or fluorescence intensity.
8. We attempt to minimize the amount of free phosphate when using anti-phosphoepitope antibodies, such as γH2A.X. For nonphosphorylation-specific antibodies, this is unnecessary.

9. For colocalization analysis, we use an ImageJ plug-in called Colocalisation Test (http://www.uhnresearch.ca/facilities/wcif/software/Plugins/colocalisation_test.html), which allows one to determine Pearson's correlation between the two channels of interest and compare them to randomized pixel intensity images (*see* http://www.macbiophotonics.ca/imagej/ for an in-depth description). We use the Costes approximation to design the random images from the second channel, and at least ten iterations to test for the chances of random colocalization.
10. We employ a quite old point scanning microscope—newer variants allow multiple position image capture as part of the standard software. Some newer models also employ an automatic autofocus correction: for instance, we have had very good experience with Nikon's PFS system on their A1R confocal.

References

1. Passos JF, Nelson G, Wang C, Richter T, Simillion C, Proctor CJ, Miwa S, Olijslagers S, Hallinan J, Wipat A, Saretzki G, Rudolph KL, Kirkwood TB, von Zglinicki T (2010) Feedback between p21 and reactive oxygen production is necessary for cell senescence. Mol Syst Biol 6:347
2. Campisi J, d'Adda di Fagagna F (2007) Cellular senescence: when bad things happen to good cells. Nat Rev Mol Cell Biol 8:729–740
3. Branzei D, Foiani M (2005) The DNA damage response during DNA replication. Curr Opin Cell Biol 17:568–575
4. Freund A, Patil CK, Campisi J (2011) p38MAPK is a novel DNA damage response-independent regulator of the senescence-associated secretory phenotype. EMBO J 30:1536–1548
5. Bensimon A, Aebersold R, Shiloh Y (2011) Beyond ATM: the protein kinase landscape of the DNA damage response. FEBS Lett 585:1625–1639
6. Smith J, Tho LM, Xu NH, Gillespie DA (2010) The ATM-Chk2 and ATR-Chk1 pathways in DNA damage signaling and cancer. Adv Cancer Res 108:73–112
7. Wang C, Jurk D, Maddick M, Nelson G, Martin-Ruiz C, von Zglinicki T (2009) DNA damage response and cellular senescence in tissues of aging mice. Aging Cell 8:311–323
8. Herbig U, Ferreira M, Condel L, Carey D, Sedivy JM (2006) Cellular senescence in aging primates. Science 311:1257
9. Krishnamurthy J, Torrice C, Ramsey MR, Kovalev GI, Al-Regaiey K, Su L, Sharpless NE (2004) Ink4a/Arf expression is a biomarker of aging. J Clin Invest 114:1299–1307
10. Dimri GP, Lee X, Basile G, Acosta M, Scott G, Roskelley C, Medrano EE, Linskens M, Rubelj I, Pereira-Smith O, Peacocke M, Campisi J (1995) A biomarker that identifies senescent human cells in culture and in aging skin in vivo. Proc Natl Acad Sci U S A 92:9363–9367
11. Chen J, Astle CM, Harrison DE (2003) Hematopoietic senescence is postponed and hematopoietic stem cell function is enhanced by dietary restriction. Exp Hematol 31:1097–1103
12. Wang C, Maddick M, Miwa S, Jurk D, Czapiewski R, Saretzki G, Langie SA, Godschalk RW, Cameron K, von Zglinicki T (2010) Adult-onset, short-term dietary restriction reduces cell senescence in mice. Aging 2:555–566
13. Nelson G, Wordsworth J, Wang C, Jurk D, Lawless C, Martin Ruiz C, von Zglinicki T (2012) A senescent cell bystander effect: senescence-induced senescence. Aging Cell 11(2):345–349
14. Rodier F, Munoz DP, Teachenor R, Chu V, Le O, Bhaumik D, Coppe JP, Campeau E, Beausejour CM, Kim SH, Davalos AR, Campisi J (2011) DNA-SCARS: distinct nuclear structures that sustain damage-induced senescence growth arrest and inflammatory cytokine secretion. J Cell Sci 124:68–81
15. Iwabuchi K, Li B, Massa HF, Trask BJ, Date T, Fields S (1998) Stimulation of p53-mediated Transcriptional Activation by the p53-binding Proteins, 53BP1 and 53BP2. J Biol Chem 273:26061–26068

16. Nelson G, Paraoan L, Spiller DG, Wilde GJ, Browne MA, Djali PK, Unitt JF, Sullivan E, Floettmann E, White MR (2002) Multi-parameter analysis of the kinetics of NF-kappaB signalling and transcription in single living cells. J Cell Sci 115:1137–1148
17. Nelson G, Buhmann M, von Zglinicki T (2009) DNA damage foci in mitosis are devoid of 53BP1. Cell Cycle 8:3379–3383
18. Wallace W, Lutz HS, Swedlow JR (2001) A workingperson's guide to deconvolution in light microscopy. Biotechniques 31:1076–1097
19. Shaner NC, Steinbach PA, Tsien RY (2005) A guide to choosing fluorescent proteins. Nat Methods 2:905–909
20. Huyen Y, Zgheib O, DiTullio RA Jr, Gorgoulis VG, Zacharatos P, Petty TJ, Sheston EA, Mellert HS, Stavridi ES, Halazonetis TD (2004) Methylated lysine 79 of histone H3 targets 53BP1 to DNA double-strand breaks. Nature 432:406–411
21. Sanders SL, Portoso M, Mata J, Bähler J, Allshire RC, Kouzarides T (2004) Methylation of histone H4 lysine 20 controls recruitment of Crb2 to sites of DNA damage. Cell 119:603–614
22. Stewart GS, Panier S, Townsend K, Al-Hakim AK, Kolas NK, Miller ES, Nakada S, Ylanko J, Olivarius S, Mendez M, Oldreive C, Wildenhain J, Tagliaferro A, Pelletier L, Taubenheim N, Durandy A, Byrd PJ, Stankovic T, Taylor AMR, Durocher D (2009) The RIDDLE syndrome protein mediates a ubiquitin-dependent signaling cascade at sites of DNA damage. Cell 136:420–434
23. Fernandez-Suarez M, Ting AY (2008) Fluorescent probes for super-resolution imaging in living cells. Nat Rev Mol Cell Biol 9:929–943

Chapter 14

Assessment and Quantification of Telomerase Enzyme Activity

Michelle F. Maritz, Laura A. Richards, and Karen L. MacKenzie

Abstract

The enzyme telomerase is activated in 80–90% of all human malignancies and immortal cell lines, where it functions to maintain the integrity of chromosomal-end structures called telomeres. Telomerase enzyme activity can be detected in whole cell lysates by a polymerase chain reaction (PCR)-based method referred to as the telomeric repeat amplification protocol (TRAP). The TRAP assay involves extension of an oligonucleotide through telomerase-mediated enzymatic addition of telomeric DNA repeats and subsequent PCR amplification of the extension products. While the TRAP assay as originally developed utilizes radioactively labelled nucleotides, protocols are provided herein for nonradioactive versions of the TRAP assay, with options for either qualitative assessment of TRAP products by polyacrylamide gel electrophoresis (standard TRAP), or quantitative analysis by real-time PCR (Q-TRAP). The Q-TRAP method poses the additional advantages of exquisite sensitivity, rapidity, and potential for adoption to a high-throughput format.

Key words: Real-time PCR, Q-TRAP, Telomeric repeat amplification protocol, Telomerase, TERT, TRAP

1. Introduction

The onset of replicative senescence is attributed (at least in part) to the shortening of specialized chromosomal-end structures referred to as telomeres (1–3). Telomeres are composed of TTAGGG DNA repeat sequence and function to protect the 3′ end of linear chromosomes from erosion and recombination (4–6). Telomeres in normal somatic cells progressively shorten with each round of cell replication and upon reaching a critically short length elicit a DNA damage signal that induces cell cycle arrest and senescence (1, 2, 7). The activation of telomerase during carcinogenesis provides a mechanism for telomere length maintenance, thereby circumventing senescence and promoting unlimited proliferation (cellular immortality).

Lorenzo Galluzzi et al. (eds.), *Cell Senescence: Methods and Protocols*, Methods in Molecular Biology, vol. 965,
DOI 10.1007/978-1-62703-239-1_14,

Telomerase is a ribonuclear protein complex that includes a reverse transcriptase as its catalytic domain (TERT), an RNA component that includes a template for the synthesis of telomeric repeats (TERC), and the RNA binding and modifying protein dyskerin, which stabilizes the RNA template (8–12). Telomerase enzyme activity was first detected in cell-free extracts isolated from the ciliate *Tetrahymena* (13). The reaction employed in those studies involved catalysis of γ-^{32}P-labelled deoxynucleoside triphosphates onto the 3′ end of a synthetic telomeric oligonucleotide. The elongation products were then precipitated and subject to polyacrylamide gel electrophoresis (PAGE) and autoradiography to reveal products with a characteristic six base repeating pattern.

The adoption of the primer extension assay to a PCR-based assay, referred to as the telomeric repeat amplification protocol (TRAP), enabled detection of telomerase with 10,000-fold increased sensitivity (14, 15). In the TRAP assay, telomerase activity within a cell lysate catalyzes addition of varying numbers of TTAGGG hexameric repeats onto the 3′ end of a telomeric primer (TS). Following primer extension at 30°C, the temperature of the reaction is increased to 95°C to inactivate telomerase activity. The extension product is then amplified by PCR using a reverse primer that is complementary to telomere repeat sequence.

The original TRAP assay involved PCR amplification in the presence of γ-^{32}P-labelled dCTP, followed by resolution of the radiolabelled PCR products by PAGE. This method was utilized to define the association between telomerase activity and human cancer cells, and then to demonstrate telomerase activity in progenitor populations, stimulated lymphoid cells, germ cells, and embryonic tissue (14, 16–19). The PCR step in the TRAP assay was subsequently modified by replacement of the reverse primer with an alternate primer, ACX. The ACX primer is complementary to four telomeric repeats, but has a single mismatched base at the third position in three of the telomeric repeats. ACX also has a six base pair anchor at the 5′ end that is neither telomeric nor complementary to telomeric repeats. These features of the ACX primer minimize primer dimer artifacts and ensure that the length of the products reflect the processivity of telomerase enzyme activity (15, 20). An additional oligonucleotide (TSNT) was also incorporated into the PCR reaction to function as internal control and to enable identification of samples containing inhibitors of *Taq* DNA polymerase, which can cause false negative results. The TSNT primer may also be used for semi-quantitation of TRAP products.

Currently, the most broadly used assays for detection and quantitation of telomerase activity are nonradioactive versions of the TRAP assay. Non-radioactive TRAP protocols include those that utilize the DNA-binding SYBR green dye to stain the gel, or incorporation of a TS primer labelled with the fluorescent dye,

Cy-5 (21). For quantitative detection of telomerase, a real-time PCR-based TRAP method (Q-TRAP) has also been developed (22, 23). The Q-TRAP method makes use of SYBR green in the PCR reaction mix for quantitative detection of amplified telomerase extension products. It is an exquisitely sensitive method that allows rapid, high-throughput quantitation of telomerase activity. In contrast to the post-PCR steps involved in PAGE visualization of TRAP products, real-time PCR analysis also poses the advantage of presenting minimal opportunity for contamination of reagents and equipment with PCR products.

This chapter describes a non-radioactive TRAP method for qualitative assessment of telomerase activity on PAGE gels, as well as the highly quantitative Q-TRAP method.

2. Materials

2.1. General Equipment

- Thermocycler or heat block at 85°C.
- Sterile ART pipette tips (see Note 1).
- 1.5 mL sterile Eppendorf tubes.
- 96-well Plate Reader Bio-Rad (595 nm) for Bradford Assay Quantification.
- Tabletop microcentrifuge.
- Chilled PCR rack for 96-well plates.
- PCR rack for 0.2 mL PCR tubes.

2.2. Equipment for Q-TRAP

- 7500 Real-Time PCR System (Applied Biosystems; Carlsbad, CA, USA).
- 96-well plate for PCR amplification and detection (Applied Biosystems).
- 96-well optical adhesive film cover.
- Tabletop centrifuge with plate holders.

2.3. Equipment for Standard TRAP

- iCycler Thermal Cycler (Bio-Rad, Hercules, CA, USA).
- Optically clear 0.2 mL PCR tubes.
- Gel electrophoresis apparatus (for a large format acrylamide gel, e.g., 16×20 cm), including gel tank, power pack, glass plates, gel pouring apparatus, and gel comb.
- Gel imaging system for detection of SYBR green or Cy-5, e.g., Typhoon (Applied Biosystems), or Versadoc (Bio-Rad) with a UV transluminator and appropriate filters for detection of SYBR green (254 nm or 302 nm).

2.4. Reagents and Solutions for Sample Preparation

- 1× CHAPS lysis buffer: 10 mM Tris–HCl pH 7.5, 1 mM $MgCl_2$, 1 mM EGTA pH 8.5, 0.5% CHAPS, 10% Glycerol, made in DEPC-treated H_2O (see Notes 2–6).
- Protease inhibitor cocktail (Roche) (see Note 7) and 0.1 M PMSF (Sigma-Aldrich, St-Louis, MI, USA) (see Note 8), to be added to 1× CHAPS or TRAPeze lysis buffer on the day the cells are lysed.

2.5. Protein Determination

- Coomassie Blue Bradford Reagent (Bio-Rad) (see Notes 9–11).
- Molecular grade bovine serum albumin (BSA).

2.6. Primers

- 0.1 μg/μL HPLC purified TS primer: 5′-AATCCGTCGA GCAGAGTT-3′ in sterile RNAse- and DNAse-free dH_2O.
- 0.1 μg/μL HPLC purified ACX primer: 5′-GCGCGG(CTTA CC)$_3$CTAACC-3′ in sterile RNAse- and DNAse-free dH_2O.

2.7. Additional Primers for Standard TRAP

- 0.1 μg/μL HPLC purified NT primer: 5′-ATCGCTTCT CGGCCTTTT-3′ in sterile RNAse- and DNAse-free dH_2O.
- 0.1 μg/μL HPLC purified TSNT primer: 5′-AATCCGTCGAGC AGAGTTAAAAGGCCGAGAAGCGAT-3′, in sterile RNAse- and DNAse-free dH_2O (see Note 12).

2.8. Alternate Primer for the Cy-5-Labeling Method of Standard TRAP

- 0.1 μg/μL HPLC purified, Cy-5 labelled TS primer: 5′-AAT CCGTCGAGCAGAGTT-3′ in sterile RNAse- and DNAse-free dH_2O.

2.9. Q-TRAP Solutions

- Q-TRAP Master Mix (see Note 13) For each of the duplicates add to the mastermix: 12.5 μL SYBR Green Master Mix (Applied Biosystems), 2.5 μL 10 mM EGTA pH 8.5, 1.0 μL 10 ng/μL ACX primer, 1.0 μL 100 ng/μL TS primer, 6.0 μL sterile, RNAse-free, DNAse-free PCR H_2O.

2.10. Standard TRAP Solutions

- 10× TRAP buffer: 200 mM Tris–HCl pH 8.0, 15 mM $MgCl_2$ (Sigma-Aldrich), 630 mM KCl, 10 mM EGTA pH 8.5, 0.5% Tween-20 (Sigma-Aldrich) in sterile nuclease-free dH_2O (see Note 14).
- Standard TRAP PCR reaction mix (see Note 15): 2.5 μL 10× TRAP buffer, 0.5 μL dNTPs (2.5 mM of each for total 10 μM of the four dNTPs), 0.5 μL 100 ng/μL TS primer, 0.5 μL 100 ng/μL NT primer, 0.5 μL 100 ng/μL ACX primer, 0.25 μL 100 ng/μL TSNT primer, 0.25 μL (5 U/μL) Ampli*Taq* DNA Polymerase (Applied Biosystems), 19 μL sterile, nuclease-free H_2O.

2.11. Reagents for PAGE for Standard TRAP

- 40% Polyacrylamide 19:1 (see Note 16).
- 50× Tris-Acetate EDTA (TAE) buffer: 2 M Tris.Cl (pH 8.0), 1 M acetic acid, 50 mM EDTA.
- *N*,*N*,*N*′,*N*′-Tetramethylethylenediamine (TEMED).
- 10% (w/v) ammonium persulphate (APS) solution (freshly prepared).
- 10× sample loading buffer (0.25% xylene cyanol, 0.25% bromophenol blue, 50% glycerol, 50 mM EDTA).
- 25 bp DNA Marker Ladder (Invitrogen, Eugene, CA, USA).
- SYBR® Green I Nucleic Acid Gel Stain (Invitrogen) (see Note 17).

3. Methods

3.1. Laboratory Set Up

1. Both the Standard TRAP and Q-TRAP are highly sensitive PCR-based techniques that are able to detect telomerase activity in a very small number of cells. Hence, a special laboratory setup and significant precautions are required to prevent PCR carry-over contamination or cross contamination from other samples. It is therefore strongly advised to designate separate areas for (a) sample extraction, (b) reagent preparation and TRAP assay setup, and (c) PCR amplification and post-PCR analysis.
2. To maintain sample and reagent integrity, the reaction should be set up on ice or a cooling rack in an RNAse-free area.
3. Since telomerase is a ribonucleoprotein complex, it is sensitive to heat, proteases and RNAse. It is therefore crucial that samples are kept on ice at all times, stored at –80°C and not frozen and thawed multiple times.
4. Keep the assay solutions (TRAP buffer, CHAPS lysis buffer, *Taq* DNA Polymerase, etc.) separate from other reagents in the lab.
5. It is advisable to use fresh aliquots of reagents as "working" stocks that are discarded after a single use.

3.2. Assay Controls

1. A known telomerase-positive cell line should be used as a positive control for the standard TRAP and to generate a standard curve for quantitation in the Q-TRAP (see Note 18). We use the SK-N-SH neuroblastoma cell line; however, any other telomerase-positive cell line may be used, e.g., MCF-7, HeLa, or HEK293. Cell pellets and lysates to be used as positive controls and standards should be prepared seperately from other samples. Prepare several stock cell pellets, each with 1×10^6 cells and store at –80°C.

2. Negative controls should be prepared in a dedicated PCR "clean-area" (see Note 19). We use UV-treated biological safety hoods. There are several options for negative controls. Since the TRAP method is highly sensitive and vulnerable to contamination, we typically use at least two of the following for each assay: heat-inactivated SK-N-SH standard stock lysate (10 ng for Q-TRAP or 1 μg for Standard TRAP). The lysate is heated to 85°C for 10 min (see Note 20); 10 ng of a lysate prepared from cells with negligible telomerase activity, e.g., an ALT-immortalized cell line or normal human fibroblasts; 1× CHAPS lysis buffer only; H_2O only or an RNAse A-treated standard lysate, e.g., SK-N-SH.

3.3. Preparation of Samples (See Note 21)

1. Detach adherent cells ($1–2 \times 10^5$) from tissue culture flasks by trypsinization. Neutralize trypsin with media containing fetal bovine serum according to standard tissue culture procedures. Transfer trypsinized cells or cells grown in suspension culture to 15 mL centrifuge tubes. Pellet the cells by centrifugation at $490 \times g$ for 8 min at 4°C. Aspirate supernatant and flick the tube to resuspend the pellet in the residual volume.
2. Wash the cells with 10 mL ice-cold phosphate-buffered saline (PBS) and centrifuge at $490 \times g$ for 8 min at 4°C.
3. Remove the supernatant and wash the cells in 1 mL of cold PBS, then transfer to a 1.5 mL Eppendorf tube. Centrifuge at $12{,}000 \times g$ for 1 min at 4°C, then carefully remove all of the supernatant and either store the pellet at –80°C, or proceed immediately to step 4.
4. Resuspend the cell pellet in ice-cold 1× CHAPS lysis buffer or TRAPeze with 1× protease inhibitors. Add 50 μL cold 1× CHAPS lysis buffer to 2×10^5 cells or 20 μL to a cell pellet of less than 2×10^5 cells. Pipette the pellet several times to ensure thorough resuspension. Vortex briefly and incubate on ice for 30 min.
5. Centrifuge the cell lysate at $12{,}000 \times g$ for 15 min at 4°C. Without disturbing the pelleted debris, carefully transfer the supernatant to a sterile 1.5 mL Eppendorf tube on ice. Aliquot the remaining lysate to a separate sterile PCR tube and use to determine protein concentration. Aliquot 20 μL of supernatant into Eppendorf tubes and freeze at –80°C for storage, or keep on ice if performing the TRAP assay on the same day.
6. Quantify protein concentrations using the Bradford assay according to the manufacturer's protocol using BSA as a standard (see Notes 9 and 10).
7. The positive control stock lysate should be prepared separately from sample preparation. In a biological safety cabinet, lyse one stock pellet in 200 μL 1× CHAPS or TRAPeze lysis buffer plus protease inhibitors as described above. Prepare a 1 μg/mL

stock of this standard control lysate and store in 5 μL aliquots at a concentration of 100 ng/μL at −80°C (see Note 22).

3.4. TRAP Reaction and Analysis (Q-TRAP Reaction)

1. Prepare the Q-TRAP master mix in a 1.5 mL Eppendorf tube. Carefully pipette 23 μL Q-TRAP master mix per well into a 96-well plate.
2. Thaw samples on ice and dilute to a concentration of 5 ng/μL in 1× CHAPS lysis buffer.
3. Prepare dilutions of a positive control to be used for the standard curve (e.g., SK-N-SH) starting from a 100 ng/μL aliquot in 1× CHAPS lysis buffer and diluting to concentrations of 12.5, 5, 2.5, 0.5, 0.25, and 0.05 ng/μL. Use these diluted samples a maximum of two times before discarding (see Note 23).
4. Add 2 μL of sample (5 ng/μL), control or standard to each well, starting with negative controls first, then samples and dilutions of the standard last, working from low concentration to high. Set up duplicates of each sample and use a new tip for every well. Keep samples on ice at all times and return the samples to −80°C at the first opportunity. Avoid multiple freeze–thaw cycles.
5. Cover the 96-well plate with the optical adhesive film cover and press it down using the provided tool. Centrifuge the 96-well plate for 30 s in the centrifuge with plate holder. Perform a four-step PCR in an ABI 7500 Real-Time Cycler with the following program: 30°C for 12 min, 95°C for 10 min, followed by 40 cycles of 95°C for 30 s, 60°C for 1 min. This is followed by a dissociaton stage of 95°C for 15 s, 60°C for 1 min, 95°C for 15 s, and 60°C for 15 s (see Note 24). The final step is an infinite hold at 4°C. After the PCR is complete, collect the 96-well plate and save the data file

3.5. Q-TRAP Data Analysis

1. Collect and evaluate real-time PCR data using the ABI sequence detection system and analysis software. Data collected using this software is displayed in an amplification plot and a melting or dissociation curve (Fig. 1a, b). Use these curves to confirm that amplification has taken place and that the dissociation curves have uniform peaks (see Note 25).
2. Eliminate background signal by setting the *baseline* fluorescence according to the instructions for the instrument. For the ABI Prism, it is recommended that a baseline is set two cycles below the first cycle that PCR amplification is evident.
3. Once the baseline is set, the software calculates a *threshold* value for fluorescence that is 10 standard deviations above the baseline fluorescence. Alternatively, the threshold can be manually adjusted and set within the linear region of the logarithmic amplification curve (see Notes 26 and 27) (Fig. 1a).

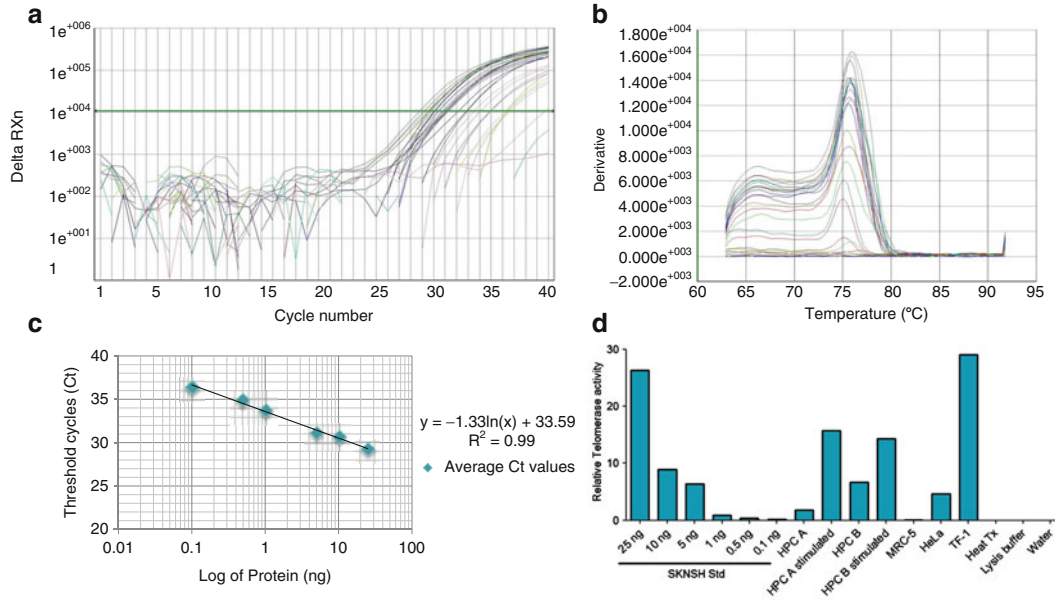

Fig. 1. *Analysis of Q-TRAP data.* (**a**) Amplification curve showing the accumulation of fluorescent PCR products (*y*-axis) amplified from each sample over 40 PCR cycles (*x*-axis). A threshold is set at the fluorescence reading where all products are in a linear phase of amplification (*green line*). The cycle number at the threshold (*Ct* value) is used to calculate relative telomerase activity (RTA) for each sample. (**b**) The dissociation curve showing uniform melting temperature of the PCR products generated by each sample. (**c**) Standard curve generated by graphing *Ct* values of SK-N-SH standards against log of protein (ng). (**d**) Graph of RTA calculated using the linear equation from the standard curve shown in **c.**

4. The threshold cycle (*Ct* value) is the cycle number at which the fluorescence signal reaches the threshold. It reflects the point at which amplicons have accumulated to a statistically significant point above the baseline (see Notes 26 and 27) (Fig. 1a). Retrieve the *Ct* value for each sample and export the data to Microsoft Excel or similar software with statistical capabilities (see Note 27). Plot a standard curve using the duplicate *Ct* values for the telomerase-positive standard dilution series (e.g., SK-N-SH) versus log10 of protein amount (Fig. 1c). Display r^2 and the linear regression equation by right clicking the format trend line button. r^2 should be >0.98 and the slope should be close to −1.4 (see Notes 28 and 29) (Fig. 1b).
5. Convert unknown test sample data to Relative Telomerase Activity (RTA) using the linear equation of your standard curve (Table 1) (Fig. 1d).
6. To ensure that the data is both reproducible and quantitative, we routinely perform the assay three times, with duplicate samples in each assay. Values are expressed as means from the three assays.

Table 1
Quantification of relative telomerase activity (RTA)

Sample	C_t-1	C_t-2	Average C_t	RTA[a] EXP((33.59-Ave C_t)/1.33)
SK-N-SH 25 ng	29.11	29.37	29.24	26.31
SK-N-SH 10 ng	30.95	30.39	30.67	8.98
SK-N-SH 5 ng	31.04	31.19	31.115	6.42
SK-N-SH 1 ng	34.05	33.43	33.74	0.89
SK-N-SH 0.5 ng	34.9	34.91	34.905	0.37
SK-N-SH 0.1 ng	36.18	36.54	36.36	0.12
HPC A	32.87	32.76	32.819	1.78
HPC A stimulated	30.08	29.73	29.919	15.79
HPC B	30.97	31.14	31.058	6.71
HPC B stimulated	30.03	30.06	30.046	14.35
MRC-5	36.29	40	38.145	0.03
HeLa	32.08	31.02	31.55	4.63
TF-1	28.7	29.51	29.105	29.12
Heat Tx	40	39.62	39.81	0.01
Lysis buffer	>40	>40	>40	0.00
Water	>40	>40	>40	0.00

[a]Equation derived from trend line for SK-H-SH standards as shown in Fig. 1c and plotted in Fig. 1d
Heat Tx heat treatment, *HPC* hematopoietic progenitor cells

3.6. Standard TRAP (Primer Extension and PCR Amplification)

1. In a PCR clean room designated for TRAP assay setup, label sterile 0.2 mL PCR tubes for the samples and controls.
2. Keep all reagents and samples on ice unless otherwise stated. Prepare the PCR reaction mix and dispense 24 μL of PCR reaction mix into the labelled tubes.
3. Thaw samples on ice and adjust the concentration to 0.5 μg/μL in 1× CHAPS lysis buffer with 1× protease inhibitors.
4. Add 1 μL of sample or control to each tube. Start with negative controls, then samples and positive controls last (see Note 30). Spin down samples in tabletop microcentrifuge and place them in the thermocycler, which should be located in a separate room to the TRAP assay setup room.
5. Run the PCR on the following four-step program *without* a hot start, which will inactivate the telomerase activity: 30°C for

30 min, 94°C for 2 min, followed by 25 cycles of 94°C for 30 s, 60°C for 30 s and 72°C for 30 s, with a final elongation step of 72°C for 5 min (see Note 24). Conclude with an infinite hold at 4°C. After the PCR amplification is complete, samples can be stored at 4°C for several days.

3.7. PAGE Analysis of Standard TRAP PCR Products (See Note 31)

1. Clean glass plates for a 16×20 cm gel apparatus with ethanol. Assemble the gel apparatus using 1 cm spacers and clamps as described by the manufacturer.
2. Prepare a 12.5% polyacrylamide gel solution as follows: 0.8 mL 50× TAE buffer, 26 mL dH_2O, 12.5 mL 40% Polyacrylamide 19:1, 0.5 mL APS (10%), 50 μL TEMED.
3. Pour the gel solution between the glass plates of the gel apparatus and carefully insert the gel comb so as not to create bubbles in the wells. Allow the gel to set in the fume hood and once set, carefully place it into the electrophoresis tank and fill the tank with 1× TAE buffer. Remove the gel comb and rinse the wells of the gel thoroughly with 1× TAE buffer to remove any residual TEMED and APS, which can degrade telomerase products. Fill the middle chamber with buffer so that wells are completely immersed. Make sure that there are no leaks.
4. Add 5 μL 10× loading dye to each PCR reactions. Load the entire PCR mixture (25 μL) from the samples and controls, as well as a 25 bp DNA molecular weight marker into the wells (see Note 32).
5. Run the gel at 60 V overnight, or at 250–300 V for 4–5 h or until the dye front reaches the bottom of the gel.
6. Carefully remove the glass plates and disassemble in a tray with sufficient 1× TAE buffer to completely immerse. To stain the gel with SYBR green (not required if using Cy5-labelled primer), prepare a 1:10,000 dilution of SYBR green in 1× TAE and dispense in another tray. Carefully transfer the gel into the SYBR green stain and incubate for 20 min at room temperature with gentle rocking.
7. After staining with SYBR green, the gel is ready for imaging on a Versa Doc (Bio-Rad), Typhoon (Amersham, Biosciences) or similar gel imaging equipment. If using Cy-5 labelled primers, gels are imaged immediately after running (without staining) using the Typhoon with settings on Cy-5 Red 633 nm/670 nm, 600 V with medium sensitivity (see Note 33).
8. The amplified telomerase products are of heterogeneous length and create a typical pattern of laddered PCR products with 6 bp increments starting at a length of 50 bp (Fig. 2). However, the furthest migrated band should be the internal TSNT control band at 36 bp (Fig. 2, lane 3). Each of the laddered telomerase PCR products represents the addition of a hexanucleotide

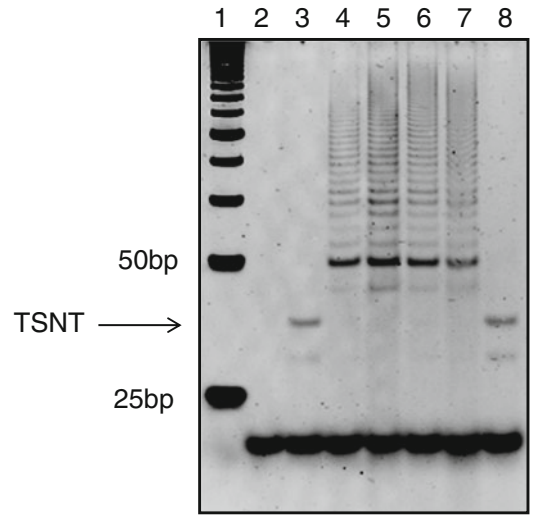

Fig. 2. *Standard TRAP products separated by polyacrylamide gel electrophoresis.* 25 μL of PCR from the standard TRAP separated by polyacrylamide gel electrophoresis, stained with SYBR Green and imaged on a Versadoc. *Lane 1*; 25 bp DNA Marker, *Lane 2*; CHAPS lysis buffer only, no TSNT, *Lane 3*; CHAPS lysis buffer with TSNT, *Lane 4*; TERT-transduced endothelial cells grown, *Lanes 5–6*; SK-N-SH neuroblastoma cell line, *Lanes 7*; HeLa cervical cancer cell line, *Lane 8*; MRC-5 normal fetal lung fibroblasts.

(TTAGGG) telomeric repeat by endogenous telomerase in the cell lysate. Negative controls should have only the internal TSNT band, while samples with high telomerase activity may have a weaker TSNT band due to competitive amplification of the TS extension products (see Notes 34 and 35) (Fig. 2, lanes 4–7).

9. For semi-quantitation of TRAP products, densitometric readings of the 6 bp increment ladder may be normalized to the TSNT signal. It is recommended that the assay is performed three times and mean values calculated from the three gels.

4. Notes

1. Make sure that all working areas are kept cleared, clean, and stocked with the required equipment. It is also recommended to have a dedicated set of pipettes for each area and to use aerosol filter pipette tips (ART).
2. Prepare all solutions in a PCR "clean room" using ART tips, sterile nuclease-free Eppendorf tubes and RNAse/DNase free H_2O.
3. It is also critical to ensure that all reagents and equipment are free of RNase and DNAse. Use sterile, nuclease-free H_2O for all buffers and solutions.

4. Molecular grade $MgCl_2$ (Sigma-Aldrich) is recommended for optimal PCR efficiency.
5. You can use commercially available TRAPeze® 1× CHAPS Lysis Buffer (Millipore), or you can make your own 1× CHAPS lysis buffer.
6. Sterilize by filtration through a 0.22 μm filter and store in 1 mL aliquots at 4°C for up to 6 months or longer periods at –20°C. β-mercaptoethanol is added to the 1× CHAPS lysis buffer to a final concentration of 5 mM on the day the buffer is used.
7. Store 100× stock at –20°C.
8. Make stock in ethanol and store at –20°C.
9. The Bradford assay is our preferred method for determination of the concentration of proteins in CHAPS lysis buffer. In our hands, the BCA protein assay produced a more substantial and variable background, which was possibly due to a reaction involving the β-mercaptoethanol in the CHAPS buffer. A high background reading may result in inaccurate protein determinations and misleading results in the TRAP assay.
10. When using the commercially bought TRAPeze® 1× CHAPS Lysis Buffer, we routinely test the reagent upon arrival using the Bradford assay for possible stock variations, which may become apparent as a high background reading in the Bradford assay).
11. Accurate determination of the amount of starting material is crucial for both the Q-TRAP and the Standard TRAP methods. In the protocols above, the amount of starting material is based on protein concentrations; however, it is also valid to base starting material on cell number equivalents.
12. The TSNT internal control primer may be used for semi-quantitation of samples analyzed by the Standard TRAP method. TSNT should be ordered at a different time or from a different company to avoid potential cross contamination with other primers. The TSNT stock should be prepared away from other PCR regents in a separate room with a dedicated pipette.
13. Prepare the Q-TRAP master mix on ice with enough reagents for the samples, standards and controls in duplicate, plus enough for an extra duplicate to allow for pipetting excess.
14. The 10× TRAP buffer should be prepared in the PCR clean area in advance and stored at –20°C in 100 μL aliquots until used. The buffer is stable for at least 6 months at –20°C.
15. Prepared from stock solutions just prior to performing the PCR amplification step. Prepare sufficient master mix for the number of samples and controls plus one.
16. Store at 4°C in the dark.

17. Prepare 20 μL aliquots of 10,000× SYBR® Green concentrate in DMSO and store at −20°C. Not needed if using Cy-5 labelled TS primer.
18. The use of positive controls is crucial for identification of false-negatives and for trouble-shooting purposes. False-negatives may result from protein degradation during processing or contamination with nucleases. In these cases, TRAP reagents should be remade.
19. The use of negative controls is essential to rule out false positive results. Negative controls in the Standard TRAP should produce no bands except the internal control band (TSNT), which is 36 bp. False positive artifacts in the standard TRAP may be recognized by variation in band migration and/or intensity. The smallest hexanucleotide band in the 6 bp incremental TRAP ladder is 50 bp and should be the most intense band (Fig. 2). The theoretical size of the ACX and TS dimers is 40 bp. In Q-TRAP, *Ct* values for negative controls should be outside the linear range of the standard curve.
20. It is possible to determine whether PCR product generated from a negative control is a PCR artifact (e.g., primer dimer) or the result of contaminating telomerase activity by analyzing a heat-treated aliquot of the sample. Heat treatment will remove contaminating telomerase activity but will not impact on artifacts caused by contaminating DNA and/or extraneous primer interactions (Fig. 3b, lane 10).
21. We prepare samples in a biological safety cabinet that is sterilized with a UV light between uses.
22. Gloves should be worn during all steps of the assay and changed after handling positive controls, samples and PCR products.
23. Change your gloves after handling SK-N-SH lysates.
24. Due to inherent variability among different PCR machines, the PCR cycling programs recommended above may need to be tested and optimal conditions empirically determined.
25. Dissociation curves of amplified products should align and have uniform peaks. Alignment of the dissociation curves at a specific melting temperature indicates a consistent DNA base content for the bulk of the PCR products. Dissociation curves that have deviating peaks may be indicative of PCR artifacts or contamination (Fig. 3b). To distinguish telomerase amplification products from artifacts and/or contamination, Q-TRAP amplified products may be resolved by PAGE (Fig. 3b) and/or samples may be analyzed using the conventional TRAP method.
26. During the real-time PCR steps of the Q-TRAP assay, the fluorescent SYBR green dye binds to double-stranded amplicons to generate fluorescent signal that accumulates in parallel with the amplification products. For quantification of the

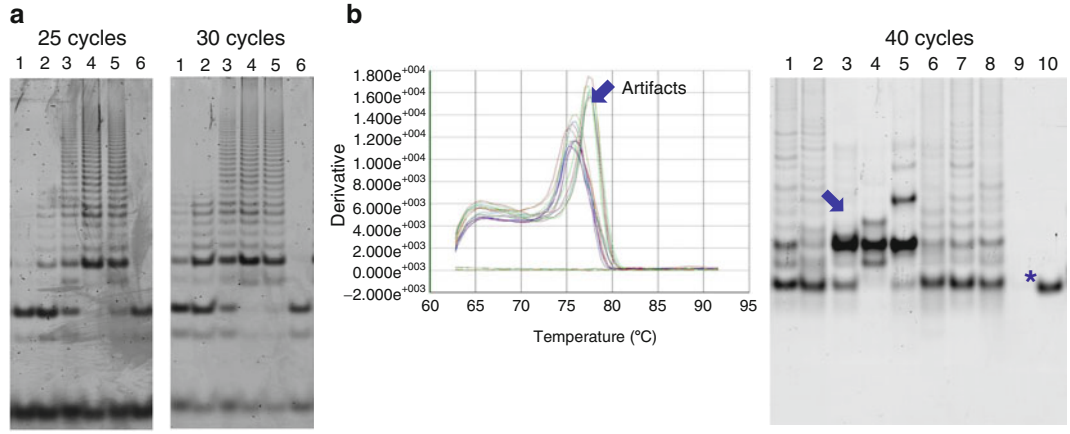

Fig. 3. *TRAP and Q-TRAP artifacts.* (**a**) Absence of high molecular weight bands following 25 cycles of standard TRAP in *lanes 1–2* suggest the presence of an inhibitor that restricts telomerase enzyme processivity. *Lanes 1–3*; ex vivo expanded myeloid cells grown under three alternate conditions. *Lane 4*; SK-N-SH neuroblastoma cell line, *Lane 5*; HeLa cervical cancer cell line, *Lane 6*; MRC-5 normal fetal lung fibroblasts. (**b**) *Left panel*; PCR artifacts evident as a shift in the peaks of the dissociation curves from Q-TRAP (*left panel*). *Right panel*; resolution of Q-TRAP products by PAGE confirmed extraneous amplification products. *Lanes 1–6*; ex vivo expanded myeloid cells grown under various conditions. Artifacts indicated by the *arrow* in *lanes 3*, *4*, *5* correspond with the shifted dissociation curves (*left panel*). *Lane 7*; HeLa cervical cancer cell line, *Lane 8*; SK-N-SH neuroblastoma cell line, *Lane 9*. MRC-5 normal fetal lung fibroblasts, *Lane 10*. Heat-treated SK-N-SH (primer artifact indicated by *asterisk*).

telomerase extension product (indicative of telomerase enzyme activity), a threshold is set for fluorescence intensity within the exponential phase of the amplification reaction. The cycle number at the threshold (*Ct*) is indicative of the starting material and hence the amount of telomerase enzyme activity in the cell lysate (22, 24).

27. An accurate threshold setting will ensure maximum sensitivity and reproducibility. We find the baseline and threshold automatically set by the ABI software allow reproducible quantitation of qTRAP data; however, these settings may be adjusted. To determine whether the automatic baseline setting is appropriate, view the amplification curves on the linear scale and check whether the earliest amplification emerges two cycles after the baseline stop value. If so, no adjustments need to be made, otherwise set the baseline limit to two cycles before the earliest amplification.

28. A standard curve with a slope of −1.4 has a dynamic linear range where the *Ct* values correlate linearly with the log10 of the standard protein concentrations. We do not use data from experiments when the slope of the regression line for standards is greater than −1.1 or less than −1.5. Re-quantitation of standard control lysate and/or additional replicates may address pipetting errors or inaccurate protein quantification, which may compromise the linearity of the

readings. Optimization of the PCR conditions may also be required to improve the standard curve.

29. Threshold cycle (*Ct*) values of telomerase-positive samples should fall within the range of the standard curve. We routinely use 10 ng of cell lysate for tumor-derived cell lines and 25 ng for primary hematopoietic cells. However, the amount of your unknown/test sample may need to be adjusted to obtain *Ct* values within the range of the standard curve. Other reports indicate that *Ct* values generally increase linearly up to 1 μg of input material, while signals are inhibited when more than 2 μg of sample is added to the reaction (22).
30. Change gloves after handling positive controls.
31. Caution should be taken when handling polyacrylamide as it is neurotoxic. Contact with the skin should be avoided. Handle acrylamide, TEMED and APS with care in the fumehood. Gel(s) should be prepared just before use.
32. Change gloves after handling PCR products.
33. Loading dye may be detected under filters used for Cy-5, thereby interfering with the image of the TRAP products. Washing the gel for 3–4 h in 1× TAE will remove the loading dye and enable acquisition of a clearer gel image.
34. In the standard TRAP assay, the TSNT internal control band may not be visible in samples with high telomerase activity because amplification of the TS extension products is competitive with TSNT amplification (Fig. 2, lanes 5 and 7; Fig. 3a, lane 4). Absence of both the TSNT internal control and the 6 bp increment ladder may indicate the presence of polymerase inhibitors or may be the result of suboptimal thermocycling. Inhibitors of the telomerase enzyme reaction may be evidenced by discontinuation of the TRAP ladder and absence of high molecular weight bands (Fig. 3a, lanes 1–2). The presence of enzyme inhibitors may be tested by repeating the assay on a dilution series. Detection of TRAP products in the diluted samples, but not the undiluted sample would be indicative of an inhibitor.
35. Primer slippage may occur during the PCR reaction as a result of the repeat sequence in the template. It may be evident as double/faint bands approximately two bases below the evenly spaced bands produced by the genuine telomerase signal.

Acknowledgments

The authors have no conflicts of interest to declare. Children's Cancer Institute Australia for Medical Research is affiliated with the University of New South Wales and Sydney Children's Hospitals

Network. Funding: National Health and Medical Research Council Career Development Fellowship (510378), National Health and Medical Research Project Grants (568704, 1007911), Cancer Council NSW Project Grant (08-03), and Cancer Institute New South Wales Scholar Award (09/RSA/1-26).

References

1. Harley CB, Futcher AB, Greider CW (1990) Telomeres shorten during ageing of human fibroblasts. Nature 345:458–460
2. Hastie ND, Dempster M, Dunlop MG, Thompson AM, Green DK, Allshire RC (1990) Telomere reduction in human colorectal carcinoma and with ageing. Nature 346:866–868
3. Olovnikov AM (1973) A theory of marginotomy. The incomplete copying of template margin in enzymic synthesis of polynucleotides and biological significance of the phenomenon. J Theor Biol 41:181–190
4. Moyzis RK, Buckingham JM, Cram LS, Dani M, Deaven LL, Jones MD, Meyne J, Ratliff RL, Wu JR (1988) A highly conserved repetitive DNA sequence, (TTAGGG)n, present at the telomeres of human chromosomes. Proc Natl Acad Sci U S A 85:6622–6626
5. McClintock B (1941) The stability of broken ends of chromosomes in Zea mays. Genetics 26:234–282
6. Blackburn EH, Gall JG (1978) A tandemly repeated sequence at the termini of the extrachromosomal ribosomal RNA genes in Tetrahymena. J Mol Biol 120:33–53
7. d'Adda di Fagagna F, Reaper PM, Clay-Farrace L, Fiegler H, Carr P, Von Zglinicki T, Saretzki G, Carter NP, Jackson SP (2003) A DNA damage checkpoint response in telomere-initiated senescence. Nature 426:194–198
8. Blackburn EH, Greider CW, Henderson E, Lee MS, Shampay J, Shippen-Lentz D (1989) Recognition and elongation of telomeres by telomerase. Genome 31:553–560
9. Greider CW, Blackburn EH (1989) A telomeric sequence in the RNA of tetrahymena telomerase required for telomere repeat synthesis. Nature 337:331–337
10. Morin GB (1989) The human telomere terminal transferase enzyme is a ribonucleoprotein that synthesizes TTAGGG repeats. Cell 59:521–529
11. Mitchell JR, Wood E, Collins K (1999) A telomerase component is defective in the human disease dyskeratosis congenita. Nature 402:551–555
12. Cohen SB, Graham ME, Lovrecz GO, Bache N, Robinson PJ, Reddel RR (2007) Protein composition of catalytically active human telomerase from immortal cells. Science 315:1850–1853
13. Greider CW, Blackburn EH (1985) Identification of a specific telomere terminal transferase activity in Tetrahymena extracts. Cell 43:405–413
14. Kim NW, Piatyszek MA, Prowse KR, Harley CB, West MD, Ho PL, Coviello GM, Wright WE, Weinrich SL, Shay JW (1994) Specific association of human telomerase activity with immortal cells and cancer. Science 266:2011–2015
15. Kim NW, Wu F (1997) Advances in quantification and characterization of telomerase activity by the telomeric repeat amplification protocol (TRAP). Nucleic Acids Res 25:2595–2597
16. Counter CM, Gupta J, Harley CB, Leber B, Bacchetti S (1995) Telomerase activity in normal leukocytes and in hematologic malignancies. Blood 85:2315–2320
17. Broccoli D, Young JW, de Lange T (1995) Telomerase activity in normal and malignant hematopoietic cells. Proc Natl Acad Sci U S A 92:9082–9086
18. Hiyama K, Hirai Y, Kyoizumi S, Akiyama M, Hiyama E, Piatyszek MA, Shay JW, Ishioka S, Yamakido M (1995) Activation of telomerase in human lymphocytes and hematopoietic progenitor cells. J Immunol 155:3711–3715
19. Wright WE, Piatyszek MA, Rainey WE, Byrd W, Shay JW (1996) Telomerase activity in human germline and embryonic tissues and cells. Dev Genet 18:173–179
20. Falchetti ML, Levi A, Molinari P, Verna R, D'Ambrosio E (1998) Increased sensitivity and reproducibility of TRAP assay by avoiding direct primers interaction. Nucleic Acids Res 26:862–863
21. Herbert BS, Hochreiter AE, Wright WE, Shay JW (2006) Nonradioactive detection of telomerase activity using the telomeric repeat amplification protocol. Nat Protoc 1:1583–1590
22. Hou M, Xu D, Bjorkholm M, Gruber A (2001) Real-time quantitative telomeric repeat

amplification protocol assay for the detection of telomerase activity. Clin Chem 47:519–524

23. Fu B, Quintero J, Baker CC (2003) Keratinocyte growth conditions modulate telomerase expression, senescence, and immortalization by human papillomavirus type 16 E6 and E7 oncogenes. Cancer Res 63: 7815–7824
24. Livak KJ, Schmittgen TD (2001) Analysis of relative gene expression data using real-time quantitative PCR and the 2(-Delta Delta C(T)) Method. Methods 25:402–408

Chapter 15

Methods for the Assessment of Telomere Status

Asako J. Nakamura

Abstract

Most methods for examining telomere functionality have relied on measurements of telomeric DNA by hybridization or quantitative PCR. While these techniques yield measures of telomeric DNA length, they generate whole-population results. However, telomeric DNA lengths on different chromatids even in the same cell are usually heterogeneous. Also, these measurements do not reveal whether a particular telomere contains the critical minimum DNA length to be functional. Therefore, in order to gain a more complete knowledge of cellular health, an alternative method that reveals the functional status of each individual telomere is needed. Based on the fact that a dysfunctional telomere induces a DNA damage response, we developed a novel technique which combines a DNA damage marker with fluorescence in situ hybridization (FISH) of telomeric DNA on metaphase chromosomes to assess the functional status of individual telomeres. This technique reveals not only whether the telomeric DNA in each chromatid is significantly shortened, but also whether the telomere has induced a DNA damage response, i.e., has become dysfunctional. We describe here in detail the protocols for simultaneous assessment of telomere length and functionality.

Key words: γH2AX, DNA damage, Fluorescence in situ hybridization, Immunofluorescence, Telomere

1. Introduction

The DNA double strand break (DSB) is one of the most potentially lethal DNA lesions, increasing cellular risk for both genomic instability and carcinogenic transformation if not repaired properly (1). To ensure proper repair, the cell contains multiple cellular pathways for DSB repair. A key factor in the recognition and subsequent repair of DNA DSBs is histone H2AX (1). Immediately after DSB induction, hundreds of H2AX molecules surrounding the DNA break site are phosphorylated by phosphoinositide 3-kinases (PI 3-kinases) (2–6). These phosphorylated H2AX,

Lorenzo Galluzzi et al. (eds.), *Cell Senescence: Methods and Protocols*, Methods in Molecular Biology, vol. 965,
DOI 10.1007/978-1-62703-239-1_15,

called γH2AX, molecules form foci at individual DSB sites, foci, which can be easily visualized by immunocytochemistry with specific antibodies against γH2AX. It is for these reasons that the use of γH2AX in the detection and quantification of DNA DSBs is expanding (7, 8).

Both normal cellular processes and exogenous genotoxic stresses induce DNA DSBs in cells (1). One normal cellular process is senescence, often associated with telomere shortening. Because DNA polymerases do not replicate the DNA double helix completely, telomerases are needed to maintain telomere length. However, since most differentiated cells lack telomerase, telomeric DNA shortens during each round of DNA replication (9, 10). At some point, the shortened telomeric DNA results in an unprotected chromatid end with DNA double strand ends (DSEs) that activate a DNA damage response (11). Many studies have demonstrated the association between the increased number of γH2AX foci and telomere shortening during both cellular senescence and mammalian aging, indicating that cellular senescence-associated shortened telomeres are also marked by the presence of DNA DSB repair proteins (12–16). In addition, telomeres may also become dysfunctional under exogenous stress, such as when the binding of telomere binding protein, telomere repeats factor 2 (TRF2), is inhibited. γH2AX forms in the telomeric chromatin, which serves to recruit other DNA DSB repair proteins (11). These findings bring attention to the idea that monitoring of DNA DSB repair proteins via γH2AX could be useful in the detection of dysfunctional telomeres. Recently, we developed a new technique to evaluate the telomere status using γH2AX immunostaining on metaphase chromosomes (16, 17) (Fig. 1). This technique permits localization of γH2AX foci to either the chromatid arms, scored as non-telomeric DNA damage, or to chromatid ends, scored as telomeric DNA damage (Fig. 2). Additionally, telomere-FISH carried out simultaneously with γH2AX immunostaining provides an independent indication of the length of telomeric DNA in these chromatids. Thus, telomeric DNA damage may be further classified by fluorescence in situ hybridization (FISH) status into (1) γH2AX positive/FISH-positive telomeres due to opened telomeric loops (Fig. 2b), and (2) γH2AX positive/FISH-negative telomeres due to shortened telomeric DNA (Fig. 2c). With these methods to characterize the status of each telomere in a cell, researchers could better evaluate telomere maintenance, cellular senescence, and organismal aging. Importantly, such methods might help measure the efficacy of telomere maintenance-targeted cancer therapy.

Below is a detailed methodological description for the assessment of dysfunctional telomeres using γH2AX immunostaining combined with telomere-FISH on metaphase chromosomes.

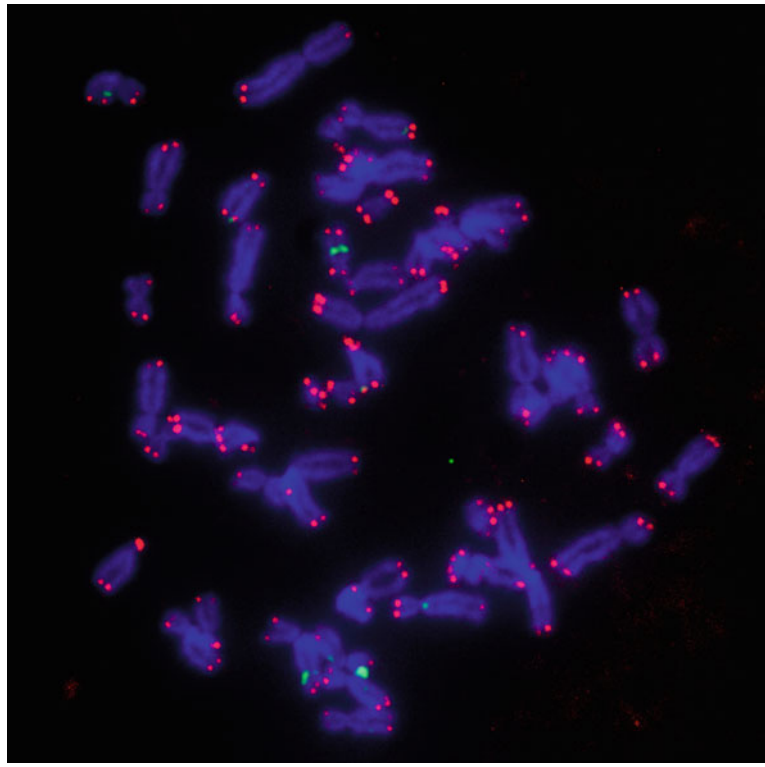

Fig. 1. Representative image of a metaphase spread with γH2AX immunostaining and telomere-FISH. Metaphase chromosomes are prepared from telomerase (hTERT) expressing-fibroblast cells (WI38). Green, γH2AX; *red*, telomere-FISH; *blue*, DNA stained with DAPI.

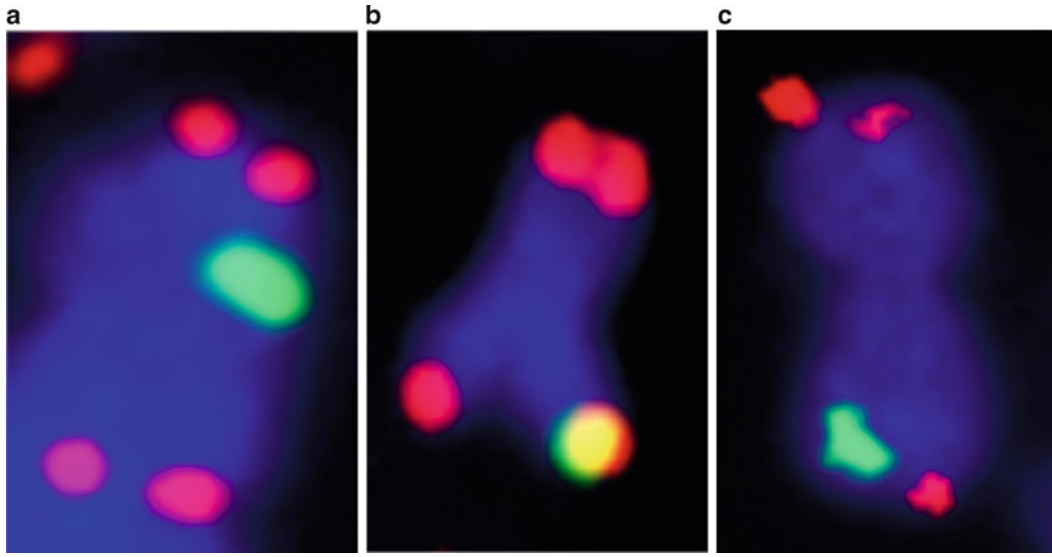

Fig. 2. Representative images of chromatids with various telomere statuses based on γH2AX staining and telomere-FISH. (**a**) γH2AX focus localizes in the chromatid arm, corresponding to non-telomeric DNA damage. (**b**) γH2AX focus localizes at chromatid end with telomere-FISH, corresponding to opened-telomeric loops. (**c**) H2AX focus localizes at chromatid end without telomere-FISH, corresponding to extremely shortened telomeres. *Green*, γH2AX; *red*, telomere-FISH; *blue*, DNA stained with DAPI.

2. Materials

2.1. Preparation of Metaphase Spreads

1. T-25 cell culture flask.
2. Colcemid, 10 μg/mL (Invitrogen, Carlsbad, CA, USA) (see Note 1).
3. Hypotonic buffer: 40 mM glycerol, 10 mM Tris–HCl (pH 7.4), 20 mM NaCl, 20 mM KCl, 1.0 mM $CaCl_2$, and 0.5 mM $MgCl_2$ (see Note 2).
4. 15 mL conical centrifuge tubes.
5. Microscopic superfrost plus slides (Thermo Fisher Scientific, Waltham, MA, USA) (see Note 3).
6. Coplin glass jars (Electron Microscopy Sciences, Hatfield, PA, USA).
7. Cytocentrifuge and supplies.
8. 80% Ethanol (EtOH) (see Note 4).
9. Acetone (see Note 5).

2.2. Immuno-cytochemistry

1. PBS-TT: (0.5% Tween-20 and 0.1% Triton X-100 in PBS) (see Note 6).
2. 5% Bovine serum albumin (BSA) in PBS (see Notes 7 and 8).
3. Liquid-repellent slide marker pen (Pap Pen) (Daido Sangyo, Tokyo, Japan).
4. Primary antibodies: mouse monoclonal anti-γH2AX (Abcam, Cambridge, MA, USA) (see Notes 9 and 10).
5. Secondary antibodies: goat anti-mouse Alexa Fluor 488-conjugated IgG (Invitrogen) (see Note 11).
6. EtOH solutions: 70, 85, and 99% EtOH (see Note 12).

2.3. Telomere-FISH

1. Telomere PNA FISH kit/Cy3 (DAKO, Glostrup, Denmark).
2. *N*,*N*-Dimethylformamide (DMF).
3. 250 mM Ethylene glycol-*bis* (succinic acid *N*-hydroxy-succinimide ester) (EGS) (Sigma-Aldrich) (see Notes 13 and 14).
4. Heat block.
5. EtOH solutions: 70, 85, and 99% EtOH (see Note 12).
6. Slide mounting medium (Electron Microscopy Science) with 50 ng/mL DAPI. (see Note 15).
7. Nail polish.
8. Epi-fluorescence inverted microscope Olympus IX70 (Olympus America, Center Valley, PA).

3. Methods

3.1. Preparation of Metaphase Spreads

1. Proliferating cell cultures grown at 37°C in T-25 flask to 80% confluence are treated with 50 ng/mL colcemid for 1.5 h. The concentration of colcemid and incubation time should be optimized for each cell type (see Note 16).
2. Gently aspirate the medium from the flask.
3. Gently add 3 mL of hypotonic buffer and rinse cells (see Note 17).
4. Gently aspirate the hypotonic buffer from the flask.
5. Add hypotonic buffer to the culture and incubate for 15 min at 37°C to swell the cells (see Notes 18 and 19).
6. After 15 min, pipet the hypotonic buffer over the surface several times to loosen the mitotic cells (see Note 20).
7. Adjust the volume of hypotonic buffer to optimize the concentration of mitotic cells to 50,000 cells/mL.
8. Prepare slides by cytospining 200 µL of cell suspension for 8 min at 366 × *g*.
9. Air-dry the specimens.
10. Incubate the slides with –20°C pre-chilled 80% EtOH at –20°C for at least 30 min.
11. Rinse the slides with –20°C pre-chilled acetone at RT for 10 s and dry (see Notes 21 and 22) (Fig. 3).

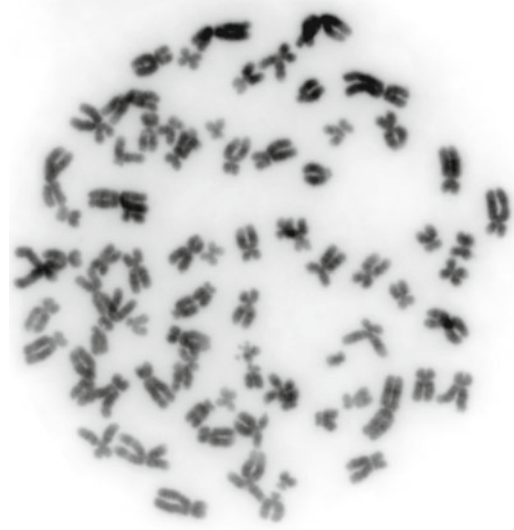

Fig. 3. Representative image of suitable metaphase spread for γH2AX staining and telomere-FISH. Metaphase chromosomes are stained by DAPI.

3.2. Immunocytochemistry

1. Mark a circle around the specimen area using a liquid-repellent slide marker pen.
2. Rehydrate specimens with PBS at RT for 5 min.
3. Incubate the specimens in PBS-TT containing 5% BSA for 1 h at RT.
4. Wash the specimens in PBS once for 5 min.
5. Incubate the specimens with the primary antibody at a 500× dilution in PBS containing 1% BSA for 2 h at RT.
6. Wash in PBS twice for 5 min each.
7. Incubate the specimens with secondary antibody at a 400× dilution in PBS containing 1% BSA for 1 h at RT. After this step, the specimen should be protected from lights.
8. Wash in PBS three times for 5 min each.

3.3. Telomere-FISH

1. Incubate the specimens with 50 mM EGS for 2.5 min at RT (see Note 23).
2. Wash in TBS three times for 5 min each.
3. Incubate the specimens with Pretreatment Solution from the DAKO FISH kit for 10 min at RT (see Note 24).
4. Wash in TBS three times for 5 min each.
5. Dehydrate the specimens with 70% pre-chilled EtOH, 85% pre-chilled EtOH and 99% pre-chilled EtOH for 2 min each at RT and air-dry (see Note 25).
6. Apply 7.5 μL of Telomere Probe solution from the DAKO FISH kit onto the specimens.
7. Place a cover slip on the specimen (18 × 18 mm).
8. Denature the specimen on a heat block for 3 min at 85°C (see Note 24).
9. Hybridize in a humid chamber for 30 min at RT. This can be a closed plastic box with damp paper towels placed in the bottom (see Note 26).
10. Immerse the slide in Rinse Solution from the DAKO FISH kit to remove the cover slip.
11. Incubate the specimen in Wash Solution from the DAKO FISH kit for 5 min at 65°C.
12. Dehydrate the specimen with 70% pre-chilled EtOH, 85% pre-chilled EtOH, and 99% pre-chilled EtOH for 2 min each in this order at RT and air-dry.
13. Add mounting medium containing DAPI and apply a cover slip. Seal the edges of the cover slip with nail polish (see Note 27).
14. Perform imaging and image analysis (see Note 28).

3.4. Imaging and Image Analysis

1. Using a fluorescent microscope, select metaphase spreads with nonoverlapping chromosomes.
2. Capture images of the whole metaphase spread.
3. Capture images of at least ten metaphase spreads from each slide.
4. Evaluate telomere status using γH2AX foci position and telomere-FISH signal by eye in images opened in Adobe Photoshop or Corel Paint Shop Pro software (see Note 29) (Fig. 2).

4. Notes

1. This colcemid solution is stored at 4°C and is ready to use, but the expiration date can differ with different manufacturers. Several other companies also sell ready-to-use colcemid solution (Cat #D1925 from Sigma-Aldrich).
2. The hypotonic solution is stored at RT and is stable at least for 1 year.
3. These slides have a positively charged-surface for better specimen attachment, and are preferred to those with silane or poly-L-Lysine coatings. MAS-GP type A slides from MATSUMAMI (Cat #S9901) are also compatible.
4. 80% EtOH should be stored at −20°C and be cold at the time of application.
5. Acetone should be stored at −20°C and be cold at the time of application.
6. PBS-TT is stored at RT. It is stable at least for 6 months.
7. 5% of BSA in PBS-TT is used for blocking.
8. 5% of BSA in PBS-TT should be prepared at the time of use.
9. This antibody is now discontinued. Several antibodies from Abcam (ab26350) or other companies (ex. 05-636: Millipore) could work with the same quality.
10. Primary antibody needs to be diluted before use with PBS containing 1% BSA.
11. Secondary antibody needs to be diluted before use with PBS containing 1% BSA.
12. EtOH should be stored at −20°C and be cold at the time of application.
13. Although several chemicals can be used for fixation, EGS is preferred for fixation in the combination of immunostaining and FISH.
14. 250 mM of EGS stock should be diluted in DMF. It is stable at RT for at least 6 months.

15. Mounting medium containing 50 ng/mL DAPI is stored at 4°C before application.
16. For an immortalized cell line, such as HeLa, we use 50 ng/mL of colcemid for 1–1.5 h. For primary human fibroblast, we use 100 ng/mL of colcemid for 3 h.
17. Perform this step gently to not disturb the mitotic cells.
18. The amount of hypotonic buffer added depends on the concentration of cells released into the buffer. For example, we use 1.5 mL of hypotonic buffer for primary cell strains and 3 mL for immortalized cell lines.
19. Optimize this incubation time by cell type. A longer incubation time creates metaphase chromosomes that are more swollen. The balance between time for colcemid treatment and time for hypotonic buffer incubation is important to obtain optimally condensed chromosomes.
20. Pipet the buffer over the growth surface forcefully enough to dislodge mitotic cells, but not so forcefully as to dislodge non-mitotic cells.
21. Although the dried slides can be stored at 4°C for up to a few days, better results are obtained if the immunostaining step is performed immediately or after overnight storage at the latest.
22. The quality of the preparations is checked by staining the specimens with DAPI and observing them under a fluorescent microscope before starting the immunostaining. If there are too few metaphase spreads or the quality of the metaphase chromosomes is poor, it is better to re-prepare the metaphase spreads. A representative image of an optimal metaphase spread is shown in Fig. 3.
23. To obtain optimum results with the combination of immunocytochemistry and FISH, it is necessary to balance the fixation and denaturing steps. Too long a fixation time will interfere with the denaturation step and degrade the FISH signal, while too long a denaturation time will degrade the immunocytochemistry signal. For human cells, a fixation time of 2.5 min and a denaturing time of 3 min works well, but for mouse cells with longer telomeric DNA, a fixation time of 3 min and a denaturing time of 5 min is better.
24. This pretreatment solution can be replaced by proteinase K solution. The concentration of proteinase K should be modified depending on the samples.
25. However, the kit's protocol mentions that the slide can be stored in 99% EtOH before conducting the telomere-FISH; this is not recommended for the combination of immunostaining with FISH. The immunostaining would be lost during storage.

Therefore, we highly recommend performing the telomere-FISH without a break.

26. For optimal results, it is essential to prevent the specimens from drying. Make sure that the chamber has sufficient humidity.
27. Before sealing with nail polish, slides should be stored at RT at least for 15 min to make sure the mounting medium spreads over the whole specimen.
28. Slides can be stored at 4°C overnight. If slides need to be stored more than a day, they should be stored at –20°C.
29. Classification is performed based on the γH2AX foci position. As mentioned above, γH2AX foci indicate both DSB and DSE. γH2AX focus localizing at chromatid arm is corresponding to non-telomeric damage (Fig. 2a). γH2AX focus localizing at chromatid ends is corresponding to telomeric damage (Fig. 2b, c) and can be further classified in to two statuses. γH2AX positive/FISH-positive telomere which is corresponding to opened telomeric loops and recognized as DSE with long telomere length (Fig. 2b). γH2AX positive/FISH-negative telomere, which is corresponding to critically short telomere and recognized as DSE (Fig. 2c).

Acknowledgment

The author thanks W.M. Bonner, National Cancer Institute, NIH, for critical reading of the manuscript.

References

1. Bonner WM, Redon CE, Dickey JS, Nakamura AJ, Sedelnikova OA, Solier S, Pommier Y (2008) gammaH2AX and cancer. Nat Rev Cancer 8:957–967
2. Rogakou EP, Pilch DR, Orr AH, Ivanova VS, Bonner WM (1998) DNA double-stranded breaks induce histone H2AX phosphorylation on serine 139. J Biol Chem 273: 5858–5868
3. Rogakou EP, Boon C, Redon C, Bonner WM (1999) Megabase chromatin domains involved in DNA double-strand breaks in vivo. J Cell Biol 146:905–916
4. Fernandez-Capetillo O, Lee A, Nussenzweig M, Nussenzweig A (2004) H2AX: the histone guardian of the genome. DNA Repair (Amst) 3:959–967
5. Stiff T, O'Driscoll M, Rief N, Iwabuchi K, Lobrich M, Jeggo PA (2004) ATM and DNA-PK function redundantly to phosphorylate H2AX after exposure to ionizing radiation. Cancer Res 64:2390–2396
6. Stiff T, Walker SA, Cerosaletti K, Goodarzi AA, Petermann E, Concannon P, O'Driscoll M, Jeggo PA (2006) ATR-dependent phosphorylation and activation of ATM in response to UV treatment or replication fork stalling. EMBO J 25:5775–5782
7. Dickey JS, Redon CE, Nakamura AJ, Baird BJ, Sedelnikova OA, Bonner WM (2009) H2AX: functional roles and potential applications. Chromosoma 118:683–692
8. Redon CE, Nakamura AJ, Zhang YW, Ji JJ, Bonner WM, Kinders RJ, Parchment RE, Doroshow JH, Pommier Y (2010) Histone gammaH2AX and poly(ADP-ribose) as clinical pharmacodynamic biomarkers. Clin Cancer Res 16:4532–4542

9. Watson JD (1972) Origin of concatemeric T7 DNA. Nat New Biol 239:197–201
10. Olovnikov AM (1973) A theory of marginotomy. The incomplete copying of template margin in enzymic synthesis of polynucleotides and biological significance of the phenomenon. J Theor Biol 41:181–190
11. Takai H, Smogorzewska A, de Lange T (2003) DNA damage foci at dysfunctional telomeres. Curr Biol 13:1549–1556
12. d'Adda di Fagagna F, Reaper PM, Clay-Farrace L, Fiegler H, Carr P, Von Zglinicki T, Saretzki G, Carter NP, Jackson SP (2003) A DNA damage checkpoint response in telomere-initiated senescence. Nature 426:194–198
13. Bakkenist CJ, Drissi R, Wu J, Kastan MB, Dome JS (2004) Disappearance of the telomere dysfunction-induced stress response in fully senescent cells. Cancer Res 64: 3748–3752
14. Herbig U, Jobling WA, Chen BP, Chen DJ, Sedivy JM (2004) Telomere shortening triggers senescence of human cells through a pathway involving ATM, p53, and p21(CIP1), but not p16(INK4a). Mol Cell 14:501–513
15. Sedelnikova OA, Horikawa I, Zimonjic DB, Popescu NC, Bonner WM, Barrett JC (2004) Senescing human cells and ageing mice accumulate DNA lesions with unrepairable double-strand breaks. Nat Cell Biol 6:168–170
16. Nakamura AJ, Chiang YJ, Hathcock KS, Horikawa I, Sedelnikova OA, Hodes RJ, Bonner WM (2008) Both telomeric and non-telomeric DNA damage are determinants of mammalian cellular senescence. Epigenetics Chromatin 1:6
17. Nakamura A, Sedelnikova OA, Redon C, Pilch DR, Sinogeeva NI, Shroff R, Lichten M, Bonner WM (2006) Techniques for gammaH2AX detection. Methods in enzymology 409:236–250

Chapter 16

Detection of Nuclear Envelope Alterations in Senescence

Clea Bárcena, Fernando G. Osorio, and José Maria Pérez Freije

Abstract

Gene mutations that cause defects in the nuclear envelope are responsible for progeroid syndromes, characterized by exacerbated cell senescence and accelerated aging. Consequently, morphological abnormalities of the nucleus represent a cellular phenotype whose analysis allows for both the characterization of the consequences of particular mutations and the assessment of the impact of approaches aimed at reversing their pathological effects. To obtain reliable results, systematic and reproducible procedures are required. Here, we describe a simple fluorescence microscopy-based protocol to detect nuclear envelope alterations in the study of cellular senescence.

Key words: Barrier to autointegration factor (BAF), Chromatin, Confocal microscopy, HGPS, Immunofluorescence, Laminopathy, Lamins, NGPS, Nuclear envelope, Progeria

1. Introduction

Cellular senescence, the irreversible cell cycle arrest triggered by dysfunctional telomeres, genotoxic stress, and oncogenic signaling, has been proposed to contribute to organismal aging since its discovery (1). This view has been supported by findings such as the reduced proliferative capacity of primary cells from advanced-age donors and the age-associated increase in the number of senescent cells in normal tissues (2). However, a causative role of cellular senescence in organismal aging has remained difficult to demonstrate conclusively (3). In this regard, the recent report by Baker et al. demonstrating that the clearance of senescent cells delays age-related phenotypes in vivo provides substantial support to the relevance of senescence for aging biology (4).

The understanding of the different cellular and molecular aspects of aging benefits from the study of segmental accelerated aging syndromes, characterized by the early manifestation of

Lorenzo Galluzzi et al. (eds.), *Cell Senescence: Methods and Protocols*, Methods in Molecular Biology, vol. 965,
DOI 10.1007/978-1-62703-239-1_16,

physiological alterations normally associated to old age (5, 6). Some human progeroid syndromes, such as Werner syndrome, are caused by defects in genomic maintenance systems (6, 7). By contrast, other accelerated aging syndromes are due to alterations in the nuclear lamina, derived from mutations in genes encoding protein components of this structure or factors involved in their maturation or dynamics. These syndromes are known as progeroid laminopathies, being Hutchinson–Gilford progeria syndrome (HGPS) (8, 9) and Nestor-Guillermo progeria syndrome (NGPS) (10, 11) paradigmatic examples of this class of accelerated aging diseases.

The nuclear lamina is a complex meshwork of proteins that underlies the inner nuclear membrane (12). The main protein components of this structure are the lamins A, C, B1, and B2, which are of high relevance to the maintenance of the nuclear shape among some other important functions including regulation of the gene expression, organization of the chromatin and signal transduction (13). Lamins A and C are encoded by the same gene, *LMNA*, through a process of alternative splicing. Lamins have a common structure consisting of an N-terminal domain, an α-helical domain, and a globular C-terminal domain. The C-terminal domain of lamins A and B ends with a CaaX motif, which undergoes farnesylation in the cysteine residue, the proteolytic removal of the –aaX peptide and the methylation of the carboxyl group of the prenylated cysteine residue (14). Unlike Lamin B, prelamin A undergoes one last proteolytic step executed by the protease FACE-1/ZMPSTE24 that removes the last 15 amino acids of the protein, including the farnesylated residue (15). HGPS is caused by a point mutation in exon 11 of *LMNA* that activates a cryptic splicing site, yielding a transcript without the last 150 bases of this exon. The resulting truncated protein, known as progerin or LAΔ50, lacks the recognition site for the second proteolytic cleavage carried out by FACE1/ZMPSTE24 and in consequence it remains constitutively farnesylated (16, 17). At the cellular level, the accumulation of this protein causes dramatic defects in the structure and function of the nuclear envelope which eventually cause accelerated cell senescence and organismal aging (18). Interestingly, accumulation of progerin and alteration of nuclear morphology have also been described in human physiological aging (19).

The investigation of the mechanisms underlying the development of progeroid laminopathies has relied on the culture of fibroblasts from patients and on the use of animal models carrying mutations in genes encoding lamina components or enzymes involved in their maturation (20). In this regard, the generation of *Face1/Zmpste24*-defficient mice by our group yielded a murine model phenocopying most physiological alterations characteristic of HGPS. This murine model allowed to identify this protease as responsible for the proteolytic cleavage (15) and enabled to define

some essential characteristics of this syndrome such as exacerbated p53 signaling (21), defects in the biology of stem cells (22), hyperactivation of autophagy (23), defective IGF signaling (24) or epigenetic alterations associated with accelerated aging (25). Moreover, Zmpste24-deficient animals together with the more recently generated *Lmna*^{G609G} knock-in mice have facilitated the preclinical in vivo testing of anti-progeria pharmacological approaches (24, 26–28).

All these studies rely largely on methods that allow testing at the cellular level the phenotypic alterations caused by particular mutations or, conversely, their reversal upon genetic of pharmacological interventions. The experimental approaches used to this end need to provide reproducible results and, at the same time, be simple enough to allow the researcher to carry out a number of experiments to obtain statistically significant results in a feasible time scale. In the context of progeroid laminopathy-related senescence, the most commonly used methods are based on the quantification of structural abnormalities of cell nuclei, since alterations in the nuclear lamina result in easily observable disruption of the normal nuclear shape. Thus, most normal cells present round or oval nuclei with a smooth surface, but in cells with nuclear envelope defects it is common to observe nuclei with a "C" shape, blebs, and infoldings. By quantifying the amount of nuclei with aberrations we can estimate the amount of harm in this individual, tissue or cell type. Importantly, this effect can be found not only in diseases related to nuclear lamina defects but also in physiological aging and other disorders including cancer (5, 19, 29). Here we describe a simple fluorescence microscopy-based protocol to detect nuclear envelope alterations in the study of cellular senescence.

2. Materials

2.1. Reagents and Solutions

- Human skin fibroblasts from control subjects (AG10803) and from HGPS patients who carried the *LMNA* p.Gly608Gly mutation (16, 17) (Coriell Cell Repository, Camden, NJ, USA).
- Human skin fibroblasts from control subjects and from NGPS patients who carried the *BANF1* p.Ala12Thr mutation (10).
- Mouse skin fibroblasts derived from control and *Lmna*$^{G609G/G609G}$ progeroid mice (18).
- Growth medium: Dulbecco's modified Eagle's medium supplemented with 10% fetal bovine serum (Gibco) and 1% antibiotic–antimycotic; stored at 4°C.
- 1× Dulbecco's Phosphate-Buffered Saline (DPBS) without Ca^{2+} and Mg^{2+}; stored at room temperature (RT).

- 0.1% Gelatin solution (w/v in distilled water); stored at 4°C.
- 4% Paraformaldehyde (PFA) solution (v/v in DPBS); stored at RT.
- 0.5% Triton X-100 (v/v in DPBS); stored at RT.
- Immunofluorescence blocking solution: 15% goat serum solution (v/v) prepared in DPBS.
- TBS-T buffer: 20 mM Tris–HCl (pH 7.4), 150 mM NaCl, and 0.05% Tween 20.
- Antibodies: Manlac-1 mouse monoclonal antibody against Lamin A/C (provided by G. Morris) and AlexaFluor-488 goat anti-mouse IgG (molecular probes).
- DAPI (4,6′-diamidino-2-phenylindole dihydrochloride, Roche) solution (1 μg/mL in mounting media for fluorescence Vectashield, Vector Labs); stored at 4°C.
- Distilled water.

2.2. Equipment

- Tissue culture 12-well plate (polystyrene flat bottom).
- Cover glasses (18 × 18 mm).
- Microscope slide glass.
- Hemocytometer.
- Tweezers.
- Inverted phase contrast microscope.
- Confocal or fluorescent microscope.

3. Methods

3.1. Cell Growth and Attachment to the Cover Glasses

- Place sterilized 18 × 18 mm cover glasses in the corresponding wells of a 12-well plate.
- Prepare gelatin-coated cover glasses by adding enough gelatin solution to cover the bottom of the dish. Incubate the plate for at least 30 min at 37°C, aspirate the excess of gelatin, and wash with DPBS.
- Count the number of cells and plate an appropriate number to each well. The recommended cellular density in the well is approximately a 50–60% of confluency (i.e., $1.25–2.5 \times 10^5$ cells per 12-well plate in the case of fibroblasts) (see Note 1).
- Allow for cell attachment overnight.
- Remove growth medium, wash twice with DPBS and fix cells with 4% PFA for 10 min at room temperature.

3.2. Lamin A/C Immunofluorescence

Wash twice with DPBS and then permeabilize cells with 0.5% Triton X-100 (v/v) prepared in DPBS for 5 min at RT.

- Aspirate the permeabilization solution, wash twice with DPBS, and block nonspecific antigen sites with 15% goat serum prepared in DPBS (v/v) for 30 min at 37°C.
- Aspirate blocking solution and incubate cells with the mouse monoclonal antibody against Lamin A/C (Manlac-1, dilution 1:50 in 15% goat serum solution) for 1–3 h at room temperature.
- Wash cells twice with TBS-T.
- Incubate cells with secondary antibody AlexaFluor-488 goat anti-mouse IgG (dilution 1:500 in 15% goat serum solution) for 1 h in the dark.
- Aspirate the antibody solution and wash twice with TBS-T.

3.3. DAPI Staining and Mounting of Fluorescence Preparations

- Prepare the microscope slides; in the place where the cover glass will be placed, add an appropriate volume of DAPI-mounting media solution to completely cover it (10–20 μL for 18 × 18 mm cover glasses) (see Note 2).
- Take carefully the cover glasses out of their well by holding them with a pair of tweezers. Wash with distilled water and place it on the correspondent slide.
- Put a piece of absorbent paper over the slide and press gently but firmly the cover glass against the slide. After that, seal the edges with varnish or similar, and keep the slides in the dark at 4°C until observation (see Note 3).

3.4. Microscopic Analysis

- An elevated number of nuclei should be analyzed in the microscope for this analysis; we suggest counting at least 200 nuclei per sample. We usually make these experiments by using a blind approach and three or more data sets per sample are recorded for the statistical analysis.
- Nuclei with a smooth oval surface are considered as normal, whereas nuclei with blebs, a vast irregular shape or multiple folds will be counted as abnormal nuclei (see Note 4) (Figs. 1 and 2).
- The statistical differences between nuclear lines are analyzed with an unpaired Student's *t* test.

4. Notes

1. This same protocol could be used for any other type of adherent cells, taking into account that some aspects such as the number of cells for plating could be variable depending on the cellular characteristics of each cell line.

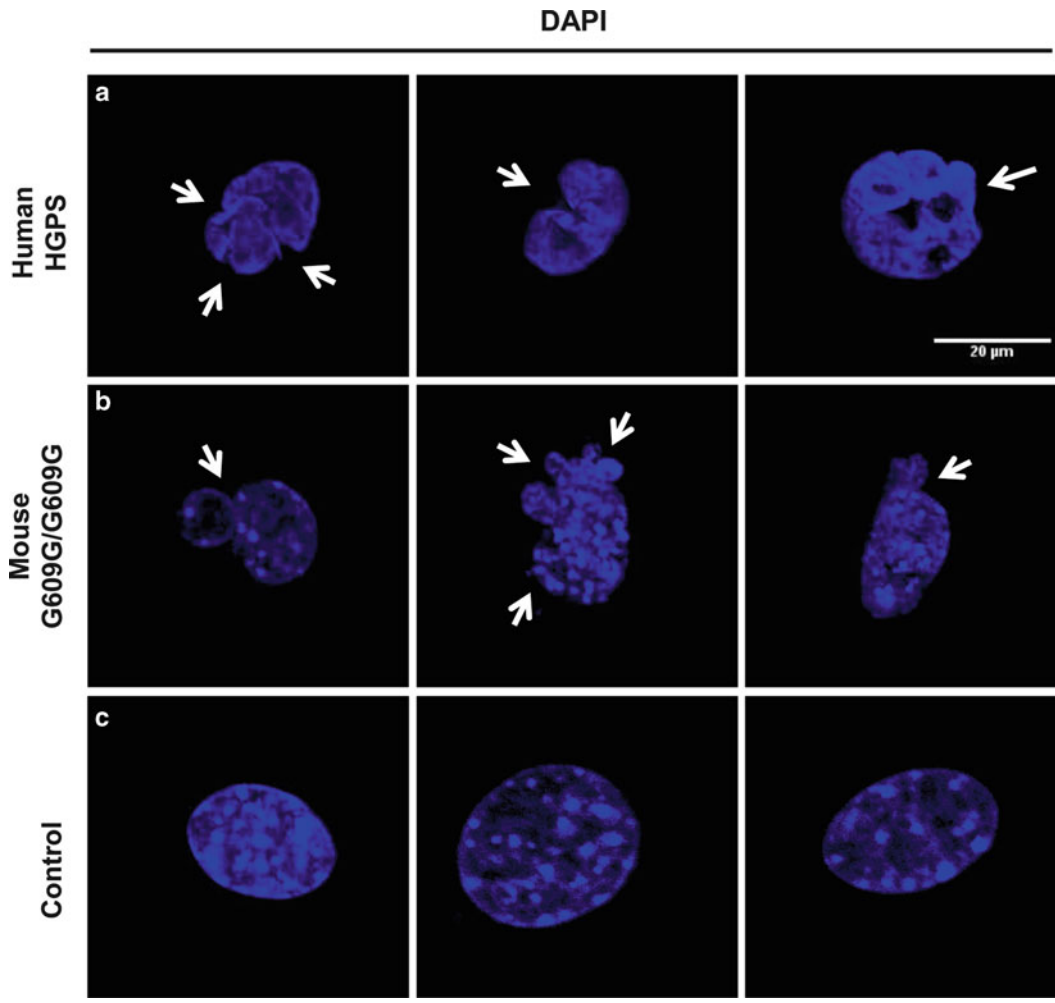

Fig. 1. Nuclear envelope alterations in progeroid laminopathies. Nuclei morphology was visualized by DAPI staining and confocal microscopy in human fibroblasts from a patient with Hutchinson–Gilford Progeria Syndrome (**a**), mouse fibroblasts carrying the mutation *Lmna*$^{G609G/G609G}$ (**b**) and wild-type murine fibroblasts as control (**c**). Three independent nuclei per genotype are shown. White *arrowheads* indicate representative examples of abnormal nuclei.

2. Permeabilization and blocking steps are not necessary for DAPI staining. If immunofluorescence is not going to be performed, go directly from Subheading 3.1, step 5 to Subheading 3.3, step 1.
3. Slides can be stored in a dark place at room temperature for up to 1 year.
4. Note that both wild-type cells and cells with a senescent phenotype derived from some sort of mutations increase the number of misshapen nuclei as they are passed in culture. This means that the number of misshapen nuclei in cells that are, for example, at passage 5 is smaller than the number of abnormal nuclei at passage 20. Thus, control cells and cells in study should be at the same passage.

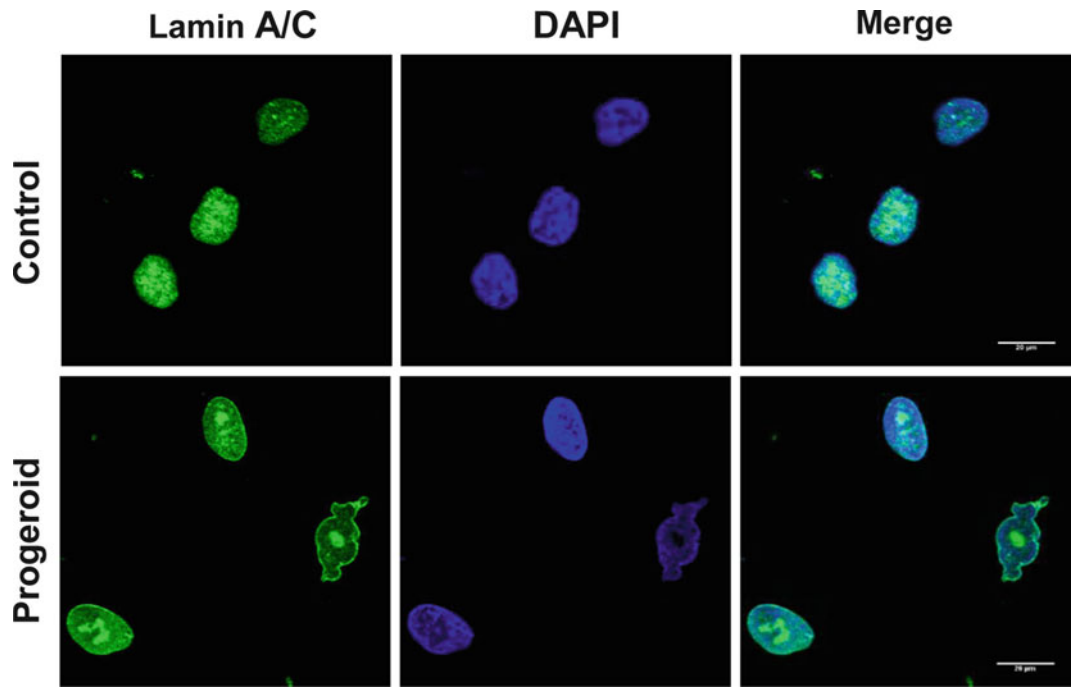

Fig. 2. Lamin A/C immunofluorescence of human fibroblasts from a Nestor-Guillermo Progeria Syndrome (NGPS) patient. Nuclear envelope architecture analyzed with an anti-lamin A/C antibody and counterstained with DAPI in control and progeroid *BANF1*$^{A12T/A12T}$ human fibroblasts. Nuclei with aberrant shapes are easily found in the fibroblasts of NGPS patients.

Acknowledgments

We thank C. López-Otín and G. Velasco for their support and assistance. We are also grateful to Prof. Glenn Morris for kindly providing anti-lamin A/C Manlac-1 antibody. The work in our laboratory is supported by grants from Ministerio de Ciencia e Innovación-Spain, Fundación Botín and European Union (FP7 MicroEnviMet). The Instituto Universitario de Oncología is supported by Obra Social Cajastur and Acción Transversal del Cáncer-RTICC. C.B. and F.G.O. are recipients of FPU fellowships from Ministerio de Educación, Cultura y Deporte-Spain.

References

1. Hayflick L (1985) Theories of biological aging. Exp Gerontol 20:145–159
2. Jeyapalan JC, Sedivy JM (2008) Cellular senescence and organismal aging. Mech Ageing Dev 129:467–474
3. Campisi J (2011) Cellular senescence: putting the paradoxes in perspective. Curr Opin Genet Dev 21:107–112
4. Baker DJ, Wijshake T, Tchkonia T, LeBrasseur NK, Childs BG, van de Sluis B, Kirkland JL, van Deursen JM (2011) Clearance of p16Ink4a-positive senescent cells delays ageing-associated disorders. Nature 479:232–236
5. Ramirez CL, Cadinanos J, Varela I, Freije JM, Lopez-Otin C (2007) Human progeroid syndromes, aging and cancer: new genetic and

epigenetic insights into old questions. Cell Mol Life Sci 64:155–170

6. Burtner CR, Kennedy BK (2010) Progeria syndromes and ageing: what is the connection? Nat Rev Mol Cell Biol 11:567–578
7. Garinis GA, van der Horst GT, Vijg J, Hoeijmakers JH (2008) DNA damage and ageing: new-age ideas for an age-old problem. Nat Cell Biol 10:1241–1247
8. Hennekam RC (2006) Hutchinson–Gilford progeria syndrome: review of the phenotype. Am J Med Genet A 140:2603–2624
9. Merideth MA, Gordon LB, Clauss S, Sachdev V, Smith AC, Perry MB, Brewer CC, Zalewski C, Kim HJ, Solomon B, Brooks BP, Gerber LH, Turner ML, Domingo DL, Hart TC, Graf J, Reynolds JC, Gropman A, Yanovski JA, Gerhard-Herman M, Collins FS, Nabel EG, Cannon RO 3rd, Gahl WA, Introne WJ (2008) Phenotype and course of Hutchinson–Gilford progeria syndrome. N Engl J Med 358: 592–604
10. Puente XS, Quesada V, Osorio FG, Cabanillas R, Cadinanos J, Fraile JM, Ordonez GR, Puente DA, Gutierrez-Fernandez A, Fanjul-Fernandez M, Levy N, Freije JM, Lopez-Otin C (2011) Exome sequencing and functional analysis identifies BANF1 mutation as the cause of a hereditary progeroid syndrome. Am J Hum Genet 88:650–656
11. Cabanillas R, Cadinanos J, Villameytide JA, Perez M, Longo J, Richard JM, Alvarez R, Duran NS, Illan R, Gonzalez DJ, Lopez-Otin C (2011) Nestor-Guillermo progeria syndrome: a novel premature aging condition with early onset and chronic development caused by BANF1 mutations. Am J Med Genet A 155A:2617–2625
12. Bridger JM, Foeger N, Kill IR, Herrmann H (2007) The nuclear lamina. Both a structural framework and a platform for genome organization. FEBS J 274:1354–1361
13. Gruenbaum Y, Margalit A, Goldman RD, Shumaker DK, Wilson KL (2005) The nuclear lamina comes of age. Nat Rev Mol Cell Biol 6:21–31
14. Meshorer E, Gruenbaum Y (2008) Gone with the Wnt/Notch: stem cells in laminopathies, progeria, and aging. J Cell Biol 181:9–13
15. Pendas AM, Zhou Z, Cadinanos J, Freije JM, Wang J, Hultenby K, Astudillo A, Wernerson A, Rodriguez F, Tryggvason K, Lopez-Otin C (2002) Defective prelamin A processing and muscular and adipocyte alterations in Zmpste24 metalloproteinase-deficient mice. Nat Genet 31:94–99
16. De Sandre-Giovannoli A, Bernard R, Cau P, Navarro C, Amiel J, Boccaccio I, Lyonnet S, Stewart CL, Munnich A, Le Merrer M, Levy N (2003) Lamin a truncation in Hutchinson–Gilford progeria. Science 300:2055
17. Eriksson M, Brown WT, Gordon LB, Glynn MW, Singer J, Scott L, Erdos MR, Robbins CM, Moses TY, Berglund P, Dutra A, Pak E, Durkin S, Csoka AB, Boehnke M, Glover TW, Collins FS (2003) Recurrent de novo point mutations in lamin A cause Hutchinson–Gilford progeria syndrome. Nature 423: 293–298
18. Osorio FG, Ugalde AP, Marino G, Puente XS, Freije JM, Lopez-Otin C (2011) Cell autonomous and systemic factors in progeria development. Biochem Soc Trans 39:1710–1714
19. Scaffidi P, Misteli T (2006) Lamin A-dependent nuclear defects in human aging. Science 312:1059–1063
20. Osorio FG, Obaya AJ, Lopez-Otin C, Freije JM (2009) Accelerated ageing: from mechanism to therapy through animal models. Transgenic Res 18:7–15
21. Varela I, Cadinanos J, Pendas AM, Gutierrez-Fernandez A, Folgueras AR, Sanchez LM, Zhou Z, Rodriguez FJ, Stewart CL, Vega JA, Tryggvason K, Freije JM, Lopez-Otin C (2005) Accelerated ageing in mice deficient in Zmpste24 protease is linked to p53 signalling activation. Nature 437:564–568
22. Espada J, Varela I, Flores I, Ugalde AP, Cadinanos J, Pendas AM, Stewart CL, Tryggvason K, Blasco MA, Freije JM, Lopez-Otin C (2008) Nuclear envelope defects cause stem cell dysfunction in premature-aging mice. J Cell Biol 181:27–35
23. Marino G, Ugalde AP, Salvador-Montoliu N, Varela I, Quiros PM, Cadinanos J, van der Pluijm I, Freije JM, Lopez-Otin C (2008) Premature aging in mice activates a systemic metabolic response involving autophagy induction. Hum Mol Genet 17:2196–2211
24. Marino G, Ugalde AP, Fernandez AF, Osorio FG, Fueyo A, Freije JM, Lopez-Otin C (2010) Insulin-like growth factor 1 treatment extends longevity in a mouse model of human premature aging by restoring somatotroph axis function. Proc Natl Acad Sci U S A 107: 16268–16273
25. Osorio FG, Varela I, Lara E, Puente XS, Espada J, Santoro R, Freije JM, Fraga MF, Lopez-Otin C (2010) Nuclear envelope alterations generate an aging-like epigenetic pattern in mice deficient in Zmpste24 metalloprotease. Aging Cell 9:947–957
26. Varela I, Pereira S, Ugalde AP, Navarro CL, Suarez MF, Cau P, Cadinanos J, Osorio FG, Foray N, Cobo J, de Carlos F, Levy N, Freije JM, Lopez-Otin C (2008) Combined treat-

ment with statins and aminobisphosphonates extends longevity in a mouse model of human premature aging. Nat Med 14:767–772

27. Fong LG, Frost D, Meta M, Qiao X, Yang SH, Coffinier C, Young SG (2006) A protein farnesyltransferase inhibitor ameliorates disease in a mouse model of progeria. Science 311:1621–1623
28. Osorio FG, Navarro CL, Cadinanos J, Lopez-Mejia IC, Quiros PM, Bartoli C, Rivera J, Tazi J, Guzman G, Varela I, Depetris D, de Carlos F, Cobo J, Andres V, De Sandre-Giovannoli A, Freije JM, Levy N, Lopez-Otin C (2011) Splicing-directed therapy in a new mouse model of human accelerated aging. Sci Transl Med 3:106ra107
29. Prokocimer M, Margalit A, Gruenbaum Y (2006) The nuclear lamina and its proposed roles in tumorigenesis: projection on the hematologic malignancies and future targeted therapy. J Struct Biol 155:351–360

Chapter 17

Measuring Reactive Oxygen Species in Senescent Cells

João F. Passos, Satomi Miwa, and Thomas von Zglinicki

Abstract

Countless studies have implicated reactive oxygen species (ROS) and mitochondrial dysfunction in the ageing process. During cellular senescence, the ultimate and irreversible loss of replicative capacity of somatic cells grown in culture, several studies have reported increased levels of ROS associated with mitochondrial dysfunction and metabolic inefficiency. Moreover, studies have revealed that interventions modulating intracellular ROS can impact on the replicative lifespan of cultured cells, suggesting that ROS play a central role in the process. In this chapter, we present several protocols used for detection of (intra- and extracellular) ROS in live cells.

Key words: Amplex® Red, DHE, DHR123, MitoSOX™, ROS, ROS indicator dyes, Senescence

1. Introduction

Accumulating data suggest a link between reactive oxygen species (ROS) and cellular senescence (1–3). Cells undergoing cellular senescence were found to accumulate oxidation products such as protein carbonyls, protein oxidative modifications (4), lipofuscin (5, 6), and DNA damage (7). Moreover, the development of fluorescent dyes able to detect ROS in live cells has shown that senescent cells have increased intracellular ROS levels when compared to young proliferating cells (7, 8).

The main source of ROS in cells is the mitochondrial electron transport chain and mitochondria have been implicated in cellular senescence. Changes in mitochondrial function have been reported during senescence (7, 9, 10), as well as damage to mtDNA (7).

It is still unclear if ROS and mitochondrial dysfunction contribute to cellular senescence or are merely associated with it. On one hand, interventions known to reduce intracellular ROS and improve mitochondrial function have been shown to consistently

Lorenzo Galluzzi et al. (eds.), *Cell Senescence: Methods and Protocols*, Methods in Molecular Biology, vol. 965,
DOI 10.1007/978-1-62703-239-1_17,

extend the replicative lifespan of cells grown in culture (7, 11, 12). These data suggest that ROS play an important causal role in cellular senescence, possibly by preventing single-stranded breaks at telomeres, which contribute to accelerated Telomere shortening (13).

On the other hand, data suggests that ROS can be generated secondarily as cells reach senescence, as a result of activation of specific signaling pathways known to be involved in cellular senescence. Activation of Ras (14), p53 (15), p21 (10, 16), and p16 (17) has been shown to induce ROS generation, contributing to the initiation of the senescent phenotype. These observations could be explained by ROS acting as signaling molecules and therefore as outcomes of a tightly regulated signaling process (18, 19). Mechanistically, it was shown that ROS produced in senescent cells contribute to a persistent activation of a DNA damage response and thus contribute to the maintenance of the phenotype (10).

While evidence is clear in establishing ROS as major players in cellular senescence, there are still technical challenges to its detection in live cells. As discussed by others, many of the fluorescent dyes used for ROS detection are nonspecific, can be misused and the interpretation of results should be met with caution (20). Thus, while fluorescent dyes have been important in accessing intracellular ROS levels during senescence, we are still uncertain about the specific ROS and the concentrations at which they are produced.

In this chapter, we present several protocols that allow us to characterize intracellular and extracellular ROS in live cells upon induction of cellular senescence. Although dichlorodihydrofluorescein diacetate (DCFH-DA) is commonly used for the fluorescent detection of ROS in cells, we have restrained from its use because (1) it is the least specific fluorophore for ROS detection, being oxidized not only by various ROS and NOS decomposition products but also by cytochrome c and other peroxidases, (2) it is prone to artifactual amplification of the fluorescence signal via redox cycling (20), and (3) it is a good substrate for various membrane transporters including the multidrug resistance protein MDR1 that is active in stem cells, compromising cellular retention and leading to badly reproducible results.

2. Materials

2.1. Cell Culture

1. Dulbecco's modified Eagle's Medium (DMEM) with 10% fetal calf serum (FCS), 1% Penicillin/Streptomycin and 1% Glutamate.
2. Solution of trypsin-EDTA (5 g of trypsin, 2 g of EDTA per liter of distilled water).

2.2. Dihydrorhodamine 123 (DHR123) Staining of Peroxides

- Dihydrorhodamine 123 (DHR123) (Life Technologies-Invitrogen), as a powder (10 mg vial, Life Technologies-Invitrogen) or as ready-to-use 5 mM stock solution in DMSO (see Note 1).

2.3. MitoSOX™ Red Staining of Mitochondrial Superoxide

- MitoSOX™ Red (50 μg vial, Life Technologies-Invitrogen), a mitochondrial superoxide indicator (see Note 2).

2.4. DHE Staining of Cellular Superoxide

- Dihydroethidium (DHE) (hydroethidine) (Life Technologies-Invitrogen), as a powder (25 mg vial or 10 vials of 1 mg) or as a stabilized 5 mM solution (see Note 3).

2.5. Amplex® Red Reagent Measurements

- The Amplex® Red reagent (Life Technologies-Molecular probes), either as in a standard Amplex® Red reagent or in the Amplex® UltraRed reagent, in vials containing 5 mg (see Note 4).
- Horseradish peroxide (HRP) (Type VI, lyophilized powder, Sigma-Aldrich) (see Note 5).
- Hydrogen peroxide solution, 30% (w/w) in H_2O, (Sigma-Aldrich); it is approximately 9.8 M.
- Fluorescence microplate reader (the one which can read from top; we use FLUOstar Omega, BMG Labtech).
- Flat bottom, black microplates.

3. Methods

3.1. DHR123 Staining (See Note 6)

1. Cells in exponential growth phase are trypsinized, collected in DMEM plus 10% FCS, counted, washed once with PBS and centrifuged for 5 min at 400×*g*.
2. Supernatant is discarded.
3. Cell pellet is resuspended in 5 mL serum free DMEM containing 15 μL DHR123 stock solution (final DHR123 concentration 30 μM).
4. Cells are incubated at 37°C for 30 min in the dark.
5. After incubation, cells are centrifuged (400×*g*, 5 min) and supernatant discarded.
6. The pellet is resuspended in 3 mL of free serum DMEM and is immediately used for analysis (see Note 7).
7. The population of live cells is defined in a FSC/SSC dot plot and apoptotic cells and debris are excluded. Median fluorescence is determined in FL1 (logarithmic), conveniently in a FSC/FL1 dot plot. Median autofluorescence of an unstained sample is also determined.

3.2. MitoSOX™ Red Staining of Mitochondrial Superoxide (See Note 8)

1. Cells in exponential growth phase are trypsinized, collected in DMEM plus 10% FCS, counted, washed once with PBS and centrifuged for 5 min at 400 × *g*.
2. Supernatant is discarded.
3. Cell pellet is resuspended in 1 mL serum free DMEM containing 1 μL MitoSOX™ stock solution (see Notes 9–12) (final MitoSOX concentration 5 μM).
4. Cells are incubated at 37°C for 10 min in the dark.
5. After incubation, cells are centrifuged (400 × *g*, 5 min) and supernatant discarded.
6. The pellet is resuspended in 3 mL of serum free DMEM and is immediately used for analysis.
7. The population of live cells is defined in a FSC/SSC dot plot and apoptotic cells and debris are excluded. Median fluorescence is determined in FL3 (logarithmic), conveniently in a FSC/FL3 dot plot. Median autofluorescence of an unstained sample is also determined (see Note 13).
8. Mitochondrial uptake of MitoSOX as a positively charged ion is membrane potential-dependent. A fluorescence increase might thus be caused by increased superoxide production, increased membrane potential, or both. To aid the interpretation of results, experiments should be complemented by measuring membrane potential in parallel samples using TMRM or JC-1, for example (10).
9. As mitochondrial superoxide levels per cell can be affected by changes in mitochondrial density, we advice the use of Mitotracker green or NAO in a parallel sample to determine mitochondrial mass (see Note 14).
10. Alternatively, one can visualize MitoSOX fluorescence in live cells by fluorescent microscopy. Cells (5×10^4) are grown in Iwaki glass bottomed dishes (Iwaki) and then incubated with the indicated MitoSOX concentration (the same as for flow cytometry). Following 10 min incubation in the absence of light, staining solution is removed, 1 mL of free serum DMEM is added and cells are immediately visualized by fluorescence microscopy (Fig. 1).

3.3. DHE Staining of Cellular Superoxide (See Notes 8 and 15)

1. Cells in exponential growth phase are trypsinized, collected in DMEM plus 10% FCS, counted, washed once with PBS and centrifuged for 5 min at 400 × *g*.
2. Supernatant is discarded.
3. Cell pellet is resuspended in 1 mL serum free DMEM containing 1 μL DHE stock solution (final DHE concentration 5 μM).

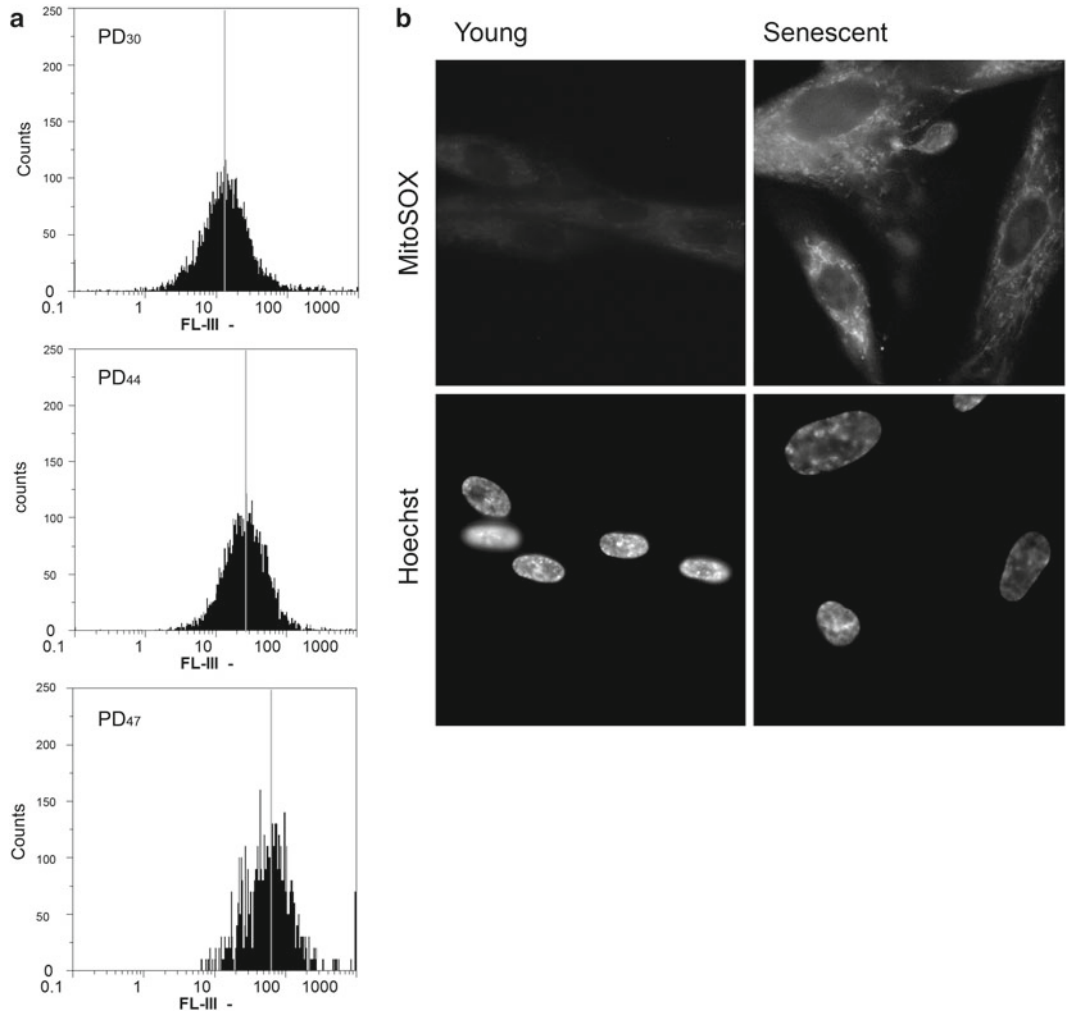

Fig. 1. (**a**) Flow cytometry histograms showing MitoSOX fluorescence distributions of human MRC5 fibroblasts at different population doublings (PD). (**b**) Fluorescent microscope images of young and senescent MRC5 fibroblasts following MitoSOX (*above*) and Hoechst (*below*) staining.

4. Cells are incubated at 37°C for 10 min in the dark.
5. After incubation, cells are centrifuged (400×*g*, 5 min) and supernatant discarded.
6. The pellet is resuspended in 3 mL of serum free DMEM and is immediately used for analysis.
7. The population of live cells is defined in a FSC/SSC dot plot and apoptotic cells and debris are excluded. Median fluorescence is determined in FL3 (logarithmic), conveniently in a FSC/FL3 dot plot. Median autofluorescence of an unstained sample is also determined.

3.4. Amplex® Red Reagent Measurements (See Note 16)

1. For preparing the working stocks for the Amplex® Red reagent (AR) (1 mM) and HRP (10 U/mL), 10 mM AR stock and 100 U/mL HRP stock should be diluted in experimental media (for example DMEM plus 10% FCS but this can be assay dependent). The working stocks should be kept on ice, and the AR working stock should be protected from light (see Note 17).
2. In order to construct the H_2O_2 standard, a stock solution needs to be prepared beforehand. H_2O_2 solution (30% w/w, which can be purchased from Sigma) should be diluted in distilled water 1,000,000 times (see Note 18).
3. Cells are trypsinized, collected in DMEM plus 10% FCS, counted, resuspended at a final concentration at a 1 million cells/mL using the experimental media and kept at 37°C.
4. Preparation of the microplate for the measurement: In a 96-well black bottom microplate, 40 μL of HRP working stock (10 U/mL) and 10 μL of AR working stock (1 mM) are pipetted to each well together with 150 μL of resuspended cells or experimental media for the blank. At least three replicates per sample (i.e., 3-wells per sample or blank) should be carried out. The final concentration of the AR is 50 μM and HRP 2 U/mL in a total of 200 μL in each well (see Notes 19 and 20).
5. Fluorescence is measured in a fluorescence microplate reader using excitation in the range of 530–560 nm and emission detection ~590 nm in a plate at 37°C. Two types of fluorescence measurements can be carried out:
   (a) End-point reading: Plates are incubated in the dark for 10 min and then measured.
   (b) Time-course reading: Fluorescence is measured kinetically for 10 min.
6. Construction of the H_2O_2 standard curve (see Note 21).
   (a) End-point reading: 0, 49, 98, 196 pmol of H_2O_2 are added to microplate (in triplicates). To do this, wells are prepared as above using the experimental media, and 5, 10, and 20 μL of H_2O_2 working stock are added corresponding to 49, 98, 196 pmol of H_2O_2 respectively. Procedure needs to be carried out fairly quickly under the protection of light.
   (b) Time course reading: This can be done either at the end of the sample reading by manually adding the H_2O_2 working stocks to the wells that have been read, or in a separate reading. Wells are prepared as above using the experimental media, and the time course reading is initialised. Reading is paused; 10 μL (for example) of the H_2O_2 stock is added to wells in triplicates and reading is resumed. This procedure can be repeated a few times. The AR fluorescence signal should increase immediately after addition of H_2O_2 and

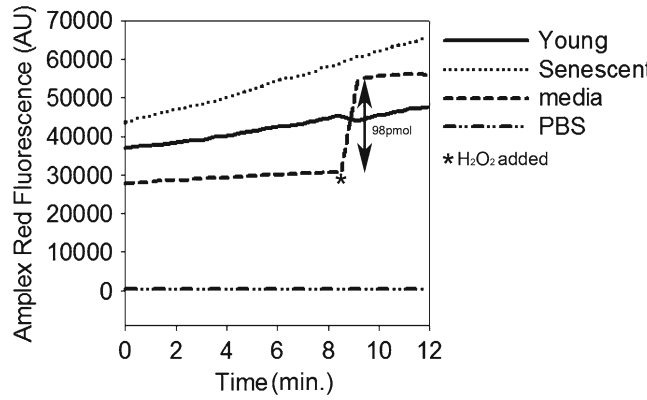

Fig. 2. A representative time-course trace of Amplex® Red assay. The rates of increase in fluorescence arbitrary units (AU) report the rate of hydrogen peroxide release to the experimental media; senescent cells have higher rates of increase than the young cells. At shortly after 8 min, a dose of hydrogen peroxide (98 pmol) is added to the well containing the media, and the increase in the AU due to the addition can be used to construct the hydrogen peroxide standard.

the difference of the fluorescence units before and after the addition corresponds to the amount of H_2O_2 added to the wells (for instance if 10 µL of the H_2O_2 working stock is added to wells, this should correspond to 98 pmol of H_2O_2) (Fig. 2).

7. Following conversion of fluorescence increase to pmol of H_2O_2 it is possible to calculate pmol H_2O_2 released from the 150,000 cells per minute.

4. Notes

1. A 10 mM stock solution of DHR123 is prepared by adding 2.89 mL DMSO to the 10 mg vial. As DHR123 is readily oxidized by air, the stock solution is immediately aliquoted under N_2 atmosphere in 100 µL each and frozen at –20°C.
2. A 5 mM stock solution is prepared by adding 13 µL DMSO to the 50 µg vial. It is advisable to divide the stock solution in 3 µL aliquots under N_2 atmosphere and freeze them at –20°C.
3. It is advisable to divide the stock solution in aliquots under N2 atmosphere and freeze them at –20°C.
4. A 10 mM stock solution can be prepared by adding 1.94 mL DMSO to each vial (containing 5 mg of the reagent), which should be aliquoted into small amounts (30–50 µL), and frozen at –20°C. All the procedures should be carried out under the protection from light.

5. The activity listed on the Certificate of Analysis of each batch can be used to convert from units to milligrams of solid. 100 U/mL stock solution can be prepared in distilled water, aliquoted, and stored frozen at –20°C. The activity of the stock solution stored in this way is found to be stable at least for 1 month.
6. Inside live cells, the colorless dihydrorhodamine 123 is oxidized, e.g., by hydrogen peroxide in the presence of peroxidases, iron or cytochrome c to form rhodamine 123. Moreover, DHR reacts also with peroxynitrite. The fluorescent product accumulates in mitochondria, even if the oxidation occurred in other organelles or the cytoplasm. Rhodamine 123 fluoresces both in FL1 (green) and FL3 (red), but we find detection to be more sensitive in FL1.
7. At room temperature and under ambient light, DHR123 fluorescence of human fibroblasts remains fairly constant for at least 1–2 h. If longer sorting times are necessary, cells should be protected from light and kept at 4°C.
8. MitoSOX™ Red reagent permeates live cells and it is targeted specifically and rapidly to mitochondria (this uptake by mitochondria is driven by the presence of a cationic triphenylphosphonium). It is a cationic derivative of DHE, which upon hydroxylation by superoxide anion emits red fluorescence (~590 nm). It becomes rapidly oxidized by superoxide but not by other ROS. However, DHE is also be oxidized by peroxynitrite or hydroxyl radicals to a product with very similar fluorescence characteristics, requiring caution in the interpretation of results as long as the superoxide-specific end product is not detected by HPLC or other analytical techniques (20). The oxidized product is highly fluorescent upon binding to nucleic acid.
9. MitoSOX™ is a derivative of ethidium bromide and should be treated with the appropriate caution. Avoid skin contact.
10. Cycles of freeze and thaw of MitoSOX™ stock solution should be avoided, and thus, storage at –20°C of aliquots of stock solution is advisable. After removal from the freezer MitoSOX™ vials and stock solutions should be allowed to warm to room temperature before use.
11. MitoSOX™ stock solutions can be immediately aliquoted under N_2 atmosphere in 5 μL each and frozen at –20°C. This allows them be stable for more than 6 months.
12. MitoSOX™ concentrations should be kept as low as possible. DHE and MitoSOX™ bind DNA easily, which greatly enhances fluorescence intensity. If the MitoSOX™ concentration is higher than the binding capacity of mitochondrial DNA, no further enhancement of the mitochondrial signal will be seen, but unspecific “spillage” into the nucleus will occur. This can

be checked by microscopy. Thus, pilot experiments should be carried out to establish dye concentration for each cell type in order to ensure that the experiments are conducted in the linear range of dye concentration.

13. For some cell types such as human fibroblasts, MitoSOX™ staining intensity is generally quite low. For that reason, when MitoSOX™ intensity is determined by flow cytometry it is essential that autofluorescence from an unstained control is subtracted, as small changes in autofluorescence can affect significantly the overall values of MitoSOX™ intensity.
14. For determination of mitochondrial mass by flow cytometry one can use Mitotracker green (a green-fluorescent mitochondrial stain which localizes to mitochondria regardless of mitochondrial membrane potential) or nonyl acridine orange (NAO) which is well retained in the mitochondria independently of mitochondrial membrane potential and binds to mitochondrial cardiolipin. NAO strongly binds to plastic including tubings in the flow cytometer and is only slowly released from these. Great care is needed not to contaminate the equipment, and unstained cells should be run as negative control after the final cleaning step.
15. DHE, also known as hydroethidine can be used to detect cellular superoxide levels. Cytosolic dihydroethidium exhibits blue fluorescence and once it is oxidized to 2-hydroxyethidium, it intercalates within DNA, staining the cell nucleus with a bright fluorescent red.
16. Amplex® Red reagent is a highly sensitive and stable probe for hydrogen peroxide (H_2O_2). In the presence of horseradish peroxidase, the Amplex® Red reagent reacts in a 1:1 stoichiometry with H_2O_2 to produce highly fluorescent resorufin; therefore it allows calculating the amount of H_2O_2 molecules being produced in the experimental system by constructing the H_2O_2 standard in parallel. The method can be applied to measure the extracellular release of H_2O_2 by cells. Advantages of the Amplex Red method are: (a) it is a direct and quantitative measurement of extracellular release of H_2O_2, (b) it is not dependent on the dye accumulation within the cells in contrast with other fluorescent ROS probes, (c) it is highly reproducible, (d) it is not necessary to remove FCS from the experimental media at the measurements. Disadvantages include: (a) the method is less sensitive because H_2O_2 is quickly degraded in most extracellular media, (b) as the method measures extracellular H_2O_2, it may not always reflect the intracellular concentration of ROS if the cells have highly active plasma membrane oxidases which can produce a large quantity of extracellular H_2O_2.
17. The working stocks of AR should be made fresh each day, and freeze–thaw cycles of the stocks should be avoided.

18. It is advisable to make a 1:1,000 dilution first, then dilute this 1,000 times again. 1 μL of this H_2O_2 working stock contains 9.8 pmol of H_2O_2.
19. Procedure has to be conducted quickly and make sure to protect AR working stock and the plate from light at all times.
20. The culture media whether containing FCS or not oxidized the AR reagent and produced a fluorescent signal in a time dependent manner, whereas PBS does not. Thus, a "blank" measurement containing AR, HRP, and media should always be conducted.
21. H_2O_2 is not stable in the culture media; we observe about half of the H_2O_2 added (at least up to micromolar range) is decomposed within 10 s in the culture media, whereas it is stable in PBS at least for 10 min. Furthermore, cells also appear to quench/consume H_2O_2, because when H_2O_2 is added to the wells with cell suspension, the fluorescence increase after H_2O_2 addition is lower than that of culture media only.

References

1. Balaban RS, Nemoto S, Finkel T (2005) Mitochondria, oxidants, and aging. Cell 120:483–495
2. Passos JF, von Zglinicki T (2005) Mitochondria, telomeres and cell senescence. Exp Gerontol 40:466–472
3. von Zglinicki T (2002) Oxidative stress shortens telomeres. Trends Biochem Sci 27:339–344
4. Ahmed EK, Rogowska-Wrzesinska A, Roepstorff P, Bulteau A-L, Friguet B (2010) Protein modification and replicative senescence of WI-38 human embryonic fibroblasts. Aging Cell 9:252–272
5. Sitte N, Merker K, von Zglinicki T, Grune T (2000) Protein oxidation and degradation during proliferative senescence of human MRC-5 fibroblasts. Free Radic Biol Med 28:701–708
6. Sitte N, Merker K, Grune T, von Zglinicki T (2001) Lipofuscin accumulation in proliferating fibroblasts in vitro: an indicator of oxidative stress. Exp Gerontol 36:475–486
7. Passos JF, Saretzki G, Ahmed S, Nelson G, Richter T, Peters H, Wappler I, Birkett M, Harold G, Schaeuble K, Birch-Machin M, Kirkwood T, von Zglinicki T (2007) Mitochondrial dysfunction accounts for the stochastic heterogeneity in telomere-dependent senescence. PLoS Biol 5:e110
8. Allen RG, Tresini M, Keogh BP, Doggett DL, Cristofalo VJ (1999) Differences in electron transport potential, antioxidant defenses, and oxidant generation in young and senescent fetal lung fibroblasts (WI-38). J Cell Physiol 180:114–122
9. Hutter E, Renner K, Pfister G, Stockl P, Jansen-Durr P, Gnaiger E (2004) Senescence-associated changes in respiration and oxidative phosphorylation in primary human fibroblasts. Biochem J 380:919–928
10. Passos JF, Nelson G, Wang C, Richter T, Simillion C, Proctor CJ, Miwa S, Olijslagers S, Hallinan J, Wipat A, Saretzki G, Rudolph KL, Kirkwood TBL, von Zglinicki T (2010) Feedback between p21 and reactive oxygen production is necessary for cell senescence. Mol Syst Biol 6:347
11. Serra V, von Zglinicki T, Lorenz M, Saretzki G (2003) Extracellular superoxide dismutase is a major antioxidant in human fibroblasts and slows telomere shortening. J Biol Chem 278:6824–6830
12. Saretzki G, Murphy MP, von Zglinicki T (2003) MitoQ counteracts telomere shortening and elongates lifespan of fibroblasts under mild oxidative stress. Aging Cell 2:141–143
13. Petersen S, Saretzki G, von Zglinicki T (1998) Preferential accumulation of single-stranded regions in telomeres of human fibroblasts. Exp Cell Res 239:152–160
14. Lee AC, Fenster BE, Ito H, Takeda K, Bae NS, Hirai T, Yu Z-X, Ferrans VJ, Howard BH, Finkel T (1999) Ras proteins induce senescence by altering the intracellular levels of

reactive oxygen species. J Biol Chem 274: 7936–7940

15. Macip S, Igarashi M, Berggren P, Yu J, Lee SW, Aaronson SA (2003) Influence of induced reactive oxygen species in p53-mediated cell fate decisions. Mol Cell Biol 23:8576–8585
16. Macip S, Igarashi M, Fang L, Chen A, Pan Z, Lee S, Aaronson S (2002) Inhibition of p21-mediated ROS accumulation can rescue p21-induced senescence. EMBO J 21: 2180–2188
17. Takahashi A, Ohtani N, Yamakoshi K, Iida S, Tahara H, Nakayama K, Nakayama KI, Ide T, Saya H, Hara E (2006) Mitogenic signalling and the p16(INK4a)-Rb pathway cooperate to enforce irreversible cellular senescence. Nat Cell Biol 8:1291–1297
18. Colavitti R, Finkel T (2005) Reactive oxygen species as mediators of cellular senescence. IUBMB Life 57:277–281
19. de Magalhaes JP, Church GM (2006) Cells discover fire: employing reactive oxygen species in development and consequences for aging. Exp Gerontol 41:1–10
20. Kalyanaraman B, Darley-Usmar V, Davies KJA, Dennery PA, Forman HJ, Grisham MB, Mann GE, Moore K, Roberts Ii LJ, Ischiropoulos H (2011) Measuring reactive oxygen and nitrogen species with fluorescent probes: challenges and limitations. Free Radic Biol Med 52:1–6

Chapter 18

Quantification of Protein Carbonylation

Nancy B. Wehr and Rodney L. Levine

Abstract

Protein carbonylation is the most commonly used measure of oxidative modification of proteins. It is most often measured spectrophotometrically or immunochemically by derivatizing proteins with the classical carbonyl reagent 2,4 dinitrophenylhydrazine (DNPH). We present protocols for the derivatization and quantification of protein carbonylation with these two methods, including a newly described dot blot with greatly increased sensitivity.

Key words: Carbonyl, 2,4-Dinitrophenylhydrazine, Dot blot, Infrared fluorescence, Protein carbonylation, Western blot

1. Introduction

Oxidative modification of proteins, both reversible and irreversible, occurs during redox signaling and other cellular processes. It also occurs as a consequence of acute or chronic oxidative stress in many conditions. The list of diseases and processes in which oxidative damage is implicated reads like a textbook of age-related diseases and includes atherosclerosis, cancer, neurodegenerative diseases such as Alzheimers and Parkinsons, and the aging process itself (1). As a consequence of the oxidative stress, cells carry an increased burden of oxidatively damaged macromolecules, including nucleic acids, lipids, and proteins. A large number of the resulting modifications of proteins have been characterized and studied (2). Protein carbonylation occurs in many of these modifications, providing an integrated assessment of oxidative damage. The National Library of Medicine's Medical Subject Headings entry for protein carbonylation notes that, "It is a standard marker for oxidative stress." (3).

The steady state level of protein carbonylation increases slowly during the first 2/3 of lifespan and then increases dramatically in

Lorenzo Galluzzi et al. (eds.), *Cell Senescence: Methods and Protocols*, Methods in Molecular Biology, vol. 965,
DOI 10.1007/978-1-62703-239-1_18,

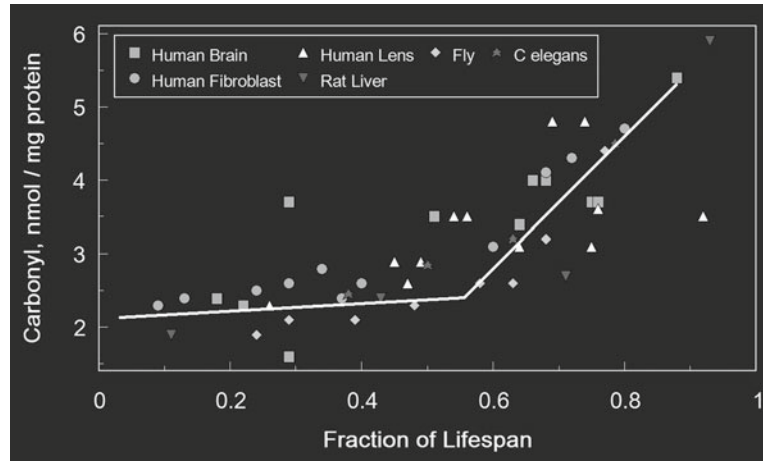

Fig. 1. Protein carbonylation increases markedly during the last third of lifespan. The data were taken from published reports: Δ, human lens (23); ●, human dermal fibroblasts in culture (24); ■, human brain at autopsy (25); ★, *Caenorhabditis elegans* (26); ▼, rat liver (27); and ◊, house fly (28).

the last 1/3 of lifespan (Fig. 1). This phenomenon can be explained theoretically by several mechanisms, but the actual underlying mechanism has not been established experimentally. While well-established to correlate with both in vivo aging and in vitro cell senescence, it remains controversial whether protein carbonylation plays a causative role in either process. However, the deleterious effects of carbonylation on protein function are well documented, providing a mechanistic basis by which protein carbonylation could have a causative role (4).

The correlation between protein carbonylation and diminished function during aging has been reported in many studies. An intriguing, early example by Carney and colleagues (5) is illustrative (Fig. 2). These investigators demonstrated that aging in gerbils was accompanied by increased protein carbonylation in the brain. The level of protein carbonylation correlated with the fractional decrease in activity of the key metabolic enzyme glutamine synthetase. As expected, the older gerbils also performed poorly on tests of cognitive function. Treatment of these older animals for 14 days with an antioxidant had the remarkable effect of reverting these three parameters to the values observed in younger animals: protein carbonylation decreased, glutamine synthetase activity increased, and cognitive function improved.

Detection and quantification of carbonylated proteins is accomplished after derivatization of the carbonyl groups. A variety of derivatizing reagents have been utilized for spectrophotometric, fluorometric, mass spectrometric, and immunochemical analysis. The most commonly employed is the classical carbonyl reagent, 2,4 dinitrophenylhydrazine (DNPH) (see Note 1), perhaps first

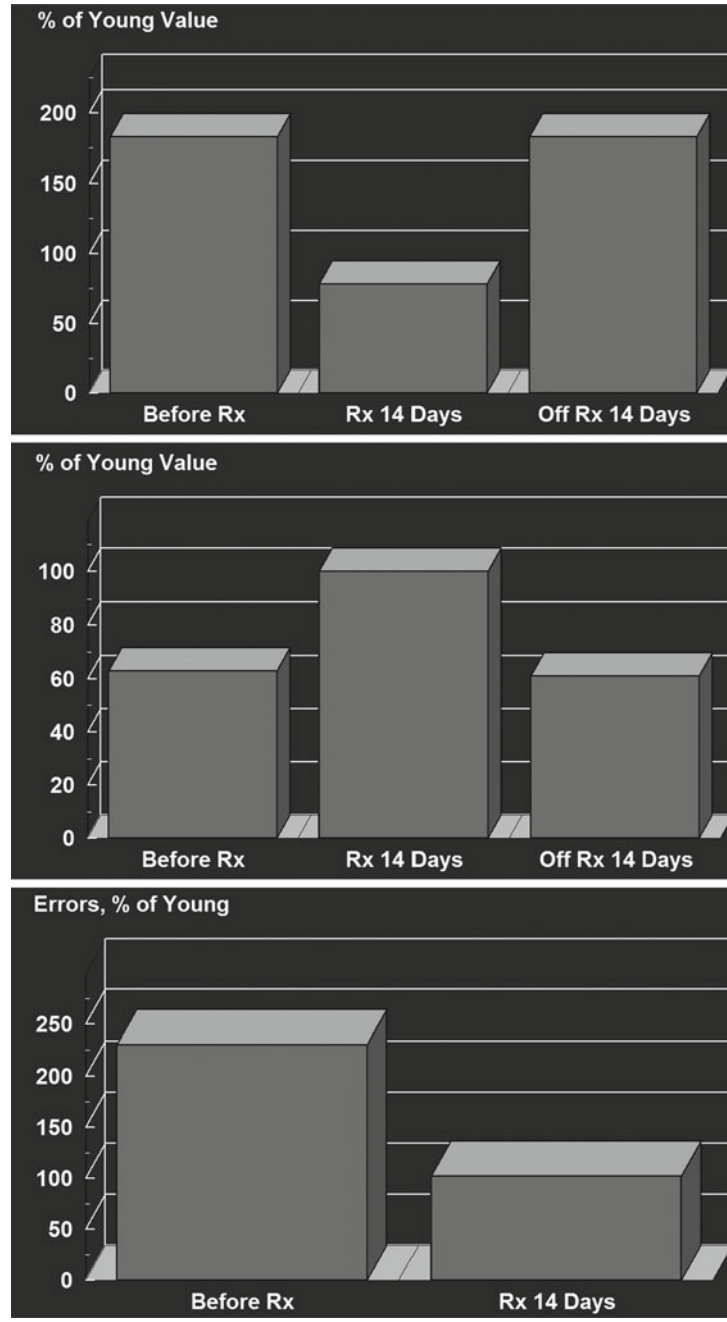

Fig. 2. Changes in the gerbil brain with aging and reversal by treatment with an antioxidant. Redrawn from (5). The gerbils were treated with an antioxidant, *N*-tert-butyl-α-phenylnitrone, for 14 days. This treatment reversed the age-related changes in the old animals and had no effect on the younger animals. Reversal required continued administration of the antioxidant; 14 days off treatment returned each parameter to the value observed before treatment. Each panel displays the results for the old animals as a percentage of the young animals. The upper panel shows brain protein carbonylation, the middle panel plots brain glutamine synthetase activity, and the lower panel presents the average number of errors on a maze.

applied to proteins by Dixon (6). Spectrophotometry was initially used for quantification of DNPH-derivatized proteins. Immunochemical detection is now more commonly utilized, either as an ELISA or as a Western blot of SDS-PAGE separated proteins. The Western blot is presently the method of choice to identify proteins that are differentially carbonylated, such as mitochondrial aconitase during aging (7). Moreover, scanning an entire lane of the blot allows determination of the total carbonyl content of the sample. Because of its much greater sensitivity, this immunochemical method has replaced the spectrophotometric method. However, the latter remains the reference method for quantification, particularly for determining the carbonyl content of standards used in other methods.

When detected with anti-DNPH antibodies carrying fluorescent labels, the Western blot is quantitative and fairly sensitive. Still, in our hands, 10–20 μg protein per sample is needed to obtain duplicate analyses. We recently developed a more sensitive dot blot method in which many samples of ~1 μL volume can be applied to one PVDF membrane, allowing convenient quantification of multiple samples with replicates (8). DNPH has limited solubility in water and many common solvents. It has limited, but sufficient solubility in strong acids, and that is the reason stock solutions are usually made in 2 M HCl. Few proteins are soluble in HCl, which will not wet PVDF membranes. These problems were obviated by employing dimethyl sulfoxide (DMSO) as solvent. It readily dissolves DNPH, wets PVDF, and is an excellent protein solvent (9). The resulting method for protein carbonylation requires ~60 ng protein for one analysis and as many samples as desired can be measured on a single PVDF membrane. It has sufficient sensitivity to allow at least triplicate determinations on individual *Drosophila* (8).

This article presents our current protocols for the spectrophotometric, Western blot, and dot blot methods. Previous publications include protocols for determination of DNPH-derivatized proteins by gel filtration and filter paper techniques and for borotritide-labeled proteins (10, 11). A number of recent reviews of proteomic methodology for determining carbonylated proteins are also available (12–15).

One should normally determine the *specific* protein carbonyl content of a sample or its component proteins and not simply the total protein carbonyl (see Note 2). This requires measurement of both the carbonyl and protein content. The specific protein carbonyl content is usually expressed with units of “mol carbonyl/mol protein” or “nmol carbonyl/mg protein.” Quantitative immunochemical detection is the most sensitive method for determining carbonyl content, but it is reliably quantitative only if the detected response is reproducible, preferably with a linear response and a wide dynamic range. Chemiluminescent detection does not have these characteristics. Fluorescent or radiochemically (I^{125}) tagged

secondary antibodies do have the desired linear response and wide dynamic range. Fluorescent-tagged secondary antibodies are readily available commercially and avoid the difficulties of in-house labeling with radioactive gamma emitters. The protocol for immunochemical detection thus employs fluorescent-tagged secondary antibodies. As explained below, we prefer use of fluorescent labels that emit in the near infrared over those that emit in the visible, but either can be used. The infrared fluorescent labels require an infrared-sensitive scanner. Our experience is limited to the Odyssey scanner (LI-COR, Lincoln, NE), but those from other manufacturers should also work.

2. Materials

2.1. Spectrophotometric Determination After Reaction with 2,4-Dinitrophenylhydrazine in 2 M HCl

- Derivatization solution: 0.2% DNPH in 2 M HCl (see Note 3).
- Derivatization blank solution: 2 M HCl.
- 20% w/v trichloroacetic acid.
- 50% absolute ethanol 50% ethyl acetate.
- 6.0 M guanidine HCl, 0.5 M potassium phosphate (pH 2.5).
- 50 μL quartz cuvette.

2.2. Immunofluorescent Western Blotting After Reaction with 2,4-Dinitrophenylhydrazine in Sodium Dodecyl Sulfate

- Derivatization solution: 20 mM DNPH in 10% trifluoroacetic acid (v/v) (see Note 3).
- Derivatization blank solution: 10% trifluoroacetic acid (v/v).
- Neutralization solution: 2 M Tris base, 30% glycerol.
- 12% sodium dodecyl sulfate (SDS). Warming the water will speed dissolution.
- Oxidized protein standards (see Note 4).
- Electrophoresis supplies: SDS PAGE gels, SDS Tris-glycine running buffer, Tris-glycine transfer buffer, as desired.
- Antibodies to the 2,4-dinitrophenyl moiety. These are available from several suppliers as monoclonal and polyclonal antibodies. We have had good experience with the goat polyclonal from Bethyl (A150-117A, Montgomery, TX). Typically a 1:10,000 dilution is used, but it is best to check the optimal dilution.
- Labeled secondary antibody to the species chosen for the primary antibody to a 2,4-dinitrophenyl moiety (see Note 5).
- 0.01% Coomassie Brilliant Blue R-250 in 50% methanol and 10% acetic acid or an equivalent stain.
- Coomassie destaining solution 40% methanol and 7% acetic acid.

- 0.01% Fast Green FCF (Sigma-Aldrich, St. Louis, MO, USA) in 30% methanol and 7% acetic acid.
- Blocking buffer tested for use in infrared fluorescence such as Odyssey blocking buffer (LI-COR, Lincoln, NE) (see Note 6).
- PBS with 0.1% Tween 20 for washing blots.
- PVDF (Immobilon-FL PVDF, Millipore, Billerica, MA) (see Note 7) or nitrocellulose membranes.

2.3. Immunofluorescent Dot Blotting After Reaction with 2,4-Dinitrophenylhydrazine in DMSO

- Stock solution: 0.5 M DNPH in dimethyl sulfoxide (DMSO); stable several months at room temperature when protected from light.
- Concentrated acetic acid and trifluoroacetic acid.
- Derivatization solution: Prepared from the stock DNPH, trifluoroacetic acid, DMSO, and water to give final concentrations of 20 mM DNPH and 0.5% trifluoroacetic acid in 92.5% DMSO. Prepare fresh daily.
- Antibodies, blocking solution, and washing solution as in Subheading 2.2.
- Fast Green FGF stain as in Subheading 2.2.
- PVDF membrane (Immobilon-FL PVDF, Millipore) (see Note 7).
- Membrane support system: 96-well polypropylene plate and a disposable plastic 96-hole grid from a Rainin tip rack to align spots above the wells.
- Rainin P-2 or other accurate small volume pipette.

3. Methods

3.1. Spectrophotometric Determination After Reaction with 2,4-Dinitrophenylhydrazine in 2 M HCl

1. Dissolve 2.0 g DNPH (dry weight) in 1,000 mL 2 M HCl.
2. Stir several hours in the dark and filter before use.
3. Protect from light. Take into account the actual content of DNPH in the reagent as most manufacturers supply DNPH with at least 30% water content.

3.1.1. Preparation of Derivatization Solution: 0.2% DNPH in 2 M HCl, 1,000 mL

3.1.2. Derivatization

1. Prepare the sample extract as desired (see Notes 8 and 9).
2. If a derivatization blank is also being prepared as is generally recommended, split the sample in half, allowing at least 200 µg protein in each 1.5 mL polypropylene tube. Concentrate by precipitation in 10% trichloroacetic acid using a slow speed centrifugation to form a loose, easily dispersed pellet. Two minutes at 2,000 × *g* is adequate.

3. Add 0.5 mL derivatization solution and vortex to suspend the sample. Treat the blank with 0.5 mL 2 M HCl without DNPH. Samples will not dissolve.
4. Allow tubes to stand 10 min at room temperature, vortexing occasionally (see Note 10).
5. Precipitate in 10% TCA; pellet using a slow speed centrifugation, carefully pouring off supernatant and draining liquid residue on a tissue.
6. Extract free DNPH from the suspended pellet with three successive 1 mL rinses with ethanol–ethyl acetate, vortexing to disperse the pellet, centrifuging for 2 min at no more than 5,000 × *g* to avoid compacting the pellet, pouring off supernatant, and draining well. Dry pellet thoroughly (see Note 11).
7. Redissolve in 200 μL 6.0 M guanidine 500 mM KCl pH 2.5, and centrifuge to remove insoluble material (see Note 12).
8. Read spectra against a blank of the same 6 M guanidine solution, measuring carbonyl at 370 nm and protein at 276 nm, calculating the results as described in Subheading 3.4.1 (see Notes 13 and 14).

3.2. Immunofluorescent Western Blotting After Reaction with 2,4-Dinitrophenylhydrazine in Sodium Dodecyl Sulfate

1. Dissolve 39.6 mg DNPH (dry weight) in 1 mL pure trifluoroacetic acid (1.54 g) in a glass tube, and dilute with vortexing to 10 mL with water.
2. Store the solution at room temperature protected from light.
3. Precipitates that appear during storage can be removed by centrifugation. Take into account the actual content of DNPH in the reagent as noted in Subheading 3.1.1.

3.2.1. Preparation of Derivatization Solution: 20 mM DNPH in 10% Trifluoroacetic Acid (v/v), 10 mL

3.2.2. Derivatization

Prepare the sample as desired (see Notes 8 and 15) and if considering dot blot assays see Note 9. Samples with protein concentrations >10 mg/mL usually require dilution to assure solubility after addition of acid. Split the sample in half if a derivatization blank is also being prepared, as is recommended when analyzing any new sample type. Prepare sufficient sample to load two identical gels with 2–5 μg total protein per lane for tissue extracts or about one-tenth that amount or less for pure proteins. Prepare carbonyl standards with at least 1, 2, and 4 pmol carbonyl per lane. Include a lane with about 0.3 μg non-oxidized protein standard to estimate protein load on the Coomassie stained gel. The volumes mentioned below always refer to the initial volume of the sample.

1. Add 1 volume of 12% SDS with mixing. Do this even if the sample contains some SDS, because it is important to have at least 6% SDS before adding the trifluoroacetic acid.
2. Add 2 volumes of the DNPH solution and mix.
3. If a blank is desired, treat it with 2 volumes of 10% trifluoroacetic acid alone.

4. Allow to stand 10 min at room temperature (see Note 10).
5. Neutralize the sample by adding roughly 1.7 volumes 2 M Tris/30% glycerol. Samples should turn golden. If not, add a little more neutralizing solution (see Note 16). Centrifuge samples.
6. Promptly load samples and standards onto duplicate gels and perform SDS gel electrophoresis (see Notes 17 and 18). Samples are not stable and should not be stored (16).
7. Transfer one gel to nitrocellulose or PVDF-FL and after transfer stain residual protein on the gel with 0.01% Coomassie Brilliant Blue R-250 stain or equivalent (see Note 19). Scan by infrared fluorescence in the 700 nm channel to determine transfer efficiency.
8. Stain and scan the gel that has not been transferred similarly to determine protein load.
9. Immunodetect the labeled proteins by infrared fluorescent Western blotting.

3.2.3. Immunological Detection (See Note 20)

1. Block the membrane 1 h.
2. Incubate 2 h with primary antibody diluted 1:10,000 in blocking buffer with 0.1% Tween 20.
3. Wash the membrane three times for 5 min with PBS containing 0.1% Tween 20.
4. Incubate 1 h with secondary antibody diluted 1:10,000 in blocking buffer with 0.1% Tween 20. Protect from light.
5. Wash the membrane three times for 5 min with PBS containing 0.1% Tween 20 and then briefly two times with water. Protect from light.
6. Detect the carbonyl signal by its infrared fluorescence in the 800 nm channel. A second fluorescent signal may be detected in the 700 nm channel. We usually use that channel to determine protein content after staining with Fast Green. We generally stain after scanning for carbonyl content since the Fast Green fluorescence might spill into the 800 nm channel (see Note 21).

3.3. Immunofluorescent Dot Blotting After Reaction with 2,4-Dinitrophenylhydrazine in DMSO

3.3.1. Preparation of Solutions

1. Stock solution of 0.5 M w/v DNPH in DMSO, 1 mL. Dissolve 99 mg DNPH (dry weight) in DMSO and bring to 1.0 mL final volume. This stock is stable at room temperature for several months protected from light. As mentioned in Subheading 3.1.1; take into account the actual content of DNPH in the reagent.
2. Derivatization solution, 5 mL: 20 mM DNPH and 0.5% trifluoroacetic acid in 92.5% DMSO. Combine 0.2 mL 0.5 M DNPH stock in DMSO, 4.4 mL DMSO, 0.025 mL trifluoroacetic acid, and 0.375 mL water in the order listed, vortexing between each addition (see Note 22).

3.3.2. Derivatization and Membrane Preparation

1. Prepare the sample as desired (see Notes 8 and 15). The buffer for dot blots can contain potassium since SDS is not present. Dry aliquots of samples and standards in a vacuum centrifuge. Skip the drying step if a DMSO solution was used for sample homogenization (see Note 23).
2. Add derivatization solution to dried proteins, including protein standards of ~150, 300, and 600 ng/μL and ~300 ng/μL for samples. Vortex vigorously. At least three carbonyl standards in the range of 0–1.0 pmol, should be included (see Note 24).
3. Wait 15 min, vortexing occasionally.
4. Set up duplicate dry PVDF membranes for protein and carbonyl blots (see Note 25). The detection limit of the Fast Green dot blot protein assay is ~150 ng. Thus, the protein measurement is done on a separate blot with more concentrated samples than those for the carbonyl blot.
5. Vortex the samples immediately before dotting. Using a Rainin P-2 or pipette of equal precision, spot a 1 μL volume of each sample and protein standard in triplicate onto PVDF and set it aside for Fast Green protein stain. Without delay, dilute the samples to approximately 60 ng/μL protein with additional derivatization solution. Vortex and spot in triplicate onto the second PVDF membrane that will be used for carbonyl determination (see Note 26).
6. Allow membranes to air dry 15 min.
7. Rinse both membranes in concentrated acetic acid twice for 2 min. After removal of the second wash, add ~5 mL acetic acid to keep the membrane wet, then add water gradually to cover the membrane. Remove the solution and replace it with water. After 5 min in the water, the membrane is ready for protein (see Note 21) or carbonyl determination as described in Subheading 3.2.3. If desired, the blots may be stored for at least 48 h before proceeding to those assays (see Note 27).

3.4. Calculations

3.4.1. Spectrophotometric Determination After Reaction with 2,4-Dinitrophenylhydrazine in 2 M HCl (10)

1. Carbonyl content may be expressed either as mol carbonyl/mol protein or as nmol carbonyl/mg protein. Carbonyl concentration in mol carbonyl/L is the sample absorbance at 370 nm divided by the molar absorptivity of the hydrazone (22,000):

$$\text{Carbonyl, M} = \frac{(A_{370})}{22{,}000}$$

2. If the molar absorptivity of the protein is known, use it for the protein calculation. If not, use $\varepsilon_{M276} = 50{,}000$ as an estimate of the molar absorptivity of a protein with average amino acid

composition and a molecular weight of 50,000 (11). The tail of the hydrazone peak absorbs in the protein region with $\varepsilon_{M276}=9{,}460$. Thus, the protein concentration is calculated with a correction for that overlap:

$$\text{Protein, M} = \frac{(A_{276} - 0.43A_{370})}{\varepsilon_{\text{M276protein}}}.$$

3. Dividing the carbonyl concentration by the protein concentration gives the specific carbonyl content of the sample with units of mol carbonyl/mol protein.
4. To summarize:

$$\text{Carbonyl, mol carbonyl/mol protein} = \frac{(A_{370})\varepsilon_{\text{M276protein}}}{(A_{276} - 0.43(A_{370})22{,}000)}.$$

5. If a blank was run, calculate it with the same equation and subtract the result from the DNPH reacted sample value.

3.4.2. Immunofluorescent Western Blotting After Reaction with 2,4-Dinitrophenylhydrazine in Sodium Dodecyl Sulfate

1. Although carbonyl can be expressed as mol carbonyl/mol protein, it is more common to use nmol carbonyl/mg protein for the Western. Using the imager software, integrate lanes in a uniform manner for all standards and samples (see Note 28).
2. Construct a calibration curve from the standards included on the blot. It should be approximately linear up to 4 pmol carbonyl/lane, so a linear regression may be fit. Do not force the regression line to include zero. Because the amount of oxidized protein standard loaded is very low, we assume that all of the protein in standards was fully transferred. The protein measurement must be accurate to obtain a valid measurement of the specific carbonyl content. The amount of protein loaded in each lane is known if a protein measurement was made on the sample before DNPH derivatization. The fractional transfer efficiency can be calculated from the protein scan of the gel before and after transfer. The protein content of each band or lane on the blot is simply:

$$(\text{Protein Loaded})(\text{Transfer Efficiency})$$

3. The specific carbonyl content of the band or lane is then obtained by dividing the carbonyl content by the protein content:

$$\text{Carbonyl, nmol/mg protein} = \frac{(\text{Carbonyl, pmol})}{(\text{Protein, } \mu\text{g})}.$$

4. Our preliminary investigations suggest that it is possible to determine both carbonyl and protein on a single western blot, obviating the need for duplicate gels to obtain the two

measurements. First scan the blot for the carbonyl signal in the 800 nm channel, then stain the blot with the Fast Green protein stain and read it in the 700 nm channel (see Note 21). Use the known protein content of the carbonyl standards to generate the standard curve for protein content.

3.4.3. Immunofluorescent Dot Blotting After Reaction with 2,4-Dinitrophenylhydrazine in DMSO

1. Integrate the scanned dots using circles of uniform diameter for standards and samples (see Note 29). The calculation is then performed as for the Western blot, Subheading 3.4.2, keeping in mind that the samples applied for carbonyl determination are more dilute than those for protein determination.

4. Notes

1. DPNH is not recommended for mass spectrometric studies. Use a method that gives a nonreversible derivatization such as reaction with a hydrazide followed by reduction to give a stable amine. A commercially available kit (Oxyblot, S7250, Millipore, Billerica, MA) is widely used for derivatization with DNPH followed by immunochemical detection, but may not be reliable because the manufacturer has made undocumented changes in composition of the reagents and the accompanying protocol (17).
2. Total carbonyl content can be misleading. For example, albumin is the dominant protein in serum, but it generally carries a low specific carbonyl content. The albumin band in a Western blot of serum will always be prominent because of the high content of albumin. In contrast, transferrin usually has a relatively high specific carbonyl content. Because the transferrin concentration in serum is much lower than that of albumin, one will miss its susceptibility to oxidative modification if the specific carbonyl content is not measured.
3. Solutions of DNPH in 2 M HCl or 10% trifluoroacetic acid develop precipitates during storage, and these can be removed by centrifugation before use. Solutions should be protected from light and are usable for months.
4. An oxidized protein stock may be prepared by oxidizing bovine albumin with copper and ascorbate (18) or by irradiation. It should be standardized by determining its carbonyl content by the spectrophotometric method. Standards of varying carbonyl content can be prepared by mixing the control and oxidized stocks. Although we have not evaluated the approach, one might be able to substitute dinitrophenylated albumin (A23018, Life Technologies, Grand Island, NY), diluting as required with unlabeled albumin.

5. We recommend using an antibody with a label, which fluoresces in the infrared region to reduce autofluorescence and increase sensitivity. If you do not have access to a scanner that operates in the infrared region, then use a label with visible region fluorescence. We do not recommend chemiluminescent detection because of the poor linear response and difficulty in calibration. When the first antibody is goat, we have typically used donkey anti-goat IgG (H+L) conjugated to IRDye 800CW (926-32214, LI-COR, Lincoln, NE) at a 1:10,000 dilution. With this antibody, fluorescence is detected in the 800 nm region, avoiding interference that may come from pre-stained molecular weight markers, plasticware, and sometimes membranes. Note that the dyes are light sensitive and care must be taken to protect such solutions and the prepared blot from light.
6. Other blocking solutions may be used but should be tested empirically for possible high background. We also use the Odyssey blocker with 0.1% Tween 20 for antibody dilutions.
7. PVDF membranes vary in their inherent infrared fluorescence, both among suppliers and from lot to lot. It is best to choose a product that is specifically tested for infrared fluorescence, such as Millipore Immobilon-FL PVDF. If it has not been tested by the manufacturer, scan a dry piece of the PVDF to assess its background fluorescence. Nitrocellulose membranes typically do not have background fluorescence issues, but they are not appropriate for many applications, because they may be damaged or even dissolved by solvents used in the application.
8. Homogenization buffer should not contain reducing agents such as dithiothreitol unless a metal chelator such as diethylene triamine pentaacetic acid (DTPA) or EDTA is present. Omission of a chelator risks oxidation of protein by adventitious metals during sample preparation through Fenton chemistry reactions leading to artifactual increases in measured carbonyl.
9. Nucleic acids are carbonyl positive, and nucleic acid contamination of extracts in the spectrophotometric carbonyl assay can cause artifactual elevation in protein carbonyl measurements. If nucleic acid contamination is suspected, streptomycin sulfate precipitation or treatment with nucleases will take care of the problem (10, 16). As a general rule, this should be done with extracts from microorganisms or cultured cells that have been transfected with vectors. It is usually is not required for extracts of higher organisms and, of course, is not needed with purified proteins.
10. A very early version of our DNPH derivatization protocol recommended a derivatization time of 1 h (10), but for many years we have recommended 10–15 min incubations to avoid

possible artifactual increases in protein-associated chromophore. Long incubations promote a non-carbonyl-dependent reaction with DNPH. Although we have not established the chemical nature of the derivative, it is consistent with formation of a hydrazide. Regardless of the chemical details, inappropriately long incubations of proteins with the DNPH reagent can cause an artifactual increase in the apparent carbonyl content.

11. Minimizing the contact time of the sample with ethanol–ethyl acetate and removing residual solvent by vacuum centrifugation has been observed to hasten dissolving of the sample in 6 M guanidine.
12. Centrifuging of the sample is recommended to avoid light scatter. Occasionally centrifugation will not remove particulates, and a light scatter correction must be made on the spectra. Light scatter increases as a power function, so a small amount of light scatter at 800 nm can cause a large artifactual increase in the 370 nm signal and thus in the calculated carbonyl values.
13. The carbonyl measurements may be read in a plate reader capable of reading UV–VIS if the exact path length of the sample solution is known or if a series of oxidized protein standards is included on the plate. This should be attempted only with very soluble proteins such as those in plasma and only after carefully inspecting representative sample spectra for scatter. UV transparent 96-well plates must be used if one wishes to measure protein in the plate reader (e.g., 3635, Corning Life Sciences, Corning, NY).
14. As an alternative to measuring protein spectrophotometrically, a microplate BCA assay can be done on the samples in 6 M guanidine after measuring the 370 nm absorbance. Protein standards must also contain the same volume of 6 M guanidine.
15. Protease inhibitor tablets should be avoided unless first tested in your immunochemical carbonyl assay. One popular tablet preparation we tested introduced smears and artifactually elevated the carbonyl measurement of Western blots. However, neither commercial nor laboratory-prepared protease inhibitor cocktail solutions have caused the problems noted with tablets. Potassium dodecyl sulfate is less soluble than SDS so the Western blot sample should not contain more than ~50 mM potassium before addition of SDS.
16. After derivatization and neutralization with the 2 M Tris base/30% glycerol, the samples may be loaded directly onto the gel and electrophoresed as usual because the sample is now in a solution similar to that used for electrophoresis by the method of Laemmli (19). Samples are not heated before analysis because heating is generally not required for reduction of disulfide

bonds, and we do not know the stability of protein-bound hydrazones to heating. When desired, β-mercaptoethanol can be added to the sample solution after neutralization. Inclusion of β-mercaptoethanol generally intensifies the bands in the chemiluminescent detection system so that it is best to either include or omit the thiol from all samples that are to be directly compared. We routinely include 2% β-mercaptoethanol.

17. The excess reagent from the sample does not interfere with gel electrophoresis or with Western blotting. This lack of interference may result from poor accessibility of the antibody to reagent on membranes, a suggestion that follows from the observation that the monoclonal antibody (D8406, Sigma, St. Louis, MO) did not detect reagent spotted directly onto the nitrocellulose. DNPH labeling of carbonylated proteins also works with isoelectric focusing gels and two-dimensional blots. Use of anti-2,4-dinitrophenyl antibodies for immunocytochemical localization of oxidized proteins and immunoaffinity purification is also feasible (20, 21), and DNPH labeled proteins immunopurified and separated on 2-D gels have been identified by MALDI-TOF analysis (21).
18. Since blot to blot variability occurs in any immunological detection, carbonyl standards must be included on each blot.
19. Coomassie Brilliant Blue R-250 quick staining method (22). Soak the gel in Coomassie Blue reagent for 10 min, destain in 30% methanol 7% acetic for 10 min, and equilibrate in water for 10 min. Measure the infrared fluorescence of the Coomassie Blue–protein complex at 700 nm in the Odyssey Imager. Coomassie G-250 stains such as Simply Blue Safestain (LC6060, Life Technologies, Grand Island, NY) can be substituted. Coomassie Blue fluoresces when bound to protein, allowing protein bands to be visualized by scanning the gel, despite high residual free Coomassie Blue.
20. The standard immunological detection protocol used in our laboratory for carbonyl Western imaging on the Odyssey Imager is provided as a guide. Incubation times have been selected for convenience and are given here because they are known to provide a linear carbonyl response. Longer incubation times with either antibody result in stronger signals, but the effect on linearity has not been studied. If desired, a second immunological target may be detected after completing the carbonyl detection. Selecting both secondary antibodies from the same species is likely to result in a lower background. Without prior testing it is not recommended to do simultaneous double detection on carbonyl blots as possible nonspecific antibody reactions may increase error.

21. Fast Green staining for protein estimate: Once the PVDF membrane is scanned for carbonyl signal in the 800 nm channel, a protein measurement can be obtained by dipping the membrane in Fast Green stain for 45 s, destaining in water, and scanning in the 700 nm channel. If validated by additional studies, this approach obviates the need for preparation of duplicate gels to separately determine carbonyl and protein. Nitrocellulose blots also may be stained with Fast Green as described previously (22).
22. We suggest preparing the DMSO derivatization solution fresh each day, although preliminary tests indicate it is stable for several days. The inclusion of 7.5% water in the derivatization mixture minimizes damage to PVDF caused by DMSO and should not be decreased.
23. An alternate homogenization technique has been tested with liver and with individual Drosophila. If homogenizing cells or tissues, the solvent is neat DMSO with 0.5% trifluoroacetic acid. No water is added to the DMSO because it will be supplied by the sample. If homogenizing a dried sample, then use 92% DMSO in water with 0.5% trifluoroacetic acid. Homogenize in a 0.5 mL microfuge tube on ice for 30 s using a plastic pestle (KT749521-0500, Kimble Chase, Vineland, NJ) and a motorized handheld homogenizer. This solvent rather effectively disrupts cell components, giving a protein recovery greater than obtained with aqueous buffers. DNA does not interfere with this dot blot method, so disruption of nuclei is not a concern. After centrifuging at 21,000 × *g* for 5 min, the supernatant can be mixed directly with DNPH derivatization solution, incubated 15 min and spotted onto the membrane.
24. We typically spot ~60 ng for samples and standards. However, the total protein content of the spot does not appear to affect the carbonyl measurement, at least when total protein is adjusted (by addition of bovine albumin) to be between 10 and 300 ng. If addition of a carrier protein is desired, for example, to avoid losses from samples of low protein content, you may add bovine albumin that is either reduced with borohydride to remove residual carbonyl or taken from a lot of low inherent carbonyl content (8). For the protein standard on the protein dot blot we use a bovine albumin solution from Pierce (23209, Rockford, IL), dried by vacuum centrifugation and diluted in derivatization solution as desired.
25. Assembly of the dotting apparatus: Lay a dry piece of PVDF membrane on a 96-well polypropylene plate and top with an alignment grid. Typically we use a flat piece of plastic with 96 holes such as that from a box of Rainin pipette tips. The assembly is taped together to avoid slippage. No backing layer

should be used because sample wicking will occur, leading to variable results. The pipette should be held vertically and the entire tip contents expelled onto the PVDF, gently touching the tip to the membrane if wished.

26. Because of the small sample volume some variation in the amount applied may occur, especially when attempting the procedure for the first time. Thus, at least triplicate dots of both protein and carbonyl samples are recommended.
27. The rinsed blots are stable for at least 2 days whether stored at −80°, in dry ice, or at room temperature. This allows blots prepared in one laboratory to be shipped to another for detection and scanning.
28. Oxidation of proteins may generate aggregates and fragments that contribute to the carbonyl content of the sample. For this reason, even when studying purified proteins, the entire lane on the gel should be integrated.
29. The dotted sample may not spread evenly on the PVDF membrane, resulting occasionally in a dense center surrounded by a more diffuse ring which should be included in the integrated area. Make sure that integration circles are large enough to accommodate the biggest dot on the blot including the diffuse ring. Use this size circle for all samples. The regression line for the carbonyl calibration curve should not be forced through zero.

References

1. Levine RL, Stadtman ER (2006) Carbonylated proteins and their implication in physiology and pathology. In: Dalle-Donne I, Scaloni A, Butterfield DA (eds) Redox proteomics: from protein modifications to cellular dysfunction and diseases. Wiley Interscience, New York, pp 123–168
2. Stadtman ER, Levine RL (2006) Chemical modification of proteins by reactive oxygen species. In: Dalle-Donne I, Scaloni A, Butterfield DA (eds) Redox proteomics: from protein modifications to cellular dysfunction and diseases. Wiley Interscience, New York, pp 3–23
3. MeSH, Medical Subject Headings. National Library of Medicine, Bethesda, MD. http://www.nlm.nih.gov/mesh/MBrowser.html. Accessed 12 Nov 2011
4. Levine RL, Stadtman ER (2001) Oxidative modification of proteins during aging. Exp Gerontol 36:1495–1502
5. Carney JM, Starke-Reed PE, Oliver CN, Landum RW, Cheng MS, Wu JF, Floyd RA (1991) Reversal of age-related increase in brain protein oxidation, decrease in enzyme activity, and loss in temporal and spatial memory by chronic administration of the spin-trapping compound N-tert-butyl-alpha-phenylnitrone. Proc Natl Acad Sci U S A 88:3633–3636
6. Dixon HB (1964) Transamination of peptides. Biochem J 92:661–666
7. Yan LJ, Levine RL, Sohal RS (1997) Oxidative damage during aging targets mitochondrial aconitase. Proc Natl Acad Sci U S A 94:11168–11172
8. Wehr NB, Levine RL (2012) Quantification of protein carbonylation by dot blot. Anal Biochem 423:241–245
9. Singer SJ (1963) The properties of proteins in nonaqueous solvents. In: Anfinsen CB (ed) Advances in protein chemistry. Academic, New York, pp 1–68
10. Levine RL, Garland D, Oliver CN, Amici A, Climent I, Lenz AG, Ahn BW, Shaltiel S, Stadtman ER (1990) Determination of carbonyl content in oxidatively modified proteins. Methods Enzymol 186:464–478

11. Levine RL, Williams JA, Stadtman ER, Shacter E (1994) Carbonyl assays for determination of oxidatively modified proteins. Methods Enzymol 233:346–357
12. Madian AG, Regnier FE (2010) Proteomic identification of carbonylated proteins and their oxidation sites. J Proteome Res 9:3766–3780
13. Toda T, Nakamura M, Morisawa H, Hirota M, Nishigaki R, Yoshimi Y (2010) Proteomic approaches to oxidative protein modifications implicated in the mechanism of aging. Geriatr Gerontol Int 10(Suppl 1):S25–S31
14. Irazusta V, Moreno-Cermeno A, Cabiscol E, Tamarit J, Ros J (2010) Proteomic strategies for the analysis of carbonyl groups on proteins. Curr Protein Pept Sci 11:652–658
15. Yan LJ, Forster MJ (2011) Chemical probes for analysis of carbonylated proteins: a review. J Chromatogr B Analyt Technol Biomed Life Sci 879:1308–1315
16. Luo S, Wehr NB (2009) Protein carbonylation: avoiding pitfalls in the 2,4-dinitrophenylhydrazine assay. Redox Rep 14:159–166
17. Wang P, Powell SR (2010) Decreased sensitivity associated with an altered formulation of a commercially available kit for detection of protein carbonyls. Free Radic Biol Med 49:119–121
18. Marx G, Chevion M (1986) Site-specific modification of albumin by free radicals. Reaction with copper(II) and ascorbate. Biochem J 236:397–400
19. Laemmli UK (1970) Cleavage of structural proteins during the assembly of the head of bacteriophage T4. Nature 227:680–685
20. Hernebring M, Brolen G, Aguilaniu H, Semb H, Nystrom T (2006) Elimination of damaged proteins during differentiation of embryonic stem cells. Proc Natl Acad Sci U S A 103:7700–7705
21. England K, Cotter T (2004) Identification of carbonylated proteins by MALDI-TOF mass spectroscopy reveals susceptibility of ER. Biochem Biophys Res Commun 320: 123–130
22. Luo S, Wehr NB, Levine RL (2006) Quantification of protein on gels and blots by infrared fluorescence of Coomassie blue and Fast Green. Anal Biochem 350:233–238
23. Garland D (1990) Role of site-specific, metal-catalyzed oxidation in lens aging and cataract: a hypothesis. Exp Eye Res 50:677–682
24. Oliver CN, Ahn BW, Moerman EJ, Goldstein S, Stadtman ER (1987) Age-related changes in oxidized proteins. J Biol Chem 262: 5488–5491
25. Smith CD, Carney JM, Starke-Reed PE, Oliver CN, Stadtman ER, Floyd RA, Markesbery WR (1991) Excess brain protein oxidation and enzyme dysfunction in normal aging and in Alzheimer disease. Proc Natl Acad Sci U S A 88:10540–10543
26. Adachi H, Fujiwara Y, Ishii N (1998) Effects of oxygen on protein carbonyl and aging in Caenorhabditis elegans mutants with long (age-1) and short (mev-1) life spans. J Gerontol A Biol Sci Med Sci 53:B240–B244
27. Starke-Reed PE, Oliver CN (1989) Protein oxidation and proteolysis during aging and oxidative stress. Arch Biochem Biophys 275:559–567
28. Sohal RS, Agarwal S, Dubey A, Orr WC (1993) Protein oxidative damage is associated with life expectancy of houseflies. Proc Natl Acad Sci U S A 90:7255–7259

Chapter 19

Assays for the Measurement of Lipid Peroxidation

Ana Cipak Gasparovic, Morana Jaganjac, Branka Mihaljevic, Suzana Borovic Sunjic, and Neven Zarkovic

Abstract

Physical and emotional stress, metabolic alterations, carcinogenesis or inflammation are conditions that can trigger oxidative stress, which is defined as a balance shift of redox reactions towards oxidation, resulting in the increase of reactive oxygen species (ROS). ROS are continuously formed in small quantities during the normal metabolism of cell, however the overproduction of ROS is cytotoxic and damages macromolecules (DNA, proteins, sugars and lipids). Polyunsaturated fatty acids (PUFAs) that are esterified in membrane or storage lipids are subject to ROS-induced peroxidation resulting in the destruction of biomembranes. Final products of lipid peroxidation (LPO) are reactive aldehydes that are relatively stable and may diffuse far from the initial site of oxidative injury and act as second messengers or free radicals. The difference between physiological and pathological oxidative stress is often the occurrence of LPO and its final toxic products. In this chapter, two classes of methods for measurement of LPO are described. The first include assays for detection of LPO at the organismal level, while the second include molecular and cellular assays that reveal the mechanistic effects of LPO on the function, morphology and viability of the cells.

Key words: ELISA, HNE, HPLC, Immunocyto/histochemistry, Lipid–derived aldehydes, LOOH, Oxidative stress

1. Introduction

1.1. Oxidative Stress

Our everyday exposure to stress, either psychological (e.g., stress at work) or environmental (e.g., pollution, cigarette smoke), provokes changes on the cellular level resulting in endogenous stress. Physical and emotional stress, infections or inflammation are conditions that can trigger overproduction of reactive oxygen species (ROS). Increase of ROS and/or decreased antioxidant defense result in the misbalance in the cell redox reactions i.e., in the state termed oxidative stress. ROS are normally formed in small quantities during metabolic processes. However, overproduction of ROS is

Lorenzo Galluzzi et al. (eds.), *Cell Senescence: Methods and Protocols*, Methods in Molecular Biology, vol. 965,
DOI 10.1007/978-1-62703-239-1_19,

cytotoxic and damages macromolecules (DNA, proteins, sugars, and lipids) (1). It is well known that LPO is generally considered to be the major mechanism of cell injury in aerobic organisms subjected to oxidative stress. LPO has a major impact on the pathology of many diseases with an oxidative etiology, such as cancer, degenerative and inflammatory diseases (2). This process proceeds through chain free radicals reactions of polyunsaturated fatty acids (PUFA). During its early stage, peroxidation of lipids results in formation of the first stabile products, lipid hydroperoxides (LOOH). The mechanism of LPO based on a radical chain reactions, starts with the abstraction of hydrogen atom producing the bisallylic radical $L^{\bullet}$ (1). The propagation steps are illustrated in reactions 2 and 3.

Initiation

$$LH \rightarrow L^{\bullet} + H^{\bullet}. \quad (1)$$

Propagation steps

$$L^{\bullet} + O_2 \rightarrow LOO^{\bullet}. \quad (2)$$

$$LOO^{\bullet} + LH \xrightarrow{k_p} LOOH + L^{\bullet}. \quad (3)$$

Termination steps

$$L^{\bullet} + L^{\bullet} \rightarrow \text{non} - \text{radical products}. \quad (4)$$

$$L^{\bullet} + LOO^{\bullet} \rightarrow \text{non} - \text{radical products}. \quad (5)$$

$$LOO^{\bullet} + LOO^{\bullet} \xrightarrow{2k_t} \text{non} - \text{radical products}. \quad (6)$$

The reaction of $L^{\bullet}$ with oxygen is close to a diffusion-controlled process, but is also reversible (reaction 2). Indeed, the peroxyl radical can undergo a very rapid fragmentation that can also serve as a useful clock for H-atom transfer from antioxidant molecules. Peroxyl radicals $LOO^{\bullet}$ can abstract a hydrogen atom to produce LOOH together with "fresh" $L^{\bullet}$ radicals to continue the chain (reaction 3). The termination steps occur either by radical–radical combination (reactions 4–6), or by attacking other molecules, such as an antioxidant or proteins.

The products of lipid degradation and decomposition are commonly expressed as conjugated dienes, as well as aldehyde end-products, which are used to assess the occurrence of oxidative stress (2).

Damage of PUFA, induced by free radicals, leads primary to the destruction of biomembranes. This can lead to changes in the permeability and fluidity of the membrane lipid bilayer while severe membrane dysfunction is usually associated with loss of viability.

Although oxidative stress has been implicated in various and numerous pathological states (e.g., inflammation, neurodegenerative diseases and cancer) LPO and oxidative stress are not only pathological but also physiological processes. Namely, oxidative stress triggers a cellular stress response thereby activating a number

of the redox-sensitive signaling cascades. At low levels oxidative stress induces protective effects but at high levels it may lead to more damaging effects. When cells are exposed to low oxidative stress levels they induce transcription factor Nrf2 that is known to regulate transcriptional activation of numerous antioxidant and detoxification enzymes (e.g., catalase). A further increase in ROS production, i.e., in oxidative stress level, can result in proinflammatory and cytotoxic effects. For example, redox-sensitive MAP kinase and NF-κB cascades are responsible for the proinflammatory effects by inducing the release of cytokines, chemokines, and adhesion molecules. Finally, high oxidative stress levels are cytotoxic and involve mitochondrial perturbation, followed by the release of proapoptotic factors and inducing apoptosis (3).

1.2. Reactive Aldehydes

Final products of LPO are reactive aldehydes such as 4-hydroxyalkenals and other similar α,β-unsaturated aldehydes. 4-Hydroxynonenal (HNE), malondialdehyde (MDA) and acrolein (4) are the most investigated aldehydes which cause increased membrane fluidity, cytosol efflux, and loss of (membrane) protein activities. As expected, vast LPO results in membrane disintegration (5) and cell death, but it cannot be resolved if it is cause or consequence of cell death (6). The α, β-unsaturated aldehydes are shown to regulate signaling kinases through function modification and thus regulate inflammation, apoptosis, and other signaling pathways (7). A great number of these aldehydes have been isolated from biological samples, where they may promote and reinforce cell damage induced by oxidative stress. Lipid-derived aldehydes are more stable than ROS and can therefore diffuse across membranes and reach the targets distant from the initial site of oxidative injury. Because of their stability and biological activity, some of them are also known as second messengers of free radicals (8, 9).

1.3. Assays for the Measurement of the Lipid Peroxidation Level

Quantification of LPO is essential to assess to role of oxidative injury in pathophysiological disorders. We can distinguish two types of methods for the measurement of LPO. The first ones include assays for the detection of the LPO level in the system, i.e., measuring the concentrations of oxidation products of lipids, proteins and DNA. The complementary methods to measurements of peroxidation are the ones measuring the concentrations of antioxidants. The second type of methods includes assays that reveal the mechanistic effect of LPO on the morphology and pathology both in vivo and in vitro. Here it has to be emphasized that in the case of reactive aldehydes it should be taken into the consideration the form of these aldehydes that is measured. Namely, they can be either free or bound to biological molecules. When they are bound, aldehydes play a real powerful biological role in cell signaling, and for this reason they are considered as bioactive markers of oxidative stress (8).

2. Materials

2.1. Common Materials

2.1.1. Disposables

- 1.5 mL microcentrifuge tubes.
- UV-dedicated cuvettes.
- Enzyme-linked immunosorbent assay (ELISA) microwell plates.
- Ni grids.
- 0.2 μm cellulose membranes.

2.1.2. Equipment

- UV/VIS spectrophotometer Varian Cary 4000.
- High-performance liquid chromatographic (HPLC) system with fluorescence detector with HPLC column ODS2, 5 μm, 4.6×150 mm.
- Microcentrifuge.
- Filtering system.
- Water bath.
- Vortex.
- HPLC system with a UV detector with a column ODS, 5 mm, 4.6×150 mm.
- Centrifuge.
- Microplate reader with filters 620 and 450 nm.
- System for electrophoresis.
- Semidry or wet blotter.
- Light microscope.
- Transmission electron microscope.

2.1.3. Common Reagents

- Phosphate buffered saline (PBS), pH 7.4: 8.08 mM Na_2HPO_4, 17.7 mM KH_2PO_4, 136.7 mM NaCl, 170 mM $CaCl_2$, 123 mM $MgCl_2$, 2.68 mM KCl.
- HNE solution: Activate HNE-dimethyl acetal by adding 1 mM HCl and incubate for 1 h at RT (see Note 1).

Ferric Thiocyanate Method Components

- Extraction solution: A cold deaerated mixture CH_2Cl_2–MeOH (2:1, v/v) (see Note 2).
- Reagent solution: Equal volumes of deaerated aqueous solution, 4.5 mM $FeSO_4 \cdot 7H_2O$ in 0.2 M HCl, and 3% deaerated methanolic solution of KSCN (see Note 3).
- 1% solution of metaphosporic acid in MeOH.

Determination of Lipid Derived Aldehydes by HPLC

- 4.4 mM MDA standard solution: 10 μL tetraethoxy-propane (TEP) in 10 mL 40% ethanol.
- 0.44 M H_3PO_4.
- 42 mM TBA.

- Alkaline methanol: Add 4.5 mL 1 M NaOH to 50 mL methanol.
- Acetonitrile/acetic acid: Mix 24 mL acetonitrile and 1 mL acetic acid.
- Mobile phase for HNE HPLC: 42% acetonitrile in distilled water.

ELISA

- BSA standards: 1% (w/v) BSA in PBS.
- Carbonate binding buffer, pH 9.6.
- Blocking solution: 5% (w/v) fat-free dry milk in PBS.
- ELISA washing buffer: 0.5 mL Tween 20/L of PBS.
- Peroxidase blocking solution: 0.1% NaN_3 and 1.5% H_2O_2 in PBS.

Immunodetection of LPO-Modified Proteins

- Nonreducing buffer for electrophoresis: 0.6055 g TRIS, 0.8766 g NaCl in 100 mL ddH_2O pH 7.5 with 1% (v/v) Triton X-100, 2% (w/v) sodium deoxycholate, and 2% (w/v) SDS. Add 1 mM PMSF immediately before use
- 10% polyacrilamide gel.
- Blocking solution: 0.5% (w/v) fat-free dry milk in PBS.
- Washing solution: 0.5 mL Tween 20/L of PBS.
- Blocking solution for ICC/IHC and ImmunoGold: 3% H_2O_2 in PBS.
- DAB (Dako, Glostrup, Denmark).
- Cacodylate buffer pH 7.2.
- Fixative for electron microscopy: 2% glutaraldehyde in cacodylate buffer.
- Post-fixative for electron microscopy: 1% osmium tetroxide in cacodylate buffer.
- Uranyl acetate.
- Reynolds lead nitrate solution.

3. Methods

3.1. Quantitative Analysis of Lipid Hydroperoxides

Spectrophotometric quantification of LOOH is used to follow accurately the initial or early stages of the LPO process (10). This method is a highly accepted and popular method of analysis, which has appeared applicable to different interdisciplinary LPO studies. At the same time, LOOH were earlier proposed as good indicators of the LPO low levels (11). Quantitative analysis of LOOH is not a straightforward task. On the one hand, LOOH molecules are unstable unless special precautions are undertaken; on the other hand, due to the lack of the characteristic chromophores, LOOH molecules are mostly devoid of convenient spectroscopic features

in the UV and VIS parts of the optical spectrum. The indirect method for determination of LOOH described here is reliable assay and does not dependent on laborious and expensive equipment. The development of the response is fast and the method is suitable for multiple sample analysis. The spectrophotometric method is based on the oxidation of ferrous with LOOH to ferric ion and subsequent complexation of the latter by thiocyanate. The analysis is to be carried out in the same solvent that is used for the extraction of lipids from the sample (deoxygenated $CHCl_3$–MeOH or a CH_2Cl_2–MeOH = 2:1, v/v mixture). In this solvent, total lipids up to 5 mg/mL do not interfere, and linear increase of the absorbance of ferric thiocyanate complex is obtained up to 20 μM LOOH. Molar absorptivity of the ferric thiocyanate complex expressed per mol of LOOH was determined as 58,440 M^{-1} cm^{-1}, based on the average of four ferric ions produced by each LOOH molecule. The estimated lowest detectable limit was about 170 pmol LOOH/mL of analyzed solution, which corresponded to about 50 pmol LOOH/mg lipid in complex natural mixtures. Thus, here, a method providing an easy, rapid, sensitive, and complete measure of hydroperoxidation of lipids is described.

1. Mix approximate amounts of deaerated solvent and deaerated extract in a volumetric flask so that total amount of lipids does not exceed 5 mg/mL.
2. Add a small amount of the deaerated reagent solution (0.04 mL of reagent solution per mL of total volume) and bring to the mark with solvent.
3. Keep the deaerated solution in dark up to 20 min, to allow for the completion of the reaction (see Note 4).
4. Measure the absorbance at 500 nm against the reagent blank (see Note 5).
5. Calculate the concentration of LOOH in the sample using molar absorptivity of the ferric thiocyanate complex 58,440 M^{-1} cm^{-1} expressed per mol of LOOH (see Note 6).

3.1.1. Microprocedure for LOOH Measurement in Fresh Plasma Samples

1. Take an aliquot of known volume of sample, e.g., 0.5 mL plasma.
2. Add 0.5 mL 1% solution of metaphosporic acid in MeOH (see Note 7).
3. Add 1 mL of ice-cold $CHCl_3$, mix thoroughly and then the mixture centrifuge at 2,000 × *g* for 5 min.
4. Collect 0.5 mL the chloroform extract, add 0.45 mL deaerated solvent mixture CH_2Cl_2–MeOH (2:1, v/v) and 0.05 mL off freshly prepared reagent solution to produce the ferric thiocianate complex.
5. After incubation for 20 min in dark and room temperature, measure the absorbance at 500 nm against a solvent mixture.
6. Measure the absorbance at 500 nm against the reagent blank.

7. Calculate the concentration of LOOH in the sample using molar absorptivity of the ferric thiocyanate complex, 58, 440M^{-1} cm^{-1}, expressed per mol of LOOH (see Note 8).

3.2. Determination of Lipid Derived Aldehydes by HPLC

Here a rapid and sensitive HPLC method is described, with either spectrofluorimetric detection for measurement of MDA-tiobarbituric acid aduct (TBA) in biological samples such as plasma, urine, and tissue samples or with UV detector for HNE detection in serum free cell culture samples (Fig. 1).

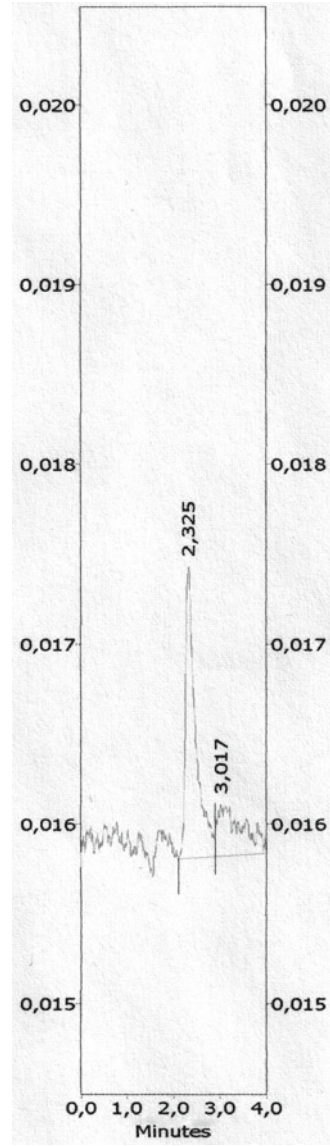

Fig. 1. Systemic oxidative stress determined by MDA presence in plasma of tumor bearing animal measured by HPLC. MDA concentration is 0.77 μM determined by standard curve (not shown).

3.2.1. MDA Determination by HPLC

1. Prepare MDA standards by serial dilution of 4.4 mM MDA standard solution to concentrations: 0, 0.31, 0.63, 1.25, 2.5, 5, and 10 mM.
2. Take a 25 μL aliquot of samples and standards and mix with 225 μL of twice distilled water, 375 μL of 0.44 M H_3PO_4 and with 125 μL of 42 mM TBA.
3. Heat all samples in boiling-water bath for 60 min and then cool them on ice (see Note 9).
4. After cooling mix the samples 1:1 with alkaline methanol.
5. Centrifuge the samples at 2,500 × *g* for 3 min.
6. Take clear supernatants and analyze by an HPLC method with fluorescence detection (excitation 527 nm, emission 550 nm) with flow adjusted to 1 mL/min (12).

3.2.2. HNE Determination by HPLC

1. Prepare HNE standards by serial dilution from HNE stock solution.
2. Take serum-free culture samples (1×10^6 cells) and mix with 300 μL ice-cold acetonitrile–acetic acid (24:1, v:v).
3. Incubate the mixture for 2 h on ice.
4. After incubation, centrifuge the samples at 8,000 × *g* at +4°C for 30 min and the supernatant is then either stored in liquid nitrogen or analyzed.
5. Inject 20 μL of each sample into the HPLC system with a UV detector. The mobile phase consisted of 42% (v/v) acetonitrile. Set the flow to 1 mL/min and the absorbance at 223 nm (13).

3.3. HNE-ELISA

One of the most popular immunological methods for measurement of specific antigen is ELISA. ELISA is based on the absorption capacity of proteins to bind to the microplate walls. Once, the antigen is bound, the detection is accomplished by interaction with the antigen-specific antibody, concentration of which is quantified by enzyme-linked to secondary antibody. In the case of aldehyde measurement, HNE-histidine adducts are measured by ELISA giving the population of this aldehyde bound to protein and thereby achieving its biological activity.

1. Prepare HNE standards by dissolving BSA in H_2O for 24 h by magnetic stirring.
2. Dilute HNE to the desired concentrations and mix with BSA solutions for 24 h at 4°C.
3. Add 200 μL carbonate binding buffer, pH 9.6 into the wells followed by 20 μL of standards or samples.
4. Incubate the plate overnight at +4°C.
5. Wash once with 400 μL H_2O.

6. Add 400 μL the blocking solution and incubate for 3 h at room temperature.
7. Wash once with 400 μL ELISA washing buffer.
8. Add 200 μL anti-HNE-His antibody and incubate for 2 h at room temperature.
9. Wash seven times with 400 μL ELISA washing buffer.
10. Add 400 μL peroxidase blocking solution and incubate for 30 min at room temperature.
11. Wash seven times with 400 μL ELISA washing buffer.
12. Add 200 μL the secondary antibody and incubate for 1 h at room temperature.
13. Wash seven times with 400 μL ELISA washing buffer.
14. Add 200 μL of TMB substrate (0.1 mg/mL) and stop the reaction after 5–10 min (ELISA Stress) or 30–60 min (ELISA Fine) by adding 2 M 50 μL H_2SO_4.
15. The absorbance is read at 450 nm with the reference filter set to 620 nm (13).

3.4. Immunoblotting of LPO-Modified Proteins

The dot blot and western blot or a protein immunoblot are techniques for detecting, analyzing, and identifying proteins (as shown in Fig. 2). The principle of these techniques is transfer of proteins to membrane, and identification of specific protein by specific

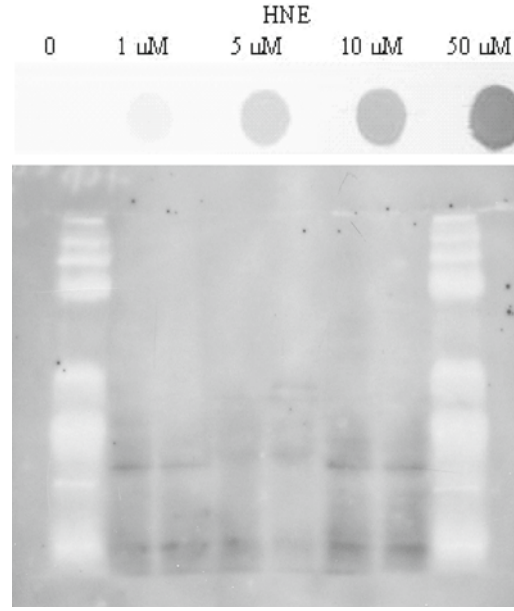

Fig. 2. Detection of LPO derived aldehydes by immunoblotting. Panel (**a**) *Dot-blot* of acrolein-protein standards detected by anti-acrolein-lysine antibody. Panel (**b**) Western blot of yeast cell treated by HNE detected by anti-HNE-histidine antibody.

antibodies. Western blot technique includes separation of proteins according to their size or 3-D structure by gel electrophoresis, while in dot-blot proteins are directly spotted onto a membrane and identified with specific antibody.

3.4.1. Western Blot Analysis of HNE/Acrolein-Modified Proteins

1. Prepare and treat cell cultures according to experimental protocol for analysis of LPO products.
2. Decant the media and wash the cells with PBS.
3. Add non-reducing buffer for electrophoresis and scrape the cells.
4. Freeze and thaw the lysates for three times in order to obtain good cell disruption.
5. Measure protein concentration according to Lowry (see Note 10).
6. Apply the samples to 10% polyacrylamide gel, and separate in the electric field.
7. After separation on the gel, proteins are to be transferred onto the membrane (pore diameter 0.2 μm) in the electric field.
8. Systems for the transfer to the membrane can be either "wet," in which the whole transfer block (gel, membrane and filter papers) are merged into the transfer buffer, or "semi-dry" in which the transfer block is soaked in the buffer. After transfer to the membrane, proteins are analyzed by immunostaining, which is common to both Western blot and dot-blot analysis and is described below.

3.4.2. Dot-Blot Analysis

In order to perform analysis of HNE or acrolein bound to proteins, cell protein lysates have to be prepared and proteins need to be quantified according to Lowry (14). For dot-blot analysis protein extracts (20 μg) should be spotted onto nitrocellulose membranes and analyzed as described below.

3.4.3. Analysis of HNE/Acrolein-Modified Proteins on the Membrane

1. After the samples are blotted onto the membrane, incubate the membrane in blocking solution (0.5% nonfat milk powder in PBS) at room temperature for 60 min.
2. Decant the blocking solution and then incubate the membrane overnight with mouse monoclonal antibodies directed against HNE-His adducts (1:45 in 1% BSA in PBS) (15), or against acrolein-Lys adducts (2 μg/mL in 5% BSA in PBS) (16).
3. Wash the blots four times for 5 min in washing solution.
4. Incubate the blot for 2.5 h with rabbit anti-mouse alkaline phosphatase-conjugated antibody (dilution 1:10,000 in PBS/1%BSA).
5. Visualize the immuno-complexes using the Enhanced AP Conjugate Substrate Kit (Bio-Rad) (17). Furthermore, the staining with alkaline phosphatase can be replaced by applying

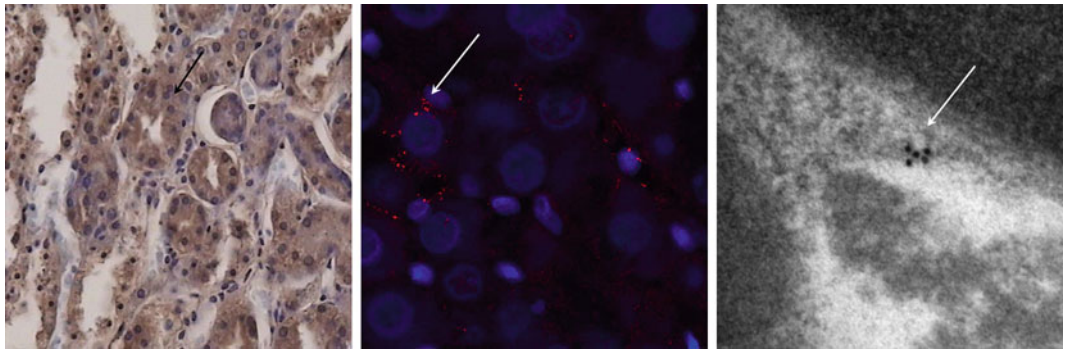

Fig. 3. Detection of LPO derived aldehydes in cells and tissues. Panel (**a**) immunohistochemical detection of HNE in kidney tissue of tumor bearing rat. Panel (**b**) Immunofluorescence detection of HNE-protein adducts in rat liver. Panel (**c**) ImmunoGold (electron microscopy) detection of HNE-protein adducts in spleen cells.

the Labelled StreptAvidin-Biotin (LSAB, Dako, Denmark) method (18) or EnVision technique followed by the 3,3′-diamino-benzidine tetrahydrochloride (DAB) visualization of the complexes (19).

6. Scan the obtained signals for quantification.

3.5. Detection of Lipid Derived Aldehydes in Cells and Tissues

The presence of lipid derived aldehydes in cells and tissue can be determined by immunocyto/histochemistry (ICC/IHC) (Fig. 3). ICC/IHC offers simple and sensitive methods for the localization of certain antigens in cells and tissues and is a routine and essential tool in diagnostic and research laboratories. The antigen of interest is detected by specific antibody-antigen interactions where the antibody has been tagged with a visible label. The complexes are visualized by a marker such as enzyme, fluorescent dye or colloidal gold. Depending on the method the samples are subsequently analyzed under light, confocal or electron microscope. Although many researchers commonly use confocal microscopy as a substitute for immunoelectron microscopy in cell biology research, confocal microscope is incapable of reliably discriminating most subcellular structures. Therefore electron microscopy represents the central tool for placing macromolecular functions within a cellular context

3.5.1. Imunocyto/ Histochemistry of HNE

1. Cut the samples which were fixed in formalin and then embedded in paraffin, to sections of 5 μm thickness.
2. Rehydrate the section through decreasing gradient of alcohol (absolute ethanol, 96%, 70% ethanol, and water).
3. Wash the section in PBS and incubate with primary antibody directed against HNE-His conjugates (20).
4. In order to block endogenous peroxidase activity, incubate the sections with 3% hydrogen peroxide in dark for 20 min.
5. Wash the sections three times for 5 min in PBS.

6. Incubate with EnVision reagent (Dako, Denmark) according to the manufacturer's instructions.
7. Wash the sections three times for 5 min in PBS.
8. Use DAB as chromogen.
9. Counterstain the sections with hematoxylin (see Note 11).

3.5.2. Subcellular Detection of HNE by Immunogold Method

10. Fix the samples in 2% glutaraldehyde in cacodylate buffer (pH 7.2).
11. Dehydrate the samples with serial dilutions of acetone (see Note 12).
12. Post-fix the samples with 1% osmium tetraoxide and infiltrate with epoxy resin by the standard procedure (21).
13. Cut ultrathin sections of samples 130 Å and mount them directly on nickel grids.
14. For immunostaining, block endogenous peroxidase activity with 3% hydrogen peroxide in PBS (see Note 13).
15. Use murine monoclonal antibodies against HNE-His and incubated for 24 h at +4°C.
16. Incubate the sections in rabbit anti-mouse (10 nm) gold probe (dilution 1:50 in PBS) (see Note 14).
17. After immunolabeling, counterstain sections with uranyl acetate and Reynolds lead nitrate solution.
18. Analyze by transmission electron microscopy.

4. Notes

1. Measure HNE concentration spectrophotometrically—measure the HNE maximal absorbance at 223 nm ($\varepsilon = 13{,}750\ M^{-1}\ cm^{-1}$).
2. We find the solution is stable for several days if protected from oxygen and light and kept in a refrigerator.
3. We find that the use of a single solution containing both reagents, Fe^{2+} and SCN^-, makes the analysis faster and easier, and overcomes the non-reproducibility caused by the addition of the Fe^{2+} reagent solution before the SCN^- reagent solution. Additionally, for developing the response, spectrophotometry of ferric thiocyanate is performed in the same solvent with which extraction of lipids is carried out, a deaerated mixture of CH_2Cl_2–MeOH (2:1, v/v).
4. The buildup of the absorbance of the ferric thiocyanate complex (the response) occurs at a rate which depends on the structure of LOOH. The composition of the ferric thiocyanate complex, $[FeNCS]^{2+}$ complex, in the solvent mixture CH_2Cl_2–MeOH is well defined over a range of concentrations, and the

stability constant is high enough to make this complex a suitable means of visualizations of Fe^{2+}-to-Fe^{3+} transformations in non-aqueous media (22).

5. If the sample extract is colored, which is often the case with natural samples, it is necessary to measure its absorbance against a different (sample) blank, which has the same composition, except for the reagent solution. In that case, the absorbance at 500 nm of the reagent blank has to be subtracted subsequently.
6. We find total lipids up to 5 mg/mL do not interfere, and linear increase of the absorbance of ferric thiocyanate complex is obtained up to 20 μM LOOH.
7. Aliquot of sample and metaphosphoric acid solution should be equal.
8. The background absorbance generated from possible interfering substances or non-hydroperoxide generated color in the assay can be measured by addition of 1 mM of triphenyphosphine and possible interference determined eliminate by subtraction from the absorbance of the LOOH in plasma sample measured at 500 nm.
9. At this point, samples can be stored for 24 h at –20°C.
10. Measuring proteins according to Bradford is not suitable, due to interference of SDS in this method, which is not the case with Lowry's method.
11. The samples should be analyzed by a pathologist. Specificity of anti-HNE immunostaining should be validated by using HeLa cells pretreated with ranging concentrations of HNE (1–100 μM) (23).
12. If working with cell samples, centrifuge the cells between each step.
13. This step makes the sections more hydrophilic. It is this step which makes antibody-binding sites visible in the transmission electron microscopy.
14. It is this step which makes antibody-binding sites visible in the transmission electron microscopy.

References

1. Esterbauer H, Schaur RJ, Zollner H (1991) Chemistry and biochemistry of 4-hydroxynonenal, malonaldehyde and related aldehydes. Free Radic Biol Med 11:81–128
2. Halliwell B, Gutteridge JMC (2007) Free radicals in biology and medicine. Oxford University Press, New York
3. Sattler KD (2010) Handbook of nanophysics. CRC, Hoboken
4. Uchida K (2003) 4-Hydroxy-2-nonenal: a product and mediator of oxidative stress. Prog Lipid Res 42:318–343
5. Dix TA, Aikens J (1993) Mechanisms and biological relevance of lipid peroxidation initiation. Chem Res Toxicol 6:2–18
6. Avery SV (2011) Molecular targets of oxidative stress. Biochem J 434:201–210

7. Leonarduzzi G, Robbesyn F, Poli G (2004) Signaling kinases modulated by 4-hydroxynonenal. Free Radic Biol Med 37:1694–1702
8. Gueraud F, Atalay M, Bresgen N, Cipak A, Eckl PM, Huc L, Jouanin I, Siems W, Uchida K (2010) Chemistry and biochemistry of lipid peroxidation products. Free Radic Res 44:1098–1124
9. Zarkovic N (2003) 4-Hydroxynonenal as a bioactive marker of pathophysiological processes. Mol Aspects Med 24:281–291
10. Mihaljevic B, Katusin-Razem B, Razem D (1996) The reevaluation of the ferric thiocyanate assay for lipid hydroperoxides with special considerations of the mechanistic aspects of the response. Free Radic Biol Med 21:53–63
11. Katusin-Razem B, Mihaijevic B, Razem D (1990) Lipid test. Nature 345:584
12. Gveric-Ahmetasevic S, Sunjic SB, Skala H, Andrisic L, Stroser M, Zarkovic K, Skrablin S, Tatzber F, Cipak A, Jaganjac M, Waeg G, Gveric T, Zarkovic N (2009) Oxidative stress in small-for-gestational age (SGA) term newborns and their mothers. Free Radic Res 43:376–384
13. Borovic S, Rabuzin F, Waeg G, Zarkovic N (2006) Enzyme-linked immunosorbent assay for 4-hydroxynonenal-histidine conjugates. Free Radic Res 40:809–820
14. Lowry OH, Rosebrough NJ, Farr AL, Randall RJ (1951) Protein measurement with the Folin phenol reagent. J Biol Chem 193:265–275
15. Waeg G, Dimsity G, Esterbauer H (1996) Monoclonal antibodies for detection of 4-hydroxynonenal modified proteins. Free Radic Res 25:149–159
16. Uchida K, Kanematsu M, Sakai K, Matsuda T, Hattori N, Mizuno Y, Suzuki D, Miyata T, Noguchi N, Niki E, Osawa T (1998) Protein-bound acrolein: potential markers for oxidative stress. Proc Natl Acad Sci U S A 95:4882–4887
17. Cipak A, Hasslacher M, Tehlivets O, Collinson EJ, Zivkovic M, Matijevic T, Wonisch W, Waeg G, Dawes IW, Zarkovic N, Kohlwein SD (2006) Saccharomyces cerevisiae strain expressing a plant fatty acid desaturase produces polyunsaturated fatty acids and is susceptible to oxidative stress induced by lipid peroxidation. Free Radic Biol Med 40:897–906
18. Jaganjac M, Prah IO, Cipak A, Cindric M, Mrakovcic L, Tatzber F, Ilincic P, Rukavina V, Spehar B, Vukovic JP, Telen S, Uchida K, Lulic Z, Zarkovic N (2011) Effects of bioreactive acrolein from automotive exhaust gases on human cells in vitro. Environ Toxicol in press; DOI: 10.1002/tox.20683
19. Spoljaric D, Cipak A, Horvatic J, Andrisic L, Waeg G, Zarkovic N, Jaganjac M (2011) Endogenous 4-hydroxy-2-nonenal in microalga Chlorella kessleri acts as a bioactive indicator of pollution with common herbicides and growth regulating factor of hormesis. Aquat Toxicol 105:552–558
20. Cherkas A, Yelisyeyeva O, Semen K, Zarkovic K, Kaminskyy D, Gasparovic AC, Jaganjac M, Lutsyk A, Waeg G, Zarkovic N (2009) Persistent accumulation of 4-hydroxynonenal-protein adducts in gastric mucosa after Helicobacter pylori eradication. Coll Antropol 33:815–821
21. Zarkovic K, Zarkovic N, Schlag G, Redl H, Waeg G. Histological aspects of sepsis-induced brain changes in a baboon model. In: Shock, sepsis, and organ failure: fifth Wiggers Bernard Conference 1996. Springer-Verlag, Heidelberg, pp 146–162
22. Mihaljević B, Ražem D (2003) Monothiocyanatoiron(III) Compelx in Dichloromethane-Methanol Solvent Mixture. Croat. Chem. Acta 76:249–255
23. Sovic A, Borovic S, Loncaric I, Kreuzer T, Zarkovic K, Vukovic T, Wag G, Hrascan R, Wintersteiger R, Klinger R, Zurak N, Schaub RJ, Zarkovic N (2001) The carcinostatic and proapoptotic potential of 4-hydroxynonenal in HeLa cells is associated with its conjugation to cellular proteins. Anticancer Res 21:1997–2004

Chapter 20

Raman Spectroscopy for the Detection of AGEs/ALEs

J. Renwick Beattie, John J. McGarvey, and Alan W. Stitt

Abstract

Raman spectroscopy is a noninvasive, nondestructive tool for capturing multiplexed biochemical information across diverse molecular species including proteins, lipids, DNA, and mineralizations. Based on light scattering from molecules, cells, and tissues, it is possible to detect molecular fingerprints and discriminate between subtly different members of each biochemical class. Raman spectroscopy is ideal for detecting perturbations from the expected molecular structure such as those occurring during senescence and the modification of long-lived proteins by metabolic intermediates as we age. Here, we describe the sample preparation, data acquisition, signal processing, data analysis and interpretation involved in using Raman spectroscopy for detecting age-related protein modifications in complex biological tissues.

Key words: Advanced glycation end-products, Advanced lipoxidation end-products, Brunch's membrane, Glycation, Raman spectroscopy

1. Introduction

1.1. AGE/ALEs in Senescence

Ageing can lead to decreased function and viability of cells and tissues. There are associations between normal physiological ageing and disease although what factors predispose to age-related disease and a departure from the "normal" ageing pathway remain obscure. As our populations become skewed towards greater longevity, ageing disorders are becoming ever-more prevalent which has far-reaching implications for morbidity and quality of life in the elderly.

Metabolic pathways are central to cell and tissue homeostasis yet they often produce cycles of reactive intermediates that need to be closely controlled by complex enzyme systems. At times when some pathways become imbalanced or overloaded these reactive intermediates can escape the rigorous controls and react with biochemical

Lorenzo Galluzzi et al. (eds.), *Cell Senescence: Methods and Protocols*, Methods in Molecular Biology, vol. 965,
DOI 10.1007/978-1-62703-239-1_20,

species such as proteins and DNA. This is further complicated by the possibility of direct oxidation of glycerides and fatty acids forming further reactive intermediates that result in additional modifications. Long-lived proteins, such as many collagens, are not readily turned over and renewed and so can accumulate these protein modifications over time. As proteins are increasingly modified, their function begin to degrade, leading to disease (1, 2).

Reactions between sugars and free amino groups on proteins, lipids and DNA are an inevitable consequence of aldehyde reactivity and many molecules in our body harbor chemically attached carbohydrate. These reactions begin with the formation of Schiff bases and ε-amino groups that rearrange to Amadori adducts. These intermediates can undergo further oxidation and dehydration reactions to form irreversible protein-bound compounds collectively termed advanced glycation endproducts (AGEs). Likewise, proteins can be modified by lipids as well as carbohydrates. During oxidative stress, reactive oxygen species attack polyunsaturated fatty acids (PUFAs) either in the cell membrane or circulating lipoprotein molecules (3). This oxidative decomposition of PUFAs initiates chain reactions that lead to the formation of a variety of reactive carbonyl species such as 4-hydroxy-trans-2-nonenal (4-HNE), acrolein (ACR), and malondialdehyde (MDA). These can generate adducts known as advanced lipoxidation endproducts (ALEs). While ALEs are often grouped together with AGEs, they should be regarded as a distinct class of adducts due to their differing reaction chemistry although most AGE/ALE adducts are highly stable at physiological pH and their accumulation in tissues depends on factors such as availability of metal ions, redox balances and longevity of the modified protein. Irrespective of their chemical derivation, AGE/ALE modifications can have a significant impact on protein structure and function by mediating protein–protein cross-linking reactions, changing tertiary structure and normal molecular function, conferring resistance to digestion or impairing receptor recognition. AGE/ALEs have been implicated in a number of diseases including neurodegeneration, cardiovascular disease, cancer, and inflammatory disorders. These modifications are sometimes referred to as markers of molecular senescence and present a very diverse group of chemical species, making simultaneous detection difficult using traditional biochemical techniques.

1.2. Raman Spectroscopy

Molecular structure is dynamic and all molecules will vibrate constantly under influence of external energy sources such as heat and light. When light shines on a sample the individual molecules can absorb some of the energy from that light and start to vibrate faster. The light is now lower in energy, and thus of longer wavelength, which means that its color has been shifted towards the red end of the spectrum. These color (energy) shifts correspond to the

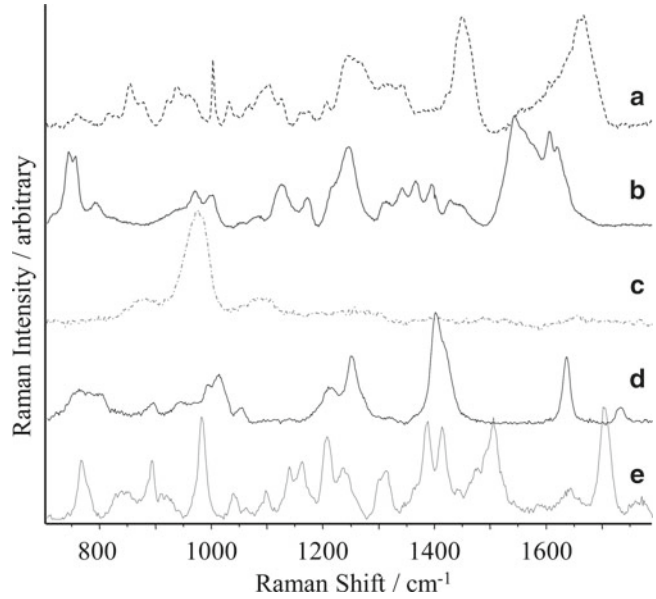

Fig.1. Raman spectra of selected reference compounds: (**a**) collagen 4, (**b**) heme, (**c**) AGE-BSA, (**d**) oleic acid, (**e**) GH-1.

vibrational energies of bonds in the scattering molecule. Each molecule exhibits very specific patterns of vibrations depending on its chemical structure and its physical interaction with neighboring molecules. This means that analyzing the changes in color allows the scientist to peer deep into the chemical and physical structure of the sample being analyzed. Figure 1 shows some selected Raman signals obtained from diverse biochemical species encountered in ocular tissue, illustrating the specificity of the method, while Table 1 lists some of the most intense bands in the spectra of selected AGE/ALEs. The reader should be cautioned against assigning a signal based on intensity at one position, but should compare the pattern of bands found against the pattern of bands in a pool of reference spectra—this search is ably assisted by spectral database software. To assist the reader in deciding if Raman spectroscopy may be of use in their application Table 2 lists some of the advantages and disadvantage of the technique (4–6).

1.3. Multivariate Statistics

Raman spectroscopic methods generate complex information in large datasets and so it is commonplace to use multivariate statistics to simplify the data and identify the most pertinent information. Principal component analysis (PCA) is the most popular *qualitative* method for reducing the data to the most limited range of basic spectral signals that, in various combinations, account for all the signals within the dataset. The results of most interest from PCA are the basic spectral signals ("loadings") and the so-called "scores," which reflect the relative contribution of these basic

Table 1
Some Raman band assignments for common moieties in AGE/ALEs

Band position wavenumber/cm^{-1}	AGE/ALE
1,734	MGO
1,697	MG-H1/MG-H2
1,690	HHE
1,685	Aminoguanidine
1,655	Acrolein
1,637	MG-H2
1,620	Acrolein
1,612	MOLD/aminoguanidine
1,580	CEL/aminoguanidine
1,534	HHE/aminoguanidine
1,460	CML/MG-H1
1,454	CEL/MGO/aminoguanidine
1,445	GOLD
1,439	MOLD
1,420	GOLD
1,417	CML/AAA
1,405	CEL
1,400	MOLD
1,390	CML
1,360	CEL
1,342	MOLD/GOLD
1,336	Aminoguanidine
1,320	CEL/CML
1,276	GO
1,038	GO
1,026	METSO
1,016	METSO
969	Aminoguanidine
930	CML
900	AAA

(continued)

Table 1
(continued)

Band position wavenumber/cm^{-1}	AGE/ALE
890	HHE
845	Acrolein
836	Acrolein/pentosidine
831	MG-H1
820	GO
809	MGO
801	Pentosidine
697	METSO
685	MGO
671	MG-H2
609	MGO

Further assignments available in refs. (4, 6, 20)

Table 2
Advantages and disadvantages of Raman spectroscopic techniques

Advantages	Disadvantages
Minimal interference from water Noncontact, noninvasive All physical states of matter Minimal sample preparation	Weak effect Expensive[a] Can be time-consuming Fluorescence can interfere
Nondestructive Spatial resolution diffraction limited Measure <1 pg material Rich chemical and physical information content Instrumentation highly adaptable	
Special techniques extend: Sensitivity (e.g., surface enhanced RS) (21) Specificity (e.g., resonance RS) (22) Spatial resolution (e.g., tip enhanced RS) (23) High fluorescence (e.g., shifted subtracted RS) (24) Sub-surface probing (e.g., spatially offset RS) (25) Larger volume (e.g., transmission RS) (26)	

[a]Cost-effective systems with good technical specifications are becoming increasingly available

spectral signals to each sample spectrum. One of the most commonly applied methods of *quantitative* analysis is partial Least Squares (PLS), in which the sample spectra are regressed against a reference parameter. The regression coefficients are the spectral bands that were used to correlate with the reference value, and are an excellent way of checking that the correlation is based on direct spectral measurement of the target analyte. A more detailed introduction to multivariate statistics is available from Umetrics AB (Umea, Sweden) (7, 8).

2. Materials

2.1. Standards

Pure reference samples for any AGE/ALE species to be targeted should be used, along with additional AGE/ALE species expected to be common and reference samples for the main bulk constituents of the tissue under investigation. For example, the authors have previously acquired a database of AGE/ALE spectra sourced from commercially available compounds:

- 2-Amino-5-(2-amino-5-hydro-5-methyl-4-imidazolon-1-yl)-pentanoic acid (MG-H2).
- 2-Aminoadipic acid.
- Acrolein.
- All-*trans* retinal.
- Carboxyethyl lysine (CEL).
- Carboxymethyl lysine (CML).
- Collagen I, III, IV, elastin, heme (Sigma-Aldrich; St Louis, MO).
- Croton aldehyde.
- Dihydropyridine-lysine (DHP-Lys).
- Glycoaldehyde.
- Glyoxal (GO).
- IMARS (pentosidine).
- MDA and AGE-modified protein (BSA), were synthesized and purified using published protocols (9, 10).
- Methionine sulfoxide.
- Methyl glyoxal (MGO).
- *N*δ-(5-hydro-4-imidazolon-2-yl)-ornithine (G-H1).
- NeoMPS (hydroimidazolones *N*δ-(5-hydro-5-methyl-4-imidazolon-2-yl)-ornithine (MG-H1).
- OXIS (4-hydroxyhexenal/HHE).

- Other AGEs/ALEs were generously donated by collaborators:
  - 4-Hydroxynonenal/HNE (Professor Koij Uchida, Nagoya University, Japan).
  - Argpyrimidine (Professor Ram Nagaraj, Department of Ophthalmology & Visual Sciences, Case Western Reserve University, Cleveland).
  - Docosahexaenoic acid/DHA and oxidized DHA (Dr Malgorzata Rozanowska, School of Optometry and Visual Sciences, Cardiff University, UK).
  - α-Crystallin (Dr Tomasz Panz, Dept of Biophysics, Jagiellonian University, Krakow).

2.2. Other Materials

- CaF_2 microscope slides as sample substrates (Crystrans, Poole, UK) (see Note 1).
- Standard methods were applied for quantification of pentosidine, CML, and CEL (11, 12).
- Standard dissection kit for preparation of tissues.
- Software capable of performing multivariate analyses (PCA, PLS), such as TheUnscrambler (Camo, Oslo, Norway), Matlab (Mathworks, Cambridge, UK).

2.3. Confocal Raman Microscope

- The Raman instrumentation employed for our studies is detailed below, but additional guidelines for choosing an optimum configuration are given in the notes section, while a more detailed and technical account of Raman instrumentation is available (13). For tissue mapping or low volume extracts a confocal Raman microscope is required, allowing measurement from volumes of the order of 1 μm^3, <1 pg of material (see Note 2).
- The specific instrumental features previously employed by the authors are offered here.
- For excitation, a 633 nm excitation laser was employed as the Bruch's membrane tissues used previously did not exhibit very strong fluorescence (10 mW at sample, focused beam diameter <1 μm, (see Note 3).
- A typical spectral "window" (i.e., the range of the spectrum detectable in one acquisition) might be 800–1,800 cm^{-1} (see Note 4).
- For Raman microscopy, microscope objectives of magnification ×10, ×50, and ×100 would be typical (see Note 5); a 0.1 μm step size motorized, computer-controlled *xyz* stage.

3. Methods

3.1. Identify the Raman Signal

1. Obtain pure reference material for the substances of interest and, if possible, a sample containing the reference material in the relevant matrix. It is important that the reference materials be as pure as possible, with no buffers present, as these will interfere with the recorded spectrum.
2. Record their Raman spectra; the exact procedure will be dependent on the instrumentation employed. Because Raman spectroscopy is sensitive to physical interactions it is important to measure the reference materials under a range of conditions and within a relevant matrix.
3. Multiple (minimum 10) spectra should be recorded from different regions of the sample to check for consistency and for microscope based assessment this should be ten grid maps (5×5 spectra with 3 μm steps between each spectrum) of separate areas.
4. PCA will highlight any deviations such as impurities, polymorphism or domain formation (see Note 6).
5. The Raman spectrum obtained from the reference material should be compared to known spectra of related molecules and tables of assignments to verify that the signal is a reasonable reflection of the expected chemical structure.
6. The Raman spectra from the pure reference samples are then loaded into spectral database software (e.g., Spectral ID, Thermo Scientific, Waltham, MA).

3.2. Sample Preparation

Raman spectroscopic techniques are applicable to matter in any state, can be used for aqueous solutions and, under appropriate circumstances are noninvasive. This means that no special sample preparations are demanded by the Raman methodology, but rather all sample preparation requirements are dependent on the biochemical aspects of the experiment. As an example, if lipids are considered important the sample cannot have been precipitated in ethanol nor can it have been paraffinated as both processes will delipidate the sample. It is preferable to keep processing of samples to a minimum. In our studies the samples were dissected and air-dried without any fixation. Raman spectroscopy is based on UV, visible or NIR radiation, allowing measurement of a sample through any substance transparent to the excitation wavelength. Thus Raman experiments can be performed using chambers or incubators to control local environment, including temperature, humidity, controlled atmospheres and pressure.

3.3. Validation of the Spectroscopic Analyses

1. Ideally a sufficiently large set of samples should be prepared, so as to allow for a separate calibration and validation set (2:1 ratio of samples). If insufficient samples exist then cross

validation can be used on a single set of data, but would be slightly optimistic about model performance.

2. The calibration should be performed over a realistic range of concentrations reflecting the range encountered in vivo (remembering, if the target analyte is likely to be localized, that its local concentration may be greater than the average concentration within the whole tissue). To calibrate the analyses for the Raman signal we measured the concentrations of a number of important AGE/ALE adducts using standard HPLC (pentosidine) and GC-MS(CML, CEL) methods (11) in a number of human Bruch's membrane.
3. These same samples were subjected to Raman analysis by recording 3 grids of 100 spectra in different areas of the sample then averaging the spectra for each grid.
4. The signal to noise ratio (S/N) of the major bands in the average spectrum of each sample should be at least 50 for the calibration.
5. Remove the background signal from the Raman spectra (14) (see Note 7).
6. Normalize the spectral intensity by dividing each point by the average intensity of a number of selected regions of the spectrum (15) (see Note 8).
7. Input the data into the statistical package, along with the chromatographically measured parameters.
8. Carry out a PLS regression, incorporating wavelength selection (this is a family of methods that identifies which wavelengths contribute most to the correlation; in The Unscrambler it is called the uncertainty test) to create a more robust model.
9. Compare the regression performance for each of the normalization procedures and select the optimal model, using this normalization procedure for future models or predictions.
10. Compare the regression coefficients with the spectra of the pure reference compounds as shown in Fig. 2 (see Note 9). In Fig. 2 the regression coefficients at the bottom of the figure are after wavelength selection of the Raman shifts most strongly correlated with the pentosidine content of the human Bruch's membrane and the main peaks are highlighted by arrows at the top.

3.4. Acquiring the Raman Data for the Sample

1. Select a suitable area of the sample. If the target analyte is highly localized it is possible to use a low spatial resolution (5–10 μm spacing) scan over a large area, follow the procedure described below, then repeat in higher resolution in an area identified from the initial screening as containing the target analyte.

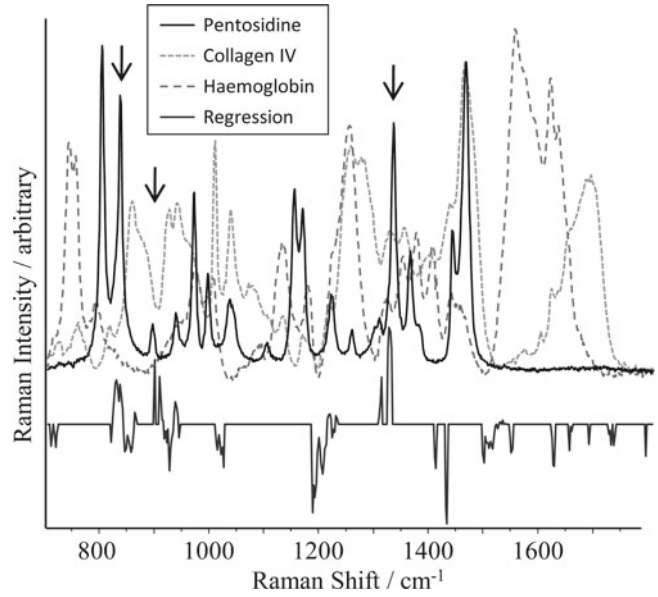

Fig. 2. Regression coefficients used to model pentosidine in human Bruch's membrane compared with the Raman spectra of purified pentosidine, collagen IV, and hemoglobin.

2. The individual spectra used to quantitatively predict the target analyte should have an S/N of at least ten (primarily due to the normalization step); For qualitative mapping the S/N can be lower, with the ultimate contrast of the chemical image determining the lower limit for S/N, as Fig. 3 illustrates.

3.5. Qualitative Mapping

1. If the spectral dataset contains a wide variation in spectral quality (as may happen in mapping uneven samples) it is not recommended that the spectral intensity of mapped data be normalized before qualitative analysis (see Note 10).
2. Import the data into the statistics package and perform a PCA.
3. Identify principal components (PCs) relating to target analytes by comparing the loadings with the reference spectra recorded initially. These loadings each contain a positive and a negative contribution from two different constituents, which can make interpretation difficult. In order to visualize the spectra related to a particular component it is necessary to weight each spectrum by its score and average the positive and negative score spectra separately. The process is illustrated in Fig. 4 and it is clear that the spectral constituents contributing to the PC are easier to identify, allowing the identification of signals for a number of AGE/ALEs.
4. Compare these signals against the database of reference signals to confirm identification or input into a linear combination analysis against a limited pool of candidate spectra (see Note 11).

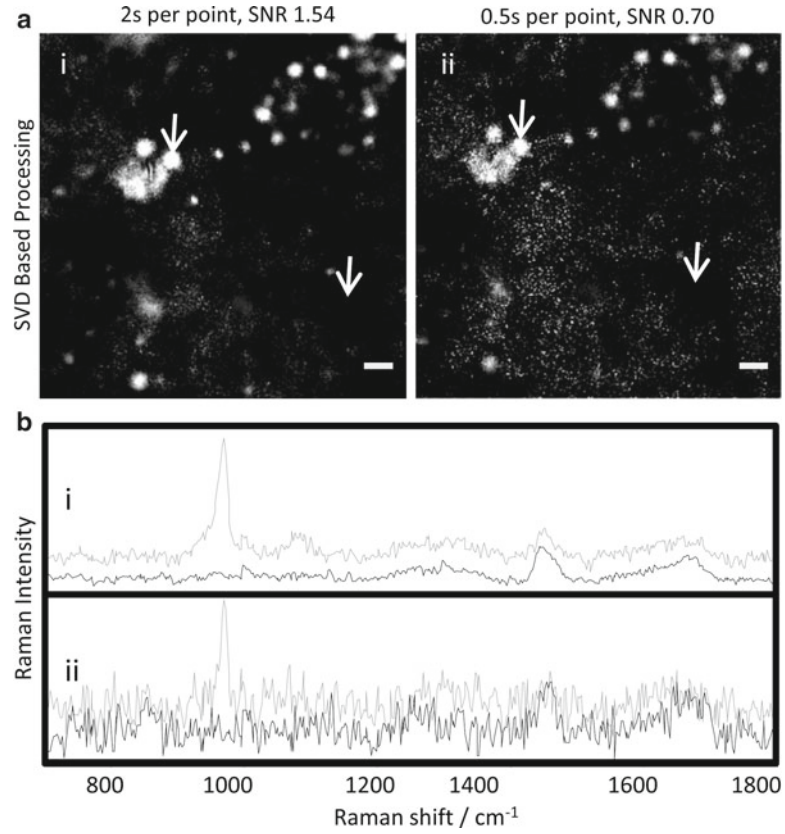

Fig. 3. (**a**) Raman maps of calcifications in Bruch's membrane using data with a mean SNR of (*i*) 1.54 and (*ii*) 0.70. (**b**) Shows the spectra for the arrowed areas with the grey spectrum corresponding to the white area, and the black spectrum to the black area.

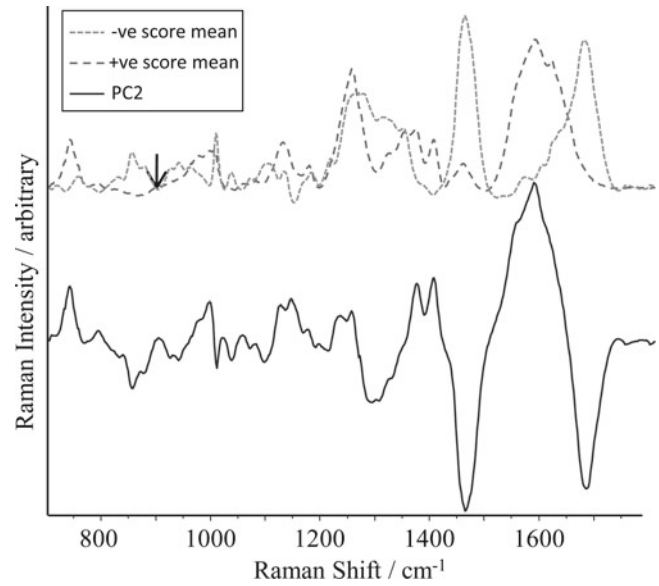

Fig. 4. PC2 loading compared with the score weighted positive (+ve) and negative (–ve) score spectra. These spectra can now be directly input into spectral databases or analyzed by linear combination analysis.

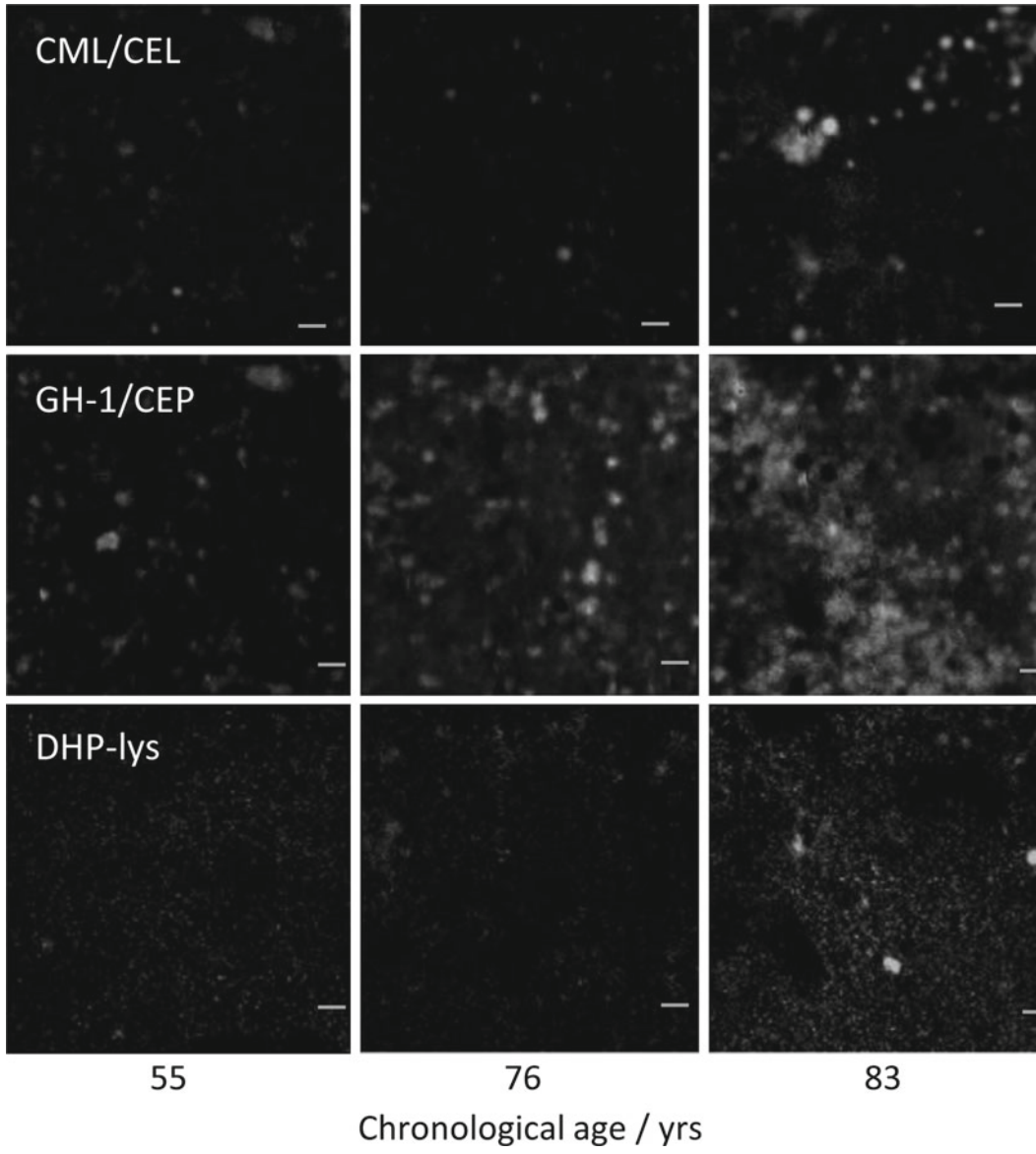

Fig. 5. Raman score maps of individual AGE/ALE constituents in human Bruch's membranes of different ages as indicated at bottom of maps.

5. The process should be stopped when the S/N of the loading reaches three.
6. The scores of the PCs can be mapped using their original coordinates in order to obtain a pseudo-image like those shown in Fig. 5.

3.6. Quantitative Mapping

1. Process the data in the same way as the calibration data were processed.
2. Import the data into the statistics package and perform a prediction using the PLS regression model created during the calibration step.
3. Use the original mapping coordinates to reconstruct a pseudocolor image of the predicted analyte.

3.7. Interpretation of Results

1. It is essential to have a comprehensive database of representative spectra available for comparison to facilitate interpretation of the Raman spectra. Use of spectral database software will compare the sample spectrum with the reference spectra and report which reference spectra are most similar to the sample. In some cases it may not be possible to obtain a pure reference spectrum of the target analyte, in which case a spectral database will not be applicable.
2. Alternatively, the sample spectrum can be compared with published spectra, tables of band assignments and comprehensive vibrational analyses of related molecules. Despite its age, Tu's book on Raman spectroscopy in biology remains a very comprehensive reference for typical spectral signals of a wide range of biochemicals (16).
3. Because of the close link between the Raman spectrum and the chemical structure of the analyte it is possible to speculate on the origin of an unidentified signal. If the spectrum of a reference sample of the suspected molecule is obtained then it can be accounted for in the original data without the need to rerecord the sample data (4).

4. Notes

1. The main issues associated with choosing a suitable substrate for the sample under investigation are minimal Raman spectral features and as low a broadband background signal as possible. CaF_2 slides give a very low background, with a single sharp peak around 325 cm^{-1}, making them an ideal substrate for many applications, but are expensive. If high throughput demands a cheaper alternative, extra white glass slides (Menzel-Gläser, Braunschweig, Germany) give a much higher background than CaF_2, but when compared to quartz, they display fewer spectral features but comparable intensity of broadband background. Standard glass gives broadband signal intensity around three times that of extra white glass. However, if the excitation wavelength is in the NIR (>750 nm) then glass (standard or extra white) gives a very strong emission that swamps the Raman signal, so that CaF_2 or quartz must be employed.

2. For larger samples (e.g., 100 μL of extracted material) a macro Raman instrument is preferable, with spot sizes available from 50 to 500 μm in diameter. For discussion on the relative merits of micro and macro Raman instrumentation see ref. 17.
3. For fluorescent samples use of 785 nm excitation is typically recommended. For nonfluorescent samples 633 nm offers the benefit of enhanced Raman scattering efficiency, optical transmission and detection efficiency as well as allowing use of extra-white glass as a substrate if cost is an important consideration. Accurate measurement of beam diameter is essential for determining spatial resolution. Measure the Raman spectrum along a line projecting over the vertical edge of a silicon wafer and measure the distance between 100 and 5t signal intensity—this distance represents the 2× standard deviation diameter of the beam intensity.
4. The size of the spectral window is inversely related to the spectral resolution of the instrument.
5. When using a high magnification objective, a water immersion lens is required for use on hydrated samples to avoid refraction problems at the sample surface.
6. PCA allows detection of any detectable impurities, which can be recognized and eliminated from the signal post-acquisition, leaving the pure signal of the target analyte.
7. The raw data acquired from a Raman experiment are generally not pure Raman spectra, but contain contributions from optical phenomena other than Raman, such as fluorescence. For this reason it is necessary to eliminate this low information broadband signal from the data set prior to quantitative analysis. A large number of methods exist, well reviewed in ref. 18 and some promising new automated methods are available (4, 19). The authors have developed a new approach based on correcting the loadings from multivariate analyses such as PCA that is ideally suited to analyzing target analytes in complex matrices (14).
8. The absolute Raman intensity is very difficult to measure reproducibly, being dependent on a very large number of factors (13) and for this reason it is necessary to standardize the intensity prior to quantitative analysis (15).
9. All the positive peaks in the regression coefficients are found in the reference pentosidine spectrum, but not all the peaks in the reference spectrum appear in the regression coefficients. Comparing the pentosidine with the collagen and heme spectra, (the dominant spectral signals in these samples), shows that the peaks not selected for the regression are overlapped by strong peaks in either the collagen or heme. The strong correspondence between the regression coefficients and the

relative intensity of the target analyte bands to the matrix Raman bands increases confidence that the regression is directly based on measuring the target analyte. If the bands do not match those in the reference material, the model is dependent upon a cross correlation that may not apply in independent samples. Wavelength selection ignores Raman shifts that are unreliable for predicting the target analyte, either because the target analyte shares intensity with the cell or because there is a third constituent unrelated to the analyte.

10. A rapid way to determine if the dataset is suitable for normalization prior to model creation is to average the dataset before and after normalization and determine if there is a significant change in the ratio of the Raman signal to the pixel-to-pixel shot noise in a baseline region of the signal. If the two are very similar in terms of signal to noise normalization will not be an issue, but if noise is enhanced it is better to create the model first and normalize by the scores after.
11. For example, PC2 is relatively easy to identify as heme versus protein without extracting the positive and negative signals, but by extracting the signals it was possible to assess the negative score spectrum against a pool of reference protein spectra and determine the composition of the spectrum to contain 15% collagen IV, 25% collagen IX, 11% Elastin, 19% fat, and 2.3% cholesterol.

Acknowledgments

Research was supported by grants from the BBSRC, UK (JREI 18471) R&D Office, Northern Ireland (SPI/2384/03) and the Medical Research Council (MRC), UK (G0600053). Leverhulme Trust (EM/2006/0049).

References

1. Monnier VM, Sell DR, Genuth S (2005) Glycation products as markers and predictors of the progression of diabetic complications. Ann N Y Acad Sci 1043:567–581
2. Stitt AW (2010) AGEs and diabetic retinopathy. Invest Ophthalmol Vis Sci 51:4867–4874
3. Aldini G, Dalle-Donne I, Facino RM, Milzani A, Carini M (2007) Intervention strategies to inhibit protein carbonylation by lipoxidation-derived reactive carbonyls. Med Res Rev 27:817–868
4. Glenn JV, Beattie JR, Barrett L, Frizzell N, Thorpe SR, Boulton ME, McGarvey JJ, Stitt AW (2007) Confocal Raman microscopy can quantify advanced glycation end product (AGE) modifications in Bruch's membrane leading to accurate, nondestructive prediction of ocular aging. FASEB J 21:3542–3552
5. Beattie JR, Pawlak AM, McGarvey JJ, Stitt AW (2011) Sclera as a surrogate marker for determining AGE-modifications in Bruch's membrane using a Raman spectroscopy-based index of aging. Invest Ophthalmol Vis Sci 52:1593–1598
6. Beattie JR, Pawlak AM, Boulton ME, Zhang J, Monnier VM, Stitt AW, McGarvey JJ (2010)

Multiplex analysis of age-related protein and lipid modifications in human Bruch's membrane. FASEB J 24:4816–4824

7. Eriksson L, Johansson E, Kettaneh-Wold N, Trygg J, Wikström C, Wold S (eds) (2006) Multi- and megavariate data analysis part II: advanced applications and method extensions, second revised and enlarged edition, vol 2, 2nd edn. Umea, Umetrics
8. Eriksson L, Johansson E, Kettaneh-Wold N, Trygg J, Wikström C, Wold S (eds) (2006) Multi- and megavariate data analysis part i: basic principles and applications, second revised and enlarged edition, vol 1, 2nd edn. Umea, Umetrics
9. Suttnar J, Cermak J, Dyr JE (1997) Solid-phase extraction in malondialdehyde analysis. Anal Biochem 249:20–23
10. Stitt AW, Li YM, Gardiner TA, Bucala R, Archer DB, Vlassara H (1997) Advanced glycation end products (AGEs) co-localize with AGE receptors in the retinal vasculature of diabetic and of AGE-infused rats. Am J Pathol 150:523–531
11. Degenhardt TP, Grass L, Reddy S, Thorpe SR, Diamandis EP, Baynes JW (1997) The serum concentration of the advanced glycation end-product N epsilon-(carboxymethyl)lysine is increased in uremia. Kidney Int 52: 1064–1067
12. Dunn JA, McCance DR, Thorpe SR, Lyons TJ, Baynes JW (1991) Age-dependent accumulation of N epsilon-(carboxymethyl)lysine and N epsilon-(carboxymethyl)hydroxylysine in human skin collagen. Biochemistry 30:1205–1210
13. McCreery RL (2000) Raman spectroscopy for chemical analysis, 1st edn. Wiley, New York
14. Beattie JR (2011) Optimising reproducibility in low quality signals without smoothing; an alternative paradigm for signal processing. J Raman Spec 42:1419–1427
15. Beattie JR, Glenn JV, Boulton ME, Stitt AW, McGarvey JJ (2009) Effect of signal intensity normalization on the multivariate analysis of spectral data in complex 'real-world' datasets. J Raman Spec 40:429–435
16. Tu AT (1982) Raman spectroscopy in biology: principles and applications. Wiley, New York
17. Bell SB, Beattie JR, McGarvey JJ, Peters KL, Sirimuthu NMS, Speers SJ (2004) Development of sampling methods for Raman analysis of solid dosage forms of therapeutic and illicit drugs. J Raman Spec 35:409–417
18. Jirasek A, Schulze G, Yu MML, Blades W, Turner RFB (2004) Accuracy and precision of manual baseline determination. Appl Spectrosc 58:1488–1499
19. Lieber CA, Mahadevan-Jansen A (2003) Automated method for subtraction of fluorescence from biological Raman spectra. Appl Spectrosc 57:1363–1367
20. Pawlak AM, Beattie JR, Glenn JV, Stitt AW, McGarvey JJ (2008) Raman spectroscopy of advanced glycation end products (AGEs), possible markers for progressive retinal dysfunction. J Raman Spec 39:1635–1642
21. Bell SEJ, Sirimuthu NMS (2008) Quantitative surface-enhanced Raman spectroscopy. Chem Soc Rev 37:1012–1024
22. Wood BR, McNaughton D (2006) Resonance Raman spectroscopy in malaria research. Expert Rev Proteomics 3:525–544
23. Stadler J, Schmid T, Zenobi R (2012) Developments in and practical guidelines for tip-enhanced Raman spectroscopy. Nanoscale 4:1856–1870. doi:10.1039/C1031NR11143D
24. Bell SEJ, Bourguignon ESO, Dennis A (1998) Analysis of luminescent samples using subtracted shifted Raman spectroscopy. Analyst 123:1729–1734
25. Matousek P, Morris MD, Everall N, Clark IP, Towrie M, Draper E, Goodship A, Parker AW (2005) Numerical simulations of subsurface probing in diffusely scattering media using spatially offset Raman spectroscopy. Appl Spectrosc 59:1485–1492
26. Everall N, Matousek P, MacLeod N, Ronayne KL, Clark IP (2010) Temporal and spatial resolution in transmission Raman spectroscopy. Appl Spectrosc 64:52–60

Chapter 21

Monitoring Oncogenic B-RAF-Induced Senescence in Melanocytes

Sieu L. Tran and Helen Rizos

Abstract

The B-RAF kinase is a downstream effector of the RAS family of proto-oncogenes and is constitutively activated in the majority of human melanomas. The common oncogenic B-RAF^{V600E} mutant cooperates with additional genetic lesions to transform immortal murine and human cells. In primary cells, however, B-RAF^{V600E} triggers a rapid cell cycle arrest that is phenotypically indistinguishable from cellular senescence. Here we describe the analyses of B-RAF-induced senescence in primary human melanocytes using recombinant lentiviruses.

Key words: B-RAF^{V600E}, Immunostaining, Melanocytes, Senescence

1. Introduction

Activating mutations in the B-RAF kinase are found in approximately 60% of human melanomas (1) and in up to 80% of benign melanocytic nevi (2). Nevi are benign tumors of melanocytes that remain growth arrested for decades and rarely develop into melanomas (3, 4), presumably because aberrant B-RAF signaling induces a potent senescence response (2, 5–8). Human nevi display some features of oncogene-induced senescence, including intact telomeres, increased p16^{INK4a} expression, and positive senescence-associated β-galactosidase (SA-β-Gal) activity (8–10), although the expression of this enzyme in human nevus cells in vivo remains controversial (11–13).

Senescent cells display a combination of markers that are not exclusive to the senescence program but in combination represent powerful predictors of this form of arrest. Senescence markers include the upregulation of p16^{INK4a}, induction of SA-β-Gal activity, the formation of senescence-associated heterochromatin foci

Lorenzo Galluzzi et al. (eds.), *Cell Senescence: Methods and Protocols*, Methods in Molecular Biology, vol. 965,
DOI 10.1007/978-1-62703-239-1_21,

Table 1
Predictive markers of oncogene-induced senescence

Senescence markers	Assay
Proliferative arrest	Ki67 and BrdU staining
Changes in cell morphology and size	Microscopy with DAPI stain
Accumulation of cell cycle regulators	Detection of $p16^{INK4a}$, $p21^{Waf1}$
Alterations in chromatin structure	DAPI stain
Expression of SA-β-Gal activity	SA-β-Gal stain
Accumulation of DNA damage	Detection of γ-H2AX
Activation of the DNA damage response	Detection of p-CHK1, p-CHK2

(SAHF), and the accumulation of DNA damage foci (reviewed in ref. 14, 15).

This chapter focuses on the analysis of senescence in primary human melanocytes expressing the oncogenic $B\text{-}RAF^{V600E}$ mutant. Using this model, senescent melanocytes can be detected using a series of well-established senescence markers and features (Table 1). These markers are easy to monitor over time and provide a robust assessment of senescence in cultured human cells.

The following section outlines some important considerations required to optimize and control senescence experiments in human melanocytes.

1.1. Human Melanocyte Model

Culture conditions are clearly important in the growth and replicative lifespan of human melanocytes (16). As with many investigators we use common supplements, including 12-*O*-tetradecanoylphorbol-13-acetate (TPA), cholera toxin, and 3-isobutyl-1-methyxanthine (IBMX), to stimulate the growth of these cells. Upon gene transduction using recombinant lentiviruses (17), we add stem cell factor to the culture media to assist cell recovery. It is also critical to replace the virus and polybrene containing media, 16–24 h posttransduction to minimize toxicity.

1.2. Transgene Expression

An important consideration when ectopically expressing oncogenes is to ensure that any effects caused by transgene expression do not simply reflect supra-physiological oncogene activity. We monitor $B\text{-}RAF^{V600E}$ activity by assessing the downstream activation of the MAPK cascade. In particular, the phosphorylation of the B-RAF kinase targets MEK and ERK (p-MEK and p-ERK) are measured using western analysis and compared to their phosphorylation in human melanoma cell lines expressing endogenous $B\text{-}RAF^{V600E}$. We only accept transgenic melanocyte data when the levels p-MEK

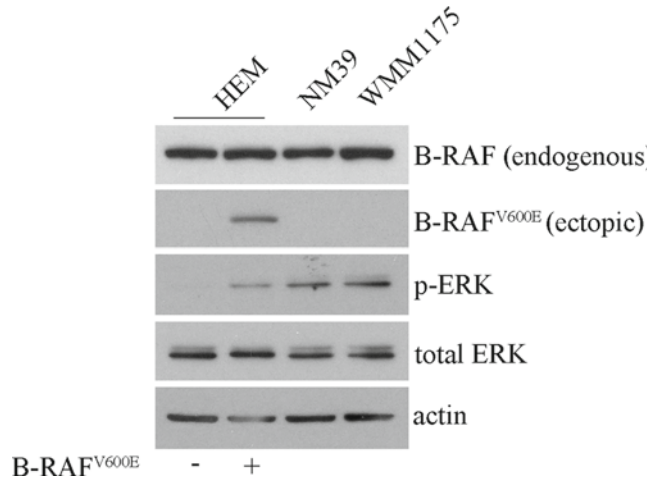

Fig. 1. Expression of the indicated proteins was determined by western blot analysis after infection of melanocytes with lentiviruses expressing copGFP (–) or B-RAF^{V600E} (+). Both the NM39 and WMM1175 melanoma cells carry the B-RAF^{V600E} oncogene.

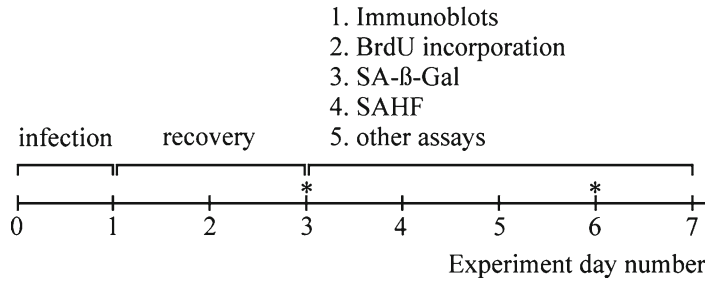

Fig. 2. Experimental time frame for melanocyte transduction and senescence analyses. Transduced cells are harvested on reference days 3 and 6.

and/or p-ERK are comparable to levels found in melanoma cell lines expressing endogenous B-RAF^{V600E} (Fig. 1).

1.3. Conducting Experiments

Optimizing the experimental time-course is also critical and depends on many factors including cell proliferation, passage number, and oncogene activity. Figure 2 outlines our typical 7-day protocol for studying the impact of activated B-RAF in human melanocytes. In order to examine multiple senescence markers (see Table 1) we recommend that at least 1×10^6 (6.7×10^6 cells/cm^2) melanocytes be harvested per time-point and per viral construct. At each time-point, adhered and suspension cells are harvested separately and enumerated. Trypan blue exclusion is used to determine the proportion of viable cells and a small fraction of the adhered cells is reseeded onto coverslips overnight for immunostaining (one coverslip per marker with DAPI nuclear staining to visualize chromatin condensation, see Fig. 3). The remaining

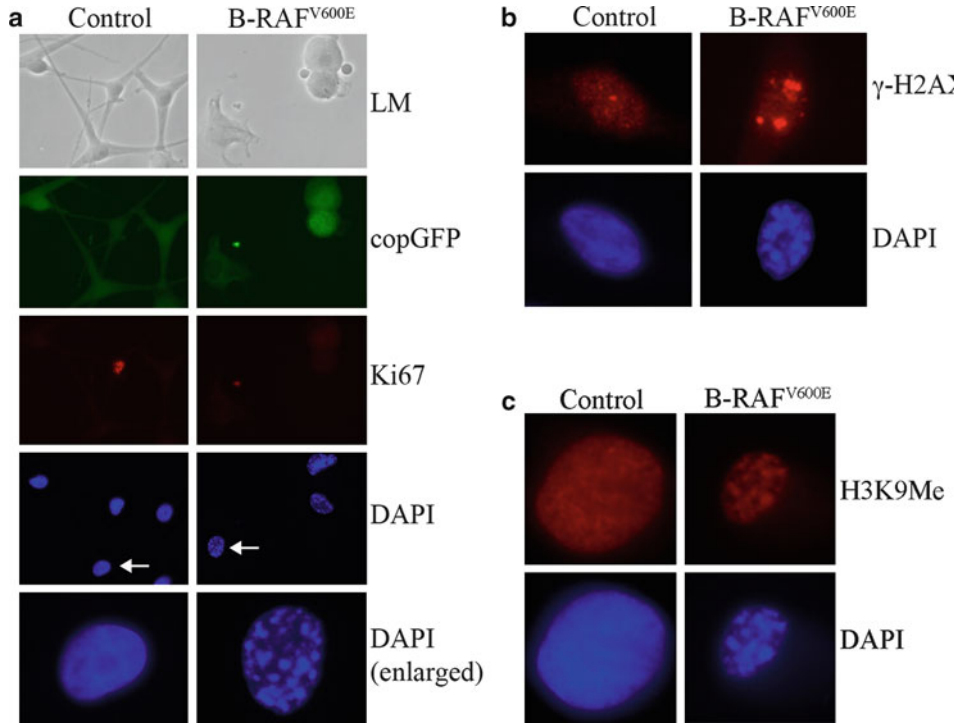

Fig. 3. Human melanocytes were infected with lentiviruses encoding B-RAF^{V600E} or copGFP (Control). (**a**) Cell proliferation (Ki67), chromatin condensation (DAPI), and transduction (copGFP) were analyzed 4 days post-transduction. Cells enlarged to show DAPI-stained chromatin foci are indicated with *arrows*. Transduced melanocytes were also stained for the DNA damage marker γ-H2AX (**b**) and the heterochromatin marker, H3K9Me (**c**) *LM* light microscopy.

adhered and suspension cells are pooled and analyzed by immunoblotting. Cell pellets are stored at −70°C until all samples are collected and are then lysed in RIPA buffer. Equal amounts of protein (35–50 μg) per sample are resolved on 12% SDS-PAGE, electroblotted on to PVDF membranes, and probed. B-RAF^{V600E}-transduced melanocytes are always compared to vector-transduced cells (Control) and ideally to wild-type B-RAF-transduced cells.

1.4. Assays

Fixed coverslips can be kept at 4°C in PBS until all samples have been collected. Ideally coverslips are stained for each marker in parallel to minimize staining variation. At least three coverslips should be seeded at days 3 and 6 (Fig. 2) to screen for (1) Ki67 expression (or BrdU incorporation) (Fig. 3), (2) γ-H2AX DNA damage foci (Fig. 3), and (3) SA-β-Gal activity (Fig. 4). We also include DAPI stain in all immunostaining to reveal SAHF (Fig. 3). Additional immunostaining markers can be included, and we often stain for common markers of heterochromatin, including histone H3 methylated at lysine 9 (H3K9Me) (Fig. 3) and nonhistone chromatin protein HMGA2 (reviewed in ref. 18).

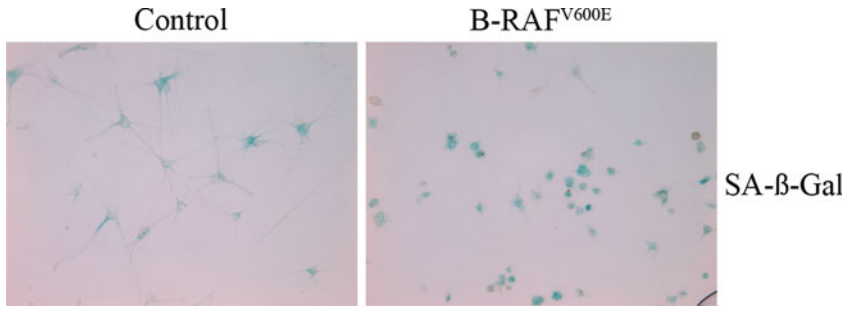

Fig. 4. SA-β-Gal activity in melanocytes infected with lentiviruses encoding B-RAF^{V600E} or copGFP (Control).

Cell pellets (adhered and suspension cells) are also collected at days 3 and 6 for western analyses of MAPK activity (p-ERK, total ERK, p-MEK, and total MEK), expression of the B-RAF transgene and senescence markers (p16^{INK4a}, p21^{Waf1}, p-CHK1, p-CHK2, γ-H2AX).

Analysis of cell morphology with particular attention to cell shape and size is routinely examined throughout the experimental time course. Senescent cells tend to be flat and larger in volume and we often measure the size of DAPI-stained nuclei as a surrogate for volume changes. Nuclear area can be accurately determined with image analysis software such as ImageJ (http://rsbweb.nih.gov/ij) or CellProfiler (http://www.cellprofiler.org). It is important to note that melanocytes induced to senescence with oncogenic B-RAF do not appear flattened or larger in size. In fact, a large proportion of B-RAF^{V600E}-transduced melanocytes become spheroidal and detach from the flask to remain viable in suspension (19).

2. Materials

2.1. Culture of Primary Dermal Melanocytes (Modified from ref. 20)

Complete growth medium for neonatal epidermal melanocytes (HEM1455): HAM'S F10 containing various growth factors that stimulate growth rate, a combination of cholera toxin and IBMX (to increase cellular cAMP levels) and TPA (to activate the protein kinase C family of enzymes) (Table 2).

2.2. Lentiviral Production

- 0.9% (w/v) NaCl in water.
- Polyethyleneimine (PEI; 40,000 nominal MW; Polysciences, Warrington, PA): 1 mg/mL in water.
- Third-generation lentivirus packaging system with compatible expression plasmid carrying B-RAF^{V600E} (see Notes 1 and 2).
- Optimem (Invitrogen, Grand Island, NY).

Table 2
Supplemented HAM'S F10 melanocyte media

Supplement[a]	Volume (mL)	Final concentration
Fetal calf serum	135	20%
Glutamine (200 mM stock)	13.5	4 mM
ITS (Becton Dickinson, Franklin Lakes, NJ)	6.7	1×
IBMX (4.5 mM stock)	15	100 μM
Cholera toxin (25 μg/mL stock; List Biological Laboratories, Campbell, CA)	3.6	135 ng/mL
TPA (27 μg/mL stock; sigma)	1.25[b]	108 nM

[a]Add to 500 mL HAM'S F10 base media; [b]TPA is labile and should be added to media immediately prior to use. Add 500 μL TPA stock per 200 mL supplemented HAM'S F10; IBMX, 3-isobutyl-1-methyxanthine

- DMEM (Lonza Group, Basel, Switzerland).
- FCS.
- Centricon Plus-70 centrifugal filter units (Millipore, Billerica, MA); 100 kDa membrane nominal molecular weight limit.
- HEK293T cells (ATCC HEK293T/17).
- U2OS cells (ATCC U-2 OS).

2.3. Lentiviral Transductions

- Polybrene (Sigma) stock at 80 mg/mL in water. Dilute this stock 1 in 10 with sterile PBS to make working stock aliquots (8 mg/mL) and store at −20°C.
- Stem cell factor (SCF; R&D systems, Minneapolis, MN) at stock concentration of 50 μg/mL (10 ng/mL final concentration in media). Store frozen aliquots at −80°C.
- Lentivirus preparations (see Subheading 3.2).
- Supplemented HAM'S F10 melanocyte media (Table 2).
- Neonatal epidermal melanocytes: low passage (<10).

2.4. Fluorescence Microscopy

2.4.1. Indirect Immunostaining

- PBS: Prepared as a 10× stock and diluted 1 in 10 for use.
- 3.7% formaldehyde fix solution: Make fresh before use by diluting concentrated formaldehyde (37%) 1 in 10 with PBS.
- Permeabilization solution: 0.1% (v/v) Triton X-100 (Sigma) in PBS.
- Blocking solution and antibody diluent: 10% (v/v) FCS in PBS.
- Mounting medium: 3% *N*-propyl gallate (Fluka Chemie, Buchs, Switzerland) dissolved in 80% glycerol in PBS.

Table 3
Antibodies used for immunostaining

Antibody	Clone	Supplier	Dilution
Ki67	MIB-1	DAKO, Glostrup, Denmark	1/300
BrdU	BU-1	Amersham Biosciences, NJ	1/40
γ-H2AX	20E3	Cell signaling, Boston, MA	1/300
AF-594	–	Molecular probes, Carlsbad, CA	1/1,000

- DNase for BrdU staining: 2,500 U of DNase I/mL of 1 × DNase buffer (Promega, Madison, WI).
- 5-Bromo-2-deoxyuridine (BrdU; Cell proliferation labeling reagent, GE Healthcare, Piscataway, NJ): Store at 4°C; for in vitro labeling, dilute 1/1,000 in prewarmed (37°C) culture medium.
- Glass coverslips (18 mm diameter).
- 12-well culture dishes.
- Antibodies (Table 3).
- 4′,6-diamidino-2-phenylindole (DAPI; Invitrogen): 2 mg/mL; dilute to 1 μg/mL for staining.

2.4.2. SA-β-Galactosidase Assay (21)

- SA-β-Gal fixative: 2% formaldehyde, 0.2% glutaraldehyde, 7.4 mM Na_2HPO_4, 1.47 mM KH_2PO_4, 137 mM NaCl and 2.68 mM KCl.
- Reaction buffer: 40 mM citric acid/sodium phosphate buffer pH 6.0, 5 mM potassium ferrocyanide, 5 mM potassium ferricyanide, 150 mM NaCl, 2 mM $MgCl_2$. Store in the dark at 4°C.
- Substrate: 5-Bromo-4-chloro-indolyl-galactopyranoside (X-Gal; Astral Scientific, Australia) stock: 20 mg/mL in dimethylformamide. Store aliquots at –20°C. Dilute X-Gal stock 1 in 20 in prewarmed reaction buffer (37°C) and filter sterilize before use (1 mg/mL final concentration).
- DAPI: 2 mg/mL; dilute to 1 μg/mL for staining.

3. Methods

3.1. Culture of Primary Dermal Melanocytes

1. HEM1455 melanocytes are cultured in supplemented HAM'S F10 media (Table 2) and seeded between 1.2 and 1.5×10^6 cells/T150 ($0.8–1 \times 10^4$ cells/cm^2) for optimal growth. Cells

will require passaging every 72–96 hours (yielding approximately one population doubling per passage). All cells are incubated and maintained at 37°C with 5% CO_2 atmosphere. Cells are routinely used for experiments prior to passage 10.

3.2. Lentiviral Production

The third-generation lentiviral packaging system is a split-genome, conditional packaging system that when combined with a self-inactivating vector construct carrying a major deletion in the 3′LTR offers the highest predictable biosafety features (17) (see Note 1). Nonetheless, it is important to adhere to strict biosafety guidelines when working with lentivirus. Please refer to your workplace safety personnel for appropriate practices and training.

1. Seed eight T150 vented flasks with 1×10^7 low passage HEK293T cells in DMEM/10%FCS and incubate under culture conditions for 16 h.
2. Make up the following two solutions:
   (a) Dilute 640 µL stock PEI in 8 mL of 0.9% NaCl.
   (b) DNA mix: 32 µg *pRSV-Rev* + 32 µg *pMD.G/VSV.G* + 32 µg *pMDLg/pRRE* + 64 µg *pCDH-copGFP* construct carrying B-RAF^{V600E} (see Note 2) in 8 mL of 0.9% NaCl.
3. Incubate the separate mixes at room temperature for 10 min.
4. Combine diluted PEI with the DNA mix and then incubate the resulting transfection mix at room temperature for 10 min to allow the formation of PEI–DNA complexes.
5. Replace media on HEK293T cells with 15 mL prewarmed (37°C) Optimem/2% FCS.
6. Add 2 mL of the transfection mix to each flask of HEK293T, gently mix, and incubate the flasks under culture conditions for 72 h.
7. Collect and pool the supernatants from the flasks and pre-filter the supernatant pool through a 0.45 µm filter.
8. Concentrate the filtrate at 3,000 rpm (1,400 × *g*) for approximately 30 min using the Centricon Plus-70 centrifugal filter units according to the manufacturer's instructions. Dilute retentate with filtrate to a final volume of ~12 mL (see Note 3).
9. Sterilize the concentrated supernatant with a syringe filter (0.2 µm).
10. Aliquot 200 µL–1 mL volumes in labeled screw capped tubes.
11. Store virus aliquots at –70°C (see Note 4).
12. Titer virus stocks by transducing U2OS cells with dilutions of virus (see Note 5).

3.3. Lentiviral Titering

1. In a 12-well culture dish, serially dilute 50 µL of virus in 500 µL volumes of DMEM/10%FCS supplemented with

16 μg/mL polybrene. Serially dilute twofold from $1/2^0$ to $1/2^{10}$.

2. Harvest and dilute U2OS cells to 6×10^4 cells/mL in DMEM/10%FCS.
3. Pipette 500 μL of the U2OS dilution (3×10^4 cells) on to each dilution of virus (final concentration of 8 μg/mL polybrene).
4. Mix thoroughly by carefully swirling the culture dish.
5. Incubate the culture dish under culture conditions for 72 h.
6. Harvest each transduced culture, fix suspended cells with paraformaldehyde for 15 min (final concentration of 1% formaldehyde).
7. Quantitate the proportion of GFP-positive transduced cells from each infection by FACS analysis (see Note 5). For constructs harboring selective markers, determine the greatest dilution of virus at which 100% of the seeded cells are resistant to the selective marker at 3 and 4 days postselection.
8. Viral titer can be calculated using the following formula:

$$\text{Viral particles / mL} = \%\text{transduced cells} \cdot \text{cells per well} \cdot 1/\text{dilution factor}.$$

3.4. Lentiviral Transductions

Seed and simultaneously transduce melanocytes with lentiviral constructs at a multiplicity of infection (MOI) to yield >80% of cells transduced. In general, MOI of 5 is sufficient.

1. Prepare the following transduction cocktail in a 15 mL tube: For 1×10^6 melanocytes use: 17 μL polybrene stock, 3.4 μL SCF stock, 5×10^6 lentivirus particles (MOI 5) and melanocyte supplement media (Table 2) to a final volume of 2 mL.
2. Dilute freshly harvested melanocytes to 1×10^6 cells/15 mL melanocyte media and dispense 15 mL volumes to T150 flasks.
3. Add 2 mL of transduction cocktail to each flask and gently mix.
4. Incubate flasks under culture conditions for 16 h.
5. Replace media with 20 mL melanocyte media supplemented with SCF (final concentration 10 ng/mL). Maintain transduced cells in media supplemented with SCF, replacing culture media at regular intervals twice weekly. Subculture cells if necessary including suspension cells.
6. Estimate the transduction efficiency by flow cytometry at 3 days posttransduction. Retain a small number of transduced melanocytes (~3×10^4) during splitting/maintenance, fix sample with 1/3 volume of 4% paraformaldehyde (final concentration 1%), and assess the proportion of cells expressing GFP.

Yields greater than 80% GFP positive cells are recommended for experiments.

7. Alternatively, lentiviral constructs expressing a puromycin resistance gene can be used to select the transduced pool by addition of 1 μg puromycin per mL of culture medium at 48 h after transduction.

3.5. Fluorescence Microscopy

3.5.1. Indirect Immunostaining

Because a significant proportion of B-RAF^{V600E}-induced senescent cells lose adherence to the culture flask, coverslips should be seeded with greater than 3×10^4 cells/coverslip (up to 5×10^4 cells/coverslip) to ensure enough cells remain adhered for staining and quantitation. It is convenient to seed coverslips for immunostaining during harvest at days 3 and 6 (Fig. 2) as this ensures the cells do not become confluent in the culture dish. Alternatively, cells can be seeded onto coverslips a few days prior to required time point. For example the day 6 coverslips can be seeded when harvesting day 3 cells for western blot.

1. Melanocytes are seeded at $3–5 \times 10^4$ cells onto a coverslip in a 12-well culture dish with 1 mL of fresh media (1 mL/well) and the cells allowed to adhere to the coverslip for 16 h under culture conditions.
2. After 16 h, wash coverslips gently with PBS twice then fix cells with 1 mL of 3.7% formaldehyde for 15 min at room temperature.
3. Remove fixative, wash coverslips with PBS and then permeabilize cells (1 mL permeabilization solution) for 10 min at room temperature.
4. Remove permeabilization solution by aspiration and wash coverslips by gently pipetting 1 mL PBS into the well then removing the volume by aspiration.
5. Add blocking solution and incubate cells at room temperature for 1 h.
6. Dilute primary antibodies (see Table 3).
7. Remove blocking solution from coverslips by aspiration and pipette 70–100 μL diluted antibody directly onto the coverslip ensuring an even coverage.
8. Incubate at room temperature for 1 h.
9. Wash coverslips three times with PBS.
10. Dilute Alexa Fluor-conjugated 594 (AF-594) secondary antibodies according to manufacturer's recommendations (see Table 3) and add DAPI to co-stain nuclei (1 μg/mL final concentration). Pipette 70–100 μL of diluted antibody directly onto the coverslip.
11. Incubate in the dark for 1 h at room temperature.

12. Wash coverslips three times with PBS and once in water.
13. Carefully lift coverslips out of the wells by lifting one edge and then removing the coverslip using forceps (see Note 6). Blot excess water by touching the edge of the coverslip onto blotting paper.
14. Mount inverted coverslips with a drop of mounting solution (17–20 μL) onto glass slides.
15. Quantitate the proportion of stained cells using fluorescence microscopy, counting at least 200 cells over multiple fields. To reduce bias, counts should be verified by several independent investigators.

3.5.2. BrdU Staining

BrdU incorporation can be used to monitor proliferative capacity and can be added to media as recommended by the manufacturer (see Subheading 2.4). Optimum incubation/incorporation times vary depending on cell type and proliferation rate (for our melanocytes a 16 h BrdU pulse will result in 5–15% BrdU positive cells).

1. Seed coverslips as described in Subheading 3.5.1, step 1, with the addition of BrdU as recommended by manufacturer.
2. 12–16 h after seeding, wash coverslips with PBS then fix and permeabilize (see Subheading 3.5.1, steps 2 and 3).
3. Wash with PBS and then incubate the coverslips with DNase to expose the incorporated BrdU. To ensure even coverage to the edge of the coverslips, DNase treatment is performed with the coverslips face down on a 70 μL drop of diluted DNase.
4. After DNase treatment for 30 min, carefully lift one edge of the coverslip and pipette anti-BrdU antibody directly into the DNase drop to an appropriate final concentration (see Table 3). Mix well by repeated pipetting but take care not to introduce bubbles.
5. Incubate for 1 h at room temperature.
6. Transfer coverslips back into a 12-well plate and wash coverslips with PBS.
7. Perform secondary antibody binding and mounting as set out in Subheading 3.5.1, steps 10–15.

3.6. SA-β-Galactosidase Assay (21)

SA-β-Gal activity is detectable at suboptimal pH (pH 6.0; see Note 7) in senescent cells due to the expansion of lysosomes in response to senescence (21, 22).

1. Seed 3–5 × 10^4 melanocytes onto coverslips in a 12-well culture plate and allow cells to adhere overnight under culture conditions.
2. Wash coverslips gently with PBS twice then fix cells with SA-β-Gal fixative for 7 min at room temperature.

3. Remove fix and wash coverslips with PBS.
4. Add prewarmed (37°C) substrate: 1 mL per well.
5. Incubate coverslips at 37°C in the dark until blue color develops within the fixed cells (up to 16 h, see Note 8).
6. Remove substrate and wash coverslips with PBS.
7. To stain nuclear DNA, incubate coverslips with 300 μL DAPI (final concentration 1 μg/mL) for several minutes, wash with PBS twice and once in distilled water.
8. Mount inverted coverslips onto glass slides with mounting solution.
9. Enumerate the proportion of blue (SA-β-Gal positive) cells with reference to control cells using a bright field microscope, counting at least 200 cells.

4. Notes

1. This protocol employs a third-generation lentiviral system (Table 4) adapted from (17). This system comprises of three plasmids, which allow the packaging of the transfer pCDH vectors.
2. The lentiviral expression vectors *pCDH-CMV-MCS-EF1-copGFP* and *pCDH-CMV-MCS-EF1-PURO* (referred to in this article as *pCDH-copGFP* and *pCDH-PURO* respectively; System Biosciences, Mountain View, CA) constitutively express cloned cDNAs under the control of the efficient CMV promoter. These vectors also encode the copepod green fluorescent protein (copGFP) or puromycin resistance (respectively) to facilitate the assessment of transduction efficiency and selection.

Table 4
Third-generation packaging systems

Vector	Gene(s)	Relevant details
pRSV-Rev	Rev	Rev gene product from HIV is involved in posttranscriptional regulation of RRE elements
pMD.G/VSV.G	VSV.G	Structural envelop protein (G protein) from the vesicular stomatitis virus (VSV)
pMDLg/pRRE	RRE, *gag*, *pol*	Harbors the REV response element (RRE) and the structural genes, *gag* and *pol* from HIV
pCDH vectors	Gene of interest	Transfer plasmid harboring gene of interest cDNA

3. Lentivirus harvest and concentration may take 2–3 h.
4. Lentivirus preparations are labile and repeat freeze/thawing should be avoided. Store single-use aliquots at –70°C.
5. For accurate titers, calculate the viral titer using virus dilutions leading to 0.1–10% transduction efficiency. Titers should be determined for each studied cell type; however to compare batches of virus preparations it is useful to calculate viral titers in an indicator cell line (e.g., U2OS). Titers generally range between 10^6 and 10^8 particles/mL.
6. Coverslips can be lifted by making a hook from the tip of a standard 21 gauge normal bevel hypodermic needle: tap the tip of the needle against a hard surface to curl the needle tip. Use the hook to catch and lift the edge of a coverslip within a well.
7. Assay pH can be optimized between pH 5.5 and 7.0 to generate the clearest differential staining between proliferating and senescent cells. Normal lysosomes have an internal pH < 5.
8. Optimal incubation times for maximum differential staining must be determined empirically for each cell type or cell line. Longer incubation times for this assay can result in more intense blue staining; however, this can also lead to a higher background staining.

Acknowledgment

We thank Drs Therese Becker and Kavitha Gowrishankar for critical reading of this manuscript. HR is a recipient of a Cancer Institute New South Wales, Research Fellowship and a NHMRC Senior Research Fellowship.

References

1. Platz A, Egyhazi S, Ringborg U, Hansson J (2008) Human cutaneous melanoma; a review of NRAS and BRAF mutation frequencies in relation to histogenetic subclass and body site. Mol Oncol 1:395–405
2. Gray-Schopfer VC, Cheong SC, Chong H, Chow J, Moss T, Abdel-Malek ZA, Marais R, Wynford-Thomas D, Bennett DC (2006) Cellular senescence in naevi and immortalisation in melanoma: a role for p16? Br J Cancer 95:496–505
3. Kuwata T, Kitagawa M, Kasuga T (1993) Proliferative activity of primary cutaneous melanocytic tumours. Virchows Arch 423:359–364
4. Maldonado JL, Timmerman L, Fridlyand J, Bastian BC (2004) Mechanisms of cell-cycle arrest in Spitz nevi with constitutive activation of the MAP-kinase pathway. Am J Pathol 164:1783–1787
5. Dankort D, Curley DP, Cartlidge RA, Nelson B, Karnezis AN, Damsky WE Jr, You MJ, DePinho RA, McMahon M, Bosenberg M (2009) Braf(V600E) cooperates with Pten loss to induce metastatic melanoma. Nat Genet 41:544–552
6. Dhomen N, Reis-Filho JS, da Rocha Dias S, Hayward R, Savage K, Delmas V, Larue L, Pritchard C, Marais R (2009) Oncogenic Braf induces melanocyte senescence and melanoma in mice. Cancer Cell 15:294–303
7. Goel VK, Ibrahim N, Jiang G, Singhal M, Fee S, Flotte T, Westmoreland S, Haluska FS,

Hinds PW, Haluska FG (2009) Melanocytic nevus-like hyperplasia and melanoma in transgenic BRAFV600E mice. Oncogene 28:2289–2298

8. Michaloglou C, Vredeveld LC, Soengas MS, Denoyelle C, Kuilman T, van der Horst CM, Majoor DM, Shay JW, Mooi WJ, Peeper DS (2005) BRAFE600-associated senescence-like cell cycle arrest of human naevi. Nature 436:720–724
9. Miracco C, De Margherita Santi M, Schurfeld K, Santopietro R, Lalinga AV, Fimiani M, Biagioli M, Brogi M, De Felice C, Luzi P, Andreassi L (2002) Quantitative in situ evaluation of telomeres in fluorescence in situ hybridization-processed sections of cutaneous melanocytic lesions and correlation with telomerase activity. Br J Dermatol 146:399–408
10. Mooi WJ, Peeper DS (2006) Oncogene-induced cell senescence–halting on the road to cancer. N Engl J Med 355:1037–1046
11. Cotter MA, Florell SR, Leachman SA, Grossman D (2007) Absence of senescence-associated beta-galactosidase activity in human melanocytic nevi in vivo. J Invest Dermatol 127:2469–2471
12. Cotter MA, Florell SR, Leachman SA, Grossman D (2008) Response to Gray-Schopfer et al. and Michaloglou et al. J Invest Dermatol 128:1583–1584
13. Michaloglou C, Soengas MS, Mooi WJ, Peeper DS (2008) Comment on absence of senescence-associated beta-galactosidase activity in human melanocytic nevi in vivo. J Invest Dermatol 128:1582–1583, author reply 1583-1584
14. Campisi J, d'Adda di Fagagna F (2007) Cellular senescence: when bad things happen to good cells. Nat Rev Mol Cell Biol 8:729–740
15. Collado M, Serrano M (2006) The power and the promise of oncogene-induced senescence markers. Nat Rev Cancer 6:472–476
16. Bennett DC (2003) Human melanocyte senescence and melanoma susceptibility genes. Oncogene 22:3063–3069
17. Dull T, Zufferey R, Kelly M, Mandel RJ, Nguyen M, Trono D, Naldini L (1998) A third-generation lentivirus vector with a conditional packaging system. J Virol 72:8463–8471
18. Adams PD (2007) Remodeling of chromatin structure in senescent cells and its potential impact on tumor suppression and aging. Gene 397:84–93
19. Becker TM, Philipsz S, Scurr LL, Fung C, Haferkamp S, Kefford RF, Rizos H (2010) Oncogenic B-RAF(V600E) promotes anchorage-independent survival of human melanocytes. J Invest Dermatol 130:2144–2147
20. Halaban R, Ghosh S, Duray P, Kirkwood JM, Lerner AB (1986) Human melanocytes cultured from nevi and melanomas. J Invest Dermatol 87:95–101
21. Dimri GP, Lee X, Basile G, Acosta M, Scott G, Roskelley C, Medrano EE, Linskens M, Rubelj I, Pereira-Smith O et al (1995) A biomarker that identifies senescent human cells in culture and in aging skin in vivo. Proc Natl Acad Sci U S A 92:9363–9367
22. Kurz DJ, Decary S, Hong Y, Erusalimsky JD (2000) Senescence-associated (beta)-galactosidase reflects an increase in lysosomal mass during replicative ageing of human endothelial cells. J Cell Sci 113(Pt 20):3613–3622

Chapter 22

Methods to Investigate the Role of SIRT1 in Endothelial Senescence

Bo Bai and Yu Wang

Abstract

Sirtuins are a family of proteins with NAD^+-dependent deacetylase or mono-ADP-ribosyltransferase activity. SIRT1, the mammalian ortholog most closely related to *Sir2* (the first gene of this family discovered in yeast), exhibits anti-senescence activity in a wide range of mammalian cells. Here, we describe the use of an ex vivo senescence model to study SIRT1 function in primary endothelial cells isolated from the porcine aorta. The methods can be applied to the investigation of the role of SIRT1 in the development of endothelial senescence and atherosclerosis.

Key words: Aorta, Atherosclerosis, Premature senescence, Primary endothelial cells, Replicative senescence, SIRT1

1. Introduction

Senescence, or finite replication of primary cells in culture, was observed and reported by Hayflick and Moorhead almost half a century ago (1). After a limited number of division cycles, cultured cells enter into a status of "replicative senescence," due mainly to the progressive erosion and eventual dysfunction of telomeres (2). In addition, premature senescence is triggered by short period exposure to agents such as hydrogen peroxide (H_2O_2) and chemicals, radiation, or energy stress, and occurs in the absence of detectable telomere shortening (3, 4).

Sirtuins are highly conserved class III histone deacetylases. The founding member *Sir2* (silent information regulator 2) was originally discovered to regulate transcription silencing in yeast by deacetylation of histones at the epsilon-amino groups of lysines (5–11). In addition to histones, mammalian sirtuins regulate the

Lorenzo Galluzzi et al. (eds.), *Cell Senescence: Methods and Protocols*, Methods in Molecular Biology, vol. 965,
DOI 10.1007/978-1-62703-239-1_22,

acetylation status of a wide range of nonhistone targets, including signaling molecules, transcription factors, and enzymes (12, 13). In 1999, Kaeberlein et al. showed that null allele of *Sir2* caused a severe reduction in the mean lifespan of *Saccharomyces cerevisiae* by about 50%, while integration of extra copies of *Sir2* increased the lifespan by up to 30% (14). Similar effects on lifespan extension were subsequently observed for this protein in *Caenorhabditis elegans* and *Drosophila melanogaster* (15–18).

There are seven members of the mammalian sirtuins (SIRT1-SIRT7), which all contain a catalytic domain with ~275 amino acids. Mutation of a conserved histidine residue (H363 of human SIRT1) within this domain abolishes the enzymatic activity and dominant negatively affects the protein functions (19). Based on phylogenetic tree analysis of the amino acid sequences, the mammalian SIRTs are further assigned into four classes (I–IV) (20). SIRT1-3 are class I sirtuins sharing high homology to Sir2 in yeast. SIRT4 and SIRT5 belong to class II and class III, respectively. The class IV sirtuins are SIRT6 and SIRT7. The differences in amino acid sequences confer profound effects on intracellular localizations and catalysis or substrate specificity of the subclass members of SIRTs (21).

Of all seven mammalian SIRTs, SIRT1 has been most extensively studied. Structurally, SIRT1 consists of a globular core and two large unordered regions at NH_2- and COOH-termini, which are in positions that may not affect the catalytic core activity but influence the intracellular localizations and interactions with other proteins (22, 23). SIRT1 is involved in a variety of biological processes, including cell growth and metabolism, gene transcription and chromosome stability, DNA repair and stress responses, etc. (24). SIRT1 has been implicated in mediating the lifespan extending effects of caloric restriction, in organisms ranging from yeast to rodents, and primates (25–27). Mice lacking SIRT1 failed to show the elevation of physical activity in response to food restriction (28). By contrast, elevation of SIRT1 in mice elicited beneficial effects resembling that of caloric restriction, such as increased metabolic activity, reduced blood cholesterol levels, and improved glucose tolerance (29). In fact, the available evidences suggest that SIRT1 mediates the antiaging effects of caloric restriction largely by regulating cellular energy metabolisms that not only benefit normal physiology, but also contribute to the prevention of aging-associated medical complications, in particular cardiovascular diseases, diabetes, and neurodegenerative disorders (30–34).

The anti-senescence function of SIRT1 has been demonstrated in mammalian cells including primary mouse embryonic fibroblasts (35), various human cancer cells (36, 37), human diploid fibroblast (38), human umbilical vein endothelial cells (39), primary porcine aortic endothelial cells (40), primary human aortic smooth muscle cells (41), endothelial progenitor cells (EPCs) (42, 43), and human

adipose tissue-derived mesenchymal stem cells (44). In most of these studies, a premature senescence phonotype can be induced by either downregulation of SIRT1 expression or inhibition of SIRT1 activity. Conversely, overexpression or activation of SIRT1 prevents both stress- and replication-induced cellular senescence by deacetylation of a plethora of intracellular protein substrates, including p53, NFκB, PGC-1α (peroxisome proliferator-activated receptor-γ coactivator 1α), eNOS, LKB1, FoxO, etc. (45).

We have been using the primary endothelial cell cultures isolated from porcine aorta or coronary artery for studying the anti-senescence functions of SIRT1 (40). These cells are relatively easy to propagate and develop cellular senescence within a shorter period of time compared to cell line-based models (46, 47).

2. Materials

Prepare all solutions and buffers using ultrapure water (deionized to attain a sensitivity of 18 MΩ-cm at 25°C). Sterilize by autoclaving at 121°C/15 psi for 20 min or by filtration through 0.2 μm membrane (Sartorius, Goettingen, Germany). Determine the pH values at room temperature. All chemicals are of analytical grade. Disposable gloves should be worn when performing the experiment. Strictly follow institutional regulations when disposing waste materials.

2.1. Dissecting Kits

- Two pairs small forceps (watchmakers'; No. 4 or 5).
- One pair small scissors (about 12.5 cm straight blades).
- One pair of ophthalmic scissors (about 10 cm straight blades).
- One scalpel (No. 3 handle, No. 22 blade).
- Steel insect pins (size 2).
- 15 cm glass dish coated with *Sylgard* and *Sylgard* 184 (Dow Corning, Midland, Michigan, USA) (see Note 1).

2.2. Solutions and Buffers for Isolation and Culture of Primary Endothelial Cells

- Earle's balanced salt solution (EBSS): 140 mM NaCl, 4 mM KCl, 1 mM Na_2HPO_4, 0.23 mM NaH_2PO_4, 5.5 mM Glucose, 1% (v/v) penicillin-streptomycin-fungizone (PSF), and 5% (v/v) FBS; pH 7.4 (see Note 2).
- Phosphate buffered saline (PBS): 137 mM NaCl, 2.7 mM KCl, 4.3 mM Na_2HPO_4, 1.47 mM KH_2PO_4 (pH 7.4) (see Note 3).
- Dulbecco's Modified Eagle Medium (DMEM), fetal bovine serum (FBS), PSF, and trypsin-EDTA are from Life Technologies (Grand Island, NY, USA). DMEM containing 15% FBS is used for maintaining the endothelial cultures.

- Autoclaved gelatin solution (1% in endotoxin-free water, store at 4°C) is used for coating the Petri dish at 37°C overnight. The gelatin solution is aspirated and the dishes washed with DMEM immediately before seeding the cells.

2.3. Solutions and Buffers for Characterization of Senescent Endothelial Cells

- Senescence-associated β-galactosidase (SA-β-gal) substrate staining solution: 150 mM NaCl, 2 mM $MgCl_2$, 5 mM potassium ferricyanide, 5 mM potassium ferrocyanide, 40 mM citric acid, 12 mM sodium phosphate, 1 mg/mL 5-bromo-4-chloro-3-indolyl-β-D-galactoside (X-gal); pH 6.
- Propidium iodide (PI) staining buffer: 100 mM Tris–HCl, pH 7.4, 150 mM NaCl, 1 mM $CaCl_2$, 0.5 mM $MgCl_2$, 0.1% NP-40, 50 μg/mL PI, and 0.1 mg/mL RNase.
- Crystal violet stock solution (5%), prepared in 20% methanol, stirred overnight, and filtered through Whatman paper. A working concentration of 0.2% is used for cell staining.

2.4. Antibodies

- Antibodies against SIRT1, LKB1, phospho-AMPK(Thr172), phospho-AMPK(Ser485), AMPK and von Willbrand factor are from Cell Signaling Technology (Beverly, MA, USA).
- Antibody against β-actin is from Santa Cruz Biotechnology (Santa Cruz, CA, USA).
- Antibodies against FLAG, peroxidase-conjugated anti-rabbit, anti-mouse and anti-goat IgG are from Sigma-Aldrich (St. Louis, MO, USA).

2.5. Assay Kits and Reagents

- Effectene transfection reagent (QIAGEN, Hilden, Germany).
- TRAPEZE XL Telomerase Detection Kit (Millipore, Billerica, MA, USA).
- TUNEL in situ Cell Death Detection Kit (Roche, Indianapolis, IN, USA).
- BCA protein assay (Thermo Fisher Scientific, Rockford, IL, USA).
- Trizol Reagent (Life Technologies, Carlsbad, CA, USA).
- SYBR Green PCR Master Mix (Qiagen, Hamburg, Germany).

3. Methods

3.1. Isolation and Culture of Primary Coronary Endothelial Cells

1. Female farm pigs (2–3 months old; 25–30 kg) are anesthetized by intramuscular injection of a mixture of tiletamine plus zolezepam (10 mg/kg each in a total volume of 5 mL) and euthanized by exsanguination. The hearts are collected and transferred into cold EBSS supplemented with 1% PSF and 5% FBS.

2. Endothelial cells can be harvested from the left circumflex, left anterior descending artery, right coronary arteries, and aorta fragment (length of 5–10 cm) attached to the heart. Separate the arteries from heart and place immediately in freshly prepared cold EBSS. After clearing all the adhering fat, arteries are cut longitudinally and pinned down for *en face* cell isolation in a glass dissecting dish covered with a layer of clear silicone (Sylgard).
3. Add sufficient cold EBSS to cover the artery fragments and rinse by gentle shaking. Discard the solution and replace with fresh EBSS (see Note 4). Repeat the washing step five times and remove the solution completely before collecting the endothelial cells.
4. Gently scrape the luminal surface of arteries with a blade and collect the fragments of endothelial lining in 30 mL of pre-warmed DMEM containing 1% PSF and 5% FBS (see Note 5). Remove extra liquid on the blade using autoclaved paper tissues before the next scraping.
5. Resuspend the cells collected in Falcon tube using sterile transfer pipettes. After centrifugation at 200 × *g* for 5 min, supernants are discarded and the centrifugation–resuspension step is repeated for two more times. The primary endothelial cells are plated in a 60 mm gelatin-coated Petri dish. The plating efficiency is about 10%. The cells are cultured in DMEM with 15% FBS at 37°C in humidified 5% CO_2 95% air. Add fresh media every 2 days.
6. At about 1 week after plating or when reaching 80% confluency, cells [referred as passage zero (P0)] are detached with trypsin-EDTA and passaged at a density of 10^3 cells/cm^2 in 100 mm gelatin-coated Petri dish. Thereafter, each of the subsequent passages are referred as passage one (P1), passage two (P2), passage three (P3), and passage four (P4).
7. A small portion of cells at different passages can be subjected to purity checking by immunocytochemistry staining of von Willebrand factor (47).

3.2. Evaluation of Cell Proliferation

1. Endothelial cell growth is evaluated by calculating the population doubling (PDL). At the end of each passage, after adding trypsin-EDTA and incubating at 37°C for 2 min, the cells are detached and resuspended in DMEM containing 5% FBS. A small volume of cell suspension is mixed with 0.4% Trypan Blue dye (diluted 1:1–1:5 depending on the number of cells). Only nonviable cells take up the dye and appear blue under a light microscope. Viable cells remain unstained and are manually counted using a haemocytometer. The growth rate of the cultured endothelial cells is progressively decreasing from P1 to P4. The cumulative PDL is around 11.34 (46) (see Note 6).

2. Cell proliferation rate is measured by crystal violet staining, a rapid and reproducible method for quantifying cell proliferation in monolayer cultures (48, 49). Cells are seeded at a density of 1×10^3/well in 96-well plates. At different time points, the media are removed and cells washed twice with PBS. Cold methanol (−20°C, 100 μL/well) is added and incubated for 30 min to fix the cells. Staining is performed by incubation with 100 μL of 0.2% crystal violet dye solution for an additional 15 min at room temperature. Excess dye is removed by gentle washing with water. After air drying the wells, stained cells are solubilized in equal volume of 1% SDS. The optical density is measured at a wavelength of 570 nm (see Note 7).
3. DNA replication rate is another indicator of cell proliferation and can be evaluated by [^{3}H-methyl]-thymidine incorporation assay (50). Cells are seeded at a density of 1×10^4/well in 24-well plates and starved for 48 h in DMEM containing 0.5% FBS prior to the addition of fresh DMEM and 15% FBS. Radio-labeling is performed by adding 1 μCi/mL of [^{3}H-methyl]-thymidine during the last 6 h of incubation. After washing with PBS for three times, DNA is precipitated with 5% trichloroacetic acid for 30 min. The precipitated DNA is subsequently solubilized with 0.2 M NaOH and neutralized with 0.2 M HCl. Cell proliferation is measured by quantifying the incorporated [^{3}H-methyl]-thymidine using a liquid scintillation counter (see Note 8).

3.3. Characterization of Senescent Endothelial Cells

1. Morphologically, the monolayer of "young" endothelial cells (P1) exhibits a typical "cobblestone" pattern, whereas the "senescent" P4 cells are enlarged and flattened with a concomitant increase in the size of the nucleus and nucleoli (Fig. 1).
2. SA-β-gal staining is used to quantitatively monitor the occurrence and accumulation of senescent cells (51–53). Cells are

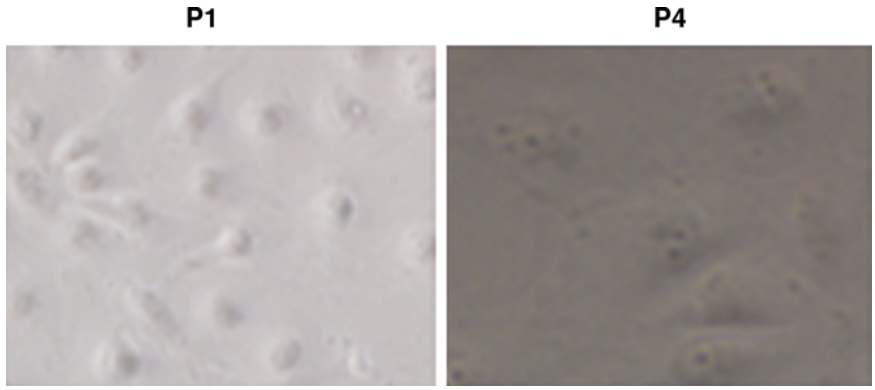

Fig. 1. Morphology of primary endothelial cells isolated from porcine aorta and cultured at passage 1 (P1) and passage 4 (P4). Magnification, 400×.

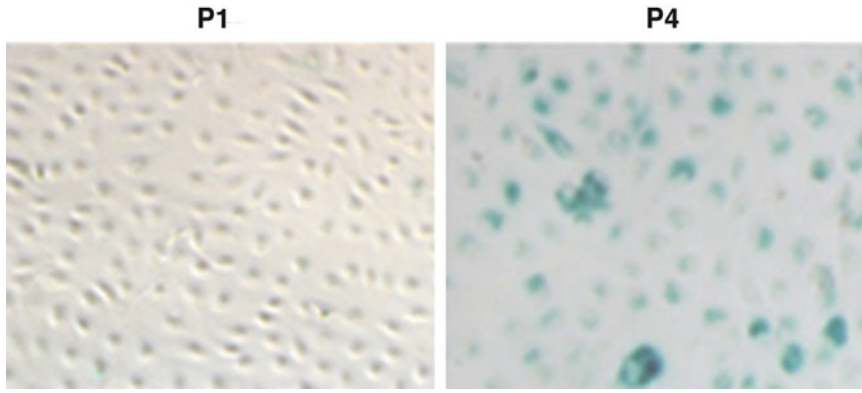

Fig. 2. SA-β-gal staining of primary endothelial cells cultured at passage 1 (P1) and passage 4 (P4). Magnification, 100×.

fixed with 2% formaldehyde/0.2% glutaraldehyde in PBS for 10 min at room temperature. After extensive washing with PBS, freshly prepared SA-β-gal substrate staining solution is added and the incubation performed at 37°C for 16 h. The substrate solution is decanted and cells washed with PBS. Glycerol solution (70%) is added and the number of stained cells evaluated with conventional microscope (see Note 9) (Fig. 2).

3. Telomerase activity is evaluated in endothelial cells collected at different passages using the Telomerase Detection Kit (40, 46). Cells are lysed by CHAPS Lysis Buffer and the protein concentrations determined by BCA assay. Cell lysates containing 1.5 μg proteins are mixed with Taq polymerase and TRAPEZE XL Reaction Mix. After incubating at 30°C for 30 min, a thermal cycling program (94°C/30 s, 59°C/30 s, 72°C/1 min) is repeated for 36 cycles followed by a single extension step (72°C/3 min, 55°C/25 min). The samples are stored at 4°C. The fluorescence of each sample is measured at the excitation/emission wavelengths of 495/516 nm for fluorescein and 600/620 nm for sulforhodamine using a fluorescence plate reader. TSR8 standards, telomerase positive control, minus telomerase control, and minus Taq polymerase control are included in the amplification process (see Note 10).

4. Premature senescence can be induced in the primary endothelial cultures. Oxidative stress is induced by adding 100 μM freshly prepared H_2O_2 and continue the incubation for 1 h (39, 46). Positive SA-β-gal stained cells can be detected after culturing for another 5 days.

3.4. Investigation of the Anti-senescence Activity of SIRT1

1. Cells at different passages are collected for measuring the mRNA expression levels of SIRT1 by quantitative PCR analysis. Total RNA is extracted using Trizol Reagent. After obtaining cDNA by reverse transcription, quantitation of target genes is

performed using SYBR Green PCR Master Mix. The primers are 5′-AGGAGGTGAATATGCCAAGC-3′ (forward) and 5′-CTGAAGAAGCTGGTGGTGAA-3′ (reverse) for SIRT1 (Sus scrofa sirtuin 1, NM_001145750.1), and 5′-AATGACC CCTTCATTGACCTCC-3′ (forward) 5′-GCTTCCCATTC TCAGCCTTGAC-3′ (reverse) for GAPDH. The mRNA levels are gradually decreased during the prolonged culture in primary endothelial cells. At P4, the SIRT1 mRNA expression is reduced by more than 70% compared to P1 cells (40).

2. SIRT1 protein expression is examined by Western blotting. Cells at different passages are solubilized in lysis buffer containing 20 mM Tris–HCl (pH 7.4), 150 mM NaCl, 1 mM EDTA, 1 mM EGTA, 1% Triton X-100, 2.5 mM sodium pyrophosphate, 1 mM β-glycerolphosphate, 1 mM Na_3VO_4, and the complete protease inhibitor cocktail. The lysates are sonicated twice for 10 s and centrifuged at $14{,}000 \times g$ for 20 min at 4°C. Protein concentration is determined by BCA assay. The samples with equal amount of protein are mixed with 5× SDS loading buffer and boiled at 95°C for 5 min before loading on SDS-PAGE. The separated proteins are transferred onto nitrocellulose membrane for probing SIRT1 with the specific primary antibody. After 1 month of culture, the SIRT1 protein amount is less than half of that in P1 cells (40).
3. Transient transfection is performed in primary endothelial cells using Effectene transfection reagent (see Note 11). Cells (4×10^5) are seeded in each well of gelatin-coated 6-well plates the day before transfection. Plasmid DNA (0.8 μg) is mixed with "buffer EC" provided in the kit to a total volume of 100 μL. Enhancer (6.4 μL) is added and the mixture incubated at room temperature for 5 min. Effectene Transfection Reagent (6 μL) is added and incubated at room temperature for another 10 min. After adding fresh medium (0.6 mL), the transfection complex is transferred drop by drop to the cell cultures. After 48–72 h, the overexpressed SIRT1 can be confirmed by Western blotting. For transient transfection in other types of multi-well plates, all the volumes are scaled up or down accordingly. Elevation of SIRT1 levels promotes the proliferation of endothelial cells and blocks the development of cellular senescence (40).
4. Inhibition or loss of SIRT1 function induces cellular senescence in primary endothelial cultures. Incubation with SIRT1 inhibitor nicotinamide (10 mM) for 48 h promotes the development of endothelial senescence (40). Similarly, knocking down of SIRT1 expression by RNA interference induces cellular senescence. Stealth siRNA is transfected into endothelial cells using LipofectamineTM 2000 transfection reagent (Invitrogen). For cells seeded in 6-well plates, 100 pmol scramble

siRNA or specific stealth siRNA is mixed with 250 μL Opti-MEM medium. LipofectamineTM 2000 is also mixed with Opti-MEM and incubated at room temperature for 5 min. Stealth siRNA and LipofectamineTM 2000 mix are then combined and incubated for a further 20 min at room temperature before adding into the culture wells containing fresh medium. The downregulation effect is confirmed by Western blotting at 48–72 h after transfection. Overexpression of a dorminant negative mutant of SIRT1 [SIRT1(H363Y)] induces cellular senescence (40). The plasmid for overexpressing the deacetylase mutant SIRT1(H363Y) is generated by site-directed mutagenesis to replace histidine at residue 363 to tyrosine. In cultured cells, overexpression of SIRT1(H363Y) is achieved by transient transfection using Effectene Transfection Reagent.

5. Hyperactivation of LKB1/AMPK signaling induces cellular senescence in primary endothelial cultures (40). Elevation of LKB1 is implemented by transient transfection using Effectene Transfection Reagent. At 48–72 h after transfection, severe senescence can be detected by SA-β-gal staining. Co-transfection with vector encoding SIRT1 blocks the pro-senescence activity of LKB1. The recombinant adenoviruses for overexpressing the constitutively active (CA-AMPK) and the dominant-negative version of AMPK (DN-AMPK) are used for studying AMPK-mediated cellular senescence. The CA-AMPK is a truncated form of AMPK catalytic subunit with Thr172 replaced by Asp. DN-AMPK contains a mutated form of AMPK with Asp157 replaced by Ala (54). Cells are infected with the recombinant adenoviruses at 50–500 pfu/cell and then incubated at 37°C for another 48 h before starting subsequent experiments (see Note 12). AMPK activity can be modulated by adding drug compounds, including the activator AICAR (2 mM) and the inhibitor compound C (5 μM). The drugs are added in the culture media for 48 h prior to senescence evaluation.

4. Notes

1. Sylgard 184 (Dow Corning) is clear silicone rubber polymerized by mixing two components (9 parts rubber solution:1 part of accelerator/catalyst). Mix and pour to the desired depth (2–5 mm) into the glass Petri dish. Allow the dishes to stand for about 1 h at room temperature for air bubbles to leave, then incubate at 55°C until polymerized (3 h to overnight). The dishes can be stored indefinitely and autoclaved.
2. Dilute 100 mL of 10× EBSS to about 800 mL with water. Adjust the pH to 7.4. Add 10 mL PSF and 50 mL FBS. Make to 1 L with water.

3. Dissolve 80 g NaCl, 2 g KCl, 14.4 g Na2HPO4, 2.4 g KH2PO4 in 800 mL of water. Adjust pH to 7.4 using HCl. Add water to a final volume of 1 L. Sterilize by autoclaving. Dilute 100 mL of 10× PBS before use.
4. Reduce the exposure time to enhance cell survival. EBSS buffer containing 1% PSF (v/v) and 5% FBS (v/v) is used to minimize the bacteria contamination and maintain the activity of the endothelial cells.
5. The media for collecting cells should be pre-warmed in a 37°C water bath. Large volume of media (over 30 mL/per wash) is recommended for resuspending the cells to minimize bacteria contamination.
6. Population doubling = (log 10*F*–log 10*I*)/0.301, where *F* is the number of cells at the end of one passage, and *I* is the number of cells seeded at the beginning of the passage. Compared to the present model, human dermal fibroblasts and human umbilical vein endothelial cells at passage 15 (PDL > 55) are considered as "senescence" cells (55). Human primary vascular smooth muscle cells reach senescence at passage 13 (56). The self-renewal capacity of human adipose tissue-derived mesenchymal stem cells is completely lost at passage 15 (44).
7. The SDS solution should be added carefully to avoid air bubbles trapped in the wells that can influence the absorbance reading. The readings are linearly related to cell number with a sensitivity of ~500 cells.
8. To ensure equal labeling, same volume of the labeling solution prepared in advance should be added into each well. The trichloroacetic acid solution should be precooled at 4°C.
9. Incubate the X-gal solution at 37°C for 1 h prior to the preparation of substrate staining solution to avoid aggregates formation during staining. Filter the freshly prepared solution before use. The staining should not be performed in a CO_2 incubator. Seal the plate with parafilm to prevent it from drying out. During staining, the plate should be kept away from light.
10. Prior to measurement, 20 μL of each reaction mix is diluted to 600 μL with 10 mM Tris–HCl pH 7.4, 150 mM NaCl, and 2 mM $MgCl_2$. The results are calculated as Total Product Generated (TPG). The net increase of fluorescein signal compared to minus telomerase control is termed ΔFL, while the net increase of sulforhodamine signal compared to minus Taq polymerase control is termed ΔR. There is a linear relationship between log(ΔFL/ΔR) and TPG. Thus, the TPG value of the samples can be calculated based on the formula generated by TSR8 standards.
11. For plasmid transient transfection, different efficiencies and toxicities are observed for transfection reagents from various

sources. Effectene is chosen after comparing five different sources of transfection reagents. The transfection can be performed in the presence of antibiotics and FBS. High purity plasmid DNA dissolved in sterile water should be used. It is not necessary to remove the Effectene–DNA complexes from the culture media.

12. For adenovirus infection, initially, the appropriate titer for each recombinant virus is determined by the addition of various dilutions to cells cultured in 6-well plates, giving a multiplicity of infection (m.o.i.) ranging from 50 to 2,000 based on 0.5–2.0×10^6 plaque-forming units/mL as measured by A260. For all infections, the viral stock is replaced with complete medium after 4–6 h and the cells incubated for two more days before starting subsequent experiment (40).

References

1. Hayflick L, Moorhead PS (1961) The serial cultivation of human diploid cell strains. Exp Cell Res 25:585–621
2. Chang E, Harley CB (1995) Telomere length and replicative aging in human vascular tissues. Proc Natl Acad Sci U S A 92:11190–11194
3. Chen QM, Prowse KR, Tu VC, Purdom S, Linskens MH (2001) Uncoupling the senescent phenotype from telomere shortening in hydrogen peroxide-treated fibroblasts. Exp Cell Res 265:294–303
4. Toussaint O, Dumont P, Dierick JF, Pascal T, Frippiat C, Chainiaux F, Sluse F, Eliaers F, Remacle J (2000) Stress-induced premature senescence. Essence of life, evolution, stress, and aging. Ann N Y Acad Sci 908:85–98
5. Brachmann CB, Sherman JM, Devine SE, Cameron EE, Pillus L, Boeke JD (1995) The SIR2 gene family, conserved from bacteria to humans, functions in silencing, cell cycle progression, and chromosome stability. Genes Dev 9:2888–2902
6. Braunstein M, Rose AB, Holmes SG, Allis CD, Broach JR (1993) Transcriptional silencing in yeast is associated with reduced nucleosome acetylation. Genes Dev 7:592–604
7. Gottlieb S, Esposito RE (1989) A new role for a yeast transcriptional silencer gene, SIR2, in regulation of recombination in ribosomal DNA. Cell 56:771–776
8. Shore D, Squire M, Nasmyth KA (1984) Characterization of two genes required for the position-effect control of yeast mating-type genes. EMBO J 3:2817–2823
9. Aparicio OM, Billington BL, Gottschling DE (1991) Modifiers of position effect are shared between telomeric and silent mating-type loci in S. cerevisiae. Cell 66:1279–1287
10. Smith JS, Boeke JD (1997) An unusual form of transcriptional silencing in yeast ribosomal DNA. Genes Dev 11:241–254
11. Rine J, Strathern JN, Hicks JB, Herskowitz I (1979) A suppressor of mating-type locus mutations in Saccharomyces cerevisiae: evidence for and identification of cryptic mating-type loci. Genetics 93:877–901
12. Guarente L (2011) Franklin H. Epstein Lecture: sirtuins, aging, and medicine. N Engl J Med 364:2235–2244
13. Haigis MC, Sinclair DA (2010) Mammalian sirtuins: biological insights and disease relevance. Annu Rev Pathol 5:253–295
14. Kaeberlein M, McVey M, Guarente L (1999) The SIR2/3/4 complex and SIR2 alone promote longevity in Saccharomyces cerevisiae by two different mechanisms. Genes Dev 13:2570–2580
15. Rogina B, Helfand SL (2004) Sir2 mediates longevity in the fly through a pathway related to calorie restriction. Proc Natl Acad Sci U S A 101:15998–16003
16. Tissenbaum HA, Guarente L (2001) Increased dosage of a sir-2 gene extends lifespan in Caenorhabditis elegans. Nature 410:227–230
17. Wang Y, Tissenbaum HA (2006) Overlapping and distinct functions for a Caenorhabditis elegans SIR2 and DAF-16/FOXO. Mech Ageing Dev 127:48–56
18. Wood JG, Rogina B, Lavu S, Howitz K, Helfand SL, Tatar M, Sinclair D (2004) Sirtuin activators mimic caloric restriction and delay ageing in metazoans. Nature 430:686–689

19. Armstrong CM, Kaeberlein M, Imai SI, Guarente L (2002) Mutations in Saccharomyces cerevisiae gene SIR2 can have differential effects on in vivo silencing phenotypes and in vitro histone deacetylation activity. Mol Biol Cell 13:1427–1438
20. Buck SW, Gallo CM, Smith JS (2004) Diversity in the Sir2 family of protein deacetylases. J Leukoc Biol 75:939–950
21. Frye RA (2000) Phylogenetic classification of prokaryotic and eukaryotic Sir2-like proteins. Biochem Biophys Res Commun 273:793–798
22. Autiero I, Costantini S, Colonna G (2009) Human sirt-1: molecular modeling and structure-function relationships of an unordered protein. PLoS One 4:e7350
23. Huhtiniemi T, Wittekindt C, Laitinen T, Leppanen J, Salminen A, Poso A, Lahtela-Kakkonen M (2006) Comparative and pharmacophore model for deacetylase SIRT1. J Comput Aided Mol Des 20:589–599
24. Finkel T, Deng CX, Mostoslavsky R (2009) Recent progress in the biology and physiology of sirtuins. Nature 460:587–591
25. Cohen HY, Miller C, Bitterman KJ, Wall NR, Hekking B, Kessler B, Howitz KT, Gorospe M, de Cabo R, Sinclair DA (2004) Calorie restriction promotes mammalian cell survival by inducing the SIRT1 deacetylase. Science 305:390–392
26. Couzin J (2004) Research on aging. Gene links calorie deprivation and long life in rodents. Science 304:1731
27. Guarente L, Picard F (2005) Calorie restriction–the SIR2 connection. Cell 120:473–482
28. Chen D, Steele AD, Lindquist S, Guarente L (2005) Increase in activity during calorie restriction requires Sirt1. Science 310:1641
29. Banks AS, Kon N, Knight C, Matsumoto M, Gutierrez-Juarez R, Rossetti L, Gu W, Accili D (2008) SirT1 gain of function increases energy efficiency and prevents diabetes in mice. Cell Metab 8:333–341
30. Longo VD, Kennedy BK (2006) Sirtuins in aging and age-related disease. Cell 126:257–268
31. Boily G, Seifert EL, Bevilacqua L, He XH, Sabourin G, Estey C, Moffat C, Crawford S, Saliba S, Jardine K, Xuan J, Evans M, Harper M-E, McBurney MW (2008) SirT1 Regulates energy metabolism and response to caloric restriction in mice. PLoS One 3:e1759
32. Guarente L (2006) Sirtuins as potential targets for metabolic syndrome. Nature 444:868
33. Hallows WC, Lee S, Denu JM (2006) Sirtuins deacetylate and activate mammalian acetyl-CoA synthetases. Proc Natl Acad Sci U S A 103:10230–10235
34. Schwer B, Verdin E (2008) Conserved metabolic regulatory functions of sirtuins. Cell Metab 7:104–112
35. Langley E, Pearson M, Faretta M, Bauer UM, Frye RA, Minucci S, Pelicci PG, Kouzarides T (2002) Human SIR2 deacetylates p53 and antagonizes PML/p53-induced cellular senescence. EMBO J 21:2383–2396
36. Jung-Hynes B, Ahmad N (2009) Role of p53 in the anti-proliferative effects of Sirt1 inhibition in prostate cancer cells. Cell Cycle 8:1478–1483
37. Ota H, Tokunaga E, Chang K, Hikasa M, Iijima K, Eto M, Kozaki K, Akishita M, Ouchi Y, Kaneki M (2006) Sirt1 inhibitor, Sirtinol, induces senescence-like growth arrest with attenuated Ras-MAPK signaling in human cancer cells. Oncogene 25:176–185
38. Huang J, Gan Q, Han L, Li J, Zhang H, Sun Y, Zhang Z, Tong T (2008) SIRT1 overexpression antagonizes cellular senescence with activated ERK/S6k1 signaling in human diploid fibroblasts. PLoS One 3:e1710
39. Ota H, Eto M, Kano MR, Ogawa S, Iijima K, Akishita M, Ouchi Y (2008) Cilostazol inhibits oxidative stress-induced premature senescence via upregulation of Sirt1 in human endothelial cells. Arterioscler Thromb Vasc Biol 28:1634–1639
40. Zu Y, Liu L, Lee MY, Xu C, Liang Y, Man RY, Vanhoutte PM, Wang Y (2010) SIRT1 promotes proliferation and prevents senescence through targeting LKB1 in primary porcine aortic endothelial cells. Circ Res 106:1384–1393
41. Takemura A, Iijima K, Ota H, Son BK, Ito Y, Ogawa S, Eto M, Akishita M, Ouchi Y (2011) Sirtuin 1 retards hyperphosphatemia-induced calcification of vascular smooth muscle cells. Arterioscler Thromb Vasc Biol 31:2054–2062
42. Balestrieri ML, Rienzo M, Felice F, Rossiello R, Grimaldi V, Milone L, Casamassimi A, Servillo L, Farzati B, Giovane A, Napoli C (2008) High glucose downregulates endothelial progenitor cell number via SIRT1. Biochim Biophys Acta 1784:936–945
43. Zhao T, Li J, Chen AF (2010) MicroRNA-34a induces endothelial progenitor cell senescence and impedes its angiogenesis via suppressing silent information regulator 1. Am J Physiol Endocrinol Metab 299:E110–E116
44. Kim YJ, Hwang SH, Lee SY, Shin KK, Cho HH, Bae YC, Jung JS (2012) miR-486-5p induces replicative senescence of human adipose tissue-derived mesenchymal stem cells and its expression Is controlled by high glucose. Stem Cells Dev 21(10):1749–1760
45. Wang Y, Liang Y, Vanhoutte PM (2011) SIRT1 and AMPK in regulating mammalian

senescence: a critical review and a working model. FEBS Lett 585:986–994

46. Lee MY, Wang Y, Vanhoutte PM (2010) Senescence of cultured porcine coronary arterial endothelial cells is associated with accelerated oxidative stress and activation of NFkB. J Vasc Res 47:287–298
47. Lee MYK, Tse HF, Siu CW, Zhu SG, Man RYK, Vanhoutte PM (2007) Genomic changes in regenerated porcine coronary arterial endothelial cells. Arterioscler Thromb Vasc Biol 27:2443–2449
48. Gillies RJ, Didier N, Denton M (1986) Determination of cell number in monolayer cultures. Anal Biochem 159:109–113
49. Kueng W, Silber E, Eppenberger U (1989) Quantification of cells cultured on 96-well plates. Anal Biochem 182:16–19
50. Wang Y, Lam JB, Lam KS, Liu J, Lam MC, Hoo RL, Wu D, Cooper GJ, Xu A (2006) Adiponectin modulates the glycogen synthase kinase-3beta/beta-catenin signaling pathway and attenuates mammary tumorigenesis of MDA-MB-231 cells in nude mice. Cancer Res 66:11462–11470
51. Debacq-Chainiaux F, Erusalimsky JD, Campisi J, Toussaint O (2009) Protocols to detect senescence-associated beta-galactosidase (SA-betagal) activity, a biomarker of senescent cells in culture and in vivo. Nat Protoc 4:1798–1806
52. Dimri GP, Lee X, Basile G, Acosta M, Scott G, Roskelley C, Medrano EE, Linskens M, Rubelj I, Pereira-Smith O et al (1995) A biomarker that identifies senescent human cells in culture and in aging skin in vivo. Proc Natl Acad Sci U S A 92:9363–9367
53. Lee BY, Han JA, Im JS, Morrone A, Johung K, Goodwin EC, Kleijer WJ, DiMaio D, Hwang ES (2006) Senescence-associated beta-galactosidase is lysosomal beta-galactosidase. Aging Cell 5:187–195
54. Woods A, Johnstone SR, Dickerson K, Leiper FC, Fryer LG, Neumann D, Schlattner U, Wallimann T, Carlson M, Carling D (2003) LKB1 is the upstream kinase in the AMP-activated protein kinase cascade. Curr Biol 13:2004–2008
55. Kim HJ, Cho JH, Quan H, Kim JR (2011) Down-regulation of Aurora B kinase induces cellular senescence in human fibroblasts and endothelial cells through a p53-dependent pathway. FEBS Lett 585:3569–3576
56. Nakano-Kurimoto R, Ikeda K, Uraoka M, Nakagawa Y, Yutaka K, Koide M, Takahashi T, Matoba S, Yamada H, Okigaki M, Matsubara H (2009) Replicative senescence of vascular smooth muscle cells enhances the calcification through initiating the osteoblastic transition. Am J Physiol Heart Circ Physiol 297:H1673–H1684

Chapter 23

Monitoring Nutrient Signaling Through the Longevity Protein p66^{SHC1}

Sofia Chiatamone Ranieri and Giovambattista Pani

Abstract

Nutrient availability and nutrient-dependent biochemical signals represent major determinants of cellular senescence and organismal aging. The present chapter describes simple procedures to reliably evaluate the response of cultured cell to nutrients through the longevity protein p66^{SHC1} and the mTOR/S6K cascade, which might be used to study cellular senescence and its chemical modulation by pharmaceutical agents in vitro.

Key words: Cell culture, Cell transfection, Glucose deprivation, Longevity, mTOR, Nutrient signaling, p66^{SHC1}, Protein phosphorylation

1. Introduction

A great deal of experimental evidence indicates that nutrient availability and energy metabolism exert major effect on the aging process, by regulating a complex network of signaling pathways involved in cell growth and proliferation, inflammation, and stress responses. Accordingly, these "nutrient-sensitive" cascades are being extensively investigated as potential targets for novel pharmacological strategies aimed at preventing senescence and age-associated diseases (1–3). Methods to simply and reproducibly address cell response to nutrients both in vivo and in vitro are therefore critically needed.

The 66 kDa adapter protein p66^{SHC1} has drawn significant attention in recent years as a longevity determinant that, through the generation of reactive oxygen species and oxidative stress in mammalian mitochondria, participates in tissue damage by several environmental stressors, therefore promoting the aging process (4).

Lorenzo Galluzzi et al. (eds.), *Cell Senescence: Methods and Protocols*, Methods in Molecular Biology, vol. 965,
DOI 10.1007/978-1-62703-239-1_23,

In fact, $p66^{SHC1}$-deficient mice live longer than their wild-type counterparts and are remarkably resistant to experimental pathologies (atherosclerosis, liver steatosis, diabetic vascular damage) reminiscent of human aging (5, 6). Original observations by us and other groups have revealed a previously unexpected role of $p66^{SHC1}$ in the intracellular signal transduction initiated by metabolic hormones (insulin) and nutritional cues (hyperglycemia, hyperlipidemia) known to have a major role in modulating organismal longevity and tissue senescence (7, 8). These studies have demonstrated that effects of $p66^{SHC1}$ on aging and senescence are related not only to the induction of oxidative damage but also, at least in part, to its role as a "nutrient sensor".

Detailed biochemical studies have shown that the response to nutrient cues are, on one side, associated with the phosphorylation of $p66^{SHC1}$on a serine (Ser 36) residue (9) and, on the other side, are largely mediated by the nutrient-sensitive cascade triggered by the mammalian Target of Rapamycin (mTOR) and its downstream target S6 Kinase (S6K) (7). Importantly, the excess activity of the latter cascade negatively regulates mammalian lifespan and has a causative role in dysmetabolism (insulin resistance), tissue damage, and inflammation associated with overnutrition and obesity in aged individuals (10–12). Moreover, several observations point to a role of mTOR, S6K, and cell hyperstimulation by nutrients in cellular damage and replicative senescence in vitro (13, 14), and in stem cell senescence/exhaustion in vivo (15).

The present protocol describes in detail simple procedures aimed at monitoring the phosphorylation status of $p66^{SHC1}$ in cultured cells exposed to nutrient cues related to diabetes and dysmetabolism [hyperglycemia, high free fatty acids (FFA), high glucosamine] and at evaluating the activation status of the mTOR/S6K cascade in different culture conditions and in particular in cells whose $p66^{SHC1}$ content has been genetically manipulated.

The described procedures can be easily utilized to investigate cultured cell responses to nutrients under a number of experimental conditions (overexpression or knockdown of specific proteins of interest as well the use of pharmacological agents) potentially relevant to cell senescence and body aging.

2. Materials

2.1. Equipment

- Standard equipment for protein electrophoresis and electrotransfer.
- Automatic film processor (XMP-2000, Kodak, Rochester, NY, USA).

2.2. Cell Culture

- HEK-293T, Human Embryonic Kidney cells expressing the SV-40 Large T antigen (ATCC/LCG Standards, Manassas, VA, USA) (see Note 1).
- Sterile plasticware (15 and 50 mL polypropylene tubes, 6-well plates, 2 and 10 mL plastic pipettes).
- Dulbecco's Modified Eagle's Medium (DMEM) containing 4.5 g/L glucose, 1 mM sodium pyruvate, 2 mM L-glutamine, nonessential amino acid mix 1:100, penicillin/streptomycin mix 1:100, and 8% fetal bovine serum (FBS).
- DMEM without glucose and FBS, containing 1 mM sodium pyruvate, 2 mM L-glutamine, nonessential amino acid mix 1:100, penicillin/streptomycin mix 1:100, 20 mM HEPES buffer (pH 7.4), and 1 mg/mL BSA.
- D-Glucose.
- Glucosamine hydrochloride.
- Mannitol.
- Palmitic acid (Sigma-Aldrich, St. Louis, MO, USA).
- Rapamycin (LC Laboratories,Woburn, MA, USA).
- pBabe-p66^{SHC1} and the corresponding empty control plasmid (see Note 2).
- Endotoxin-free Plasmid DNA purification kit (Qiagen, Hilden, Germany).
- EFFECTENE® transfection reagent (Qiagen).

2.3. Cell Lysis and SDS-PAGE

- Cell lysis buffer: 150 mM NaCl, 50 mM Tris–HCl pH 8, 2 mM EDTA, 1% v/v Triton X-100, 0.1% v/v SDS, 1:1,000 Protease Inhibitor cocktail, 1 mM PMSF, 1 mM Sodium Orthovanadate, 20 mM Sodium Fluoride, 20 mM Beta-glycerophosphate (Sigma-Aldrich).
- 30% Acrylamide/bisacrylamide solution (ratio 29:1) (Fisher Molecular Biology, Rome).
- Ammonium persulfate.
- Bromophenol blue.
- Glycine.
- Glycerol.
- Methanol.
- 0.1% w/v Ponceau S Red in 5% acetic acid.
- *N*,*N*,*N*′,*N*′-Tetramethylethylenediamine (TEMED).
- Tris base.
- Polyethylene glycol sorbitan monolaurate (Tween-20®).
- Broad Range Prestained protein ladder (ProSieve QuadColor protein marker, Lonza, Basel, Switzerland).

- 0.45 μm pore size nitrocellulose membrane (PROTRAN®, Whatman International Limited, Dassel, Germany).
- TBS-T: 10 mM Tris–HCl (pH 7.4), 150 mM NaCl, 0.5% v/v Tween-20.
- Primary antibodies: Anti-p66^{SHC1} polyclonal rabbit antiserum (Upstate Biotechnology/Millipore, Billerica, MA, USA); anti-phosho-p66^{SHC1} (Ser 36) mouse monoclonal clone 6E10 (Alexis Biochemicals, Lausen, Switzerland); anti-phosho-S6K1 (Thr 389); anti-phospho-S6 (Ser 235-236); anti-phospho-4EBP1 (Thr 37-46); anti-4EBP1 (Cell Signaling Technology, Beverly, MA, USA); anti-S6K1 clone 18 and anti-actin goat polyclonal (Santa Cruz Biotechnology Inc., Santa Cruz, CA, USA).
- Secondary HRP-conjugated reagents: HRP-conjugated-goat anti-rabbit IgG (Bio-Rad, Hercules, CA, USA); HRP-conjugated-goat anti-mouse IgG (Amersham GE-HealthCare, Piscataway, NJ, USA); HRP-conjugated donkey anti-goat/sheep IgG (Chemicon/Millipore, Billerica, MA, USA).
- Enhanced chemoluminescence (ECL) reagent and autoradiography films (Amersham/GE-HealthCare, Pittsburg, PA, USA).

3. Methods

3.1 Monitoring p66^{SHC1} Phosphorylation on Ser 36 in Response to Nutrient Availability

3.1.1. Overexpression of Human p66^{SHC1} in 293T Cells (See Note 3)

1. The day before transfection (ideally 16–24 h) seed 293T (see Note 4) cells at 150,000 cells/800 μL complete medium/well in a 12-well sterile plate (see Note 5). Put the plate back in the incubator (humidified, 5% CO_2, 37°C) until transfection.
2. After overnight incubation transfect cells with transfection-grade (endotoxin-free) plasmid DNA, using the EFFECTENE transfection reagent according to the manufacturer's instruction with small changes (see Notes 6 and 7). Transfect the appropriate number of wells with the p66^{SHC1} construct and the empty control, based on your experimental design (see below). Put the plate back in the incubator for 48 h.

3.1.2. Cell Stimulation

1. Forty-eight hours after transfection aspirate medium from cells and replace it with 1 mL pre-warmed DMEM without glucose and FCS (starvation medium). Add back nutrients as desired. Examples are high/low glucose (4.5 and 0.9 g/L, respectively, from a 50 g/L stock in PBS), Glucosamine (1–2 mM from a 100 mM stock in PBS), Palmitate/BSA (1 mM from a 10 mM stock in PBS/NaOH, see Note 8) alone or in combination. Use mannitol (stock 50 g/L in PBS) to compensate for decreased osmolarity in samples with no or low glucose.
2. Put the cells back in the incubator for additional 48 h (see Note 9).

3.1.3. Cell Lysis

1. Cells can be lysed directly in the culture wells after careful removal of medium and floating cells (see Note 10). Aspirate medium, transfer the plate on ice, and add 110 μL/well of cold lysis buffer with inhibitors (see Note 11). Cover the plate with lid to avoid evaporation, swirl the plate, and leave it on ice for 2–5 min. Then collect cells by flushing with pipet all over the well and transfer lysates into clean 1.5 mL tubes (see Note 12).
2. Leave tubes on ice for 10–15 min, with occasional tapping or vortexing; spin down in the bench-top centrifuge at maximum speed (14,000 rpm/21,000 × *g* in our equipment) at 4°C (use a refrigerated centrifuge or put your microfuge in the cold room) for 10 min.
3. Transfer supernatants in clean tubes and discard pellets. Measure protein concentration by your favorite method (see Note 13). Prepare samples by mixing protein lysates with 6× Laemmli gel loading SDS buffer (see Note 14), to a final protein concentration of 1 mg/mL.

3.1.4. Protein Electrophoresis and Electrotransfer

1. Pour a 8% polyacrylamide gel (10% if you wish to monitor also phosho-S6 and phosho-4EBP1 in the same experiment) (see Note 15). Load 40 μL of sample (40 μg of protein)/well alongside with the prestained protein ladder, and run the gel until the front dye reaches the bottom (see Note 16).
2. Transfer proteins onto nitrocellulose membrane according to your standard electroblotting protocol (we use 1 h × gel at 330 mA).
3. Stain the membrane with Ponceau S Red a 0.1% Ponceau S/5% acetic acid solution to confirm homogeneous protein transfer (see Note 17).
4. Destain the membrane with TBS-T and incubate it at RT in 5% v/v dry milk/TBS-T (blocking solution) for 1.5–2 h on a rocking plate (see Note 18).
5. Remove the membrane from the blocking solution. Put the membrane on a glass plate and, using a sharp blade and a ruler, cut it into strips corresponding to different molecular weight ranges, based on protein markers (Fig. 1a) (see Note 19). The 50–100 kDa range is where you expect to see p66SHC1; keep the lower strip(s) for actin, pS6 or p4EBP1.

3.1.5. p66SHC1-phospho (Ser 36) and Total p66SHC1 Immunostaining

1. Prepare 1:1,000 solutions of your primary reagents in 3% milk/TBST (see Note 20).
2. Incubate membranes O/N with an appropriate volume of solution (at least 5 mL for a 2.5 cm × 9 cm strip in a small box, see Note 21) at 4°C with gentle agitation.

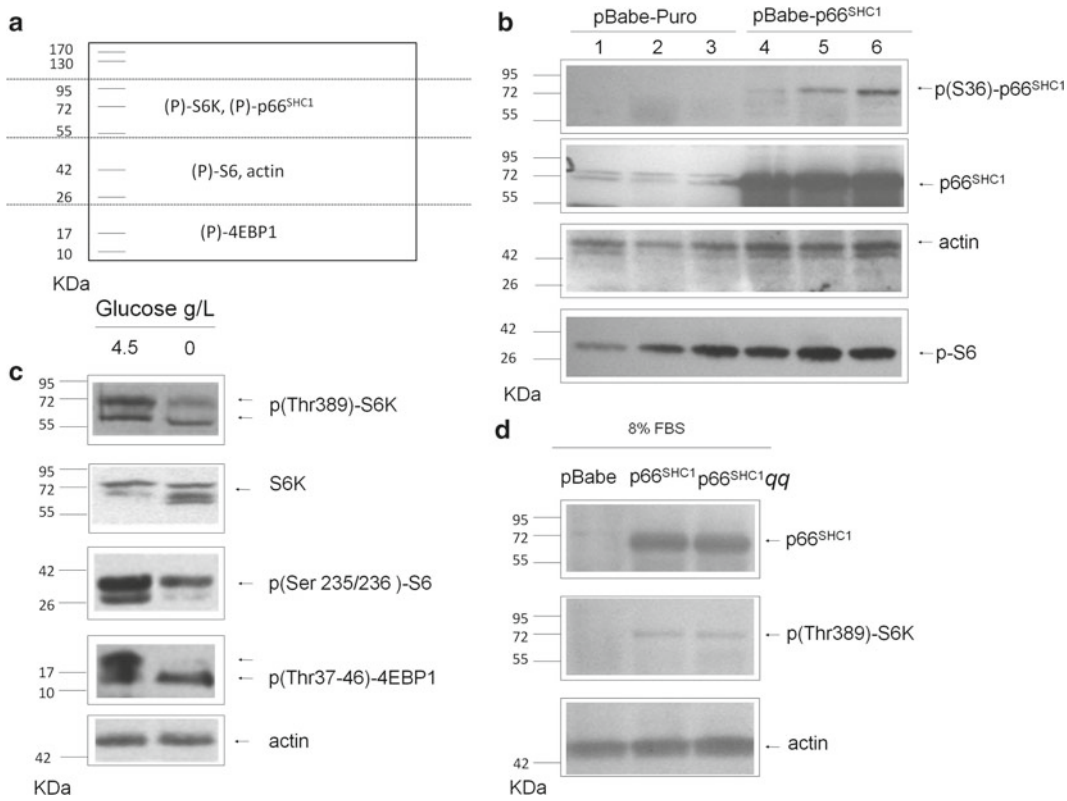

Fig. 1. (**a**) Scheme illustrating how to cut the nitrocellulose membrane for the simultaneous detection of p66^{SHC1}, of different components of the mTOR/S6K cascade and of the loading control (actin). *Short lines* on the left indicate prestained molecular weight markers as appear on the membrane; the corresponding weights are also indicated. (**b**) Detection of p66 ^{SHC1} phosphorylation on Serine 36 in glucose-free medium (lanes 1 and 4), in the presence of 2 mM glucosamine (lanes 2 and 5) and in 4.5 g/L glucose (lanes 3 and 6). Phosphorylation signal can be easily appreciated in p66^{SHC1} transfected (lanes 4–6) but not in mock-transfected cells (lanes 1–3). Note that overexpression of p66^{SHC1} increases the phosphorylation of S6, particularly in glucose-free medium (compare lanes 1 and 4) and in 2 mM glucosamine (lanes 2 and 5). Actin band is displayed as loading control. All the panels were obtained from the same membrane; anti-p-p66^{SHC1} and anti-tot-p66^{SHC1} were performed on the same piece of membrane sequentially, without membrane "stripping" in SDS. (**c**) Analysis of the mTOR/S6K cascade in cells exposed to high glucose and to a glucose-free medium. Glucose withdrawal reduces the phosphorylation of S6K, S6, and 4EBP-1. For S6K and 4EBP1 protein dephosphorylation is revealed by attenuation or disappearance of the uppermost, slowest migrating band. Total S6K and actin are displayed as loading controls. (**d**) Activation of S6K by p66^{SHC1} in complete medium (8% FBS, high glucose). The same strip (*upper*) was sequentially stained for p-S6K and for total p66^{SHC1}. The lower strip was immunostained for actin as loading control. p66^{SHC1} *qq* is a redox-inactive mutant of p66^{SHC1} that displays equal expression level and stimulatory effect on S6K compared to the wild-type isoform (7).

3. Proceed with washes and secondary reagents (anti-mouse IgG for anti-pSer36 p66^{SHC1} and anti-rabbit IgG for anti-total p66^{SHC1}) by standard WB procedure.
4. Detect immunocomplexes by ECL and autoradiography (Fig. 1) (see Note 22). Compare p36Ser-p66^{SHC1} band intensities among different treatments (e.g., high glucose versus no glucose) and relate them to signals obtained in the corresponding anti-total p66^{SHC1} immunoblot (see Note 23).

3.2. Monitoring mTOR/S6K Cascade Response to p66SHC1 and Nutrients

This part of the protocol largely overlaps with the monitoring p66SHC1 phosphorylation (see Subheading 3.1), but focuses on the assessment of mTOR signaling to downstream effectors S6K, S6, and 4EBP1 in response to nutrients and/or overexpression of p66SHC1.

3.2.1. Seeding and Transfection of 293T Cells

1. Transfection of cell with p66SHC1 (see Subheading 3.1.1). To monitor the mTOR cascade in parental, non-transfected cells, seed 1.5–2 × 10^5 cells/1 mL complete medium/well in a 12-well plate 16/24 h before cell stimulation.
2. Cell stimulation. Perform cell stimulation as described previously (see Subheading 3.1.2), but preferably incubate cells for no longer than 24 h (see Note 24); add an experimental control with the mTOR inhibitor Rapamycin (200 nM) (see Notes 25 and 26).

3.2.2. Cell Lysis

1. Lyse cells as described above (Subheading 3.1.3).

3.2.3. Protein Electrophoresis and Electroblotting (See Subheading 3.1.4)

1. Pour 8 or 10% acrylamide gel to optimally visualize phospho-S6 kinase, 10% to co-visualize p-S6 K and p-S6, 12% to co-visualize p-S6K, p-S6, and p-4EBP1 (poor resolution of the S6K bands). After protein transfer and blocking, cut the membrane into strips to be hybridized with different antibodies as outlined in Fig. 24.1a (higher than 50 kDa for p-S6K, 50–25 kDa for p-S6, 25–10 kDa for p-4EBP1) (see Note 27).
2. Immunodetection of p-S6K, p-S6, and p-4EBP-1. Use the appropriate primary and secondary reagents. For interpretation of phospho-S6K patterns see Note 28. On the same membrane (subsequently) or on a twin membrane (in parallel) perform staining for total S6K, S6, and 4EBP1, in order to distinguish changes in phosphorylation from differences in protein expression levels (see Note 29). Stain the 50–25 kDa strip for actin to confirm equal protein loading throughout the lanes. Sequential staining of the same membrane with different antisera can be performed without further manipulation (i.e., "stripping" in SDS/DTT) of the membrane, provided that target bands do not overlap.

4. Notes

1. 293T cells have very low growth requirements and medium/serum source and lot do not appear to be critical in our experience.

2. Expression constructs encoding human full length $p66^{SHC1}$ under the control of a mammalian promoter such (pBabe-$p66^{SHC1}$ and the corresponding empty control plasmid, pBabe-Puro) can be obtained from Prof. P.G. Pelicci (Istituto Europeo di Oncologia, Milan, Italy) under a Material Transfer Agreement. Alternatively, a similar construct can be requested from the Addgene repository (Plasmid 10972: pcDNA3.1his $p66^{SHC1}$) or purchased from ORIGENE (Rockville, MD, USA; untagged cDNA in the pCMV6-XL6 backbone). As control (empty) the plasmids pBabe-Puro (Addgene, plasmid 1764), PcDNA3.1 (Clontech) or pCMV6-XL6 (Origene) might be used.
3. Expression levels of $p66^{SHC1}$ in most cell types tend to be relatively low, although the protein can be induced under several stress conditions (16). $p66^{SHC1}$ overexpression in 293T cells highly facilitates the analysis of protein phosphorylation, while maintaining relatively constant the total amount of protein. Additionally, 293T represents a suitable and widely investigated model of cell response to nutrient signaling. If a different cell line needs to be used, or endogenous $p66^{SHC1}$ has to be investigated, one should consider the possibility of enriching $p66^{SHC1}$ by immunoprecipitation from large volumes of protein lysates. The rabbit antiserum from Upstate Biotechnology/Millipore works very well for this application.
4. 293T cells are routinely maintained in complete DMEM plus 8–10% FCS. We usually split cells 1:5 every 3 or 4 days, with a medium change at day 2. Higher dilutions are not recommended since (a) cells doubling is delayed at very low density, and (b) unwanted clonal selection may occur, thus changing the characteristics of the cell population over passages.
5. During the first half hour after plating occasionally swirl the plate to allow homogeneous distribution of the cells on the well surface and avoid crowding in the middle of the well.
6. Unlike recommended, we noticed that changing the medium immediately before transfections reduces transfection efficiency; cells should be transfected in the same medium in which they were seeded the day before.
7. The protocol involves incubation of DNA with an "Enhancer" (5 min) before dendrimers are added. Amounts and ratio of DNA, Enhancer, and Effectene should be optimized. We use 0.5 μg DNA, 4 μL of Enhancer, and 5 μL of transfection reagent/well in 12-well plate; a master mix for up to three wells can be prepared in the same 1.5 mL tube.
8. Palmitate is broadly used to model the effect of free fatty acids (FFA) on cultured cells. Palmitic acid (5.2 mg/mL, 20 mM) should be dissolved in hot (70°C) 0.1 N NaOH, and the clear

solution so obtained immediately mixed with an equal volume of 200 mg/mL BSA in PBS. This yields a 10 mM solution of Palmitate in 1.6 mM BSA (molar ratio ~6:1), to be diluted 1:10 in the cell medium (the solution may turn a bit cloudy at some point, but dissolves rather well in the cell medium). We recommend using a vehicle control in addition since high concentrations of BSA are toxic for some cell lines. As an alternative to Palmitate, the Fatty Acid Supplement (in BSA) from Sigma-Aldrich could be used at 1:10–1:20 dilution.

9. In samples containing glucose medium may turn yellow by the end of the incubation due to accumulation of lactate. This does not affect viability of 293T cells, and medium change is not required.
10. In alternative, cells can be detached in their own medium by pipetting up and down few times, and transferred in 1.5 mL tubes. After a brief centrifugation (30 s at 14,000 rpm) supernatants are discarded and pellets lysed directly in the tube. This method is preferable if a significant fraction of live cells have detached from the plate surface during experimental manipulations (e.g., medium change) or incubation time. One potential drawback is that dead cells are also collected in the pellet.
11. We prepare 100× stocks of inhibitors [50× for Sodium Fluoride (NaF) and Beta-Glycerophosphate] in water and store them at −20%. Repeated freeze-thaw cycles do not seem to decrease their activity. Sodium fluoride is toxic if swallowed, and irritating to eyes and skin; contact with acids liberates very toxic gas. Do not inhale dust and wear suitable protective clothing. PMSF is also toxic if swallowed or inhaled and causes burns. Sigma-Aldrich sells a 100 mM (100×) solution in ethanol that avoids operator exposure to the powder. Wear gloves and eye protection.
12. Avoid bubbling. It may help to set the pipet at a volume lower than the one to be collected (i.e., 80 μL to collect 110 μL).
13. Several reagents and kits for protein quantification are available on the market. We use DC Protein Assay from Bio-Rad; colorimetric reaction is performed in 96-well plate and read (at 570 nm) by an ELISA plate reader. This allows using very small volumes of your sample for protein determination.
14. A general procedure for SDS-PAGE and protein transfer to nitrocellulose can be found in Sambrook J, Fritsch EF, Maniatis T (1989) Molecular cloning: a laboratory manual, 2nd edn, pp. 18.47–18.75. Cold Spring Harbor Laboratory Press, Cold Spring Harbor, New York.
15. Acrylamide is toxic if swallowed and harmful if inhaled or in contact with skin. Prolonged exposure may cause cancer. Gels should be poured under the fume hood and with suitable hand

and eye protection. Precast gels are a good although expensive alternative. Other reagents employed in SDS-PAGE, like ammonium persulfate and TEMED, are also harmful and require hand/face protection.

16. These volumes are suited for a 10-well, 1.5 mm thick mini-gel (Bio-Rad Mini Protean). Bigger gels allow larger loading volumes. Increasing protein loading (up to 100–120 μg) may help improving detection sensitivity.
17. Submerge the membrane in a sufficient volume of Ponceau S solution, gently agitate few seconds and pour the stain back in the bottle. Rinse the membrane 2–3 times with water; red bands will appear on a white/pinkish background. Remove the stain with 1–2 washes in TBS-T. Although optional, Ponceau S staining is valuable to score gross loading differences among samples (to be annotated in your protocol) or the presence of blank areas usually due to the formation of air bubbles during protein transfer. Note that Ponceau S is irritating to eyes, respiratory system, and skin, and should be handled with gloves.
18. One hour or less at 37°C (you need a water-bath with shaker) also works well, if you are in a rush.
19. Parallel hybridization of multiple strips from the same membrane with different antibodies is advisable whenever possible to save time and reduce costs; moreover it minimizes the intra-sample variation and makes loading controls more reliable. However, avoid cutting the membrane unless you are reasonably sure of where your bands of interest are going to migrate. For instance, phosphorylation may determine significant changes in band migration compared to the predicted protein size, and, additionally, protein ruler can sometimes be far from accurate although internally consistent.
20. Unlike recommended by most vendors, solutions of most primary antibodies can be reused several times before losing activity. Sodium Azide (NaN_3) should be added at 0.1 or 0.5% v/v as preservative. Note that Azide is very toxic if swallowed, liberates toxic gas in contact with acids, and should be therefore handled with the precautions indicated in the accompanying Material Safety data Sheet (MSDS).
21. We use plastic containers for nails/screws that have multiple independent compartments of the right size in one single box. This is also very convenient for handling during washes.
22. A relatively short film exposure (2 min with amplifying screen) is usually sufficient to detect phospho-$p66^{SHC1}$. Ser-36 phosphorylation of $p66^{SHC1}$ is easily detectable in whole cell lysates upon overexpression of the protein, and nutrient-related changes usually rather obvious. If desired, a positive control can be obtained by treating cells with 1 mM hydrogen peroxide for 30 min.

If signal intensity is an issue, p66SHC1 immunoprecipitation followed by anti-p-Ser36 immunoblotting can represent a valid alternative approach (see Note 3).

23. When assessing nutrient-related changes in p66SHC1 phosphorylation, reference to total p66SHC1 amount is necessary. An anti-total p66SHC1 immunoblot can be prepared in parallel from the same samples. In alternative, we suggest to re-hybridize for total p66SHC1 the strip previously stained with the phospho-specific mAb. Since anti-total p66SHC1 signal is usually much stronger than the phosphorylation signal (although remaining in the linear range) and secondary reagents are different (anti-rabbit IgG and anti-mouse IgG, respectively), this procedure is fairly reliable to assess total p66SHC1 content and increases the internal consistency of the control.
24. We noticed that while 48 h are necessary to detect nutrient-related changes in p66SHC1 phosphorylation, nutrient effects on the mTOR cascade are best seen at 24 h in serum-free medium.
25. Rapamycin is insoluble in water, but can be dissolved in DMSO or ethanol. We prepare 1 mg/mL stocks in DMSO, to be further diluted in PBS to 20 μg/mL, and finally given to cells 1:100 (final 200 ng/mL, approximately 200 nM). Avoid filtering the 20 μg/mL sub-dilution, since this may lead to some loss of activity (probably due to incomplete solubilization).
26. S6K/S6 phosphorylation in cells over-expressing p66SHC1, although detectable in the absence of growth factors, is amplified in the presence of insulin (100 ng/mL) or fetal calf serum in the medium (8% v/v), or simply by refeeding with fresh complete medium the day before the assay.
27. Hyperphosphorylated S6K migrates just above the BSA band that is usually clearly recognizable by Ponceau S staining. BSA may sometimes be spotted also in immunoblots as a large faint shadow that distorts the shape of the lane. This may help identifying the phospho-S6K band when the signal is not very strong or multiple bands appear in the same molecular weight range.
28. While anti-p-S6 (Ser 235-236) detects a single sharp band around 34 kDa, both anti-pS6K (Thr 389) and p-4EBP1 (Ser 37-46) detect multiple phosphorylated bands, likely reflecting different degrees of phosphorylation at sites different from the one recognized by the antiserum. In general, the uppermost, slowest migrating band represents the most heavily phosphorylated and presumably active isoform of the corresponding protein (Fig. 1c). Dephosphorylation of S6K or 4EBP1, for instance in the absence of glucose, will lead to the disappearance of higher bands, and also to the paradoxical and

potentially misleading increase in the intensity of lower bands. This aspect should be taken into consideration while interpreting the results.

29. Antibodies against different phosphorylation sites of 4EBP-1 are available from CST as a sampler kit.

Acknowledgments

This work was supported by the Associazione Italiana per la Ricerca sul Cancro (AIRC grant IG8634/2009), by the Italian Ministry of University/Catholic University (linea D1, MIUR ex 60%) and by Italian Ministry of University, PRIN 2008, grant 2008T7WRTM_003.

References

1. Jasper H, Jones DL (2010) Metabolic regulation of stem cell behavior and implications for aging. Cell Metab 12:561–565
2. Zoncu R, Efeyan A, Sabatini DM (2011) mTOR: from growth signal integration to cancer, diabetes and ageing. Nat Rev Mol Cell Biol 12:21–35
3. Sinclair DA (2005) Toward a unified theory of caloric restriction and longevity regulation. Mech Ageing Dev 126:987–1002
4. Migliaccio E, Giorgio M, Mele S, Pelicci G, Reboldi P, Pandolfi PP, Lanfrancone L, Pelicci PG (1999) The p66shc adaptor protein controls oxidative stress response and life span in mammals. Nature 402:309–313
5. Koch OR, Fusco S, Ranieri SC, Maulucci G, Palozza P, Larocca LM, Cravero AA, Farre SM, De Spirito M, Galeotti T, Pani G (2008) Role of the life span determinant P66(shcA) in ethanol-induced liver damage. Lab Invest J Tech Meth Pathol 88:750–760
6. Cosentino F, Francia P, Camici GG, Pelicci PG, Luscher TF, Volpe M (2008) Final common molecular pathways of aging and cardiovascular disease: role of the p66Shc protein. Arterioscler Thromb Vasc Biol 28:622–628
7. Ranieri SC, Fusco S, Panieri E, Labate V, Mele M, Tesori V, Ferrara AM, Maulucci G, De Spirito M, Martorana GE, Galeotti T, Pani G (2010) Mammalian life-span determinant p66shcA mediates obesity-induced insulin resistance. Proc Natl Acad Sci USA 107:13420–13425
8. Berniakovich I, Trinei M, Stendardo M, Migliaccio E, Minucci S, Bernardi P, Pelicci PG, Giorgio M (2008) p66Shc-generated oxidative signal promotes fat accumulation. J Biol Chem 283:34283–34293
9. Pinton P, Rimessi A, Marchi S, Orsini F, Migliaccio E, Giorgio M, Contursi C, Minucci S, Mantovani F, Wieckowski MR, Del Sal G, Pelicci PG, Rizzuto R (2007) Protein kinase C beta and prolyl isomerase 1 regulate mitochondrial effects of the life-span determinant p66Shc. Science 315:659–663
10. Um SH, D'Alessio D, Thomas G (2006) Nutrient overload, insulin resistance, and ribosomal protein S6 kinase 1, S6K1. Cell Metab 3:393–402
11. Harrison DE, Strong R, Sharp ZD, Nelson JF, Astle CM, Flurkey K, Nadon NL, Wilkinson JE, Frenkel K, Carter CS, Pahor M, Javors MA, Fernandez E, Miller RA (2009) Rapamycin fed late in life extends lifespan in genetically heterogeneous mice. Nature 460:392–395
12. Selman C, Tullet JM, Wieser D, Irvine E, Lingard SJ, Choudhury AI, Claret M, Al-Qassab H, Carmignac D, Ramadani F, Woods A, Robinson IC, Schuster E, Batterham RL, Kozma SC, Thomas G, Carling D, Okkenhaug K, Thornton JM, Partridge L, Gems D, Withers DJ (2009) Ribosomal protein S6 kinase 1 signaling regulates mammalian life span. Science 326:140–144
13. Panieri E, Toietta G, Mele M, Labate V, Ranieri SC, Fusco S, Tesori V, Antonini A, Maulucci G, De Spirito M, Galeotti T, Pani G (2010) Nutrient withdrawal rescues growth factor-deprived cells from mTOR-dependent damage. Aging 2:487–503
14. Demidenko ZN, Blagosklonny MV (2008) Growth stimulation leads to cellular senescence

when the cell cycle is blocked. Cell Cycle 7:3355–3361

15. Chen C, Liu Y, Liu R, Ikenoue T, Guan KL, Liu Y, Zheng P (2008) TSC-mTOR maintains quiescence and function of hematopoietic stem cells by repressing mitochondrial biogenesis and reactive oxygen species. J Exp Med 205:2397–2408
16. Trinei M, Giorgio M, Cicalese A, Barozzi S, Ventura A, Migliaccio E, Milia E, Padura IM, Raker VA, Maccarana M, Petronilli V, Minucci S, Bernardi P, Lanfrancone L, Pelicci PG (2002) A p53-p66Shc signalling pathway controls intracellular redox status, levels of oxidation-damaged DNA and oxidative stress-induced apoptosis. Oncogene 21:3872–3878

Chapter 24

Profiling the Metabolic Signature of Senescence

Florian M. Geier, Silke Fuchs, Gabriel Valbuena, Armand M. Leroi, and Jacob G. Bundy

Abstract

Aging is a complex process, which involves changes in different cellular functions that all can be integrated on the metabolite level. This means that different gene regulation pathways that affect aging might lead to similar changes in metabolism and result in a metabolic signature of senescence. In this chapter, we describe how to establish a metabolic signature of senescence by analyzing the metabolome of various longevity mutants of the model organism *Caenorhabditis elegans* using gas chromatography-mass spectrometry (GC-MS). Since longevity-associated genes exist for other model organisms and humans, this analysis could be universally applied to body fluids or whole tissue samples for studing the relationship between senescence and metabolism.

Key words: Aging, Metabolomics, *Caenorhabditis elegans*, Cellular senescence, GC-MS

1. Introduction

1.1. Metabolism and Aging

Metabolism and aging are intimately linked (1). Studies in yeast, *Drosophila melanogaster*, *Caenorhabditis elegans*, and mammals have shown that many ways of extending lifespan—caloric restriction (2), reducing insulin-like signaling (3), altering mitochondrial activity (4), autophagy (5), or lipid peroxidation (6)—also perturb, and depend on, alterations of metabolism (1). The link between aging and metabolism has been generally studied by quantifying transcript or protein levels of metabolism-related genes (7, 8). More recent studies have begun to focus on the metabolites themselves. Such metabolomics (9) (or "metabonomics") (10) studies generally depend on the untargeted quantification of the concentrations of dozens or hundreds of metabolites. Since metabolite concentrations are the result of many regulatory changes, the hope is that such studies might give a much more direct picture of how metabolism

Lorenzo Galluzzi et al. (eds.), *Cell Senescence: Methods and Protocols*, Methods in Molecular Biology, vol. 965,
DOI 10.1007/978-1-62703-239-1_24,

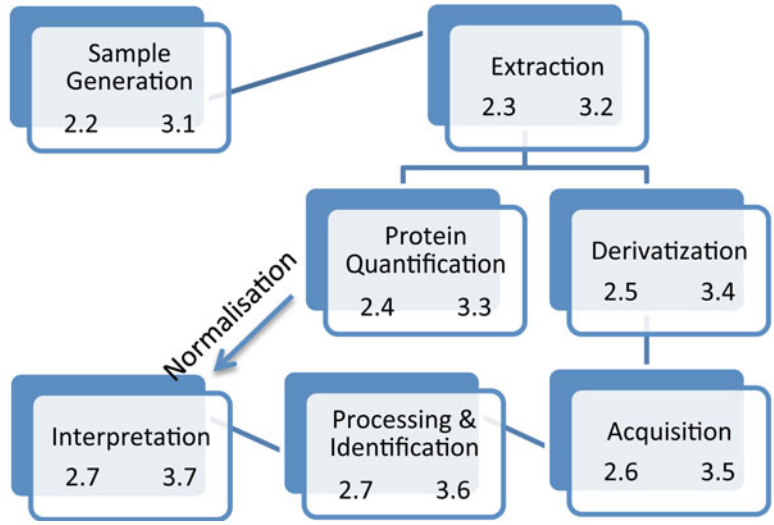

Fig.1. Workflow of a metabolic profiling experiment. Numbers refer to method sections.

influences the rate of aging. Most metabolomic studies of aging have focused on the search for "biomarkers", that is, they have surveyed aging cells or animals with a view to identifying what metabolites change (11–13). Recently, however, we sought to identify metabolites that might causally contribute to aging by studying the metabolomes of a series of longevity-extension mutations in *C. elegans* (14). It is an optimized (15) version of this protocol that we report here. It can be used to study many aspects of metabolism in worms, but also any other organism or (clinical) tissue samples.

1.2. The Metabolite Profiling Workflow

We begin with an overview of the workflow of a typical metabolite profiling experiment (Fig. 1).

1.2.1. Experimental Design

Metabolomic data are noisy. The noise arises from two sources: biological variations and technical variations, due to fluctuations in the extraction process or differences in the analytical equipment. For this reason, any metabolomic study needs adequate sample replication. The number of replicates needed cannot be specified without knowing the treatment means and variances; however, in our experience an initial survey of differences in metabolite profiles between worms of different ages or genotypes requires 5–10 replicate samples.

This level of replication means that replicate samples will often not be prepared in parallel. Since conditions can vary subtly from day to day, it's easy to introduce unwanted "batch effects." Some of these batch effects will come from the culturing of the worms themselves (e.g., variation in temperature, density, and food); others may arise from the postmortem preparation of the samples (variation in extraction procedures, reagents, etc.). For this reason,

if it is not possible to culture, kill, extract, and analyze all samples at the same time, then a suitable blocked design should be adopted. It is desirable to obtain an estimate of the technical variance by dividing samples and processing them in different extraction and analysis runs.

1.2.2. Sample Extraction

Since living organisms such as bacteria or worms respond promptly to their environments, it is necessary to minimize handling and then rapidly halt their metabolisms. Most samples need to be washed. In the case of worms, which have been grown on bacterial lawns, as much bacterial debris should be removed as possible. But, inevitably, there is a trade-off between sample purity and degradation.

Once the samples have been cleaned, their metabolisms must be halted as instantaneously as possible so that a true representation of in vivo metabolite concentrations can be obtained (16–19). This is best done by snap freezing in liquid nitrogen. The resulting pellets are then stored frozen until extracted directly into the extraction solvents. These solvents should be cooled to ensure precipitation of proteins, halting any further metabolic changes.

The tissues then need to be "disrupted" to release the metabolites into solution. Worms have tough cuticles, so mechanized aids can be used for this. The solvents chosen determine the yield of recovered metabolite classes. Monophasic solutions, such as simple alcohol/water mixtures, that are miscible with wet tissues/cells are widely used (we use 80% methanol). Alternatively, the classic Bligh and Dyer methanol/chloroform extraction method (20) can be used. Although this extraction method was originally designed for lipids, it is now widely used for parallel polar metabolite extraction, with analysis of the polar fraction that results from splitting the solution into two phases following sample extraction (15, 21, 22). Besides these, there are also many other protocols optimized for other metabolite groups, such as lipids (23). Different extraction strategies will be more or less successful depending on the precise analytical criteria used to define success, such as number of metabolites detected, precision of measurements, and the choice of analytical platform (15).

1.2.3. Analytical Platforms

The two major analytical platforms for metabolomics are nuclear magnetic resonance (NMR) spectroscopy and mass spectrometry (MS). Each has particular advantages and drawbacks. NMR is a fully quantitative and near-universal detector but is relatively insensitive (24–26); MS is very sensitive to low metabolite concentrations, but its performance may be biased toward certain compound classes (27). MS is typically used with a prior chromatographic separation step. Liquid chromatography (LC) is suitable for metabolites that can be ionized; Gas chromatography (GC), which is used in our protocol, requires the molecules to be volatile or made volatile by derivatization and thus has an upper mass limit of around

650 Da (9). It is not suitable for certain classes of highly polar and/or labile metabolites, such as nucleotides. The choice of chromatographic column and solvents (LC) and derivatization procedures (GC) depends on the particular metabolite classes that are of interest.

1.2.4. Data Analysis

Once the data have been acquired, they must be processed prior to statistical analysis (28). The exact procedures depend on the analytical platform the type of statistical analysis that will be used. LC-MS and GC-MS methods generally require a peak deconvolution step in order to align and extract metabolite features. These steps are usually integrated in the vendor's own software package, but there are also freely available tools (29–33). Data are commonly normalized to compensate for differences in extracted biomass or ionization efficiency (34).

Data analysis itself consists of mining the extracted metabolite features (GC/LC) or whole spectrum (NMR) for biomarkers that discriminate samples. Multivariate methods can either be supervised or unsupervised, i.e., the algorithm does or does not use knowledge about sample class membership to discriminate these. Commonly used unsupervised methods are principal component analysis (PCA) and hierarchical clustering (HC). Techniques based on supervised partial-least-squares regression (PLS) have frequently been used in metabolomics studies (30, 35, 36), although of course a wealth of other approaches exist (35, 37, 38). Data may also be rescaled. We often log-transform the data before multivariate analysis. However, it should be kept in mind that transformation can also introduce problems, for instance by emphasizing peaks close to the noise (39). More detailed approaches to scaling are discussed elsewhere (40).

After interesting metabolite peaks have been flagged up for further investigation, their chemical identity may be assigned using public metabolite libraries, such as HMDB (41), metlin (42), GOLMdb (43), or commercial/in-house databases such as the NIST (44) and Fiehn (45) libraries for GC-MS. It may be appropriate to use univariate statistical methods, if necessary with correction for multiple testing, to confirm the statistical significance of individual metabolite features.

Once metabolites have been provisionally identified, there are several possible ways of confirming their identity. We refer the reader to the metabolomics standards initiative (46) proposed minimum reporting standards for chemical analysis (47). These standards state that assignments based on library matches alone should be regarded as putative provisional assignments only, and confirmation requires at least two independent kinds of data (e.g., a matching retention time and mass spectral data of an authentic metabolite standard) (48).

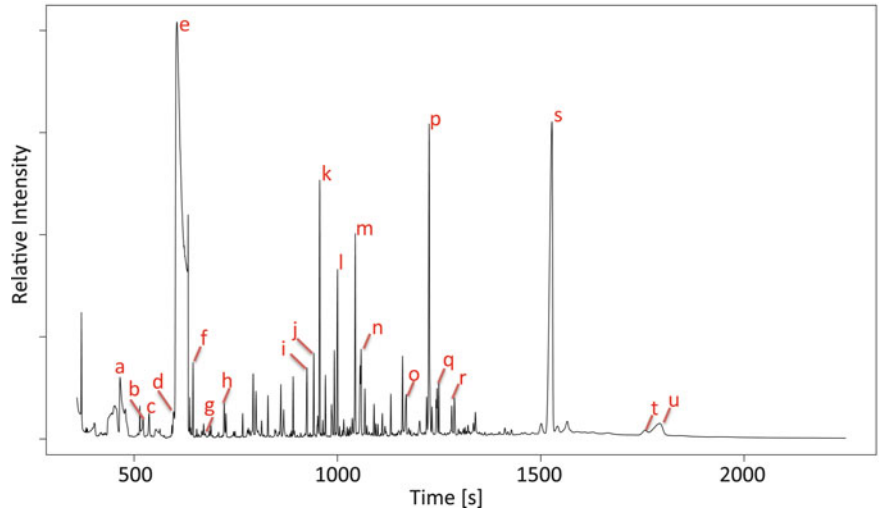

Fig. 2. Typical GC-MS chromatogram of a *Caenorhabditis elegans* tissue extract with selected peaks annotated (chromatogram shows total ion chromatogram, i.e., sum signal of all masses): (*a*) lactate, (*b*) leucine, (*c*) proline, (*d*) serine, (*e*) phosphate (contaminant from washing buffer), (*f*) glycine, (*g*) fumarate, (*h*) beta-alanine, (*i*) putrescine, (*j*) 2-aminoadipate, (*k*) glycerol-1-phosphate, (*l*) myristic acid d_{27} (internal standard for retention time locking), (*m*) glucose, (*n*) lysine, (*o*) *N*-acetyl-histidine, (*p*) tyrosine, (*q*) spermidine, (*r*) glucose-6-phosphate, (*s*) sucrose (contaminant from gradient centrifugation), (*t*) cholesterol, (*u*) adenosine phosphates.

1.2.5. Summary

There are many ways of analyzing the metabolomes of aging organisms. The protocol we describe has been optimized for use in *C. elegans*. In this protocol, metabolites are extracted from a tissue pellet, using 80% methanol, prior to a two-step derivatization procedure and untargeted GC-MS analysis. The free software package AMDIS (49) is used in conjunction with the Fiehn GC-MS database (45) to extract and annotate metabolite peaks (Fig. 2). After post-processing, the data are normalized by quantifying the protein content of the remaining cell pellet. Univariate and multivariate statistics are then used to help identify biomarkers and patterns of cellular aging.

2. Materials

2.1. Sample Generation

Comprehensive information on the materials and procedures can be found in the freely available reference WormBook (50).

- *C. elegans* strains can be obtained from the Caenorhabditis Genetics Center (CGC), Minnesota (50) (see Note 1).
- Nematode growth medium plate (NGM): Autoclave 3 g NaCl, 17 g agar, 2.5 g peptone, and 975 mL dH_2O. After cooling to ~50°C add 1 mL of autoclaved 1 M $MgSO_4$ and $CaCl_2$ each. Also add 25 mL of autoclaved phosphate buffer (108.3 g

KH_2PO_4, 35.6 g K_2HPO_4, water to 1 L) and 1 mL of a sterile filtered (0.22 μm) 5 mg/L cholesterol in ethanol. Pour agar into 9 cm petri dishes, filling 2/3 of the volume and let cool overnight. Leave on at room temperature for 2 days to check for contamination. Store in a sealed bag, refrigerated for a month.

- Seeded NGM plate: NGM plate seeded with a lawn of 100 μL of an LB overnight culture of *Escherichia coli* strain OP50 and incubated at 37°C. Keep in a sealed bag and refrigerated for a maximum of 2 weeks.
- M9 buffer: 3 g KH_2PO_4, 6 g Na_2HPO_4, 5 g NaCl, 1 mL 1 M $MgSO_4$, and water to 1 L. Autoclave.
- Bleach solution: 0.5 mL 5 N NaOH with 1 mL bleach (5%). Make fresh before use.
- 15 mL conical tubes.
- 200 mL pipette with sterile tips.
- Temperature-controlled incubator.

2.2. Extraction

- 200 μL and 1 mL pipette.
- 1 mL positive displacement pipette, with tips suitable for organic solvents.
- Dry ice inside a polystyrene box (amount is depending on number of samples and duration of overall procedure).
- 80% Methanol. Keep sealed and cool for a maximum of a week.
- 2.0 mL graduated screw cap tubes with caps (Starlabs) filled with 200 μL of appropriate zirconia beads (i.e., 0.1 mm beads for *C. elegans* and cells, 1 mm for tissue) (see Note 2).
- Bead-Beater (e.g., Precellys 24 from Bertin or FastPrep from MP Biomedicals).
- 15 mL conical tubes (one per sample).
- Vacuum concentrator with rotor (e.g., Eppendorf 5301) suitable for 2 mL glass Agilent autosampler vials (see below).

2.3. Protein Quantification

- 0.2 M NaOH.
- 15 mL conical tubes.
- Bradford reagent (Sigma-Aldrich).
- Flat, clear bottom 96-well plate.
- 96-well plate-compatible absorbance reader, with filter for 595 nm.

2.4. Derivatization

- 10 mL glass syringe.
- (Dry) inert gas (i.e., nitrogen).

- 5 mL plastic syringe.
- Air balloon.
- FAME mix: Saturated fatty acid methyl esters of linear length of C_8, C_9, C_{10}, C_{12}, C_{14}, C_{16}, C_{18}, C_{20}, C_{22}, C_{24}, C_{26}, C_{28}, and $C_{30,}$ for retention index calculations.
- Internal standard mix: 3 mg/mL myristic acid-d27, 2 mM ^{13}C-glucose, 2 mM 2,3,3-d3-Leucine in 1:1 methanol:water. Consider making a larger, more concentrated stock, aliquoted into several small vials (batches), stored frozen (–40°C).
- 40 mg/mL methoxyamine HCl in anhydrous pyridine. Prepare fresh and keep, closed inside the vial, wrapped with Parafilm for a maximum of 1 week inside a fridge (see Note 3).
- 1 mM 2-fluorobiphenyl in anhydrous pyridine (see Note 3).
- *N*-methyl-*N*-(trimethylsilyl) trifluoroacetamide (MSTFA) + 1% trimethylchlorosilane (TMCS) derivatizing solution (Sigma-Aldrich). Once opened, keep for a maximum of a week inside a fridge, wrapped in parafilm.
- 2 mm glass vial with screw cap (Agilent Technologies Inc., Santa Clara, CA).
- Flat bottom, silanized glass vial insert (Agilent).
- Vial heater or temperature-controlled incubator.

2.5. Acquisition

- Gas chromatograph (e.g., Agilent 6890 with split/splitless injector). *Inlet:* Inject 1 μL at 250°C, split ratio 1:5–1:10, with 3–10 mL/min helium into glass-wool split liner; *Oven:* 1 mL/min constant flow of helium, oven ramp from 60°C (1 min hold) to 325 at 10°C/min, 10 min hold before cool down to 70°C; 37.5 min total runtime. For exact settings see manual of Agilent Fiehn Library.
- Mass spectrometer with single quadrupole detector (e.g., Agilent 5973 MSD) with transfer line at 290°C and electron impact ionization at 70 eV, filament source at 290°C, quadrupole at 250°C, scanning over a range of m/z 50–600 at 2 spectra/s and starting after a 5.90 min solvent delay.
- FC43 (perfluorotributylamine) for autotune with manufacturer-specific tune settings.
- Autosampler (e.g., Agilent 7693).
- DB5-MS column, 30 m length, 0.25 mm inner diameter, 0.25 μm film, 95% dimethyl 5% diphenyl polysiloxane (Agilent).
- Conical single glass-wool split/splitless liner and septum (Agilent).
- Analytical grade helium as carrier gas.
- Agilent ChemStation software.

2.6. Data Processing and Analysis

A Microsoft windows computer and the following software are required:

- Agilent ChemStation.
- Retention-time-locked Fiehn Library (Agilent).
- AMDIS (NIST) (49), downloadable from http://chemdata.nist.gov/mass-spc/amdis/.
- Gevin (51) and Matlab (Mathworks).
- R, downloadable from http://cran.r-project.org/, install relevant packages by typing *install.packages("gplots")* inside R.

3. Methods

This protocol uses chemicals, which require special safety precautions such as handling under a fume hood. Please familiarize yourself with the hazards associated with each chemical by reading their material safety datasheets (MSDS).

3.1. Sample Generation

We grow five replicates, of a wild-type (N2) and several long-lived knockout mutant strains at 1 replicate per NGM plate (see Note 4). For preparation of growth materials and worm handling aseptic techniques are to be used whenever possible.

1. Grow nematodes at 20°C on seeded NGM plates until the majority of worms start to lay eggs (~3.5 days) (50).
2. Perform synchronization (50) for each replicate: Wash nematodes into a conical tube with 4 mL of M9 buffer and spin 2 min at 1,300 × *g*; aspirate worms with a glass pipette and transfer into bleach solution. Shake vigorously every 2 min for 10 min. Spin down to pellet and wash twice with M9 buffer. Let the embryos hatch in M9 buffer overnight at 20°C and then transfer growth arrested L1 larvae onto seeded NGM plates (see Note 5).
3. Grow worms at 20°C until L4 (see Note 6).
4. Harvest by washing each replicate into a conical tube with a few milliliter of M9 buffer and let them settle to a pellet (~15 min.).
5. Consider cleaning worms by washing pellet with M9 buffer.
6. Transfer pellet into a bead-beater tube, using a 200 µL syringe and snap-freeze instantly.
7. Store at −80°C until extraction.

3.2. Sample Extraction

Perform all work with the pellet frozen on dry ice.

1. Label bead-beater tubes with pencil/printer labeled tags (solvent spills may wash off marker pens used directly on plastic).

2. Transfer frozen samples into the bead-beater tubes (if not already frozen inside those).
3. Using a positive displacement pipette, add 0.8 mL of cold (≤4°C) methanol, to compliment the 200 μL to 1 mL 80% methanol, whilst keeping samples on dry ice.
4. Insert the tubes into the bead-beater and run at 6,500 rpm for 40 s (see Note 7).
5. Spin down samples at 10,000 × *g* for 5 min at 4°C.
6. Using a Pasteur pipette, carefully transfer the supernatant to a 15 mL conical tube, avoiding the debris of the precipitated protein pellet.
7. Add 1.5 mL of 80% methanol to bead-beater tube and re-extract using another round of bead-beating by repeating step 4.
8. Repeat steps 5 and 6 joining the two extracts.
9. Using 80% methanol top up to a defined volume (e.g., 2 mL) and pool an equal aliquot of each sample into one quality control (QC) sample (52) of appropriate concentration (i.e., if there are ten samples, take 200 μL each).
10. If several aliquots of the sample set are desired (e.g., for using several analytical platforms or rerunning samples at a later time point), split the samples in the desired ratio. Consider storing samples in the vials that will be used for derivatization (silanized glass vials).
11. Evaporate the samples to dryness in the vacuum concentrator without heating.
12. Store at −80°C or if not available at −40°C until analysis.

3.3. Protein Quantification (Optional)

As often samples have a different biomass, their total signal intensity may vary, resulting in higher errors if compared directly. To compensate, normalizing to the total protein content of each sample has proven to be a reliable method. We use the following Bradford assay.

1. Transfer the protein pellets (and beads) from step 6 above into a 15 mL conical flask, using 2 mL of 0.2 M NaOH to rinse. Vortex.
2. Denature the protein pellet by incubating 20 min at 98°C.
3. Centrifuge at 5,000 × *g* for 5 min after allowing to cool down.
4. Dilute as necessary (see Note 8).
5. Add 5 μL to a 96-well plate, and mix with 250 μL Bradford reagent.
6. Create a calibration curve (from 0.1 to 2 mg/mL), by dissolving BSA in 0.2 NaOH and proceeding as in steps 4 and 5.
7. Slightly mix by shaking the plate and incubate for 5 min.

8. Read absorbance at 595 nm.
9. Construct a calibration function in Excel, based on the recorded calibration curve.
10. Calculate a normalization factor for each sample based on the calibration equation and the individual readings.

3.4. Derivatization

Our protocol is based on a method from Kind et al. (45), in order to guarantee compatibility with their retention-time-locked metabolite database (distributed by Agilent). Once derivatized, samples degrade with time. Thus immediate analysis is necessary and samples to be derivatized per batch should be limited to 30 at most (~1 day batch). When splitting a large dataset into smaller batches, make sure samples are appropriately distributed to avoid confounding sample treatments with batches. Typically, samples should be run in randomized blocks—e.g., if an experiment had 5 treatment groups and 10 replicates in each group, i.e., 50 samples in total, and so had to be run in two batches, then treatments 1 + 2 + 3 should not be run as the first and 4 + 5 as the second batch. Instead, it would be better to run five replicates of each group per batch and then randomize the sample order within the batch. Also prepare a derivatization blank, i.e., derivatize inside a clean vial, to check for contaminants and peaks of the derivatization chemicals.

It is important to use positive displacement pipettes in all steps, to ensure accurate dispensing of organic solvents. Handling of pyridine and MSTFA must be done in a fume hood.

1. Make sure the mass spectrometer is in working order (check "Data acquisition" steps 1–5) as derivatized samples will need to be run immediately.
2. Add 25 μL of internal standard mix.
3. Thoroughly dry sample in the vacuum concentrator.
4. Add 20 μL of methoxyamine solution, cap, dissolve pellet by vortexing, and spin down sample (no vacuum) (see Note 9).
5. Incubate 90 min at 30°C inside a heater block. Gently agitate at various times (~every 20 min).
6. Add 80 μL MSTFA, cap, agitate by vortexing and spin down (no vacuum).
7. Incubate 30 min at 37°C using a heater block.
8. Spin down for 5 min and transfer to silanized vial insert using a glass pipette. Ensure non-dissolved debris is not carried over.
9. Add 20 μL injection standard solution, cap, and proceed to acquisition.

3.5. Data Acquisition

1. Ensure the syringe wash vials are topped up and the waste vials are empty.
2. Tune the mass spectrometer via the autotune function and evaluate tune, according to the manufacturer's documentation.
3. Run an underivatized methanol sample to check for contaminants in the system and column bleeding (deterioration). Change liner and septum, if needed.
4. Consider running the FAME mix to evaluate retention time calibration.
5. When setting up the run-list (sequence), proceed as with the selection of samples for different batches (described above): Randomize or choose a run order orthogonal to sample classes (i.e., replicate 1 of all groups, replicate 2 of all groups). Start the sequence with the prepared QC sample and reinject every five samples. Finish with a QC sample.
6. At the end of each sequence, do run another methanol blank to check for carryover or contamination build up during the sequence.

3.6. Data Processing

Peak identification and post-processing.

1. Convert data files from vendor format to an open format (e.g., netCDF) using the vendor's software (e.g., Agilent ChemStation).
2. Use AMDIS and a database in-house, Fiehn db (45), NIST (44), Golm db (43) to deconvolve and annotate peaks. For exact use, refer to the manual.
3. Use the Matlab code "Gavin" (51) to reintegrate peaks and fill the gaps in those samples where a compound was not detected. A step-by-step instruction is included in the download.

3.7. Data Analysis

The data matrix obtained in Subheading 3.6 can be analyzed in various ways. Prior to statistical analysis, data should be normalized, to compensate for differences in sampled biomass. The factors determined from the protein quantification in Subheading 3.3 should be used for this. Alternatively, normalization to total spectral area may be a sufficient approximation in most cases (53). There are many software packages available for data analysis, and an enormous range of potential statistical analyses that could be carried out. It was not our intention here to offer a guide to omics data analysis, which is a separate subject; instead, we have directed the interested reader to appropriate reviews. However, we will describe how to create a clustered heat map using the free statistical software package R, as this simple first step provides a convenient graphical summary of large datasets.

We commonly use two types of clustered heatmaps. Either (a) each individual sample is included as a row in the data matrix,

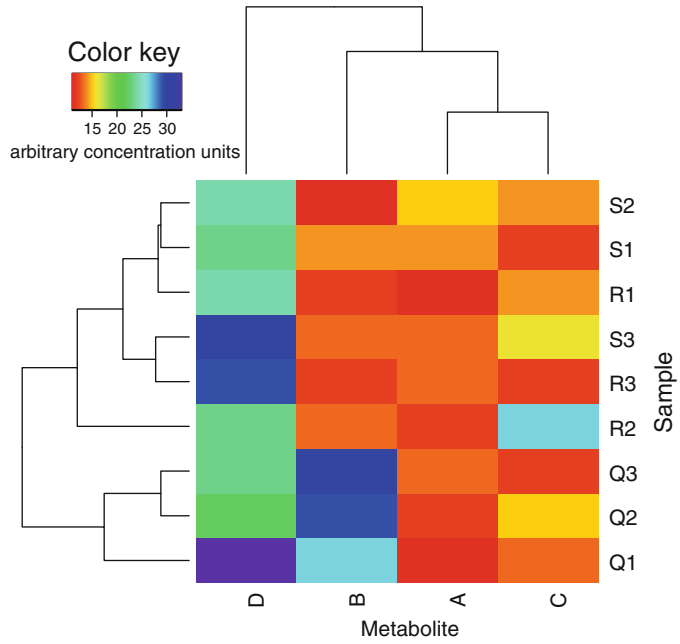

Fig.3. Clustered heatmaps allow for easy identification of metabolite patterns. This figure provides an example with three different experimental treatments (sample groups, Q, R, and S), three replicates, and four selected metabolites (**a**–**d**). Two of the groups (S and R) appear similar. However group Q can clearly be discriminated, due to an increased concentration of metabolite B compared to R and S. Metabolite C in sample R, replicate two suggests to be an outlier.

which takes into account the variation of each sample. An example of such a heatmap is displayed in Fig. 3. This type of heatmap can be used to spot outlying samples and helpful when estimating dataset quality by examining the behavior of the QC samples.

Another variant (b) is to pool all replicates of an experimental treatment per single row by calculating their arithmetic mean. If the means are then scaled with respect to the control group (i.e., wild-type/no treatment/time 0), the relative distance to control, best expressed as $\log_2$ fold-change, is obtained. So long as there is a large number of replicates, this can be much easier to interpret than when each biological sample is treated as an individual row.

Pre-processing heatmap (a) (NB, it is assumed that all of these data manipulations are performed in a user-friendly software such as Microsoft Excel, but any appropriate software package can be chosen).

1. Normalize with respect to total protein measurements for each sample.
2. Make sure data are ordered as a matrix with rows being the individual samples and columns metabolites.
3. Save as comma separated value file (.csv).

Pre-processing heatmap (b).

1. Normalize with respect to total protein measurements for each sample.
2. Calculate the arithmetic mean for all replicates of an experimental treatment for each metabolite.
3. Divide the average metabolite concentration for each group by the value of the control group.
4. Make sure data are ordered as a matrix with rows being the group/control ratios and columns metabolites.
5. Save as comma separated value file.

Making the clustered heatmap in R (R commands are in *italics*).

1. Start R.
2. Load library: *library(gplots)*, if library cannot be found, install by *install.packages("gplots")*.
3. Load the sample—metabolite matrix, saved as csv into R: *data<- read.csv("filename.csv")*. If the first line contains metabolite names, use the parameter *header=TRUE*, if the first row contains the sample (a) or group (b) names, set the parameter *row.names=1*.
4. Convert the R data frame to a matrix: *data<- data.matrix(data)*.

logdata<- log10(data)

and $\log_2$ transformation for (b):

logdata<- log2(data) (*see* **Note 10**).

5. We recommend a $\log_{10}$ transformation for (a):
6. Create heatmap:
heatmap<-*heatmap.2(logdata,col=rainbow(100,start=0,end=0.75))*.
7. Tweak the heatmap by adjusting the options, which can be viewed by: *?heatmap.2*.
8. When satisfied, the heatmap can be exported as an image file. For extended information on multivariate data analysis we recommend consultation of the literature (28, 30, 35, 54).

4. Notes

1. Some (life-extending) mutations are embryonic lethal and therefore must be induced via RNAi, by feeding *E. coli* containing the appropriate RNAi vector. For *C. elegans*, a whole-genome RNAi library is commercially available (55). Please consult literature for exact experimental procedures (58).
2. Prefilled tubes may be purchased at a higher price. However, prefilling of bead-beater tubes can be efficiently done with a

self-made dispenser. Simply cut away the sides of an Eppendorf tube, down to the volume needed, but keeping the lid and lash as handle.

3. For the derivatization to succeed, the solvents used must be kept anhydrous. Thus care must be taken while dispensing the pyridine from the stock bottle. We use a (dry) glass syringe for dispensing. A plastic syringe, connected to a balloon filled with inert gas (e.g., nitrogen) is used to substitute for the dispensed volume, without the risk of moisture from the air to enter.
4. For GC-MS one 9 cm plate per replicate yields sufficient signal intensity. However, if required, several plates may be pooled to obtain one replicate.
5. If after bleaching the yield of L1 larvae is too low, repeat and make sure you bleach many gravid hermaphrodites (at an early onset of egg-laying). Consider a shorter exposure to bleach, check that the pH is neutral after the final washing step, and make sure eggs are pelleted into the vial and are not lost during washing.
6. Other live-stages may be used as well. However, during the adult stage, the offspring will spoil synchronization of the culture. This can either be overcome by chemical (mitosis inhibitors) (56) or mechanical means (sorting) (57), but may impact on worm physiology.
7. It is crucial to ensure that the samples stay cool (≤4°C) the whole time to prevent degradation of labile compounds. Keep on dry ice, whenever possible. Test the bead-beater cycle with a blank sample. If the dry ice cooled sample is warm after the cycle, reduce cycle duration (and consider intermittent cooling).
8. Find right dilution by keep adding different concentrations/volumes of a representative sample to the 250 µL Bradford reagent and see when color lies well within calibration curve (brown to dark blue). In case individual measurements lie at the edge or beyond the calibration curve (color very similar to 0 or 2 mg/mL wells), perform another measurement (inside a new well) for those with adjusted concentration/volume and take into account when calculating the scaling factor.
9. Some samples are difficult to dissolve in pyridine. Consider sonication for 10 min after vortexing. If even then a crystal-like pellet remains, proceed with the protocol, as these might be insoluble inorganic salts.
10. If the integrated intensities of some metabolites are negative or zero (which may happen if the concentration was low to baseline), a log-transformation may not be allowed. In this case a small constant offset can be added to each value to rise all intensities above zero, prior to log-transformation (39).

Acknowledgments

Manuel Liebeke is thanked for the fruitful discussions of the manuscript. FMG acknowledges the AXA Research Fund for funding.

References

1. Kenyon CJ (2010) The genetics of ageing. Nature 464:504–512
2. McCay CM, Crowell MF (1934) Prolonging the life span. Sci Mon 39:405–414
3. Kenyon C, Chang J, Gensch E, Rudner A, Tabtiang R (1993) A C. elegans mutant that lives twice as long as wild type. Nature 366: 461–464
4. Finkel T, Holbrook NJ (2000) Oxidants, oxidative stress and the biology of ageing. Nature 408:239–247
5. Eisenberg T, Knauer H, Schauer A, Buttner S, Ruckenstuhl C, Carmona-Gutierrez D, Ring J, Schroeder S, Magnes C, Antonacci L, Fussi H, Deszcz L, Hartl R, Schraml E, Criollo A, Megalou E, Weiskopf D, Laun P, Heeren G, Breitenbach M, Grubeck-Loebenstein B, Herker E, Fahrenkrog B, Frohlich KU, Sinner F, Tavernarakis N, Minois N, Kroemer G, Madeo F (2009) Induction of autophagy by spermidine promotes longevity. Nat Cell Biol 11:1305–1314
6. Shmookler Reis RJ, Xu L, Lee H, Chae M, Thaden JJ, Bharill P, Tazearslan C, Siegel E, Alla R, Zimniak P, Ayyadevara S (2011) Modulation of lipid biosynthesis contributes to stress resistance and longevity of C. elegans mutants. Aging 3:125–147
7. Lund J, Tedesco P, Duke K, Wang J, Kim SK, Johnson TE (2002) Transcriptional profile of aging in C. elegans. Curr Biol 12:1566–1573
8. Holt SJ, Riddle DL (2003) SAGE surveys C. elegans carbohydrate metabolism: evidence for an anaerobic shift in the long-lived dauer larva. Mech Ageing Dev 124:779–800
9. Fiehn O, Kopka J, Dormann P, Altmann T, Trethewey RN, Willmitzer L (2000) Metabolite profiling for plant functional genomics. Nat Biotechnol 18:1157–1161
10. Nicholson JK, Lindon JC, Holmes E (1999) 'Metabonomics': understanding the metabolic responses of living systems to pathophysiological stimuli via multivariate statistical analysis of biological NMR spectroscopic data. Xenobiotica 29:1181–1189
11. Butler JA, Ventura N, Johnson TE, Rea SL (2010) Long-lived mitochondrial (Mit) mutants of Caenorhabditis elegans utilize a novel metabolism. FASEB J 24:4977–4988
12. Martin FP, Spanier B, Collino S, Montoliu I, Kolmeder C, Giesbertz P, Affolter M, Kussmann M, Daniel H, Kochhar S, Rezzi S (2011) Metabotyping of Caenorhabditis elegans and their culture media revealed unique metabolic phenotypes associated to amino acid deficiency and insulin-like signaling. J Proteome Res 10:990–1003
13. Rezzi S, Martin FP, Shanmuganayagam D, Colman RJ, Nicholson JK, Weindruch R (2009) Metabolic shifts due to long-term caloric restriction revealed in nonhuman primates. Exp Gerontol 44:356–362
14. Fuchs S, Bundy JG, Davies SK, Viney JM, Swire JS, Leroi AM (2010) A metabolic signature of long life in Caenorhabditis elegans. BMC Biol 8:14
15. Geier FM, Want EJ, Leroi AM, Bundy JG (2011) Cross-platform comparison of Caenorhabditis elegans tissue extraction strategies for comprehensive metabolome coverage. Anal Chem 83:3730–3736
16. Liebeke M, Bundy JG (2011) Tissue disruption and extraction methods for metabolic profiling of an invertebrate sentinel species. Metabolomics 8:819–830
17. Rabinowitz JD, Kimball E (2007) Acidic acetonitrile for cellular metabolome extraction from Escherichia coli. Anal Chem 79:6167–6173
18. Tredwell GD, Edwards-Jones B, Leak DJ, Bundy JG (2011) The development of metabolomic sampling procedures for Pichia pastoris, and baseline metabolome data. PLoS One 6:e16286
19. Meyer H, Liebeke M, Lalk M (2010) A protocol for the investigation of the intracellular Staphylococcus aureus metabolome. Anal Biochem 401:250–259
20. Bligh EG, Dyer WJ (1959) A rapid method of total lipid extraction and purification. Can J Biochem Physiol 37:911–917
21. Masson P, Alves AC, Ebbels TM, Nicholson JK, Want EJ (2010) Optimization and evaluation of metabolite extraction protocols for

untargeted metabolic profiling of liver samples by UPLC-MS. Anal Chem 82:7779–7786

22. Want EJ, O'Maille G, Smith CA, Brandon TR, Uritboonthai W, Qin C, Trauger SA, Siuzdak G (2006) Solvent-dependent metabolite distribution, clustering, and protein extraction for serum profiling with mass spectrometry. Anal Chem 78:743–752
23. Matyash V, Liebisch G, Kurzchalia TV, Shevchenko A, Schwudke D (2008) Lipid extraction by methyl-tert-butyl ether for high-throughput lipidomics. J Lipid Res 49:1137–1146
24. Beckonert O, Keun HC, Ebbels TM, Bundy J, Holmes E, Lindon JC, Nicholson JK (2007) Metabolic profiling, metabolomic and metabonomic procedures for NMR spectroscopy of urine, plasma, serum and tissue extracts. Nat Protoc 2:2692–2703
25. Fan WMT (1996) Metabolite profiling by one- and two-dimensional NMR analysis of complex mixtures. Prog Nucl Mag Res Spectrosc 28:161–219
26. Bothwell JH, Griffin JL (2011) An introduction to biological nuclear magnetic resonance spectroscopy. Biol Rev Camb Philos Soc 86:493–510
27. Want EJ, Nordstrom A, Morita H, Siuzdak G (2007) From exogenous to endogenous: the inevitable imprint of mass spectrometry in metabolomics. J Proteome Res 6:459–468
28. Want E, Masson P (2011) Processing and analysis of GC/LC-MS-based metabolomics data. Methods Mol Biol 708:277–298
29. Melamud E, Vastag L, Rabinowitz JD (2010) Metabolomic analysis and visualization engine for LC-MS data. Anal Chem 82:9818–9826
30. Xia J, Wishart DS (2011) Web-based inference of biological patterns, functions and pathways from metabolomic data using MetaboAnalyst. Nat Protoc 6:743–760
31. Carroll AJ, Badger MR, Harvey Millar A (2010) The MetabolomeExpress Project: enabling web-based processing, analysis and transparent dissemination of GC/MS metabolomics datasets. BMC Bioinformatics 11:376
32. Pluskal T, Castillo S, Villar-Briones A, Oresic M (2010) MZmine 2: modular framework for processing, visualizing, and analyzing mass spectrometry-based molecular profile data. BMC Bioinformatics 11:395
33. Smith CA, Want EJ, O'Maille G, Abagyan R, Siuzdak G (2006) XCMS: processing mass spectrometry data for metabolite profiling using nonlinear peak alignment, matching, and identification. Anal Chem 78:779–787
34. Veselkov KA, Vingara LK, Masson P, Robinette SL, Want E, Li JV, Barton RH, Boursier-Neyret C, Walther B, Ebbels TM, Pelczer I, Holmes E, Lindon JC, Nicholson JK (2011) Optimized preprocessing of ultra-performance liquid chromatography/mass spectrometry urinary metabolic profiles for improved information recovery. Anal Chem 83:5864–5872
35. Trygg J, Holmes E, Lundstedt T (2007) Chemometrics in metabonomics. J Proteome Res 6:469–479
36. Stacklies W, Redestig H, Scholz M, Walther D, Selbig J (2007) pcaMethods–a bioconductor package providing PCA methods for incomplete data. Bioinformatics 23:1164–1167
37. Ebbels TM, Keun HC, Beckonert OP, Bollard ME, Lindon JC, Holmes E, Nicholson JK (2007) Prediction and classification of drug toxicity using probabilistic modeling of temporal metabolic data: the consortium on metabonomic toxicology screening approach. J Proteome Res 6:4407–4422
38. Cloarec O, Dumas ME, Craig A, Barton RH, Trygg J, Hudson J, Blancher C, Gauguier D, Lindon JC, Holmes E, Nicholson J (2005) Statistical total correlation spectroscopy: an exploratory approach for latent biomarker identification from metabolic 1H NMR data sets. Anal Chem 77:1282–1289
39. Rocke DM, Durbin B (2003) Approximate variance-stabilizing transformations for gene-expression microarray data. Bioinformatics 19:966–972
40. van den Berg RA, Hoefsloot HC, Westerhuis JA, Smilde AK, van der Werf MJ (2006) Centering, scaling, and transformations: improving the biological information content of metabolomics data. BMC Genomics 7:142
41. Wishart DS, Tzur D, Knox C, Eisner R, Guo AC, Young N, Cheng D, Jewell K, Arndt D, Sawhney S, Fung C, Nikolai L, Lewis M, Coutouly MA, Forsythe I, Tang P, Shrivastava S, Jeroncic K, Stothard P, Amegbey G, Block D, Hau DD, Wagner J, Miniaci J, Clements M, Gebremedhin M, Guo N, Zhang Y, Duggan GE, Macinnis GD, Weljie AM, Dowlatabadi R, Bamforth F, Clive D, Greiner R, Li L, Marrie T, Sykes BD, Vogel HJ, Querengesser L (2007) HMDB: the human metabolome database. Nucleic Acids Res 35:D521–D526
42. Smith CA, O'Maille G, Want EJ, Qin C, Trauger SA, Brandon TR, Custodio DE, Abagyan R, Siuzdak G (2005) METLIN: a metabolite mass spectral database. Ther Drug Monit 27:747–751
43. Kopka J, Schauer N, Krueger S, Birkemeyer C, Usadel B, Bergmuller E, Dormann P, Weckwerth W, Gibon Y, Stitt M, Willmitzer L, Fernie AR, Steinhauser D (2005) GMD@CSB. DB: the golm metabolome database. Bioinformatics 21:1635–1638

44. Stein SE, Scott DR (1994) Optimization and testing of mass-spectral library search algorithms for compound identification. J Am Soc Mass Spectrom 5:859–866
45. Kind T, Wohlgemuth G, do Lee Y, Lu Y, Palazoglu M, Shahbaz S, Fiehn O (2009) FiehnLib: mass spectral and retention index libraries for metabolomics based on quadrupole and time-of-flight gas chromatography/mass spectrometry. Anal Chem 81: 10038–10048
46. Sansone SA, Fan T, Goodacre R, Griffin JL, Hardy NW, Kaddurah-Daouk R, Kristal BS, Lindon J, Mendes P, Morrison N, Nikolau B, Robertson D, Sumner LW, Taylor C, van der Werf M, van Ommen B, Fiehn O (2007) The metabolomics standards initiative. Nat Biotechnol 25:846–848
47. Sumner LW, Amberg A, Barrett D, Beale MH, Beger R, Daykin CA, Fan TWM, Fiehn O, Goodacre R, Griffin JL, Hankemeier T, Hardy N, Harnly J, Higashi R, Kopka J, Lane AN, Lindon JC, Marriott P, Nicholls AW, Reily MD, Thaden JJ, Viant MR (2007) Proposed minimum reporting standards for chemical analysis. Metabolomics 3:211–221
48. Kind T, Fiehn O (2010) Advances in structure elucidation of small molecules using mass spectrometry. Bioanal Rev 2:23–60
49. Stein SE (1999) An integrated method for spectrum extraction and compound identification from gas chromatography/mass spectrometry data. J Am Soc Mass Spectrom 10:770–781
50. Stiernagle T (2006) Maintenance of C. elegans. WormBook: the online review of C. elegans biology, pp 1–11
51. Behrends V, Tredwell GD, Bundy JG (2011) A software complement to AMDIS for processing GC-MS metabolomic data. Anal Biochem 415:206–208
52. Sangster T, Major H, Plumb R, Wilson AJ, Wilson ID (2006) A pragmatic and readily implemented quality control strategy for HPLC-MS and GC-MS-based metabonomic analysis. Analyst 131:1075–1078
53. Dieterle F, Ross A, Schlotterbeck G, Senn H (2006) Probabilistic quotient normalization as robust method to account for dilution of complex biological mixtures. Application in 1H NMR metabonomics. Anal Chem 78:4281–4290
54. Steuer R, Morgenthal K, Weckwerth W, Selbig J (2007) A gentle guide to the analysis of metabolomic data. Methods Mol Biol 358:105–126
55. Kamath RS, Fraser AG, Dong Y, Poulin G, Durbin R, Gotta M, Kanapin A, Le Bot N, Moreno S, Sohrmann M, Welchman DP, Zipperlen P, Ahringer J (2003) Systematic functional analysis of the Caenorhabditis elegans genome using RNAi. Nature 421: 231–237
56. Davies SK, Leroi AM, Bundy JG (2012) Fluorodeoxyuridine affects the identification of metabolic responses to daf-2 status in Caenorhabditis elegans. Mech Ageing Dev 133:46–49
57. Casadevall i Solvas X, Geier FM, Leroi AM, Bundy JG, Edel JB, DeMello AJ (2011) High-throughput age synchronisation of Caenorhabditis elegans. Chem Commun (Camb) 47:9801–9803
58. Ahringer J (ed) (2006) Reverse genetics, WormBook (ed) The C. elegans Research Community, WormBook, doi: 10.1895/wormbook.1.47.1, http://www.wormbook.org

Chapter 25

Genome-Wide RNAi Screening to Identify Regulators of Oncogene-Induced Cellular Senescence

Narendra Wajapeyee, Sara K. Deibler, and Michael R. Green

Abstract

RNA interference (RNAi) is a powerful research tool that can be used to turn off—or silence—the expression of a specific gene. In recent years, RNAi screening on a genome-wide scale has provided the opportunity to identify factors and pathways involved in complex biological processes in a systematic and unbiased manner. Here we describe a genome-wide RNAi screening strategy to identify genes that are required for a particular type of cellular senescence called oncogene-induced senescence. The approach we describe is a general screening strategy that can be applied to the study of other forms of cellular senescence, including replicative senescence.

Key words: Functional genomics, Genome-wide, Oncogene-induced senescence, Positive-selection screen, RNA interference, siRNA, shRNA

1. Introduction

Genome-wide RNA interference (RNAi) screens provide an opportunity to identify the regulators of a biological pathway or phenomenon in an unbiased manner. Several factors must be considered when designing a successful RNAi screen. General guidelines for choosing the appropriate RNAi library (e.g., shRNA vs. siRNA, retroviral vs. lentiviral) and screening strategy (single-well vs. pooled format; positive vs. negative selection, etc.) have been covered in detail elsewhere, and the reader is referred to several excellent reviews on these topics (1–4).

When designing a genome-wide RNAi screen for regulators of oncogene-induced senescence, there are several critical parameters to consider. First, it is important to choose a cell line in which the oncogene induces senescence in all the oncogene-expressing cells. Obtaining a high degree of senescence is crucial for reducing the rate of false positive results and thus decreasing the "background" of the

Lorenzo Galluzzi et al. (eds.), *Cell Senescence: Methods and Protocols*, Methods in Molecular Biology, vol. 965,
DOI 10.1007/978-1-62703-239-1_25,

screen. Second, it is important to choose an appropriate negative control to assess the background of the screen. In most cases, a control non-silencing shRNA or luciferase siRNA is suitable. Third, it is critical to choose an assay (or assays) for validating the candidates identified from the primary RNAi screen that is robust enough to clearly distinguish true positives from false positives.

In addition to issues of background and distinguishing false from true positives, there are other parameters to consider regarding the feasibility of the screen. For example, it is important to determine whether knockdown of a single gene is sufficient to bypass oncogene-induced senescence in the context of the cell line and oncogene used. Furthermore, if using a pool-based strategy, it is important to establish whether a positive shRNA can yield the desired phenotype when present as part of a mixed pool of shRNAs.

For these reasons, before starting a genome-wide RNAi screen, we strongly recommend that the researcher perform either a targeted experiment using known regulators of oncogene-induced senescence, or a small-scale pilot screen using two to three shRNA pools. This step will allow the researcher to optimize RNAi screening conditions as well as understand the technical challenges that could be faced when performing the screen and validating the candidates.

The RNAi screen we describe below is based upon a previous publication by our group in which we identified genes required for oncogenic BRAF to induce senescence in human primary foreskin fibroblasts (PFFs) (5). In brief, we used a positive-selection strategy to identify genes that, when knocked down, allowed cells to bypass oncogene-induce senescence. We used the retroviral (pSM2-based) human shRNA^{mir} library (release 1.20; Open Biosystems), which consists of ~62,400 shRNAs directed against ~28,000 human genes (for a list of other commercially available genome-wide RNAi libraries, see Table 1). The shRNAs were divided into ten pools, which were packaged into retrovirus particles and used to stably transduce PFFs. The cells were then infected with a retrovirus expressing oncogenic BRAF (BRAF^{V600E}). Cells that bypassed the BRAF^{V600E}-mediated cellular proliferation block formed colonies, which were pooled and expanded, and the shRNAs were identified by sequence analysis. Positive candidates were confirmed by stable transduction of PFFs with a single shRNA directed against each candidate gene, infection with the BRAF^{V600E}-expressing retrovirus, and quantification of cellular proliferation. Confirmed candidate shRNAs were then tested in a secondary screen for their ability to bypass the proliferation block in BRAF^{V600E}-expressing primary human melanocytes.

The approach described here is a general screening strategy that could be performed using other oncogenes and/or primary human (or mouse) cell lines. Furthermore, this general screening strategy could, in principle, be applied to identify genes required for other types of cellular senescence, including replicative senescence.

Table 1
List of human and mouse shRNA/siRNA libraries available for genome-wide RNAi screens

Library	Supplier/ Institute	Targeted genes	Total shRNA or siRNA	shRNA or siRNA/gene	Targeted organisms	Vector	Type of library	Features
GIPZ lentiviral	Thermo Scientific	"Entire mouse genome" "Entire human genome"	62,000 62,000	~2	Human Mouse	pGIPZ	Lentiviral	RNA pol II promoter Turbo GFP Puromycin selection marker Can infect nondividing cells
TRIPZ inducible shRNA	Thermo Scientific	~16,000 human annotated genes ~15,950 mouse annotated genes	~159,000	~4–5	Human Mouse	pLKO.1	Lentiviral	Human U6 promoter Inducible Puromycin Can infect nondividing cells
MISSION shRNA	Sigma-Aldrich	~16,000 human annotated genes ~15,950 mouse annotated genes	~159,000	~4–5	Human Mouse	pLKO.1	Lentiviral	Human U6 promoter Puromycin Can infect nondividing cells
NKI	NKI	~8,000 human genes 15,000 mouse genes	24,000 30,000	~3 ~2	Human Mouse	pRSC	Retroviral	RNA Pol III promoter Puromycin selection
GeneNet shRNA	System biosciences	39,000 mouse genes 47,400 human genes	150,000 200,000	4	Human Mouse	HIV- and FIV-based	Lentiviral	Fluorescent proteins such as GFP etc. Puromycin selection
siGenome SMARTpool siRNA	Thermo Scientific	18,236 human genes		~4	Human		siRNA-based	Four mRNA regions targeted at once to reduce false negatives Guaranteed 75% silencing
Silencer siRNA	Ambion	12,585 human genes 11,134 mouse genes	37,755 33,402	~3	Human Mouse		siRNA-based	Can be used in low concentration (>30 nM) Off-target, polymorphic, and antiviral inducing regions have been eliminated

2. Materials

2.1. Generation of Retroviral Particles, Determination of the Multiplicity of Infection, and Cell Infection

- Genome-wide shRNA library (Table 1) and a control shRNA, such as a non-silencing shRNA.
- Phoenix-gp helper-free retrovirus producer cell line (Garry Nolan, Stanford University; l).
- pCI-VSVG plasmid (Addgene).
- Transfection reagent, such as Effectene (Qiagen).
- 0.45 μM filters (Millipore).
- HEK-293 cells (ATCC).
- Culture medium: DMEM high glucose (1×, liquid, with L-glutamine and sodium pyruvate; Life Technologies), 10% FBS (Invitrogen) and Penicillin–Streptomycin (Invitrogen).
- Polybrene (Sigma Aldrich).
- Puromycin.
- Crystal violet staining solution: 40% methanol, 10% acetic acid, 50% ddH_2O, 0.01% crystal violet.
- BJ fibroblasts (ATCC).
- pBABE-Zeo/$BRAF^{V600E}$ retroviral vector (see ref. 6).
- Zeocin.

2.2. Isolation of Genomic DNA and Identification of Candidate shRNAs by DNA Sequencing

- Trypsin-EDTA (0.25%, Invitrogen).
- Genomic DNA preparation buffer: 100 mM NaCl, 10 mM Tris–HCl (pH 8.0), 25 mM EDTA (pH 8.0), 0.5% (v/w) SDS, 50 μL of Proteinase K.
- Phenol–Chloroform–Isoamyl alcohol (25:24:1).
- Chloroform.
- NaCl (5 M).
- Ethanol (70 and 100% solutions).
- TE buffer (1×): 10 mM Tris–HCl, 1 mM EDTA, pH 8.0.
- Spectrophotometer or NanoDrop.
- 5× Go-Taq PCR buffer (Promega).
- Taq DNA polymerase (Invitrogen).
- Primers for sequencing shRNA inserts in pSM2 library: For-pSM2 (5′-GCTCGCTTCGGCAGCACATATAC-3′) and Rev-pSM2 (5′-GAGACGTGCTACTTCCATTTGTC-3′).
- DNase and RNase free Agarose for gel electrophoresis.
- Ethidium bromide solution (10 mg/mL).
- QIAquick gel extraction kit (Qiagen).
- pGEM-T Vector system I (Promega).

- Bacterial competent cells that allow for blue/white selection, such as DH5α, and that have a transformation efficiency of $>10^6$ colonies/μg.
- LB-Agar plates with 100 μg/mL ampicillin, 40 μL X-gal (50 mg/mL), and 10 μL IPTG (1 M).
- LB liquid.
- QIAprep Miniprep kit (Qiagen).
- SP6 sequencing primer (sequence 5′-ATTTAGGTGACAC TATAG-3′).

3. Methods

Carry out all procedures at room temperature unless otherwise specified.

3.1. Generation of Retroviral Particles

1. Plate 3×10^6 Phoenix-gp cells in 10 individual 100 mm tissue culture dishes. Plate one additional dish, which will be infected with a retrovirus expressing a control non-silencing shRNA.
2. After 36 h, transfect cells with 10 μg pooled shRNA plasmid DNA (see Note 1), 1 μg Gag–pol plasmid DNA and 1 μg pCI-VSVG plasmid DNA using transfection reagent as per the supplier's instructions.
3. After 48 h, collect the culture supernatants, which contain retroviral particles.
4. Filter the culture supernatants using 0.45 μM filters. Aliquot 1 mL supernatant into microfuge tubes and freeze at −80°C (see Note 2).

3.2. Determining the Multiplicity of Infection for Retroviral shRNA Pools

1. Plate 1×10^5 HEK-293 cells in each well of a 6-well plate, using one plate for each pool.
2. Perform serial dilutions of each retroviral shRNA pool. First, label six microfuge tubes as "10^{-1}," "10^{-2}," "10^{-3}," "10^{-4}," "10^{-5}," and "10^{-6}." Add 1080 μL of DMEM media with 10% FBS/Pen-Strep to all six tubes. Add 120 μL of retroviral supernatant to the first tube, resulting in a 1/10 dilution (10^{-1}). Mix and remove 120 μL of the 10^{-1} dilution and add it to the second tube to create a 10^{-2} dilution. Repeat to generate 10^{-3}, 10^{-4}, 10^{-5}, and 10^{-6} dilutions.
3. Label the wells of the 6-well plates as "10^{-1}," "10^{-2}," "10^{-3}," "10^{-4}," "10^{-5}," and "10^{-6}." Aspirate the media from all the wells and add 1 mL of serially diluted retroviral supernatant with Polybrene (10 μL/mL) to the appropriate well.
4. After 24 h, remove the media and add 2 mL of fresh DMEM media with 10% FBS/Pen–Strep.

5. After 24 h, add puromycin (1.0 μg/mL) to select for cells carrying the retroviral shRNA.
6. Change the media with puromycin every 3 days.
7. Between day 10 and 14, depending upon the size of the colonies, stain the colonies that survive puromycin selection using crystal violet staining solution. Colonies comprising 1,000 or more cells are considered to be the right size for staining.
8. Calculate the multiplicity of infection (MOI) of the retroviral supernatants as follows:

   MOI (particle forming units (pfu)/mL) = Number of colonies × dilution factor × 10.

   For example, if you observe five colonies in the 10^{-4} dilution plate, the calculation will be: $5 \times 10^4 \times 10 = 5 \times 10^5$ pfu/mL (see Note 3).

3.3. Infection and Selection of Cells After Transduction with Retroviral shRNA Pools

1. Plate 1.2×10^6 BJ fibroblasts in 10 individual 100 mm tissue culture dishes.
2. After 24 h, transduce the BJ fibroblasts with retroviral shRNA pools in a total volume of 5 mL of DMEM media with 10% FBS/Pen–Strep and Polybrene (10 μg/mL) to achieve infection at an MOI of 0.2 (see Note 4).
3. After 24 h, change the media and add 10 mL of DMEM media with 10% FBS/Pen–Strep.
4. After 24 h, add puromycin (1.0 μg/mL) to enrich the cells that carry integrated shRNAs. Change the media after 3 days with fresh puromycin. It usually takes 6 days to completely select cells carrying shRNAs.

3.4. Transduction of shRNA-Carrying Cells with Activated $BRAF^{V600E}$

1. Plate 1.2×10^6 BJ fibroblasts infected with individual shRNA pools in 10 individual 100 mm tissue culture dishes.
2. Transduce the cells with retroviral pBABE-Zeo/$BRAF^{V600E}$ at an MOI of 20 (see Note 5). Retroviral $BRAF^{V600E}$ can be prepared and titrated using the same methodology as that mentioned above for generating the retrovirus particles for the pooled shRNA DNA (see Subheading 3.1).
3. Select the transduced cells with zeocin (100 μg/mL) for 6–9 days to enrich for the cells that are infected with pBABE-Zeo/$BRAF^{V600E}$. Change the media every 3 days with fresh media.
4. Allow the cells to grow 4–6 weeks after infection with $BRAF^{V600E}$.

3.5. Isolation of Genomic DNA from Cells that Bypass Oncogene-Induced Senescence

1. For all ten pools, trypsinize and isolate the surviving cells that are able to bypass $BRAF^{V600E}$-induced senescence.
2. Lyse the cells in genomic DNA preparation buffer. Use 1.0 mL lysis buffer per 1×10^6 cells.
3. Incubate the lysate at 42°C overnight.

4. The next day, mix 500 μL of the lysate with 500 μL of phenol–chloroform–isoamyl alcohol.
5. Vigorously mix by shaking and centrifuge at 2,300 ×*g* for 5 min at room temperature.
6. Remove the upper aqueous phase and transfer into a fresh microfuge tube.
7. Mix 500 μL of the phenol–chloroform–isoamyl alcohol-extracted lysate with 500 μL chloroform.
8. Vigorously mix by shaking and then centrifuge at 2,300 ×*g* for 5 min at room temperature.
9. Remove the upper aqueous phase and transfer into a fresh microfuge tube.
10. Add 100 μL of 5 M NaCl to 400 μL of lysate, mix by tapping and add 1 mL of 100% ethanol. Mix by inverting the tube.
11. Store the tube at –20°C for 1 h.
12. Spin the samples at 9,300 ×*g* for 30 min.
13. Add 1 mL of 70% ethanol to wash the pellet and spin the samples at 9,300 ×*g* for 10 min.
14. Pour off the ethanol and invert the microfuge tube on a paper towel to drain the residual traces of ethanol.
15. Dry the genomic DNA pellet at room temperature.
16. Dissolve the genomic DNA in 200 μL 1× TE per 10^6 cells.
17. Leave the genomic DNA in 1× TE at 60°C overnight to completely dissolve the genomic DNA.
18. Quantify the amount of genomic DNA using a spectrophotometer or NanoDrop at double stranded DNA setting at 260 nm wavelength.

3.6. Identification of Integrated shRNAs by DNA Sequencing

1. To amplify the retroviral shRNA integrated into the genomic DNA, set up the following PCR:

Components	Volume
5× Go-Taq PCR buffer	10 μL
Taq polymerase (5 units/μL)	1 μL
Genomic DNA	2 μL (100 ng (50 ng/μL))
For-pSM2 (10 pmol/μL)	1 μL
Rev-pSM2 (10 pmol/μL)	1 μL
dd H_2O	35 μL

2. Run the PCR products on a 1% agarose gel with 10 μL ethidium bromide (10 mg/mL stock) and elute from the gel using a Qiagen Gel elution kit.

3. Ligate 100 ng of the eluted PCR product with the TA vector using the TA cloning Kit (Promega) as per the manufacturer's instructions.
4. Perform an overnight ligation at 16°C.
5. The next day, transform half of the ligation mixture into bacterial competent cells. Plate the transformation mixture onto LB-Agar plates containing 100 μg/mL Ampicillin, 40 μL of X-gal (50 mg/mL), and 10 μL of IPTG (1 M).
6. Place the LB-Agar plates in a 37°C incubator for at least 16 h, until the white colonies and blue colonies can be clearly distinguished.
7. Inoculate white colonies into tubes containing 3 mL of LB liquid with 100 μg/mL Ampicillin. Grow overnight at 37°C. The number of colonies required to be sequenced will depend upon the number of colonies that rescued oncogene-induced senescence.
8. Isolate plasmid DNA from white colonies using Qiagen's miniprep kit as per the manufacturer's instructions.
9. Sequence the plasmid DNA using the SP6 primer.
10. To identify the target gene corresponding to the shRNA, perform a Nucleotide BLAST search using the shRNA sequence as a query.

3.7. Secondary Screen to Confirm the Candidates Identified from the Genome-Wide RNAi Screen

1. Select the individual shRNA corresponding to the candidate gene from the RNAi library and prepare the retrovirus as described above in Subheading 3.1.
2. For each candidate shRNA to be tested, plate 1×10^5 BJ fibroblasts in a well of a 6-well plate and infect with the retrovirus particle(s).
3. After 24 h, change the media and add 2 mL of DMEM media with 10% FBS/Pen–Strep.
4. After 24 h, add puromycin (1.0 μg/mL) to enrich the cells that carry integrated shRNAs. Change the media after 3 days with fresh puromycin. It usually takes 6 days to completely select cells carrying shRNAs.
5. Validate the candidates by using several assays to assess if the knockdown delays or bypasses oncogene-induced senescence. These assays include colony formation (5), senescence-associated β-galactosidase (7), immunoblotting for p16 (8, 9), and histone H3 lysine 9 (H3K9) acetylation (8, 9).
6. Validate the positive candidate shRNAs using a second shRNA, unrelated in sequence to the first shRNA, to rule out "off-target" effects (see Note 6).

4. Notes

1. To perform the screen in a pooled strategy, shRNAs from the library are required to be assembled into several pools. The total shRNA library contains 65,000 shRNAs. Using automatic robotics, we assembled 10 pools, each containing 6,500 shRNAs, using plasmid DNA as the source material.
2. It is important to note that freeze-thawing will lead to reduced titer. Therefore, we recommend avoiding multiple freeze-thawing cycles.
3. Aim for an MOI of at least ~2×10^5 pfu/mL.
4. Infection at a low MOI of 0.2 will ensure that each cell receives no more than one shRNA, ensuring that the observed phenotype is due to the loss of expression of a single gene.
5. The purpose of transducing the cells at an MOI of 20 is to ensure that all cells are infected with the BRAFV600E virus.
6. In any RNAi experiment it is critical to rule out the possibility that the results observed with a single shRNA (or siRNA) are due to an off-target effect. We recommend performing the following experiments to rule out off-target effects. First, for all shRNAs verified in the above-mentioned assays in Subheading 3.7 of the protocol, we recommend analyzing a second, unrelated shRNA directed against the same gene. These second shRNAs, similar to the first shRNAs, should be tested for their ability to bypass $BRAF^{V600E}$-induced senescence, and for target gene knockdown by qRT-PCR.

Acknowledgments

M.R.G. is an investigator of the Howard Hughes Medical Institute. Narendra Wajapeyee is a Kimmel Scholar for Translational Cancer Research and is supported by grants from American Association for Cancer Research, Leukemia Research Foundation, and Elsa U. Pardee Foundation.

References

1. Ashworth A, Bernards R (2010) Using functional genetics to understand breast cancer biology. Cold Spring Harb Perspect Biol 2:a003327
2. Mullenders J, Bernards R (2009) Loss-of-function genetic screens as a tool to improve the diagnosis and treatment of cancer. Oncogene 28:4409–4420
3. Lizardi PM, Forloni M, Wajapeyee N (2011) Genome-wide approaches for cancer gene discovery. Trends Biotechnol 29:558–568
4. Westbrook TF, Stegmeier F, Elledge SJ (2005) Dissecting cancer pathways and vulnerabilities with RNAi. Cold Spring Harb Symp Quant Biol 70:435–444

5. Wajapeyee N, Serra RW, Zhu X, Mahalingam M, Green MR (2008) Oncogenic BRAF induces senescence and apoptosis through pathways mediated by the secreted protein IGFBP7. Cell 132:363–374
6. Michaloglou C, Vredeveld LC, Soengas MS, Denoyelle C, Kuilman T, van der Horst CM, Majoor DM, Shay JW, Mooi WJ, Peeper DS (2005) BRAFE600-associated senescence-like cell cycle arrest of human naevi. Nature 436:720–724
7. Dimri GP, Lee X, Basile G, Acosta M, Scott G, Roskelley C, Medrano EE, Linskens M, Rubelj I, Pereira-Smith O et al (1995) A biomarker that identifies senescent human cells in culture and in aging skin in vivo. Proc Natl Acad Sci U S A 92:9363–9367
8. Narita M, Narita M, Krizhanovsky V, Nunez S, Chicas A, Hearn SA, Myers MP, Lowe SW (2006) A novel role for high-mobility group a proteins in cellular senescence and heterochromatin formation. Cell 126:503–514
9. Narita M, Nunez S, Heard E, Narita M, Lin AW, Hearn SA, Spector DL, Hannon GJ, Lowe SW (2003) Rb-mediated heterochromatin formation and silencing of E2F target genes during cellular senescence. Cell 113:703–716

Chapter 26

An Integrated Approach for Monitoring Cell Senescence

Tatiana V. Pospelova, Zhanna V. Chitikova, and Valery A. Pospelov

Abstract

Cellular senescence is considered as a crucial mechanism of tumor suppression that helps to prevent the growth of cells at risk for neoplastic transformation. In normal cells, cellular senescence induces an irreversible cell cycle arrest in response to telomere dysfunction, oncogene activation, genotoxic stress and a persistent DNA damage response (DDR). This process is accompanied by dramatic changes in cell morphology as well as in the activity of several signaling pathways. The senescent phenotype is multifaceted. In addition to an obligatory proliferation arrest, senescent cells manifest various senescence markers: mTOR-mediated hypertrophic growth (cell size increase), cell flattening, senescence-associated β galactosidase (SA-β gal) staining, expression of negative cell cycle regulators p53, $p21^{Waf1}$ and $p16^{Ink4a}$, specific chromatin reorganization including DNA segments with chromatin alterations reinforcing senescence (DNA-SCARS), senescence-associated secretory phenotype (SASP) and other features. Here, we describe the protocols that are used to study histone deacetylase inhibitor (HDACI)-induced cellular senescence in transformed cells with a special emphasis on the morphological features of senescence.

Key words: Apoptosis, Autophagy, Cell cycle arrest, DNA damage response, γH2AX foci, HDAC inhibitors, Hypertrophy, mTOR signaling, $p21^{Waf1}$, p53, Senescence

1. Introduction

Cellular senescence was originally defined as "irreversible" cell cycle arrest caused by the replicative exhaustion of human diploid fibroblasts in vitro (1). Later, Serrano et al. (2) showed that ectopic expression of oncogenic Ras induces growth arrest and a senescent-like phenotype in normal human fibroblasts. Senescence of cells in culture is a suitable model for identification and characterization of senescence effectors: chromatin modifications, epigenetic gene regulation, DNA damage response (DDR) signaling, and autophagy (3). Growth arrest is established and maintained by the p53 and $p16^{Ink4a}$/pRB pathways. In the majority of tumor cells, there are various defective negative cell cycle regulators (p53/pRb) or an elevated expression of the positive regulators (cyclin D1,

Lorenzo Galluzzi et al. (eds.), *Cell Senescence: Methods and Protocols*, Methods in Molecular Biology, vol. 965,
DOI 10.1007/978-1-62703-239-1_26,

CDKs, c-myc) that allows the cells to avoid "irreversible" cell cycle arrest and senescence in response to various DNA damage and stress factors.

Conventional therapy of p53-defected tumor cells is ineffective due to the inability to stop proliferation and induce senescence or apoptosis. Many senescence-inducing stimuli generate a persistent DDR signaling associated with DNA double-strand breaks (DSBs) which are a signal for activation of ATM/ATR and downstream pathways, including p53 activation and the accumulation of DNA repair foci marked by γH2AX (4). Activation of DDR signaling can be a trigger for switching on senescence in normal cells and in some types of tumor cells and it is essential for establishing and maintaining senescent phenotypes (5). However, persistent DDR signaling can arise upon the induction of senescence by non-DNA damaging inducers such as HDAC inhibitors or over-expression of CDK inhibitors $p21^{Waf1}$ and $p16^{Ink4a}$ (6). HDACIs relax chromatin structure without physically damaging DNA and promote the accumulation of γH2AX foci, probably interfering with DDR signaling pathways. The number of γH2AX foci increases with the length of HDACIs treatment, so there is a temporal correlation with the dynamics of senescence. Therefore, it is reasonable to include γH2AX foci persistence in a growing list of senescence markers.

Numerous data indicate that multiple signal transduction pathways may be involved in the process of cell senescence. One of the hallmarks of senescent cells is the formation of senescence-associated heterochromatin foci (SAHF) that provides repression of E2F-regulated target genes (7). SAHF formation is connected with the function of p16/pRB and p53 pathways, but senescence without SAHF implies that it is a non-mandatory marker (8). HDACIs are capable of inducing cell cycle arrest in tumor cells with a dysfunctional p53/Rb pathway. This seems to be encompassed by the p53-independent activation of $p21^{Waf1}$ transcription (9) that leads to irreversible G1/S cell cycle arrest (10). The question of which molecular events in the cell and how they initiate the senescence program eventually giving rise to a number of morphological markers will be answered in the nearest future. Cellular senescence exemplifies the most important morphological markers:

1. Suppression of DNA replication.
2. Cell hypertrophy. The size of cells is increased several-fold, when the cell cycle is blocked but the activity mTORC1 and the process of translation remains high.
3. Cell flattening. The senescent cells become flattened due to the formation of the actin stress fibers and the accumulation of focal adhesion contacts that are in correlation with an almost complete suppression of migratory properties in transformed cells (10).

4. Senescence-associated β galactosidase (SA-β gal) activity. Senescent cells express a SA-β gal marker (11).
5. SAHF-foci. Formation of senescence-associated heterochromatic foci (SAHF) that correlate with the irreversibility of senescence (7).
6. γH2AX foci. Accumulation γH2AX foci in senescent cells (6).
7. DNA-SCARS. Senescent cells harbor persistent nuclear foci, which are called the DNA segments with chromatin alterations reinforcing senescence (5).
8. SASP - Senescence-associated secretory phenotype comprising the secretion of numerous cytokines, growth factors and proteases (12).

HDACI-induced senescence is associated with the chromatin remodeling and activation of signaling pathways that eventually form the specific cellular phenotype. Protein accumulation in HDACI-arrested cells due to the activation of rapamycin-sensitive mTOR signaling (mTORC1) leads to cellular hypertrophy. The majority of HDACI-induced morphological and growth features cancels in the presence of specific pharmacological inhibitor of mTORC1 signaling—rapamycin (13) thereby demonstrating that the activation of mTOR signaling is a necessary step in HDACI mediated senescence.

This chapter contains the protocols that are routinely used in our experimental work to describe morphological markers of senescence induced by HDAC inhibitors in rodent embryonic fibroblasts transformed with E1A and c-Ha-ras oncogenes. Murine cell lines remain a popular model for studying the mechanisms of cellular senescence and aging owing to a unique opportunity to use mice with knockouts and derive the possibility from their cells to study the role of relevant genes and signaling pathways in this process. It should be noted that the appearance of senescence markers indicates a complex process, which depends on many factors, first and foremost, the epigenetic status of the cell.

2. Materials

2.1. Common Materials

- Assorted disposable sterile pipettes.
- Set of mechanical pipettes and tips.
- Tissue culture plates, 35, 60, and 100 mm in diameter.
- 6-well tissue culture plates.
- Cell counting chamber.
- 18 × 18 mm cover glasses.

- Microscope slides.
- Forceps.
- Humid chamber (see Note 1).
- Whatman paper.
- Parafilm.
- 1.5 mL microcentrifuge tubes.
- 15 mL polypropylene centrifuge tubes, sterile.
- Laminar flow hood.
- Tissue culture incubator adjusted at 37°C, 5% CO_2 humidified atmosphere.
- Benchtop orbital shaker suitable for 6-well plates and set to the speed of 60 rpm.
- Microcentrifuge with temperature control.
- Tabletop minicentrifuge.
- Light microscope equipped with ×10, ×20, and ×40 lenses and digital camera.
- Fluorescent or confocal microscope equipped with ×63 or ×100 lens, argon-ion (488 nm), helium–neon (543 nm), UV (405 nm) lasers, CCD camera, and image analysis software.
- Flow cytometer equipped with argon-ion (488 nm) laser.
- Dulbecco's Modified Eagle Medium (DMEM) containing 2 mM L-glutamine, 1 mM sodium pyruvate, 4.5 g/L glucose, 100 U/mL penicillin, and 0.1 mg/mL streptomycin (see Note 2).
- Fetal calf serum (FCS) (see Note 3).
- Trypsin-EDTA 0.25%.
- Phosphate-buffered saline (PBS) 1× (cell culture grade), sterile, pH 7.4.
- PBS 1×: 137 mM NaCl, 2.7 mM KCl, 8 mM Na_2HPO_4, and 1.5 mM KH_2PO_4 (pH 7.4).
- Methanol.
- Formaldehyde 3.7% solution in PBS: Mix 36.5–38% formalin solution with PBS with a ratio 1:10 (see Note 4).
- Tap water.
- Ultrapure water.
- Permeabilizing buffer: 0.2% Triton X-100 in PBS.
- Washing buffer: 0.1% Tween-20 in PBS (PBS-T).
- Blocking solution: Bovine serum albumin (BSA) 3% in PBS.
- Antibodies dilution buffer: 3% BSA solution in PBS-T.
- Tris-buffered saline (TBS) 1×: 0.5 M Tris–HCl, 1.5 M NaCl (pH 7.4).

- Permount mounting medium (Thermo Fisher Scientific, Waltham, MA, USA).
- ProLong Gold antifade mounting medium with DAPI (Invitrogen, Life Technologies Corporation, Eugene, CA, USA).
- Clear nail polish.
- Propidium iodide 1 mg/mL solution in water: dilute 1 mg of propidium iodide (Sigma-Aldrich, St. Louis, MO, USA) in 1 mL of ultrapure water, aliquot, and store at –20°C, protect from light.
- 100 mg/mL RNAse A solution, DNAse free (Qiagen, Hilden, Germany) (see Note 5).
- Staining solution: 0.4% (w/v) crystal violet, 30% (v/v) ethanol and 10% (v/v) acetic acid in ultrapure water.
- Alexa-Fluor 488 mouse anti-rabbit antibody (Invitrogen, Life Technologies Corporation).
- Alexa-Fluor 546 rabbit anti-mouse antibody (Invitrogen Life Technologies Corporation).

2.2. Tissue Culture Maintenance and Induction of Senescence

- Vacuum pump with a waste collection flack.
- Water bath set at 37°C.
- Inverted light microscope for cell culture work.
- 0.4% Trypan blue solution.
- Senescence inducing reagent, for example HDAC inhibitor sodium butyrate.

2.3. Analysis of Senescent Cells Morphology by Hematoxylin and Eosin Staining

- Glass rod.
- Hematoxylin Mayer's ready to use aqueous solution (Dako, Glostrup, Denmark).
- Eosin ready-to-use aqueous solution (Dako).

2.4. Senescence-Associated β Galactosidase Activity Assay

- X Gal stock solution: 40 mg/mL 5-bromo-4-chloro-3-indolyl-β-D Galactopyranoside (Sigma-Aldrich) in DMSO (see Note 6).
- SA-β gal staining solution: 5 mM potassium ferrocyanide, 5 mM potassium ferricyanide, 2 mM $MgCl_2$ in PBS (pH to 6.6) (see Note 2).

2.5. Actin Cytoskeleton and Focal Adhesion Contacts Visualization in Senescent Cells

- Anti-vinculin rabbit monoclonal antibody (Cell Signaling Technology, Danvers, MA, USA).
- Rhodamine-phalloidin (Invitrogen Life Technologies Corporation).

2.6. Cell Area Measurements with Immunofluorescent Confocal Microscopy, Analysis of γH2AX Foci Formation in the Nucleus and Cell Size Measurement and Cell Cycle Analysis by Flow Cytometry

- Anti-*N*-cadherin antibody (Santa Cruz Biotechnology, Santa Cruz, CA, USA).
- Anti-phosphorylated histone H2AX (Ser 139) mouse antibody (Cell Signaling Technology, Inc. Danvers, MA 01923).
- Saponin 10% solution (0.1 g/mL of saponin (Sigma-Aldrich) in PBS) (see Note 7).

2.7. Cell Proliferation Assay with Bromodeoxyuridine Immunofluorescent Staining

1. pH indicator paper, pH 0–14.
2. Bromodeoxyuridine (BrdU) (BD Biosciences, San Jose, CA, USA).
3. DNA denaturing reagent (2 M HCl solution in ultrapure water) (see Notes 8 and 9).
4. Anti-BrdU mouse monoclonal antibody (Millipore, Billerica, MA, USA).

2.8. Two-Parametric Laser Scanning Flow Cytometry Method for Detection of γH2AX Accumulation in Senescent Cells

1. Ethanol 70%.
2. BSA-TBS-T solution (1% BSA, 0.2% Tween-20 in TBS).
3. Antibody to phosporylated histone H2AX (Ser 139) rabbit antibody (Cell Signaling Technology).

2.9. Anchorage-Independent Growth in Soft Agar

1. Water bath set at 40°C.
2. Stock agar 3% (0.033 g/mL bacteriological agar (Invitrogen, Carlsbad, CA) in ultrapure water) (see Note 10).

2.10. Cell Migration Through the Porous Membrane

1. 24-well cell culture plates.
2. 8.0 μm pore size Boyden chambers (BD Biosciences).
3. Cotton swabs.

3. Methods

3.1. Tissue Culture Maintenance

1. Grow the cells in DMEM supplemented with 10% FCS.
2. Change the culture medium every other day.
3. Monitor the cells every day using a microscope to control the cell growth density and the absence of contamination.

4. Split the cells every 3–4 days when they reach 80% confluence. To this aim:
5. Pre-warm the medium and other solutions to 37°C in the water bath before use. To this aim:
   (a) Aspirate the medium from the cell culture plates using a pipette or a vacuum pump.
   (b) Rinse the cells twice with 1 mL of sterile PBS (see Note 11).
   (c) Trypsinize the cells (see Note 12).
   (d) Add 1–3 mL of fresh DMEM with 10% FCS to the cells and pipette them up and down several times to break the clumps and obtain single cell suspension.
   (e) Count the cells and test their viability using trypan blue staining assay (see Note 13).
   (f) Plate the cells in the new cell culture dish for propagation (see Note 14). To keep the cell line, periodically cryo-conserve the cells with indication of the passage number.

3.2. Induction of Cell Senescence

1. Seed the cells in a density of 5×10^3 cells/cm^2 in DMEM supplemented with 10% FCS (see Note 15). Put the cover glasses in 35 mm culture dishes or 6-well plates for histological and immunofluorescent staining experiments, use 35 or 60 mm culture plates without glasses for other assays.
2. Allow the cells to grow for 24 h and perform the appropriate senescent inducing treatment. Incubate the cells in the tissue hood at 37°C, 5% CO_2 humidified atmosphere. Change the culture medium to a fresh one containing a HDAC inhibitor every other day.
3. Harvest or fix the cells 24, 72, and 120 h after treatment.

3.3. Histochemical Assays for the Determination of the Morphological Markers of Senescence

3.3.1. Analysis of Senescent Cell Morphology by Hematoxylin and Eosin Staining

1. Discard the culture medium and wash the cells three times with PBS (see Note 16).
2. Fix the cells with 2 mL of ice-cold methanol (–20°C) for 4 min at 4°C.
3. Discard methanol; wash the cells three times with PBS, 5 min each.
4. Add 2 mL of hematoxylin solution and incubate for 3 min at room temperature (see Note 17).
5. Remove hematoxylin from the cells, wash them three times (5–10 min in total) with tap water (see Note 17). After that rinse the cells three times with ultrapure water (see Note 18).
6. Add 2 mL of eosin solution (see Note 20) and incubate for 3 min at room temperature (see Notes 17 and 21).
7. Discard eosin solution; wash the cells three times with ultrapure water.

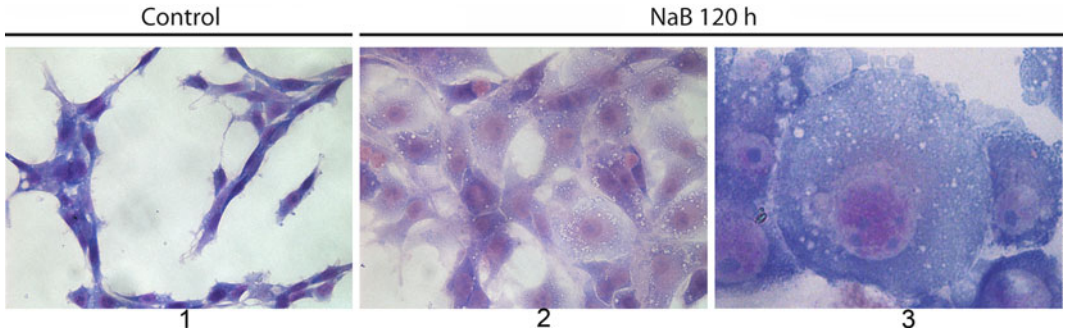

Fig. 1. Morphology of the senescent cells. The senescent cells demonstrate an increase in cell size, change of nuclear–cytoplasmic ratio and vacuolization of the cytoplasm. E1A + c-Ha-ras cells growing on cover glasses were untreated (**a**) or incubated with 4 mM NaB for 120 h (**a**, **c**). Cells were fixed with methanol and stained with hematoxylin and eosin. Images were acquired in bright field microscopy. (**a**) and (**b**) Magnification 100×, (**c**) magnification 400×. The description of the protocol is provided in Subheading 3.3.1.

8. Allow the glasses to dry at room temperature (see Note 22).
9. Put a drop of Permount on the microscope slide using a glass rod. Place the cover glass on it with care to avoid air bubbles formation (see Note 23). Allow Permount to spread evenly between the glasses.
10. Carefully seal the edges of the cover glass with a thin layer of nail polish. Store the samples at 4°C.
11. Acquire the images with a digital camera using a light microscope and magnification ×20 or ×40. As a result of staining, the nuclei should appear dark blue and the cytoplasm should be various shades of pink (Fig. 1).

3.3.2. Senescence-Associated β Galactosidase Activity Assay

1. Discard the culture medium and wash the cells three times with PBS.
2. Fix the cells with 3.7% formaldehyde solution for 15 min at room temperature.
3. Discard formaldehyde solution and wash the cells with PBS three times, 5 min each.
4. Prepare staining solution by mixing of 10 μL X Gal solution with 1 mL of X Gal buffer in a microcentrifuge tube (see Note 24).
5. Place the cover glasses with the forceps on parafilm in the humid chamber.
6. Add 200 μL of staining solution on each cover glass. Cover the humid chamber with a lid. Incubate the cells overnight at 37°C in non-CO_2 environment in the dark (see Note 25).
7. Discard the staining solution. Place the glasses back in to the plates and wash with PBS three times, 5 min each.
8. Blot the excess of liquid from the cover glasses with the Whatman paper by touching it only with the edges of the glass. Use the forceps to hold the glass.

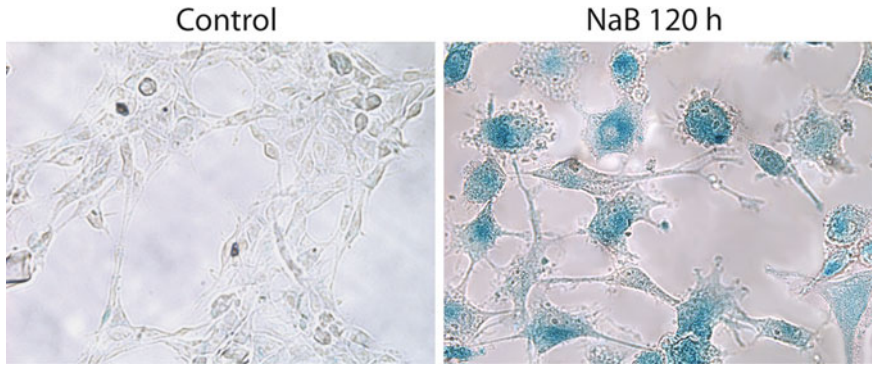

Fig. 2. Senescent E1A + c-Ha-ras cells demonstrate SA-β gal staining. The senescent cells demonstrate SA-β Galactosidase activity and develop blue staining. E1A + c-Ha-ras cells growing on cover glasses were untreated (control) or incubated with 4 mM NaB for 120 h, fixed with 3.7% formaldehyde solution and stained for the acid SA-β Galactosidase with X Gal solution as described in Subheading 3.3.2. Images were acquired in phase-contrast at magnification 200×.

9. Add 5–7 μL of ProLong Gold antifade reagent on the microscope slide and place the cover glass on it with care, avoid air bubbles formation (see Note 23).
10. Carefully seal the edges of the cover glasses with nail polish and leave to dry for 15 min at room temperature. Store the samples at 4°C in the dark.
11. Determine the percentage of blue SA-β gal positive cells using a microscope, lens ×40, and take the pictures of the representative fields in the phase contrast (see Note 26) (Fig. 2).

3.4. Visualization of Senescent Markers by Immunofluorescence

3.4.1. Actin Cytoskeleton and Focal Adhesion Contact Visualization in Senescent Cells

1. Discard the culture medium from the plates (see Note 16). Wash the cells three times with PBS (see Note 27).
2. Add 2 mL of 3.7% formaldehyde solution to the cells and incubate for 15 min at room temperature in the dark for fixation (see Note 28).
3. Discard the formaldehyde solution and wash the cells with PBS three times, 5 min each.
4. Add 2 mL of PBS containing 0.2% Triton X-100. Leave for 20 min at room temperature for permeabilization.
5. Discard Triton X-100 solution; wash the cells with PBS three times, 10 min each.
6. Place the cover glasses on parafilm with forceps in the humid chamber. Avoid bubble formation between the glass and parafilm.
7. Pipette 200 μL of 3% BSA blocking solution on each cover glass (see Notes 29–31). Cover the humid chamber with a lid. Incubate for 1 h at room temperature.
8. Prepare anti-vinculin antibody solution of desirable concentration in 3% BSA in PBST (see Notes 31–34).

9. Discard BSA and pipette 200 μL of primary antibody solution on each cover glass.
10. Incubate in the humid chamber for 1 h at room temperature or overnight at 4°C.
11. Discard the antibody solution.
12. Place the glasses in to the 6-well plate using the forceps and wash with PBST three times, 10 min each (see Note 35).
13. Change parafilm in the humid chamber to a new one.
14. Prepare a fresh solution of rhodamine-phalloidin and Alexa-Fluor 488 conjugated secondary antibody in 3% BSA in PBST. Mix gently by pipetting (see Notes 32, 33, 36, and 37).
15. Put the glasses on parafilm in the humid chamber.
16. Pipette 200 μL of rhodamine-phalloidin and secondary antibody solution per each glass. Incubate for 1 h at room temperature in the dark (see Note 38).
17. Remove antibody solution from the glasses. Place the glasses in to a 6-well plate and wash three times with PBST 10 min each.
18. Blot the excess liquid from the cover glasses with the Whatman paper, touching it only with the edges of the glass. Use forceps to hold the glass.
19. Add 5–7 μL of ProLong Gold antifade reagent on the microscope slide and place the cover glass on it with care, avoid air bubbles formation (see Note 23).
20. Carefully seal the edges of the cover glasses with nail polish and leave to dry for 15 min at room temperature. Store the samples at 4°C in the dark.
21. Acquire the images of the representative fields with the fluorescent or confocal microscope, lenses ×63, ×100 (Fig. 3).

3.5. Methods for the Quantitative Characterization of the Cell Senescence

3.5.1. Cell Area Measurement Based on Immunofluorescent Staining of Cell Membrane Protein

1. To determine the cell area, perform the staining (see Subheading 3.4.1) using the primary antibody against *N*-cadherin and secondary Alexa-Fluor 488 conjugated antibody (see Note 39).
2. Acquire the images of the cells in the *x*–*y* and *x*–*z* planes with the fluorescent or confocal microscope, lens ×63 or ×100. Determine the cell area with an Image-J program analyzing the data obtained in horizontal sections (*x*–*y* plane) and measure the cell thickness at the maximum of the nucleus diameter in the images of *x*–*z* plane (Fig. 4).

3.5.2. Analysis of γH2AX Foci Formation in the Nucleus

1. Perform the staining (see Subheading 3.4.1) using the primary antibody against phosporylated histone H2AX and secondary Alexa-Fluor 546 fluorescent-tagged rabbit anti-mouse antibody (see Notes 39 and 40).

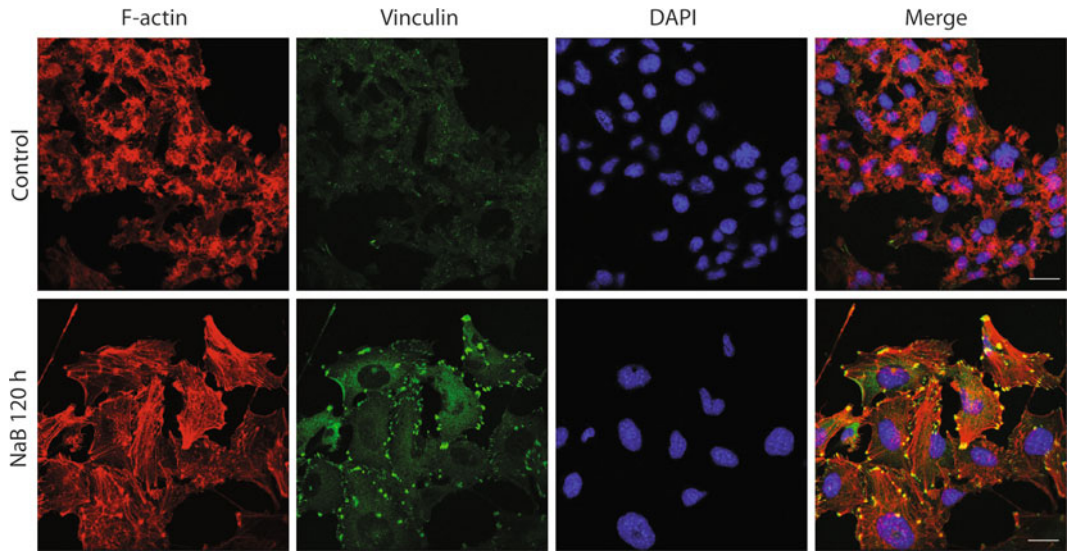

Fig. 3. Flattening of the senescent cells. Cell flattening upon senescence is associated with accumulation of the vinculin containing focal adhesions and formation of actin stress fibers. E1A + c-Ha-ras cells growing on cover glasses were untreated (control) or incubated with 4 mM NaB for 120 h and then fixed with 3.7% formaldehyde solution. The immunofluorescent staining was performed with anti-vinculin antibody to visualize the focal adhesions (*green*) and rhodamine-phalloidin (*red*) to detect F-actin, nuclei were stained with DAPI. Images were acquired with a confocal microscope equipped with CCD camera. Scale bar = 20 μm. The protocol is described in Subheading 3.4.1.

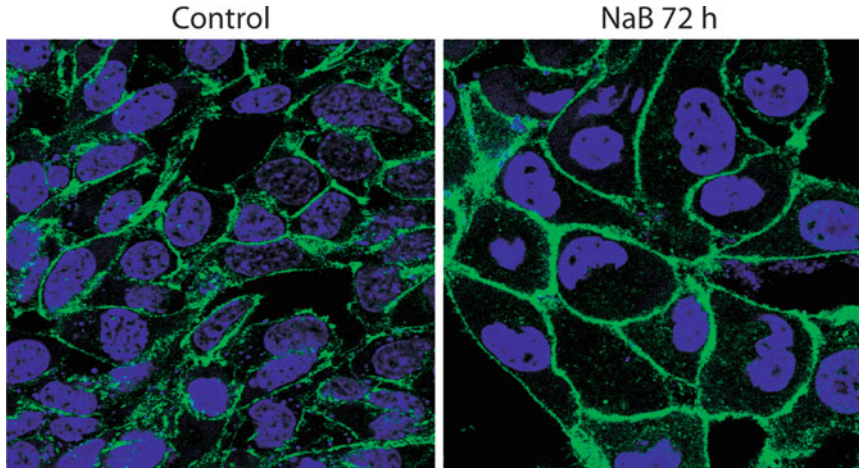

Fig. 4. Senescent cells demonstrate the increased cell size (hypertrophy). E1A + c-Ha-ras cells growing on cover glasses were untreated (control) or incubated with 4 mM NaB for 72 h and then fixed with 3.7% formaldehyde solution. Cell membranes were stained with the antibody to N-cadherin and secondary antibody Alexa-Fluor 488. Images were acquired with a confocal microscope equipped with CCD camera. The cell area can be calculated in the program Image J. The detailed protocol is described in Subheading 3.5.1.

2. Acquire the images of the representative fields with the fluorescent or confocal microscope, lens ×63 or ×100. Calculate the percentage of the cells containing γH2AX foci and an average amount of foci per cell with an Image-J program (Fig. 5).

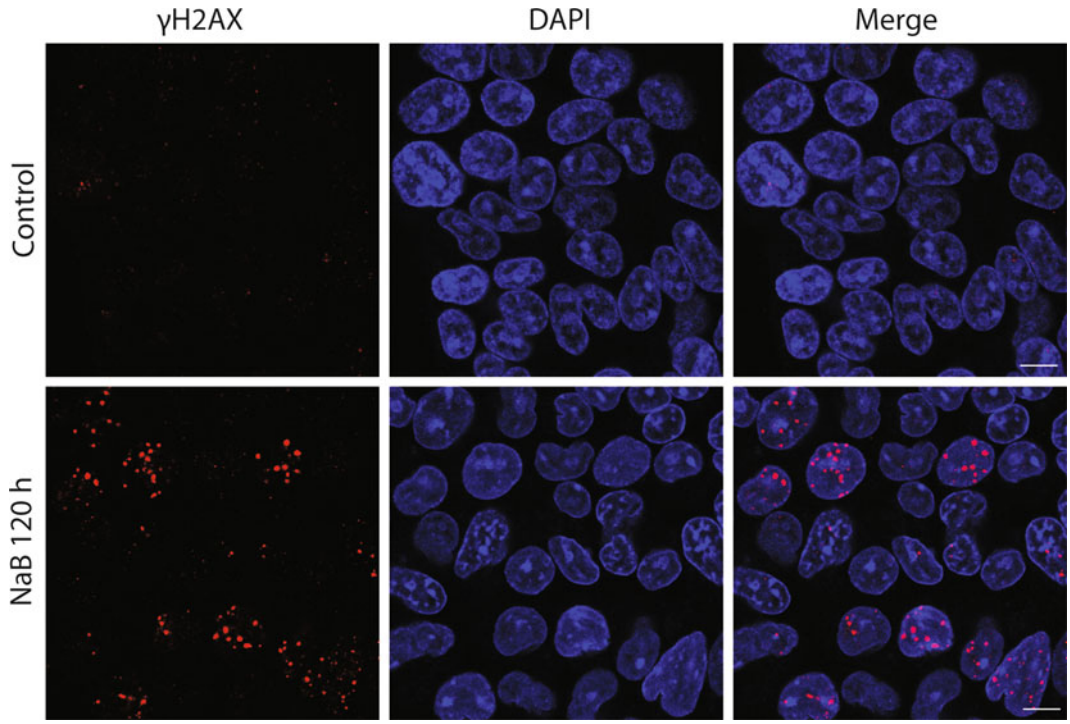

Fig. 5. Senescent cells accumulate γH2AX foci. The cells show accumulation of γH2AX foci upon senescence induced by NaB. E1A + c-Ha-ras cells growing on cover glasses were untreated (control) or incubated with 4 mM NaB for 120 h and then fixed with 3.7% formaldehyde solution. The immunofluorescent staining for γH2AX foci was performed with the antibody to phosphorylated H2AX (Ser 139) and Alexa-Fluor 546 conjugated secondary antibody, nuclei were stained with DAPI. The images were acquired with a confocal microscope equipped with CCD camera. Scale bar = 7.5 μm. *See* Subheading 3.5.2 for detailed protocol.

3.5.3. Cell Size Measurement and Cell Cycle Analysis by Flow Cytometry

1. Collect the medium from the plates in to the 15 mL polypropylene tubes, place on ice (see Note 41).
2. Wash the cells once with 1 mL of ice-cold PBS to remove the traces of serum, transfer the PBS to the tube with medium.
3. Trypsinize the cells at room temperature to obtain single-cell suspension and transfer them to the tube with the medium (see Note 12).
4. Rinse the plate with 1 mL of ice-cold PBS and transfer it to 15 mL tube to collect all the cells for the analysis.
5. Centrifuge at 100 × *g* for 5 min at 4°C and discard the supernatant.
6. Wash the cells with 1 mL of ice-cold PBS. For that, resuspend the cells in PBS, mix by gentle pipetting or vortex at low speed of rotation to disaggregate the clumps, and centrifuge at 100 × *g* for 5 min at 4°C. Discard the supernatant and repeat the washing one more time.
7. Resuspend the pellet in 1 mL of ice-cold PBS and count the cells.

8. Transfer 2×10^6 cells to the microcentrifuge tube.
9. Centrifuge at $100 \times g$ for 5 min at 4°C and discard the supernatant.
10. Resuspend the pellet in 1 mL of PBS containing 0.01% of saponin. Mix gently by pipetting or vortex at low speed.
11. Incubate for 10 min on ice for permeabilization.
12. Centrifuge at $100 \times g$ for 5 min at 4°C and discard the supernatant.
13. Wash the cells three times with ice-cold PBS.
14. Resuspend the cells in 1 mL of PBS containing 40 μg/mL of propidium iodide and 0.1 mg of RNAse A (see Note 42). Incubate for 20 min at 37°C.
15. The samples can be stored for 1 week in the dark at 4°C, though we recommend analyzing them preferably within 24 h. Carefully mix the cell suspension by pipetting before the analysis to disaggregate the cell clusters.
16. Acquire the data by means of light scattering flow cytometry. Analyze not less than 1×10^4 cells from each sample for statistically significant results. Measure the fluorescence of propidium iodide excited with a 488 nm argon-ion laser for DNA content and forward light scatter (FSC) for the cell size. Perform the analysis of the data using the ModFit LT program (VSH, USQ). Calculate the average values on the histograms of forward scattering with the Win MDI program version 2.8.

3.5.4. Cell Proliferation Assay with Bromodeoxyuridine Immunofluorescent Staining

BrdU incorporation

1. Remove the medium from the cells growing on the cover glasses.
2. Rinse the cells once with sterile PBS to remove the traces of the inhibitor which was used for senescence induction.
3. Add 2 mL of fresh DMEM supplemented with 10% FCS and containing 10 μM of BrdU (see Note 43).
4. Place the cells in the tissue culture incubator at 37°C, 5% CO_2 humidified atmosphere for 1–4 h (see Note 44).

Staining procedure

1. Discard the medium and wash the cells three times with ice-cold PBS.
2. Fix the cells with 2 mL of ice-cold methanol (–20°C) for 4 min at 4°C.
3. Discard methanol and wash the cells with PBS three times, 5 min each.
4. Add 2 mL of 2 M HCl and incubate for 20 min at room temperature for DNA denaturation (see Note 45).

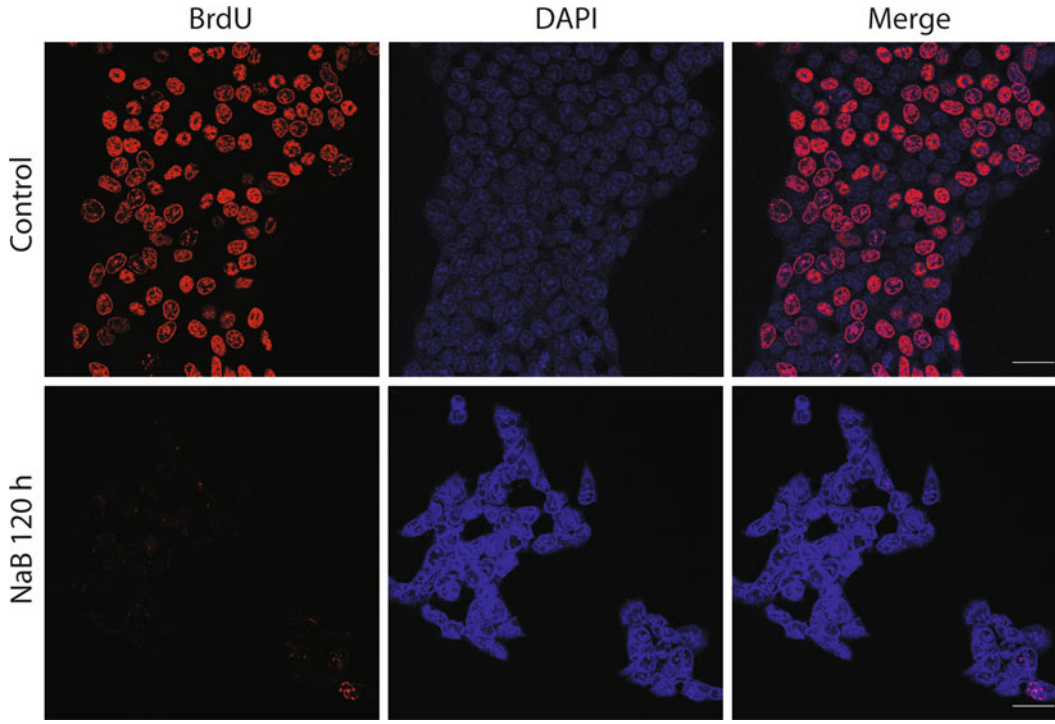

Fig. 6. Senescent cells do not incorporate BrdU. Senescent cells do not show proliferative activity according to a BrdU assay. The cells growing on cover glasses were untreated (control) or incubated with 4 mM NaB for 120 h and fixed with methanol followed by DNA denaturation for 20 min with 2 M HCl. After that, cells were blocked in 3% BSA in PBST for 1 h, incubated with anti-BrdU antibodies and Alexa-Fluor 546 rabbit anti-mouse antibody, nuclei were stained with DAPI. Images were acquired with Leica TCS SP2 confocal microscope equipped with CCD camera, lens ×63. Scale bar = 7.5 μm. *See* Subheading 3.5.4 for the detailed protocol.

5. Discard HCl solution and wash the cells with PBS five times, 5 min each (see Note 46). Check the pH of PBS at the last wash with an indicator paper to ensure that the pH is neutral.
6. Place the cover glasses on parafilm in the humid chamber, pipette 200 μL of 3% BSA blocking solution and incubate for 1 h at room temperature.
7. Prepare anti-BrdU antibody solution by diluting it in 3% BSA-PBST at the ratio 1:50–1:100 (see Note 33).
8. Discard BSA and add 200 μL of anti-BrdU antibody solution per each cover glass. Incubate for 1 h at room temperature or overnight at 4°C.
9. Continue as described above in steps 11–22 (see Subheading 3.4.1) Use Alexa-Fluor 546 secondary antibody diluted 1:1,000 in 3% BSA in PBST (see Notes 33 and 39).
10. Calculate the percentage of the cells incorporating BrdU using fluorescent or confocal microscope, lenses ×63, ×100. Acquire the images of the representative fields (Fig. 6).

3.5.5. Two-Parametric Laser Scanning Flow Cytometry for Detection of γH2AX Binding in Senescent Cells

1. Discard the medium from the plates. Wash the cells two times with ice-cold TBS to remove the traces of serum (see Notes 27 and 40).
2. Trypsinize the cells (see Note 12).
3. Resuspend the cells in 1 mL of fresh DMEM supplemented with 10% FCS to neutralize trypsin. Mix gently by pipetting to obtain single-cell suspension and transfer it to the microcentrifuge tube (see Note 41).
4. Centrifuge the cells at 100×*g* for 5 min at 4°C. Discard the supernatant.
5. Wash the cells with 1 mL of TBS. For that, resuspend the pellet in ice-cold TBS, mix by gentle pipetting or vortex at low speed of rotation to disaggregate the clumps and then centrifuge at 100×*g* for 5 min at 4°C. Discard the supernatant. Repeat the procedure one more time.
6. Resuspend the cells in 0.5 mL of TBS. Add the equal volume of 3.7% formaldehyde solution (see Note 40), incubate for 15 min on ice for fixation.
7. Centrifuge the cells at 100×*g* for 5 min at 4°C. Discard the supernatant and wash the cells twice in TBS.
8. Resuspend the cells in 100 μL of TBS; add 900 μL of ice-cold (–20°C) 70% ethanol (see Notes 47 and 48). Incubate for 2 h at –20°C (see Note 49).
9. Centrifuge the cells at 100×*g* for 5 min at 4°C. Remove the supernatant carefully and resuspend the pellet in 1 mL of BSA-TBS-T. Repeat the step twice.
10. Resuspend the cells in 100 μL of BSA-TBS-T containing 1 μg of primary antibody against phosphorylated H2AX (see Notes 32 and 33).
11. Incubate with gentle shaking at 4°C overnight.
12. Add 1 mL of BSA-TBS-T and centrifuge at 100×*g* for 5 min at room temperature. Repeat the procedure twice.
13. Resuspend the cells in 100 μL of BSA-TBS-T (see Note 50) containing Alexa-Fluor 488 mouse anti-rabbit secondary antibody diluted 1:200.
14. Incubate with gentle shaking for 60 min in the dark.
15. Add 1 mL of BSA-TBS-T; incubate for 20 min.
16. Centrifuge the cells at 100×*g* for 5 min and discard the supernatant.
17. Resuspend the cells in 1 mL of BSA-TBS-T and centrifuge for 5 min at 100×*g*. Repeat the procedure twice.
18. Resuspend the cells in 0.5 mL of TBS; add 0.5 μL of RNAse A and 5 μL of propidium iodide solutions. Incubate for 30 min in the dark.

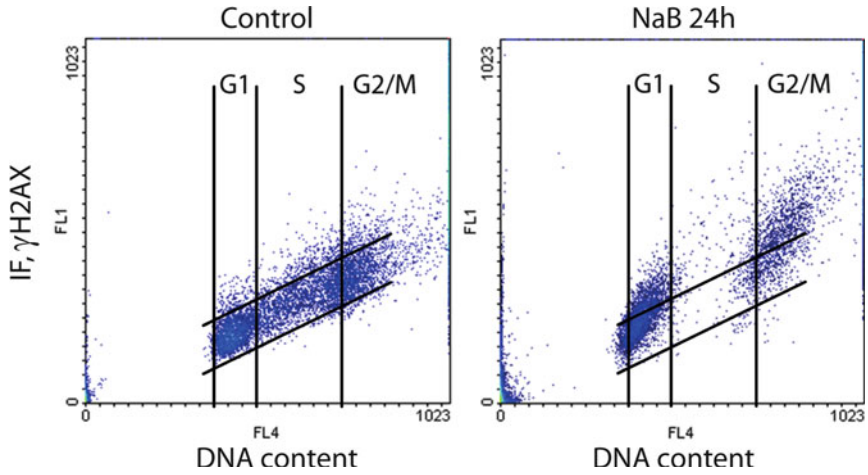

Fig. 7. The ability of cells to bind antibody to γH2AX increases upon senescence according to flow cytometry data. Bivariate distributions of DNA content versus γH2AX are shown. Notice, S phase cells are almost absent in NaB-treated cells. E1A + c-Ha-ras cells were untreated (control) or incubated with 4 mM NaB for 24 h. Cells were stained with propidium-iodide (PI) and antibody to γH2AX (Ser 139) and subjected to two-parametric flow cytometry. Results are present as DNA content (*x*-axis) versus γH2AX levels (*y*-axis). The mean value of γH2AX immunofluorescence can be calculated for G1, S, and G2 subpopulations. The detailed protocol is described in Subheading 3.5.5.

19. Measure the fluorescence induced by the excitation of a 488 nm argon ion laser using a flow cytometer. Analyze the flow cytometry data with the WinMDI 2.8 program (Fig. 7).

3.6. Suppression of the Transformed Phenotype of Cells Upon Senescence

Cellular senescence is a crucial anticancer mechanism that prevents the growth of cells at the risk for neoplastic transformation. However, some tumor cells retain the ability to senesce in vivo in response to chemotherapy. In these cases the induced senescence is associated with tumor regression. Senescence of tumor cells in vitro can change the main features of the transformed phenotype such as the ability to proliferate in clonal density, anchorage independent growth in semisolid media (agar, Methocel), and high migratory and invasive properties.

3.6.1. Ability of the Cells to Proliferate in Clonal Density (Clonogenic Assay)

Preparation of the cells for clonogenic assay

1. Discard the medium from the plates.
2. Wash the cells two times with sterile PBS to remove the traces of serum (see Note 11).
3. Trypsinize the cells (see Note 12).
4. Add 1 mL of fresh DMEM with 10% FCS to the cells to neutralize the trypsin. Mix gently by pipetting to obtain single-cell suspension.
5. Count the cells accurately (see Note 51).
6. Calculate the amount of the cells and medium required for the experiment (see Note 52).

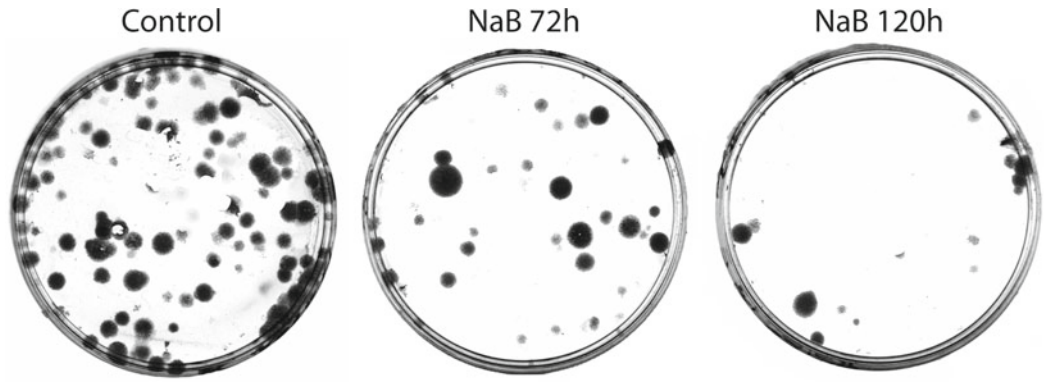

Fig. 8. Cellular senescence suppresses proliferation at the single-cell density (clonogenic assay). The senescent cells lose the ability to proliferate in low density upon senescence in time-dependent manner. E1A+c-Ha-ras cells were untreated (control) or incubated with 4 mM NaB for 72 and 120 h. The cells were trypsinized and 200 cells per 35 mm dish were plated. Cells were grown for 14 days and the colonies then were stained with crystal-violet solution and counted under the microscope equipped with 10× lens. The images were acquired with a digital camera. The detailed protocol is described in Subheading 3.6.1.

7. Prepare the desirable concentration of cell suspension in a 15 mL centrifuge tube (see Note 53).
8. Pipette 3 mL of cell suspension in the well of a 6-well plate (see Note 51).
9. Incubate the cells at 37°C, 5% CO_2 in a humidified atmosphere for 1–4 weeks (see Notes 54 and 55).

Fixation and staining of the colonies

1. Discard the medium and wash the cells twice with PBS.
2. Add 1 mL of crystal violet staining solution; incubate for 15 min at room temperature in the chemical hood (see Note 56).
3. Discard the crystal violet solution and wash the cells three times with tap water.
4. Allow the plates to dry at room temperature.
5. Count the clones using a light microscope, lens ×10, and acquire the images of the plates with a digital camera (Fig. 8).

3.6.2. Anchorage-Independent Growth in Soft Agar

1. Discard the medium from the plates.
2. Wash the cells two times with sterile PBS to remove traces of the serum (see Note 11).
3. Trypsinize the cells (see Note 12).
4. Add 1 mL of fresh DMEM with 10% FCS to the cells to neutralize the trypsin. Mix gently by pipetting to obtain single-cell suspension.
5. Count the cells accurately (see Note 51).
6. Calculate the amount of the cells and medium required for the experiment (see Note 52).

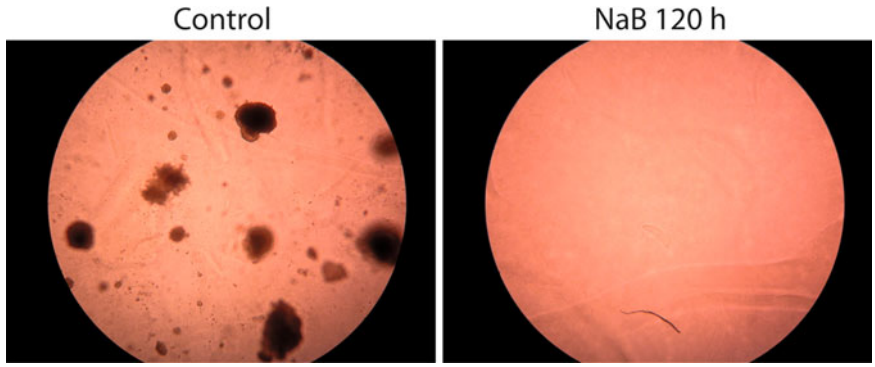

Fig. 9. Senescent cells do not proliferate in soft agar. Senescent E1A + c-Ha-ras cells are unable to proliferate and form the colonies in semisolid agar. The cells were left untreated (control) or incubated with 4 mM NaB for 120 h. Then they were trypsinized and seeded in DMEM with 10% FCS and containing 0.33% agar at density of 1,000 cells per well of 6-well plate. After 14 days the colonies were counted under the microscope equipped with 10× lens and the representative sections were photographed. See Subheading 3.6.2 for the detailed description of the protocol.

7. Prepare the desirable concentration of cell suspension in a 15 mL centrifuge tube (see Note 57).
8. Add 10% of stock agar solution of the final volume of the cell suspension, mix carefully (see Notes 58–60).
9. Pipette 3 mL of the cell suspension in the well (see Note 51).
10. Incubate the cells at 37°C, 5% CO_2 humidified atmosphere for 1–4 weeks (see Note 61).
11. Count the colonies using light microscope magnification ×10 or ×20 and acquire the images with a digital camera (Fig. 9).

3.6.3. Cell Migration and Wound Healing Assay

1. Grow cells to approximately 80–90% of confluence. Discard the medium.
2. Add 3 mL of fresh DMEM supplemented with 10% FCS and treat the cells with the appropriate inhibitor as long as necessary to induce senescence (see Note 62).
3. After that make a wound using a sterile 100 µL plastic tip.
4. Aspirate the medium carefully and rinse the cells twice with 1 mL of sterile PBS to remove the detached and broken cells (see Note 63).
5. Add 3 mL of fresh DMEM supplemented with 10% FCS and inhibitor (see Note 64).
6. Incubate the cells at 37°C, 5% CO_2 humidified atmosphere for 24 h.
7. Acquire images of the same area of the wound every day using the light microscope, lens ×10, and digital camera.
8. To investigate the irreversible effect of the chemical senescent inducer, change the medium to fresh one without inhibitor, place the cells in the incubator, and acquire images of the wound after 24 h (Fig. 10).

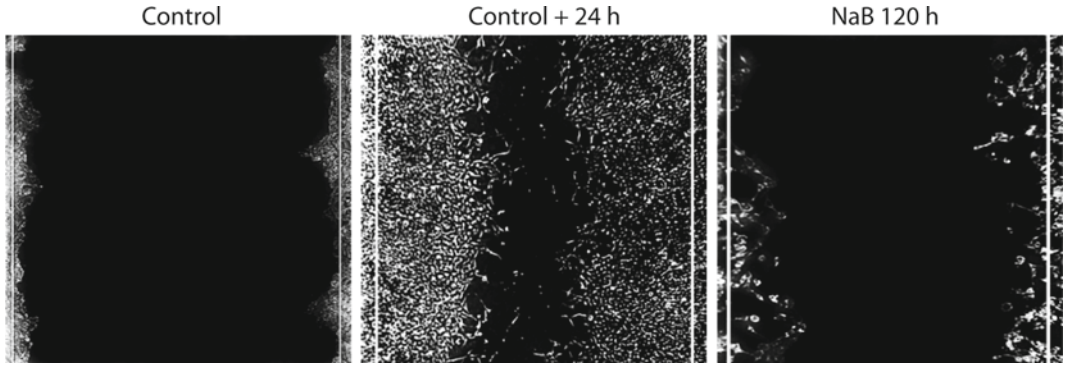

Fig. 10. Senescent cells have a reduced ability to migrate into the wound. The cell motility assay was performed as described in Subheading 3.6.3. Cells were grown to 80% of confluence and treated with 4 mM of NaB for 120 h. After that the wound was made by a 200 μL tip and cells were photographed (control) and then incubated for additional 24 h to allow the wound to repair. The cells with the wound but grown untreated were used as the positive control (control + 24 h).

3.6.4. Cell Migration Through the Porous Membrane

Preparation of the Boyden chambers

1. To prepare the Boyden chambers to work add 750 μL of DMEM with 10% FCS to each well of 24-well plate.
2. Using the sterile forceps carefully place the Boyden chambers into the wells with the medium; avoid bubble formation (see Note 65).

Preparation of the cells

1. Discard the medium from the cells.
2. Wash the cells two times with sterile PBS to remove the traces of serum (see Note 8).
3. Trypsinize the cells (see Note 12).
4. Add 1 mL of fresh DMEM with 10% FCS to the cells to neutralize the trypsin. Mix gently by pipetting to obtain single-cell suspension.
5. Count the cells accurately (see Note 51).
6. Prepare the cell suspension of the appropriate concentration (see Note 66) in DMEM without FCS (see Note 67). Use the sterile 15 mL polypropylene tube. Mix carefully but not vigorously by swirling and pipetting.
7. Add 300 μL of the cell suspension in to each insert of the Boyden chamber.
8. Incubate the cells at 37°C, 5% CO_2 humidified atmosphere overnight (see Note 68).

Fixation and staining of migrated cells

1. Carefully discard the medium from the Boyden chambers.
2. Remove the cells from the inner surface of the membranes using cotton swabs. Do not touch the bottom side of the membrane with migrated cells.

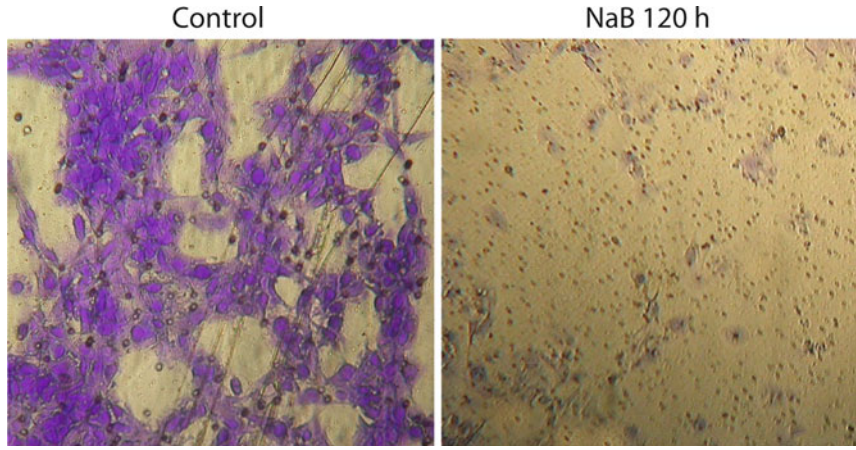

Fig. 11. Cells do not migrate through the porous membrane upon NaB-induced senescence. Untreated E1A + c-Ha-ras cells (control) and cells incubated with NaB 120 h were trypsinized and counted. 750 μL of DMEM with 10% FCS was added to the wells of 24-well plate, after that 500 cells in 300 μL DMEM without FCS were placed in the upper section of the Boyden chamber. The chambers were incubated for 24 h, then the medium was removed, the cells were fixed with 3.7% formaldehyde solution and stained with crystal violet. Migrated cells were counted using the microscope (lens 10×), the images were acquired with a digital camera. The detailed protocol is described in Subheading 3.6.4.

3. Using forceps transfer the Boyden chambers to a new 24-well plate containing 750 μL of 3.7% formaldehyde solution in PBS (see Note 66).
4. Fix the cells for 15 min at room temperature.
5. Remove the formaldehyde solution from the wells.
6. Add 750 μL of PBS into the wells to wash the cells. Discard the PBS. Repeat the washing twice.
7. Add 750 μL of crystal violet solution into the wells to stain the migrated cells.
8. Incubate for 15 min at room temperature in the chemical hood (see Note 57).
9. Discard the crystal violet solution.
10. To wash the membranes add 750 μL of PBS into the wells of the plate. Repeat the washing two more times or until discarded PBS becomes clear.
11. Allow the membranes to dry at room temperature.
12. Remove the membranes from the inserts with a scalpel and forceps. Keep the cell layer intact.
13. Place a drop of Permount on the microscope slide using a glass rod and mount the membranes facing the cell side down.
14. Carefully seal the edges of the membranes with a thin layer of nail polish. Leave the samples at room temperature.
15. Acquire the images using the microscope equipped with a digital camera, lenses ×10 or ×20, and count the migrated cells (Fig. 11).

4. Notes

1. To make the humid chamber use the flat bottom container with the lid or cell culture dish of 150 mm diameter. Put wet Whatman paper on the bottom and cover it with parafilm. Make sure that there are no bubbles between the layers. Uneven surface causes an unbalanced distribution of the solutions on the cover glasses and irregular staining of the samples.
2. Store at 4°C.
3. Store at –70°C.
4. Prepare fresh solution before use.
5. In case RNAse A is not DNAse free, boil the stock solution for 5 min in the water bath.
6. Aliquot and store at –20°C protected from light.
7. Warm up to 37°C for better dilution, aliquot, and store at –20°C.
8. Add concentrated acid to the water but not the opposite way around to avoid splashing the concentrated acid as a result of heat release and boiling.
9. Store at room temperature.
10. Melt agar in the microwave oven, sterilize in autoclave. Keep the stock agar solution at 4°C. Melt in the microwave oven and keep in the water bath at 40°C before use.
11. FCS contains the proteins which repress the protease activity of trypsin.
12. Leave 1 mL of trypsin over the cells until they get round and start to detach. For best results put the plate in the incubator at 37°C. Monitor the process under the microscope. Alternatively, withdraw trypsin and wait until the cells get round. Then add 1 mL of DMEM supplemented with 10% FCS and resuspend the cells in the medium.
13. To perform cell viability assay, dilute trypan blue 1:10 with PBS, then mix the cell suspension with diluted trypan blue 1:5 in the microcentrifuge tube. Immediately proceed to counting, do not keep the cells in trypan blue for a long time. Count the number of live cells (clear) and dead cells (blue) and calculate the concentration of viable cells (cells/mL) and % of viability.
14. The amount of cells which should be transferred to the new culture plate for propagation depends on the cell line and the proliferation rate.
15. It is extremely important to determine the optimal density for each cell line. The cell may undergo apoptosis if plated in an

insufficient density or will not respond the treatment if the density is too high. This parameter also influences the development of flattening and increase in cell size.

16. Protect the cells from drying during the entire staining procedure. Once the solution is removed, it should be replaced by the next one.
17. To obtain a desirable intensity of staining, the incubation time with hematoxylin as well as eosin can vary.
18. Tap water has a slightly alkaline reaction which is necessary for hematoxylin staining development. To obtain differential staining and more intense blue color of the nuclei, it is possible to add few drops (5–10 drops per L) of ammonium hydroxide solution to alkalify water. Using warm tap water helps to accelerate the staining development as well.
19. It is important to wash the cells with ultrapure water to normalize the pH otherwise eosin staining will develop weakly.
20. Filter eosin solution before use in case of precipitation.
21. Eosin is a water soluble dye; therefore the excess staining can be corrected by washing with water.
22. The remaining water dissolves eosin in the sample and leads to a loss of staining.
23. Start to lower the cover glass from one side touching the mounting medium and let it fall slowly. Use the forceps to hold the cover glass.
24. X Gal staining solution may precipitate if added to cold X Gal buffer. Pre-warm the solutions to 37°C before use for better dilution.
25. The presence of CO_2 can change the pH of the staining solution and may lead to incorrect results.
26. To acquire the images combining SA-β gal and nuclei staining use the fluorescent microscope equipped with UV laser.
27. It is important to remove the traces of DMEM, since it contains the pH indicator phenol red, which is a source of autofluorescence and causes the background noise.
28. Do not use methanol for fixation of the samples. Methanol impairs the phalloidin-binding site on F-actin and abolishes the staining.
29. As an alternative, it is possible to add 100 μL of BSA or antibodies solutions on parafilm and then place the cover glass upside down (with the cell side facing the liquid phase). It helps to save the antibodies and produces more even distribution of the solutions on the glass area. To obtain reliable results from staining, avoid the air bubbles when putting the cover glass on solutions. This method is not recommended for cells with low adhesive characteristics.

30. Optimize the concentrations of the BSA blocking solution and antibodies solutions to reduce the background and nonspecific staining and obtain the optimal signal level.
31. While BSA and primary antibody solutions are stable for some time at 4°C if 0.01% of sodium azide is added, we recommend preparing fresh solutions before use for best results.
32. Do not vortex antibody solutions, it may alter their functionality. Mix gently by pipetting.
33. To determine the optimal concentration of antibody, perform the staining using a series of dilutions before starting the experiment. Use 1:50 up to 1:2,000 dilutions for the primary antibodies and rhodamine-phalloidin, and 1:500–1:2,000 for Alexa-Fluor 488 and Alexa-Fluor 546 conjugated secondary antibody. The optimal concentration for the antibodies against BrdU usually varies between 1:50 and 1:150 dilutions.
34. Essential controls. Control of the primary antibodies specificity: perform the staining as described in the protocol but skip the incubation with the fluorochrome-tagged secondary antibody. Control the specificity secondary antibody: follow the staining protocol but do not apply primary antibody solution after the blocking, instead of that incubate the cells with the secondary antibodies only.
35. For a more efficient wash, use a benchtop orbital shaker at a low speed of rotation, 50–100 rpm is optimal.
36. Briefly centrifuge the secondary antibody using tabletop minicentrifuge in order to remove the precipitated antibody and thereby reduce artifacts and background.
37. Antibodies and reagents conjugated with fluorochromes as well as their solutions and stained cells should be protected from light.
38. Do not store rhodamine-phalloidin and secondary antibody solution.
39. Do not add rhodamine-phalloidin into the secondary antibody solution.
40. To detect the phosphorylated isoforms of the proteins prepare all solution in TBS instead of PBS to prevent false-positive results due to phosphorylation by PBS component.
41. Place the cells in the tubes preliminarily chilled on ice. Perform all the work with the cells on ice with the solutions chilled to 4°C if not otherwise mentioned.
42. Prepare a fresh working solution containing 40 μg/mL propidium iodide and 0.1 mg RNAse A in PBS at room temperature before use.
43. Protect the BrdU reagent, solutions, and stained cells from light.

44. The time of the BrdU treatment depends on the cell line.
45. DNA has to be denatured to make the incorporated BrdU accessible for anti-BrdU antibodies.
46. Instead of using the neutralizing solution we increase the number of washes and control the pH after the washing. This change does not influence the results.
47. The adhesion properties of the cells change after ethanol treatment and cells can be removed with supernatant if the liquid flow is too fast.
48. Add ethanol carefully in drops while swirling the tube to mix the suspension.
49. The cells can be kept at –20°C up to 2 weeks.
50. Starting from this point the solutions, incubation and working conditions are at room temperature.
51. It is extremely important to count the cells accurately and place an equal amount of cells on each well to obtain correct results. Mix the cell suspension regularly to prevent sedimentation.
52. Perform the assay in triplicate to achieve significant results.
53. Determine the optimal cell concentration for the investigated cell line before the experiment starts. To make that, use the series of dilutions from 100 to 1,000 cells per well and perform the clonogenic assay. Some cell lines are not able to form the clones if seeded at a very low density; whereas being plated at high density may overlap the growing colonies and cannot be counted.
54. Keep the plates in the incubator until the colonies in the untreated control visible to the naked eye as they form but not overlap.
55. Carefully add fresh medium supplemented with serum every 5 days.
56. Crystal violet staining solution contains acetic acid, which causes irritation of the respiratory tract.
57. To determine the optimal cell concentration, perform the soft agar assay before starting the experiment using a series of dilutions from 10^3 to 10^4 cells per well.
58. Do not use agar with a temperature of more than 40°C; it may kill the cells.
59. Work with only one tube at once to avoid premature agar hardening.
60. It is important to pipette softly to avoid bubbles formation in the agar containing solution. The bubbles may lead to a mistake in the analysis and fail the experiment. In the meantime the cells

should be distributed in agar solution as evenly as possible to prevent fusion of the clones formed by adjacent cells.

61. To obtain the optimal results, monitor the formation of the clones and their size once a week using the microscope. Do not shake the plates; movement of the agar layer may have negative effect on the clone formation and influence the validity of data.
62. Change the medium to a fresh one containing an inhibitor every other day.
63. Removing the detached cells prevents acquisition of incorrect data associated with cell sedimentation and subsequent proliferation in the wound area.
64. Add the medium carefully to avoid cells wash off, direct the non-vigorous liquid flow to the dish wall but not to the bottom.
65. Place the insert at a small angle and lower it down slowly to prevent bubble formation.
66. Determine the optimal concentration before starting the experiment. For that, perform the assay using a series of dilutions with concentrations from 10^3 to 10^6 cells per well. Note that some cell lines are difficult to grow if seeded at a low density whereas in case of a density that is too high the migrated cells cannot be counted.
67. FCS in the lower chamber acts as a chemoattractant for the cells and forces them to migrate through the porous membrane.
68. Depending on the cell type the time of incubation may vary between 2 and 24 h.

Acknowledgments

We thank members of our laboratory Drs. Svetlana Svetlikova, Maria Abramova, Alexander Kukushkin, Svetlana Zubova, Tatiana Bykova, Vasily Romanov, and Elena Bukreeva for their constant support and help during preparation of this chapter. We are grateful to Sergei Gordeev for help in figure preparation and Ksenia Strunnikova for critical reading of manuscript. The work was supported by Russian Foundation for Basic Research (RFBR): No. 12-04-01393-a (VAP) and No. 10-04-01152 (TVP), Russian Academy of Sciences Program "Molecular and Cell Biology" and grant from the St. Petersburg State University, Contract № 1.37.122.2011.

References

1. Hayflick L (1965) The limited in vitro lifetime of human diploid cell strains. Exp Cell Res 37:614–636
2. Serrano M, Lin AW, McCurrach ME, Beach D, Lowe SW (1997) Oncogenic ras provokes premature cell senescence associated with accumulation of p53 and p16INK4a. Cell 88: 593–602
3. Young AR, Narita M, Ferreira M, Kirschner K, Sadaie M, Darot JF, Tavare S, Arakawa S, Shimizu S, Watt FM, Narita M (2009) Autophagy mediates the mitotic senescence transition. Genes Dev 23:798–803
4. d'Adda di Fagagna F (2008) Living on a break: cellular senescence as a DNA-damage response. Nat Rev Cancer 8:512–522
5. Rodier F, Munoz DP, Teachenor R, Chu V, Le O, Bhaumik D, Coppe JP, Campeau E, Beausejour CM, Kim SH, Davalos AR, Campisi J (2011) DNA-SCARS: distinct nuclear structures that sustain damage-induced senescence growth arrest and inflammatory cytokine secretion. J Cell Sci 124:68–81
6. Pospelova TV, Demidenko ZN, Bukreeva EI, Pospelov VA, Gudkov AV, Blagosklonny MV (2009) Pseudo-DNA damage response in senescent cells. Cell Cycle 8:4112–4118
7. Narita M, Nunez S, Heard E, Narita M, Lin AW, Hearn SA, Spector DL, Hannon GJ, Lowe SW (2003) Rb-mediated heterochromatin formation and silencing of E2F target genes during cellular senescence. Cell 113:703–716
8. Di Micco R, Sulli G, Dobreva M, Liontos M, Botrugno OA, Gargiulo G, dal Zuffo R, Matti V, d'Ario G, Montani E, Mercurio C, Hahn WC, Gorgoulis V, Minucci S, d'Adda di Fagagna F (2011) Interplay between oncogene-induced DNA damage response and heterochromatin in senescence and cancer. Nat Cell Biol 13: 292–302
9. Abramova MV, Pospelova TV, Nikulenkov FP, Hollander CM, Fornace AJ Jr, Pospelov VA (2006) G1/S arrest induced by histone deacetylase inhibitor sodium butyrate in E1A+Ras-transformed cells is mediated through down-regulation of E2F activity and stabilization of beta-catenin. J Biol Chem 281:21040–21051
10. Romanov VS, Abramova MV, Svetlikova SB, Bykova TV, Zubova SG, Aksenov ND, Fornace AJ Jr, Pospelova TV, Pospelov VA (2010) p21(Waf1) is required for cellular senescence but not for cell cycle arrest induced by the HDAC inhibitor sodium butyrate. Cell Cycle 9:3945–3955
11. Dimri GP, Lee X, Basile G, Acosta M, Scott G, Roskelley C, Medrano EE, Linskens M, Rubelj I, Pereira-Smith O et al (1995) A biomarker that identifies senescent human cells in culture and in aging skin in vivo. Proc Natl Acad Sci U S A 92:9363–9367
12. Rodier F, Coppe JP, Patil CK, Hoeijmakers WA, Munoz DP, Raza SR, Freund A, Campeau E, Davalos AR, Campisi J (2009) Persistent DNA damage signalling triggers senescence-associated inflammatory cytokine secretion. Nat Cell Biol 11:973–979
13. Demidenko ZN, Zubova SG, Bukreeva EI, Pospelov VA, Pospelova TV, Blagosklonny MV (2009) Rapamycin decelerates cellular senescence. Cell Cycle 8:1888–1895

Chapter 27

Robust Multiparametric Assessment of Cellular Senescence

Clara Correia-Melo, Diana Jurk, and João F. Passos

Abstract

Cellular senescence, the irreversible loss of replicative capacity, is both a tumor suppressor mechanism and a contributor to the age-related loss of tissue function. However, the role of cellular senescence in vivo has been unclear, mostly because of the absence of cellular markers specific enough to identify the state (senescent or proliferating) of individual cells in tissues. Recently, we have tested the robustness of multiple senescence candidate markers by comparing them to a dynamic stimulation model, which estimates the fraction of senescent cells with high precision. We found that the absence of the proliferation markers Ki67 and PCNA combined with high density DNA damage foci (>5 γH2AX foci per nucleus) was the best quantitative indicator of cellular senescence. In this chapter, we describe protocols for the dual immunofluorescence-based quantification of Ki67/PCNA and γH2AX in both fixed cells and paraffin-embedded tissues.

Key words: Cellular senescence, γH2AX, Immunofluorescence, Ki-67, PCNA

1. Introduction

Cellular senescence, the irreversible cell-cycle arrest of somatic cells was first described by Hayflick and Moorhead (1). Evidence suggests that cellular senescence has important consequences in vivo. On one hand, it can act as a tumor-suppressor mechanism as several studies have demonstrated (2–4). In this context senescence can be seen as a potential beneficial process, which prevents the spread of damage to the next cell generation.

On the other hand, senescent cells have also been implicated in the impaired tissue regeneration which is observed in several organs during ageing. Data also indicates that senescent cells can affect the surrounding microenvironment and induce hyperproliferation of cancer cells, neoplastic progression, and tissue damage (5–8). Thus, qualitative and quantitative assessment of cellular senescence both in vitro and in vivo is of great importance when studying ageing and age-related diseases. Despite the increasing research in the

Lorenzo Galluzzi et al. (eds.), *Cell Senescence: Methods and Protocols*, Methods in Molecular Biology, vol. 965,
DOI 10.1007/978-1-62703-239-1_27,

field, the role of cellular senescence in vivo is still relatively unclear, mostly because of the absence of robust and specific cellular markers, which can be used to identify senescent cells in tissues.

When compared to their proliferating counterparts, senescent cells comprise changes in a wide variety of parameters when cultured in vitro including gene expression patterns (9), protein processing and metabolism (5, 10), cellular and nuclear size, shape and structure, resistance to apoptosis, mitochondrial function and production of reactive oxygen species (ROS) (11, 12), accumulation of age pigment (lipofuscin) (13), and increased activity of β galactosidase (14).

Despite the extensive list of observed changes in vitro, the absence of specific markers exclusive to senescent cells represents the main obstacle to detect them in living tissues.

One of the most widely used markers is a histochemical assay for β-galactosidase activity at pH6 (senescence-associated β galactosidase, SA-βgal) (14). However, this method is technically tricky at least in some tissues, requires the use of cryosections and has resulted, in some instances, in contradictory data (15, 16). The use of DNA damage foci as markers for telomere- or non-telomere DNA damage-induced cellular senescence in vivo has recently been proposed as marker for the detection of senescent cells (17, 18). The DNA damage response (DDR), triggered by uncapped telomeres or non-telomeric DNA damage, is one of the most prominent initiators of senescence (19). This response is characterized by activation of sensor kinases (ATM/ATR, DNA-PK), formation of DNA damage foci containing activated H2AX (γH2AX) and ultimately induction of cell-cycle arrest through activation of checkpoint proteins, notably p53 (TP53) and the cyclin-dependent kinase inhibitor 1 (CDKN1A) (20). The cyclin-dependent kinase inhibitor 1, also termed p21, is a crucial transcriptional target of p53 and mediator of p53-dependent senescence (21). However, p21 also mediates a transient DNA-damage induced growth arrest. It is thought that rapid DNA repair quickly terminates p53–p21 signalling, whereas slow, incomplete, or faulty repair results in sustained signalling and senescence. In any case, decreased levels of p53, p21, or DDR proteins such as ATM or CHK2 prevent telomere- or damage-induced senescence (22, 23). Consequently, the application of p21 or other DDR proteins as markers of cellular senescence might not be indicators of the permanent cell cycle arrest characteristic of senescence.

Recently, our group has proposed that a combination of Ki-67 or PCNA negativity (both proliferation markers) and γH2AX positivity (DNA damaged foci marker) can be used to assess the senescent state of cells both in vitro cultures of cells and in mice tissue sections. We first estimated fraction of senescent cells in human and mouse fibroblasts with high precision from observed growth curves using a dynamic simulation mathematical model. Then, we

tested several candidate senescent markers and compared them with the results from the model. Using this method we demonstrated that the combination of Ki67 negativity with high γH2AX foci density (>5 per nucleus) in fibroblasts provided the best fit to the mathematical model (24). Moreover, we reported that this marker combination, which can easily be performed in paraffin-embedded tissues, gives quantitative senescent cell frequency estimates in mouse intestinal sections similar to the ones found by SA-βgal histochemistry.

In this chapter, we describe these methods in detail and how they can be used to identify senescent cells both in vitro and in vivo.

2. Materials

2.1. Immunofluorescence Staining of Ki67 and γH2AX in Fixed Cells

2.1.1. Cell Culture

- Dulbecco's modified Eagle's medium (DMEM) with 10% fetal bovine serum, 1% penicillin–streptomycin, and 1% glutamate.
- 1× Phosphate buffered saline (PBS).
- 19 mm Ø Coverslips (VWR International, Radnor, PA, USA).
- 12 Well cell culture plates (Corning, Corning, NY, USA).

2.1.2. Immunofluorescence Staining of Ki67 and γH2AX in Fixed Cells

- 2% Paraformaldehyde (2% neutral buffered formaldehyde).
- PBG-Triton: 0.2% fish skin gelatin, 0.5% bovine serum albumin (BSA), and 0.5% Triton X-100 in PBS.
- Rabbit polyclonal antibody anti-Ki67 (Abcam, Cambridge, MA, USA).
- Mouse monoclonal anti-γH2AX (Upstate Biotechnology, Billerica, MA, USA).
- Anti-mouse Fluorescein-conjugated secondary antibody AlexaFluor 594 (Molecular Probes, Eugene, CA, USA).
- Anti-rabbit Fluorescein-conjugated secondary antibody AlexaFluor 488 (Molecular Probes).
- VECTASHIELD HardSet Mounting Medium (Vector labs, Burlingame, CA, USA).
- Glass slides.

2.2. Immunofluorescence Staining of PCNA and γH2AX in Paraffin Tissue Sections

2.2.1. Deparaffinization and Rehydration

- Histoclear (Fisher scientific, Waltham, MA, USA).
- Ethanol (100, 90 and 70%).
- Distilled water.

2.2.2. Antigen Retrieval

- Domestic (850 W) or scientific microwave.
- Microwaveable vessel to hold approximately 400–500 mL.
- 0.01 M citrate buffer pH 6.

2.2.3. Immunofluorescence Staining of PCNA and γH2AX in Paraffin Tissue Sections

- Hydrophobic pen.
- T-TBS: 10 mM Tris–HCl, 0.88% NaCl, 0.25% Triton X-100 in distilled water (pH = 7).
- M.O.M.™ Mouse kit (Vector Labs, Burlingame, CA, USA).
- Normal goat serum PK-6101 Rabbit IgG Vectastain ABC Kit (Vector Labs): this kit includes the normal goat serum and the biotinylated goat anti-rabbit IgG antibody.
- Rabbit monoclonal anti-γH2AX (Cell Signaling, Beverly, MA, USA).
- Mouse monoclonal anti-PCNA (Abcam, Cambridge, UK).
- Biotinylated goat anti-rabbit IgG antibody.
- Anti-mouse Fluorescein-conjugated secondary antibody AlexaFluor 594 (Invitrogen, Eugene, CA, USA).
- Fluorescein Avidin DCS (Vector Labs).
- DAPI staining solution (Partec, Münster, Germany).
- VECTASHIELD HardSet Mounting Medium (Vector Labs).

3. Methods

One trait of senescent cells is their inability to express genes required for cellular proliferation and/or DNA replication, even in a promitogenic environment. This feature distinguishes senescence from quiescence, another non-proliferative state that is readily rescued in response to mitogenic stimuli. It has been shown that the fraction of Ki67-positive nuclei declines continuously with population-doublings in human fibroblasts and mesothelial cells (25, 26). With increased population-doublings cells also accumulate DNA damage foci. Senescent fibroblasts display molecular markers characteristic of cells bearing persistent DNA double-strand breaks. DNA double strand breaks as well as telomere uncapping are able to trigger a DNA damage response by phosphorylation of Ser-139 of histone H2AX histone (γH2AX), facilitating the focal assembly of checkpoint and DNA repair proteins (27). The frequency of cells positive for γH2AX increases steeply as cultures approach replicative senescence, however, it is not by itself a good marker for cellular senescence as we have demonstrated in fibroblasts cultures. Moreover, it is well established that a DNA damage response initiates DNA repair, which may culminate in resumed cell proliferation and can also be induced due to replication stress, leading to transiently stalled replication forks (28).

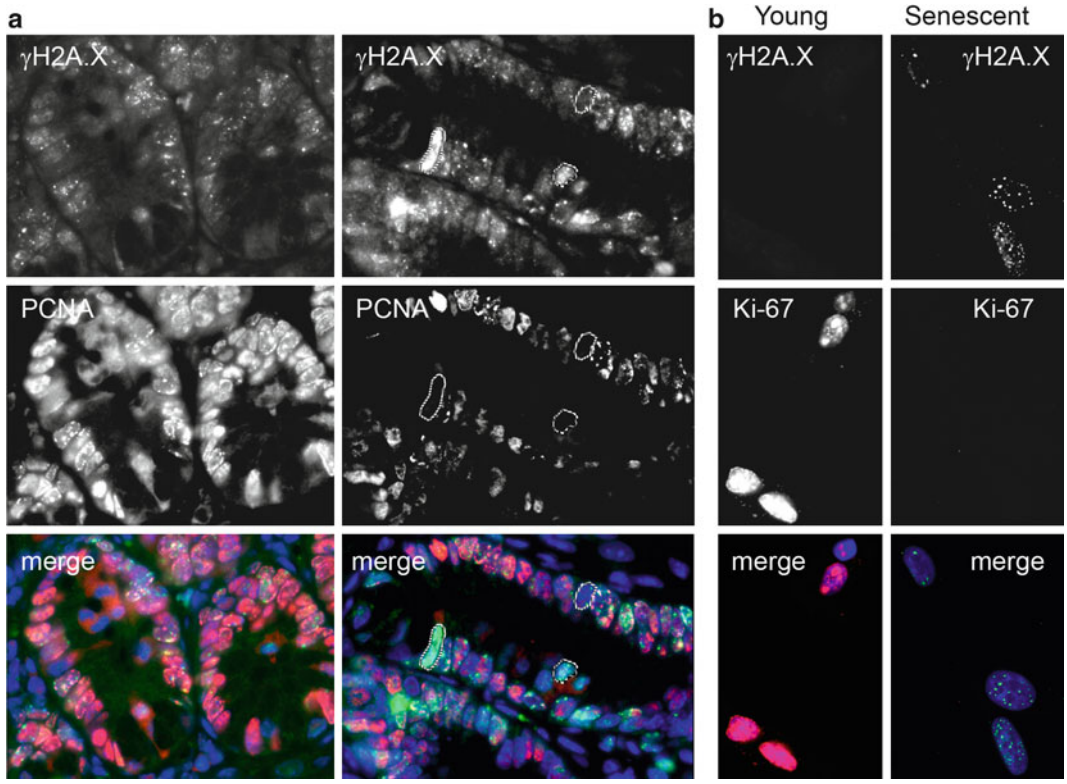

Fig. 1. Assessment of senescent cells in sections of mice intestine and in human fibroblasts. (**a**) Immunofluorescence staining of PCNA and γH2AX in paraffin embedded mice small intestine at 9 months of age. In some crypts all γH2AX foci are associated with proliferation marker PCNA (*left panels*), while in others one can find enterocytes which are negative for PCNA and positive for γH2AX. (**b**) Immunofluorescence Staining of Ki67 and γH2AX in MRC5 human fibroblasts. Young fibroblasts have low numbers of γH2AX foci and most cells are positive for proliferation marker Ki67 (*left panels*). Senescent fibroblasts have generally more than five γH2AX foci per nucleus and are negative for Ki67 (*right panels*).

Below we describe a protocol for immunofluorescence dual staining for PCNA/Ki67 and γH2AX in fixed cells grown in culture (see Subheading 3.1) and in paraffin embedded tissue sections (see Subheading 3.2) (Fig. 1).

3.1. Immunofluorescence Staining of PCNA/Ki67 and γH2AX in Fixed Cells (See Note 1)

3.1.1. Cell Culture

1. Seed 3×10^4 cells in 19 mm Ø coverslips in 12 well plates. Incubate cells at 37°C with 5% CO_2 for the period of time that the experiment requires (do not allow cells to be confluent by the time of the immunostaining) (see Note 1).
2. Rinse cells twice in 1× PBS (see Note 2).

3.1.2. Cell Fixation

1. Incubate cells in 1 mL of 2% paraformaldehyde in 1×PBS for 10 min at room temperature (see Note 3).
2. Remove paraformaldehyde and wash cells three times for 5 min with 1× PBS.

3.1.3. Immunofluorescence Staining

1. For permeabilization incubate cells for 45 min at room temperature with 1 mL PBG-Triton (see Note 4).
2. Remove the permeabilization solution and add 400 μL of the rabbit polyclonal antibody anti-Ki67 (first primary antibody) in a 1:250 dilution (diluted in PBG-Triton), to each coverslip.
3. Incubate cells for 1 h at room temperature with gentle agitation.
4. Wash cells three times for 5 min each with PBG-Triton.
5. Apply the anti-rabbit Fluorescein-conjugated secondary antibody AlexaFluor 488 in a 1:4,000 dilution (diluted in PBG-Triton).
6. Wash cells twice with PBG-Triton for 5 min each.
7. Add 400 μL of the Mouse monoclonal anti-γH2AX (second primary antibody) in a 1:2,000 dilution (diluted in PBG-Triton) (see Note 5).
8. Incubate 45 min to 1 h at room temperature.
9. Wash cells twice with PBG-Triton for 5 min.
10. Apply the anti-mouse Fluorescein-conjugated secondary antibody AlexaFluor 594 in a 1:4,000 dilution (diluted in PBG-Triton).
11. Incubate cells for 45 min to 1 h.
12. Wash cells three times for 5 min each with 1× PBS.
13. Add 400 μL of DAPI to each coverslip for nuclear counterstain.
14. Incubate cells for 10 min.
15. Wash cells three times for 5 min each with 1× PBS.
16. Add 20 μL of the Vectashield mounting media to a glass slide and mount the coverslip upside down. Allow mounting media to polymerize (see Note 6).
17. Image cells in a fluorescence microscope.

3.2. Immunofluorescence Staining of PCNA/Ki67 and γH2AX in Paraffin Tissue Sections (See Note 7)

Tissue sections are best mounted on 4% APES (amino-propyl-triethoxy-silane) coated slides in order to avoid tissues to detach from the slides.

3.2.1. Deparaffinization and Rehydration

1. Place paraffin tissue sections in two changes of histoclear for 5 min each.
2. Place tissue sections in two changes of 100% ethanol for 5 min each, followed by one change in 90 and 70% ethanol for 5 min each.

3. Place tissue sections in two changes of distilled water for 5 min. Keep slides in the water until the microwave antigen retrieval solution has been prepared. At no time from this point onwards should the slides be allowed to dry out! (see Note 7).

3.2.2. Antigen Retrieval

A major cause of variation in the reproducibility of immunohistochemical staining is induced by tissue fixation and, to a lesser degree, tissue processing. Most laboratories use 4% neutral-buffered formaldehyde (10% formalin) for tissue fixation, which introduces cross-links with proteins. The aldehyde group from formaldehyde can react with nitrogen atoms of proteins forming a cross-link –CH2– called a methylene bridge. Studies indicate that the most frequent type of cross-link formed by formaldehyde is between the nitrogen atom at the end of the side-chain of lysine and the nitrogen atom of a peptide linkage (29). In order to improve exposure of epitopes for immune detection, an antigen retrieval protocol should precede the immunostaining.

1. Remove the tissue sections from water and place them in the microwaveable vessel with the Citrate Buffer (see Note 8).
2. Place the vessel in the microwave. Set to full power (800–850 frequency) and wait until the solution comes to the boil. After the start of boiling reduce from high to medium power (400–450 frequency) for 10 min from this point (see Note 9).
3. When 10 min has elapsed, remove the vessel and allow tissue sections to cool down for 20–30 min (see Notes 10 and 11).
4. Rinse tissue sections in three changes of distilled water for 5 min each.
5. Continue with immunohistochemical staining protocol.

3.2.3. Immunofluorescence Staining

1. Delimit tissue sections with a hydrophobic pen to avoid loss of solution and minimize volume usage during incubation periods (see Note 12).
2. Block no-specific binding with blocking solution containing normal goat serum (1:60) and BSA (0.1%) in PBS for 30 min at RT (see Note 13).
3. Prepare working solution for primary antibody incubation. Dilute γH2AX antibody 1:250 in blocking solution (PBS/BSA/NGS), apply to the sections and incubate overnight at 4°C in a humidified chamber (see Note 14).
4. Wash tissue sections in PBS three times for 5 min.
5. Prepare working solution for secondary antibody incubation by adding biotinylated anti-rabbit Ig 1:200 in blocking solution (PBS/BSA/NGS). Apply to the sections and incubate for 30 min at RT in a humidified chamber.

6. Wash tissue sections in PBS three times for 5 min.
7. Dilute Fluorescein Avidin DCS 1:500 in PBS and apply to the sections for 20 min (protect from light) (see Note 15).
8. Wash tissue sections in 1×PBS for 5 min.
9. Wash tissue sections in T-TBS twice for 5 min.
10. Block nonspecific binding with M.O.M.™ Mouse Ig Blocking Reagent, for 1 h at room temperature (M.O.M.™ Mouse Ig Blocking Reagent: 90 μL to 2.5 mL T-TBS).
11. Wash tissue sections in T-TBS twice for 5 min each.
12. Incubate tissue sections for 5 min in working solution of M.O.M.™ Diluent (M.O.M.™ Diluent: add 600 μL of Protein Concentration to 7.5 mL T-TBS).
13. Tip excess of M.O.M.™ Diluent off sections. Dilute PCNA primary antibody 1:1,000 in M.O.M.™ Diluent. Incubate sections in diluted second primary antibody over night at 4°C in a humidified chamber. Place the remaining M.O.M.™ Diluent solution at 4°C for further usage.
14. Wash tissue sections in T-TBS twice for 5 min each.
15. Prepare working solution with M.O.M.™ Diluent and fluorescent labeled (Alexa 594) anti-mouse secondary antibody (1:2,000), apply to the section and incubate in the dark at RT in a humidified chamber for 30 min (see Note 15).
16. Wash tissue sections in T-TBS twice for 5 min each.
17. Wash tissue sections in PBS for 5 min.
18. Apply ready to use DAPI staining solution on the slides and incubate for 10 min.
19. Wash tissue sections in PBS three times for 5 min.
20. Mount slides with Vectashield mounting media. Allow mounting media to harden (see Note 6).

4. Notes

1. Cells should be reproducibly subconfluent at the time of usage. Therefore, size of coverslips and cell culture plates can be adjusted to each experiment since cells should be subconfluent by the time of fixation.
2. Do not allow cells to dry at any time. Perform washing and incubation steps with gentle agitation. From step 5 onwards perform all steps keeping cells in the dark since fluorescence antibodies are light sensitive.
3. Following fixation, cells can be store at −80°C for posterior staining. In this case, remove paraformaldehyde and wash cells

once with 1× PBS. Remove 1× PBS leaving only 200 μL in order for the cells not to dry. Store cells immediately at –80°C.

4. Permeabilization conditions (type of detergent, length of incubation time) must be adjusted according to the cell type used; however, this protocol has been used in cancer cell lines, stem cells and fibroblasts successfully.
5. Antibody dilutions are given as a starting example only; concentrations must be titrated out for every combination of cell strain and antibody. Nevertheless, the indicated concentrations have been shown to work for several types of cancer cells, stem cells, and fibroblasts.
6. When using non-hardening mounting media slides can be imaged immediately after mounting. DAPI incorporated mounting media is also available, in this case skip DAPI nuclear counterstain and mount coverslips into the glass slide (DAPI incorporated mounting media can give a blue background). Before imaging cells by fluorescence microscopy, clean carefully the coverslips with a paper tissue embedded in 70% ethanol to remove any PBS crystals which can be formed after coverslips dry out. This gives rise to considerable better image quality.
7. Once the slides have been deparaffined and rehydrated, drying out will cause nonspecific antibody binding and consequently high background staining.
8. Do not allow tissue sections to dry at any time. From step 2 onwards perform washing with gentle agitation. From step 3 onwards perform all steps keeping slides in a humidified chamber and after step 6 all procedures should be performed in the dark since fluorescence antibodies are light sensitive.
9. Use a sufficient volume of antigen retrieval solution in order to cover the slides. This should be by at least a few centimeters above the slides if using a non-sealed vessel to avoid tissues to dry due to evaporation during boiling.
10. Ten minutes is only a suggested antigen retrieval time. Less than 10 min may leave the antigens under-retrieved, leading to weak staining. More than 10 min may leave them over-retrieved, leading to nonspecific background staining and also increasing the chances of sections dissociating from the slides. A control experiment is recommended beforehand, where slides of the same tissue section are retrieved for 5, 10, 15, 20, 25 and 30 min before being immunohistochemically stained to evaluate optimum antigen retrieval time for the particular antibody being used.
11. Cooling down of slides is essential to allow easy handling and for the antigenic site to reform after being exposed to such high temperature.

12. T-TBS solution easily diffuses through the slide surface. If tissue sections are not delimited using a hydrophobic pen, tissues can easily dry out during incubation periods. Do not allow tissues sections to dry out at any time.
13. Some tissues might need further blocking with avidin/biotin due to high endogenous avidin and biotin which can lead to background staining (especially recommended for liver sections; avidin/biotin blocking kit, Vector labs).
14. If PCNA staining is performed on day 1 and γ-H2AX staining is performed on day 2 we recommend using a directly labeled secondary anti-rabbit antibody (e.g., Alexa 488) as Avidin DCS could lead to some unspecific binding.
15. Longer incubation periods may result in increased background staining.

Acknowledgments

We would like to thank Rhys Anderson for providing immunofluorescence images of human fibroblasts. CCM is funded by a studentship from FCT via the GABBA program, University of Porto, and JP is funded by a BBSRC David Phillips Fellowship.

References

1. Hayflick L, Moorhead PS (1961) The serial cultivation of human diploid cell strains. Exp Cell Res 25:585–621
2. Sager R (1991) Senescence as a mode of tumor suppression. Environ Health Perspect 93:59–62
3. Campisi J (2001) Cellular senescence as a tumor-suppressor mechanism. Trends Cell Biol 11:S27–S31
4. Braig M, Schmitt CA (2006) Oncogene-induced senescence: putting the brakes on tumor development. Cancer Res 66:2881–2884
5. Campisi J (2000) Cancer, aging and cellular senescence. In Vivo 14:183–188
6. Krtolica A, Parrinello S, Lockett S, Desprez P-Y, Campisi J (2001) Senescent fibroblasts promote epithelial cell growth and tumorigenesis: a link between cancer and aging. Proc Natl Acad Sci USA 98:12072–12077
7. Liu D, Hornsby PJ (2007) Senescent human fibroblasts increase the early growth of xenograft tumors via matrix metalloproteinase secretion. Cancer Res 67:3117–3126
8. Krtolica A, Campisi J (2002) Cancer and aging: a model for the cancer promoting effects of the aging stroma. Int J Biochem Cell Biol 34: 1401–1414
9. Shelton DN, Chang E, Whittier PS, Choi D, Funk WD (1999) Microarray analysis of replicative senescence. Curr Biol 9:939–945
10. Sitte N, Merker K, von Zglinicki T, Grune T (2000) Protein oxidation and degradation during proliferative senescence of human MRC-5 fibroblasts. Free Radic Biol Med 28:701–708
11. Passos JF, Nelson G, Wang C, Richter T, Simillion C, Proctor CJ, Miwa S, Olijslagers S, Hallinan J, Wipat A, Saretzki G, Rudolph KL, Kirkwood TBL, von Zglinicki T (2010) Feedback between p21 and reactive oxygen production is necessary for cell senescence. Mol Syst Biol 6:347
12. Passos JF, Saretzki G, Ahmed S, Nelson G, Richter T, Peters H, Wappler I, Birkett M, Harold G, Schaeuble K, Birch-Machin M, Kirkwood T, von Zglinicki T (2007) Mitochondrial dysfunction accounts for the stochastic heterogeneity in telomere-dependent senescence. PLoS Biol 5:e110
13. Sitte N, Merker K, Grune T, von Zglinicki T (2001) Lipofuscin accumulation in proliferating

fibroblasts in vitro: an indicator of oxidative stress. Exp Gerontol 36:475–486

14. Dimri GP, Lee X, Basile G, Acosta M, Scott G, Roskelley C, Medrano EE, Linskens M, Rubelj I, Pereira-Smith O et al (1995) A biomarker that identifies senescent human cells in culture and in aging skin in vivo. Proc Natl Acad Sci USA 92:9363–9367
15. Kurz DJ, Decary S, Hong Y, Erusalimsky JD (2000) Senescence-associated (beta)-galactosidase reflects an increase in lysosomal mass during replicative ageing of human endothelial cells. J Cell Sci 113(Pt 20):3613–3622
16. Severino J, Allen RG, Balin S, Balin A, Cristofalo VJ (2000) Is beta-galactosidase staining a marker of senescence in vitro and in vivo? Exp Cell Res 257:162–171
17. von Zglinicki T, Saretzki G, Ladhoff J, d'Adda di Fagagna F, Jackson SP (2005) Human cell senescence as a DNA damage response. Mech Ageing Dev 126:111–117
18. Wang C, Jurk D, Nelson G, Martin-Ruiz C, von Zglinicki T (2009) DNA damage response and cellular senescence in aging mice. Aging Cell 8:311–323
19. d'Adda di Fagagna F (2008) Living on a break: cellular senescence as a DNA-damage response. Nat Rev Cancer 8:512–522
20. Sherr CJ, McCormick F (2002) The RB and p53 pathways in cancer. Cancer Cell 2: 103–112
21. Brown JP, Wei W, Sedivy JM (1997) Bypass of senescence after disruption of p21CIP1/WAF1 gene in normal diploid human fibroblasts. Science 277:831–834
22. Gorgoulis VG, Vassiliou LV, Karakaidos P, Zacharatos P, Kotsinas A, Liloglou T, Venere M, Ditullio RA Jr, Kastrinakis NG, Levy B, Kletsas D, Yoneta A, Herlyn M, Kittas C, Halazonetis TD (2005) Activation of the DNA damage checkpoint and genomic instability in human precancerous lesions. Nature 434: 907–913
23. Bartkova J, Horejsi Z, Koed K, Kramer A, Tort F, Zieger K, Guldberg P, Sehested M, Nesland JM, Lukas C, Orntoft T, Lukas J, Bartek J (2005) DNA damage response as a candidate anti-cancer barrier in early human tumorigenesis. Nature 434:864–870
24. Lawless C, Wang C, Jurk D, Merz A, Zglinicki T, Passos JF (2010) Quantitative assessment of markers for cell senescence. Exp Gerontol 45: 772–778
25. Kill IR, Faragher RG, Lawrence K, Shall S (1994) The expression of proliferation-dependent antigens during the lifespan of normal and progeroid human fibroblasts in culture. J Cell Sci 107:571–579
26. Faragher RG, Kill IR, Hunter JA, Pope FM, Tannock C, Shall S (1993) The gene responsible for Werner syndrome may be a cell division "counting" gene. Proc Natl Acad Sci USA 90:12030–12034
27. d'Adda di Fagagna F, Reaper PM, Clay-Farrace L, Fiegler H, Carr P, von Zglinicki T, Saretzki G, Carter NP, Jackson SP (2003) A DNA damage checkpoint response in telomere-initiated senescence. Nature 426:194–198
28. Ward IM, Chen J (2001) Histone H2AX is phosphorylated in an ATR-dependent manner in response to replicational stress. J Biol Chem 276:47759–47762
29. Werner M, Chott A, Fabiano A, Battifora H (2000) Effect of formalin tissue fixation and processing on immunohistochemistry. Am J Surg Pathol 24:1016–1019

Chapter 28

Assessing Chronological Aging in Bacteria

Stavros Gonidakis and Valter D. Longo

Abstract

Bacteria, which are often considered as avid reproductive organisms under constant selective pressure to utilize available nutrients to proliferate, might seem an inappropriate model to study aging. However, environmental conditions are rarely supporting the exponential growth that is most often studied in laboratories. In the wild, *Escherichia coli* inhabits environments of relative nutritional paucity. Not surprisingly, under such circumstances, members of an *E. coli* population age and progressively lose the ability to reproduce, even when environmental conditions provide such an opportunity. Here, we review the methods to study chronological aging in bacteria and some of the mechanisms that may contribute to their age-dependent loss of viability.

Key words: Aging, *Escherichia coli*, Oxidative DNA damage, Protein carbonylation, Rifampicin, Stress resistance, Time-lapse microscopy

1. Introduction

Inoculation and maintenance of a bacterial population in the same environment without the addition or removal of cells or nutrients is termed batch culture. It differs from continuous culture systems whereby either a fraction of cells is serially transferred to fresh medium at a certain point before stationary phase (serial passage) or cells are constantly removed and fresh nutrients added to the same incubation vessel (chemostat) (1). When inoculated into fresh LB (see "Subheading 1" below for details) and maintained at 37°C in batch culture, an *Escherichia coli* population goes through five distinct phases that can be described in terms of changes in the number of cells over time and are shown in Fig. 1 (1). The exact timing of those phases is dependent on both the strain and the technique used during the experiment. The time periods that will be herein mentioned are based on experiments with strain BW25113 (2).

Lorenzo Galluzzi et al. (eds.), *Cell Senescence: Methods and Protocols*, Methods in Molecular Biology, vol. 965,
DOI 10.1007/978-1-62703-239-1_28,

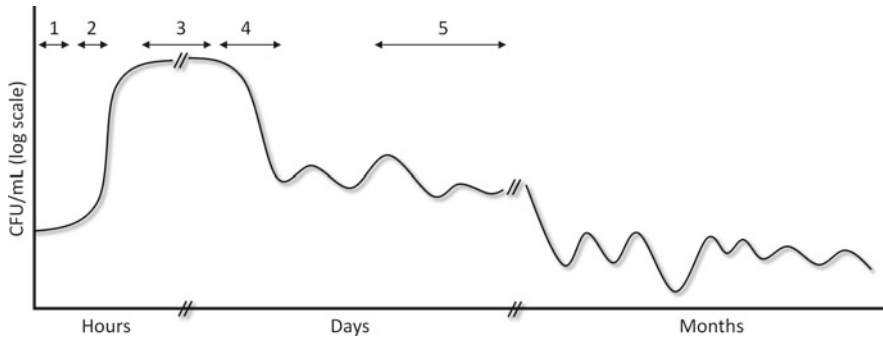

Fig. 1. A schematic of *Escherichia coli* life cycle in LB batch culture; adapted from ref. 1.

The period when no increase in biomass using optical density measurements can be detected is called lag phase (phase 1 in Fig. 1). It is worth noting that cells removed from cultures that have spent more time in stationary phase (see below) display longer lag phases compared to cells removed from "younger" cultures (3). Following lag phase, the culture exhibits an exponential increase in the number of cells, during the so-called log phase (phase 2 in Fig. 1), which is arguably the most intensively studied physiological state. As time progresses during log phase, the following four changes occur, among others: excreted metabolic by-products accumulate in the medium, pH increases from 7.5 to approximately 8.5, cell density also increases and growth rate declines, marking the onset of stationary phase (phase 3 in Fig. 1). Inoculation of *E. coli* cells into conditioned medium obtained from early stationary phase cultures (after 12 h of incubation) results in cell proliferation detected as an increase in optical density at 600 nm (OD600, our unpublished observation). This observation rules out the possibility that cessation of proliferation is the result of nutrient exhaustion, increase in pH or the accumulation of growth-inhibiting metabolic by-products in the medium and points to cell density increase as the most important physiological trigger for stationary phase entry.

The maximum cell density reached is approximately 2×10^9 cells/mL. After approximately 18 h in stationary phase, during which no change in the number of cells is observed, the population exhibits a marked decline in the number of living organisms, referred to as the death phase of the *E. coli* life cycle in LB (phase 4 in Fig. 1). By the end of the death phase, 90–99% of the original population loses the ability to form colonies when plated on nutrient agar medium. The progressive loss of viability during the death phase of the *E. coli* life cycle, reminiscent of the age-dependent loss of function and increase in death rate that is defined as aging in higher organisms, makes *E. coli* an important model organism to understand aging in prokaryotes but also a system to identify and understand the fundamental factors that modulate aging in all organisms.

During phase 5 (Fig. 1), the number of cells per milliliter remains relatively constant for periods of up to 5 years without the addition of nutrients (1). Despite this stability at the macroscopic level, the surviving population undergoes many cycles of death and proliferation of mutants adapted to the changing conditions created during the experiment. This phenomenon has been termed GASPing, which stands for growth advantage in stationary phase (4). Although quite interesting in terms of mechanisms of evolutionary adaptation, it is outside the scope of an investigation into the mechanisms of senescence. It is therefore apparent that continuous culture systems are unsuitable for the study of chronological aging in bacteria, since the culture is maintained in a proliferating state throughout the duration of these experiments.

1.1. Studying Stationary Phase Survival in E. coli

Two different types of nutrient media can be used to study stationary phase survival in *E. coli*, namely complex media and defined-minimal media. The former contain a mixture of amino acids, peptides and carbohydrates (see Notes 1 and 2), while the latter contain specific inorganic compounds that provide the bacteria with all the elements they require, as well as a defined carbon and energy source (usually glucose). The most commonly used complex and defined media are LB and M9 minimal medium, respectively.

The nutrients available in unbuffered LB versus minimal media and the pH eventually reached are quite different (also depending on the carbon source used in minimal media) and, as a result, physiological changes and other phenomena observed during the stationary phase of the bacterial life cycle will not always coincide among different media (Fig. 2). Perhaps the most important functional distinction between stationary phase in LB compared to stationary phase in minimal medium is that in the latter, stationary phase is reached due to the exhaustion of a specific nutrient required

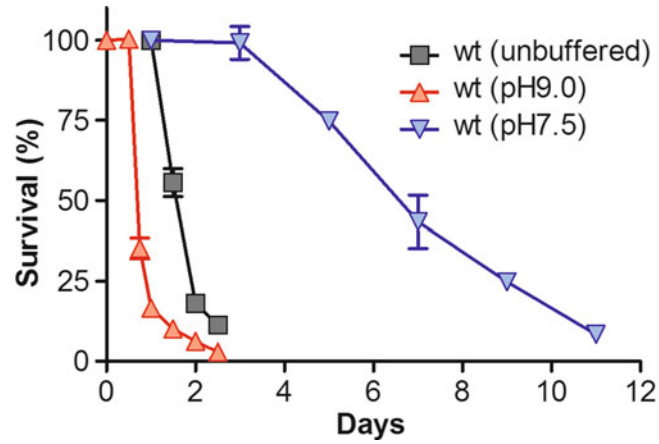

Fig. 2. Chronological aging of bacteria in unbuffered, alkaline, or neutral pH LB medium; redrawn based on data published in ref. 16.

for the production of biomass. The limiting nutrient is chosen by the investigator and is commonly the phosphate, nitrogen or carbon source. Under such conditions, the survival and underlying physiology of *E. coli* cells starved for a specific nutrient is examined. By contrast, cessation of proliferation of a population maintained in LB is not triggered by nutrient exhaustion (see above). A lot of work has been done on the stationary phase physiology of *E. coli* under conditions of starvation for a specific nutrient; the information extracted from these studies should not be extrapolated to stationary phase in LB without sufficient experimental verification.

Despite the differences in the proximal causes of stationary phase entry, the life cycle of stationary phase *E. coli* in different fresh media is quite similar, characterized by a log phase followed by death (5) and the expression of the GASP (6). The physiological differences between cells proliferating in LB and M9 minimal medium containing 0.4% glucose as the carbon source have been described using a microarray analysis of gene expression. Higher expression of amino acid and pyrimidine biosynthetic genes, as well as glucose metabolism genes was observed in minimal medium compared to LB (7). On the other hand, LB-grown cultures had increased expression compared to minimal medium of gluconeogenic genes and genes that mediate the breakdown of small molecules.

Reports of the abundance of *E. coli* in its aquatic habitats vary from 0.01 to 10/mL in pristine well water and mountain streams (8) to 100–1,000/mL in the watersheds of grazed pastures (9). These studies used the colony-forming ability as a measure of the abundance of bacteria. However, a considerable proportion of bacteria in aquatic environments is metabolically active as judged, for example, by electron transfer activity, but cannot form colonies when transferred on rich nutrient medium (10). This physiological state has been termed viable, but not culturable (VBNC) and its contribution to the ecology of enteric bacteria has been intensively studied. The last cited reference enumerates as many as 47 different techniques that have been used to accurately assign bacteria to the correct place of the physiological spectrum that ranges from active proliferation to death. It therefore becomes apparent that any account of the viability of *E. coli* in its secondary environment is heavily dependent on the methodology used to quantify viability. Detailed examination of the relative merits of these techniques is outside the scope of this text.

Some studies report that, in river water, the loss of culturability is paralleled by a decrease in direct counts (number of cells visible under the microscope) obtained by acridine orange and viable counts estimated using yeast extract and nalidixic acid and therefore conclude that *E. coli* should not enter the VBNC state in such a habitat (11). Others report a progressive loss of colony-forming units (CFU's) in seawater, while metabolic activity assayed by the ability of a functioning electron transport chain to reduce

2-(*p*-iodophenyl)-3-*p*-nitrophenyl-5-phenyltetrazolium chloride remains constant, thus suggesting that the VBNC state is indeed a part of the physiology of *E. coli* in aquatic environments (12). Total cell counts obtained by microscopy appear to remain constant even after extended incubation (56 days in ref. 11) reflecting a preservation of the integrity of the membrane of otherwise dead bacteria. It is worth mentioning that the seemingly straightforward observation of colonies after incubation on solid nutrient media used to measure colony-forming ability is complicated by the fact that *E. coli* loses the ability to form colonies on Endo agar, a medium commonly used to detect enteric microorganisms, while retaining the ability to form colonies on trypticase soy agar (13). Attempting a generalization based on several published studies, Rozen and Belkin suggest that the ability to form colonies on nutrient plates is the first loss of *E. coli* when faced with conditions approximating seawater in vitro, while other metabolic capabilities are either retained or lost at differing rates (14). Thus, a significant part of the life of *E. coli* in soil and aquatic habitats may be spent in the VBNC state.

On the other hand, during stationary phase incubation in LB, colony-forming ability and viability do seem to coincide, according to the study of Ericsson *et al.* (15). In this study, stationary phase *E. coli* maintained in nutrient broth were trapped, stained with the fluorescent dyes SYTO 9 and propidium iodide, and observed using fluorescence microscopy after the addition of fresh nutrient medium (15). Bacteria fluorescing green (SYTO 9) have intact membranes, whereas red bacteria have damaged membranes that allow propidium iodide to enter. Upon fresh nutrient addition, none of the cells stained red divided and 93.3% of cells stained green did. These results argue against the existence of viable but not culturable cells during stationary phase in complex medium, such that viability, survival and culturability can be considered generally equivalent under the experimental conditions described above. Therefore, according to the life cycle (Fig. 1), a long-lived *E. coli* population is one that survives longer in stationary phase (phase 3 in Fig. 1) compared to the control population.

Based on this technique, a genome-wide screen for long-lived single-gene knock-out mutants in *E. coli* was performed and several strains that exhibit extended stationary phase survival compared to wt, independently if the cultures' pH (Fig. 2) were found. The extended survival of these mutants was dependent on the hypoxia-inducible transcription factor ArcA and on the production of acetate, one of the metabolic by-products of fermentation (16). The metabolic switch from TCA cycle/respiration to glycolysis and glycerol production was recently reported as a central component of the lifespan extension observed in the *Saccharomyces cerevisiae tor1*Δ and *sch9*Δ mutants (17). Such mechanisms of lifespan extension are expected to be dependent on a broad metabolic repertoire

that confers the ability to grow and survive both in the presence and absence of oxygen. A metabolic model for lifespan extension in the nematode worm *Caenorhabditis elegans*, which cannot survive in the absence of oxygen, also invoked the reduced use of aerobic respiration in favor of fermentative malate dismutation, producing acetate and succinate, as a common metabolic adaptation of most long-lived mutants described for this species (18). Recently, several studies implicated HIF-1, a functional homolog of ArcA found in metazoans, in lifespan regulation in *C. elegans* (19–21). Thus, the metabolic alterations leading to extended stationary phase survival in the bacterium *E. coli* might reveal the conservation of fundamental lifespan-regulating mechanisms.

1.2. Protein Carbonylation

Protein carbonyls are carbon–oxygen double bonds formed at the side chains of the amino acids arginine, lysine, proline, and threonine (22). Unlike other oxidative modifications like disulfide bond formation, these modifications are irreversible, rendering the degradation of the affected proteins the only means of limiting the dysfunction caused by their presence. A time-dependent accumulation of protein carbonyls is observed during stationary phase in *E. coli* (24), with some proteins showing increased susceptibility (TCA cycle enzymes, among others) (23). Populations lacking both cytosolic superoxide dismutases display a higher amount of protein carbonylation and also a more rapid loss of viability during stationary phase. On the other hand, incubation of a stationary phase population in the absence of oxygen causes a significant lifespan extension (24). The use of radioselectan equilibrium density-gradient centrifugation allows the separation of a stationary phase population of *E. coli* to a high-density and a low-density fraction. Desnues *et al.* showed that the high density fraction displays increased expression of catalase, enhanced protein carbonylation and preferential loss of viability compared to the low-density fraction (25). These observations provided credence to the notion that oxidative deterioration of proteins is causally linked to stationary phase death in *E. coli*.

In another study, an age-dependent accumulation of protein carbonyls was observed in the wild type (wt) strain incubated in LB buffered at pH 7.5, but protein carbonyls were reduced in the long-lived *lipA* strain (26), consistent with the hypothesis that age-dependent death in *E. coli* is associated with the accumulation of protein carbonyls. However, the *lipA acs* mutant survived longer than the wt strain, despite having a similar protein carbonylation load to wt. It is possible that a compensatory, longevity-assuring mechanism is activated in the *lipA* strain to counteract the increased protein carbonylation caused by the lack of Acs. However, the most parsimonious interpretation for these data is the lack of a causal association between stationary phase survival and protein carbonylation in *E. coli*.

In an early attempt to tackle the mechanistic basis of aging, Harman proposed in 1956 that free radicals (such as the ones that give rise to protein carbonylation) generated as a consequence of oxidative metabolism cause aging (27). Studies providing evidence for this theory in many different model systems have been performed since it was first put forward. An account of this vast volume of work is outside the scope of this text; the interested reader is directed to a recent review (28). However, more recently a number of studies have challenged the generality of the free radical theory of aging. The nematode worm *C. elegans* has five sod genes. A recent report found that lack of any one of those genes, as well as combined deficiency of two to three genes has no effect on the organism's lifespan (29). Instead, lack of the mitochondrial SOD further extends the lifespan of the long-lived clk-1 mutant. Overexpression of the mitochondrial SOD in mice does not protect against age-related neurological defects and produces a 4.3% mean lifespan extension (30), which is much smaller in magnitude compared to the effects observed with mice deficient in the growth hormone axis (31).

Using an evolutionary biology approach, Jobson *et al.* compared the nonsynonymous and synonymous evolution of approximately 5.7 million sites in 25 species and correlated these changes to the species' lifespan. Despite the limited capacity of such an associational approach to reach valid conclusions about a phenotype as complex as aging, the authors found that genes involved in oxidative stress defense, including the superoxide dismutases, have not been involved in the selection process that led to increased lifespans in mammals (32). The authors found such evidence for genes involved in lipid composition. However, it is likely that: (a) even though free radicals may be one of the major mediators of age-dependent cellular damage the overexpression of specific antioxidant enzymes is not a sufficiently sophisticated intervention to insure that toxic levels of free radicals are reduced while the normal levels of free radicals, which participate in cellular function, are not affected, (b) Similarly, genes involved in oxidative damage may not have been involved in the selection process leading to lifespan extension because altered function of each gene alone would be expected to have both beneficial and detrimental effects.

Thus, although there is strong evidence for the involvement of superoxide in certain diseases, such as amyotrophic lateral sclerosis, its role in lifespan regulation is mixed across different model systems and experimental circumstances. As mentioned above, there is also mixed evidence about the involvement of oxidative damage in bacterial senescence. The available data suggests that although protection against oxidative stress may lead to a modest lifespan extension, it may be only a small part of the longevity promotion effect induced by interfering with the central regulators of aging, such as the evolutionarily conserved, nutrient-responsive growth hormone/insulin growth factor I signaling pathway (31).

1.3. Oxidative DNA Damage

Rifampicin is a broad-spectrum bacteriostatic drug that acts by inhibiting subunit β of the RNA polymerase, encoded by *rpoB* in *E. coli* (33). Point mutations in this gene prevent binding of the drug to its target, allowing growth of the mutant strain in the presence of the antibiotic. The occurrence of rifampicin-resistant mutants (which represent mostly base substitutions) has therefore been used as an indirect measure of DNA damage in *E. coli* (34). To our knowledge, the role of DNA damage in the stationary phase survival/aging of *E. coli* has not been studied. Although the extended lifespan phenotype we unveiled (16) could provide fertile ground for the exploration of this subject, no time-dependent increase in DNA damage was observed by enumeration of rifampicin-resistant mutants in the wt strain (2). The reason for this could either be technical or biological. On the technical side, the assay used might not be sensitive enough to detect age-dependent DNA damage occurring during a survival experiment, since the *rpoB* locus might not be a representative target of the genome-wide DNA damage occurring under these conditions. The biological explanation is that stationary phase death in *E. coli* happens independently of damage to DNA; a technique that measures DNA damage across larger regions of the genome should be used to further explore this issue. It is worth noting however, that we observed a time-dependent increase in oxidative DNA damage in the mutant lacking both cytosolic superoxide dismutases (*sodA sodB*) (2), consistent with previous reports about both static (35) and proliferating (36) populations of this mutant.

1.4. Stress Resistance

One of the hallmarks of stationary phase in *E. coli* is the development of resistance to heat and oxidative stress. Cells starved for carbon or nitrogen were markedly more resistant than proliferating cells to incubation at 57°C or exposure to 15 mM hydrogen peroxide (37). Furthermore, starved cultures exhibited greater resistance than growing cultures preadapted to heat or hydrogen peroxide before treatment with the respective stressors. The RNA polymerase of *E. coli* is made up of a core component and one of several sigma subunits; the identity of the sigma subunit is modulated by environmental conditions and confers sequence selectivity to the polymerase. In broad terms, the sigma 70 subunit (encoded by *rpoD*) is used predominantly during log phase and the sigma S subunit (encoded by *rpoS*) during stationary phase (38). The latter protein mediates stationary phase resistance to heat (39) and oxidative stress (40), and also contributes to glycogen synthesis (41). *E. coli* strains with extended stationary phase survival also exhibit enhanced resistance to heat stress and to paraquat treatment (16). Paraquat is a herbicide that catalyzes the formation of intracellular superoxide, by successive rounds of reduction by intracellular reducing agents and oxidation by oxygen to form superoxide (42). Stress resistance is coupled to longevity in several model organisms (43),

perhaps reflecting an evolutionarily conserved physiological state that channels resources away from reproduction and towards maintenance and protection functions (44).

1.5. Chronological Versus Replicative Aging

The study of stationary phase *E. coli* populations as a model system for aging should be contrasted with another observation about the organism's physiology that has recently been associated with aging. This observation is that cell division in *E. coli*, although morphologically symmetrical, produces two functionally different progeny. Daughter cells that inherit one of the two poles of the mother cell ("old pole") show progressively slower growth rates compared to daughter cells inheriting the "new pole" (45). The mechanistic basis for aging in this organism is thought to be the asymmetrical segregation of some aging-inducing factor in cells inheriting the old pole following binary fission. Therefore, some sort of time-dependent functional asymmetry between "parent" and "offspring" is tightly linked to the aging process even in organisms without a clear germline/soma separation. This finding has implications on the evolutionary biology of aging, since it is inconsistent with the disposable soma theory of aging, which states that organisms age because of limited resources allocated to the maintenance of somatic cells due to the need to maintain the germ cells that are responsible for the propagation of the species. Hence, the *E. coli* findings obtained using time-lapse microscopy raise the possibility that aging can occur in an organism without a clear germline/soma separation.

In a different study, cells receiving the old pole were shown to preferentially accumulate protein aggregates (46), providing a possible mechanistic link to the aging-inducing factor accumulating in old pole cells mentioned above. These observations are reminiscent of the replicative lifespan of *S. cerevisiae* that has been extensively used to model the aging process of mitotic tissues in higher organisms (47), whereas the chronological lifespan of yeast is regarded as a more suitable model for the aging of post-mitotic tissues and organisms (48). It would be of interest to test the correlation between inheritance of old poles and stationary phase survival; such an experiment would be quite demanding technically though, as the observation of functionally asymmetrical division was performed using time-lapse microscopy (45) and the establishment of a stationary phase population under such conditions is not straightforward. Conversely, it would also be interesting to identify any effects of mutations affecting stationary phase survival on the replicative aging of *E. coli*.

1.6. Conclusion

In summary, as for eukaryotes, *E. coli* age chronologically and this process can be postponed by dietary restriction or by mutations in a number of genes involved in metabolism. Although both DNA and protein damage can accumulate during aging in *E. coli*, it is not known whether this damage is a cause or consequence of

aging and viability loss. The conservation of key age-dependent macromolecular damage phenotypes together with the role of genes that control the hypoxia response in regulating lifespan in both bacteria and higher eukaryotes, indicate that some of the most fundamental mechanisms of aging are conserved from bacteria to mammals. The simplicity of *E. coli* makes it a valuable model to test the evolutionary theories of aging.

2. Materials

2.1. Common Materials

2.1.1. Consumables

- pH test strips.
- 125-mm Petri dishes.
- 16-mm glass test tubes.
- 125-mL Erlenmeyer flasks.

2.1.2. Equipment

- Incubator with controlled humidity.
- Orbitally rotating platform.
- pH meter.

2.1.3. Reagents

- LB medium: 1% bacto tryptone (see Note 1), 0.5% yeast extract (see Note 2), 0.5% (w/v) NaCl. For solid medium, add 1.5% agar. Sterilized by autoclaving.
- HEPES (*N*-(2-hydroxyethyl)-piperazine-*N*′-ethanesulfonic acid) buffer: 1 M stock, sterilized by autoclaving and kept at room temperature.
- AMPSO (*N*-(1,1-dimethyl-2-hydroxyethyl)-3-amino-2-hydroxypropanesulfonic acid) buffer: 1 M stock, sterilized by autoclaving and kept at room temperature.
- NaCl, 0.5% (w/v), sterilized by autoclaving.

2.2. Quantification of Protein Carbonyls

- Y-PER protein extraction reagent (Thermo Fisher Scientific Inc—Pierce, Rockford, IL USA).
- BCA protein assay kit (Thermo Fisher Scientific Inc—Pierce).
- Oxyblot protein oxidation detection kit (Millipore—Chemicon, Billerica, MA, USA).
- Slot blot apparatus.
- PVDF membrane.
- Blocking buffer: PBS (pH 7.4), 0.05% (v/v) Tween-20, 1% (w/v) BSA.
- Washing buffer: PBS (pH 7.4), 0.05% (v/v) Tween-20.
- Chemiluminescent horseradish peroxidase (HRP) detection reagent.

2.3. Quantification of Oxidative DNA Damage

- Rifampicin, stock solution of 120 mg/mL in ethanol, stored at –20°C.

2.4. Assaying Stress Resistance

- Methyl viologen dichloride hydrate (see Note 3).

2.5. Time-Lapse Microscopy

- Temperature-controlled (Cube and Box incubation system, Life Imaging Services, Reinach, Switzerland) automated microscope (Zeiss 200 M; Zeiss, Jena, Germany), along with filters from Chroma, Rockingham, Vermont, USA.
- MetaMorph microscope control software (Universal Imaging, Downingtown, PA, USA).
- CoolSNAP HQ CCD camera (Princeton Instruments, Trenton, NJ, USA).

3. Methods

3.1. Enumeration of Colony-Forming Units

1. A small (approximately 50 μL) sample is collected from the frozen stock (maintained at –70°C) and streaked onto a fresh LB agar plate.
2. After incubating the plate overnight at 37°C, inoculate 2–3 colonies into 1 mL of LB (see Note 4).
3. Overnight culture is inoculated (1:1,000) into fresh medium. Cultures are incubated in 3 mL of LB in 16-mm diameter test tubes rotating orbitally at 220 rpm for 12 h; stationary phase has been reached after this period (see Note 5).
4. At this point, if working with various mutant strains, cell density can be adjusted to approximately 1.5×10^9/mL (density of BW25113 strain) by resuspending a pellet containing the desired number of cells in cell-free spent medium of the same strain.
5. If working with different mutant or wild type (wt) strains reaching different pH at stationary phase, the pH can be adjusted to 8.5 (pH of stationary phase wt culture in initially unbuffered LB) by adding AMPSO buffer to a final concentration of 100 mM that has been brought to the desired pH with 10 M NaOH (see Notes 6 and 7).
6. Cultures are incubated at 37°C and 70% relative humidity and CFU's are measured over time by removing an aliquot, serially diluting in 0.5% NaCl that has been sterilized by autoclaving, followed by colony enumeration after plating on LB agar plates that are incubated for approximately 16 h at 37°C (see Note 8). Hence, enumeration of live bacteria using this method is

dependent on the ability of a non-proliferating bacterium from the liquid culture to resume growth when transferred onto solid nutrient media, resulting in the formation of a colony visible by the naked eye.

3.2. Quantification of Protein Carbonyls

Oxidative damage in the form of protein carbonyls has been used as a biomarker of protein damage and cellular senescence in *E. coli*.

1. An *E. coli* strain is inoculated in 25 mL of LB in a 125-mL flask by a 1:1,000 transfer from an overnight 1 mL LB culture (see Note 9).
2. At 3 h after inoculation, 3 mL are removed from the culture to provide the log phase sample.
3. 2.5 mL of 1 M HEPES buffer is added to the culture at 12 h after inoculation, that is the onset of stationary phase (see Note 10).
4. On days 1, 3, and 5, 1.5-mL samples are collected in Eppendorf tubes. The samples are centrifuged, supernatant aspirated off and the pellets are flash-frozen by incubating in crushed dry ice for 2 min. The frozen pellets are subsequently stored at –70°C.
5. After all samples have been collected, they are removed from the freezer and thawed on ice.
6. Each pellet is then resuspended in 100 μL of Y-PER protein extraction reagent (Pierce) and incubated for 20 min at room temperature.
7. Cell debris is pelleted by centrifuging for 5 min at 14,000×*g* and the supernatant used as the protein extract during the subsequent steps.
8. Protein concentration is quantified in duplicate using the BCA protein assay kit (Pierce, see Note 11).
9. The Oxyblot protein oxidation detection kit (Chemicon) is used to quantify the amount of protein carbonyls in each sample starting with 8 μg of protein for each sample in a volume of 5 μL.
10. Each protein aliquot is denatured by the addition of 5 μL, 12% SDS.
11. 10 μL of 1× 2,4-dinitrophenylhydrazine (DNPH) solution is then added and the solutions incubated at room temperature for 15 min to derivatize the protein carbonyls.
12. 7.5 μL of neutralization solution is then added.
13. All samples are subsequently transferred to a PVDF membrane using a slot blot apparatus and the Western blot performed as follows.
14. The membrane is consecutively incubated for 1 h each at room temperature first with a rabbit anti-DNP antibody and then with a HRP-conjugated goat anti-rabbit IgG antibody, both in blocking buffer with gentle shaking.

15. The membrane is rinsed twice with washing buffer between the two antibody incubations and after the second incubation.
16. Chemiluminescent HRP detection reagent is layered on top of the membrane and incubated for 1 min at room temperature.
17. An autoradiography film is then exposed for 30 s on top of the membrane and subsequently developed in the darkroom.
18. Signal intensity is quantified using the Image J software (http://rsbweb.nih.gov/ij/).

3.3. Quantification of Oxidative DNA Damage

1. Cultures are processed as described in Subheading 2 with HEPES (pH 7.5) in a volume of 25 mL in 125-mL Erlenmeyer flasks.
2. Rifampicin-resistant mutants are quantified by plating on LB plates containing the antibiotic at 120 μg/mL after washing once with 0.5% NaCl.
3. The colonies grown in rifampicin are enumerated and normalized by the total number of CFU's at each time-point (see Note 12).

3.4. Assaying Stress Resistance

1. To assay heat shock resistance, cultures are buffered with AMPSO after 12 h of incubation as described in Subheading 3.1, returned to the incubator and 4 h later (16 h after inoculation) are subjected to a 5-min incubation in a 54°C water bath without shaking and CFU's enumerated before and after the treatment.
2. For the measurement of resistance to paraquat (methyl viologen dichloride hydrate), cultures are prepared in the same way and paraquat (see Note 3) is added to 500 μM at 12 h after inoculation. CFU's are enumerated before and after a 12-h incubation at 37°C.

3.5. Time-Lapse Microscopy

Protocol adapted from (45):

1. A wild-type strain of *E. coli* is modified to express yellow fluorescent protein under the control of the lactose operon repressor and the Pl promoter of lambda phage (49).
2. Cells are inoculated onto microscope cavity slides from exponentially growing liquid cultures, such that the colonies and cells grow exponentially in a single plane on the surface of a solid matrix of LB-agarose (NaCl concentration of 5 g/L, see Note 13). The slides are incubated in a temperature-controlled automated microscope at 30°C for up to 6 h (see Notes 14 and 15).
3. Up to seven fields containing one to four cells each are manually identified at the start of the experiment and stored in the MetaMorph microscope control software.

4. Fluorescent images are recorded at each field with time points taken generally every 4 min for the first 160 min, then every 2 min for the remaining time (see Notes 16 and 17).
5. Images are taken with a CoolSNAP HQ camera at 100× magnification; the resulting images have a spatial dimension of 0.064 μm per pixel (see Notes 18 and 19).

4. Notes

1. Tryptone is marketed as a pancreatic digest of casein. Casein (80%) and whey (20%) are the fundamental protein components of milk. Casein is a mixture of proteins that contains all of the common amino acids. After it is separated from the other components of milk, it is subjected to enzymatic hydrolysis using pancreatic enzymes that contain, among others, trypsin and chymotrypsin. The resulting substance contains varying amounts of all the amino acids, both free and as part of peptides, and very little carbohydrate (4.3 mg/g).
2. Yeast extract, an animal-free peptone, is manufactured by the controlled autolysis of cultures of the baker's yeast *S. cerevisiae*. Apart from amino acids, it also contains a significant amount of carbohydrate (163 mg/g) and also several micronutrients that include B-complex vitamins. All information regarding the contents of LB was extracted from the BD Bionutrients™ technical manual, third edition revised, which is available from the manufacturer's website.
3. A fresh solution of paraquat is prepared using sterile de-ionized water before each use to ensure that the drug does not break down during extended storage.
4. Survival experiments can also be carried out in a various minimal media (e.g., M9 or M63) with the addition of the different carbon sources at the desired concentrations (e.g., M9 medium containing 0.5% glucose). The recipe for these media can be found in standard laboratory manuals (e.g., the one edited by Maniatis).
5. In case a higher degree of aeration compared to the one provided by test-tubes is required, cultures can be maintained in 10 mL of LB in orbitally shaking 125-mL Erlenmeyer flasks.
6. The pH can be adjusted to a neutral value (7.5, since the intracellular pH of *E. coli* over a range of extracellular pH values is 7.4–7.8 (50)) by the addition of 100 mM HEPES buffer to the culture.
7. Spontaneous and adjusted pH for the different strains can be quantified using either a pH electrode or pH test strips.

8. The period of incubation of these LB agar plates need not be precisely measured, but care should be taken to allow enough time for any late-appearing colonies to emerge and be counted.
9. To minimize the fraction of culture removed for each sampling, larger culture volumes are required compared to those for the survival experiments described above.
10. The quantification of protein carbonyls during a survival experiment is more appropriately carried out at an external pH of 7.5 (rather than 8.5) so as to increase the time-window available for the detection of any age-dependent changes.
11. All extracts are diluted using water to equalize the protein concentration to that of the least concentrated sample.
12. Care should be taken in order to measure any late-emerging colonies on the rifampicin plates. These colonies need to be restreaked on rifampicin-containing plates to ensure that they are indeed resistant and to rule out the possibility that they arose due to the breakdown of the antibiotic.
13. The slide cavities are sealed with silicone grease and contained sufficient oxygen and nutrients to allow unhindered growth and fluorescence for the length of the experiment.
14. The entire microscope is contained within the incubator, eliminating temperature variation.
15. The conditions described for time-lapse microscopy result in an excess of nutrients and a protected environment without external causes of cell mortality.
16. A subset of six colonies is recorded every 40 s for improved time resolution.
17. The excitation light does not affect the cellular growth rate.
18. Excitation light (480–520 nm) is limited to 5% of the output of a 100-W Hg vapor lamp, with an exposure of 2 s.
19. Emission wavelengths are 505–565 nm.

References

1. Finkel SE (2006) Long-term survival during stationary phase: evolution and the GASP phenotype. Nat Rev Microbiol 4:113–120
2. Gonidakis S (2010) Molecular genetics of longevity in *Escherichia coli*. Ph.D. thesis. University of Southern California, Los Angeles
3. Pin C, Baranyi J (2008) Single-cell and population lag times as a function of cell age. Appl Environ Microbiol 74:2534–2536
4. Zambrano MM, Siegele DA, Almiron M, Tormo A, Kolter R (1993) Microbial competition: Escherichia coli mutants that take over stationary phase cultures. Science 259:1757–1760
5. Nystrom T, Larsson C, Gustafsson L (1996) Bacterial defense against aging: role of the Escherichia coli ArcA regulator in gene expression, readjusted energy flux and survival during stasis. EMBO J 15:3219–3228
6. Farrell MJ, Finkel SE (2003) The growth advantage in stationary-phase phenotype conferred by rpoS mutations is dependent on the pH and nutrient environment. J Bacteriol 185:7044–7052
7. Wei Y, Lee JM, Richmond C, Blattner FR, Rafalski JA, LaRossa RA (2001) High-density microarray-mediated gene expression profiling of Escherichia coli. J Bacteriol 183:545–556

8. Hartl DL, Dykhuizen DE (1984) The population genetics of Escherichia coli. Annu Rev Genet 18:31–68
9. Doran JW, Linn DM (1979) Bacteriological quality of runoff water from pastureland. Appl Environ Microbiol 37:985–991
10. Roszak DB, Colwell RR (1987) Survival strategies of bacteria in the natural environment. Microbiol Rev 51:365–379
11. Bogosian G, Sammons LE, Morris PJ, O'Neil JP, Heitkamp MA, Weber DB (1996) Death of the Escherichia coli K-12 strain W3110 in soil and water. Appl Environ Microbiol 62:4114–4120
12. Garcia-Lara J, Martinez J, Vilamu M, Vives-Rego J (1993) Effect of previous growth conditions on the starvation-survival of Escherichia coli in seawater. J Gen Microbiol 139:1425–1431
13. Morinigo MA, Cornax R, Castro D, Martinez-Manzanares E, Borrego JJ (1990) Viability of Salmonella spp and indicator microorganisms in seawater using membrane diffusion chambers. Antonie Van Leeuwenhoek 57:109–117
14. Rozen Y, Belkin S (2001) Survival of enteric bacteria in seawater. FEMS Microbiol Rev 25:513–529
15. Ericsson M, Hanstorp D, Hagberg P, Enger J, Nystrom T (2000) Sorting out bacterial viability with optical tweezers. J Bacteriol 182: 5551–5555
16. Gonidakis S, Finkel SE, Longo VD (2010) Genome-wide screen identifies Escherichia coli TCA-cycle-related mutants with extended chronological lifespan dependent on acetate metabolism and the hypoxia-inducible transcription factor ArcA. Aging Cell 9:868–881
17. Wei M, Fabrizio P, Madia F, Hu J, Ge H, Li LM, Longo VD (2009) Tor1/Sch9-regulated carbon source substitution is as effective as calorie restriction in life span extension. PLoS Genet 5:e1000467
18. Rea S, Johnson TE (2003) A metabolic model for life span determination in Caenorhabditis elegans. Dev Cell 5:197–203
19. Chen D, Thomas EL, Kapahi P (2009) HIF-1 modulates dietary restriction-mediated lifespan extension via IRE-1 in Caenorhabditis elegans. PLoS Genet 5:e1000486
20. Mehta R, Steinkraus KA, Sutphin GL, Ramos FJ, Shamieh LS, Huh A, Davis C, Chandler-Brown D, Kaeberlein M (2009) Proteasomal regulation of the hypoxic response modulates aging in C. elegans. Science 324:1196–1198
21. Zhang Y, Shao Z, Zhai Z, Shen C, Powell-Coffman JA (2009) The HIF-1 hypoxia-inducible factor modulates lifespan in C. elegans. PLoS One 4:e6348
22. Nystrom T (2005) Role of oxidative carbonylation in protein quality control and senescence. EMBO J 24:1311–1317
23. Dukan S, Nystrom T (1998) Bacterial senescence: stasis results in increased and differential oxidation of cytoplasmic proteins leading to developmental induction of the heat shock regulon. Genes Dev 12:3431–3441
24. Dukan S, Nystrom T (1999) Oxidative stress defense and deterioration of growth-arrested Escherichia coli cells. J Biol Chem 274: 26027–26032
25. Desnues B, Cuny C, Gregori G, Dukan S, Aguilaniu H, Nystrom T (2003) Differential oxidative damage and expression of stress defence regulons in culturable and non-culturable Escherichia coli cells. EMBO Rep 4:400–404
26. Gonidakis S, Finkel SE, Longo VD (2010) E. coli hypoxia-inducible factor ArcA mediates lifespan extension in a lipoic acid synthase mutant by suppressing acetyl-CoA synthetase. Biol Chem 391:1139–1147
27. Harman D (1956) Aging: a theory based on free radical and radiation chemistry. J Gerontol 11:298–300
28. Muller FL, Lustgarten MS, Jang Y, Richardson A, Van Remmen H (2007) Trends in oxidative aging theories. Free Radic Biol Med 43:477–503
29. Van Raamsdonk JM, Hekimi S (2009) Deletion of the mitochondrial superoxide dismutase sod-2 extends lifespan in Caenorhabditis elegans. PLoS Genet 5:e1000361
30. Hu D, Cao P, Thiels E, Chu CT, Wu GY, Oury TD, Klann E (2007) Hippocampal long-term potentiation, memory, and longevity in mice that overexpress mitochondrial superoxide dismutase. Neurobiol Learn Mem 87:372–384
31. Longo VD, Finch CE (2003) Evolutionary medicine: from dwarf model systems to healthy centenarians? Science 299:1342–1346
32. Jobson RW, Nabholz B, Galtier N (2009) An evolutionary genome scan for longevity-related natural selection in mammals. Mol Biol Evol 27:840–847
33. Jin DJ, Gross CA (1988) Mapping and sequencing of mutations in the Escherichia coli rpoB gene that lead to rifampicin resistance. J Mol Biol 202:45–58
34. Garibyan L, Huang T, Kim M, Wolff E, Nguyen A, Nguyen T, Diep A, Hu K, Iverson A, Yang H, Miller JH (2003) Use of the rpoB gene to determine the specificity of base substitution mutations on the Escherichia coli chromosome. DNA Repair (Amst) 2:593–608
35. Benov L, Fridovich I (1995) A superoxide dismutase mimic protects sodA sodB

Escherichia coli against aerobic heating and stationary-phase death. Arch Biochem Biophys 322:291–294

36. Farr SB, D'Ari R, Touati D (1986) Oxygen-dependent mutagenesis in Escherichia coli lacking superoxide dismutase. Proc Natl Acad Sci U S A 83:8268–8272
37. Jenkins DE, Schultz JE, Matin A (1988) Starvation-induced cross protection against heat or H2O2 challenge in Escherichia coli. J Bacteriol 170:3910–3914
38. Hengge-Aronis R (2002) Stationary phase gene regulation: what makes an Escherichia coli promoter sigmaS-selective? Curr Opin Microbiol 5:591–595
39. Hengge-Aronis R, Klein W, Lange R, Rimmele M, Boos W (1991) Trehalose synthesis genes are controlled by the putative sigma factor encoded by rpoS and are involved in stationary-phase thermotolerance in Escherichia coli. J Bacteriol 173:7918–7924
40. Conter A, Gangneux C, Suzanne M, Gutierrez C (2001) Survival of Escherichia coli during long-term starvation: effects of aeration, NaCl, and the rpoS and osmC gene products. Res Microbiol 152:17–26
41. Hengge-Aronis R, Fischer D (1992) Identification and molecular analysis of glgS, a novel growth-phase-regulated and rpoS-dependent gene involved in glycogen synthesis in Escherichia coli. Mol Microbiol 6:1877–1886
42. Hassan HM, Fridovich I (1977) Regulation of the synthesis of superoxide dismutase in Escherichia coli. Induction by methyl viologen. J Biol Chem 252:7667–7672
43. Miller RA (2009) Cell stress and aging: new emphasis on multiplex resistance mechanisms. J Gerontol A Biol Sci Med Sci 64: 179–182
44. Longo VD, Mitteldorf J, Skulachev VP (2005) Programmed and altruistic ageing. Nat Rev Genet 6:866–872
45. Stewart EJ, Madden R, Paul G, Taddei F (2005) Aging and death in an organism that reproduces by morphologically symmetric division. PLoS Biol 3:e45
46. Lindner AB, Madden R, Demarez A, Stewart EJ, Taddei F (2008) Asymmetric segregation of protein aggregates is associated with cellular aging and rejuvenation. Proc Natl Acad Sci U S A 105:3076–3081
47. Steinkraus KA, Kaeberlein M, Kennedy BK (2008) Replicative aging in yeast: the means to the end. Annu Rev Cell Dev Biol 24: 29–54
48. Fabrizio P, Longo VD (2003) The chronological life span of Saccharomyces cerevisiae. Aging Cell 2:73–81
49. Elowitz MB, Levine AJ, Siggia ED, Swain PS (2002) Stochastic gene expression in a single cell. Science 297:1183–1186
50. Slonczewski JL, Rosen BP, Alger JR, Macnab RM (1981) pH homeostasis in Escherichia coli: measurement by 31P nuclear magnetic resonance of methylphosphonate and phosphate. Proc Natl Acad Sci U S A 78:6271–6275

Chapter 29

Assessing Organismal Aging in the Filamentous Fungus *Podospora anserina*

Heinz D. Osiewacz, Andrea Hamann, and Sandra Zintel

Abstract

Podospora anserina is an extensively studied model organism to unravel the mechanism of organismal aging. This filamentous fungus is short-lived and accessible to experimentation. Aging and lifespan are controlled by genetic and environmental traits and, in this model, have a strong mitochondrial etiology. Here, we describe methods and protocols to manipulate and study the aging process in *P. anserina* at different levels including biochemistry, cell biology, genetics, and physiology.

Key words: Aging, Apoptosis, Healthspan, Lifespan, Mitochondrial functions, *Podospora anserina*

1. Introduction

In contrast to most other filamentous fungi all wild-type isolates of *Podospora anserina* are characterized by a limited lifespan. This phenotype has been first described by George Rizet in the early 1950s and termed the "senescence syndrome" (1, 2). *P. anserina* efficiently reproduces by sexual reproduction. After fertilization a fruiting body (perithecium) is formed that contains a large number of ascospores. These meiospores give rise to the formation of a macroscopically visible colony, termed a mycelium, which represents an individual and consists of highly branched filamentous cells (hyphae). Mycelial growth occurs by the elongation of the hyphal tips at the periphery. After a strain-specific period of linear growth, mycelia turn to senescence by reducing the growth rate and changing their morphology. Senescent cultures are characterized by an increased pigmentation and a reduced formation of aerial hyphae (Fig. 1). At the microscopic level the peripheral hyphae appear as undulated filaments, which at the final stage burst. While transfer of pieces from a juvenile and pre-senescent culture to new growth substrate gives rise to new colonies, inoculation of such pieces from the growth front of a

Lorenzo Galluzzi et al. (eds.), *Cell Senescence: Methods and Protocols*, Methods in Molecular Biology, vol. 965,
DOI 10.1007/978-1-62703-239-1_29,

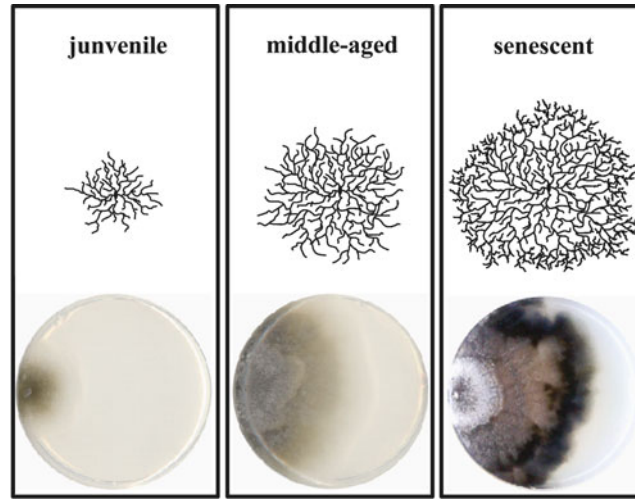

Fig. 1. Schematic illustration and culture plates of the phenotypic appearance of a juvenile, middle-aged, and senescent *Podospora anserina* culture. A mycelial piece of a freshly germinated ascospore was inoculated on a petri dish containing M2 medium and incubated at 27°C under constant light until the culture turned to senescence. In comparison to the juvenile and middle-aged mycelium the senescent mycelium is characterized by increased pigmentation, decreased formation of aerial hyphae, and a reduced growth rate.

senescent mycelium does not. The period of growth, either measured as time (in days) or as the distance of growth (in centimeters) is recorded as the lifespan of an individual and is characteristic for any given wild-type strain and mutant.

Early genetic experiments revealed a genetic basis of senescence. In *P. anserina* it is possible to perform reciprocal crosses using isolated male gametes with only very little cytoplasm to fertilize the female gametangia, the so-called protoperithecia, which contribute most of the cytoplasm to the resulting progeny. These kind of formal genetic investigations revealed that aging is controlled by both nuclear as well as extranuclear genetic traits (3, 4). Already in the late 1970s and early 1980s, long before mitochondrial DNA (mtDNA) were demonstrated to be of relevance for human aging and disease, DNA species in mitochondria, termed plasmid-like DNAs (plDNAs) were reported to accumulate during aging. The additional DNA species originate from the standard mtDNA, (5–9). More than 30 years of subsequent research resulted in the elucidation of a complex network of pathways affecting aging and lifespan of *P. anserina*. Mitochondria, the "power plants" of eukaryotic cells, do play a key role. Overall a complex network of interacting pathways including those governing mtDNA stability/instability, mtDNA repair, the generation and scavenging of reactive oxygen species (ROS), copper metabolism, proteostasis, mitochondrial dynamics, and apoptosis emerged to be of relevance for aging in *P. anserina* (for review see ref. 10–17). However, there is still much more to understand in this rather "simple" aging model.

In particular, the mechanistic details about the role of the individual pathways, their components, and their interactions remain to be elucidated in the future. From this kind of research, important perspectives for a general understanding of biological aging that also holds true in "higher" organisms like mammals will be continued to be elaborated.

In this treatise we provide a selection of protocols for assessing aging and senescence in *P. anserina*. For more details about the life cycle of *P. anserina* as well as the basis and the experimental set-up of formal genetic experiments the reader is referred to earlier publications (18–20).

2. Materials

Growth media, solutions and buffers are prepared with ultrapure water (Millipore™ GmbH, Schwalbach, Germany), analytical grade reagents and sterilized for 20 min at 121°C, 2 bar. Unless otherwise noted all solutions and growth media are stored at room temperature (RT).

2.1. Growth Media

In nature, the filamentous ascomycete *P. anserina* grows on herbivores dung. The fungus is cultivated in the laboratory under defined conditions on different liquid or solid media. Cultures are usually grown at 27°C under continuous light (18). Cultures are grown in liquid media under agitation at 160 rpm.

- "Biomalz–Mais"-Medium (BMM): 50 g cornmeal is incubated overnight at 60°C in 1 L water. Subsequently, the cornmeal suspension is filtered through a cotton cloth. 0.8% biomalt is added to the liquid (cornmeal extract) and pH is adjusted with KOH (6.5) followed by sterilization. For solid medium add 2% agar prior to sterilization. Agar plates can be stored at 4°C for 1–2 months.
- Complete medium (CM): 1 g KH_2PO_4, 0.5 g KCl, 0.5 g $MgSO_4 \times 7\ H_2O$, 10 g glucose-monohydrate, 3.7 g NH_4Cl, 2 g yeast extract, 2 g tryptone, 1 mL stock solution A, adjust pH to 6.5 with KOH, add water to a volume of 1 L, sterilization.
  - Stock solution A: 0.1% $ZnSO_4 \times 7\ H_2O$, 0.1% $FeCl_2 \times 4\ H_2O$, 0.1% $MnCl_2 \times 2\ H_2O$. Dissolved in water and sterilized.
- Minimal medium 2 (M2): 0.25 g KH_2PO_4, 0.3 g K_2HPO_4, 0.25 g $MgSO_4 \times 7\ H_2O$, 0.5 g urea, and 10 g dextrin are dissolved in water with a final volume of 1 L before 2% agar is added. After sterilization 50 µL biotine (0.05 mg/mL),

200 µL thiamine (250 mg/L) and 100 µL micronutrient stock solution are added (see Note 1).

  - Micronutrient stock solution: 5 g citric acid × H_2O, 5 g $ZnSO_4 \times 7\ H_2O$, 1 g $Fe(NH_4)_2(SO_4)_2 \times 6\ H_2O$, 0.25 g $CuSO_4 \times 5\ H_2O$, 0.05 g $MnSO_4 \times H_2O$, 0.05 g $Na_2MoO_4 \times 2\ H_2O$, 0.05 g H_3BO_4; dissolved in 100 mL water and filtered through a pore size of 0.2 µm.

- Spore germination medium: This medium is used for ascospores germination. BMM is supplemented with 60 mM ammonium acetate and 2% agar. Plates can be stored at 4°C for 1–2 months.
- Transformation medium: 3.7 g ammonium chloride, 2 g tryptone, 1 g yeast extract, 10 g glucose-monohydrate, 342.3 g sucrose, 20 mL stock solution 1, 20 mL stock solution 2. Adjust pH to 6.0 (for hygromycin-containing medium) or to pH 7.5 (for phleomycin-containing medium), add water to a volume of 1 L, 1.2% agar. After sterilization add—if required—hygromycin (final concentration 100 µg/mL) or phleomycin (final concentration 6 µg/mL).
  - Stock solution 1: 7.5 g KH_2PO_4, 2.5 g KCl, 2.7 g $MgSO_4 \times 7\ H_2O$ in 100 mL water, sterilized.
  - Stock solution 2: 0.005 g $ZnSO_4 \times 7\ H_2O$, 0.005 g $FeSO_4 \times 7\ H_2O$, 0.005 g $CuSO_4 \times 5\ H_2O$, 0.005 g $MnSO_4 \times H_2O$ in 100 mL water, sterilized.

2.2. Solutions and Buffers

- Antifoam dilution: 20% antifoam Y-30 Emulsion (Sigma-Aldrich, St. Louis, USA) in water.
- CsCl solution: 5.7 M CsCl, 0.1 M EDTA, pH 7.4, sterilized (see Note 2).
- Desalinization solution: 25% acetone, 25% ethanol, 50% H_2O (see Note 3).
- DMPC: 900 mL water, 99 mL 50% ethanol is added with 1 mL DMPC (Dimethyl pyrocarbonate), incubated at RT for at least 30 min, sterilized.
- DTT stock solution (1 M): 3.09 g DTT dissolved in 20 mL 0.01 M NaAc (pH 5.2) and filter-sterilized.
- GTC/β mercaptoethanol: 5.5 M guanidinium thiocyanate (GTC), 25 mM sodium citrate, 10 mL 10% *N*-lauroyl sarcosine, and 200 mL with H_2O After sterilization 0.2 M β mercaptoethanol is added (see Note 4).
- Mito buffer 1: 10 mM Tris–HCl, 1 mM EDTA, 0.33 M sucrose (pH 7.5).
- Mito buffer 2: 0.2% BSA in Mito buffer 1.

- Native running buffer (10×): 0.25 M Tris–HCl, 1.9 M glycine (pH 8.3).
- Native sample loading buffer (6×): 3 mL glycerine, 3.75 mL 0.5 M Tris–HCl (pH 7.0), 0.1 g bromophenol blue in H_2O.
- Oxygen buffer: 0.3 M sucrose, 10 mM KH_2PO_4, 5 mM $MgCl_2$, 1 mM EGTA, 10 mM KCl, 0.2% BSA. Adjust pH to 7.2 (with NaOH).
- PEG: 60% polyethylene glycol (PEG) 4,000, 50 mM $CaCl_2 \times 2H_2O$, 10 mM Tris–HCl (pH 7.5).
- Potassium phosphate buffer (0.1 M, pH 7.8): 13.2 mM K_2HPO_4, 86.8 mM KH_2PO_4.
- Potassium phosphate buffer (10 mM, pH 7): 1.32 mM K_2HPO_4, 8.68 mM KH_2PO_4.
- 1.5 M Tris: 181.71 g/L Tris–HCl (pH 8.9).
- Protein extraction buffer: 50 mM HEPES (pH 7.4), 100 mM NaCl, 0.1 mM EDTA, 0.1% CHAPS, 1 mM DTT (see Note 5).
- STC: 1 M sorbitol, 10 mM Tris–HCl (pH 7.5), 50 mM $CaCl_2 \times H_2O$.
- TENS: 10 mM Tris–HCl (pH 8.0), 1 mM EDTA, 100 mM NaCl, 2% SDS.
- TPS: 200 g/L sucrose, 45 mM KH_2PO_4, 5 mM Na_2HPO_4, H_3PO_4 (pH 5.5).

2.3. Special Equipment

- Cellophane foil (583 Gel Dryer, Bio-Rad, California, USA).
- Waring blender.
- Hemocytometer.
- Glass wool.
- Gauze.
- Liquid nitrogen.
- Mortar.
- Pestle.
- Quartz glass cuvette.
- Photometer.
- Glass beads (0.5 mm diameter).
- BeatBeater (Roth®, Karlsruhe, Germany).
- Nettle cloth, filter tubes (Amicon Ultra-15, Ultracel-3k, Millipore™ GmbH, Schwalbach, Germany).
- Light table.
- Race tubes (glass tubes with 45 cm length, 1.5 cm diameter).
- Oxygen electrode.

3. Methods

1.5–2 mL microcentrifuge tubes are centrifuged using a centrifuge 5417R (Eppendorf, Hamburg, Germany). Centrifugation of 50 mL tubes is performed with Varifuge 3.0 (Heraeus, Hanau, Germany). A Sorvall RC 5B (DuPont®, Wilmington, USA) is used for centrifugation of GSA or SS34 centrifuge tubes (rotors: Super-Lite™ GSA SLA-1500 or Sorvall SS34). Ultracentrifugation is performed in a Sorvall WX Ultra 80 centrifuge (Thermo Scientific, Massachusetts, USA) using the TH 641 swinging bucket rotor (DuPont®, Wilmington, USA).

3.1. Phenotypic Analyses

In general, phenotypic studies are performed with genetically defined strains originating from mononucleate ascospores. Such spores are formed in 1–2% of the asci of a perithecium. They are the result of an untypical formation of ascospores, which in the vast majority, do contain two nuclei and therefore may be heterogenous. Genetically homogenous mononucleate ascospores can clearly be identified in the dissection microscope by their smaller size. These spores are isolated, germinated, and generally used for subsequent experiments including lifespan determination (18, 20).

3.1.1. Cultivation

P. anserina grows on standard cornmeal agar (BMM) at 27°C under constant light according to Esser (18). Mycelia are stored at 4°C until next usage (see Note 6). Every 3–6 months the stored mycelia have to be freshly inoculated on a new petri dish to keep a strain alive.

3.1.2. Strain Library

For longer periods of time, strains are kept in a strain library. Therefore, a piece of mycelium is placed on BMM solid medium (~10 mL) in a thin glass tube, incubated at 27°C at constant light for 3–5 days and can then be stored at 4°C. To keep stored strains alive, strains have to be regrown on a new BMM containing glass tube within a period of 9–12 months.

3.1.3. Mating by Confrontation of Two Growing Cultures of Different Mating Types

For fertilization one piece of mycelium of two different cultures with opposite mating types are placed on a petri dish containing 30 mL M2 medium (Fig. 2a). The growing colonies come into contact. In this zone, spermatia of one mating type fertilize the protoperithecia (ascogones) of the opposite mating type in a reciprocal manner. After an incubation of 8–12 days at 27°C under constant light, perithecia occur as macroscopically visible fruiting bodies (Fig. 2b, c).

3.1.4. Fertilization by Spermatization

This kind of fertilization allows performing defined reciprocal crosses of two strains. In brief, a genetically defined culture serving as the female parent (but contains both female as well as male

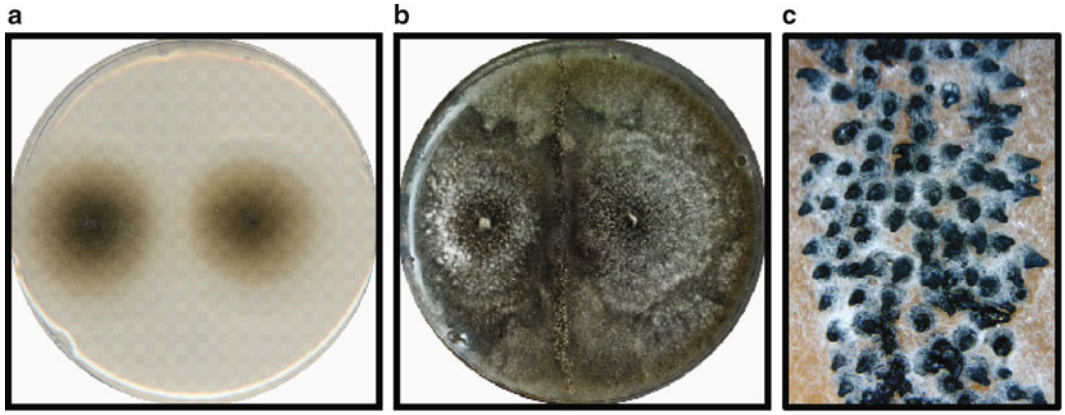

Fig. 2. Confrontation mating of two cultures of different mating types. (**a**) For fertilization, one piece of mycelium of mating type *plus* (+) and of mating type *minus* (–) are placed a few centimeters away on a petri dish containing M2 medium. (**b**) The hyphal tips of both cultures grow toward the middle of the petri dish. At the contact zone fertilization takes place and perithecia (fruiting bodies) develop. (**c**) Enlarged section of the perithecia building zone. Numerous perithecia are formed, containing ascospores.

gametangia) is fertilized by a solution of collected "pure spermatia" of another strain with the opposite mating type. The donor and acceptor strains can be switched in respect to the phenotype of interest (e.g., short-lived vs. long-lived). Reciprocal crosses of this type provide information of whether or not a specific phenotype is inherited by nuclear or extranuclear genetic traits.

1. Homokaryotic mycelia of opposite mating types (+ or –) are allowed to overgrow the surface of separate M2 (or BMM) containing petri dishes for 7–10 days at 27°C under constant light.
2. Spermatia, a nonmotile sperm cell, of the one colony (serving as male partner) are harvested by flooding the mycelium on the petri dish with 3–5 mL of sterile water.
3. After an incubation of 5 min, the solution of the released spermatia is transferred onto the mycelium of the colony of the opposite mating type (serving as female partner).
4. After an incubation of 5 min the suspension is removed. Mature perithecia (fruiting bodies) develop within 1–2 weeks under constant light at 27°C.
5. Spores can be manually isolated in the dissection microscope, and subsequently be analyzed (e.g., for inheritance of a specific mutation, for physiological and molecular characteristics).

3.1.5. Isolation and Germination of Ascospores

All cultures used for genetic analyses are monokaryotic and derived from irregular asci containing small spores.

Perithecia are flask-shaped structures with an opening pore (ostiole) through which the ascospores can be released (Fig. 3a). The perithecium contains a rosette full of asci (Fig. 3b). One ascus usually contains four binucleate spores including the two products

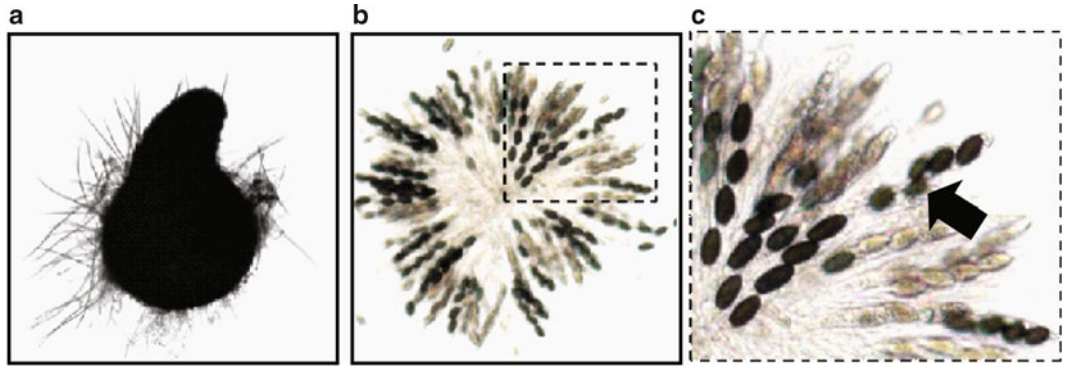

Fig. 3. Isolation of ascospores. (**a**) Perithecia (fruiting bodies) are *flask shaped* structures, which are formed after fertilization between two different cultures of opposite mating type. (**b**) The perithecium contains a rosette of asci, the specialized meiosporangia (meiospore containers) of the ascomycetes. (**c**) Magnification of the rosette. Each ascus usually contains four ascospores. Occasionally (1–2% of all asci), two mononuclear homokaryotic ascospores (see *arrow*) instead of one binuclear heterokaryotic ascospore are formed which differ in their sizes. Such asci are five to eight-spored depending on the number of mononucleate ascospores.

of a half-tetrad. The vast majority of these spores are heterokaryotic for the mating-type, possessing the mating type +/−. Only in rare cases the mating type of dinucleate ascospores is +/+ or −/−. Occasionally, as the result of a disturbed spindle apparatus two mononuclear homokaryotic ascospores are formed instead of one binuclear heterokaryotic ascospore. The mononucleate ascospores are smaller in size than binucleate spores (Fig. 3c, arrow). These homokaryotic ascospores give rise to self-sterile (+ or −) cultures, which are used to perform crosses, and for genetic analyses.

1. Under a dissection microscope the perithecium is perforated using a heat sterilized dissection pin (see Note 7).
2. A rosette of asci is transferred onto a petri dish containing prep-agar (8% agar dissolved in water) and gently dissected with the dissection pin.
3. The smaller spores of an irregular ascus are separated and transferred to spore germination medium.
4. For germination, the isolated ascospores are incubated at 27°C in the dark for 2–3 days.

3.1.6. Generation of Mycelium of Defined Age

1. In order to obtain *P. anserina* cultures of a defined age, mycelia derived from freshly germinated mononucleate ascospores are placed on one side of a petri dish containing 30 mL M2 medium.
2. As soon as the growth front reaches the other side of the petri dish, a new plate with M2 is inoculated with a piece of mycelium of the culture obtained from the growth front.
3. Subsequently the growth front of the growing mycelium is marked every other day until the senescent culture stops growing and displays hyperpigmentation.

4. Senescent cultures are obtained from mycelia shortly before growth arrest to inoculate fresh plates for follow-up experiments (e.g., RNA or protein isolation).
5. For isolation of mitochondria, nucleic acids, or other compounds from senescent cultures, pieces of a senescent culture from a position 3 days before growth stop are placed on solid medium for 3 days and then transferred to Fernbach flasks containing 150 mL CM and incubated without shaking under constant light at 27°C for 4–5 days.
6. The resulting mycelium is subsequently used for analyses.

3.1.7. Growth Rates

Growth rates of a colony are analyzed by measuring the growth of the mycelium every second day. A piece of mycelium from a monokaryotic culture is placed on a M2 (30 mL) containing petri dish. The incubation followed by 27°C and constant light. Growth rates are calculated as growth distance per day of incubation (cm/day).

3.1.8. Fertility

The formation of female and male reproduction structures of *P. anserina* differs in the amount of energy requirement. The male gametes, the spermatia, are small cells that do hardly contain cytoplasm and therefore do not transmit mitochondria to the cross. The female reproduction structures, the trichogyne and the ascogon, however, are much larger and provide the vast majority of mitochondria and cytoplasmic material. Due to the different size and the different developmental steps involved in the formation, the ability to form these structures is differentially affected in certain mutants. To assess the male and female fertility of a given strain reciprocal crosses are performed.

Determination of the female fertility

1. A piece of freshly germinated mycelium of both, the wild type and a strain of interest with the opposite mating type is placed in the middle of a M2 containing petri dish and incubated for 7–14 days at 27°C under constant light until the mycelium has completely overgrown the plate.
2. Spermatia (male gametes) are harvested by flooding the mycelial surface of the wild type for 5 min with 5 mL sterile water.
3. 6 drops of 400 μL of the spermatia suspension are transferred on the mycelium of the tested strain (see Note 8).
4. After 5 min of incubation, the drops are gently removed and the spermatized mycelium is incubated at 27°C under constant light until perithecia develop (2–3 days).
5. The fruiting bodies, which are resulting from fertilization of the protoperithecia, are scanned and the resulting picture file is evaluated with the help of an image processing program like "Photoshop 5.0" (Adobe). For this, every counted perithecium

is marked by a dot, allowing the exact determination of the number of perithecia per spermatization area. The total number of fruiting bodies/μL spermatia solution is determined.

Determination of the male fertility

1. A piece of mycelium is placed in the middle of a M2 containing petri dish and incubated for 7–14 days at 27°C under constant light until the mycelium has completely overgrown the plate.
2. Spermatia (male gametes) are harvested by flooding the mycelial surface for 5 min with 5 mL sterile water.
3. After 10 min at 18,000 × *g* centrifugation of the spermatia suspension, the supernatant is carefully removed up to 0.2 mL and the sediment is resuspended in the residual liquid.
4. The number of spermatia is finally determined microscopically using a hemocytometer.

3.1.9. Resistance Against Different Stressors

To determine the resistance of a *P. anserina* cultures against a stressor in the medium, the growth rate is measured as described above (see Subheading 3.1.7). Mycelia of monokaryotic isolates are grown on M2 containing petri dishes supplemented with different stressors (e.g., 20–150 μM paraquat, 0.04–0.1% hydrogen peroxide, 100–400 μM copper, 2.5–10 μg/mL ethidium bromide, or 0.5–10 mM DTT). Plates with hydrogen peroxide are kept in the dark to protect hydrogen peroxide from degradation. Heat shock experiments are done at 37°C and constant light.

3.1.10. Lifespan Determination

The lifespan of *P. anserina* is analyzed using juvenile monokaryotic mycelia from 2 days old germinated ascospores. Mycelial pieces are placed on race tubes containing 50 mL M2. Race tubes allow the growth of colonies for a longer period of time (e.g., 3 months) under defined conditions. (Fig. 4) (see Note 9). The lifespan is defined as the time period, recorded in days, of linear hyphal growth. After that time, the hyphal tips at the growth front of the

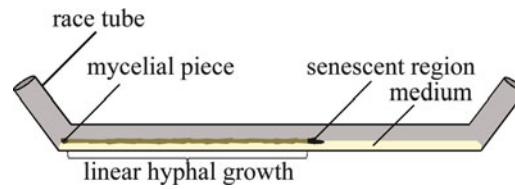

Fig. 4. Determination of the lifespan. Scheme illustrating the determination of the lifespan of *Podospora anserina*. A mycelial piece of a juvenile monokaryotic culture from 2 days old germinated ascospore is placed on one site of the race tube containing M2 medium. The race tube is incubated at 27°C under constant light conditions. Every other day the growth front is marked until it stops to grow continuously and displays an increased pigmentation (senescent region).

mycelium do not continue to grow, formation of aerial hyphae is reduced and the pigmentation is increased. Survival curves are calculated allowing the determination of the median lifespan.

3.2. Genetic Manipulations

For *P. anserina* techniques to construct specific genetically modified strains have been developed. As prerequisites a general transformation procedure based on the generation, transformation, regeneration, and selection of transformants had to be achieved. Transformation is performed with spheroplasts generated by incubation of chopped mycelium with lytic enzyme mixtures able to disrupt the fungal cell wall.

In *P. anserina* DNA introduced into spheroplasts becomes efficiently integrated into the genome. Integration is only targeted to homologous sequences when sequences on the genome and the transforming plasmids are characterized by long matching nucleotide stretches (i.e., greater than 3 kbp).

In order to replace (delete) a gene of interest by a selectable marker gene the corresponding marker needs to be enclosed by long sequences of 3 kbp of the sequence up- and downstream of the gene of interest. The construction of such vectors is generally possible but rather inefficient by conventional cloning techniques. A more effective procedure for construction of deletion strains of *P. anserina* has been described, which employs the use of cosmid vectors containing large flanking regions of the gene of interest (21). Alternatively, a procedure described by El-Khoury et al. utilizing a specific mutant strain (Δ*PaKu70*) for gene replacement experiments is used. This method is characterized by a highly efficient homologous recombination machinery (22). In this strain, about 500 bps of matching nucleotide stretches are sufficient for efficient homologous recombination.

For the construction of over-expressing strains the gene of interest is generally placed downstream of a strong promoter like the *PaGpd* or the *PaMt1* promoter (23, 24). Constructs containing a non-disrupted version of the gene of interest is selected by Southern Blot analyses and subsequently analyzed for transcript levels and—if a suitable antibody is available—for protein level.

3.2.1. Transformation of P. anserina

To generate specific mutant strains (e.g., over-expression or deletion strains) over-expressing plasmids or deletion cosmids are transformed into *P. anserina* wild-type strain "s." The production, regeneration, and integrative transformation of *P. anserina* spheroplasts is performed as described (25, 26).

Preparation of spheroplasts

In order to transform *P. anserina*, the cell wall must partially be removed using glucanex as a lytic enzyme mixture (see Note 10). All steps are performed under sterile conditions to exclude

contaminations (e.g., *Saccharomyces spec* or *Aspergillus spec* which are able to grow on that medium).

1. The mycelium of wild-type strain "s" grows 2–3 days on 6–8 BMM containing petri dishes at 27°C and constant light.
2. Mycelia are then inoculated in 6–8 CM containing flasks (200 mL) which are incubated at 27°C, constant light by shaking (see Note 11).
3. After 3 days of growth, the cultured mycelia are harvested by filtration through gauze. A maximum of 20 g mycelia (moist mass) are washed with TPS.
4. Mix per 1 g of the mycelia with 5 mL of a glucanex suspension to a final volume of 20 mg glucanex/mL suspension in TPS (see Note 12).
5. The glucanex-mycelium mixture is chopped using a Waring blender (2 × 5 s low and 2 × 5 s high) and transferred to a flask which is incubated at 35°C for 90 min by carefully shaking.
6. The digestion process is controlled microscopically using a few μL of the mycelia suspension (see Note 13).
7. In order to separate the mycelia from the spheroplasts and to terminate the digestion process, the suspension is filtered through two layers of gauze and once through glass wool stuffed funnels in 50 mL falcon tubes.
8. After centrifugation (10 min at 1,500 × *g*) the spheroplast pellets are dissolved in 1 mL TPS, centrifuged 10 min at 1,500 × *g*. The pellet is resuspended again in 1 mL TPS.
9. The washing step is repeated for three times again and finally the spheroplasts are resuspended 1 mL TPS.
10. The number of spheroplasts/μL is counted with a hemocytometer.
11. Protoplasts can be transformed immediately or stored at −80°C (see Note 14).

Transformation

1. Per transformation experiment 10^7 spheroplasts are used and kept during the whole experiment on ice.
2. Spheroplasts are centrifuged at 1,500 × *g*, RT for 10 min, resuspended in 200 μL STC and kept on ice.
3. For the transformation 10 μg DNA (e.g., plasmids, cosmids) are used in a final volume of 40 μL.
4. As a negative control the plasmid phph-1 (Roche, Risch, Switzerland) and as a positive control the plasmid pAN7-1 (27) are used (see Notes 15 and 16).
5. To determine the regeneration ability of the spheroplasts, to one aliquots of spheroplasts 40 μL of sterile water instead of DNA are added.

6. After addition of DNA or water, the spheroplasts are incubated for 30 min on ice.
7. Subsequently, 50 µL PEG is added, carefully mixed, and incubated for 20 min on ice.
8. The reaction batch is transferred into 5 mL PPN tubes. 2 mL PEG in 500 µL steps are added and incubated for 30 min on ice followed by incubation for 10 min at RT.
9. After an addition of 4 mL STC, the samples are gently mixed.
10. 800 µL aliquots of the transformation mixture are mixed with 4 mL overlay-agar (transformation medium with 0.5% agar instead of 1.2% agar, including selection marker), mixed briefly and transferred to a petri dish containing the transformation medium (including selection marker).
11. Regeneration control: 1 mL of each dilution series (10^{-1}–10^{-6} in STC or H_2O) are mixed with 4 mL overlay-agar (transformation medium with 0.5% agar instead of 1.2% agar, without selection marker) and transferred to plates with transformation medium (without selection marker).
12. After 4 days of incubation at 27°C and continuous light the regeneration rate is determined.
13. The regeneration rate (mycelia/10^7 spheroplasts) indicates how many spheroplasts are able to form a mycelium. Therefore the number of growing colonies is determined which result from regenerated spheroplasts. Mycelia that appear on the water control plates result from insufficient cell wall digestion of the mycelia and must be subtracted from the value of the STC batch. The regeneration rate should at least be 0.4%.
14. After 14 days, the positive and negative control is analyzed and the transformation efficiency is calculated. The transformation efficiency indicates how many transformants occurred per µg transformed DNA and should be 1–2 transformants/µg DNA.
15. Grown colonies are individualized on BMM containing petri dishes and incubated at 27°C at constant light to enable an increase in size. In parallel, a piece of mycelium is transferred to BMM containing petri dishes with a corresponding selection marker to verify the resistance resulting from the potential integration of the DNA of interest.
16. To investigate the selected transformants in more detail, DNA is isolated and Southern blot analyses are performed.

3.3. Molecular Methods

P. anserina is accessible to molecular analyses. Wild-type strains, randomly selected mutants, and specifically constructed strains can efficiently be characterized by molecular techniques relying on the specific isolation of DNA, RNA, proteins, and other cellular compounds.

3.3.1. Isolation of DNA

Isolation of DNA from *P. anserina* is performed by a modified protocol of the method described by Lecellier and Silar (28).

1. Pieces of mycelium are allowed to overgrow the surface of a BMM containing petri dish covered with cellophane foil for 2–3 days at 27°C under constant light.
2. The cultured mycelium is easily harvested by simply scraping it from the cellophane foil with a spatula.
3. The mycelium is transferred into a 2 mL microcentrifuge tube containing 1 mL TENS.
4. Next the samples are frozen and thawed (liquid nitrogen and a water bath at 70°C) three times to destroy the cell walls.
5. Cell debris is sedimented by centrifugation at 18,000 × *g*, RT for 10 min.
6. To precipitate the DNA in solution, the supernatant is transferred to a fresh 2 mL microcentrifuge tube, mixed with 1 volume phenol and centrifuged at 3,300 × *g*, RT for 5 min.
7. Step 6 is repeated with phenol–chloroform–isoamyl alcohol (mixing ratio 25:24:1) and with only chloroform–isoamyl alcohol (mixing ratio 24:1) (see Note 17).
8. The DNA is precipitated by adding 1 volume isopropyl alcohol (–20°C) to the supernatant and mixed thoroughly.
9. After 20 min centrifugation at 20,000 × *g* and 4°C the pelleted DNA is air-dried before it is dissolved in 100 µL 0.3 M sodium acetate (pH 5.2) at 37°C for 15 min.
10. 2 volumes of ethanol (100%, –20°C) are added and incubated for 15 min at –80°C. Samples are centrifuged for 20 min at 20,000 × *g* and 4°C.
11. The pellet is washed with 200 µL ethanol (70%, –20°C), centrifuged at 20,000 × *g*, 4°C for 10 min.
12. The pellet is again air-dried and resuspended, depending on pellet size, in 30–50 µL sterile water.

3.3.2. Isolation of RNA

1. Pieces of mycelium are allowed to overgrow the surface of 2–3 BMM (or M2) containing petri dish for 2–5 days at 27°C under constant light.
2. The cultured mycelium is harvested by scraping it from the agar (as less agar as possible) with a spatula and transferred in 2–3 flasks containing 200 mL CM.
3. Incubation follows for 2–5 days under constant light at 27°C by shaking.
4. The mycelia are harvested by filtration through four layers of gauze.
5. The mycelia (4–8 g moist mass) are pulverized in liquid nitrogen using mortar and pestle (see Note 18).

6. The powder is decanted in a SS34 reaction tube (see Note 19) and resuspended in ~15 mL GTC/β mercaptoethanol by thoroughly mixing.
7. After incubation at 60°C for 10 min, the samples are centrifuged at 12,000 × *g* for 10 min (see Note 20).
8. The supernatant is transferred to an ultracentrifuge tube filled with 3 mL CsCl solution.
9. Samples are centrifuged 18 h at 200,000 × *g* and 20°C.
10. The supernatant is carefully removed with a pipette until the CsCl cushion is reached and the ultracentrifuge tube is subsequently decanted.
11. The RNA, a transparent pellet, is washed with 200 µL 70% ethanol/DMPC-H_2O.
12. Depending on the size of the RNA pellet the RNA is dissolved in 200–800 µL DMPC-H_2O and transferred to a microcentrifuge tube (see Note 21).
13. The dissolved RNA is added with 1/10 volume 3 M sodium acetate (pH 5.0) and 3 volumes ethanol to precipitate the RNA at –80°C for at least 30 min.
14. After centrifugation at 20,000 × *g*, 0°C for 15 min, the RNA pellet is washed by adding 70% ethanol/DMPC-H_2O and centrifuged again at 20,000 × *g*, 0°C for 15 min.
15. The RNA pellet is air-dried and resuspended, depending on pellet size, in 100–300 µL DMPC-H_2O at 60°C for max. 1 h.
16. The samples are immediately used or aliquoted and stored at –80°C until use (e.g., transcript analyses using Northern blot analysis, RT-PCR to investigate the expression of specific gene or whole transcriptome analyses).

3.3.3. Isolation of Total Protein Extract

1. Mycelium from a *P. anserina* strain overgrows the surface of a cellophane foil covered M2 (or BMM) containing petri dish for 2–3 days at 27°C under constant light.
2. The cultured mycelium is inoculated in flasks containing 200 mL CM which is then incubated for 3 days at 27°C and constant light by shaking (see Note 22).
3. The mycelium (1–4 g) is harvested by filtration through two layers of gauze (see Note 23).
4. The harvested mycelium is pulverized in liquid nitrogen using mortar and pestle (see Note 24).
5. The powder is decanted in a 2 mL microcentrifuge tube and resuspended in protein extraction buffer (50 µL/100 mg pulverized mycelium) by 5 min of thorough mixing.
6. The homogenized powder is subsequently centrifuged at 12,000 × *g* and 4°C for 10 min to pellet cell debris.

7. The supernatant is recovered (see Note 25) and protein concentration is determined according to the method of Bradford (29).
8. The samples are immediately used or aliquoted and stored at −80°C until use.

3.3.4. Isolation of Mitochondria

1. To isolate functional mitochondria according to Gredilla et al. (30) mycelia are inoculated on 5–10 BMM or M2 containing petri dishes covered with cellophane foil.
2. After incubation of 2–3 days under constant light and 27°C, mycelia are transferred to flasks with 200 mL CM (see Note 22).
3. After growing under shaking at 27°C for 2–3 days, the mycelia are harvested by filtration through two layers of gauze.

   The following steps are carried out at 4°C with cooled solutions, plastic, and glass wares:

4. In order to disrupt the cell wall, the mycelia (in portions of max. 5 g mycelium) are crushed 2 × 15–20 s with at least 1 min break in between by glass beads (0.5 mm diameter) in a BeadBeater (Roth®, Karlsruhe, Germany) with Mito buffer 2 containing 20–50 µL antifoam dilution (see Note 26).
5. The homogenate is filtered through a nettle cloth, where mitochondria are able to pass through while large fragments (e.g., hyphae, cell wall) are kept back.
6. The filtrate is split into two GSA centrifuge tubes. After centrifugation at 600 × *g*, 4°C for 10 min, smaller fragments are filtered through glass wool stuffed funnels and transferred to SS34 centrifuge tubes.
7. The mitochondria are pelleted by centrifugation at 12,000 × *g* at 4°C for 20 min.
8. The supernatant, which includes cytoplasmic proteins, is aliquoted (500 µL to 10 mL, depending on the concentration).
9. The pelleted mitochondrial fraction, which also contains vacuoles, is dissolved in 1 mL Mito buffer 1, transferred to 1.5 mL microcentrifuge tubes for sedimentation of particulate material for 2–3 min.

At this point, the mitochondrial fraction can be purified in two different ways: The differential centrifugation allows isolation of functional mitochondria, which can be used for physiological measurements. Ultrapure mitochondrial samples for Western Blot analysis and activity measurements are isolated by sucrose gradient to separate mitochondria from vacuoles. These samples are strongly reduced in physiological function.

Differential centrifugation protocol

1. The mitochondrial supernatants are transferred to SS34 centrifuge tubes, which are filled up to a ¾ volume with Mito buffer 1.

2. After centrifugation for 20 min at 15,000 × *g* and 4°C, the supernatants are discarded.
3. The pellet is composed of two components, an interior part (dark brown vacuoles) and an exterior part where mitochondria are enriched. The vacuoles are removed (see Note 27) and the mitochondria are dissolved without generating air bubbles in Mito buffer 1 (maximum volume: 300–600 µL).

Sucrose gradient centrifugation protocol:

1. The mitochondrial supernatants are transferred to SS34 centrifuge tubes which are filled up to a ¾ volume with Mito buffer 1.
2. After centrifugation for 20 min at 15,000 × *g* and 4°C, the supernatants are discarded.
3. The pellet is dissolved in 1 mL Mito buffer 1, transferred on top of the sucrose gradient (4 mL 50%, 4 mL 36%, and 2 mL 20% sucrose solution) and centrifuged for 60 min at 100,000 × *g*, 4°C.
4. The mitochondria, visible as a "milky" band in the middle of the centrifugation tube, are pipetted off the sucrose gradient and transferred to a fresh SS34 centrifuge tube, which is then filled up to a ¾ volume with Mito buffer 1 to wash the sucrose away.
5. After centrifugation at 4°C, 15,000 × *g* for 20 min, the mitochondria are dissolved free from air bubbles in Mito buffer 1 (maximum volume: 300–600 µL).
6. Protein concentration of the cytoplasmic and mitochondrial fraction is measured according to the method of Bradford (29). The samples are immediately used or aliquoted and stored at −80°C until use.

3.3.5. Isolation of Secreted Proteins

1. Mycelia from *P. anserina* are allowed to overgrow the surface of 2 BMM petri dishes covered with cellophane foil, followed by incubation at 27°C under constant light for 2–3 days.
2. The cultured mycelia are inoculated in 2 CM containing flasks (150 mL CM) which are incubated for 4 days at 27°C under constant light without shaking (see Note 28).
3. After incubation the liquid CM medium is separated from the mycelium by filtration though gauze (see Note 29) and enriched by using filter tubes (Amicon Ultra-15, Ultracel-3k, Millipore™ GmbH, Schwalbach, Germany).
4. Supernatants are mixed with protease inhibitor cocktail (PIC, 1:100 dilution) to prevent protein degradation and aliquoted into 2 mL microcentrifuge tubes.
5. The secreted proteins are precipitated by adding 2 volumes of ethanol and 2 volumes of acetone at −20°C for 2 days, and then centrifuged at 4°C and 20,000 × *g* for 30 min.

6. 1 mL desalinization solution is added to the pellets and mixed thoroughly for 1 min. The samples are incubated over night at −20°C.
7. The desalting procedure (step 6) is repeated twice.
8. Pellets are dried and resuspended 30–50 µL protein extraction buffer at RT.
9. Protein concentration is measured according to the method of Bradford (29). The samples are stored at −80°C until use.

3.4. Physiological Studies

3.4.1. "In-Gel" Enzyme Activity Assay

The described enzyme activities can be measured spectroscopically. However, the advantage of measuring the activity "in-gel" is the possibility to dissect the different enzymes by separating them in a native acrylamide gel. Since *P. anserina* has different SODs and catalases, the "in-gel" activity assay allows the assignment of the activity to the different isoenzymes.

"In-gel" SOD activity assay

For staining of the gels, nitro blue tetrazolium chloride (NBT), riboflavin and tetramethylenediamine (TEMED) as well as dimethylformamide are used as described (31).

1. Following resolving and stacking gel were used:
   Resolving gel (10%): 3.3 mL 30% acrylamide (acrylamide–bisacrylamide 27.5: 1), 2.2 mL 1.5 M Tris–HCl (pH 8.9), 4.5 mL H_2O, 50 µL 10% APS (0.01 g/100 µL H_2O), 16.7 µL TEMED (see Note 30).

   Stacking gel (5%): 850 µL 30% acrylamide (acrylamide–bisacrylamide 27.5: 1), 850 µL 1.5 M Tris–HCl (pH 8.9), 3.3 mL H_2O, 50 µL 10% APS (0.01 g/100 µL H_2O), 5 µL TEMED (see Note 30).
2. 75–150 µg protein samples are loaded on a native acrylamide gel (5% stacking gel, 10% resolving gel) and separated electrophoretically at 100 V and RT in native running buffer until the dye of the native loading dye has reached the bottom of the gel.
3. Next the gel is rinsed with a 0.1 M potassium phosphate buffer (pH 7.8) before incubated in the dark for 20 min on a rocking platform in 10 mL potassium phosphate buffer with 400 µL NBT solution (50 mg/mL NBT, dissolved in 70% dimethylformamid) (see Note 31).
4. Subsequently the solution is discarded and the gel is soaked in 10 mL potassium phosphate buffer supplemented with 10 µL TEMED and 200 µL riboflavin solution (1 mg/mL riboflavin, dissolved in 0.1 M potassium phosphate buffer) (see Note 32). Incubation occurs in the dark for 20 min on a rocking platform.

5. Thereafter, the gel is illuminated on a light table for 5–10 min to initiate the photochemical reaction. Regions of SOD activity remain white while the rest of the gel becomes dark purple.
6. When the bands have appeared, the gel is washed with water and imaged by scanning (see Note 33).

"In-gel" catalase activity assay

The "in-gel" catalase staining method is done as previous described by Woodbury et al. (32).

1. Following resolving and stacking gel were used:
   Resolving gel (10%): 3.3 mL 30% acrylamide (acrylamide–bisacrylamide 27.5: 1), 2.2 mL 1.5 M Tris–HCl (pH 8.9), 4.5 mL H_2O, 50 µL 10% APS (0.01 g/100 µL H_2O), 16.7 µL TEMED (see Note 30).
   Stacking gel (5%): 850 µL 30% acrylamide (acrylamide–bisacrylamide 27.5: 1), 850 µL 1.5 M Tris–HCl (pH 8.9), 3.3 mL H_2O, 50 µL 10% APS (0.01 g/100 µL H_2O), 5 µL TEMED (see Note 30).
2. The secreted protein samples are loaded on a native acrylamide gel and separated electrophoretically at 70 V and 4°C overnight (15 h) in native running buffer.
3. Following the electrophoresis, the gel is washed three times 15 min in water and incubated in a 900 µM H_2O_2 solution for 10 min in the dark on a rocking platform.
4. Subsequently, the gel is transferred into 30 mL freshly prepared solution containing 2% ferric chloride ($FeCl_3$) and 2% potassium ferricyanide ($K_4(Fe(CN)_6)$).
5. The gel tray is gently agitated over a light table until a green color appears in the gel.
6. After rinsing the gel with water, it is documented for further analysis.

3.4.2. Photometric Measurement of Catalase Activity

Quantitative photometric measurement of H_2O_2 degradation is performed in quartz glass cuvettes by quantifying the absorption at 240 nm in intervals of 10 s for a total of 10 min.

1. The cuvette is loaded with 300 µL of a 10 mM potassium phosphate buffer (pH 7.0) and 100 µL of a 300 mM H_2O_2 solution dissolved in 10 mM potassium phosphate buffer are added.
2. After reaching a constant absorption, 100 µL of a 0.02 µg/µL protein solution, dissolved in 10 mM potassium phosphate buffer, is added.
3. The percentage absorption decrease (ΔAbs) at 240 nm per time, representing the catalase activity, is calculated based on the amount of the linear slope after addition of the protein solution (catalase activity = ΔAbs/µg protein × s).

3.4.3. Oxygen Measurements of Physiologically Coupled Mitochondria

Oxygen consumption is measured using Clark type electrodes. In principle the measurement is based on the electrochemical reduction of oxygen at a negatively polarized electrode. These electrodes can be purchased from e.g., Rank Brothers Ltd (Cambridge, England). A special high-resolution respirometer is produced by the Oroboros company (OROBOROS® INSTRUMENTS GmbH, Innsbruck, Austria), allowing the highly sensitive measurement of oxygen flux rates of less than 1 pmol/s cm^3. This is especially relevant if the oxygen consumption of isolated mitochondria is determined.

To assess mitochondrial function, especially impairments in the respiratory chain, mitochondria with intact inner mitochondrial membrane preserving the membrane potential, have to be isolated. To demonstrate the intactness of the mitochondria, "state 4" (oxygen consumption of isolated mitochondria in the absence of ADP and inhibitors, basal respiration rate) and "state 3" (oxygen consumption of isolated mitochondria in the presence of ADP, maximal oxygen consumption rate associated with ATP production) respiration rates are measured. If the membrane potential is preserved, electron transport should lead to the oxidative phosphorylation of ADP. In "state 4" by addition of a substrate to the mitochondria, the formation of reducing equivalents ($NADH + H^+$, $FADH_2$) is stimulated. By introducing "state 3" through the addition of ADP, ATP production and thus the activity of the respiratory chain is promoted. In "state 3," compared to "state 4," there is an increased oxygen uptake, due to improved oxygen consumption caused by the production of ATP.

Before measurement, the oxygen electrode has to be calibrated according to manufacturer's instructions (e.g., regular replacement of teflon membrane, measurement of basal line after complete removal of oxygen by sodium dithionite).

The measurement of the oxygen consumption in the presence of KCN (inhibitor of cytochrome c oxidase, complex IV) or SHAM (salicylhydroxamic acid, inhibitor of the alternative oxidase AOX) allows a deduction on the composition of the respiratory chain. For example, copper-deficiency leads to the activation of PaAOX, which is able to replace the copper-containing complex IV as alternative terminal oxidase.

Oxygen measurement

1. 300 µg mitochondria are loaded with the oxygen buffer in a cuvette.
2. The cuvette is sealed free of air and the recording is started. The decrease in oxygen concentration of the buffer will be recorded until a constant oxygen consumption rate is reached.
3. Then, pyruvate/malate as substrates are added (final concentration: 20 mM/5 mM) and "state 4" respiration is recorded.

4. As soon as a constant value is reached, ADP is added (final concentration: 300 μM), to trigger "state 3" respiration.
5. As soon as a constant value is reached, SHAM (final concentration: 4 mM) is added to inhibit the AOX or KCN (final concentration: 2 mM) to inhibit COX (see Note 34).
6. The ratio of the oxygen uptake of "state 4" and "state 3" is set at 100%. The oxygen uptake during inhibition of COX or the AOX is assigned accordingly.

4. Notes

1. After the medium is cooled to 60°C, biotin, thiamine, and micronutrient stock solution is added to the medium, because the nutrient solutions are not heat resistant. Solutions are stored at 4°C.
2. Due to evaporation during sterilization the density is altered and is set with DMPC-H_2O to the refraction index of 1.400.
3. The desalinization solution is stored at –20°C. After prolonged storage of the solution ice crystals can occur, indicating that the concentration of acetone is too low due to evaporation. The solution has to be prepared freshly.
4. GTC without β mercaptoethanol is stable for 3 months. After adding 0.2 M β mercaptoethanol, buffer is stable for 1 month.
5. Add CHAPS and DTT after sterilization or just before use. Optionally, Protease Inhibitor Cocktail (PIC Set IV (Calbiochem Merck, Darmstadt, Germany)) at a 1:100 dilution is added.
6. Senescent mycelium kept in the refrigerator returns to a juvenile state.
7. The dissection pin is sterilized in the flame of a Bunsen burner and subsequently cooled down in the agar of an agar plate.
8. Dilute the spermatia suspension 1:1 with sterile water.
9. Alternatively, petri dishes containing 30 mL M2 can also be used.
10. Glucanex (Novo Nordisk, Bagsværd, Denmark) contains a glucanase, extracted from the fungus *Trichoderma harzianum*, and is used in the wine production to improve clarification and filtration. In *P. anserina*, it digests the cell wall.
11. The mycelium must be carefully scraped from the medium without transferring too much agar medium into the liquid medium.

12. Before the mycelium is added to the glucanex/TPS suspension, the suspension must first be sterilized by filtration.
13. If the cell walls are not sufficiently digested, the mycelium must be incubated longer in the glucanex suspension, but not more than 2.5–3 h of incubation.
14. When the spheroplasts are used immediately, we achieved good regeneration rates. However, during prolonged storage at –80°C, the cells lose the ability to regenerate.
15. phph-1 (Roche, Risch, Switzerland), a plasmid which contains the hygromycin resistance marker but with a frame-shift that leads to a nonfunctional gene expression. This plasmid serves as a negative control.
16. pAN7-1, a plasmid which contains a hygromycin B resistance cassette from *Escherichia coli* (27) and therefore serves as a positive control.
17. Isoamyl alcohol is used for a clear phase separation.
18. Do not allow thawing, otherwise RNA-degrading enzymes are active.
19. Optionally, the pulverized mycelia can be stored at –20°C for some hours until all samples are harvested and pulverized.
20. In the meanwhile, the ultracentrifuge tubes are filled with 3 mL CsCl solution.
21. RNA pellet is easier and completely dissolved when incubated at 60°C.
22. Senescent cultures are inoculated in Fernbach flasks (150 mL CM) and incubated for 4–5 days at 27°C and constant light without shaking.
23. To remove the remaining liquid medium, which dilutes the sample, the mycelium was patted dry with tissues.
24. Do not allow thawing, otherwise proteases are activated again and proteins would be degraded.
25. If required, supernatant is centrifuged again to ensure complete removal of cell debris.
26. It is important to avoid air bubbles which can damage the mitochondria. Antifoam is a reagent which prevents air bubbles.
27. The vacuoles are removed by scraping this part of the pellet off and take it off with a pipette tip.
28. Incubation in liquid medium follows without shaking to prevent cell damage and consequential resultant contamination with total cell extract.
29. Do not squeeze the mycelia due to contaminations with total cell extract.

30. APS and TEMED are added shortly before casting the gels because the polymerization will start after addition.
31. Always prepare the NBT solution fresh just before use.
32. Always prepare the riboflavin solution fresh just before use.
33. Staining and activity bands will intensify over the next 1–4 days.
34. Be careful by handling with SHAM and KCN, because both substances are very toxic.

References

1. Rizet G (1953) Impossibility of obtaining uninterrupted and unlimited multiplication of the ascomycete *Podospora anserina*. C R Hebd Seances Acad Sci 237:838–840
2. Rizet G (1953) Longevity of strains of *Podospora anserina*. C R Hebd Seances Acad Sci 237:1106–1109
3. Marcou D (1961) Notion de longevité et nature cytoplasmatique du determinant de senescence chez quelques champignons. Ann Sci Nat Bot 12:653–764
4. Esser K, Keller W (1976) Genes inhibiting senescence in the ascomycete *Podospora anserina*. Mol Gen Genet 144:107–110
5. Kück U, Kappelhoff B, Esser K (1985) Despite mtDNA polymorphism the mobile intron (plDNA) of the COI gene is present in ten different races of *Podospora anserina*. Curr Genet 10:59–67
6. Stahl U, Lemke PA, Tudzynski P, Kück U, Esser K (1978) Evidence for plasmid like DNA in a filamentous fungus, the ascomycete *Podospora anserina*. Mol Gen Genet 162: 341–343
7. Kück U, Esser K (1982) Genetic map of mitochondrial DNA in *Podospora anserina*. Curr Genet 5:143–147
8. Cummings DJ, Belcour L, Grandchamp C (1979) Mitochondrial DNA from *Podospora anserina*. II. Properties of mutant DNA and multimeric circular DNA from senescent cultures. Mol Gen Genet 171:239–250
9. Osiewacz H, Esser K (1984) The mitochondrial plasmid of *Podospora anserina*: a mobile intron of a mitochondrial gene. Curr Genet 8:299–305
10. Osiewacz HD (2002) Aging in fungi: role of mitochondria in *Podospora anserina*. Mech Ageing Dev 123:755–764
11. Osiewacz HD, Hamann A (1997) DNA reorganization and biological aging. A review. Biochemistry (Mosc) 62:1275–1284
12. Osiewacz HD (2002) Genes, mitochondria and aging in filamentous fungi. Ageing Res Rev 1:425–442
13. Osiewacz HD, Brust D, Hamann A, Kunstmann B, Luce K, Müller-Ohldach M, Scheckhuber CQ, Servos J, Strobel I (2010) Mitochondrial pathways governing stress resistance, life, and death in the fungal aging model *Podospora anserina*. Ann N Y Acad Sci 1197:54–66
14. Luce K, Weil AC, Osiewacz HD (2010) Mitochondrial protein quality control systems in aging and disease. Adv Exp Med Biol 694: 108–125
15. Osiewacz HD (2011) Mitochondrial quality control in aging and lifespan control of the fungal aging model *Podospora anserina*. Biochem Soc Trans 39:1488–1492
16. Scheckhuber CQ, Osiewacz HD (2008) *Podospora anserina*: a model organism to study mechanisms of healthy ageing. Mol Gen Genet 280:365–374
17. Osiewacz HD, Hermanns J (1992) The role of mitochondrial DNA rearrangements in aging and human diseases. Aging (Milano) 4:273–286
18. Esser K (1974) *Podospora anserina*. In: King RC (ed) Handbook of genetics. Plenum Press, New York, pp 531–551
19. Esser K, Tudzynski P (1980) Senescence in fungi. In: Thimann KV (ed) Senescence in plants. CRC, Boca Raton, pp 67–83
20. Osiewacz HD, Scheckhuber CQ (2002) Senscence in *Podospora anserina*. In: Osiewacz HD (ed) Molecular biology of fungal development. Marcel Dekker, New York, pp 87–108
21. Hamann A, Krause K, Werner A, Osiewacz HD (2005) A two-step protocol for efficient deletion of genes in the filamentous ascomycete *Podospora anserina*. Curr Genet 48:270–275
22. El-Khoury R, Sellem CH, Coppin E, Boivin A, Maas MF, Debuchy R, Sainsard-Chanet A (2008) Gene deletion and allelic replacement

in the filamentous fungus *Podospora anserina*. Curr Genet 53:249–258

23. Ridder R, Osiewacz HD (1992) Sequence analysis of the gene coding for glyceraldehyde-3-phosphate dehydrogenase (gpd) of *Podospora anserina*: use of homologous regulatory sequences to improve transformation efficiency. Curr Genet 21:207–213
24. Averbeck NB, Borghouts C, Hamann A, Specke V, Osiewacz HD (2001) Molecular control of copper homeostasis in filamentous fungi: increased expression of a metallothionein gene during aging of *Podospora anserina*. Mol Gen Genet 264:604–612
25. Stumpferl SW, Stephan O, Osiewacz HD (2004) Impact of a disruption of a pathway delivering copper to mitochondria on *Podospora anserina* metabolism and life span. Eukaryot Cell 3:200–211
26. Osiewacz HD, Skaletz A, Esser K (1991) Integrative transformation of the ascomycete *Podospora anserina*: identification of the mating-type locus on chromosome VII of electrophoretically separated chromosomes. Appl Microbiol Biotechnol 35: 38–45
27. Punt PJ, Oliver RP, Dingemanse MA, Pouwels PH, van den Hondel CA (1987) Transformation of Aspergillus based on the hygromycin B resistance marker from *Escherichia coli*. Gene 56:117–124
28. Lecellier G, Silar P (1994) Rapid methods for nucleic acids extraction from Petri dish-grown mycelia. Curr Genet 25:122–123
29. Bradford MM (1976) A rapid and sensitive method for the quantitation of microgram quantities of protein utilizing the principle of protein-dye binding. Anal Biochem 72:248–254
30. Gredilla R, Grief J, Osiewacz HD (2006) Mitochondrial free radical generation and lifespan control in the fungal aging model *Podospora anserina*. Exp Gerontol 41:439–447
31. Flohe L, Otting F (1984) Superoxide dismutase assays. Methods Enzymol 105:93–104
32. Woodbury W, Spencer AK, Stahman MA (1971) An improved procedure using ferricyanide for detecting catalase isozymes. Anal Biochem 44:301–305

Chapter 30

Assessing Chronological Aging in *Saccharomyces cerevisiae*

Jia Hu, Min Wei, Mario G. Mirisola, and Valter D. Longo

Abstract

Saccharomyces cerevisiae is one of the most studied model organisms for the identification of genes and mechanisms that affect aging. The chronological lifespan (CLS) assay, which monitors the survival of a non-dividing population, is one of the two methods to study aging in yeast. To eliminate potential artifacts and identify genes and signaling pathways that may also affect aging in higher eukaryotes, it is important to determine CLS by multiple methods. Here, we describe these methods as well as the assays to study macromolecular damage during aging in yeast, with a focus on genomic instability.

Key words: Aging, Caloric restriction, Genomic instability, Mutation frequency

1. Introduction

Studies using the *Saccharomyces cerevisiae* aging model have uncovered lifespan regulatory pathways that are partially conserved in higher eukaryotes. Here, we describe the standard procedures used to study chronological aging/senescence in yeast. We highlight the importance of utilizing multiple approaches to analyze yeast chronological lifespan (CLS) to rule out system bias and identify genes and signaling pathways that may also affect aging in higher eukaryotes. The methods described here provide straightforward approaches to determine CLS and genomic integrity while avoiding the artifacts that can be caused by the accumulation of toxic levels of acids in the medium or the regrowth of subpopulation of cells within the nondividing cultures.

Lorenzo Galluzzi et al. (eds.), *Cell Senescence: Methods and Protocols*, Methods in Molecular Biology, vol. 965,
DOI 10.1007/978-1-62703-239-1_30,

2. Materials

2.1. Common Materials

- Dextrose (20%, w/v) stock solution.
- Sterile 18.2 MΩ·cm ultrapure water; used for media preparation, serial dilution, and survival analysis in water experiments.
- Synthetic complete dextrose (SDC) medium (Table 1). Medium is prepared without glucose. After sterilization by autoclaving, glucose is added at the desired level. For SDC solid medium, add 20 g/L Bacto™ Agar.

Table 1
Synthetic complete glucose (SDC) medium

Component	g/L
D-Glucose	20
Ammonium sulfate	5
Nitrogen base (-AS/-AA)	1.8
NaH_2PO_4	1.4
	mg/L
Adenine	80
L-Arginine	40
L-Aspartic acid	100
L-Glutamic acid	100
L-Histidine	80
L-Isoleucine	60
L-Leucine	120
L-Lysine	60
L-Methionine	80
L-Phenylalanine	60
L-Serine	400
L-Threonine	200
L-Tryptophan	80
L-Tyrosine	40
L-Valine	150
Uracil	80

SDC (18) is supplemented with a four-fold excess of histidine, leucine, tryptophan, and uracil to compensate the auxotrophies in the DBY746 strain. Similar supplementations should be carried out based on the autotrophies of the genetic background used. Adjust to pH 6.0 with NaOH.

- Synthetic complete (SC) medium with various carbon sources: SC medium without carbon source; SC medium supplemented with low glucose (e.g., 0.5%, w/v) or other carbon sources such as ethanol (e.g., 0.8%, w/v), glycerol (1–3%, w/v), or acetic acid (10–100 mM).
- Amino acid dropout media:
  - SDC Arg– Can+ medium for Can^r frequency assay: SDC without arginine, with L-canavanine sulfate (60 μg/mL).
  - SDC Arg– Can+ 5FOA+ medium for gross chromosomal rearrangement (GCR) frequency assay: SDC without arginine, L-canavanine sulfate (60 μg/mL), and 5-fluoroorotic acid (5FOA, 1 mg/mL).
  - SDC Trp– medium for Trp^+ reversion and in situ viability assay: SDC without tryptophan.
  - SDC Lys– medium for frame-shift mutation frequency assay: SDC without lysine.
  - SC His– Gal+ medium for homologous/homeologous recombination frequency assay: SC without histidine, with galactose (2%, w/v).
- Yeast extract peptone dextrose (YPD) medium: 10 g/L Bacto™ Yeast Extract, 20 g/L Bacto™ Peptone, 20 g/L Bacto™ Agar. Dissolve in water (up to 900 mL). Autoclave and add glucose stock (20%) to a final concentration of 2%. Mix well and pour the plates.
- Yeast strain: DBY746 *MAT*α *leu2*-3,112 *his3*Δ1 *trp1*-289a *ura3*-52 GAL+.

3. Methods

3.1. Yeast CLS in Liquid Culture

1. From the frozen stock, streak strain of interest onto a YPD plate. Incubate the plate at 30°C for 2–3 days. Inoculate a single colony into 1–2 mL synthetic complete dextrose medium (SDC) and incubate overnight with shaking (220 rpm) at 30°C (see Note 1).
2. Dilute the overnight culture into fresh SDC medium (usually 10 mL) to OD_{600}: ~0.1 (~1:100 dilution) and incubate with shaking (220 rpm) at 30°C (see Notes 2 and 3). This time point is considered day 0 of the chronological aging. Note that the use of aluminum foil caps (Fig. 1) minimizes evaporation and also reduces exposure of culture to oxygen (see Notes 4 and 5).
3. Starting at day 3, remove two aliquots of 10 μL from the flask, dilute 10,000 times in sterile water, plate 10 μL of the diluted

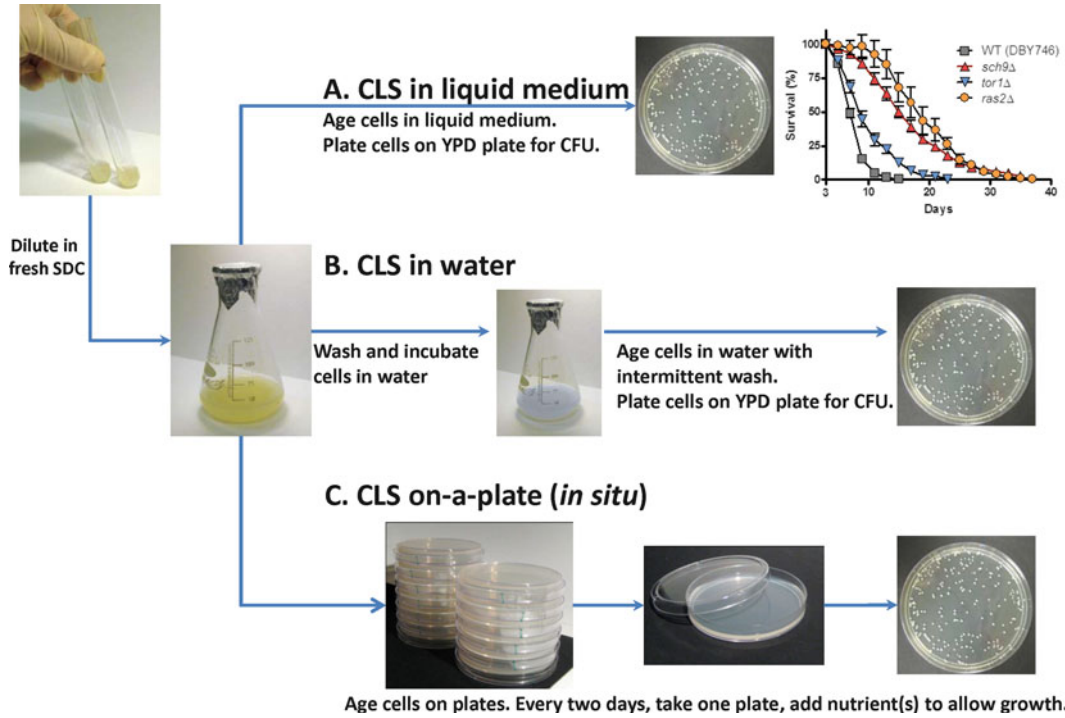

Fig. 1. Yeast chronological lifespan (CLS) analyses. Inoculate freshly streaked colony into 1 mL SDC medium and let grow overnight. (**a**) For a typical liquid SDC CLS analysis, the overnight cultures are diluted (1:100) in to fresh SDC medium to a final volume of 10 mL (with flask to culture volume of 5:1). This time point is considered day 0. Every 2 days, aliquots from the culture are properly diluted and plated onto YPD plates for Colony Forming Units (CFUs) evaluation. Viability at day 3, when the yeast had reached the stationary phase, is considered to be the initial survival (100%). Representative results of chronological survival of the wild-type (DBY746), *sch9*Δ, *tor1*Δ, and *ras2*Δ are shown (replotted from Wei (1)). (**b**) For extreme CR/starvation, cells from 3-day-old SDC culture are washed three times with sterile water and resuspended in water. Every 2–4 days, cells from the water cultures are washed to remove nutrients released from dead cells. (**c**) Chronological survival on solid medium. Day 1 SDC cultures are diluted and plated onto agar plates (extreme calorie restriction) or tryptophan dropout (SC-TRP) plates. Plates are incubated at 30°C for the duration of the assay. Every 2 days, one plate from each set is retrieved and appropriate nutrients are added to allow growth.

culture (i.e., 10^4–10 μL) onto YPD plates every 2 days (see Note 6). Incubate plates at 30°C for 2–3 days and count colony forming unit (CFU).

4. The day 3 CFU number is considered to be the 100% survival. Dilution factors of aging culture in the subsequent days should be adjusted to ensure ~20–100 colonies per plate can be counted (e.g., 10^4–10, 10^4–30, and 10^3–10 μL). For wild-type cells (DBY746 background), the culture reaches the 50% survival by days 6–7 and 1% survival around day 11; for the BY4741 background the 50% survival is reached after approximately 15 days (see Note 7).

3.2. Yeast CLS in Water

This water assay for CLS serves three purposes: (1) it prevents any regrowth (GASP) which would invalidate the CLS assay (see Note 7); (2) it allows the assessment of CLS independently of the composition and age-dependent modification of the extracellular medium; (3) it serves as a way to assess survival under extreme calorie restriction condition, which represents a starvation environment frequently encountered by microorganisms.

1. Proceed as in steps 1–3 in Subheading 3.1.
2. Remove conditional medium by centrifuging (1,400 × *g* for 5 min) at room temperature.
3. Wash the cell pellet with sterile water (equal volume as the original culture) three times.
4. Resuspend cell pellet in water (equal volume as the original culture), incubate with shaking (220 rpm) at 30°C.
5. Every 2 days, aging culture must be washed with sterile water and resuspended in equal volume of water to remove any nutrients or metabolites (see Note 8). Attention should be paid to aseptic practices as water cultures are particularly prone to contamination during the advanced phases of survival.
6. Perform viability assay by sampling the aging culture as described in Subheading 3.1. This starvation condition will lead to a doubling of mean CLS in the wild-type DBY746 strain (1).

3.3. Yeast CLS on Solid Medium

The in situ viability system that utilizes the auxotrophy of the DBY746 strain (*trp*1) circumvents the regrowth/GASP problem mentioned above and can be used to test the effect of constant exposure to the selected external nutrients or stimuli on yeast CLS (2). This in situ viability assay is also more closely related to the yeast replicative lifespan (RLS) model where cells are constantly exposed to abundant nutrients for the duration of lifespan analysis (see Note 9). The tryptophan deficiency was selected since it is one of the deficiencies that does not result in reduction of CLS due to starvation.

1. Proceed as in steps 1–3 in Subheading 3.1.
2. Dilute the culture with sterile water to 100–200 cell/10 μL (usually 10^4-fold dilution of the day 3 culture) and 1,000 cells/10 μL (10^3-fold dilution).
3. Plate two aliquots of 10–30 μL of diluted culture onto one tryptophan dropout SDC plate. For each strain, prepare a set of 8–20 plates and labele according to plating density (e.g., 10^4-fold diluted, plate 10 μL or 10^4-10, 10^4–30, 10^3–10, and 10^3–30 μL), which ensures that 10–100 colonies can be counted in anticipation of decreasing viability during aging.
4. Incubate the plate set at 30°C for the duration of the lifespan analysis (see Note 10).

5. On the day of plating and every 2 days subsequently, remove one plate and slowly and drop-wise add 0.5 mL tryptophan (2 mg/mL) to allow viable cells to grow. Incubate the plate at 30°C for additional 2–3 days. Record the CFU as the viability of the day of tryptophan addition. The CFU on day 3 is considered 100% survival.

Variations of in situ viability assay:

1. For extreme calorie restriction conditions, age cells on agar plates (see Subheading 3.2). Add 1 mL 2× YPD instead of tryptophan on subsequent days to allow growth and CFU count.
2. For carbon source-specific growth conditions, age cells on plates with tryptophan dropout synthetic complete medium but with various carbon sources, e.g., various concentrations of glucose (calorie restriction by glucose limitation, e.g., 0.5 or 0.05% vs. the standard 2% glucose), various carbon sources such as ethanol, glycerol, acetic acid, can be used in place of glucose (3). Add 1 mL glucose/tryptophan solution (20% glucose and 1 mg/mL tryptophan) to allow growth and CFU count.

3.4. Nuclear DNA Mutation Frequency During Chronological Aging

Canavanine resistance (Can^r). Mutations in the plasma membrane arginine permease (CAN1/YEL063) render cells resistant to the arginine analogue L-canavanine. Spontaneous frequency of a wide variety of mutations can be evaluated by monitoring the frequency of canavanine resistance (Can^r) in chronologically aging cultures. Sequencing of the CAN1 gene in Can^r colonies collected at different time points can provide the age-dependent mutation spectrum data (with Mutation Surveyor, SoftGenetics) (4).

Base substitutions (Trp$^+$ reversion). Strains with *trp1*-289 contain an amber mutation (C403T) in the *TRP1*/YDR007W coding sequence. The frequency of *trp1*-289/wild-type reversion allows the estimation of the frequency in base substitutions during yeast chronological aging (5).

Frame-shift mutations. The Lys$^-$ strain EH150 (*MATa*, *lys2ΔBglII*, *trp1*-Δ, *his3*-Δ*200*, *ura3-52*, *ade2-1o*) harbors a *lys2ΔBgl*II mutation that was constructed by inserting four nucleotides to create a *Bgl*II restriction enzyme site in the *LYS2* gene. The resulting +4 shift in the open reading frame results in auxotrophy for lysine that can be reversed by small insertion/deletion mutations (6, 7).

Gross chromosomal rearrangements (GCRs). *HXT13*/YEL069C is located 7.5 kb telomeric to *CAN1* (YEL063C) on chromosome V. Stains carrying *hxt13::URA3* can be used to measure mutation frequency in both *CAN1* and *URA3* genes, which render cells resistance to L-canavanine and 5-fluoroorotic acid (5FOA), respectively. Considering the low frequency of point mutations that occur in both genes, analysis of the Can^r 5FOA^r frequency provides an estimation of GCRs by assessing the lack of both genes (8).

Homologous and homeologous recombinations. To monitor the level of homologous (100%) and homeologous (91%) recombinations during chronological aging, strains harboring *HIS3*::intron-IR-*URA3* with either 100% homologous inverted repeats (IRs) (pSR406) or 91% homeologous IRs (pSR407) at the *HIS3* locus are studied (9). Recombination between the IRs allows the expression of functional His3 protein.

1. In parallel to normal viability assay (see Subheading 3.1), remove an appropriate amount of cells from the aging cultures (see Notes 11 and 12).
   (a) For Can^r mutation, start with ~2×10^7 cells (~200 µL of day 3 SDC culture).
   (b) For Trp^+ reversion, start with ~10^8 cells (500–1,000 µL of day 3 culture).
   (c) For Lys^+ frame-shift mutation, start with ~10^8 cells (500–1,000 µL of day 3 culture).
   (d) For GCRs, start with 2–3×10^8 cells (2–3 mL of day 3 culture).
   (e) For homologous and homeologous recombination, start with ~5×10^7 cells (200–500 µL of day 3 culture).
2. Pellet the cells in a bench-top centrifuge (1,400 × *g* for 5 min).
3. Resuspend cells in 1 mL sterile water, and pellet the cells again.
4. Resuspend cell pellet in 100 µL of water. Plate cells,
   (a) For Can^r mutation, on SDC Arg– Can+ plates.
   (b) For Trp^+ reversion, on SDC Trp– plates.
   (c) For Lys^+ frame-shift mutation, on SDC Lys– plates.
   (d) For GCRs, on SDC Arg– 5FOA+ plates.
   (e) For homologous and homeologous recombination, on SC His– Gal+ plates (see Note 13).
5. Count CFUs after a 3–4 days' incubation at 30°C. The mutation frequency is normalized to the number of viable cells (as described in Subheading 3.1).

Complementary to the in situ viability assay (Subheading 3.2), age-dependent Trp^+ reversion, Lys^+ frame-shift mutation, recombination, or Can^r can also be studied in cells aged on plates.

1. Proceed as step 1–3 in Subheading 3.2.
2. Suspend cells in water at ~10^8 cells/100 µL. Plate 20–200 µL of cells suspension on to Trp-, Lys-, His-dropout, or Can+ SDC plates.
3. Incubate plates at 30°C for the duration of the CLS assay.
4. Every 2 days (or at the time point of interest), score the newly emerging colonies.

5. Mutation frequency is estimated by normalizing newly emerging colonies to the total number of viable cells of the specific day (as described in Subheading 3.2).

4. Notes

1. CLS assay should be carried out using freshly streaked cells. Master plates should be kept at 4°C and plates >1 week old should be discarded. Three inoculums from independent colonies should be prepared for each strain to provide biological replicas.
2. Maintain a 1:5 ratio of culture/flask volume (e.g., 10 mL culture in a 50 mL flask) to ensure proper mixing and aeration.
3. The standard CLS in liquid culture can be augmented to study the effects of various nutrients on chronological aging. For example, dilution of overnight culture in glucose-limited SC medium (e.g., 0.5 or 0.05% glucose instead of the standard 2% in SDC) leads to lower population saturation density on day 3, but much extended mean (50% survival) and maximal (10% survival) lifespans.
4. The uses of different flask closures greatly affect aeration, evaporation rate, and metabolism of microorganism cultures (10–12). The commonly used loose plastic cap and cotton plugs result in high evaporation rate under the standard shaking speed. Due to the long-lasting nature of the chronological aging study, we chose to use aluminum foil cap (Fig. 1), which leads to less than 15% volume loss at the end of a typical 2-weeks long CLS experiment and still allows a level of oxygen sufficient for cell growth on non-fermentable carbon sources. Moreover, the use of plastic caps that allow maximum aeration will cause early depletion of ethanol and increased accumulation of acetic acid.
5. Special attention should be paid to culture conditions, such as culture density (due to evaporation), acidification, and accumulation of various metabolites when interpreting experimental results. In a typical CLS experiment, accumulation of metabolites leads to medium acidification (13, 14). Depending on the culture volume, shake speed, type of flask closure, and strain of interest, the pH of the medium normally drops from 6 to 3–4. Constant adjustment of pH by addition of NaOH or buffer solution (e.g., MES) is *not* recommended since it often leads to regrowth/GASP.
6. For short-lived strains, daily assessment of viability is recommended. Viability can also be confirmed by live/dead staining, e.g., FUN1 (Invitrogen). Dot assay could also be used to

obtain the approximate survival rate of an aging culture as an initial estimation of viability and lifespan (15).

7. In the liquid culture, a small fraction of the surviving cells may reenter the cell cycle using the remaining nutrients or those released from lysed dead cells to proliferate, a phenotype termed regrowth or GASP (growth advantage in stationary phase). This phenotype is often associated with increased oxidative stress and/or decreased protection in the cell (14, 16). We define regrowth as an increase in viability or stabilization in viability for three consecutive samplings in the high mortality phase during chronological aging. CLS analysis in water or on plate can eliminate the complication of regrowth (see Subheadings 3.2 and 3.3).
8. During yeast chronological aging, dead cells lyse and release nutrients. Accumulation of various metabolites affects extra- and intracellular pH, signaling, and viability of yeast. Intermittent wash of aging culture removes metabolites whose generation may be strain-specific and reduces potential systematic bias such as selecting cells resistant to media acidification or acetic acid cytotoxicity.
9. The survival curve of approximately 200 wild-type DBY746 cells plated on SC Trp– plates supplemented with 2% glucose is reminiscent of that in the standard liquid SDC medium (3). However, certain amino acid auxotrophy may lead to a dramatic reduction of chronological survival, which may be strain specific. For example, survival of DBY746 is much reduced on SDC Leu– plates.
10. Water loss due to evaporation could pose a problem for the long-term in situ chronological aging study. Every 2–4 days, dropwise add 0.5–1.0 mL sterile water to each plate and return the plates to incubator without disturbance.
11. Percoll density gradient fractionation can be used to isolate quiescent and non-quiescent cells to evaluate their contribution in nuclear DNA mutations in chronologically aged cells (4, 17).
12. Age-dependent mutation frequency varies greatly depending on the strain background, genetic manipulation, culture conditions, as well as regrowth/gasp and extremely low survival. Preliminary experiments should be carried out to determine the mutation frequency range before performing the full-scale lifespan analysis. Multiple biological replicas should be included in the study; and, both liquid and in situ viability/mutation assays should be carried out to corroborate the results.
13. Galactose is used to induce the expression of *HIS3* in the recombination frequency assay. For strains with slow growth on galactose, after overnight incubation at 30°C, drop-wise add 1 mL 20% glucose onto the plates, return plates to 30°C incubator.

References

1. Wei M, Fabrizio P, Hu J, Ge H, Cheng C, Li L, Longo VD (2008) Life span extension by calorie restriction depends on Rim15 and transcription factors downstream of Ras/PKA, Tor, and Sch9. PLoS Genet 4:e13
2. Madia F, Gattazzo C, Fabrizio P, Longo VD (2007) A simple model system for age-dependent DNA damage and cancer. Mech Ageing Dev 128:45–49
3. Wei M, Fabrizio P, Madia F, Hu J, Ge H, Li LM, Longo VD (2009) Tor1/Sch9-regulated carbon source substitution is as effective as calorie restriction in life span extension. PLoS Genet 5:e1000467
4. Madia F, Wei M, Yuan V, Hu J, Gattazzo C, Pham P, Goodman MF, Longo VD (2009) Oncogene homologue Sch9 promotes age-dependent mutations by a superoxide and Rev1/Polzeta-dependent mechanism. J Cell Biol 186:509–523
5. Capizzi RL, Jameson JW (1973) A table for the estimation of the spontaneous mutation rate of cells in culture. Mutat Res 17:147–148
6. Heidenreich E, Novotny R, Kneidinger B, Holzmann V, Wintersberger U (2003) Non-homologous end joining as an important mutagenic process in cell cycle-arrested cells. EMBO J 22:2274–2283
7. Heidenreich E, Wintersberger U (1998) Replication-dependent and selection-induced mutations in respiration-competent and respiration-deficient strains of *Saccharomyces cerevisiae*. Mol Gen Genet 260:395–400
8. Chen C, Kolodner RD (1999) Gross chromosomal rearrangements in *Saccharomyces cerevisiae* replication and recombination defective mutants. Nat Genet 23:81–85
9. Datta A, Adjiri A, New L, Crouse GF, Jinks Robertson S (1996) Mitotic crossovers between diverged sequences are regulated by mismatch repair proteins in *Saccaromyces cerevisiae*. Mol Cell Biol 16:1085–1093
10. Chain EB, Gualandi G (1954) Aeration studies. II. Rend Ist Sup Sanit 17:1109–1163
11. Schultz JS (1964) Cotton closure as an aeration barrier in shaken flask fermentations. Appl Microbiol 12:305–310
12. McDaniel LE, Bailey EG (1969) Effect of shaking speed and type of closure on shake flask cultures. Appl Microbiol 17:286–290
13. Burtner CR, Murakami CJ, Kennedy BK, Kaeberlein M (2009) A molecular mechanism of chronological aging in yeast. Cell Cycle 8:1256–1270
14. Fabrizio P, Battistella L, Vardavas R, Gattazzo C, Liou LL, Diaspro A, Dossen JW, Gralla EB, Longo VD (2004) Superoxide is a mediator of an altruistic aging program in *Saccharomyces cerevisiae*. J Cell Biol 166:1055–1067
15. Smith DL Jr, McClure JM, Matecic M, Smith JS (2007) Calorie restriction extends the chronological lifespan of *Saccharomyces cerevisiae* independently of the Sirtuins. Aging Cell 6: 649–662
16. Fabrizio P, Pletcher SD, Minois N, Vaupel JW, Longo VD (2004) Chronological aging-independent replicative life span regulation by Msn2/Msn4 and Sod2 in *Saccharomyces cerevisiae*. FEBS Lett 557:136–142
17. Allen C, Buttner S, Aragon AD, Thomas JA, Meirelles O, Jaetao JE, Benn D, Ruby SW, Veenhuis M, Madeo F, Werner-Washburne M (2006) Isolation of quiescent and nonquiescent cells from yeast stationary-phase cultures. J Cell Biol 174:89–100
18. Guthrie C, Fink GR (1991) Guide to yeast genetics and molecular biology. Methods Enzymol 194:1–863

Chapter 31

Assessing Aging and Senescent Decline in *Caenorhabditis elegans*: Cohort Survival Analysis

Eirini Lionaki and Nektarios Tavernarakis

Abstract

The nematode *Caenorhabditis elegans* provides a versatile and expedient platform for the genetic and molecular dissection of mechanisms underlying senescent decline and aging. Indeed, pioneering studies in this organism revealed the first genes and pathways directly influencing lifespan. In this chapter, we present routine, mainstream methods, developed for monitoring aging and senescent decline in *C. elegans*. These procedures allow the assessment of lifespan parameters on solid growth media that are typically used for rearing nematodes.

Key words: Aging, *Caenorhabditis elegans*, Lifespan, Longevity, Nematode, Senescent decline, Stochastic death, Survival analysis

1. Introduction

Aging and senescent decline are global phenomena that affect all living organisms. Senescence at the level of the whole organism can be broadly defined as the declining ability to maintain homeostasis and cope with inevitable spontaneous decay of cells, tissues organs, and biological systems, through time. Organismal senescence, or aging, involves all the obvious changes associated with old age that can be referred to as senescent decline. Although aging is largely driven by random and stochastic degenerative processes, it is extensively influenced by both genetic and environmental signals (1). The field of aging research has made significant progress and gained increasing attention during the last 50 years; however many mysteries still remain unresolved.

The roundworm *Caenorhabditis elegans*, a tiny (~1 mm total length), free-living, soil-dwelling nematode is one of the first and most widely used model organisms for aging research. Under standard laboratory cultivation conditions (20°C), animals complete a

Lorenzo Galluzzi et al. (eds.), *Cell Senescence: Methods and Protocols*, Methods in Molecular Biology, vol. 965,
DOI 10.1007/978-1-62703-239-1_31,

life cycle (egg to sexually mature adult) in 3.5 days. During this period, worms go through four successive larval stages (termed L1–L4), separated by molting events. After animals reach adulthood, they survive for a conveniently short period of about 2–3 weeks at 20°C. *C. elegans* is easily and inexpensively maintained in the laboratory, both on solid and in liquid media, feeding mainly on bacteria *E. coli* (monoxenic media), at temperatures that range from 15 to 25°C. Because *C. elegans* is a poikilotherm, its life cycle and lifespan are greatly influenced by the environmental temperature (2, 3). The predominant sexual form is the hermaphrodite but males also appear in populations at a low frequency (~0.1%), and can be used in genetic crosses. The reproductive period of a hermaphrodite lasts for the first 5 days of adulthood. One wild-type adult lays approximately 300 fertilized eggs within this period.

The body of *C. elegans* is transparent, permitting the detailed study of its embryonic and post-embryonic development. The complete cell lineage, from zygote to adult has been precisely mapped (4, 5). An adult hermaphrodite comprises 959 somatic cells, all of which are post-mitotic. The *C. elegans* germ line is an immortal lineage that gives rise to diploid germ cells, which in turn undergo meiotic division and differentiation, producing initially sperm and subsequently oocytes. By contrast, the soma of *C. elegans*, which is made up of 959 post-mitotic cells, experiences senescent decline, and gradually develops phenotypes that can be easily recognized as aging. Typical examples of such phenotypes are a decline and then pause of progeny production, progressively slower movement, darker hue due to accumulation of fat and the age pigment lipofuscin, reduced ultradian rhythms (feeding and defecation frequencies), and others. These easily discernible phenotypes, coupled with a relatively short lifespan and the capacity to establish genetically identical populations through clonal self-reproduction make *C. elegans* a particularly useful and convenient organism for the study of the biology of aging. Additional, relevant features, which benefit experimental efforts are the uncomplicated and flexible genetic manipulation (RNAi, introduction of transgenes, gene knock outs), the fully mapped nervous system and the extended arsenal of tools for in vivo imaging of cellular and developmental processes.

In this chapter, we describe a well-established method for acquiring and processing survival data for the nematode. We provide detailed information for cohort analysis of animals grown on solid growth media, including population synchronization techniques, censoring of death events, recording and analysis of survival data, and finally construction of survival curves. Alternative methods of acquiring survival data suitable for implementation in high-throughput and longitudinal studies are described in the accompanying chapter (see Chapter 32).

2. Materials

- Wormpick: Cut 3 cm of platinum wire (90% platinum, 10% iridium wire, 0.010 inches diameter; e.g., Tritech Research, Los Angeles, CA) and flatten one end using pincers or a light hammer. Break off the thin part of a glass Pasteur pipette. Melt the glass at the site of breakage on a Bunsen burner and attach the sharp end of the platinum wire. When using the wormpick always sterilize the tip over a flame.
- Nematode Growth Medium Agar (NGM) plates: For 1 L, add 3 g NaCl, 2.5 g Bacto-Peptone, 0.2 g streptomycin, 17 g agar, double distilled (dd) H_2O up to 975 mL. Add a magnetic stirrer in the medium and autoclave it. Let it cool down (with stirring) to approximately 55°C and then add 25 mL Phosphate Buffer 1 M pH 6.0 (sterile), 1 mL $CaCl_2$ 1 M (sterile), 1 mL $MgSO_4$ 1 M (sterile), 1 mL cholesterol 5 mg/mL (sterile) and 1 mL nystatin 10 mg/mL (sterile). Pour 11.5 mL of NGM agar in each plate.
- Cholesterol stock 5 mg/mL: For 100 mL, add 0.5 g cholesterol in 100 mL of absolute ethanol. Stir to dissolve. Store at 4°C (see Note 1).
- Nystatin suspension 10 mg/mL: For 50 mL, add 0.5 g nystatin, in 70% ethanol in dd H_2O. This is going to be a suspension, so it needs shaking prior to use (see Note 2).
- Streptomycin stock 100 mg/mL: For 10 mL, add 1 g of streptomycin in 10 mL of dd H_2O. Shake until the streptomycin is dissolved. Filer-sterilize the solution and store at 4°C.
- Phosphate buffer 1 M: For 1 L, add 102.2 g KH_2PO_4, 57.06 g K_2HPO_4, adjust the volume to 1 L with dd H_2O and autoclave.
- Luria Bertani (LB) medium and agar plates containing streptomycin: For 1 L, add 10 g Bacto-tryptone, 5 g yeast extract, 10 g NaCl. Adjust pH to 7.0 with NaOH, adjust volume to 1 L with dd H_2O and autoclave. For LB agar plates add 20 g of agar to the previous mixture and a magnetic stirrer prior to autoclaving. After autoclaving let the mixture cool down to 55°C (with stirring when it is LB agar) add 1 mL of streptomycin stock 100 mg/mL and poor into petri dishes (10 mm diameter).
- Petri dishes (60 mm × 15 mm).
- Peristaltic pump.
- Dissecting microscope.
- Incubator for stable temperature.
- *E. coli* strain OP50-1.

3. Methods

3.1. Preparation of NGM Plates with Bacterial Lawn (Seeded Plates)

1. Streak the bacterial *E. coli* strain OP50-1 on LB agar plates containing the antibiotic streptomycin (6).
2. Incubate for 16–18 h at 37°C.
3. Pick a single colony and inoculate 50 mL of LB for ~4–6 h at 37°C.
4. Disperse 100–200 μL of OP50-1 culture on a medium plate and spread it with the tip of a glass pipette or with a glass rod in order to form a circle in the center of the plate surface (see Note 3).
5. Incubate the plates at room temperature overnight to allow the bacterial lawn to grow before transferring worms to the plate.

3.2. Choosing Parental Worms

1. Add five (5) L4 larvae on a freshly seeded NGM plate. Prepare five (5) such plates.
2. Incubate the plates at 20°C (see Note 4).
3. Four days later the plates contain mixed worm population from which we can start the lifespan experiment (Fig. 1, step 1) (see Note 5).

3.3. Synchronizing Populations

There are several ways of synchronizing populations to be used in the assay. The most common are described in the following paragraphs, and summarized in Fig. 1 (step 2: a, b, c).

3.3.1. Egg Preparation from Gravid Adults

1. Starting from a plate with a well-fed, mixed population (prepared in Subheading 3.2) that contains plenty of gravid adult worms, embryos are gathered by dissolving the bodies of embryo-bearing, gravid adult worms in sodium hypochlorite solution (see Note 6).
2. Disperse the egg suspension using a glass pipette in 2–3 seeded plates, and allow eggs to hatch for 3 days in a 20°C incubator.
3. By the end of the third day, randomly pick worms (L4 larvae) from this synchronous population and transfer them to new plates (10–15 worms per plate), to begin the lifespan experiment.

Depending on whether or not post-embryonic development is included in the lifespan assay, either the day of hatching or the first day of adulthood may be set as day 1 of experiment (Fig. 1, step 2a).

3.3.2. Egg-Laying for a Short Period of Time

An alternative way of acquiring synchronized embryos is to allow gravid adults to lay their eggs for a short period of time (a few hours) on freshly seeded plates (Fig. 1, step 2b).

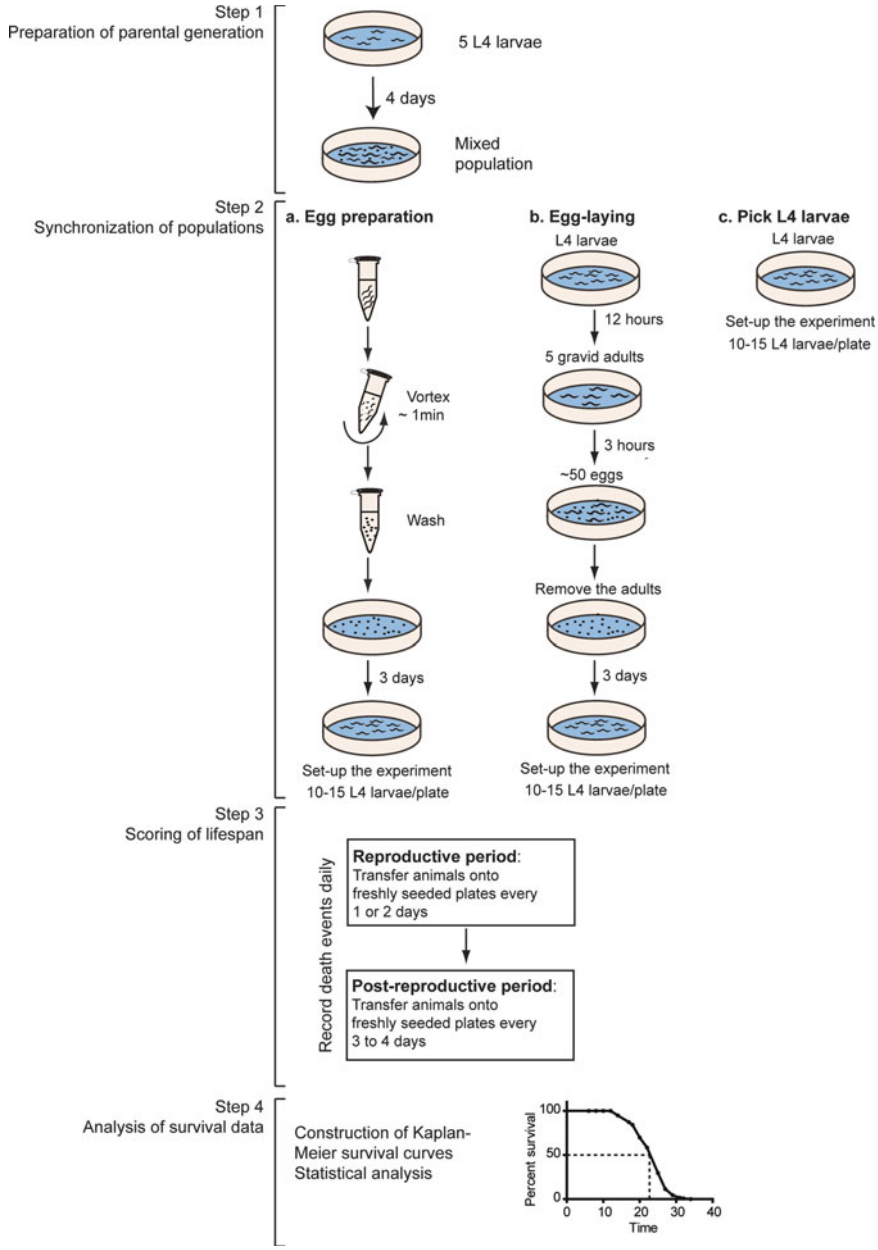

Fig. 1. Lifespan assay on solid media. The schematic shown here summarizes the protocol, including preparation of the parental generation grown under ad libitum conditions, and the subsequent synchronization of experimental populations. Three different procedures are depicted: (**a**) Egg preparation by lysing gravid adult worms, (**b**) egg-laying for a few hours on freshly seeded plates, and (**c**) manual picking of L4 larvae. Worms are transferred to freshly seeded plates every other day during their reproductive period, and every 3–4 days during the post-reproductive period. Death events are recorded daily. The acquired survival data are analyzed using GraphPad Prism software and a Kaplan–Meier survival plot is constructed.

1. One day before egg-laying, select L4 larvae (starting from a mixed population, see Subheading 3.2) and transfer them to freshly seeded NGM plates.
2. Let the larvae mature overnight at 20°C, until they start laying eggs.
3. Transfer five adults per plate and let them lay eggs for 3 h.
4. Remove the adults from the plate and let the eggs hatch, to begin a synchronous population. When working with the standard wild-type strain (N2), this procedure will give approximately 50 eggs/plate (see Note 7). Day 1 of the assay can be set as either the day of hatching, or the first day of adulthood.

3.3.3. Picking L4 Larvae

This type of synchronization is chosen when the duration of the post-embryonic development period is not included in the assay. L4 animals are selected from mixed populations (prepared in Subheading 3.2). Pick with a platinum wire and transfer to separate plates to start the experiment. Day 1 of this experiment will be the first day of adulthood (Fig. 1, step 2c).

3.4. Setting up the Experiment

An adequately sized population for a lifespan assay typically includes about 100 animals (see Note 8). Usually, experiments are started with populations of more than 100 worms, because it is expected that about 20% of animals will be removed from the assay later on as "censored" (see Subheading 3.5.3).

1. Prepare ten freshly seeded plates per worm population/strain (see Note 9).
2. Transfer 10–15 worms per plate.
3. Annotate plates with numbers from 1 to 10, in order to follow worms on each plate separately (see Note 10).
4. Prepare a chart where the number of alive, dead, and censored worms will be noted each day.

3.5. Scoring Lifespan

In summary, this part of the experiment includes the following steps:

1. Counting of worms daily and transferring when necessary (see below) onto fresh pre-annotated plates.
2. Removing dead and censored worms form the plates.
3. By the end of the experiment, when the worm population shrinks, pool noncontaminated worms from different plates on the same plate.

3.5.1. Reproductive Period: Progeny Separation

1. During the egg-laying period (approximately the first week of adulthood), worms should be transferred to fresh plates daily or every other day, to separate them from their progeny. The egg-laying period may differ between different strains, so the daily transfer routine can be extended or shortened accordingly.

During the reproductive period, it is important that the worms are monitored and recorded every day.

2. To maintain population synchrony without having to transfer parental worms every day, strains with temperature-sensitive fertility defects have been used (for example *fer-15(b26)* or *glp-4(bn2)* mutants). Both these mutants are fertile when grown at 15°C but become sterile when grown at 25°C, starting at the L1 stage. The *fer-15(b26)* allele blocks sperm production at high temperature, while the *glp-4(bn2)* mutation prevents efficient germ line proliferation (7, 8). These fertility mutants have been also used in cases where the genetic trait to be monitored causes deleterious phenotypes (i.e., hatching of eggs inside the uterus) (9).
3. Alternatively, 5-fluoro-2-2deoxyuridine (FUdR), an inhibitor of DNA synthesis that blocks egg-hatching may be used. In this case, L4 worms are transferred to FUdR-containing plates (concentration 120 μM) (see Note 11). The drug can cause complete sterility by inhibiting egg-hatching, within 5 h of its application (10). Lower concentrations of FUdR (25 μM) have also been used successfully (11). However, recent data have shown that FUdR in some cases can affect the overall lifespan of the animals, so it must be used with caution (12, 13).

3.5.2. Post-reproductive Period: Scoring of Lifespan

After, animals stop laying eggs, they can be transferred every 3–4 days or even once a week, depending on the availability and the quality of the food source (see Note 12). However, worms should be counted daily, for deaths to be scored on time and for the removal of censored worms from the plate.

3.5.3. Censoring Individual Death Events

Animals are excluded from analysis (censored) when they display obvious defects that interfere with normal aging, or have been otherwise compromised by experimental mishandling or accidents. Examples of such censoring instances can be:

1. Internal hatching of eggs (bag-of-worms phenotype or bagging): Hermaphrodites carrying internally hatched eggs usually do not move. Upon inspection, newly hatched worms can be spotted moving inside the animal. The mother is literally eaten by its progeny, up until larvae escape by penetrating the cuticle. It is important to remove these animals early on, because worms that escape from bagging parents may already be old enough to be mixed with their parental generation on the plate, altering the results of the experiment.
2. Vulva protrusion: The vulva protrusion phenotype should be dealt with caution as it can also be a trait accompanying some mutant strains. In general, it is advisable to remove animals with vulva protrusion that also show additional signs of sickens such as impaired movement or paralysis.

3. Vulva rupture: These worms appear to drag their intestine that has spilled out of their body cavity through the opening of the vulva.
4. Paralysis or uncoordinated movement: These phenotypes, when not attributed to mutant alleles carried by the strain itself, indicate injury or experimental mishandling, which can affect animal lifespan and skew the outcome of the assay.
5. Bacterial or fungal contamination: Contamination of NGM plates with bacteria not indented for feeding or with fungi may have a detrimental impact on animal survival (see Note 13).

3.5.4. Scoring Death Events

As they grow older worms gradually stop moving and only forage for food by just moving their head. Ultimately they also cease foraging, but they may remain alive for several more days. Worms are scored as dead if they fail to respond to repeated light prodding on the head and tail.

3.6. Data Analysis

The Kaplan–Meier analysis is the most common method used for processing and plotting survival data. The graph generated presents the percentage of animals surviving at each observation point plotted against time. The advantage of the Kaplan–Meier survival analysis is that it takes into account censoring events. The curve usually comprises horizontal steps with progressively lower magnitude (beginning at 100%; Fig. 2). In this case, survival in between different sample observation points is considered steady. Two Kaplan–Meier survival curves corresponding to different populations can be compared by means of several statistical tools like the log-rank test (or Mantel-Cox test), the Gehan-Breslow-Wilcoxon test, and the Cox hazard regression. The key parameters, derived from survival analysis, which are used to interpret and compare survival data are the mean and maximum lifespan values. Mean lifespan is the time interval by which half of the population (50% of the total number of animals, nor including censored individuals) is dead. Maximum lifespan is defined by the time of death of the longest-lived survivor within the population. Maximum lifespan is also alternatively calculated as the mean lifespan of the longest-lived 10% of the population (Fig. 2).

There are several software applications that perform survival data analysis based on the Kaplan–Meier method. Microsoft Excel (Microsoft Corporation, Redmond, WA, USA) is an extensively used application for a wide range of statistical analyses. Specific Excel add-ins can be obtained and installed for easier analysis of survival data (14). Origin is another software package (OriginLab Corporation, Northampton, USA) for scientific graphs and data analysis that is capable of generating Kalpan–Meier plots. GraphPad Prism (GraphPad Software Inc., San Diego, USA) is an additional, useful software application for scientific graphing, including survival curve construction and analysis.

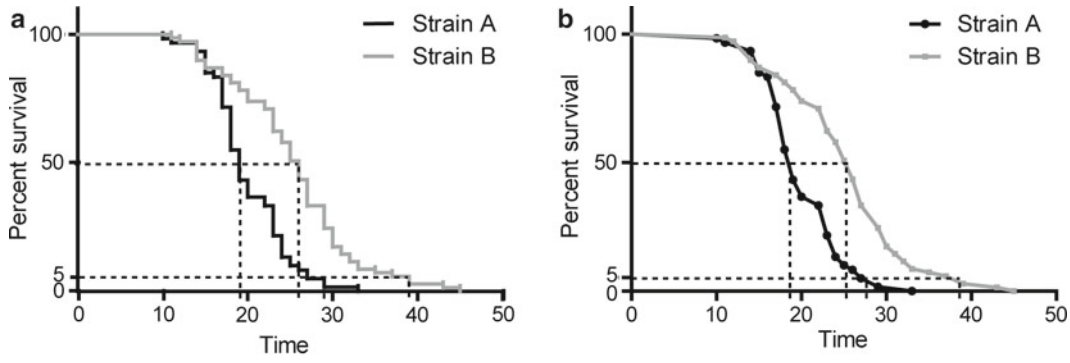

	A	B
Median lifespan:	19	26
Maximum lifespan (10%):	28	39
Absolute Maximum lifespan:	33	45

Fig. 2. Examples of survival curves. The GraphPad Prism software was used for the construction of Kaplan–Meier survival curves for each of the two hypothetical strains A and B. The same set of data is used for the construction of the two different types of curves: the staircase type shown in panel (**a**), where points are connected with steps, and the point-to-point fit in panel (**b**), where the points are connected with *straight lines*. Two *dashed lines* starting from 50 and 5% survival (*Y* axis) intersect the two curves at different points. For each curve, the projections of these points on the *X* axis, indicate the median lifespan of the total population, and the median lifespan of the upper 10% of the longest-lived survivors in the population (maximum lifespan), respectively. The median and maximum lifespan of each strain are shown in panel (**c**). Both the Log-rank test and the Gehan-Breslow-Wilcoxon test estimate the difference between the two survival curves to be statistically significant, with p values < 0.001.

4. Notes

1. Caution: do not flame or autoclave!
2. Caution: do not flame or autoclave! Store at 4°C in a dark bottle or wrap the bottle in aluminum foil since it is photosensitive.
3. Do not spread the bacterial lawn close to the edges of the plate. Worms tend to stay within the bacterial lawn and by extending it near the ends, the probability of worms crawling on the sides of the plate and dying by desiccation increases.
4. It is not uncommon that genetic or environmental manipulations have different effects on lifespan at different temperatures. For this reason a comprehensive analysis should include lifespan assays at different temperatures (within the 15–25°C range of rearing temperatures).
5. Several studies with diverse species indicate that parental age or stress experienced by the parental generation affects progeny physiology and lifespan (3, 15–17). For this reason it is important that synchronous worm populations assayed derive from synchronous parents grown under optimal conditions.

6. Egg preparation from gravid adult worms: gather animals from plates containing mixed worm populations, using 1 mL of sterile water per plate and transfer them to 1.5 mL microcentrifuge tubes. Spin down shortly and resuspend worms in sodium hypochlorite solution (bleach) (0.5 N NaOH, 20% bleach). Vortex for about 1 min, until animal bodies are completely dissolved (check the tube under a dissecting microscope to monitor when lysis is complete). Eggs, protected by the egg shell, are resistant to this treatment. When only eggs are visible in solution, spin down and wash extensively the egg preparation (2–3 times) with sterile water. Washing off the bleaching solution is important for the survival of embryos.
7. If more embryos are needed, the number of plates, the number of gravid adults per plate, or the duration of the egg-laying can be increased accordingly.
8. Largest populations provide more statistically reliable survival data.
9. Given that the quality of bacterial food and the composition/condition of the solid medium, which are important components of the microenvironment that can cumulatively affect survival lifespan of a population, it is important to keep these parameters steady throughout the study. Plates should be no more than 2 weeks old and always freshly seeded. Moreover, it is important to use the same batch of seeded NGM plates for all different worm populations within one experiment, to ensure that all populations age within comparable microenvironments and survival data are directly comparable.
10. Annotation of the plates confers better control over the course of an experiment. For example, animals on specific plates can be monitored separately from the rest of the population allowing to animals in contaminated plates to be discarded without adversely affecting the outcome of the experiment.
11. Preparation of FUdR-containing plates: make a stock solution of FUdR at a concentration 40 mM in dd H_2O (by adding 984 mg in 100 mL dd H_2O). Filter-sterilize the solution, aliquot and freeze at –20°C. Add 3 mL of the stock solution in 1 L NGM agar after it cools down to 55°C, just before pouring plates.
12. If drugs are used in the food source or if RNAi by feeding is performed, the stability of the compounds examined or the ability of the HT115 *E. coli* strain to induce double-stranded RNA after several days should be taken into account, to determine the frequency of transferring. Typically, for feeding RNAi experiments, dsRNA levels and consequently target gene knockdown is not considered efficient after 4 days on the same plate. Therefore transferring frequency should be adjusted accordingly.

13. Contamination problems are already mitigated by the use of the *E. coli* strain OP50-1, a uracil auxotroph resistant to streptomycin, and also by the addition of streptomycin and nystatin in NGM agar plates. However, contaminations may still appear during the course of an experiment, originating from the NGM agar plates, the feeding bacterial cultures used or airborne contaminants. Hence, sterilization practices should be meticulously implemented and all necessary safety measures taken when performing animal transfers and population observations. In cases of extensive contamination, affected plates should be removed from the experiment. Transferring worms from contaminated plates would risk spreading the contamination to the rest of the population. If contamination is less extensive, transferring animals more often or passing them through a clean intermediate plate for about an hour prior to moving them to their final destination may rid animals of contaminants. However, if contamination persists for several days, contaminated animals should be removed from the experiment.

Acknowledgement

Work in the authors' laboratory is funded by grants from the European Research Council (ERC), the European Commission Framework Programmes, and the Greek Ministry of Education.

References

1. Kenyon CJ (2010) The genetics of ageing. Nature 464:504–512
2. Conti B (2008) Considerations on temperature, longevity and aging. Cell Mol Life Sci CMLS 65:1626–1630
3. Klass MR (1977) Aging in the nematode *Caenorhabditis elegans*: major biological and environmental factors influencing lifespan. Mech Ageing Dev 6:413–429
4. Sulston JE, Horvitz HR (1977) Post-embryonic cell lineages of the nematode, *Caenorhabditis elegans*. Dev Biol 56:110–156
5. Sulston JE, Schierenberg E, White JG, Thomson JN (1983) The embryonic cell lineage of the nematode *Caenorhabditis elegans*. Dev Biol 100:64–119
6. Brenner S (1974) The genetics of *Caenorhabditis elegans*. Genetics 77:71–94
7. Beanan MJ, Strome S (1992) Characterization of a germ-line proliferation mutation in *C. elegans*. Development 116:755–766
8. Roberts TM, Ward S (1982) Membrane flow during nematode spermiogenesis. J Cell Biol 92:113–120
9. Neumann-Haefelin E, Qi W, Finkbeiner E, Walz G, Baumeister R, Hertweck M (2008) SHC-1/p52Shc targets the insulin/IGF-1 and JNK signaling pathways to modulate lifespan and stress response in *C. elegans*. Genes Dev 22:2721–2735
10. Mitchell DH, Stiles JW, Santelli J, Sanadi DR (1979) Synchronous growth and aging of *Caenorhabditis elegans* in the presence of fluorodeoxyuridine. J Gerontol 34:28–36
11. Gandhi S, Santelli J, Mitchell DH, Stiles JW, Sanadi DR (1980) A simple method for maintaining large, aging populations of *Caenorhabditis elegans*. Mech Ageing Dev 12:137–150
12. Aitlhadj L, Sturzenbaum SR (2010) The use of FUdR can cause prolonged longevity in mutant nematodes. Mech Ageing Dev 131:364–365

13. Van Raamsdonk JM, Hekimi S (2011) FUdR causes a twofold increase in the lifespan of the mitochondrial mutant gas-1. Mech Ageing Dev 132:519–521
14. Khan HA (2006) SCEW: a Microsoft Excel add-in for easy creation of survival curves. Comput Methods Programs Biomed 83:12–17
15. Priest NK, Mackowiak B, Promislow DE (2002) The role of parental age effects on the evolution of aging. Evol Int J Org Evol 56:927–935
16. Vijendravarma RK, Narasimha S, Kawecki TJ (2010) Effects of parental larval diet on egg size and offspring traits in Drosophila. Biol Lett 6:238–241
17. Leshem M, Schulkin J (2011) Transgenerational effects of infantile adversity and enrichment in male and female rats. Dev Psychobiol 54: 169–186

Chapter 32

High-Throughput and Longitudinal Analysis of Aging and Senescent Decline in *Caenorhabditis elegans*

Eirini Lionaki and Nektarios Tavernarakis

Abstract

Caenorhabditis elegans is becoming a multipurpose tool for genetic and chemical compound screening approaches aiming to identify and target the molecular mechanisms underlying senescent decline, aging, and associated pathologies. In this chapter, we describe specialized methods that have been developed to facilitate such screening strategies using *C. elegans*. The first section provides detailed procedures for the assessment of lifespan parameters on liquid growth media that are typically used for rearing nematodes. In the second section, we consider methodologies optimized for high-throughput survival analysis, applicable to large-scale chemical compound or genetic screening ventures. Finally, we discuss recently developed microfluidics tools for the noninvasive monitoring of behavioral and physiological traits in longitudinal studies of aging and senescent decline.

Key words: Aging, *Caenorhabditis elegans*, Drug screening, Lifespan, Longitudinal studies, Microfluidics, Nematode, Senescent decline, Stochastic death, Survival analysis

1. Introduction

Caenorhabditis elegans is a model organism that is particularly suited for large-scale, high-throughput approaches to dissect and target mechanisms underlying senescent decline and age-associated pathologies. The small size and transparent body, coupled with a short lifespan and prolific clonal reproduction provide a unique combination of advantages that decisively facilitate such studies. In this chapter, we describe methods based on liquid worm cultures that build on these features and advantages of *C. elegans*, to monitor and quantify parameters and phenotypes associated with senescent decline and aging.

Lorenzo Galluzzi et al. (eds.), *Cell Senescence: Methods and Protocols*, Methods in Molecular Biology, vol. 965,
DOI 10.1007/978-1-62703-239-1_32,

The first method described here has proven particularly useful for nematode-based, high-throughput drug screening approaches (1–3). It allows lifespan assessment of *C. elegans* animals in 96-well plate liquid cultures. Survival assays in liquid media reproduce results obtained with lifespan experiments on solid media both for wild-type (N2) worms in different temperatures and for mutants strains with altered lifespan (3). Because this method of lifespan determination is relatively not labor-intensive and also amenable to automation, it can be readily integrated into automated drug screening platforms.

The increasing need for screening large libraries of chemical compounds to identify molecules that promote survival under different conditions (acute stress (4), bacterial infections (5)) led to the development of high-throughput methods for lifespan assessment. In this chapter, we describe a dedicated method or high-throughput analysis and screening of several thousands of compounds simultaneously, based again on liquid cultures in multi-well plates. This method uses survival after stress (a few hours) as a predictor of long-term lifespan (a few weeks) (4). Survival after stress is often linked to the normal lifespan of the animal. The connection between lifespan and stress resistance has been shown for different kinds of stressors (6–8). This approach is much shorter compared to performing lifelong survival analysis and can be easily combined with identification of drugs that affect worm survival after acute stress (thermal stress, oxidative stress, etc.). It can also be implemented for the examination of multiple genetic mutants simultaneously, to investigate how molecular pathways are implicated in stress responses (for an extended discussion of high-throughput screens in *C. elegans* see ref. 9).

The third method described in this chapter exploits a microfluidic device suitable for longitudinal studies and monitoring of age-related changes and senescent decline, in a noninvasive manner, throughout the lifetime of single animals. Detailed study of age-related changes is important because they reveal mechanisms implicated in the aging process, they indicate cause-and-effect relationships between these mechanisms and aging, and some may also be used as biomarkers for the assessment of the biological age of an organism. Microfluidics technologies and devices have recently been developed that greatly facilitate such analyses by allowing long-term observation of age-related traits in single animals (10). These devices can also be utilized in longitudinal studies that combine exposing of worms to chemical or other stressors at specific time points through life. They are also excellent tools for downstream analysis of chemicals or metabolites generated by the worm itself (for example pheromones).

2. Materials

2.1. Lifespan Assay in Liquid Media

- Luria Bertani (LB) medium and agar plates containing streptomycin: For 1 L, add 10 g Bacto-tryptone, 5 g yeast extract, 10 g NaCl. Adjust pH to 7.0 with NaOH, adjust volume to 1 L with dd H_2O, and autoclave. For LB agar plates add 20 g of agar to the previous mixture and a magnetic stirrer prior to autoclaving. After autoclaving let the mixture cool down to 55°C (with stirring when it is LB agar) add 1 mL of streptomycin stock 100 mg/mL and poor into petri dishes (10 mm diameter).
- 2 Streptomycin stock 100 mg/mL: For 10 mL, add 1 g of streptomycin in 10 mL of dd H_2O. Shake until the streptomycin is dissolved. Filer-sterilize the solution and store at 4°C.
- Nystatin suspension 10 mg/mL: For 50 mL, add 0.5 g nystatin, in 70% ethanol in dd H_2O. This is going to be a suspension, so it needs shaking prior to use (*see* **Note 1**).
- Hypochloride solution: For 10 mL, add 1 mL NaOH 5 N, 2 mL bleach, 7 mL double-distilled (dd) H_2O.
- M9 buffer: For 1 L, add 6 g Na_2HPO_4, 3 g KH_2PO_4, 5 g NaOH, 0.25 g $MgSO_4{\cdot}7H_2O$ (or 1 mL of $MgSO_4$ 1 M solution). Add dd H_2O up to 1 L and autoclave.
- Potassium Phosphate Buffer pH 6.0: For 1 L, add 136 g KH_2PO_4, adjust pH to 6.0 with 5 M KOH, add dd H_2O water up to 1 L and autoclave.
- Trace metal solution: For 1 L, add: 1.86 g Na_2EDTA, 0.69 g $FeSO_4{\cdot}7H_2O$, 0.20 g $MnCl_2{\cdot}4H_2O$, 0.29 g $ZnSO_4{\cdot}7H_2O$, 0.016 g $CuSO_4$. Add dd H_2O up to 1 L, autoclave, and store in the dark.
- Potassium citrate Buffer 1 M: For 1 L, add 268.8 g tripotassium citrate, 26.3 g citric acid monohydrate and dd H_2O up to 900 mL. Adjust pH to 6.0 with 5 M KOH, add dd H_2O up to 1 L and autoclave.
- S-basal medium: For 1 L, add: 5.9 g NaCl, 50 mL of 1 M Potassium Phosphate Buffer pH 6.0 (*see* above for details). Adjust the volume with dd H_2O up to 1 L and autoclave. Let the medium cool down and add 1 mL of 5 mg/mL cholesterol (dissolved in ethanol).
- S-complete medium: for 1 L, add: 977 mL S-basal medium, 10 mL 1 M Potassium citrate pH 6 (sterile) (*see* above for details), 10 mL Trace metal solution (sterile), 3 mL 1 M $CaCl_2$ (sterile), 3 mL 1 M $MgSO_4$ (sterile). Use sterile technique, do not autoclave.

- 0.6 mM Fluorodeoxyuridine (FUDR): For 67 mL, dissolve 10 mg FUDR in 67 mL sterile S-complete medium. Filter-sterilize the solution, aliquot and store at −20°C.
- Flat bottom 96-well plates.
- Plate mixer.
- Transparent adhesive plate sealers.
- *Escherichia coli* strain OP50-1.
- Incubator for stable temperature.

2.2. Automated High-Throughput Assessment of C. elegans Survival After Acute Stress

- COPAS Biosort instrument (Union Biometrica Inc., Holliston, USA).
- SYTOX Green fluorescent dye (Life Technologies Corporation, Eugene, Oregon, USA).
- Microtiter plate-reading fluorometer (Thermo Labsystems, Beverly, USA).
- Epi-fluorescence microscope.
- Black wall clear bottom 384-well plates.
- Transparent adhesive plate sealers.

2.3. Lifespan Assessment on a Chip: The Microfluidics Approach

- Microfluidic device: Photolithography is used to pattern raised features of SU-8 photoresist (Microchem Corp., Newton, MA, USA) on silicon wafer (Silicon Sense, Inc., Nashua, NH, USA). This silicon master serves as a template for replica molding with poly(dimethyl siloxane) (PDMS, Dow Corning Sylgard 184, Corning, NY). Subsequently, masters are treated with tridecafluoro (1,1,2,2 tetrahydrooctyl) trichlorosilane (Gelest, Inc., Philadelphia, PA, USA) (10).
- Polyethylene tubing.
- Syringe.

3. Methods

3.1. Lifespan Assay in Liquid Media

3.1.1. Preparation of Feeding Bacteria

1. An outline of this protocol is presented in Fig. 1. Starting from a freshly streaked culture of OP50-1 *E. coli* bacteria on an LB, streptomycin-containing agar plate, pick a single colony and inoculate 5 mL LB/streptomycin medium (see Note 2).
2. Incubate overnight (12–16 h) at 37°C, shacking at 250 rpm.
3. The following day, inoculate 500 mL LB/streptomycin using 500 μL of the overnight-saturated culture (1/1,000 dilution) and incubate at 37°C shacking for ~12 h until saturation.
4. Transfer the bacterial culture in a pre-weighted sterile centrifuge tube, and centrifuge for 10 min at 3,000 × *g*.

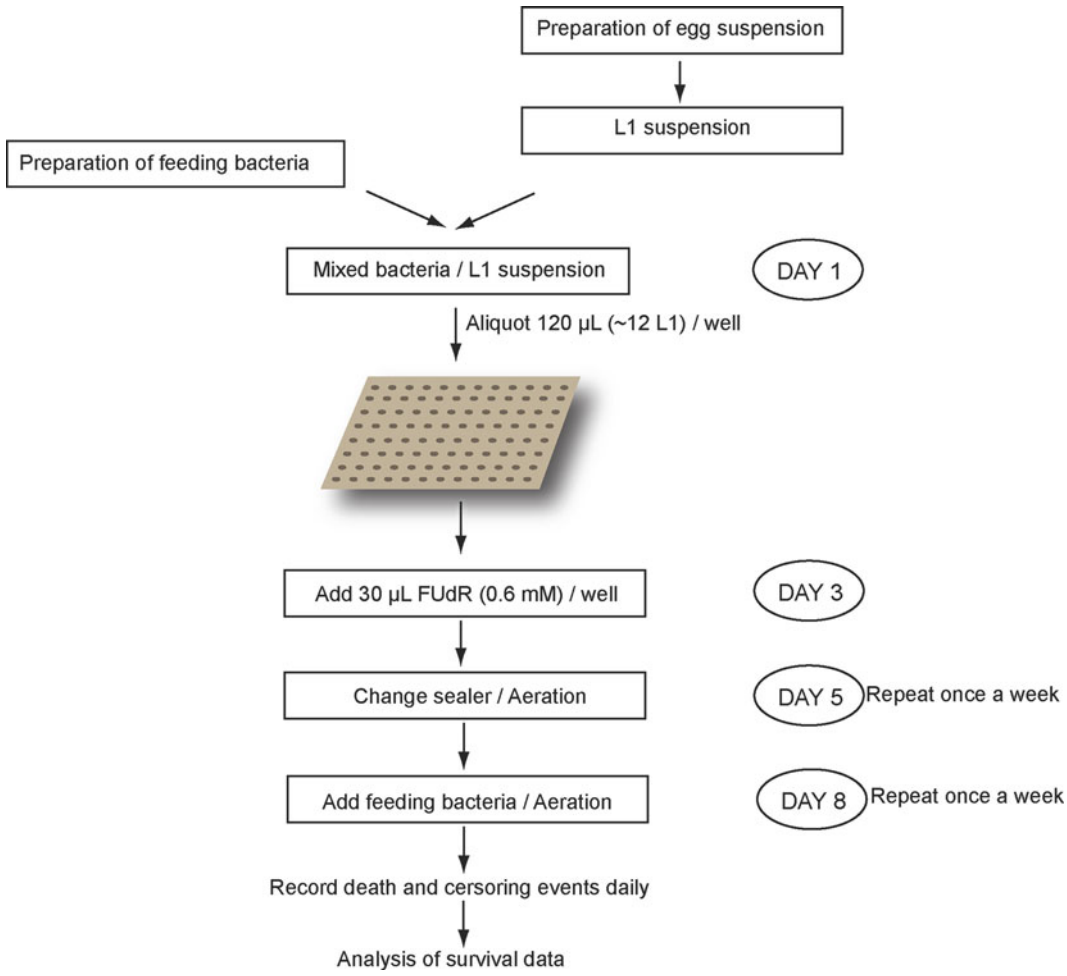

Fig. 1. Lifespan assay in 96-well plates. Briefly, this protocol involves the preparation of synchronous L1 larvae in S-complete medium, mixing them with bacterial suspension and dispersing them in the 96-well plate, at a concentration of ~12 worms per well. Just before larvae reach adulthood, FUdR is added to sterilize the population. Feeding bacteria are added once per week and the sealer is also changed once per week to allow aeration. Death and censoring events are recorded daily and analysis of the survival data follows the completion of the experiment.

5. Discard the LB medium and wash the cells twice with sterile water.
6. After the second wash, discard carefully all the remaining water and weight the cell pellet.
7. Resuspend the cell pellet in S-complete medium to a final concentration of 100 mg/mL (see Note 3). No cell clumps should remain after resuspension in S-complete medium. After adding the S-complete medium, resuspend the pellet by shacking for 15–60 min at 250 rpm at room temperature.
8. Resuspended bacteria can be stored at 4°C, for up to 2 weeks.

3.1.2. Population Synchronization

Preparation of synchronous worm populations for liquid cultures is easily accomplished by means of the egg-preparation technique (see Chapter 31).

1. Prepare 3 NGM agar plates with mixed worm population (see Note 4 and Chapter 31).
2. Collect worms by washing plates with 5–10 mL of sterile water (see Note 5) and transfer animals to a sterile tube.
3. Let worms settle to the bottom of the tube for about 5 min.
4. Remove supernatant and add 3 mL of freshly prepared sodium hypochlorite solution.
5. Vortex for about 1 min until worm bodies are dissolved and only eggs are obvious under the dissecting microscope.
6. Spin down the egg preparation for 2 min at 300×*g*.
7. Wash the egg pellet three times with 5 mL of sterile water (see Note 6).
8. Wash eggs once with 5 mL of S-complete medium (see Note 6).
9. After the final centrifugation, resuspend eggs in 5 mL S-complete medium and transfer to a 50 mL sterile canonical tube.
10. Add another 35 mL of sterile S-complete medium and incubate overnight with gentle shacking on a nutator mixer.
11. Eggs will hatch during their overnight incubation in the S-complete medium. By next morning the tube will contain a suspension of L1 larvae (see Note 7).

3.1.3. Setting Up the Experiment

Preparation of L1 Larvae and Feeding Bacteria Suspension

1. Mix the L1 suspension by inverting the tube several times.
2. Spot 10 μL drops on NGM agar plates (make sure to mix directly before each pipetting). Measure the number of worms in each drop. Measure at least ten drops and estimate the mean number of worms per milliliter of suspension.
3. Adjust the final volume so that worm concentration in the suspension is approximately 100 worms/mL. If the estimated worm concentration is less than 100 worms/mL, spin down worms shortly and remove the appropriate amount of medium, to achieve the desired concentration.
4. Add streptomycin (to a final 200 μg/mL) and the antifungal drug nystatin (final concentration 10 μg/mL) to avoid contamination (see Note 2).
5. Add an appropriate volume of feeding bacteria in S-complete media (prepared in Subheading 3.1.1) to a final concentration of 6 mg/mL. The bacterial suspension will be further diluted by later adding the FUdR solution.

Transfer Animals to 96-Well Plates

It is important to use 96-well plate with transparent flat bottom.

1. Mix the worm suspension thoroughly by inverting the tube several times.
2. Disperse 120 μL of the suspension in each well. Mix the suspension often, because the larvae are quickly swimming downwards and their concentration on the surface changes.
3. Each well should contain approximately 12 L1 larvae.
4. Count worms in all wells and note the number of worms in each well.
5. Remove the wells that contain more than 18 worms from the assay. These wells are likely to run out of food earlier than the rest of the wells.
6. Seal the plate with a transparent adhesive sealer, to avoid contamination and evaporation of the samples.
7. Mix the plate on a micro-plate mixer for 2 min.
8. Put the plate in a 20°C incubator for 2 days.

Sterilize the Worms with FUdR

FUdR sterilizes L4 worms without significantly affecting adult physiology or aging (see Chapter 31). It can be used in a range of concentrations from 25 to 400 μM (11, 12). It should not be added to the culture before animals reach the L4 stage of development (approximately 2 days after the L1 larvae have been transferred to the 96-well plate), because it will affect their development (see Note 8).

1. Prepare an FUdR stock solution in S-complete medium at a concentration 0.6 mM.
2. Add 30 μL of the stock in each well containing late L4 larvae.
3. Seal again the micro-plate with an adhesive sealer.
4. Shake the plate for 2 min on a micro-plate shaker.
5. Return the plate back into the 20°C incubator.

Worms stop producing eggs within a few hours of FUdR addition. Eggs that will be already produced within this time frame will not develop normally in the presence of FUdR so they will not interfere with the assay by mixing with parents.

3.1.4. Feeding and Aeration of Worms in Liquid Cultures

To prevent starvation of worms, feeding bacteria need to be added once a week in each well.

1. Mix the feeding bacteria suspension kept in the refrigerator by inverting the tube several times.
2. Transfer an adequate fraction of the suspension into a fresh sterile tube and leave on the bench for 15–20 min to warm up to room temperature.

3. Remove the sealer from the micro-plate (next to a Bunsen burner to maintain sterile conditions).
4. Add 5 μL of bacterial suspension in each well and seal the plate again.
5. Mix the cultures for 2–3 min on a micro-plate shaker.
6. Return it into the 20°C incubator.

To allow fresh oxygen to enter culture wells, the tape sealer needs to be removed twice a week.

1. Remove the old sealer.
2. Leave the plate uncovered for 2 min, next to a Bunsen burner (to maintain sterile conditions).
3. Put a new sealer and shake for 2 min on a micro-plate shaker.
4. Return the plate into the 20°C incubator (see Note 9).

3.1.5. Scoring of Lifespan

Prepare a worksheet where the number of live, dead, and censored animals will be noted and monitor the cultures every 1–2 days.

1. Remove the plate from the 20°C incubator.
2. Mix the plate for 2–3 min to induce animal movement.
3. Monitor the plate every 1–2 days under the dissecting microscope without removing the tape sealer.

Scoring of live worms is based upon their motility and their body shape (5) (see Note 10). Live worms move (subtle movements can be visualized at higher magnification) and their body typically assumes a sinusoidal posture. Dead worms don't move and their body shape is usually like a rigid rod. Score and record the live and dead worms in each well every day. Do not remove dead animals from the assay wells. Some worms may appear as dead 1 day but then the next day they may move again.

3.1.6. Survival Data Analysis

The Kaplan–Meier analysis is the most common method used for processing and plotting survival data. The graph generated depicts the percentage of animals surviving at each observation point plotted against time. Several software applications perform survival data analysis based on the Kaplan–Meier method. Microsoft Excel (Microsoft Corporation, Redmond, Washington, USA) is an extensively used application for a wide range of statistical analyses. Specific Excel add-ins can be obtained and installed for easier analysis of survival data (13). Origin is another software package (OriginLab Corporation, Northampton, USA) for scientific graphs and data analysis that is capable of generating Kalpan–Meier plots. GraphPad Prism (GraphPad Software Inc., San Diego, USA) is an additional, useful software application for scientific graphing that also includes survival curve construction and analysis. For further information on survival data analysis see Chapter 31.

3.2. Automated High-Throughput Assessment of C. elegans Survival After Acute Stress

In summary, synchronous worm populations of the same larval stage are selected by an automated large particle flow-sorting system and subsequently dispensed into 384-well plates containing a fluorescent dye, SYTOX green. Following stress, the dye stains only dead animals, and the overall survival of a population will be calculated based on the individual fluorescent curves that determine the time of death for each, single animal-containing well. The *fer-15(b26)* temperature sensitive sterile mutant strain can be used to avoid progeny interference (see Note 11).

3.2.1. Preparation of fer-15(b26) Sterile Populations

Solid Media

1. Grow mixed populations of *fer-15(b26)* mutant worms at 15°C to maintain fertility (see Note 4).
2. Transfer (with a wormpick) five young adult worms per plate, on 5 NGM agar plates (25 worms, total) and incubate at 25°C for 3–4 days. The progeny of *fer-15(b26)* worms will develop into sterile adults. The total number of worms needed depends on the experimental design. However, one NGM plate will hold approximately 1,500 worms, and ideally, the percentage of adult worms in the overall population should not exceed 25% at the beginning of the experiment.

If larger worm populations are needed, then preparation of a liquid culture is a more convenient alternative.

Liquid Media

1. Prepare feeding bacteria as described in Subheading 3.1.1, and three medium NGM agar plates with mixed worm population grown at 15°C to maintain fertility.
2. Add 475 mL of S-complete medium and 25 mL of feeding bacteria in a 2 L flask
3. Collect the worms from the NGM agar plates and prepare eggs by treatment with hypochlorite solution.
4. Add the eggs in the flask with the S-complete medium and the feeding bacteria.
5. Incubate at 25°C shaking at 160 rpm.
6. Worms should clear the bacteria from the culture in approximately 3–4 days (see Note 12).
7. Collect worms by tilting the flask and aspirating the supernatant after allowing animals to settle at the bottom.
8. Transfer worms in a sterile canonical tube.

3.2.2. Preparation of 384-Well Plate Cultures

Using 384-well plates not only multiplies the number of samples that can be assayed simultaneously but also improves the detection of signal coming from dead worms, as in 96-well plates worms can stay in the periphery of the well, introducing high variation in the detected results.

1. Inoculate 5 mL of LB/streptomycin with a single OP50-1 colony and incubate at 37°C shacking overnight.
2. In the next morning, add 50 μL of the saturated culture into 50 mL of fresh LB/streptomycin medium and incubate at 37°C, shacking until OD_{600} is about 0.2.
3. Spin down cells for 10 min at 3,000 × *g*.
4. Resuspend in equal volume (50 mL) of S-complete medium.
5. Wash twice in S-complete medium.
6. Add the antibiotics, streptomycin (200 μg/mL final concentration) and nystatin (10 μg/mL final concentration).
7. Dispense 20 μL of the bacterial suspension in S-complete medium in each well (see Notes 13 and 14).
8. Add SYTOX Green dye in each well at a final concentration 1 μM (see Note 13).

3.2.3. Automated Selection and Distribution of Age-Matched Individuals in 384-Well Plates with the COPAS Biosort Platform

Animals of different larval stages within a mixed population can be separated and sorted by large particle flow cytometry. The COPAS (Complex Object Parametric Analyser and Sorter; Union Biometrica Inc., Holliston, USA) Biosort platform has a specially engineered fluidic path and flow cell optimized to separate eggs, all larval stages and adults from mixed *C. elegans* populations. This system is capable of sorting worms using physical and optical properties, such as length and internal complexity (5, 14).

1. Once mixed population of sterile *fer-15(b26)* worms have been established, animals are collected in conical tubes and resuspended in M9 buffer containing 0.01% Triton X-100.
2. Wash 2–3 times in the same buffer.
3. Samples are passed through a 180 μM nylon mesh filter to remove larger clumps of eggs and debris.
4. Estimate the worm concentration in the sample (as described in Subheading 3.1.3). Adjust to 1 worm/μL using M9 (see Note 12).
5. Place the worm suspension to the sample cup a COPAS Biosorter, following the manufacturer's instructions, and proceed to dispense them. You may select both the developmental stage of worms in the assay and the number of worms per well.
6. Seal the plate with a transparent adhesive plate sealer to avoid evaporation and contamination.
7. Shake the plate using a plate mixer at 1,800 rpm.

3.2.4. Thermotolerance Assay and Fluorescence Data Analysis

Assay Conditions and Data Acquisition

Animals are dispersed in 384-well plates (1 worm per well). Acute thermal stress is induced at 35–37°C, either in an incubator or inside the fluorometer used for detection, for precise temperature control. Fluorescence quantification is performed with a microtiter plate-reading fluorometer (Thermo Labsystems, Beverly, USA). Fluorescence intensity is measured in each well every 30 min, over a 24 h period, with 20 ms integration time for each well. Reading of a 382-well plate is typically completed in about 30 s. The excitation wavelength for the SYTOX Green Dye is 485 nm, with emission wavelength at 538 nm.

Individual fluorescence intensity curves are examined to determine the time at which there is a significant increase in fluorescence over baseline. This point is considered the actual time of death (4). After acquiring all time points of death, a Kaplan–Meier plot can be generated and used to estimate and compare mean lifespan values after specific thermal or other insults (see Subheading 3.1.6 and Chapter 31).

Survival at Specific Time Points After an Insult: Multiple Worms Per Well

1. Dispense bacteria and/or drug-containing media in 384-well plates at a final volume of 55 mL.
2. Add up to 15 sterile adult worms per well (total volume 15 μL), using the automated COPAS Biosorter.
3. Perform stress resistance assays as dictated by the experimental design for each specific stressor.
4. Add SYTOX dye in each well, to a final concentration of 1 μM, a few hours after treatment (to allow death events).
5. Mix for 15 s on a microtiter plate mixer.
6. Incubate at RT for 15 min.
7. Capture images from each well separately using an automated fluorescence microscope (see Note 15). Two images should be captured from each well: one fluorescence image in which only dead worms will be visible (stained with SYTOX) and one bright-field image in which all the animals are visible.

Collected images are analyzed to determine the ratio of the total SYTOX-positive area in each well (fluorescence image), divided by the total area occupied by all worms in the same well (bright-field image). This ratio is indicative of the percentage of survival in each well (5, 9). This analysis can be automated by using the open-source cell image analysis software CellProfiler (5, 15). For additional information on whole-animal, high-throughput analyses based on *C. elegans* see also ref. 9.

3.3. Lifespan Assessment on a Chip: The Microfluidics Approach

3.3.1. The Microfluidic Device

Microfluidic devices are typically fabricated with poly-dimethylsiloxane (PDMS), a biocompatible material, which is mechanically malleable, permeable to O_2 and CO_2, and nontoxic. In addition, it is transparent for wavelengths above 230 nm, allowing bright-field and fluorescence imaging analysis. Directly after sealing the devise on PDMS-coated glass substrate, the walls are coated with 2-(methoxy(polyethyleneoxy)$_{6-9}$propyl) trimethoxysilane (mPEG-silane) to reduce bacterial absorption that would interfere with continuous liquid flow and would obscure the observation of the worms.

The device contains circular chambers (of 1.5 mm diameter) for growing individual worms. Each chamber is linked on one side, to a channel which allows loading of individual worms and the continuous flow of S-complete medium, and from the opposite side, to a conical 7.5 mm-long clamp channel. The width of the clamp wide side is 100 μm, and is proximal to the chamber, allowing an adult worm to enter the clamp. The other side of the clamp is narrow (25 μm), so that animals may be reversibly restricted and immobilized within the clamp. If animal immobilization is not required, an alternative design can be used, where the clamp is replaced by a constant width channel (100 μm). The flow of liquid through each chamber is regulated by a screw valve, located above the channel on the side of each clamp, proximal to the inlet of the device.

3.3.2. Loading Animals into Micro-Chambers

1. Synchronize worms by allowing synchronous gravid adults to lay eggs on NGM agar plates (see Chapter 31).
2. Incubate plates at 24°C for 2 days. At this point, most worms will be at the L4 larval stage.
3. Preload the device with S-complete medium containing OP50 bacteria at a concentration 10^9 cells/mL (using the network outlet of the device).
4. Once the device is saturated with the feeding bacteria suspension in S-complete medium, add worms from the outlet, one at a time.
5. Add a single worm into the network outlet.
6. Connect a syringe (containing bacterial suspension in S-complete medium) to the network outlet via a polyethylene tubing. Note that all the valves need to be open during this procedure.
7. Depress the plunger of the syringe manually. The resulting flow will carry the worm through the network channels into a random chamber.
8. Once the first worm reaches a chamber, close the valve of the corresponding channel, so that the flow of liquids in this chamber is blocked (see Note 16).

9. Continue until all the chambers are filled with L4 larvae (this procedure takes about 1 min/worm).
10. Within 6 h after loading, worms are big enough not to fit in the orifice proximal to the outlet and thus the continuous flow of liquid from the inlet can begin (see Note 17).

3.3.3. Maintenance of Worms in the Device

Feeding of animals while in the device is achieved by a continuous flow of bacterial suspension (from the inlet to the outlet) at a flow rate of 300 μL/h. In total, 25 mL of fresh bacterial suspension in S-complete medium is added to the inlet reservoir each day. To remove any bacterial aggregates, debris or dust particle that could clog the channels of the device, each bacterial suspension is filtered through a 5 μm porous polycarbonate membrane, before loading into the inlet reservoir. The liquid that passes through the device, exits through the outlet and gathers into a waste reservoir.

Over time, bacteria from the inlet reservoir settle and form aggregates at the junction of tubing connecting the reservoir and the inlet of the device. To prevent clogging of device channels, a bypass outlet is built into the device. Every 1–2 days, fresh bacterial suspension is flushed down the inlet tubing and into the inlet of the device and diverted to the bypass outlet (by closing of appropriate valves on the device), thus removing sediment and aggregated bacteria from the inlet of the device. The waste from the bypass outlet is collected into a third reservoir.

The continuous flow of liquid through the chambers also serves to remove eggs laid by the hermaphrodite in the chamber. If aggregates of eggs form that cannot pass through the 25 μm diameter orifice towards the network outlet, eggs may hatch inside the chamber. In this case, L1 larvae are easily removed with the flow and are separated from the mother. Thus, the synchrony of the population is maintained throughout the experiment (see Note 18).

3.3.4. Immobilizing Animals into Clamps

As mentioned above a microfluidic device provides the opportunity to monitor senescent decline in *C. elegans* by monitoring age-related changes of individual worms throughout lifetime. For longitudinal studies, it is important to choose phenotypes that can be monitored noninvasively so that worms are minimally disturbed by the act of observation. To this end, reversible immobilization takes place in the clamp. For example, to immobilize a worm in chamber 1:

1. Close all the valves of chambers 2–16.
2. Reverse the direction of flow from the network outlet to the inlet, by raising the reservoir connected to outlet in a higher position than the inlet reservoir.
3. For as long as the flow is reversed, the worm is immobilized in the clamp and observation can take place.
4. To return worm back in the chamber, just reverse the direction of flow.

4. Notes

1. Caution: Do not flame or autoclave! Store at 4°C in a dark bottle or wrap the bottle in aluminum foil since it is photosensitive.
2. In addition to the OP50-1 bacteria, two *E. coli* strains available at the *Caenorhabditis* Genetics Center (CGC; http://www.cbs.umn.edu/CGC/) are resistant to antibiotics: the OP50-GFP strain which is resistant to Ampicillin (16) and the OP50-NeoR, resistant to neomycin (17). Since, in this assay worms remain in the same well until their death, it is very important to avoid contamination by using antibiotics and exercising good lab practice. To add more antibiotics in the S-complete medium, OP50 bacteria we can be transformed with plasmids that bear the respective selection marker genes. For example, OP50-1 bacteria can be transformed with the empty pL4440 RNAi vector, which confers resistance to ampicillin, which can then be added together with streptomycin and nystatin in the S-complete medium.
3. A bacteria concentration of 100 mg/mL corresponds to about 2×10^{10} cells/mL. The OD_{600} of the suspension should be around 25. Caution: the measurement of the OD_{600} in a spectrophotometer should be performed with a diluted sample (1/50 dilution) so that the measured OD is below 1.0, within the linear range of the spectrophotometer. Otherwise the measurement will not be accurate.
4. Preparation of mixed worm populations involves transferring of five (5) L4 larvae on a freshly seeded Nematode Growth Media (NGM) plate and incubating at 20°C for four (4) days. For detailed information on the preparation and seeding of NGM plates see Chapter 31 (Chapter 31).
5. Caution: Use sterile conditions!
6. After each wash, spin down eggs for 2 min at $1{,}500 \times g$ at room temperature.
7. To verify that all eggs hatch during the night, drop 20 μL of L1 suspension on a clean NGM agar plate and monitor under a dissecting microscope.
8. The exact time of FUdR addition can vary when the experiment is performed at different temperatures or when strains with shorter or longer post-embryonic developmental periods are used. It must always be added when worms are well into the L4 larval stage.
9. Alternatively one can use gas permeable adhesive seal which allows air exchange, but prevents evaporation.

10. Moving into liquid media is much easier then moving onto solid media.
11. For antimicrobial drug screening studies, a mutant strain more susceptible to infections (*sek-1(km4)*; available at the CGC), is used to increase the sensitivity of the assay.
12. Monitor worm culture progress by removing aliquots and examining under a dissecting microscope. Ideally the percentage of adult worms in the sample should be no more than 25%.
13. When performing screens for anti-microbial substances, OP50 bacteria in the wells may be substituted for microbes causing infection (5, 18). The presence of bacteria in the wells generally increases baseline fluorescence when working with SYTOX Green. For this reason, bacterial concentration in wells should not exceed 5×10^8 cells/mL. It is also helpful to include no-worm control wells to monitor bacteria-specific background fluorescence with time. The medium dispensing step can be automated by using reagent dispenser machines (for example Multidrop Combi reagent dispenser; Thermo Fisher Scientific, Massachusetts, USA).
14. The chemical compounds to be tested can be added at this step. DMSO (Dimethyl sulfoxide) is a common diluent of many chemical compounds. However, DMSO concentration above 0.6% may adversely affect worm lifespan.
15. Versatile imaging devices are available that enable automated image acquisition from multiwall plates. The High-throughput Digital Imager (HiDI 2100; Elegenics, California, USA), is such a devise incorporating two functionally distinct modules: a plate management module and an image acquisition and management system (14).
16. Closing the valve of a chamber occupied by a worm, will stop liquid flow through this chamber, thus preventing entry of additional animals in the same chamber.
17. L4 larvae are particularly convenient for loading the device, as within a few hours (6–12) they grow to become efficiently trapped within the chambers.
18. The probability of death by internal hatching of progeny (bagging) is increased up to 30–35% when worms are grown in liquid cultures (10). These animals are censored during the experiment.

Acknowledgment

Work in the authors' laboratory is funded by grants from the European Research Council (ERC), the European Commission Framework Programmes, and the Greek Ministry of Education.

References

1. Petrascheck M, Ye X, Buck LB (2007) An antidepressant that extends lifespan in adult Caenorhabditis elegans. Nature 450:553–556
2. Braungart E, Gerlach M, Riederer P, Baumeister R, Hoener MC (2004) Caenorhabditis elegans MPP + model of Parkinson's disease for high-throughput drug screenings. Neurodegener Dis 1:175–183
3. Solis GM, Petrascheck M (2011) Measuring Caenorhabditis elegans lifespan in 96 well microtiter plates. J Vis Exp pii:2496
4. Gill MS, Olsen A, Sampayo JN, Lithgow GJ (2003) An automated high-throughput assay for survival of the nematode Caenorhabditis elegans. Free Radic Biol Med 35:558–565
5. Moy TI, Conery AL, Larkins-Ford J, Wu G, Mazitschek R, Casadei G, Lewis K, Carpenter AE, Ausubel FM (2009) High-throughput screen for novel antimicrobials using a whole animal infection model. ACS Chem Biol 4:527–533
6. Lithgow GJ, Walker GA (2002) Stress resistance as a determinate of C. elegans lifespan. Mech Ageing Dev 123:765–771
7. Vanfleteren JR (1993) Oxidative stress and ageing in Caenorhabditis elegans. Biochem J 292(Pt 2):605–608
8. Barsyte D, Lovejoy DA, Lithgow GJ (2001) Longevity and heavy metal resistance in daf-2 and age-1 long-lived mutants of Caenorhabditis elegans. FASEB J 15:627–634
9. O'Rourke EJ, Conery AL, Moy TI (2009) Whole-animal high-throughput screens: the C. elegans model. Methods Mol Biol 486:57–75
10. Hulme SE, Shevkoplyas SS, McGuigan AP, Apfeld J, Fontana W, Whitesides GM (2010) Lifespan-on-a-chip: microfluidic chambers for performing lifelong observation of C. elegans. Lab Chip 10:589–597
11. Mitchell DH, Stiles JW, Santelli J, Sanadi DR (1979) Synchronous growth and aging of Caenorhabditis elegans in the presence of fluorodeoxyuridine. J Gerontol 34:28–36
12. Gandhi S, Santelli J, Mitchell DH, Stiles JW, Sanadi DR (1980) A simple method for maintaining large, aging populations of Caenorhabditis elegans. Mech Ageing Dev 12:137–150
13. Khan HA (2006) SCEW: a Microsoft Excel add-in for easy creation of survival curves. Comput Methods Programs Biomed 83: 12–17
14. Burns AR, Kwok TC, Howard A, Houston E, Johanson K, Chan A, Cutler SR, McCourt P, Roy PJ (2006) High-throughput screening of small molecules for bioactivity and target identification in Caenorhabditis elegans. Nat Protoc 1:1906–1914
15. Carpenter AE, Jones TR, Lamprecht MR, Clarke C, Kang IH, Friman O, Guertin DA, Chang JH, Lindquist RA, Moffat J, Golland P, Sabatini DM (2006) Cell Profiler: image analysis software for identifying and quantifying cell phenotypes. Genome Biol 7:R100
16. Labrousse A, Chauvet S, Couillault C, Kurz CL, Ewbank JJ (2000) Caenorhabditis elegans is a model host for Salmonella typhimurium. Curr Biol 10:1543–1545
17. Giordano-Santini R, Milstein S, Svrzikapa N, Tu D, Johnsen R, Baillie D, Vidal M, Dupuy D (2010) An antibiotic selection marker for nematode transgenesis. Nat Methods 7: 721–723
18. Tampakakis E, Okoli I, Mylonakis E (2008) A C. elegans-based, whole animal, in vivo screen for the identification of antifungal compounds. Nat Protoc 3:1925–1931

Chapter 33

Assessing Senescence in Drosophila Using Video Tracking

Reza Ardekani, Simon Tavaré, and John Tower

Abstract

Senescence is associated with changes in gene expression, including the upregulation of stress response- and innate immune response-related genes. In addition, aging animals exhibit characteristic changes in movement behaviors including decreased gait speed and a deterioration in sleep/wake rhythms. Here, we describe methods for tracking *Drosophila melanogaster* movements in 3D with simultaneous quantification of fluorescent transgenic reporters. This approach allows for the assessment of correlations between behavior, aging, and gene expression as well as for the quantification of biomarkers of aging.

Key words: Aging, Biomarkers, *Drosophila melanogaster*, GFP, In vivo imaging, 3D video tracking

1. Introduction

Aging of living organisms (senescence) has traditionally been assayed by lifespan, and altered lifespan is still generally considered the "gold standard" for verifying interventions in aging (1). However, assay of lifespan is problematic in that it takes a long time to determine, and once determined there is limited additional information that can be obtained from the animal. For these reasons there has been extensive interest in identifying predictive biomarkers of aging, i.e., parameters that can be assayed in a non-destructive way in young animals that will be indicative of aging rate, future performance and lifespan (2–4). Aging in both Drosophila and mammals is characterized by changes in gene expression including upregulation of stress response and innate immune response genes (5–8). Expression of transgenic reporter constructs derived from such genes correlates with Drosophila lifespan (9, 10) and is predictive of remaining lifespan when assayed in young animals including Drosophila (7, 11) and *C. elegans* (12). Movement behaviors are also promising as aging biomarkers: aging in Drosophila and humans is characterized by

Lorenzo Galluzzi et al. (eds.), *Cell Senescence: Methods and Protocols*, Methods in Molecular Biology, vol. 965,
DOI 10.1007/978-1-62703-239-1_33,

reduced gait speed (13) and disrupted sleep/wake cycles (14, 15), and gait speed is predictive of remaining lifespan in elderly humans (16). We have previously reported methods that allow for 3D video tracking of *Drosophila melanogaster* movement behaviors (17), while simultaneously quantifying gene expression in aging flies using fluorescent reporter proteins (18, 19). Video tracking in 3D has also been applied to studies of aging in additional fly species (20). We have recently developed a system called FluoreScore that utilizes two synchronized cameras and recorded videos and provides a simplified operating system and a user-friendly interface (21). FluoreScore allows for quantification of fluorescent transgenic reporter expression in groups of free moving flies and provides 3D movement patterns with simultaneous fluorescence quantification for single flies. Here we provide a detailed protocol for FluoreScore, including instructions on assembling the hardware and running the software.

2. Materials

2.1. Hardware

The physical setup consists of the following parts:

- Desktop computer with FW800 PCI-E cards to connect the cameras.
- 2× video cameras (Grasshopper type GRAS-20S4C, Point Grey Research, Scottsdale, AZ).
- 2×8mm Megapixel fixed focal lens (Edmund Optics Inc., Barrington, NJ).
- 2× Adaptor with external SM30 threads and internal SM1 threads (SM1A15, Thorlabs Inc, Newton NJ).
- 2× Lens tube, Ø1″, 0.3″ long (SM1L03, Thorlabs Inc, Newton, NJ).
- 2× blue LED lights (Blue 3 Watt LED MR16 bulb, Super Bright LEDs, Inc., St. Louis, MO).
- 2× MR16/MR11 Socket—GX5.3/GZ4 (MR16S, Super Bright LEDs, Inc., St. Louis, MO).
- 2× 12V DC Single Color LED Dimmer (LDK-8A, Super Bright LEDs, Inc., St. Louis, MO).
- 2×0700C24F 17W Xitanium LED Driver, 700mA, plus Power Cord (XI-LED120A, LED Supply, Randolph, VT).
- 2×Xitanium Driver Connector (1365323-1, LED Supply, Randolph, VT).
- MDF-GFP filter set (Thorlabs Inc, Newton, NJ).
  - 2× MF469-35 filters (pass range: ~450–490 nm).
  - 2× MF525-39 filters (pass range: ~500–550 nm).

- Standard glass Drosophila culture vial as observation chamber.
- Aluminum Breadboard, 24″ × 24″ × 1/2″ (MB2424, Thorlabs Inc., Newton, NJ).
- 2× Mounting Post, Length = 14″ (P14, Thorlabs Inc., Newton, NJ).
- 2 × 1.5″ Mounting Post Bracket (C1505, Thorlabs Inc., Newton, NJ).
- 2 × 3″ One-Arm Package, Two Knuckles, 3″ Shaft (NT53-885, Edmond Optics Inc., Barrington, NJ).
- 2× Mounting Post Base Ø2.40″ × 0.50″ High (PB2, Thorlabs Inc., Newton, NJ).
- 2× U-shaped Base Support Stand, Cast Iron (12985-078, VWR, Brisbane, CA).
- 2× Talon Rod, Aluminum 457 mm (60079-381, VWR, Brisbane, CA).
- 2 × Talon 3-Prong Dual Adjust Extension Clamp (21570-302, VWR, Brisbane, CA).
- Cardboard box.

Cameras are connected to the desktop computer via FW800 PCI-E cards. A low-end desktop computer is used, including Intel 64-bit Quad-Core Xeon Processors (2.13 GHz/Core) with 6GB of RAM and running Windows 7 enterprise (64 bit). The two LED lights have the MF469-35 filters fitted in front of them using electrician's tape, and are pointed toward the observation chamber. These filters pass light in the range of approximately 450–490 nm, which overlaps the eGFP absorption peak at approximately 488 nm. Each camera has an Edmund Optics 8 mm Megapixel fixed focal lens, with an MF525-39 filter fixed in front using lens tube and adaptor. The emission peak for eGFP is approximately 509 nm and is within the pass-range of the filter (500–550 nm). The observation chamber is a standard glass Drosophila culture vial. The bottom of the vial and the vial stopper are covered with nonreflective black cotton cloth. For longer tracking periods where water and nutrition are required we have found that grape agar media (Genesee Scientific, San Diego, CA) produces the least background. Typical fly media was found to produce significant background, which can be reduced by adding dark food coloring. Plastic (polystyrene) Drosophila culture vials can also be used but reflect more light, and although these reflections can be removed in processing, glass vials are preferable (see Note 1). After making cameras and lights rigid and stable on the breadboard, using mounting posts for the cameras and ring stands and clamps for the lights, the setup (lights, cameras, observation chamber) is isolated from outside light by covering with a cardboard box. The chamber and other parts are accessible from one side of the box that can be opened and closed to make a light-tight seal.

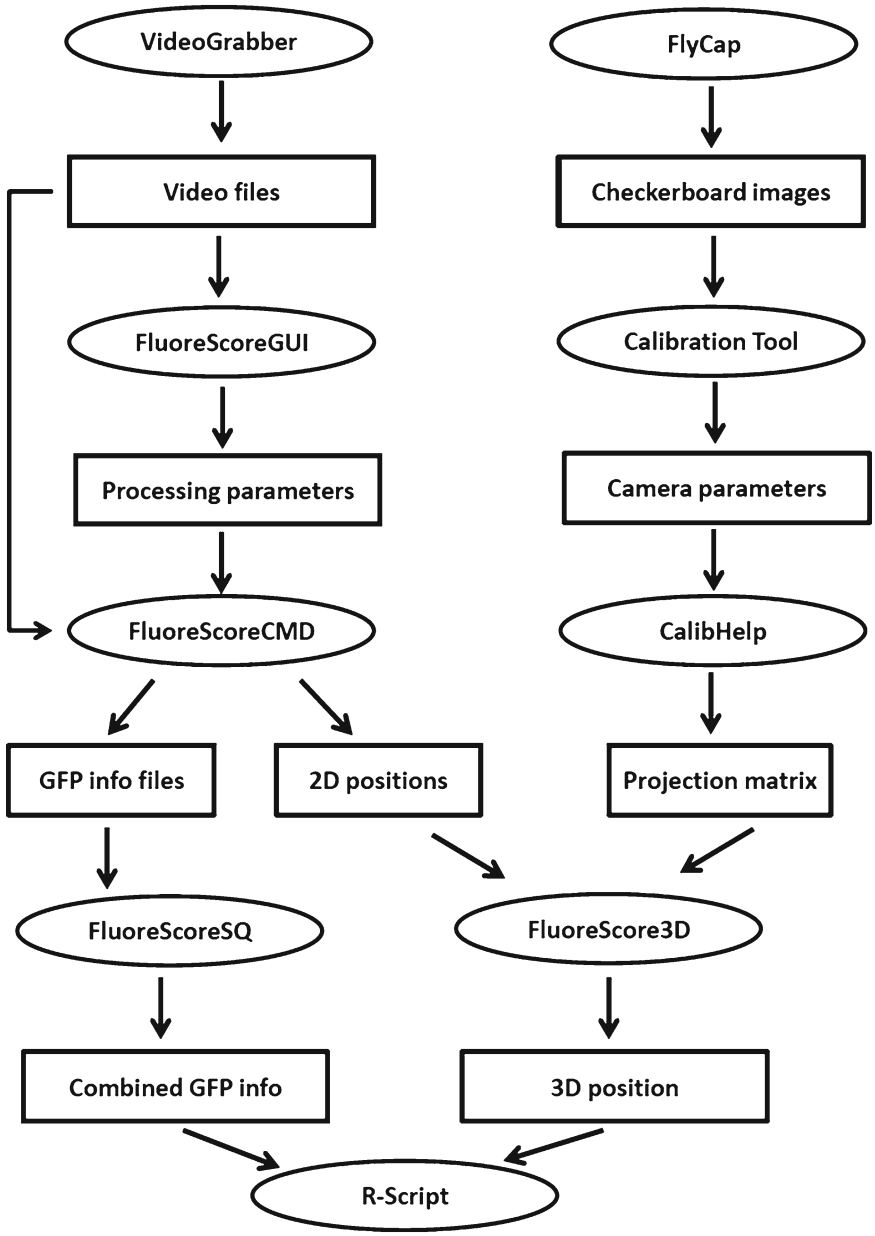

Fig. 1. FluoreScore suite modules and data flow. Each module is shown in an *ellipse*. Input and outputs are shown in a *rectangle*. *Arrows* show data flow between different components.

2.2. Software

The FluoreScore software suite has multiple modules. Each module is implemented independently to facilitate ease of use and future developments. Figure 1 shows components and data-flow of the FluoreScore suite. Custom software called VideoGrabber is

used to capture videos from the cameras (http://code.google.com/p/video-grabber/). VideoGrabber exploits FlycapSDK software (provided by Point Grey Research with the cameras) to capture synchronized videos from multiple cameras. Cameras are calibrated using software called Camera Calibration Tools, which is freely available at http://www.cs.ucl.ac.uk/staff/Dan.Stoyanov/calib/.

In addition, we provide five additional custom software modules, written in Visual Studio C++ (2005):

- CalibHelp (version 1.0): converts intrinsic and extrinsic parameters of cameras generated by Camera Calibration Tools to a projection matrix.
- FluoreScoreGUI (version 1.0): includes a graphical user interface (GUI) and is used to determine processing parameters such as the detection threshold. It also can be used to process videos, for example for extracting GFP information as well as 2D position of flies.
- FluoreScoreCMD (version 1.0): for experiments involving longer tracking periods the user needs to process multiple videos. A command line version of FluoreScore (FluoreScoreCMD) is provided that allows for batch processing of videos.
- FluoreScoreSQ (version 1.0): removes noise and irrelevant measurements from the data. In particular, it removes the data from objects with size smaller than a user-chosen threshold. In addition it combines the data from the two cameras.
- FluoreScore3D (version 1.0): generates 3D tracking using the 2D positions generated by FluoreScoreCMD.

More details about each module are provided in the next heading. FluoreScore suite is freely available at http://fluorescore.cmb.usc.edu.

3. Methods

Here, we describe the methods for conducting experiments, assuming that the hardware setup is ready. More specifically, cameras are connected to a workstation and have a full view of the chamber (see Note 2) and lighting conditions are appropriate (see Note 3). The major steps for running experiments after having the hardware setup and flies ready are as below:

1. Recording videos.
2. Calibrating cameras for 3D reconstruction.
3. Parameter findings.

4. (Batch) processing of videos and obtaining GFP and 3D trajectories.
5. Data analysis.

Details are described for each step and sub-step.

3.1. Recording Videos

A custom program called VideoGrabber is used to record compressed videos (see Note 4).

Steps for recording videos are:

1. Create a new folder, copy "VideoGrabber.exe" to the folder and run it by double clicking on it.
2. Indicate the number of frames that you want to record. If the videos are recorded at 30 fps, this means for each second you will record 30 frames. For example to record a 5 min video, you will need to input 7,200 (= 5 min × 60 s/min × 30 fps).
3. After indicating other options including display On/Off (choose Off) and recording option (choose openCV AVI) as well as the number of cameras (input 2) the display will show the camera configuration GUI where you can define the resolution, frame rate, and other options for videos. A typical setting is resolution 800 × 600, frame rate 30 fps, and YUV 422 color space for recording.
4. After pressing ok, it will ask about the codec; press Enter to choose the default codec, which is FFDS and stands for ffdshow codec (see Note 5) and it will begin to grab frames from the cameras and save them in a file. It will show a "done!" message after it grabs the number of frames that you have indicated at step 2.

3.2. Calibrating the Cameras

To reconstruct 3D points the projection matrix must be obtained for each camera. The camera projection matrix P describes the mapping between the real 3D points (X, Y, Z) to the 2D points (x, y) in the image (22). Freely available software called Camera Calibration Tools is used to find the intrinsic and extrinsic parameters of the cameras. A small custom program called "CalibHelp" converts these parameters to a projection matrix for the cameras.

3.2.1. Camera Calibration Tool

Camera Calibration Tools (http://www.cs.ucl.ac.uk/staff/Dan.Stoyanov/calib/) has been developed by Daniel Stoyanov. This software calibrates cameras using multiple images of a checkerboard in different positions. The checkerboard should be an N × N grid with squares of the same size. Figure 2a shows a 13 × 13 checkerboard that we used for calibration, and the 10 × 10 square in the middle of the checkerboard was used as follows: Each corner is marked by a number to indicate the x-axis and y-axis and origin. Since we want to keep the axes and the origin the same in all 2D

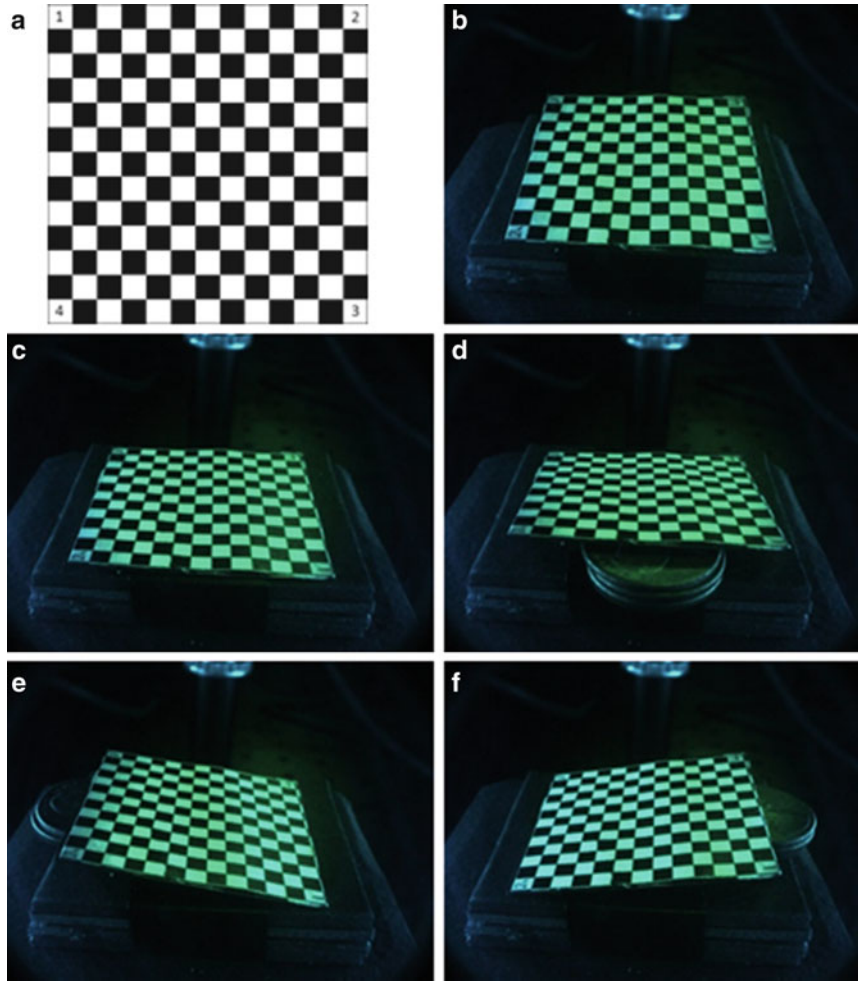

Fig. 2. Camera Calibration. (**a**) Sample checkerboard for calibration. (**b**–**f**) Checkerboard in five different orientations. Except for position one, at each position one side of the checkerboard is elevated to cover different 3D points in space and provide more sample points for Camera Calibration Tools.

images, we indicate them with a number to make sure the origin (O) is the same for all 2D images.
The steps for calibration are:

1. Create an $N \times N$ checkerboard (at least 5×5).
2. Take five different images for each camera and in each image incline the checkerboard at different angles (Fig. 2b–e).
3. Add images to the Camera Calibration Tool, define the size of the checkerboard (here 10×10) and choose the corners for each image. Make sure the order of choosing the corners stays

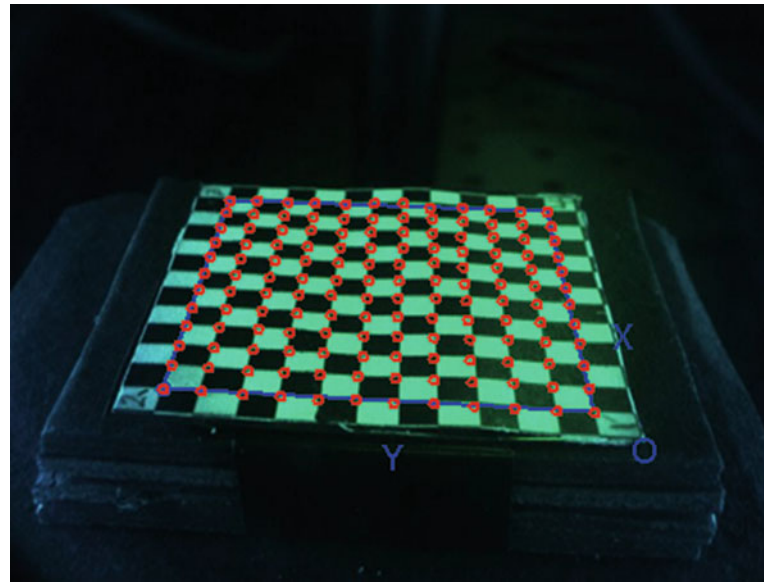

Fig. 3. Camera Calibration Tools. Camera Calibration Tools selects the vertex of each square in the checkerboard.

the same (i.e., corner1 → corner 2 → corner 3 → corner 4). After selecting corners, Calibration Tool extracts intersection points of inner squares (Fig. 3).

4. Press the calibration button for each camera and save the project. All intrinsic and extrinsic parameters will be saved in an output file.

For more details please refer to the manual of Camera Calibration Tool that is available online.

3.2.2. CalibHelp

This program converts intrinsic and extrinsic parameters into a projection matrix. To use CalibHelp, copy "CalibHelp.exe" to the same folder where the output of Camera Calibration Tool is located and run it. It will create a file named "projMat.txt" in the same folder. This file contains the projection matrix of the cameras, which will be used by the FluoreScore3D module to generate 3D points from 2D points (see Note 6).

3.3. Parameter Finding

1. There are three parameters that should be determined before processing using FluoreScoreGUI. The most important one is the threshold for detecting flies (21). The optimal value for this threshold will vary based on the lighting conditions and specific experimental setup. Once the user starts to (pre)process a video, they can see what will be detected with different thresholds. In the processed window flies should be marked, and background pixels should be minimized or eliminated. Figure 4 shows examples of detected fly silhouettes with different threshold values (see Note 7).

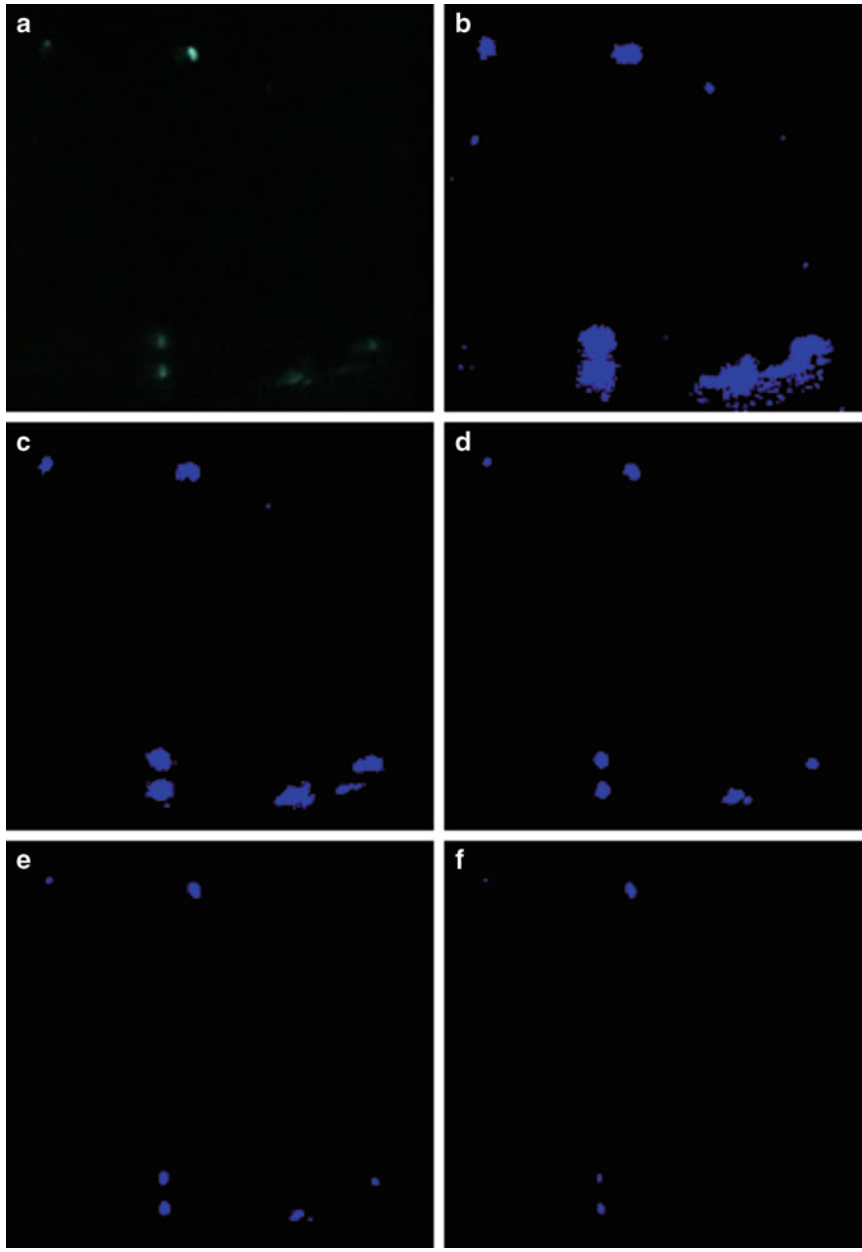

Fig. 4. Selecting threshold for silhouette detection. (**a**) Original image from the camera. (**b**–**f**) Detected components using different thresholds: threshold = 5 (**b**), threshold = 10 (**c**), threshold = 20 (**d**), threshold = 30 (**e**), or threshold = 50 (**f**). Different thresholds lead to different detected components. FluoreScoreGUI enables the user to see the detected components and choose appropriate thresholds.

2. Because of the LED lights, sometimes there is glare in videos on the wall of the vial or on the base of the chamber. To exclude such glare from the analysis, the user can define a processing mask for each view by free-hand drawing; the mask marks regions that will not be included in the quantification. FluoreScoreGUI saves the mask in a .jpg file, which is used as an input parameter for FluoreScoreCMD so that it can be applied to multiple videos recorded under the same conditions (see Subheading 3.4.1).
3. To make the processing faster as well as more accurate the user can also define a region of Interest (ROI) in a view, which is a rectangle that just covers the chamber in the view. By defining an ROI, FluoreScore does not process the part of the images that are not useful, thereby increasing processing speed. An ROI rectangle is defined by two points (top-left and bottom-right). These points are saved in a text file and used as input parameters for FluoreScoreCMD.

3.4. Processing Videos

After finding parameters, the user can start processing the videos. Processing videos has several steps. The first step is to generate from the videos the raw data files that contain GFP values and 2D positions of the fly, using FluoureScoreGUI or FluoreScoreCMD. The next step is to process the data and combine the information from both views using FluoreScoreSQ. These files along with the projection matrix file (see Subheading 3.2) will be used in FluoreScore3D to generate 3D position of the fly.

3.4.1. FluoreScoreCMD

FluoreScoreCMD should be called from the command-line to start processing videos. It will generate two CSV files for each view. One file contains 2D positions of the flies in that view. The other file contains intensity information on detected flies. More specifically, for each frame, intensity values (between 0 and 256) are calculated for red, blue, and green channels for pixels that represent flies. For each channel the pixels are separated into four bins based on the pixel intensity values. For example, for the green channel, pixels are separated into bins G1, G2, G3 and G4 of increasing intensity. For each fly, the histogram of pixel intensity values is calculated along with the sum of intensities for each bin of the histogram. Below, the input parameters and command line format for FluoreScoreCMD are shown.

Command:

FluoreScoreCMD.exe <a1> <a2> … <a16>

a1: inputAviFile for View 1

a2: threshold value for View1, should be between 0 and 127

a3: inputAviFile for View 2

a4: threshold value for View2, should be between 0 and 127

a5: showing videos while processing (y or n).

a6: Number of frames to process, put −1 to the whole video

a7: Mask file name for view 1 (jpg file)

a8: X-coordination of top-left for view 1, min = 0, max = 800

a9: Y-coordination of top-left for view 1, min = 0, max = 600

a10: X-coordination of down-right for view 1, min = 0, max = 800

a11: Y-coordination of down-right for view 1, min = 0, max = 600

a12: Mask file name for view 1 (jpg file)

a13: X-coordination of top-left for view 1, min = 0, max = 800

a14: Y-coordination of top-left for view 1, min = 0, max = 600

a15: X-coordination of down-right for view 1, min = 0, max = 800

a16: Y-coordination of down-right for view 1, min = 0, max = 600

Example:

FluoreScoreCMD.exe Case_View0.avi 15 Case_View1.avi 15 y −1 mask1.jpg 200 200 400 400 mask2.jpg 100 100 500 500

3.4.2. FluoreScoreSQ

1. After processing videos from each view, FluoreScoreSQ is used for de-noising and for combining information from both views. FluoreScoreSQ combines the intensity values from two views and generates a CSV file including the intensity values for each frame. Moreover, if there are some detected components whose size is smaller than a chosen threshold, they will be removed (see Notes 8 and 9). Below, the use of FluoreScoreSQ is exemplified.

Command:

FluoreScoreSQ.exe <a1> <a2> <a3> <a4> <a5>

a1: input intensity CSV file for view 1 (contains intensity info and is generated by FluoreScore)

a2: input intensity CSV file for view 2 (contains intensity info and is generated by FluoreScore)

a3: output CSV file for combined results of view 1 and view 2

a4: fly number (should be 1 for 3D tracking)

a5: threshold of the size of fly in pixels (with current setup it would be around 20–50)

Example:

FluoreScoreSQ.exe 0_0.csv 0_1.csv 0.csv 0_pos1.csv 0_pos2.csv 1 20

3.4.3. FluoreScore3D

2. FluoreScore3D uses the 2D position files for each view as well as the projection matrix file, and generates 3D position for each frame where 2D positions were available in both views (see Notes 10 and 11). FluoreScore3D is used as described below:

Command:

FluoreScore3D.exe <a1> <a2> <a3> <a4>

a1: input CSV file for view 1 (contains 2D positions of fly, is generated by FluoreScore)

a2: input CSV file for view 2 (contains 2D positions of fly, is generated by FluoreScore)

a3: projmat.txt (generated in Subheading 3.2.1)

a4: output CSV file containing 3D position of the fly

Example:

FluoreScore3D.exe experiment_pos1.csv experiment_pos2.csv projmat.txt experiment_3dpos.csv

3.4.4. Batch Processing

Experiments involving longer tracking periods will generate multiple videos. For example, if an experiment is for 48 h, VideoGrabber (with default settings) will generate 48 1-hour video segments. Processing these videos one by one is laborious. Because we have provided command line versions of the software modules, it is straightforward to have a BAT file that runs all the modules on

multiple videos. A file called "runFSInBatch.bat" is provided that processes all segments of an experiment at once (see Note 12). Below, the use of FluoreScoreBatch.bat is shown:

Command:

FluoreScoreBatch.bat <a1> <a2>

a1: first hour to be processed

a2: last hour to be processed

Example:

FluoreScoreBatch.bat 1 48

3.4.5. Data Analysis

After running the previous modules, GFP data as well as the 3D positions of the fly have been calculated. R is then used to perform basic statistical analysis, including mean and standard deviation, calculation of motion parameters including velocity and frequency of directional heading changes, and data visualization.

4. Notes

1. When preparing the chamber make sure the following steps are done; (a) clean the chamber with water followed by ethanol, using cotton swabs. (b) Clean the chamber plug using scotch tape to remove any lint and prevent background reflection. (c) Put flies into the chamber and push the plug into the vial until 2.0 cm from the bottom. (d) Place observation vial in defined location in front of the cameras. For optimal results the cameras should be inclined slightly downwards towards the observation chamber. A stand for the observation chamber can be fixed in place in front of the cameras; we have used stacked plastic eppendorf tube racks, taped together, with a circle drawn on top to indicate the location for placement of the observation chamber. We have also found it useful to tape pieces of thick black paper to the top of the stand to create a slot into which the observation chamber fits. The ring stands holding the LED lights can be moved closer or further away from the observation chamber to optimize lighting conditions and to make lighting equal for the two cameras; alternatively lighting can be adjusted using the LED Dimmers.
2. Once the cameras are calibrated they should not be moved or rotated; make sure they are sturdy and fixed in place before starting the calibration process.

3. To get the best signal possible make sure there is no light changing during an experiment. To do so make sure that the observation chamber and cameras are completely isolated from outside light.
4. The data storage capacity of the operating system employed here requires that files be smaller than 2 GB; therefore VideoGrabber will record videos in separate files of a length of 108,000 frames (equal to 1 h at 30 fps).
5. Recording uncompressed videos requires a lot of space and storing long experiments is practically impossible. VideoGrabber can record compressed videos. However the appropriate codec should be installed. More specifically, to be able to read/write compressed videos, codecs are needed. There are many codecs available for this task. We chose "ffdshow" due to its compatibility with openCV library and high compression rate. It is freely available at (http://sourceforge.net/projects/ffdshow/).
6. HelpCalib writes the projection matrices of cameras in "projmat.txt" with the same order that they have been added in Camera Calibration Tool. It is arbitrary to choose which camera be the "first" view. However, the order should be same for the FluoreScore3D to assign projection matrices to cameras correctly (see Note 10).
7. To choose an appropriate threshold for fly detection adjust the threshold such that the fly is detected in the majority of frames, and background (scattered) pixels are eliminated. Once you find the optimal threshold make sure you keep it the same across any additional samples that you wish to compare so that data are analyzed consistently.
8. Fly Size choice means the minimum size of the fluorescent region of the fly, as that is what is being detected. If this parameter is set too large, you will never detect flies. At the same time you want to set it large enough that you filter noise (which is mostly small connected components consisting of a few pixels). Larger settings will tend to eliminate frames where your fly is farther away and/or oriented such that only a part of the fluorescent region is detected. This is not ideal for a movement assay as you want to detect your fly in as many frames as possible. Typical values for expression specifically in eye tissue is 15–20, and for expression throughout the fly ~50.
9. Fly Number usually is equal to the number of flies in the observation chamber. However, it is possible to have multiple flies in the observation chamber and to set Fly Number to a smaller value if you want to recognize only a subset of the flies (for example the brightest or biggest, depending upon how the detection threshold and fly size have been set).

10. The order of inputs is important. Make sure the first file (view 1 csv file) belongs to the camera that is chosen to be the "first" view in the calibration step.
11. There are some frames in which a fly is not visible in either view. In these frames the 3D position of the fly cannot be obtained because two views of 2D points are needed to be able to perform 3D reconstruction.
12. To be able to use the batch file make sure you do not change the name of the video files that are generated by VideoGrabber.

Acknowledgement

This work was supported by grants from the Department of Health and Human Services to ST (HG02790) and to JT (AG011833). We thank Ravi Prakash for help writing CalibHelp and Anurag Biyani for providing VideoGrabber.

References

1. Salmon AB, Richardson A, Perez VI (2010) Update on the oxidative stress theory of aging: does oxidative stress play a role in aging or healthy aging? Free Radic Biol Med 48:642–655
2. Sprott RL (2010) Biomarkers of aging and disease: introduction and definitions. Exp Gerontol 45:2–4
3. Pincus Z, Slack FJ (2011) Developmental biomarkers of aging in *Caenorhabditis elegans*. Dev Dyn 239:1306–1314
4. Piazza JR, Almeida DM, Dmitrieva NO, Klein LC (2010) Frontiers in the use of biomarkers of health in research on stress and aging. J Gerontol B Psychol Sci Soc Sci 65:513–525
5. Zahn JM, Sonu R, Vogel H, Crane E, Mazan-Mamczarz K, Rabkin R, Davis RW, Becker KG, Owen AB, Kim SK (2006) Transcriptional profiling of aging in human muscle reveals a common aging signature. PLoS Genet 2:e115
6. Pletcher SD, Macdonald SJ, Marguerie R, Certa U, Stearns SC, Goldstein DB, Partridge L (2002) Genome-wide transcript profiles in aging and calorically restricted *Drosophila melanogaster*. Curr Biol 12:712–723
7. Landis GN, Abdueva D, Skvortsov D, Yang J, Rabin BE, Carrick J, Tavaré S, Tower J (2004) Similar gene expression patterns characterize aging and oxidative stress in *Drosophila melanogaster*. Proc Natl Acad Sci USA 101: 7663–7668
8. Tower J (2009) Hsps and aging. Trends Endocrinol Metab 20:216–222
9. King V, Tower J (1999) Aging-specific expression of Drosophila hsp22. Dev Biol 207: 107–118
10. Wheeler JC, Bieschke ET, Tower J (1995) Muscle-specific expression of Drosophila hsp70 in response to aging and oxidative stress. Proc Natl Acad Sci USA 92:10408–10412
11. Yang J, Tower J (2009) Expression of hsp22 and hsp70 transgenes is partially predictive of drosophila survival under normal and stress conditions. J Gerontol A Biol Sci Med Sci 64: 828–838
12. Rea SL, Wu D, Cypser JR, Vaupel JW, Johnson TE (2005) A stress-sensitive reporter predicts longevity in isogenic populations of *Caenorhabditis elegans*. Nat Genet 37:894–898
13. Jones MA, Grotewiel M (2011) Drosophila as a model for age-related impairment in locomotor and other behaviors. Exp Gerontol 46: 320–325
14. Koh K, Evans JM, Hendricks JC, Sehgal A (2006) A Drosophila model for age-associated changes in sleep:wake cycles. Proc Natl Acad Sci USA 103:13843–13847
15. Rakshit K, Krishnan N, Guzik EM, Pyza E, Giebultowicz JM (2012) Effects of aging on the molecular circadian oscillations in Drosophila. Chronobiol Int 29:5–14

16. Studenski S, Perera S, Patel K, Rosano C, Faulkner K, Inzitari M, Brach J, Chandler J, Cawthon P, Connor EB, Nevitt M, Visser M, Kritchevsky S, Badinelli S, Harris T, Newman AB, Cauley J, Ferrucci L, Guralnik J (2011) Gait speed and survival in older adults. JAMA 305:50–58
17. Grover D, Tower J, Tavare S (2008) O fly, where art thou? J R Soc Interface 5:1181–1191
18. Grover D, Yang J, Ford D, Tavare S, Tower J (2009) Simultaneous tracking of movement and gene expression in multiple *Drosophila melanogaster* flies using GFP and DsRED fluorescent reporter transgenes. BMC Res Notes 2:58
19. Grover D, Yang J, Tavare S, Tower J (2008) Simultaneous tracking of fly movement and gene expression using GFP. BMC Biotechnol 8:93
20. Zou S, Liedo P, Altamirano-Robles L, Cruz-Enriquez J, Morice A, Ingram DK, Kaub K, Papadopoulos N, Carey JR (2011) Recording lifetime behavior and movement in an invertebrate model. PLoS One 6:e18151
21. Ardekani R, Huang YM, Sancheti P, Stanciauskas R, Tavaré S, et al. (2012) Using GFP Video to Track 3D Movement and Conditional Gene Expression in Free-Moving Flies. PLoS ONE 7(7): e40506. doi:10.1371/journal.pone.0040506
22. Hartely R, Zisserman A (2004) Multiple view geometry in computer vision, 2nd edn. Cambridge University Press, Cambridge

Chapter 34

Assessing Vascular Senescence in Zebrafish

Sandra Donnini, Antonio Giachetti, and Marina Ziche

Abstract

Zebrafish, a diurnal vertebrate characterized by gradual senescence, is an excellent model for studying age-dependent diseases, such as neurodegenerative diseases. Cerebral amyloid angiopathy (CAA) caused by amyloid β (Aβ) deposition around brain microvessels is a human neurovascular degenerative disease that is characterized by an early onset of recurrent stroke episodes, vascular brain degenerative changes, and moderate to severe clinical presentations. Recently, by using the zebrafish model, we investigated whether Aβ peptides cause endothelial cells to enter senescence at an early stage of vascular development. During early embryonic zebrafish development, the presence of senescence-associated biomarkers, such as β-galactosidase and the cyclin-dependent kinase inhibitor p21, has been shown to be predictive of the premature aging phenotype. By measuring β-galactosidase activity and p21 expression in whole-mount zebrafish embryos exposed to Aβ, we demonstrated that these oxidative peptides promote vascular senescence at an early stage of development, a harbinger of vascular clinical symptoms in adult. This chapter describes the methods for studying cell senescence in zebrafish, detailing protocols for β-gal activity and the in situ p21 hybridization in whole-mount zebrafish embryos.

Key words: Amiloid β peptides, β-Galactosidase, Cerebral amyloid angiopathy, Cyclin-dependent inhibitor p21, In situ hybridization, Vascular senescence

1. Introduction

The interest in the age-associated cerebrovascular diseases stems from the recognition that brain vessels dysfunction concurs to the progression, and perhaps to the aggravation of neurodegenerative pathologies, among which Alzheimer's disease is the most prominent. Cerebral amyloid angiopathy (CAA) is a cerebrovascular disease, characterized by deposition of amyloid peptides around brain vessels, hypoperfusion, and aberrant vessels (1–3). CAA, frequently coexisting with Alzheimer disease, is primarily an age-related disease, and, therefore, appears to be a suitable model for exploring the relationship between aging and development of cerebrovascular diseases. Furthermore, numerous dominant hereditary human

Lorenzo Galluzzi et al. (eds.), *Cell Senescence: Methods and Protocols*, Methods in Molecular Biology, vol. 965,
DOI 10.1007/978-1-62703-239-1_34,

CAA variants, which originate from genetic mutations in the amyloid precursor protein (APP), give rise to different disease phenotypes. The best known, the Dutch mutant, features early onset of recurrent stroke episodes (occurring as early as in the fourth decade), and severe clinical presentation (4). In this context, given the long-term interest of our laboratory in the vascular effects of amyloid peptides, in order to investigate whether natural Amyloid β (Aβ) or the Aβ-Dutch peptides would cause endothelial cells to enter senescence at an early stage of vascular development, we used the zebrafish model at the embryonic/larval stages, when blood vessels develop very rapidly (5).

Among the models of human senescence, zebrafish (*Danio rerio*) has emerged as a highly promising model for studies of vertebrate senescence (6, 7). The optical transparency of zebrafish at embryonic and larval stages, combined with the small size and high fecundity has made them a preferred vertebrate of developmental biologists. Zebrafish is a diurnal vertebrate which lives for approximately 3–5 years and show gradual senescence similar to humans. With age, they often display spinal curvature, related to muscle abnormalities (8), increased lipofuscin (aging pigment) in the liver, similar to mice and humans (9), and retinal atrophy (10). In aged zebrafish, senescence-associated β-galactosidase (SA-β-gal) activity has been detected in skin (11). Further, SA-β-gal activity early in the development correlates with an accelerated aging phenotype in zebrafish.

Here, we describe the protocol to study the senescence marker β-gal in embryos zebrafish exposed to Aβ peptides, and in histological sections, to determine β-gal staining in vessels.

We also describe a novel approach for investigating senescence in zebrafish, which consist in measuring the expression of the messenger RNA for p21, a cyclin-dependent inhibitor that induces cell cycle arrest, a typical feature of cell senescence (12–14). In situ hubrydization in whole-mount embryos is a method widely used to evaluate the expression pattern of developmentally regulated genes (15–18). By measuring β-galactosidase activity and p21 expression in whole-mount zebrafish embryos exposed to Aβ, we demonstrated that these oxidative peptides promote vascular senescence at an early stage of vascular development, a harbinger of vascular clinical symptoms in adult.

2. Materials

2.1. Common Materials

- Zebrafish AB strain (see Note 1).
- Fish water (Instant Ocean, 0.01% Methylene Blue).
- Petri dishes.

- Pronase solution (100 μg/mL; Protease from Streptomyces griseus; Sigma, cat. no. P6911).
- 1-Phenyl-2-thiourea (PTU, Sigma, cat. no. P7629) (see Note 2).
- Sterile distilled water.
- Dulbecco's phosphate-buffered saline (PBS, Sigma, cat. no. D-5652).
- Paraformaldehyde (PFA, Sigma, cat. no. P-6148) (see Note 3).
- Ethanol absolute (Sigma, cat. no. 459844) (see Note 4).
- Glycerol >99% (Sigma, cat. no. G6279) (see Note 5).
- Images are taken with a Leica microscope DM6000B equipped a Leica DCF480 digital camera and the software LAS (Leica Application Suite) (Leica, Germany).
- Planachromatic objectives.

2.2. SA-β-Gal Staining

- Paraformaldeyde/phosphate-buffered saline 4%.
- SA-β-galactosidase detection kit (Millipore-Chemicon, Billerica, MA, USA) (see Note 6).
- Components:
  - 100× Fixing Solution: One 1.5 mL vial.
  - 10× Staining Solution A: One 15 mL bottle.
  - 10× Staining Solution B: One 15 mL bottle.
  - X-gal Solution: Two 1.5 mL vials.
- 30–50–70% EtOH in water.
- NaN_3 0.1% (Sigma-Aldrich, St. Louis, MO, USA) (see Note 7).
- Glycerol 70% in water (Sigma-Aldrich).
- LR White resin (London Resin Company; Working, Surrey, UK) (see Note 8).
- Reichert Ultra-cut "E" (see Note 9).

2.3. p21 In Situ Hybridization

- p21 plasmid or genomic p21.
- PCR master mix (Promega, Madison, WI, USA) (see Note 10).
- Trizma base (Sigma-Aldrich).
- Ethylenediaminetetraacetic acid (EDTA) (Sigma-Aldrich) (see Note 11).
- Boric acid (Sigma-Aldrich).
- Agarose (Sigma-Aldrich) (see Note 12).
- Transcription buffer (Promega).
- DL-Dithiothreitol (DTT) (Promega) (see Note 13).
- DIG RNA labeling mix (UTP) (Roche, Basel, Switzerland).
- RNasein (Promega).

- T3 RNA-Polymerase (Promega).
- T7 RNA-Polymerase (Promega).
- RNase free DNAse I (Roche).
- NaOH (Sigma-Aldrich).
- RNAlater (Sigma-Aldrich).
- Methanol (MeOH) (Sigma-Aldrich) (see Note 14).
- NaCl (Sigma-Aldrich).
- KCl (Sigma-Aldrich).
- $MgSO_4$ (Sigma-Aldrich).
- $Ca(NO_3)$ (Sigma-Aldrich).
- HEPES (Sigma-Aldrich).
- H_2O_2 (Sigma-Aldrich) (see Note 15).
- KOH (Sigma-Aldrich).
- Tween 20 (Sigma-Aldrich) (see Note 16).
- Proteinase K (10 mg/mL) (Roche Diagnostics).
- Formamide (Sigma-Aldrich) (see Note 17).
- Citric acid trisodium salt (Sigma-Aldrich).
- Citric acid monohydrate (Sigma-Aldrich).
- Heparin sodium salt (Sigma-Aldrich).
- tRNA from wheat germ type V, lyophilized powder (Sigma-Aldrich).
- Phenol solution saturated with 0.1 M citrate buffer, pH 4.3 (Sigma-Aldrich) (see Note 18).
- Chloroform (Sigma-Aldrich) (see Note 19).
- Sodium acetate (Merck, Darmstadt, Germany).
- Sheep serum (Sigma-Aldrich).
- Albumin from bovine serum (BSA, Sigma-Aldrich).
- Sheep anti-digoxigenin-AP Fab fragments (Roche Diagnostics).
- HCl (Sigma-Aldrich) (see Note 20).
- $MgCl_2$ (Sigma-Aldrich).
- Nitro blue tetrazolium (NBT, Sigma-Aldrich) (see Note 21).
- 5-Bromo 4-chloro 3-indolyl phosphate (BCIP, Sigma-Aldrich) (see Note 22).
- *N*,*N*-dimethylformamide anhydrous, 99.8% (Sigma-Aldrich) (see Note 23).
- $Na_2HPO_4 \cdot 12H_2O$ (Fluka-Sigma-Aldrich).
- NaH_2PO_4 (Merck).
- Stop solution (see Note 24).

- 10× PBS, pH 5.5, stock solution (see Note 25).
- PBT (see Note 26).
- 20× SSC stock solution (see Note 27).
- Blocking buffer (see Note 28).
- Alkaline Tris buffer (see Note 29).
- Microcon YM-50 columns (Millipore).
- Sigmaspin post-reaction purification columns (Sigma-Aldrich).

3. Methods

3.1. SA-β-Gal Staining

1. Zebrafish are raised and maintained at 28°C on a 14 h light/10 h dark cycle. Embryos are collected by natural spawning in fish water (Instant Ocean, 0.01% Methylene Blue) in Petri dishes, and their age is expressed in hours post fertilization (hpf) or in days post fertilization (dpf), according to Kimmel (14).
2. Dechorionate embryos with pronase solution (100 μg/mL) at 6 hpf (see Note 30).
3. Treat with 0.003% phenylthiourea (PTU) at 24 hpf to prevent pigmentation (see Note 31).
4. Administer Aβ from 12 somites stage (somitogenesis) until 7 dpf (larval stage) of zebrafish development, every 24 h (see Note 32).
5. Fix zebrafish larvae (7 dpf) at room temperature for 2 h in 4% paraformaldehyde/phosphate-buffered saline (see Note 33).
6. Wash three times in PBS 1×, 15 min each wash.
7. Make up the senescence staining mixture as recommended by the vendor (Millipore-Chemicon). Add 1 mL to embryos and incubate for 4 h at 37°C. We have used the SA-Galactosidase Detection Kit (Millipore-Chemicon).
8. Wash animals three times in 1× PBS, 15 min each washes.
9. Zebrafish can be stored at 4°C in 1× PBS and 0.1% NaN_3 or in 70% glycerol at 4°C.
10. Photograph all animals under the same conditions and quantify SA-β-gal activity using a selection tool in Adobe Photoshop for blue color range, according to Kishi et al. (10).
11. Take images with microscope (Fig. 1).

For histological analysis

1. Start from step 5 above: fix zebrafish larvae for 4 h at room temperature in 4% paraformaldehyde/PBS.
2. Stain the larvae as described above (steps 6–8).

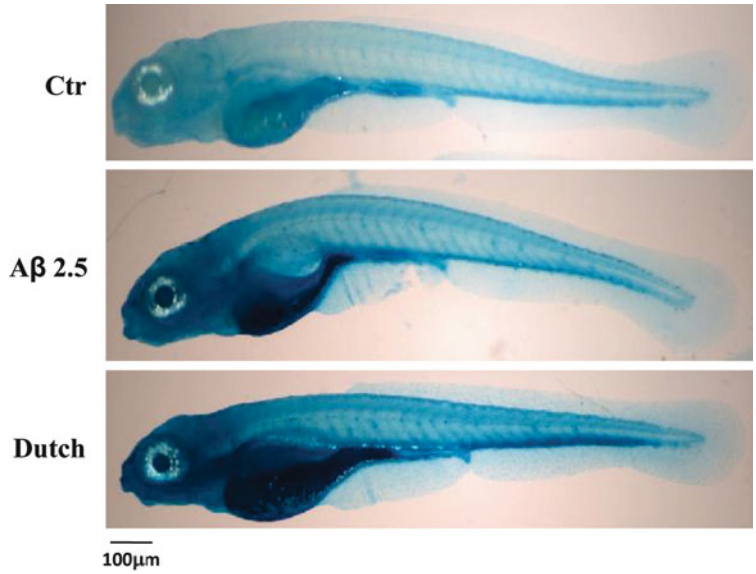

Fig. 1. β-Gal activity in whole-mount zebrafish at 7 dpf. Zebrafish were exposed to Aβ repeated treatment (2.5 μM) (images at ×3.2). Image adapted from ref. 5.

3. Dehydrate the embryos in 30–50–70% EtOH at room temperature.
4. Immerse the larvae in a mixture 2:1 LR White resin (London Resin Company; Working, Surrey, UK): 70% EtOH for 5 min.
5. Wash in PBS 1× 10 min.
6. Immerge in pure LR White resin, overnight on a rotary device.
7. Embed the larvae at 50°C with LR white resin.
8. Each larvae are sectioned on a Reichert Ultra-cut "E" at 3 μm.
9. Stain with basic fuxine for light microscopy.
10. Take images (Fig. 2).

3.2. p21 In Situ Hybridization

1. For the p21 probe (also known as *cdkn1a*) set up 100 μL PCR in a 0.5 mL sterile tube as follow:

Template DNA	0.5 μL	(10–100 ng)
Forward primer (500 ng/mL)	0.5 μL	(250 ng)
Reverse primer (500 ng/mL)	0.5 μL	(250 ng)
PCR master mix (2×)	50 μL	(1×)
Sterile water up to	100 μL	

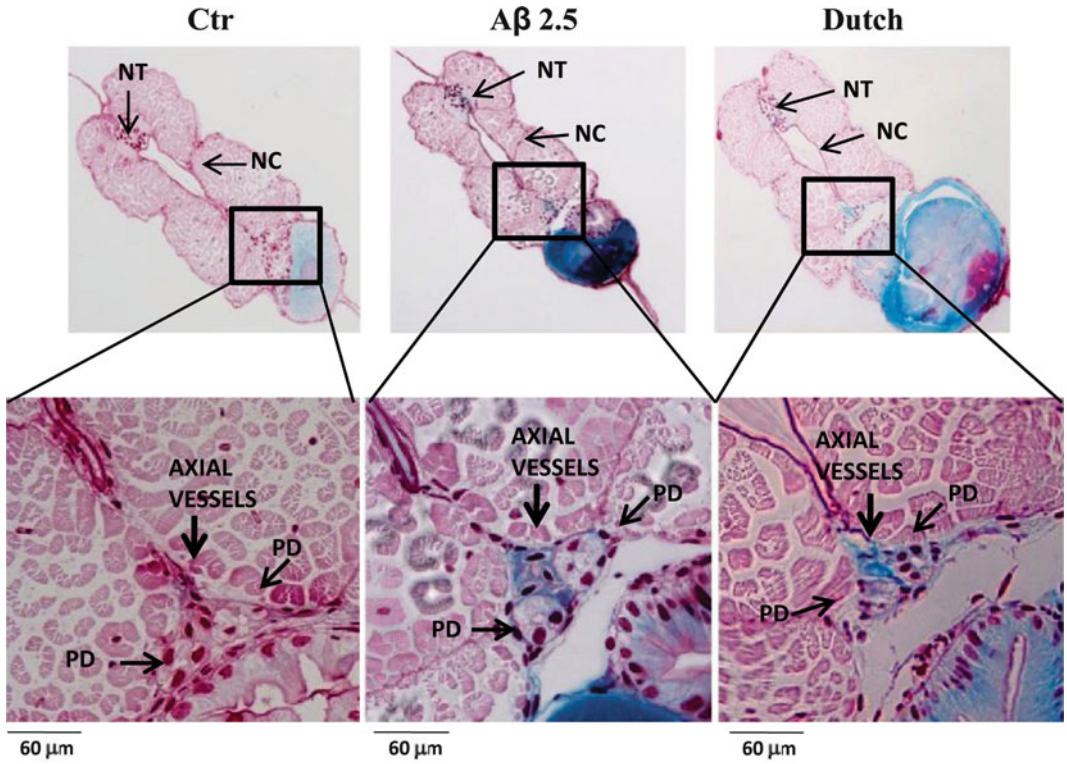

Fig. 2. *Top \nel*: β-Gal-positive vessels in larvae trunk (transversal section, ×40), taken from whole mounts reported in Fig. 1. *Bottom panel*: enlarged areas show axial vessels β-Gal positive (*arrows*). NT, neural tube; NC, notochord; PD, pronephric ducts. Image adapted from ref. 5.

p21 forward: *5′-ATGCAGCTCCAGACAGATGA-3′*,

p21 reverse: *5′-CGCAAACAGACCAACATCAC-3′* (see Note 34).

2. Run the PCR using the follow conditions: 4 min at 95°C, 40 cycles as follows: 30 s at 95°C, 30 s at 55°C, and 1 min at 72°C; 7 min at 72°C.
3. Add the 100 μL PCR to a Microcon YM-50 column and add 400 μL of sterile water. Centrifuge for 15–20 min at 1,000×*g* at room temperature.
4. Place the Microcon column into a new microfuge tube, add 20 μL of sterile water, vortex briefly, and then turn the Microcon column upside down. Spin for 1 min at 1,000×*g* at room temperature to recover the DNA (see Note 35).
5. Check the quality, quantity, and size of the PCR amplification product by loading 1/20 of the preparation on a 1% (w/v) agarose gel in 1× TBE buffer.

6. Add to a microfuge tube:

Template DNA from PCR	2.5 µL	200 ng
5× Transcription buffer	1 µL	1×
DTT (0.1 M)	0.5 µL	10 mM
DIG-RNA labeling mix (10×)	0.5 µL	1×
RNAsein (40 U/mL)	0.25 µL	10 U
T3 or T7 RNA polymerase (20 U/mL)	0.25 µL	5 U

7. Mix and incubate for 2 h at 37°C (see Note 36).
8. Add 2 µL of RNase-free DNase I and 18 µL of sterile water. Mix and incubate for 30 min at 37°C.
9. Stop the reaction by adding 1 µL of sterile 0.5 M EDTA and 9 µL of sterile water.
10. Place a Sigmaspin post-reaction purification column on top of a microfuge tube. Centrifuge for 15 s at 750×*g*.
11. Break the base of the column and discard the lid. Spin for 2 min at 750×*g*.
12. Place the column on a new microfuge tube. Add the RNA template on top of the resin. Centrifuge for 4 min at 750×*g*. Discard the column.
13. Add 1 µL of sterile EDTA 0.5 M and 9 µL of RNAlater to the sample (see Note 37).
14. Visualize 1/20 of the synthesized RNA on 1% (w/v) agarose gel in 1× TBE buffer after 30 min of electrophoresis at 230 V.
15. Fix embryos (72 hpf, after dechorionation) for 2 h at room temperature in 4% paraformaldehyde/phosphate buffered saline, then wash twice in PBS-Tween, 5 min each, at room temperature (see Note 38).
16. Dehydrate the embryos in 100% methanol (MeOH) for 15 min at room temperature and store at −20°C until processed (see Note 39).
17. Rehydrate embryos into successive dilutions of methanol in 1× PBS: 5 min in 75% (v/v) methanol; 5 min in 50% (v/v) methanol; and 5 min in 25% (v/v) methanol.
18. Wash four times, 5 min per wash, in 100% PBT.
19. Permeabilize the embryos by digestion with proteinase K (10 µg/mL in 1× PBS) at room temperature (40 min) (see Note 40).
20. Stop the proteinase K digestion by incubating the embryos for 20 min in 4% (w/v) paraformaldehyde in 1× PBS.
21. Transfer the embryos from to 1.5 mL sterile Eppendorf tubes (up to 50 embryos per tube).

22. Prehybridize the embryos for at least 3 h at 62°C in hybridization buffer (50% formamide, 5× SSC, 50 μg/mL heparin, 500 μg/mL tRNA, 0.1% Tween 20, 1 M citric acid pH 6.0) (see Note 41).
23. Discard the hybridization buffer and replace with 400 μL of hybridization buffer containing 200 ng of antisense DIG-labeled RNA probe. Hybridize overnight at 62°C (see Note 42).
24. Incubate for 10 min the embryos with 200 μL of hybridization buffer (without RNase-freetRNA and heparin) warmed at 62°C.
25. Gradually change the hybridization buffer to 2× SSC: wash once in each of the following: 75% hybridization buffer, 50% hybridization buffer, 25% hybridization buffer and 100% 2× SSC. Perform washes in a 62°C water bath with gentle shaking, 10 min each wash.
26. Wash twice, for 30 min/wash, in 0.2× SSC at 62°C.
27. Gradually replace 0.2× SSC with PBT: wash once at room temperature, in agitation, in 200 μL of the following solutions: 75% 0.2× SSC, 50% 0.2× SSC, 25% 0.2× SSC and 1× PBT, 10 min each wash.
28. Incubate the embryos for 3–4 h at room temperature in blocking buffer under agitation (see Note 43).
29. Incubate in 200 μL of anti-DIG antibody solution diluted at 1/10,000 with blocking buffer overnight at 4°C with gentle agitation.
30. Discard the antibody solution and wash the embryos briefly in PBT.
31. Wash six times, 15 min/wash, in PBT at room temperature with gentle shaking.
32. Briefly dry the embryos on a sheet of absorbent paper.
33. Incubate the embryos at room temperature three times, 5 min/wash, in alkaline Tris buffer with agitation.
34. Transfer the embryos to 1.5 mL microfuge tubes.
35. Remove the alkaline Tris buffer and replace with 0.7-mL staining solution prepared fresh and kept in the dark (see Note 44).
36. Transfer the embryos to 12-well ceramic plates. Monitor the color reaction periodically under a dissecting microscope, lit from above. Keep the embryos in the dark between checks.
37. Stop the reaction by transferring the embryos to 1.5-mL Eppendorf tubes containing 1 mL stop solution.
38. Transfer embryos to a 6-well plate containing 100% glycerol. Shake gently overnight at room temperature in the dark.
39. Mount the embryos in 100% glycerol and observe microscopically.
40. Take images (Fig. 3).

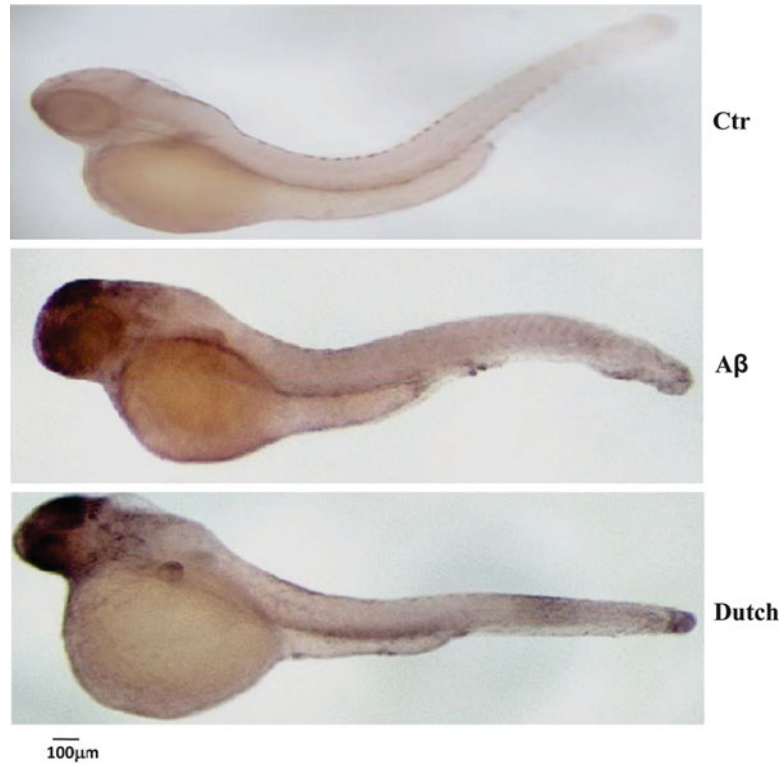

Fig. 3. p21-In situ hybridization in embryos at 72 hpf. Lateral (×4) view of control and treated embryos (Aβ and Dutch peptides at 2.5 μM), showing p21 mRNA expression in whole body, with enrichment in the head. Image adapted from ref. 5.

4. Notes

1. All animal experiments should be performed in accordance with the relevant authorities' guidelines and regulations.
2. Poison. Highly toxic, may be fatal if swallowed or inhaled. Experimental teratogen. Irritant. Use safety glasses, gloves, and dust mask and ensure good ventilation if powdered product may get into the atmosphere.
3. Noxious substance. Avoid inhalation and contact with the eye and skin. Use protective clothes during preparation and application. To prepare 4% PFA (see Subheading 2.1), dissolve 4 g of paraformaldehyde in 1× PBS and heat until the powder has dissolved completely. When the powder is completely dissolved, cool the solution until it reaches room temperature (18–25°C). This solution, stored at room temperature, can be used for a couple of days. Never boil the solution because paraformaldehyde will be degraded and the medium will acidify due to the formation of formic acid.
4. Avoid inhalation and contact with the eye and skin.

5. This substance is not classified as dangerous, it may act as a mild irritant for the eyes, skin, and respiratory system.
6. Store X-gal solution protected from light at –20°C, and other kit components at 4°C. All components supplied are stable for 1 year. X-gal solution, contains the 5-bromo-4-chloroindol-3-yl beta-D-galactopyranoside (XGal) and *N*,*N*-dimethylformamide (DMF), which are defined as dangerous substances or hazardous chemicals as defined in European Community Directives 67/548/EEC or 1999/45/EC, and Hazard Communication Standard 29 CFR 1910.1200. Wear eye protection, and gloves to prevent skin contact. Use this product with adequate ventilation. Similarly, 10× Staning Solution A contains Potassium hexacyanoferrate (III) (Red prussiate), and Potassium hexacyanoferrate (II) trihydrate (Yellow prussiate), 100× fixing solution contains glutaraldehyde and methanol and, finally, 10× Staining Solution B contains Sodium chloride, Sodium dihydrogenorthophosphate, Citric acid, and Magnesium chloride, all of which are defined as dangerous substances or hazardous chemicals as defined in European Community Directives 67/548/EEC or 1999/45/EC, and Hazard Communication Standard 29 CFR 1910.1200.
7. NaN_3, sodium azide is toxic by ingestion and under acidic conditions may release the highly toxic gas hydrazoic acid. It should be manipulated carefully and under an appropriate fume hood.
8. The resin contains 80% polyhydroxy substituted bisphenol A dimethacrylate resin, 19.6% C12 methacrylate ester, 0.9% benzoyl peroxide. The resin is of very low viscosity and designed to penetrate biological tissue being an embedding resin. Hence care should be taken to minimize skin contact. Be careful if allergy to methacrylates is known. Avoid all contact with eyes. The resin should be kept cool (4°C) to prevent premature polymerization.
9. Methacrylates resins as LR White are hydrophilic and tend to wet the block surface because they attract water. Dry the block face with filter paper, and if necessary, use an antistatic device (gun) to eliminate electrostatic charging.
10. Work careful to avoid contamination, use appropriate tips with filter RNAse/DNase free and wear gloves.
11. To prepare 0.5 M EDTA (see Subheading 3.2, step 8), dissolve 186.1 g of EDTA in 800 mL of water. Add 15 g of NaOH pellets and make up to 1 L by adding water when all pellets are dissolved. EDTA may behave as a mild irritant for the eyes, skin, and respiratory system.
12. Not a hazardous substance or mixture according to Regulation (EC) No. 1272/2008. Avoid dust formation, breathing vapors,

mist, or gas. During the preparation of the gel, avoid boiling and bubbles.

13. DTT is a hazardous substance that can cause skin irritation and severe ocular damage.
14. Avoid inhalation and contact with the eye and skin.
15. Hydrogen peroxide solution should be prepared fresh immediately before use.
16. Stock solution is prepared by diluting 200 mL of Tween 20 with 800 mL of sterile water. After complete homogenization of the solution, store at room temperature. Protect the solution from light.
17. Tween 20 may behave as a mild irritant for the eyes, skin, and respiratory system.
18. The solution is extremely destructive to tissue of the mucous membranes and upper respiratory tract, eyes, and skin. Be very careful. Wear suitable protective clothing, gloves and eye/face protection. Wear respiratory protection.
19. Caution, chloroform is harmful, and irritating to eyes and skin. Harmful if swallowed. Limited evidence of a carcinogenic effect. Harmful: danger of serious damage to health by prolonged exposure through inhalation and if swallowed. Probable Carcinogen. Target organ(s): liver and cardiovascular system. Use only in a chemical fume hood. Wear chimica resistant gloves.
20. Caution, hazard solution, causes severe skin burns and eye damage. May cause respiratory irritation. Wear respiratory protection. Avoid breathing vapors, mist or gas. Ensure adequate ventilation. Evacuate personnel to safe areas.
21. Dissolve 50 mg of NBT in 0.7 mL of *N*,*N*′-dimethylformamide and 0.3 mL of sterile water and store at –20°C for max 6 months.
22. Dissolve 50 mg of BCIP in 1 mL of *N*,*N*′-dimethylformamide anhydrous and store at –20°C for max 6 months.
23. *N*,*N*′-dimethylformamide is a dangerous substance as defined in European Community Directives 67/548/EEC or 1999/45/EC, and Hazard Communication Standard 29 CFR 1910.1200. Wear gloves to prevent skin contact. Use this product with adequate ventilation.
24. Mix 1× PBS, pH 5.5, with 1 mM EDTA, and 0.1% Tween 20 (v/v) and store at room temperature.
25. Dissolve 10.8 g of Na_2HPO_4, 65 g of NaH_2PO_4, 80 g of NaCl and 2 g of KCl in 1 L of water.
26. Mix 1× PBS, and 0.1% Tween 20 (v/v) and store at room temperature.

27. Dissolve 175.3 g of NaCl and 88.2 g of Citric acid trisodium salt in 1 L of water and store at room temperature.
28. Mix 1× PBT, 2% sheep serum (v/v), BSA 2 mg/mL, and store at 4°C.
29. 100 mM Tris–HCl, pH 9.5, 50 mM $MgCl_2$,100 mM NaCl and 0.1% Tween 20 (v/v).
30. Dissolve 1 g of protease in 100 mL of 0.3× Danieau buffer, incubate for 2 h at 37°C, aliquot in 5-mL tubes and store at –20°C. The Danieu buffer should be prepared as follow: mix 2.9 M NaCl (60 mL), 70 mM KCl (30 mL), 40 mM $MgSO_4 7H_2O$ (30 mL), 60 mM $Ca(NO_3)_2$ (30 mL), 0.5 M HEPES (pH 7.2) (30 mL), H_2O to 1,000 mL. Pronase softens the chorion. In this stage, approximately half of the population should be dechorionated after rinsing. To remove any remaining chorions, pass the embryos gently through a Pasteur capillary pipette with a small opening. Once dechorionated, the embryos are very fragile and should be manipulated gently.
31. PTU solution prevents the formation of melanin pigments and greatly facilitates visualization of the final signal. PTU is an inhibitor of tyrosinase, an enzyme required for melanin synthesis. PTU affects early development: do not treat embryos before the end of gastrulation. Further a reduction of cell viability in catecholaminergic neuronal cells has been reported after PTU treatment. These effects can be avoided by using the hydrogen peroxide for dechorionation.
32. Aβ (1–40) peptides, WT or bearing the Duch mutation—were synthesized at Espikem (University of Florence, Italy). In all cases peptides were purified by reverse phase high-pressure liquid chromatography, eluting as a single peak, and their respective molecular masses corroborated by mass spectrometry. Peptides were first dissolved to 1 mM in cold (4°C) hexafluoroisopropanol (HFIP,) in a chemical fume hood to break down β-sheet structures and disrupt hydrophobic forces in aggregated Aβ. HFIP was allowed to evaporate, and the resulting clear peptide films were vacuum dried. Before use, HFIP-treated peptides were dissolved to 5 mM in anhydrous dimethyl sulfoxide (DMSO) and further diluted (1–25 μM) in fish water.
33. Alternatively, embryos can be left in fixing solution overnight at 4°C.
34. In addition to the use of antisense RNA probes, a sense (control) RNA probe of the corresponding gene should be performed to provide indications about the background signal that may appear. Primers should generate linear DNA containing one T3 or T7 RNA polymerase promoter, which should be located at 3′ (for antisense probes) or 5′ (for sense probes) of

the cDNA or exon of interest. The sequences to include the T3 or T7 RNA polymerase promoter in the appropriate primer are T3: 5′-CATTAACCCTCACTAAAGGGAA-3′ or T7: 5′-TAAT ACGACTCACTATAGGG-3′ (reverse primer for antisense probes, forward primer for sense probes). Sequences should be located at the 5′ extremity of the primer. Be careful not to contaminate the PCRs. Use sterile tubes and filter tips and wear gloves. Alternatively to PCR amplification, cDNAs in plasmids can be linearized using restriction enzymes that have a unique site located 5′ (for antisense probes) or 3′ (for sense probes) to the insert. Purification of linear DNA can be achieved by phenol/chloroform extraction followed by ethanol precipitation.

35. Centrifuge for 1 min only to avoid overdrying of the sample. Purified PCR products can be stored for several months at –20°C.
36. In this chapter, we describe the approach using the synthesized p21 RNA probe tagged with digoxygenin uridine-5′-triphosphate. Following hybridization, the transcript is visualized by immunohistochemistry using an anti-digoxygenin antibody conjugated to alkaline phosphatase.
37. Purified digoxygenin-labeled antisense (or sense) RNA can be stored for months at –20°C.
38. Alternatively, embryos can be left in fixing solution overnight at 4°C.
39. This step is necessary for permeabilization of embryos even if you do not want to store them. These embryos can be stored at –20°C for several months. Use MeOH and not ethanol because ethanol causes a higher background.
40. This step permeabilizes the embryos and allows the RNA probe to penetrate. It is important to use the times indicated for proteinase K treatment. There are different times of treatment for each developmental stage. Under-digestion would not allow the probe to get in, whereas over-digestion will alter the morphology of the embryo.
41. The prehybridized embryos can be stored in hybridization medium at –20°C for up to several weeks.
42. Do not use excessive amounts of RNA probe. This increases background labeling. This high hybridization temperature and the percentage of formamide in the hybridization buffer ensure high stringency of hybridization and decrease the occurrence of cross-hybridization.
43. These high-stringency washes prevent nonspecific hybridization of the probe.
44. The staining solution should be light yellow. If it turns pink, prepare a fresh solution to prevent background staining. Stain for 30 min to overnight.

Acknowledgments

This work was supported by Ministero dell'Istruzione, dell'Università e della Ricerca (MIUR), PRIN project 2008.

References

1. Revesz T, Holton JL, Lashley T, Plant G, Frangione B, Rostagno A, Ghiso J (2009) Genetics and molecular pathogenesis of sporadic and hereditary cerebral amyloid angiopathies. Acta Neuropathol 118:115–130
2. Wisniewski T, Ghiso J, Frangione B (1991) Peptides homologous to the amyloid protein of Alzheimer's disease containing a glutamine for glutamic acid substitution have accelerated amyloid fibril formation. Biochem Biophys Res Commun 179:1247–1254
3. Solito R, Corti F, Fossati S, Mezhericher E, Donnini S, Ghiso J, Giachetti A, Rostagno A, Ziche M (2009) Dutch and Arctic mutant peptides of beta amyloid(1-40) differentially affect the FGF-2 pathway in brain endothelium. Exp Cell Res 315:385–395
4. Maat-Schieman M, Roos R, van Duinen S (2005) Hereditary cerebral hemorrhage with amyloidosis-Dutch type. Neuropathology (J Japan Soc Neuropathol) 25:288–297
5. Donnini S, Solito R, Cetti E, Corti F, Giachetti A, Carra S, Beltrame M, Cotelli F, Ziche M (2010) Abeta peptides accelerate the senescence of endothelial cells in vitro and in vivo, impairing angiogenesis. FASEB J (Fed Am Soc Exp Biol) 24:2385–2395
6. Kishi S, Uchiyama J, Baughman AM, Goto T, Lin MC, Tsai SB (2003) The zebrafish as a vertebrate model of functional aging and very gradual senescence. Exp Gerontol 38: 777–786
7. Donnini S, Cantara S, Morbidelli L, Giachetti A, Ziche M (2006) FGF-2 overexpression opposes the beta amyloid toxic injuries to the vascular endothelium. Cell Death Differ 13:1088–1096
8. Poleo G, Brown CW, Laforest L, Akimenko MA (2001) Cell proliferation and movement during early fin regeneration in zebrafish. Dev Dyn (Am Assoc Anat) 221:380–390
9. Jung T, Bader N, Grune T (2007) Lipofuscin: formation, distribution, and metabolic consequences. Ann N Y Acad Sci 1119:97–111
10. Kishi S, Bayliss PE, Uchiyama J, Koshimizu E, Qi J, Nanjappa P, Imamura S, Islam A, Neuberg D, Amsterdam A, Roberts TM (2008) The identification of zebrafish mutants showing alterations in senescence-associated biomarkers. PLoS Genet 4:e1000152
11. Jowett T, Lettice L (1994) Whole-mount in situ hybridizations on zebrafish embryos using a mixture of digoxigenin- and fluorescein-labelled probes. Trends Genetics TIG 10:73–74
12. Santoriello C, Deflorian G, Pezzimenti F, Kawakami K, Lanfrancone L, d'Adda di Fagagna F, Mione M (2009) Expression of H-RASV12 in a zebrafish model of Costello syndrome causes cellular senescence in adult proliferating cells. Dis Model Mech 2:56–67
13. Lu WJ, Abrams JM (2006) Lessons from p53 in non-mammalian models. Cell Death Differ 13:909–912
14. Kimmel CB, Ballard WW, Kimmel SR, Ullmann B, Schilling TF (1995) Stages of embryonic development of the zebrafish. Dev Dyn (Am Assoc Anat) 203:253–310
15. Furthauer M, Lin W, Ang SL, Thisse B, Thisse C (2002) Sef is a feedback-induced antagonist of Ras/MAPK-mediated FGF signalling. Nat Cell Biol 4:170–174
16. Furthauer M, Reifers F, Brand M, Thisse B, Thisse C (2001) Sprouty4 acts in vivo as a feedback-induced antagonist of FGF signaling in zebrafish. Development 128:2175–2186
17. Furthauer M, Thisse C, Thisse B (1997) A role for FGF-8 in the dorsoventral patterning of the zebrafish gastrula. Development 124:4253–4264
18. Tsang M, Friesel R, Kudoh T, Dawid IB (2002) Identification of Sef, a novel modulator of FGF signalling. Nat Cell Biol 4:165–169

INDEX

Lorenzo Galluzzi et al. (eds.), *Cell Senescence: Methods and Protocols*, Methods in Molecular Biology, vol. 965,
DOI 10.1007/978-1-62703-239-1, © Springer Science+Business Media, LLC 2013

D

E

F

G

H

I

K

L

M

N

O

P

Q

R

S

T

V

Y

Z